University of Fribourg (Switzerland)

Department of Biology

UNIVERSITÉ DE FRIBOURG
UNIVERSITÄT FREIBURG

Nutrient and Energy Sensing in Yeast: The Crosstalk of the SNF1/AMPK and TORC1/mTORC1 Pathways

THESIS

Presented to the Faculty of Science and Medicine of the University of Fribourg
(Switzerland) in consideration for the award of the academic grade of
Doctor of Philosophy in Biochemistry

by
Marco Caligaris
from
Lecco, Italy

Thesis N°: 8099
UNIPRINT
2024

Accepted by the Faculty of Science and Medicine of the University of Fribourg (Switzerland) upon the recommendation of:

Prof. Robbie J. Loewith, University of Genève, Genève, Switzerland
Dr. Sébastien Leon, Université de Paris, CNRS, Institut Jacques Monod, Paris, France
Prof. Urs Albrecht, University of Fribourg, Fribourg, Switzerland

Fribourg, 21.01.2025

Thesis Supervisor:	Dean:
…………………………………….	…………………………………….
Prof. Claudio De Virgilio	Prof. Ulrich Ultes-Nitsche

“Don't Panic.”

— Douglas Adams, *The Hitchhiker’s Guide to the Galaxy*

Index

LIST OF ABBREVIATIONS **9**

SUMMARY **18**

RÉSUMÉ **21**

GENERAL INTRODUCTION **24**

1. The SNF1 complex **25**
  1.1. Components of the SNF1 complex 26
  1.2. Upstream regulation of SNF1 27
    1.2.1. The SNF1 activating kinases (SAKs) 27
    1.2.2. The protein phosphatase 1 (PP1) 28
    1.2.3. Model of SNF1 regulation 29
  1.3. Downstream signaling 31
  1.4. Genetic modulation of SNF1 activity 35
  1.5. Conservation of the SNF1 complex 36
    1.5.1. Components of the AMPK complex 37
    1.5.2. Upstream regulation of AMPK 38
    1.5.3. AMPK downstream signaling 39
2. The TORC1 complex **40**
  2.1. Components of the TORC1 complex 40
  2.2. Upstream regulation of TORC1 42
    2.2.1. The Rag GTPases 42
      2.2.1.1. GEFs and GAPs for Gtr1 and Gtr2 45
    2.2.2. Pib2 46
    2.2.3. TORC1 pools in yeast cells 47
  2.3. Downstream signaling 48
    2.3.1. Tap42 and protein phosphatases 48
    2.3.2. Other direct and indirect TORC1 targets 50
  2.4. Molecules modulating TORC1 activity 51
  2.5. Conservation of the TORC1 complex 52
    2.5.1. Components of mTORC1 52
    2.5.2. Upstream regulation of mTORC1 53
      2.5.2.1. Nutrient-mediated regulation of mTORC1 53
      2.5.2.2. Hormones-mediated regulation of mTORC1 57
      2.5.2.3. mTORC1 pools in mammalian cells 58
    2.5.3. mTORC1 downstream signaling 59
3. The Yeast Protein Kinase Sch9 Functions as a Central Nutrient-Responsive Hub That Calibrates Metabolic and Stress-Related Responses **61**

3.1. Introduction 61
3.2. Contribution to this chapter: 62
4. Crosstalk between the SNF1/AMPK and TORC1/mTORC1 signaling pathways 84
4.1. SNF1/AMPK regulation of TORC1/mTORC1 84
4.2. TORC1/mTORC1 regulation of SNF1/AMPK 87
4.3. SNF1 and TORC1 converge on common targets in budding yeast 88
CHAPTER 1: SNF1/AMPK FINE-TUNES TORC1 SIGNALING IN RESPONSE TO GLUCOSE STARVATION 90
1. Introduction 91
2. Key contributions of this chapter 92
CHAPTER 2: THE NUTRIENT-RESPONSIVE CDK PHO85 PRIMES THE SCH9 KINASE FOR ITS ACTIVATION BY TORC1 125
1. Introduction 126
2. Key contributions of this chapter 128
CHAPTER 3: IDENTIFICATION OF SPATIALLY DISTINCT POOLS OF SNF1/AMPK AND THEIR TARGETS IN YEAST 173
3.1. INTRODUCTION 174
3.1.1. The SNF1 β-subunits 174
3.1.1.1. The role of the β-subunits in regulating SNF1 localization 176
3.1.1.2. Localization and regulation of AMPK complexes in mammalian cells 177
3.1.1.3. Modulation of SNF1 activity via the β-subunits 178
3.2. RESULTS 180
3.2.1. Targeted mutagenesis and functional analysis of SNF1 pools in yeast 180
3.2.2. Targeted localization and activity of SNF1-specific probes in yeast cellular compartments 186
3.2.3. Functional analysis of SNF1 pools in yeast via monitoring ACC1^{Probes} 190
3.2.4. Phosphoproteomic profiling of SNF1 complexes 194
3.2.5. Impact of β-subunit deletions on Snf1 levels and stability 204
3.3. DISCUSSION 206
CHAPTER 4: PROXIES INTRODUCE BIAS IN DECODING TORC1 ACTIVITY .. 211
1. Introduction 212
2. Key contributions of this chapter 213
GENERAL DISCUSSION 222
Mechanistic insights on SNF1 regulation of TORC1 activity 223
Phosphorylation and functional modulation of Sch9 by nutrient-sensing pathways 226
Spatial regulation and target specificity of SNF1 in yeast 228
MATERIAL AND METHODS 231

Material and Methods 232
Supplementary tables 242
REFERENCES 255
APPENDIX 282
Acknowledgments 283
Curriculum Vitae 285

LIST OF ABBREVIATIONS

1NM-PP1: 1-NaphthylMethyl PyrazoloPyrimidine 1
2NM-PP1: 2-NaphthylMethyl PyrazoloPyrimidine 1
4E-BP1: eIF4E Binding Protein 1
AC1-5: ACC Central 1-5
Acc1: Acetyl-CoA Carboxylase 1
ADP: Adenosine DiPhosphate
Adr1: Alcohol Dehydrogenase II synthesis Regulator 1
AID: AutoInhibitory Domain
Ala: ALAnine
AMP: Adenosine MonoPhosphate
AMPK: AMP-activated protein Kinase
AMPKRs: AMPK Related kinases
AP-3: Adaptor Protein 3
Apl5: clathrin Adaptor Protein complex Large chain 5
Apl6: clathrin Adaptor Protein complex Large chain 6
Apm3: clathrin Adaptor Protein complex Medium chain 3
Aps3: clathrin Associated Protein complex Small subunit 3
as: Analog Sensitive
Asp: ASPartate
Atg1: AuTophaGy related 1
Atg11: AuTophaGy related 11
Atg13: AuTophaGy related 13
Atg8: AuTophaGy related 8
ATP: Adenosine TriPhosphate
ATPase: Adenosine TriPhosphatase
BC: Biotin Carboxylase
Bcy1: Bypass of CYclic-AMP requirement
Bmh1/2: Brain Modulosignalin Homolog 1/2
CAD: C-terminal TORC1-Activating Domain
CaMKK2: Ca^{2+}/calModulin-dependent Kinase 2
cAMP: Cyclic Adenosine MonoPhosphate
Cat8: CATabolite repression 8
CBM: Carbohydrate Binding Module
CBS: Cystathionine β-Synthase
Cdc55: Cell Division Cycle 55

Cdc60: Cell Division Cycle 60
Crm1: Chromosome Region Maintenance 1
Cryo-EM: CRYOgenic Electron Microscopy
CSRE: carbon source-responsive element
CT: CarboxylTransferase
Cyr1: CYclic AMP Requirement
DENN: Differentially Expressed in Normal and Neoplastic cells
Deptor: DEP-domain containing mTOR-interacting protein
DMSO: DiMethylSulfOxide
EDTA: EthyleneDiamine Tetraacetic Acid
EGO-TC: Ego Ternary Complex
Ego1: Exit from rapamycin-induced GrOwth arrest 1
Ego2: Exit from rapamycin-induced GrOwth arrest 2
Ego3: Exit from rapamycin-induced GrOwth arrest 3
EGOC: Exit from rapamycin-induced GrOwth arrest Complex
eIF2α: Eukaryotic Initiation Factor 2α
Elm1: ELongated Morphology 1
ER: Endoplasmic Reticulum
Fab1: Forms Aploid and Binucleate cells 1
FAT: FKBP12 rapamycin Associated protein [FRAP], ATM, TRRAP
FATC: C-terminal FAT
FKBP12: FK506 Binding Protein 12
FLCN: FoLliCuliN
FNIP1/2: FolliculiN Interacting Protein 1/2
Fpr1: Fk506-sensitive Proline Rotamase 1
FRB: FKBP12-Rapamycin Binding
FYVE: Fab 1, YOTB, Vac 1, and EEA1
GAAC: General Amino Acid Control
GABA: Gamma-AminoButyric Acid
Gal83: GALactose metabolism 83
GAP: GTPase Activating Protein
Gap1: General Amino acid Permease 1
GATOR1: GAP Activity TOward Rags 1
GATOR2: GAP Activity TOward Rags 2
Gcn2: General Control Non-derepressible 2

Gcn4: General Control Non-derepressible 4

GDI: Guanine nucleotide Dissociation Inhibitor

GDP: Guanosine DiPhosphate

GEF: Guanine nucleotide Exchange Factors

GFP: Green Fluorescent Protein

Glc: GLuCose

Glc7: GLyCogen 7

Gln3: GLutamiNe metabolism 3

Glu: GLUtamate

GLUT4: GLUcose Transporter type 4

Gpa2: G-Protein Alpha subunit

GTP: Guanosine TriPhosphate

GTPase: Guanosine TriPhosphatase

Gtr1: GTp binding protein Resemblance 1

Gtr2: GTp binding protein Resemblance 2

HEAT: Huntingtin, Elongation factor 3, a subunit of PP2A, and TOR1

HM: Hydrophobic Motif

HOPS: HOmotypic fusion and vacuole Protein Sorting)

Hxt2: HeXose Transporter 2

Hxt4: HeXose Transporter 4

IAA: Indole-3-Acetic Acid

Iml1: Increased Minichromosome Loss 1

IPTG: Isopropyl β- d-1-thiogalactopyranoside).

IR: Insulin Receptor

IRS: Insulin Receptor Substrates

KD: Kinase Domain

KICSTOR: KPTN, ITFG2, C12orf66 and SZT2-containing regulator of mTORC1

Kog1: Kontroller Of Growth 1

LAMTOR1: Late endosomal/lysosomal Adaptor, MAPK, and mTOR activator 1

LAMTOR2: Late endosomal/lysosomal Adaptor, MAPK, and mTOR activator 2

LAMTOR3: Late endosomal/lysosomal Adaptor, MAPK, and mTOR activator 3

LAMTOR4: Late endosomal/lysosomal Adaptor, MAPK, and mTOR activator 4

LAMTOR5: Late endosomal/lysosomal Adaptor, MAPK, and mTOR activator 5

LB: Luria-Bertani

LeuRS: LEUcyl-tRNA Synthetases

LFC: Lysosomal FLCN Complex
LKB1: Liver Kinase B1
Lst4: Lethal with Sec Thirteen 4
Lst7: Lethal with Sec Thirteen 7
Lst8: Lethal with Sec Thirteen 8
LYCHOS: LYsosomal CHOlesterol Signaling
Meh1: Multicopy suppressor of Ers1 Hygromycin B sensitivity 1
Mig1: Multicopy Inhibitor of GAL gene expression 1
Mig2: Multicopy Inhibitor of GAL gene expression 2
Mms21: Methyl MethaneSulfonate sensitivity 21
Msn2: Multicopy suppressor of SNF1 mutation 2
Msn4: Multicopy suppressor of SNF1 mutation 4
MST: MicroScale Thermophoresis
Mtc5: Maintenance of Telomere Capping 5
mTORC1: Mechanistic Target Of Rapamycin Complex 1
NES: Nuclear Export Signal
NID: N-terminal TORC1-Inhibiting Domain
NLS: Nuclear Localization Signal
Npr1: Nitrogen Permease Reactivator 1
Npr2: Nitrogen Permease Regulator 2
Npr3: Nitrogen Permease Regulator 3
OD$_{600nm}$: Optical Density at 600 nm
ORF: Open Reading Frame
PAS: Phagophore Assembly Site
PDK1: 3-Phosphoinositide-Dependent protein Kinase 1
Pho8: PHOsphate metabolism 8
Pho80: PHOsphate metabolism 80
Pho85: PHOsphate metabolism 85
PI[3,5]P$_2$: PhosphatidylInositol-3,5-bisPhosphate
PI3K: PhosphoInositide 3-Kinase
PI3P: PhosphatidylInositol-3-Phosphate
Pib2: PhosphatidylInositol-3-phosphate Binding 2
PIKKs: PhosphatidylInositol Kinase-related Kinases
PIP2: PhosphatidylInositol (4,5)-bisPhosphate
PIP3: PhosphatidylInositol (3,4,5)-trisPhosphate

PKA: Protein Kinase A

Pma1: Plasma Membrane ATPase

PP1: Protein Phosphatase type 1

PP2A: Protein Phosphatase type 2A

PP6: Protein Phosphatase 6

Pph21: Protein Phosphatase 21

Pph22: Protein Phosphatase 22

PRAS40: Proline-rich Akt substrate 40

PTM: Post-Translational Modification

Rag: RAs-related GTP binding protein

Ras1: homologous to RAS proto-oncogene 1

Ras2: homologous to RAS proto-oncogene 2

RBR: Rag Binding Region

Rck2: Radiation sensitivity Complementing Kinase 2

RD: Regulatory Domain

Rds2: Regulator of Drug Sensitivity 2

Reg1: REsistance to Glucose repression 1

Reg2: REsistance to Glucose repression 2

Rhb1: RHeB homolog 1

Rheb: RAS Homolog Enriched in the Brain

rpm: Revolutions Per Minute

Rps6: Ribosomal Protein of the Small subunit 6

Rtc1: Restriction of Telomere Capping 1

Rts1: Rox Three Suppressor 1

S6K1: S6 Kinase 1

Sak1: SNF1 Activating Kinase 1

SAKs: SNF1 Activating KinaseS

SAM: S-AdenosylMethionine

SAMTOR: S-AdenosylMethionine sensor upstream of mTORC1

Sap155: Sit4 Associated Protein 155

Sap185: Sit4 Associated Protein 185

Sap190: Sit4 Associated Protein 190

Sap4: Sit4 Associated Protein 4

SC: Synthetic Complete

Sch9: Scott Cameron HindIII library clone number 9

SD: Synthetic Defined
SD: Synthetic Dropout
SDS: Sodium Dodecyl Sulfate
Sea2: SEh1-Associated 2
Sea3: SEh1-Associated 3
Sea4: SEh1-Associated 4
SEAC: SEh1-Associated Complex
SEACAT: SEAC subcomplex Activating TORC1 signaling
SEACIT: SEAC subcomplex Inhibiting TORC1 signaling
Sec13: SECretory 13
Seh1: SEc13 Homolog 1
Ser: SERine
Ser3: SERine requiring 3
Ser33: SERine requiring 33
Sfp1: Split Finger Protein 1
Shp1: Suppressor of High-copy PP1
SILAC: Stable Isotope Labeling by Amino acids in Cell culture
Sip1: SNF1-Interacting Protein 1
Sip2: SNF1-Interacting Protein 2
Sip4: SNF1-Interacting Protein 4
Sit4: Suppressor of Initiation of Transcription 4
SLC38: SoLute Carrier family 38
Slm4: Synthetic Lethal with Mss4
Snf1: Sucrose Non Fermenting 1
SNF1: Sucrose Non Fermenting 1 complex
Snf4: Sucrose Non Fermenting 4
SnRK: SNF1-Related protein Kinase
ssDNA: Salmon Sperm DNA
STRE: STress Response Element
Suc2: SUCrose 2
SUMO: Small Ubiquitin-like MOdifier
TAK1: Transforming growth factor-β-Activated Kinase
Tap42: Two A phosphatase Associated Protein 42
Tat2: Tryptophan Amino acid Transporter 2
TCA cycle: TriCarboxylic Acid cycle

TCA: TriChloroAcetic acid
Tco89: Tor Complex One subunit with 89 kDa
TFEB: Transcription Factor EB
TGN: Trans-Golgi Network
Tip41: Tap42 Interacting Protein 41
Tor1: Target Of Rapamycin 1
Tor2: Target Of Rapamycin 2
TORC1: Target Of Rapamycin Complex 1
TORC2: Target Of Rapamycin Complex 2
TOROID: TORC1 Organized in Inhibited Domain
TOS: TOR Signaling
Tos3: Target Of Sbf 3
Tpd3: tRNA Processing Deficient 3
Tpk1-3: Takashi's Protein Kinase 1-3
TRAIL: Tumor necrosis factor-Related Apoptosis-Inducing Ligand
TSC: Tuberous Sclerosis Complex
TSC1: Tuberous Sclerosis Complex 1
TSC2: Tuberous Sclerosis Complex 2
ULK1: Unc-51-Like autophagy-activating Kinases 1
Ulp1: UbL-specific Protease 1
Ure2: UREidosuccinate transport 2
v-ATPase: Vacuolar ATPase
Vac14: VACuolar segregation 14
Vac7: VACuolar segregation 7
Vam6: VAcuolar Morphogenesis 6)
Vma1: Vacuolar Membrane ATPase
Vps11: Vacuolar Protein Sorting 11
Vps16: Vacuolar Protein Sorting 16
Vps18: Vacuolar Protein Sorting 8
Vps27: Vacuolar Protein Sorting 27
Vps33: Vacuolar Protein Sorting 33
Vps39: Vacuolar Protein Sorting 39
Vps41: Vacuolar Protein Sorting 41
Y2H: Yeast Two-Hybrid
YPD: Yeast extract Peptone Dextrose

Ypk1: Yeast Protein Kinase 1

Ypk2: Yeast Protein Kinase 2

Ypk3: Yeast Protein Kinase 3

Ypt1: Yeast Protein Two 1

SUMMARY

In eukaryotic organisms, regulating metabolism and growth in response to nutrient availability and cellular energy status is crucial for survival. The conserved SNF1/AMPK and TORC1/mTORC1 protein complexes act as key nutrient and energy sensors, facilitating rapid adaptation to changing conditions. SNF1/AMPK promotes catabolic and stress response pathways when cellular energy or glucose levels are low. Conversely, TORC1/mTORC1 inhibits these processes and stimulates anabolic metabolism, protein synthesis, and growth when nutrients and amino acids are abundant.

In the first chapter of this PhD thesis we explored the regulatory mechanism by which SNF1/AMPK inhibits mTORC1/TORC1 in the budding yeast *Saccharomyces cerevisiae*. Using SILAC-based phosphoproteomics, genetic, biochemical, and physiological analyses, we identified SNF1-dependent phosphorylation sites on the upstream regulator of TORC1 Pib2, and the downstream effector Sch9. This chapter extends Pib2's role in integrating glucose and amino acid signals to control TORC1. In parallel, it demonstrates that SNF1 phosphorylation of Sch9 at its N-terminal region counteracts the phosphorylation of a critical C-terminal TORC1-target residue within Sch9. The combined effects of SNF1-mediated phosphorylation of Pib2 and Sch9 are sufficient for short-term TORC1 inhibition in glucose-starved cells, only measured with respect to Sch9 phosphorylation.

In chapter two we investigated the synthetic lethality caused by the loss of the protein kinase Sch9 when combined with the loss of the cyclin-dependent kinase (CDK) Pho85 or its inhibitor Pho81, both crucial for phosphate sensing and cell cycle regulation. We found that the CDK-cyclin pairs Pho85-Pho80 and Pho85-Pcl6/Pcl7 become essential for growth in the absence of Sch9. These pairs regulate the activity and distribution of the phosphatidylinositol-3-phosphate 5-kinase Fab1 on endosomes and vacuoles, which generates phosphatidylinositol-3,5-bisphosphate (PI[3,5]P_2). This, in turn, recruits TORC1 and Sch9. Additionally, Pho85-Pho80 directly phosphorylates Sch9 at Ser^{726} and Thr^{723}, priming it for subsequent phosphorylation and activation by TORC1. Furthermore, we discovered that the loss of the transcription factor Pho4 rescues the synthetic lethality caused by the loss of Pho85 and Sch9, indicating that both pathways converge on Pho4, which is linked to a feedback loop involving the high-affinity phosphate transporter Pho84 that fine-tunes Sch9-mediated responses.

In chapter three we focused on identifying SNF1 targets phosphorylated at various cellular compartments. The SNF1 β-subunits are needed for SNF1 kinase activity, acting as scaffolds for the α- and γ-subunits, aiding in substrate recognition, and regulating SNF1 complex localization. Under high glucose conditions, SNF1 is mostly inactive and cytosolic. Upon carbon starvation, SNF1 is activated and either translocates to the nucleus with Gal83, docks to vacuolar membranes with Sip1, or remains in the cytoplasm with Sip2. To investigate the specific roles of these SNF1 complexes, we used CRISPR/Cas9 to introduce amino acid substitutions in the β-subunits, creating yeast strains with only one functional SNF1 complex. After confirming that our mutations do not cause compensatory effects, we employed SILAC-based phosphoproteomics, interactomics, and TurboID proximity labeling to identify the target profiles of these SNF1 pools. In this study, we confirmed previously identified SNF1 targets and clarified which specific SNF1 pool is involved in their regulation. Additionally, we discovered new putative SNF1 targets, specifically phosphorylated in each cellular compartment, which will require further detailed investigation to understand their roles and regulatory mechanisms.

In chapter four we examined and compared the most commonly used TORC1 activity readouts in yeast, specifically Sch9 phosphorylation at Thr^{737} and Rps6 phosphorylation at Ser^{232} and Ser^{233}. We revealed that these effectors show different phosphorylation patterns in response to rapamycin treatment or changes in nitrogen availability, suggesting that the choice of TORC1 proxies can bias the interpretation of TORC1 activity.

RÉSUMÉ

Chez les organismes eucaryotes, la régulation du métabolisme et de la croissance en réponse à la disponibilité des nutriments et à l'état énergétique cellulaire est cruciale pour la survie. Les complexes protéiques conservés SNF1/AMPK et TORC1/mTORC1 agissent comme des capteurs clés de nutriments et d'énergie, facilitant une adaptation rapide aux conditions changeantes. SNF1/AMPK favorise les voies cataboliques et de réponse au stress lorsque les niveaux d'énergie ou de glucose cellulaires sont bas. À l'inverse, TORC1/mTORC1 inhibe ces processus et stimule le métabolisme anabolique, la synthèse des protéines et la croissance lorsque les nutriments et les acides aminés sont abondants.

Dans le premier chapitre de cette thèse de doctorat, nous avons exploré le mécanisme de régulation par lequel SNF1/AMPK inhibe mTORC1/TORC1 chez la levure bourgeonnante *Saccharomyces cerevisiae*. En utilisant la phosphoprotéomique basée sur SILAC, ainsi que des analyses génétiques, biochimiques et physiologiques, nous avons identifié des sites de phosphorylation dépendants de SNF1 sur le régulateur en amont de TORC1, Pib2, et sur l'effecteur en aval, Sch9. Ce chapitre étend le rôle de Pib2 dans l'intégration des signaux de glucose et d'acides aminés pour contrôler TORC1. Parallèlement, il démontre que la phosphorylation de Sch9 par SNF1 à son extrémité N-terminale empêche la phosphorylation d'un résidu critique cible de TORC1 à l'extrémité C-terminale de Sch9. Les effets combinés de la phosphorylation médiée par SNF1 de Pib2 et Sch9 sont suffisants pour une inhibition à court terme de TORC1 dans les cellules privées de glucose, mesurée uniquement par rapport à la phosphorylation de Sch9.

Dans le deuxième chapitre, nous avons étudié la létalité synthétique causée par la perte de la kinase protéique Sch9 lorsqu'elle est combinée à la perte de la kinase dépendante des cyclines (CDK) Pho85 ou de son inhibiteur Pho81, tous deux cruciaux pour la détection du phosphate et la régulation du cycle cellulaire. Nous avons découvert que les paires CDK-cycline Pho85-Pho80 et Pho85-Pcl6/Pcl7 deviennent essentielles pour la croissance en l'absence de Sch9. Ces paires régulent l'activité et la distribution de la phosphatidylinositol-3-phosphate 5-kinase Fab1 sur les endosomes et les vacuoles, ce qui génère du phosphatidylinositol-3,5-bisphosphate (PI[3,5]P_2). Cela, à son tour, recrute TORC1 et Sch9. De plus, Pho85-Pho80 phosphoryle directement Sch9 sur Ser^{726} et Thr^{723}, le préparant pour une phosphorylation et une activation ultérieure par TORC1. En outre, nous avons découvert que la perte du facteur de transcription Pho4 sauve la létalité synthétique causée par la perte de Pho85 et Sch9, indiquant que les deux voies convergent sur Pho4, qui est lié à une boucle de rétroaction impliquant le transporteur de phosphate à haute affinité Pho84, ajustant finement les réponses médiées par Sch9.

Dans le troisième chapitre, nous nous sommes concentrés sur l'identification des cibles de SNF1 phosphorylées dans divers compartiments cellulaires. Les sous-unités β de SNF1 sont nécessaires à l'activité de la kinase SNF1, agissant comme des échafaudages pour les sous-unités α et γ, aidant à la reconnaissance des substrats et régulant la localisation du complexe SNF1. En présence de niveaux élevés de glucose, SNF1 est principalement inactif et cytosolique. En cas de privation de carbone, SNF1 est activé et soit transloqué dans le noyau avec Gal83, soit se fixe aux membranes vacuolaires avec Sip1, soit reste dans le cytoplasme avec Sip2. Pour étudier les rôles spécifiques de ces complexes SNF1, nous avons utilisé CRISPR/Cas9 pour introduire des substitutions d'acides aminés dans les sous-unités β, créant des souches de levure avec un seul complexe SNF1 fonctionnel. Après avoir confirmé que nos mutations ne causent pas d'effets compensatoires, nous avons employé la phosphoprotéomique basée sur SILAC, l'interactomique et le marquage de proximité TurboID pour identifier les profils cibles de ces pools SNF1. Dans cette étude, nous avons confirmé les cibles SNF1 précédemment identifiées et clarifié quel pool SNF1 spécifique est impliqué dans leur régulation. De plus, nous avons découvert de nouvelles cibles putatives de SNF1, spécifiquement phosphorylées dans chaque compartiment cellulaire, qui nécessiteront des investigations plus détaillées pour comprendre leurs rôles et mécanismes de régulation.

Dans le chapitre quatre, nous avons examiné et comparé les lectures d'activité TORC1 les plus couramment utilisées chez la levure, en particulier la phosphorylation de Sch9 sur Thr^{737} et la phosphorylation de Rps6 sur Ser^{232} et Ser^{233}. Nous avons révélé que ces effecteurs montrent des schémas de phosphorylation différents en réponse au traitement par la rapamycine ou aux changements de disponibilité en azote, suggérant que le choix des rapporteur peut biaiser l'interprétation de l'activité de TORC1.

GENERAL INTRODUCTION

In eukaryotic organisms, regulating metabolism and growth in response to nutrient availability and internal cellular energy status is crucial for survival. The conserved SNF1/AMPK and TORC1/mTORC1 protein families are considered two of the main nutrient and energy sensors in eukaryotic cells, enabling rapid adaptation to changes in energy, nutrient, and environmental conditions.

1. The SNF1 complex

In the budding yeast *Saccharomyces cerevisiae*, the protein kinase complex SNF1 (Sucrose Non-Fermenting 1) ensures the proper coordination between nutrient availability and stress condition with cell growth, cell cycle, and stress response (Coccetti et al., 2018). Its rapid activation following nutrient depletion or environmental stress (Hong & Carlson, 2007; K. J. Simpson-Lavy & M. Kupiec, 2023) induces metabolic (Humston et al., 2011) and transcriptional (Nicastro et al., 2015b) changes, allowing adaptation to stringent growing conditions (**Figure 1**) (Coccetti et al., 2018; Hedbacker & Carlson, 2008).

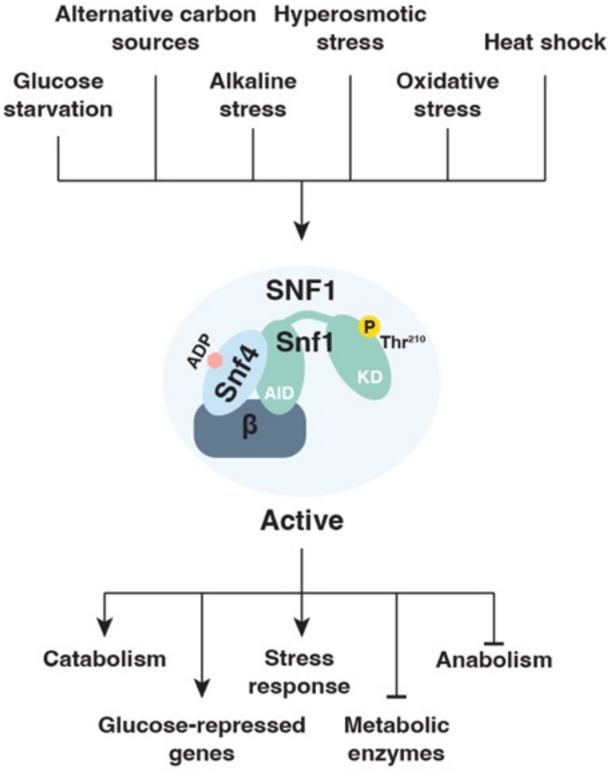
Alternative carbon sources
Hyperosmotic stress
Heat shock
Glucose starvation
Alkaline stress
Oxidative stress
SNF1
ADP
Snf4
Snf1
P
Thr210
AID
KD
β
Active
Catabolism
Stress response
Anabolism
Glucose-repressed genes
Metabolic enzymes

Figure 1. Schematic representation of the inputs and outputs of SNF1 activation.
SNF1 can be activated by glucose starvation, growth on alternative carbon sources, and various environmental stresses, such as alkaline conditions, hyperosmotic stress, oxidative stress, and heat shock (Hedbacker & Carlson, 2008; Hong & Carlson, 2007). When active, SNF1 promotes catabolism, the expression of glucose-repressed genes, and stress responses, and, in parallel, inhibits anabolism and metabolic enzymes (Hedbacker & Carlson, 2008).

1.1. Components of the SNF1 complex

The SNF1 complex in yeast consists of an α-catalytic subunit (Snf1), three different β-subunits (Gal83, Sip1, and Sip2), and a γ-regulatory subunit (Snf4) (Hedbacker & Carlson, 2008).

The *SNF1* (Sucrose Non-Fermenting 1) gene was identified in 1981 in yeast strains incapable of growing on sucrose or carbon sources alternative to glucose (Carlson et al., 1981). A *snf1Δ* strain exhibits growth deficiency in YEP (Yeast Extract Peptone) -glycerol, YEP-ethanol, and YEP-0.2% glucose (Carlson et al., 1981). It also shows a slower growth rate, compared to a wild-type strain in liquid YEP medium containing 0.1% glucose, but a similar rate in YEP-7.5% glucose (Carlson et al., 1981). This indicates that SNF1 is not only involved in the regulation of the metabolism of different carbon sources, but is also crucial for supporting growth in the presence of low levels of glucose (Carlson et al., 1981). These findings underscore the importance of this gene in supporting yeast growth under scarce conditions, leading to numerous further studies centered on this protein kinase. *SNF1* encodes a serine/threonine protein kinase, recognizing the consensus motif *ββXX**S/T**XXXΦ* (where *β* indicates basic residues (*i.e.* histidine, arginine, and lysin) and *Φ* indicates hydrophobic residues) (Dale et al., 1995). At the structural level, Snf1 features the Kinase Domain (KD) at the N-terminus region, while the C-terminus contains a Regulatory Domain (RD), which includes a region named AutoInhibitory Domain (AID) (**Figure 2A**) (Crute et al., 1998; Sanz et al., 2016). When the RD and the AID domains interact, SNF1 adopts an inactive conformation (Chen et al., 2009). The phosphorylation of the residue Thr^{210}, located in the activation loop (T-Loop) of Snf1 is a necessary step to activate Snf1 (**Figure 2A**) (Crute et al., 1998). Finally, Snf1 is a cytosolic protein during the growth in high glucose but becomes enriched in the nucleus after glucose depletion and activation (Vincent et al., 2001).

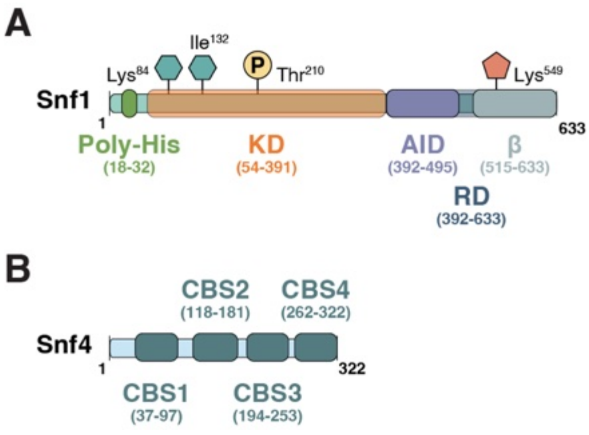

Figure 2. Schematic representation of the domains of α- and γ-type subunits of SNF1.

(**A**) Domains in Snf1: Poly-His (Poly Histide stretch), KD (Kinase Domain), RD (Regulatory Domain), AID (AutoInhibitory Domain), β (region of interaction with the β-subunits). The blue pentagons represent the ATP binding site (Lys^{84}) and the gatekeeper residue (Ile^{132}); the orange pentagon indicates the SUMOylated site (Lys^{549}); the yellow circle represents the phosphorylated residue Thr^{210} in the T-loop (K. Simpson-Lavy & M. Kupiec, 2023) (**B**) Domains in Snf4: the CBS1-4 (Cystathionine β-Synthase) domains.

Snf1 can be associated with three different β-subunits: Gal83 (GALactose metabolism 83), Sip1 (SNF1-Interacting Protein 1), and Sip2 (SNF1-Interacting Protein 2) (Hedbacker & Carlson, 2008). They serve as a scaffold for the interaction between Snf1 and Snf4, regulate the localization of the complex, and are involved in substrate recognition (Sanz et al., 2016).

The γ-subunit Snf4 (Sucrose Non-Fermenting 4) has a regulatory function, controlling the conformational status of the SNF1 complex (Hedbacker & Carlson, 2008; Leech et al., 2003). Snf4 contains four tandem repeats of a structural module called CBS (Cystathionine β-Synthase) (**Figure 2B**), which can bind AMP (Adenosine Monophosphate), ADP (Adenosine Diphosphate), and ATP (Adenosine Triphosphate) and seems to be involved in the regulation of SNF1 activation (Sanz et al., 2016; Wilson et al., 1996).

1.2. Upstream regulation of SNF1

1.2.1. The SNF1 activating kinases (SAKs)

Snf1 requires to be phosphorylated on the Thr^{210} residue in the T-loop to reach full activation (McCartney & Schmidt, 2001). This event is promoted by three upstream kinases, named SAKs (SNF1 Activating KinaseS) (Hedbacker & Carlson, 2008): Sak1 (SNF1 Activating Kinase 1), Tos3 (Target Of Sbf 3), and Elm1 (ELongated Morphology 1) (Hedbacker & Carlson, 2008). They are considered to be constitutively active and partially redundant kinases (Hedbacker & Carlson, 2008; Hedbacker et al., 2004a; Hong et al., 2003) that phosphorylate Snf1 on Thr^{210} both *in vitro* and *in vivo* (Hong & Carlson, 2007). A *sak1Δ tos3Δ elm1Δ* strain behaves like a *snf1Δ* showing a growth defect on raffinose or glycerol-ethanol media (Hong et al., 2003). It is still not clear how these upstream protein kinases are regulated, with PKA (Protein Kinase A) being the only kinase known to phosphorylate Sak1 on Ser^{1074}, albeit with only a modest effect on its activity (Barrett et al., 2012). Nevertheless, It has been shown that their activity can outcompete the dephosphorylation event of the phosphatase PP1 (Protein Phosphatase 1) after nutrient starvation or different environmental stresses (Hong & Carlson, 2007).

Sak1 is considered the main SNF1 upstream protein kinase (Elbing et al., 2006a; Hedbacker & Carlson, 2006, 2008; Hedbacker et al., 2004a). Sak1 can form stable complexes with Snf1 both *in vitro* (Elbing et al., 2006a; Elbing et al., 2006b) and *in vivo* (Liu et al., 2011) by associating with the Snf1 catalytic domain (Elbing et al., 2006b; Liu et al., 2011). Under high glucose conditions, Sak1 is cytosolic, but it relocates to the vacuolar membrane after glucose depletion (Hedbacker et al., 2004a). The predominant role of Sak1 is attributed to its C-terminal domain (residues 519 to 1142), which, when fused to Tos3 and Elm1, significantly increases their interaction with Snf1 and their activity (Liu et al., 2011). The catalytic domain of Sak1 is located between amino acids 130 and 500, but the upstream N-terminal portion (residues 87 to 129) is necessary to activate Snf1 *in vivo* (Rubenstein et al., 2006). There is evidence for Snf1 regulating Sak1, as Snf1-dependent phosphosites have been detected in the C-terminus of Sak1, although their physiological role remains unclear (Liu et al., 2011). Finally, Sak1 is crucial for the correct localization of the Snf1-Gal83-Snf4 complex. Accordingly, *sak1Δ* strains show impaired nuclear localization of SNF1 under glucose de-repressed conditions (Hedbacker et al., 2004a).

Tos3 and Elm1 contribute differently to cellular regulation under various growth conditions. Tos3 activates SNF1 when cells grow on non-fermentable carbon sources (Kim et al., 2005), while Elm1 localizes at the bud neck, emphasizing its role in controlling cell morphology and cell cycle progression (Sutherland et al., 2003). Additionally, both Tos3 and Elm1 exhibit weaker interactions with Snf1 compared to Sak1 (Elbing et al., 2006a).

Sak1 shares a high sequence identity with Tos3 (Hedbacker & Carlson, 2008; Kim et al., 2005; Rubenstein et al., 2006). Similarly to Sak1, the C-terminus of Tos3 is crucial for activating Snf1, although Tos3 plays a more marginal role in phosphorylating Snf1-Thr^{210} (Rubenstein et al., 2006) and, in contrast to Sak1, Tos3 remains cytosolic even during carbon starvation conditions (Kim et al., 2005).

Elm1, on the other hand, has a lower sequence identity compared to the other two SAKs (Hedbacker & Carlson, 2008; Rubenstein et al., 2006). Indeed, Elm1 has an additional role in regulating the mitotic phase of the cell cycle and maintaining proper cellular morphology (Hedbacker & Carlson, 2008; Rubenstein et al., 2006). In fact, the deletion of its C-terminal region or the entire ORF (Open Reading Frame) results in an elongated cell morphology (Hedbacker & Carlson, 2008; Rubenstein et al., 2006).

1.2.2. The protein phosphatase 1 (PP1)

The regulation of the activation status of Snf1 is dependent on the activity of Protein Phosphatase 1 (PP1). The catalytic subunit Glc7 (GLyCogen 7), associated with the regulatory subunit Reg1 (REsistance to Glucose repression 1), can dephosphorylate Snf1-Thr^{210} when cells are growing in the presence of glucose (Hedbacker & Carlson, 2008). Interestingly, the activity of Glc7-Reg1 does not seem to be regulated by glucose levels (Rubenstein et al., 2008).

Reg1 is essential to guarantee efficient dephosphorylation of Snf1, and in a *reg1Δ* strain, SNF1 is constitutively active because Glc7 alone cannot efficiently dephosphorylate Thr^{210} (Sanz et al., 2016). Therefore, the deletion of *REG1* is frequently used as a genetic strategy to induce hyperactivation of SNF1 even in the presence of glucose (Adachi et al., 2017). Reg1 shows cytosolic localization under all growth conditions (Hedbacker & Carlson, 2008) and interacts with the SNF1 complex through the kinase domain of the α subunit, an interaction that is stronger after glucose depletion (Ludin et al., 1998). Additionally, Reg1 is phosphorylated by SNF1 during glucose limitation on Ser^{75}, Ser^{775}, and Ser^{825}, while it is dephosphorylated after glucose readdition by Glc7 (Kanshin et al., 2017; Sanz et al., 2000).

The Glc7-Reg2 complex (REsistance to Glucose repression 2) is also involved in Snf1-Thr^{210} dephosphorylation after glucose readdition, playing a role during prolonged carbon starvation (24h) (Maziarz et al., 2016; K. J. Simpson-Lavy & M. Kupiec, 2023). Interestingly, the overexpression of *REG2* can complement *REG1* deletion (Maziarz et al., 2016).

The PP2A-like (Protein Phosphatase type 2A) subunit Sit4 (Suppressor of Initiation of Transcription 4) has been shown to have a partially overlapping activity with PP1 towards the SNF1 signaling pathway. In line with this, *SIT4* deletion causes an increase in glycogen accumulation and defective Snf1-Thr^{210} dephosphorylation (Ruiz et al., 2011), and, similarly to Reg1, Sit4 interacts directly with Snf1 (Ruiz et al., 2011).

1.2.3. Model of SNF1 regulation

The activation of SNF1 in low glucose requires two independent steps: the phosphorylation of Thr^{210} by the SAKs and the binding of Snf4 to the AID (**Figure 3**) (McCartney & Schmidt, 2001; Sanz et al., 2016). It is the interaction between the KD and the AID that controls the conformational change between the low and high activity forms (Chen et al., 2009). Indeed, in cells growing in media with high levels of glucose, KD and AID interact, keeping SNF1 in a closed inactive form (Leech et al., 2003). On the contrary, in cells growing on media with low levels of glucose, Snf4 binds the Snf1 AID domain, releasing the KD from autoinhibition and allowing SNF1 to perform its kinase activity (Leech et al., 2003). In fact, a *snf4Δ* strain is not able to grow on alternative carbon sources because, even if activated, SNF1 remains in the closed inactive conformation. A simultaneous deletion of the AID in a *snf4Δ* strain can suppress this phenotype (Leech et al., 2003).

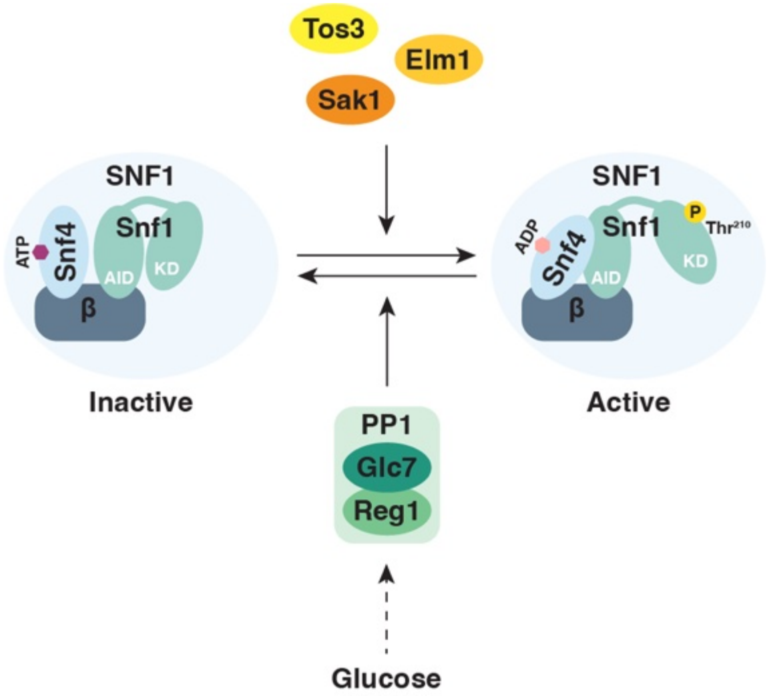

Figure 3. Scheme depicting the mechanisms of activation and inactivation of SNF1.
During energy depletion, the Snf1 subunit is phosphorylated on Thr^{210} by the three upstream SNF1 activating kinases (Sak1, Tos3, and Elm1) to become active and assume an open conformation. This conformational change is also promoted by the binding of ADP to Snf4 and the interaction of Snf4 with the Snf1 AID domain. In the presence of glucose, the phosphate PP1 (Glc7-Reg1) dephosphorylates Snf1-Thr^{210}, inactivating SNF1 and promoting the conformational change to the catalytically inactive form. This inactivation is also favored by the binding of ATP to Snf4.

The link between the energy status of the cell and SNF1 activity can be explained by the fact that AMP can bind to the Snf4-CBS domains (Wilson et al., 1996). This event does not allosterically activate SNF1, like it does for AMPK in mammalian cells (Wilson et al., 1996). In yeast, it has been shown that the binding of ADP to Snf4 induces a conformational change (**Figure 3**) (Mayer et al., 2011). A model that explains the complex regulation mechanisms of the activation status of SNF1 in response to energy levels involves the binding of ADP to Snf4, which induces a conformational change that protects Snf1-Thr^{210} from Glc7-Reg1-dependent dephosphorylation (Sanz et al., 2016). The hypothesis is that Reg1-Glc7 is always bound to SNF1, but Thr^{210} is accessible only when Snf4 is ATP-bound (Sanz et al., 2016). When ADP is bound to Snf4, a conformation change occurs, and Reg1-Glc7 cannot dephosphorylate Thr^{210} on Snf1 anymore, allowing Sak1-, Tos3-, and Elm1-mediated phosphorylation of Thr^{210} to predominate (**Figure 3**) (Sanz et al., 2016).

Interestingly Snf1 presents a stretch of 12 histidines at its N-terminus (**Figure 2A**), which has been proposed to behave as a pH sensor (K. Simpson-Lavy & M. Kupiec, 2023; Simpson-Lavy & Kupiec, 2022). In the presence of high glucose levels, the plasma membrane

Pma1 (Plasma Membrane ATPase) exports protons outside the cells, and the vacuolar membrane Vma1 (Vacuolar Membrane ATPase) pumps protons inside the vacuole, preserving a mildly alkaline cytoplasmic pH (~7.8) (Martinez-Munoz & Kane, 2017). In this condition, the polyhistidine stretch is deprotonated, favoring the SNF1 close/inactive conformation (Simpson-Lavy & Kupiec, 2022). On the contrary, when glucose levels are low, the cytosolic pH decreases (~5.7) due to a reduction in Pma1 and Vma1 activities (Isom et al., 2018). As a consequence, the Snf1 polyhistidine stretch becomes protonated, favoring the open/active SNF1 conformation (Simpson-Lavy & Kupiec, 2022). Deletion of this stretch leads to an increase of 50% in SNF1 activity, monitored by transcript measurement (K. Simpson-Lavy & M. Kupiec, 2023).

1.3. Downstream signaling

SNF1 regulates the transcription of over 400 genes and is involved in various cellular processes, including the metabolism of alternative carbon sources, respiration, gluconeogenesis, cell cycle regulation, intracellular transport and trafficking, chromatin modification, and the transcription apparatus (Coccetti et al., 2018; Hedbacker & Carlson, 2008; Nicastro et al., 2015b). To achieve this, the SNF1 complex interacts with 216 proteins, 92 of which have been identified as direct substrates (Coccetti et al., 2018).

Mig1 (Multicopy Inhibitor of GAL gene expression 1) is considered one of the main targets of SNF1 (**Figure 4**). Mig1 is a transcriptional repressor that is phosphorylated by SNF1 under low glucose conditions, promoting its export from the nucleus (Papamichos-Chronakis et al., 2004; Treitel et al., 1998). Mig1 represses 90 genes that are expressed following SNF1 activation, including *SUC2* (SUCrose 2), which encodes the enzyme invertase that hydrolyzes sucrose; *HXT2* (HeXose Transporter 2) and *HXT4* (HeXose Transporter 4), which encode two high-affinity glucose transporters necessary during glucose depletion; and genes encoding enzymes involved in the TCA cycle (TriCarboxylic Acid cycle) (Coccetti et al., 2018). Interestingly, the region of Mig1 mediating nuclear import and export (residues 261-400) (De Vit et al., 1997) contains many SNF1-dependent phosphosites (DeVit & Johnston, 1999; Ostling & Ronne, 1998; Smith et al., 1999; Treitel et al., 1998). In response to alkaline stress, SNF1 phosphorylates and inhibits Mig2 (Multicopy Inhibitor of GAL gene expression 2) (**Figure 4**), a protein closely related to Mig1 (Chandrashekarappa et al., 2016; Serra-Cardona et al., 2014). In response to ER (Endoplasmic Reticulum) stress, SNF1 becomes active and, through the inhibitory phosphorylation of both Mig1 and Mig2, allows the expression of *ATG39*, thereby promoting ER-phagy (Mizuno et al., 2020). Notably, it has been shown that Glc7-Reg1 may be involved in the dephosphorylation of Mig1 (Shashkova et al., 2017).

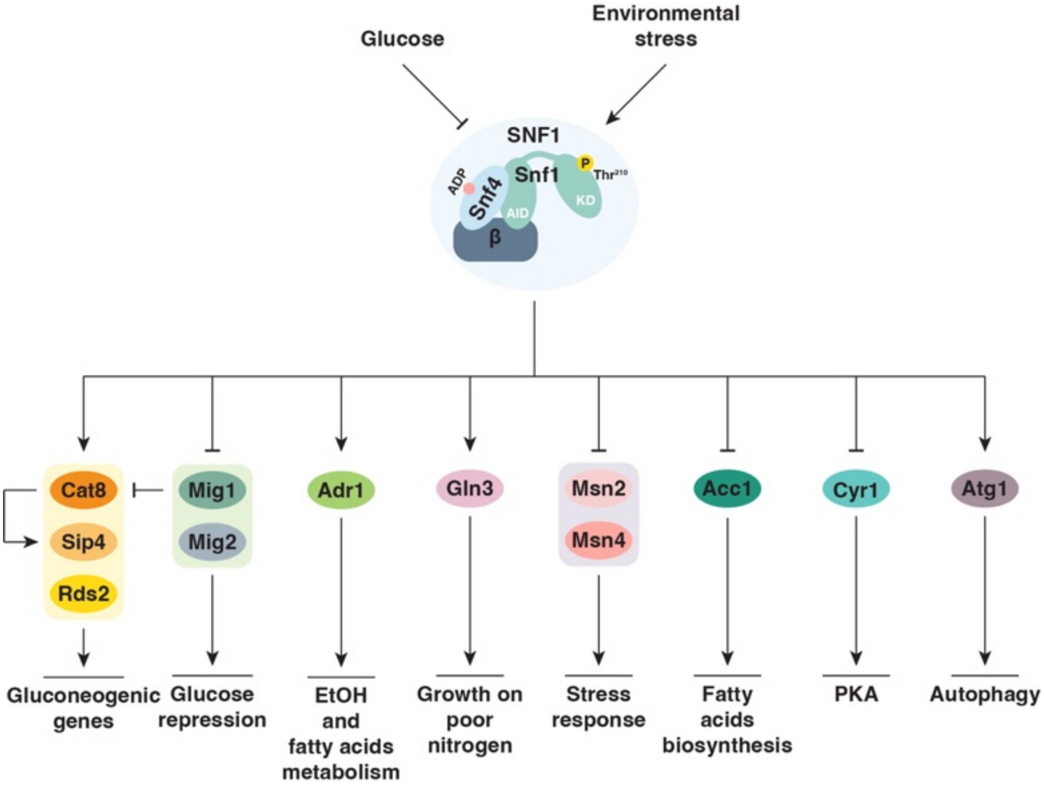
Glucose
Environmental stress
SNF1
ADP
Snf4
Snf1
P
Thr210
KD
AID
β
Cat8
Sip4
Rds2
Mig1
Mig2
Adr1
Gln3
Msn2
Msn4
Acc1
Cyr1
Atg1
Gluconeogenic genes
Glucose repression
EtOH and fatty acids metabolism
Growth on poor nitrogen
Stress response
Fatty acids biosynthesis
PKA
Autophagy

Figure 4. Scheme depicting the known direct SNF1 targets.
In the absence of glucose or under environmental stress conditions, active SNF1 phosphorylates various proteins to induce transcriptional and metabolic rearrangements in yeast cells, leading to the activation or inhibition of specific signaling pathways. For details, refer to the text.

SNF1 promotes the transcription of gluconeogenic genes through the activation of the transcription factors Cat8 (CATabolite repression 8), Sip4 (SNF1-Interacting Protein 4), and Rds2 (Regulator of Drug Sensitivity 2) (**Figure 4**) (Roth et al., 2004; Sanz et al., 2016; Vincent & Carlson, 1999; Young et al., 2003). Gluconeogenic genes have promoters containing a carbon source-responsive element (CSRE) with the consensus sequence *YCCRTTNRNCGG* (where Y represents C or T, R represents A or G, and N represents any base), which can be directly bound by Cat8, Sip4, and Rds2 (Roth et al., 2004; Sanz et al., 2016; Vincent & Carlson, 1999; Young et al., 2003). Notably, the expression of Cat8 is repressed by Mig1 when glucose levels are high (**Figure 4**) (Hedges et al., 1995). When transcribed, Cat8 promotes the transcription of Sip4 (**Figure 4**), the promoter of which contains a CSRE (Vincent & Carlson, 1998). Moreover, SNF1 promotes the expression of genes needed for ethanol and fatty acid metabolism through the activation of the transcription factor Adr1 (Alcohol Dehydrogenase II synthesis Regulator 1) (**Figure 4**) (Ratnakumar et al., 2009; Sanz et al., 2016; Young et al., 2003).

Another target of SNF1 is the enzyme Acc1 (Acetyl-CoA Carboxylase 1) (**Figure 4**), which catalyzes the carboxylation of acetyl-CoA to malonyl-CoA (Shi et al., 2014). In this case, SNF1 does not act at the transcriptional level but directly phosphorylates Acc1, inhibiting its enzymatic activity by phosphorylating the residue Ser^{1157} and hindering the respective carboxylation step (Shi et al., 2014). Consequently, similar to a *snf1Δ* strain, an $acc1^{S1157A}$ mutant exhibits an aberrant accumulation of fatty acids (Shi et al., 2014). Acc1 functions as a homodimer and presents two catalytic domains: the Biotin Carboxylase (BC) and the CarboxylTransferase (CT) domains, along with a central region formed by five domains (namely AC1-5 (ACC Central)) (Wei et al., 2016). Ser^{1157} is situated in a loop of the AC4 region (Wei et al., 2016), and in the dephosphorylated and active state, the CT and BC domains of the two subunits pair (Wei et al., 2016). Upon SNF1 phosphorylation at Ser^{1157}, the BC domains dissociate, and the homodimer assumes a continuum of conformations, ranging from a bent to a straight shape, corresponding to an inactive state (Wei et al., 2016).

The GATA-type transcription factor Gln3 (GLutamiNe metabolism 3) regulates the expression of genes necessary for growth on non-preferential nitrogen sources, such as proline, GABA (Gamma-AminoButyric Acid), or urea (Hofman-Bang, 1999). When nitrogen and amino acid levels are high, Gln3 remains inactive, localized in the cytoplasm and phosphorylated by the kinase complex TORC1 (Target Of Rapamycin Complex 1) (Target Of Rapamycin Complex 1) (Bertram et al., 2002). Under low glucose conditions, SNF1 phosphorylates and activates Gln3 (**Figure 4**), even in the presence of nitrogen and amino acids, conditions under which Gln3 would be expected to be inactive and cytosolic (Bertram et al., 2002; Perez-Sampietro et al., 2013; K. J. Simpson-Lavy & M. Kupiec, 2023). Thereby, SNF1-dependent phosphorylation promotes the nuclear relocalization of Gln3 (Bertram et al., 2002).

PKA is indirectly regulated by SNF1, specifically at the level of the upstream acting adenylate cyclase (Cyr1; CYclic AMP Requirement) (**Figure 4**) (Nicastro et al., 2015a). In the presence of glucose, Cyr1 is stimulated either by the G-protein Gpa2 (G-Protein Alpha subunit) or by Ras1 or Ras2 (homologous to RAS proto-oncogene 1 or 2), converting AMP into cAMP (Cyclic Adenosine MonoPhosphate) (Plank, 2022). cAMP binds to the homodimer of Bcy1 (Bypass of CYclic-AMP requirement), causing its dissociation from the PKA homodimer of catalytic subunits (either Tpk1, Tpk2, or Tpk3; Takashi's Protein Kinase 1-3), thereby allowing their activation (Plank, 2022). Under low glucose conditions, SNF1 directly phosphorylates Cyr1, causing its inhibition, which leads to a reduction in cAMP levels and consequently decreases PKA activation (Nicastro et al., 2015a).

To finely tune the stress response, SNF1 phosphorylates the transcription activators Msn2 (Multicopy suppressor of SNF1 mutation 2) and Msn4 (Multicopy suppressor of SNF1 mutation 4) (**Figure 4**) (De Wever et al., 2005). Under rich growth conditions, PKA phosphorylates and inhibits Msn2, retaining it in the cytosol (De Wever et al., 2005; Gorner et al., 2002). Upon carbon starvation, PP1 dephosphorylates Msn2, promoting its import into the nucleus, where it can induce the transcription of STRE-driven (STress Response Element) genes (De Wever et al., 2005). Since prolonged stress responses can have damaging effects on cellular growth and proliferation, it has been proposed that once cells adapt to glucose starvation, SNF1 phosphorylates Msn2 to counteract its nuclear import, thus attenuating the stress response (De Wever et al., 2005; Hedbacker & Carlson, 2008; Mayordomo et al., 2002; Petrenko et al., 2013).

Autophagy is a cellular process that favors growth in restrictive conditions by promoting the degradation and recycling of organelles and molecules (Nakatogawa et al., 2009). The main step of autophagy is the formation of a double-membrane structure, namely the phagophore, which matures into a vesicle-like organelle called the autophagosome (Nakatogawa et al., 2009). The autophagosome then fuses with the vacuole, where organelles and molecules are degraded (Nakatogawa et al., 2009). The Atg1 complex promotes the formation of the phagophore, thanks to the activity of the kinase Atg1 (AuTophaGy related 1) (Nakatogawa et al., 2009). Autophagy induction can be measured in different ways. One method involves the translocation of GFP-Atg8 (Green Fluorescent Protein; AuTophaGy related 8) to the vacuole (Nair et al., 2011). When autophagy is occurring, GFP-Atg8 is sent together with the autophagosome to the vacuole (Nair et al., 2011; Nakatogawa et al., 2009). When the autophagosome is lysed, its content gets degraded, including Atg8, but GFP tends to accumulate inside the vacuole due to its higher resistance to degradation (Nair et al., 2011). Alternatively, the autophagic flux can be measured via the Pho8$^{\Delta60}$ (PHOsphate metabolism 8) phosphatase enzymatic assay (Klionsky, 2007; Noda et al., 1995). The truncated version of the phosphatase Pho8 (Pho8$^{\Delta60}$) can be delivered to the vacuole only via the autophagy route (Klionsky, 2007; Noda et al., 1995). There, in the lumen, it is cleaved and becomes catalytically active (Klionsky, 2007; Noda et al., 1995). Therefore, only in cells with high autophagic flux is it possible to measure a high Pho8$^{\Delta60}$ enzymatic activity (Klionsky, 2007; Noda et al., 1995). SNF1 positively regulates autophagy by directly phosphorylating and activating Atg1 (**Figure 4**) in the presence of Atg11 (AuTophaGy related 11) (Wang et al., 2001; Yao et al., 2020). In a *snf1Δ* strain, there is a noticeable defect in the translocation of GFP-Atg8 (Green Fluorescent Protein; AuTophaGy related 8) to the vacuole (Yi et al., 2017) and in Pho8$^{\Delta60}$ activation, indicating a reduction in autophagic flux (Wang et al., 2001).

Moreover, when SNF1 expression was blocked using the auxin-inducible degron system (AID system), autophagy was not induced during carbon starvation (Adachi et al., 2017). On the contrary, in *reg1Δ* strains (*i.e.* constitutive active SNF1), autophagy was induced even when cells were grown in high glucose conditions (Adachi et al., 2017). More recently, it has been shown that carbon starvation induces the release of Ca^{2+} from the main reservoir, *i.e.* from the vacuole into the cytoplasm (Yao et al., 2024). This triggers the activation of the kinase Rck2 (Radiation sensitivity Complementing Kinase 2), which phosphorylates Atg11 (Yao et al., 2024). Phosphorylated Atg11 can bind the proteins Bmh1/2 (Brain Modulosignalin Homolog 1/2), which recruits the Snf1-Sip1-Snf4 complex that then activates Atg1, allowing the initiation of carbon starvation-induced autophagy (Yao et al., 2024).

1.4. Genetic modulation of SNF1 activity

There are different ways to genetically modulate and inhibit the kinase activity of SNF1. Mutation of Snf1-Thr^{210} to alanine (T210A; kinase-inactive mutant) dramatically reduces SNF1 activity both *in vitro* and *in vivo* (Estruch et al., 1992). In contrast, the $snf1^{K84R}$ allele behaves like a kinase-dead version. Lys^{84} is the ATP-binding site and a conserved residue in protein kinases, whose mutation can impair catalytic activity (Celenza & Carlson, 1989). It has been noted that the T210A mutation is more effective at inhibiting SNF1 activity *in vitro* than the K84R mutation, likely due to the conformational changes induced by the former (Nicastro et al., 2015a). On the other hand, the G53R mutation results in increased catalytic activity compared to wild-type cells (Estruch et al., 1992). Indeed, strains expressing the $snf1^{G53R}$ allele can recover from *SNF4* deletion, restoring growth on raffinose and invertase expression (Estruch et al., 1992).

To express a Snf1 variant whose activity can be modulated as needed, an analog-sensitive (as) allele can be created (Shirra et al., 2008). Proteins in the kinase superfamily typically have a large hydrophobic residue in the ATP-binding pocket, called the gatekeeper, which controls sensitivity to small inhibitors (Knight & Shokat, 2007). An alanine or glycine mutation of this amino acid induces a change in the ATP-binding pocket, allowing the binding of bulky ATP analogs (Knight & Shokat, 2007). The Snf1 gatekeeper is Ile^{132}, and its mutation to glycine confers sensitivity to the ATP analog 2NM-PP1 (2-NaphthylMethyl PyrazoloPyrimidine 1) and partially also to 1NM-PP1 (1-NaphthylMethyl PyrazoloPyrimidine 1) (Chandrashekarappa et al., 2013; Shirra et al., 2008). The $snf1^{I132G}$ (also referred to as $snf1^{as}$) mutant can complement a *SNF1* deletion in the absence of the inhibitor, exhibiting growth on alternative carbon sources and invertase induction (Shirra et al., 2008). However, 2NM-PP1 reduces the growth rate and *SUC2* transcription to levels seen in cells growing exponentially under glucose-rich conditions (Shirra et al., 2008). In control experiments, 2NM-PP1 affects only the analog-sensitive version of Snf1, without impacting wild-type strains (Shirra et al., 2008).

Snf1 can also be inhibited by SUMOylation (Simpson-Lavy & Johnston, 2013). This Post-Translational Modification (PTM) involves the addition of the SUMO (Small Ubiquitin-like MOdifier, also known as Smt3) ubiquitin-like protein to Lys^{549} of Snf1 by the E3 SUMO ligase Mms21 (Methyl MethaneSulfonate sensitivity 21) (**Figure 2A**) (Crozet et al., 2014; Simpson-Lavy & Johnston, 2013). In high glucose, Mms21 SUMOylate Snf1, while during the growth in galactose, the deSUMOylase Ulp1 (UbL-specific Protease 1) deSUMOylate Snf1 (Simpson-Lavy & Johnston, 2013). This PTM promotes the folding of Snf1 into its inactive conformation and its ubiquitination, leading to Snf1 degradation, thereby affecting both its activity and protein levels (Simpson-Lavy & Johnston, 2013; K. J. Simpson-Lavy & M. Kupiec, 2023).

1.5. Conservation of the SNF1 complex

The AMPK protein family is conserved throughout all eukaryotes and serves as a metabolic sensor, responding to variations in energy levels and nutrient status to induce quick adaptation (Crozet et al., 2014; Hardie & Ashford, 2014; Polge & Thomas, 2007). The ortholog of SNF1 in plants is called SnRK (SNF1-Related Protein Kinase) and AMPK (AMP-Activated Protein Kinase) in metazoans (Roustan et al., 2016). Although the mechanisms for activating these proteins can vary among organisms (Coccetti et al., 2018; Crozet et al., 2014; Gonzalez et al., 2020), their structure is highly conserved (Polge & Thomas, 2007). The kinase complex consists of an αβγ heterotrimeric configuration, and different orthologs of each subunit may be components of the complex, depending on the organism (Polge & Thomas, 2007). Another conserved aspect is that the α catalytic subunit must be phosphorylated on a conserved threonine residue in the T-loop to assume a catalytically active conformation (Hardie & Ashford, 2014; McCartney et al., 2005; Polge & Thomas, 2007; Stein et al., 2000). Furthermore, this conservation extends to the consensus motif recognized by these kinases (**Figure 5**) (Dale et al., 1995; Halford et al., 2003; Marin et al., 2015).

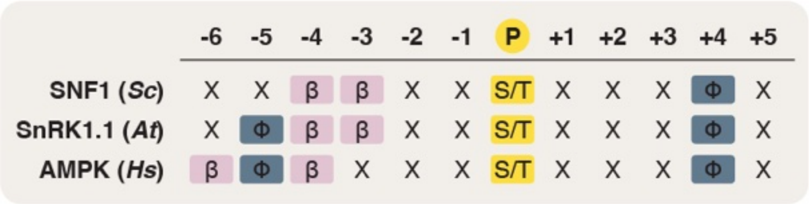

	-6	-5	-4	-3	-2	-1	P	+1	+2	+3	+4	+5
SNF1 (*Sc*)	X	X	β	β	X	X	S/T	X	X	X	Φ	X
SnRK1.1 (*At*)	X	Φ	β	β	X	X	S/T	X	X	X	Φ	X
AMPK (*Hs*)	β	Φ	β	X	X	X	S/T	X	X	X	Φ	X

Figure 5. SNF1, AMPK, and SnRK1.1 target similar consensus motifs.

β indicates basic residues (*i.e.* histidine, arginine, and lysin); Φ indicates hydrophobic residues.

1.5.1. Components of the AMPK complex

In mammalian cells, two α-subunits (AMPKα1 and AMPKα2), two β-subunits (AMPKβ1 and AMPKβ2), and three γ-subunits (AMPKγ1, AMPKγ2, and AMPKγ3) can be part of the AMPK complex (**Table 1**) (Crozet et al., 2014; Hardie & Ashford, 2014; Herzig & Shaw, 2018; Mihaylova & Shaw, 2011; Steinberg & Carling, 2019). The AMPK isoforms are differentially expressed across different tissues and cell types (Herzig & Shaw, 2018; Trefts & Shaw, 2021). Some differences have been reported at the biochemical level for the different isoforms, even though there is not yet evidence of different substrate specificity (Trefts & Shaw, 2021).

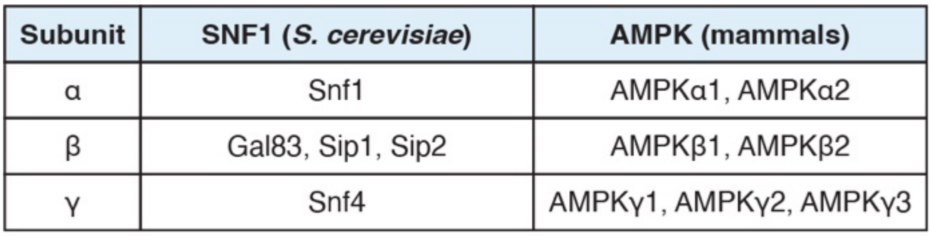

Subunit	SNF1 (*S. cerevisiae*)	AMPK (mammals)
α	Snf1	AMPKα1, AMPKα2
β	Gal83, Sip1, Sip2	AMPKβ1, AMPKβ2
γ	Snf4	AMPKγ1, AMPKγ2, AMPKγ3

Table 1. SNF1 and AMPK components in *S. cerevisiae* and mammals, respectively.

Similarly to SNF1, AMPKα-type subunits contain an AID and a KD (Herzig & Shaw, 2018; Trefts & Shaw, 2021), which need to be phosphorylated in the T-loop on the residue Thr^{172} to achieve full activation (Herzig & Shaw, 2018; Willows et al., 2017). The AID and the C-terminal domain, containing the RD, are connected by an α-linker (Steinberg & Hardie, 2023). AMPKβ1/2 subunits present a myristoylation site at the N-terminus, like Sip1 and Sip2, a conserved CBM, and an αγ binding domain at the C-terminus (Trefts & Shaw, 2021). Their myristoylation promotes AMPK activity and stability (Warden et al., 2001), and their association with autophagosomes and mitochondria (Herzig & Shaw, 2018; Liang et al., 2015). AMPKγ subunits have a role in sensing the energy status of the cell, thanks to the CBS domain, which can specifically bind adenine nucleotides (Herzig & Shaw, 2018; Trefts & Shaw, 2021).

In a similar manner to SNF1, the AMPK complex can also be SUMOylated (Crozet et al., 2014). Differently from what occurs in yeast, it is the AMPKβ2 subunit that was reported to be SUMOylated with the SUMO2 isoform, which promotes the formation of poly-SUMO2 chains (Crozet et al., 2014). SUMOylation seems to compete with ubiquitination, therefore enhancing the activity of the AMPK complex, observed by monitoring the phosphorylation of the activatory threonine (Thr^{172}) and the AMPK target ACC1 (Crozet et al., 2014).

1.5.2. Upstream regulation of AMPK

The canonical activation of AMPK requires three independent events: the phosphorylation of the T-loop, the allosteric binding of AMP, and the inhibition of Thr^{172} dephosphorylation (Gonzalez et al., 2020; Steinberg & Hardie, 2023). The main difference between *S. cerevisiae* SNF1 and mammalian AMPK is that the latter can be allosterically activated by AMP, which is considered a cellular signal for energy deficiency (Gonzalez et al., 2020). The allosteric binding of AMP to the CBS3 domain in the AMPKγ subunit allows the interaction of the α-linker in AMPKα1/2 with the phosphorylated T-loop (Steinberg & Hardie, 2023). This allows the dissociation of the AID from the KD, causing the allosteric activation of AMPK (Steinberg & Hardie, 2023). As a consequence, the KD and the RD come into proximity, protecting Thr^{172} from dephosphorylation (Steinberg & Hardie, 2023). Recently, the SAPS3 containing PP6 complex was identified as a phosphatase that dephosphorylated $pThr^{172}$ of AMPK *in vitro*, while PP2A and PP2C can dephosphorylate also $pThr^{172}$ *in vitro* (Yang et al., 2023).

The first identified upstream regulator of AMPK was the tumor suppressor kinase LKB1 (Liver Kinase B1), which is mutated in 20% of the patients with non-small cell lung cancer (Gonzalez et al., 2020; Hardie & Ashford, 2014; Herzig & Shaw, 2018; Hollstein et al., 2019; Trefts & Shaw, 2021), which can phosphorylate and activate 12 other kinases, namely AMPKRs (AMPK Related kinases) (Gonzalez et al., 2020; Hollstein et al., 2019; Lizcano et al., 2004). LKB1 is in complex with the pseudo-kinase STRADα/β and the adapter protein MO25α/β, forming the LKB1 complex (Steinberg & Hardie, 2023). This complex is constitutively active, even though the expression levels of its components can be regulated by micro-RNAs or ubiquitination (Steinberg & Hardie, 2023). AMPK can also be phosphorylated by CaMKK2 (Ca^{2+}/calModulin-dependent Kinase 2) and TAK1 (Transforming growth factor-β-Activated Kinase 1) (Gonzalez et al., 2020; Hardie & Ashford, 2014; Herzig & Shaw, 2018; Steinberg & Hardie, 2023; Trefts & Shaw, 2021). In response to hormones and changes in ion concentrations, CaMKK2 can become active and regulate AMPK (Hardie & Ashford, 2014; Trefts & Shaw, 2021). Since the ER is involved in maintaining Ca^{2+} homeostasis, it has been proposed that the ER can be an alternative source of AMPK activation (Trefts & Shaw, 2021). TAK1 responds to different transmembrane receptors, including the receptor for Tumor necrosis factor-Related Apoptosis-Inducing Ligand (TRAIL) (Hardie & Ashford, 2014; Steinberg & Hardie, 2023). Accordingly, knockdown cell lines for TAK1 failed to activate AMPK in response to the stimulation of TRAIL (Steinberg & Hardie, 2023). Nevertheless, this activation mechanism is still not clear, and there are insights suggesting that TAK1 may activate AMPK in response to lysosomal damage (Steinberg & Hardie, 2023).

1.5.3. AMPK downstream signaling

AMPK inhibits cell growth under nutrient-scarce conditions by acting on various signaling pathways and modulating multiple cellular processes. To achieve this, AMPK inhibits mTORC1 both directly and indirectly (for more details, see **Paragraph 4.1**). Similar to observations in yeast, autophagy is promoted by AMPK's direct phosphorylation of ULK1 (Unc-51-Like Autophagy-Activating Kinase 1), the mammalian ortholog of Atg1, on different residues (Egan et al., 2011; Herzig & Shaw, 2018; Mihaylova & Shaw, 2011; Sadria et al., 2022; Tian et al., 2015). Moreover, AMPK subunits have been identified as ULK1 interactors in MS analyses (Mihaylova & Shaw, 2011). Additionally, ULK1 is active in its AMPK-dependent phosphorylated form (Herzig & Shaw, 2018; Kim et al., 2011; Mihaylova & Shaw, 2011).

AMPK regulates mitochondrial homeostasis by inducing mitophagy via ULK1 activation (Hung et al., 2021; Mihaylova & Shaw, 2011), by promoting mitochondrial biogenesis through PGC-1α transcription (Malik et al., 2023; Mihaylova & Shaw, 2011), and and by facilitating mitochondrial fission (Toyama et al., 2016). Another role of AMPK is in metabolism regulation. Similar to the yeast SNF1, AMPK directly phosphorylates and inhibits ACC1 and ACC2, thereby reducing fatty acid biosynthesis (Carling et al., 1987; Mihaylova & Shaw, 2011; Steinberg & Carling, 2019). AMPK also inhibits cholesterol synthesis by directly phosphorylating HMGR (HMG-CoA Reductase) both *in vivo* and *in vitro*, leading to lower serum and liver cholesterol levels (Mihaylova & Shaw, 2011; Steinberg & Carling, 2019).

In a tissue-specific manner, AMPK regulates glucose uptake and lipase activity (Mihaylova & Shaw, 2011). For example, AMPK promotes the plasma membrane translocation of the Glucose Transporter type 4 (GLUT4) to increase glucose uptake by indirectly preventing its retention in the Golgi apparatus (Steinberg & Carling, 2019). Another similarity with yeast is the extensive transcriptional rearrangement that occurs in an AMPK-dependent manner. AMPK phosphorylates and regulates various transcription factors, coactivators, acetyltransferases, histone deacetylases, and histones themselves (Mihaylova & Shaw, 2011). Finally, in addition to its role in cell growth and metabolism, AMPK controls cell polarity and cytoskeletal dynamics (Mihaylova & Shaw, 2011).

2. The TORC1 complex

In *S. cerevisiae*, the TORC1/mTORC1 kinase complex governs another pivotal signaling pathway that coordinates nutrient availability with growth and cell division. This pathway's function is to stimulate cellular processes essential for growth in environments with high levels of nitrogen and amino acids while suppressing processes associated with growth inhibition and stress response (De Virgilio & Loewith, 2006b).

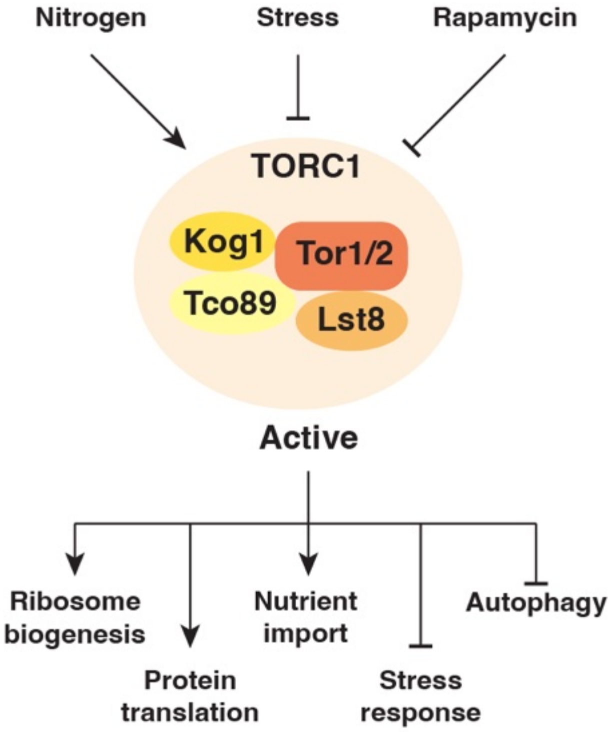

Figure 6. A schematic representation of the inputs and outputs of TORC1 activation.
TORC1 primarily reacts to nitrogen availability, while being inhibited under stress conditions or by the macrolide rapamycin (De Virgilio & Loewith, 2006b). When active, TORC1 enhances ribosome biogenesis, protein translation, and nutrient import, while simultaneously suppressing stress response and autophagy (De Virgilio & Loewith, 2006b). (Image adapted from (De Virgilio & Loewith, 2006b)).

2.1. Components of the TORC1 complex

The TORC1 structure is highly conserved across eukaryotes, comprising a dimer of a heterocomplex (Baretic et al., 2016; Prouteau et al., 2023; Prouteau et al., 2017; Wullschleger et al., 2006). In yeast, this complex includes the catalytic subunit Tor1 or Tor2 (Target of Rapamycin 1 or 2), the conserved subunits Kog1 (Kontroller Of Growth 1) and Lst8 (Lethal with Sec Thirteen 8), and the non-conserved subunit Tco89 (Tor Complex One subunit with 89 kDa) (De Virgilio & Loewith, 2006b; Wullschleger et al., 2006).

TOR1 and *TOR2* were identified as genes whose mutations confer dominant rapamycin resistance (Heitman et al., 1991; Wullschleger et al., 2006). Rapamycin is a lipophilic macrolide that was discovered in 1975 as an antifungal agent produced by *Streptomyces hygroscopicus*, a bacterial strain isolated from Rapa Nui island, which inspired the drug's name (De Virgilio & Loewith, 2006b; Wullschleger et al., 2006). Subsequently, rapamycin's anticancer and immunosuppressant properties were recognized, heightening the interest in this molecule (De Virgilio & Loewith, 2006b; Wullschleger et al., 2006). To inhibit TORC1, rapamycin binds the cofactor FKBP12 (FK506-Binding Protein 12) in mammalian cells, which is the ortholog of Fpr1 (Fk506-sensitive Proline Rotamase 1) in budding yeast (De Virgilio & Loewith, 2006b). *TOR1* and *TOR2* encode two Ser/Thr protein kinases belonging to the PhosphatidylInositol Kinase-related Kinases (PIKKs) family (De Virgilio & Loewith, 2006b; Wullschleger et al., 2006). At the N-terminus, they contain two tandem HEAT (Huntingtin, Elongation factor 3, a subunit of PP2A, and TOR1) repeats, which interact with Kog1, followed by a FAT (FKBP12 rapamycin Associated protein [FRAP], ATM, TRRAP) domain that is common to all PIKK family members and facilitates interactions with other proteins (**Figure 7**) (Maegawa et al., 2015; Qi et al., 2022). Following the FAT domain, Tor1 and Tor2 contain the FRB (FKBP12-Rapamycin Binding) domain, the binding site for the Fpr1-rapamycin complex, and the protein kinase domain (**Figure 7**) (Maegawa et al., 2015; Qi et al., 2022). At their C-termini, both kinases also contain the FATC (C-terminal FAT) domain (**Figure 7**), which serves as a potential scaffolding domain (Maegawa et al., 2015; Qi et al., 2022). *tor1Δ* strains exhibit a slow-growth phenotype, whereas *tor2Δ* or *tor1Δ tor2Δ* strains are inviable, with the latter arresting in G0 of cell cycle (De Virgilio & Loewith, 2006b). Either Tor1 or Tor2 can be part of the TOR1-complex, but only Tor2 serves as the protein kinase in TORC2 (Target Of Rapamycin Complex 2), which has a role that is dinstinct from the one of TORC1 (Gaubitz et al., 2015; Gaubitz et al., 2016; Wullschleger et al., 2006). TORC1 regulates growth, proliferation, protein synthesis, and metabolism (Chantranupong et al., 2015; De Virgilio & Loewith, 2006b; Loewith & Hall, 2011), while TORC2 primarily controls survival, membrane tension, sphingolipid, and ceramide biosynthesis (Eltschinger & Loewith, 2016; Gaubitz et al., 2015; Gaubitz et al., 2016). Notably, only TORC1 is sensitive to rapamycin due to a different conformation of the complex then TORC2, which cannot be bound by the inhibitor Fpr1 when associated with rapamycin (Gaubitz et al., 2015; Gaubitz et al., 2016).

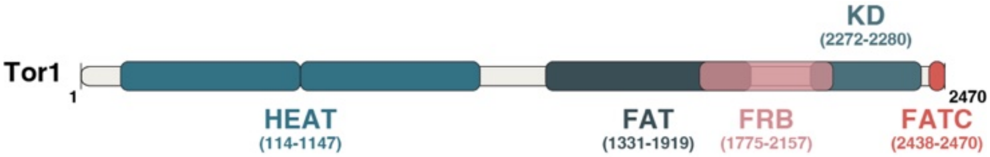

Figure 7. Schematic representation of the structure of Tor1.

Scheme depicting the structure of Tor1 and its main domains: HEAT (Huntingtin, Elongation factor 3, a subunit of PP2A, and TOR1) repeats, FAT (FKBP12 rapamycin Associated protein [FRAP], ATM, TRRAP), FRB (FKBP12-Rapamycin Binding), KD (Kinase Domain), and FATC (C-terminal FAT).

The Lst8 subunit of TORC1 and TORC2 functions as an interaction scaffold, facilitating connections between Tor1/2 and downstream effectors, as well as between Tor1/2 and other complex subunits (De Virgilio & Loewith, 2006b). It is hypothesized that Lst8 might be a substrate for upstream regulators of TORC1, potentially playing a role in transmitting downstream signals (De Virgilio & Loewith, 2006b).

Kog1 acts as a scaffold, recruiting substrates and facilitating their interaction with Tor1 (De Virgilio & Loewith, 2006b). It also regulates TORC1 activity by being a target of upstream regulators, particularly interacting with the Rag GTPases (De Virgilio & Loewith, 2006b; Hughes Hallett et al., 2015; Prouteau et al., 2023). Both Lst8 and Kog1 are essential proteins (Loewith et al., 2002).

In contrast, the Tco89 subunit is not essential, as *tco89Δ* strains remain viable (Reinke et al., 2004). Unlike Lst8 and Kog1, which are highly conserved in eukaryotes, Tco89 is only expressed in fungi related to *S. cerevisiae* (De Virgilio & Loewith, 2006a). Strains lacking *TCO89* are hypersensitive to rapamycin and exhibit growth defects and temperature sensitivity (Reinke et al., 2004). Additionally, *TCO89* deletion is synthetically lethal with *TOR1* deletion (Reinke et al., 2004). This protein contains numerous serine and threonine residues and is highly phosphorylated *in vivo* (De Virgilio & Loewith, 2006a; Hu et al., 2019).

2.2. Upstream regulation of TORC1

TORC1 activity is tightly regulated by several upstream factors that respond to amino acid availability (Péli-Gulli et al., 2015; Teng & Hardwick, 2019), some of which are conserved from yeast to mammals (Nicastro et al., 2017). The two primary regulatory branches involve the highly conserved Rag GTPases and the Pib2-controlled pathway (Teng & Hardwick, 2019).

2.2.1. The Rag GTPases

TORC1 activity is regulated by Rag GTPases (RAs-related GTP binding proteins), specifically Gtr1 (GTP binding protein resemblance 1) and Gtr2 (GTP binding protein resemblance 2), which can bind and hydrolyze GTP (Guanosine TriPhosphate) (Nakashima et al., 1999; Nicastro et al., 2017). Both proteins have an extended C-terminal region necessary for forming the Gtr1-Gtr2 heterodimer (Nicastro et al., 2017; Powis et al., 2015; Zhang et al., 2019). In the presence of amino acids, Gtr1 is loaded with GTP and Gtr2 with

GDP (Guanosine DiPhosphate), enabling them to activate TORC1 (**Figure 8**) (Binda et al., 2009; Dubouloz et al., 2005; Nicastro et al., 2017; Powis et al., 2015). When Gtr2 hydrolyzes GTP to GDP and Gtr1 is GTP-loaded, the heterodimer adopts a conformation that exposes a surface capable of interacting with the TORC1 subunits Kog1 and Tco89 (Binda et al., 2009; Gao & Kaiser, 2006; Nicastro et al., 2017). Conversely, under nitrogen-poor conditions, Gtr1 hydrolyzes GTP to GDP, and Gtr2 becomes GTP-loaded (**Figure 8**) (Binda et al., 2009; Gao & Kaiser, 2006; Nicastro et al., 2017). This results in a conformational change that likely reduces interaction with TORC1, preventing its activation (Binda et al., 2009; Gao & Kaiser, 2006; Nicastro et al., 2017).

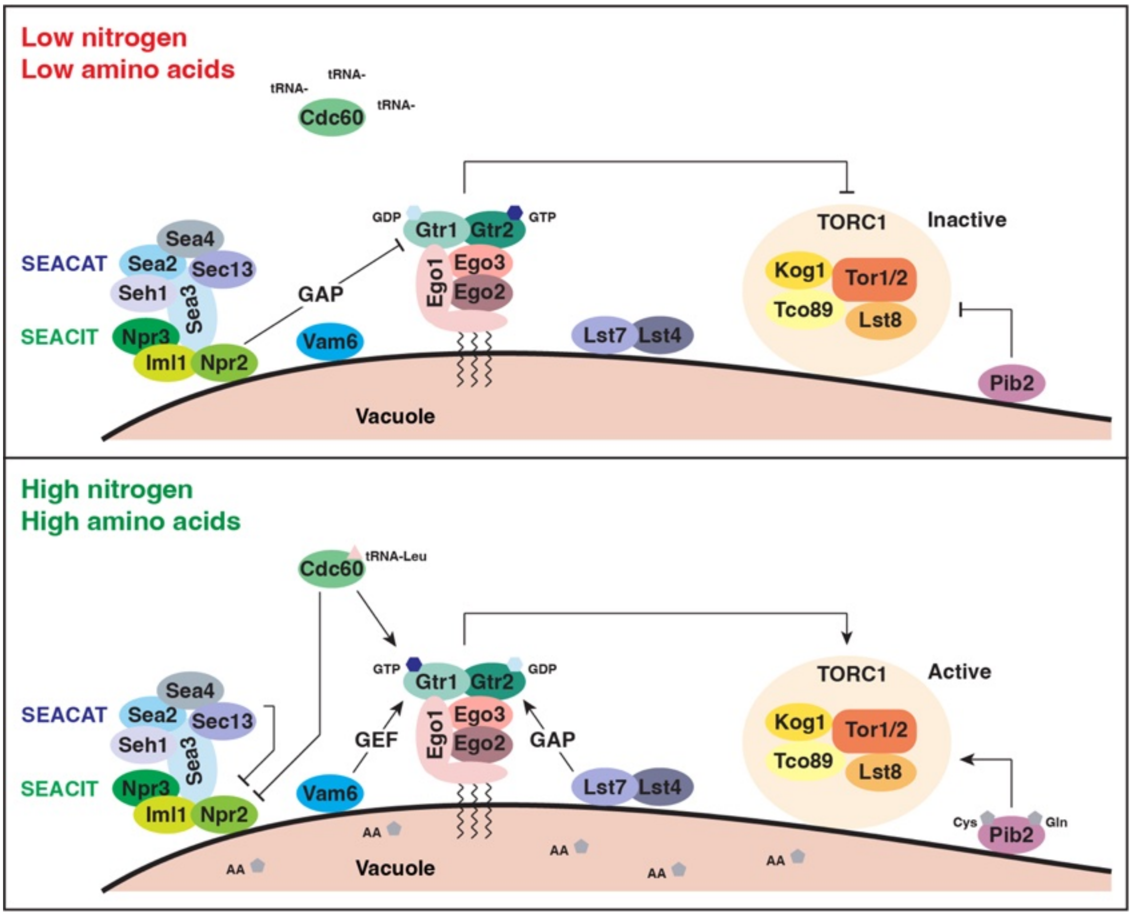
Low nitrogen
Low amino acids
tRNA-
tRNA-
tRNA-
Cdc60
GDP
Gtr1
Gtr2
GTP
TORC1
Inactive
Sea4
SEACAT
Sea2
Sec13
Seh1
Sea3
GAP
Ego1
Ego3
Ego2
SEACIT
Npr3
Iml1
Npr2
Vam6
Lst7
Lst4
Kog1
Tor1/2
Tco89
Lst8
Pib2
Vacuole
High nitrogen
High amino acids
Cdc60
tRNA-Leu
GTP
Gtr1
Gtr2
GDP
TORC1
Active
Sea4
SEACAT
Sea2
Sec13
Seh1
Sea3
GEF
Ego1
Ego3
Ego2
GAP
SEACIT
Npr3
Iml1
Npr2
Vam6
Lst7
Lst4
Kog1
Tor1/2
Tco89
Lst8
Cys
Pib2
Gln
AA
AA
AA
AA
AA
Vacuole

Figure 8. Mechanisms of TORC1 activation and inactivation.

When nitrogen and amino acid levels are low, SEACIT, through its GAP activity towards Gtr1, and the inhibitory action of Pib2 maintain TORC1 in an inactive state. In contrast, when nitrogen and amino acid levels are high, SEACAT inhibits SEACIT, and Cdc60 binds to Leu-tRNA, likely competing with SEACIT for Gtr1 binding. Simultaneously, Vam6 promotes the GTP-bound state of Gtr1 via its GEF activity, while Lst4-Lst7 acts as a GAP for Gtr2, promoting its GDP-bound state. Additionally, Pib2 directly senses the presence of glutamine (Gln) and cysteine (Cys), leading to TORC1 activation. Active TORC1 then promotes ribosome biogenesis, protein translation, and nutrient import, while inhibiting stress responses and autophagy. (Image adapted from (Nicastro et al., 2017)).

Rag GTPases are located at the vacuolar membrane, although they do not directly bind to it. Their interaction is mediated by the EGO-TC (EGO-Ternary Complex), which consists of the proteins Ego1/Meh1 (Exit from rapamycin-induced GrOwth arrest 1/Multicopy suppressor of Ers1 Hygromycin B sensitivity 1), Ego2 (Exit from rapamycin-induced GrOwth arrest 2), and Ego3/Slm4 (Exit from rapamycin-induced GrOwth arrest 3/Synthetic Lethal with Mss4) (Binda et al., 2009; Dubouloz et al., 2005; Nicastro et al., 2017; Powis et al., 2015). The EGO-TC, acting as a scaffold, associates with the Gtr1-Gtr2 heterodimer to form the EGOC (EGO Complex) (**Figure 8**) (Binda et al., 2009; Nicastro et al., 2017; Powis et al., 2015; Zhang et al., 2019). Ego1 has a myristoylated and palmitoylated N-terminus, enabling its binding to the vacuolar and endosomal membranes (Nicastro et al., 2017; Powis et al., 2015; Zhang et al., 2019). Additionally, it features a rope-like structure that wraps around and stabilizes the other EGOC components (Zhang et al., 2019). The interaction surface between the EGO-TC and Gtr1-Gtr2 is formed by the N-terminus of Ego1 and Ego3 (Zhang et al., 2019). Although Ego2 interacts with Ego1 and Ego3 (Nicastro et al., 2017; Powis et al., 2015; Zhang et al., 2019), it does not directly interact with Gtr1-Gtr2 (Zhang et al., 2019). The EGO-TC is essential for recruiting Gtr1-Gtr2 and TORC1 to the vacuolar surface and thereby enables proper control of TORC1 in response to amino acids (Nicastro et al., 2017; Powis et al., 2015).

The EGOC proteins are transported from the Trans-Golgi Network (TGN) to the vacuolar membrane via the AP-3 (Adaptor Protein 3) and HOPS (HOmotypic fusion and vacuole Protein Sorting) complex pathway (Hatakeyama et al., 2019). AP-3 acts as an adaptor complex, providing a membrane-binding site for the formation of the protein coat necessary for vesicle budding from the Golgi apparatus (Cowles et al., 1997). This heterotetrameric complex is conserved from yeast to mammalian cells (Cowles et al., 1997), with in *S. cerevisiae* the four subunits of this complex being Apl6 (clathrin Adaptor Protein complex Large chain 6), Apl5 (clathrin Adaptor Protein complex Large chain 5), Apm3 (clathrin Adaptor Protein complex Medium chain 3), and Aps3 (clathrin Associated Protein complex Small subunit 3) (Cowles et al., 1997). Deletions of either *APL5* or *APL6* result in the mislocalization of the EGOC to the plasma membrane (Hatakeyama et al., 2019), underscoring their crucial role in the proper delivery of EGOC to the vacuolar surface. In parallel, the HOPS complex mediates the fusion of vesicles formed via the AP-3 pathway with the vacuolar membrane (Shvarev et al., 2022). This heterohexameric complex consists of the proteins Vps11/Pep5, Vps16, Vps18/Pep3, Vps33, Vps39, and Vps41 (Vacuolar Protein Sorting 11-16-18-33-39-41) (Kuhlee et al., 2015). Deletion of *VPS39* (also known as *VAM6*) and *VPS41* causes vacuolar fragmentation and partial relocalization of Ego1 to the plasma membrane (Hatakeyama et al., 2019).

2.2.1.1. GEFs and GAPs for Gtr1 and Gtr2

The GTP and GDP loading status of Rag GTPases is regulated by two main types of proteins: Guanine nucleotide Exchange Factors (GEFs) and GTPase Activating Proteins (GAPs) (Gonzalez & Hall, 2017).

The active state of Gtr1-GTP is promoted by the GEF Vam6 (VAcuolar Morphogenesis 6) (Binda et al., 2009; Valbuena et al., 2012). Deleting *VAM6* results in recovery defects post-rapamycin treatment, whereas its overexpression enhances rapamycin resistance (Binda et al., 2009). Vam6 exhibits GEF activity both *in vitro* and *in vivo*, promoting the Gtr1-GTP loaded state and subsequent TORC1 activation (**Figure 8**) (Binda et al., 2009). Vam6 is not the sole GEF for Gtr1; the cytosolic leucine sensor LeuRS (LEUcyl-tRNA Synthetase), also known as Cdc60 (Cell Division Cycle 60), plays a similar role (Bonfils et al., 2012; Powis & De Virgilio, 2016). When nitrogen and amino acid levels are high, LeuRS binds to leucine, interacts with Gtr1, and promotes the GTP-bound state through an incompletely understood mechanism (**Figure 8**) (Bonfils et al., 2012; Gonzalez & Hall, 2017; Powis & De Virgilio, 2016).

The inactive state of Gtr1^{GDP} is promoted by the GAP activity of the SEACIT (SEAC Inhibiting TORC1) subcomplex in yeast (Nicastro et al., 2017; Panchaud et al., 2013a, 2013b). SEACIT comprises the proteins Npr2 (Nitrogen Permease Regulator 2), Npr3 (Nitrogen Permease Regulator 3), and Iml1/Sea1 (Increased Minichromosome Loss 1) (Increased Minichromosome Loss 1) (Nicastro et al., 2017; Panchaud et al., 2013a, 2013b). SEACIT's activity is counteracted by the SEACAT (SEAC Activating TORC1) subcomplex (Nicastro et al., 2017; Panchaud et al., 2013a), which includes Seh1 (SEc13 Homolog 1), Sec13 (SECretory 13), Rtc1/Sea2 (Restriction of Telomere Capping 1/SEh1-Associated 2), Mtc5/Sea3 (Maintenance of Telomere Capping 5/SEh1-Associated 3), and Sea4 (SEh1-Associated 4). Together, SEACIT and SEACAT form the SEAC (SEh1-Associated protein Complex) (Nicastro et al., 2017; Panchaud et al., 2013a), whose structure has been recently resolved by Cryo-EM (CRYOgenic Electron Microscopy) (Tafur et al., 2022). The SEAC appears as a dimer with a central core, previously assigned as SEACAT, and two identical flexible wings, previously assigned as SEACIT, with Sea3 being the connector between them, allowing a stable interaction between the two modules (Tafur et al., 2022). The wing module SEACIT, via interaction with the EGOC and another yet unidentified interactor, is localized on the vacuolar membrane (Tafur et al., 2022). Initially, Iml1/Sea1 was identified as the GAP for Gtr1 during nitrogen starvation, due to the presence of a presumed catalytic arginine residue (Arg^{943}) (Nicastro et al., 2017; Panchaud et al., 2013a). However, thanks to the newly resolved structure, it was possible to identify Npr2-Arg^{84} as the catalytic residue that stimulates the GAP activity of SEAC (Tafur et al., 2022). Indeed, Arg^{84} is accessible to solvent and opposite to the core-wing interface, allowing it to enhance the GTPase activity of Gtr1 and promote the GDP-bound inactive state, which causes TORC1 inhibition (**Figure 8**) (Tafur et al., 2022). Conversely, in the presence of amino acids, Npr2 is dephosphorylated by PP2A (Protein Phosphatase type 2A), leading to its dissociation from other SEACIT subunits (**Figure 8**) (Nicastro et al., 2017; Panchaud et al., 2013a), introducing the idea of Npr2 as a hub receiving inputs to regulate the GTPase activity of Gtr1 and thereby the activation status of TORC1. When nitrogen and amino acid levels are high, TORC1 activity is stimulated by the indirect inhibitory effect of the core module SEACAT on the wing module SEACIT (**Figure 8**) (Nicastro et al., 2017; Panchaud et al., 2013a; Tafur et al., 2022). SEACAT may recruit nutrient sensors, which then may regulate the SEACIT GAP activity (Tafur et al., 2022).

The active state of Gtr2-GDP is promoted by the heterodimeric complex Lst4-Lst7 (Lethal with Sec Thirteen 4 and 7), which has GAP activity (Nicastro et al., 2017; Péli-Gulli et al., 2017; Péli-Gulli et al., 2015). Deleting *LST4* and/or *LST7* reduces TORC1 activity and increases rapamycin sensitivity (Péli-Gulli et al., 2015). In exponentially growing cells, Lst4-Lst7 are primarily located in the cytosol, with a small fraction on the vacuolar surface (Pacitto et al., 2015; Péli-Gulli et al., 2017; Péli-Gulli et al., 2015). Upon amino acid readdition, the complex becomes active as a GAP, interacting with Gtr1-Gtr2 and promoting GTP hydrolysis to GDP in Gtr2 (**Figure 8**) (Péli-Gulli et al., 2015). However, the mechanism by which amino acids influence Lst4-Lst7 GAP activity remains unclear (Péli-Gulli et al., 2015). Notably, TORC1 feedback inhibits of Lst4-Lst7 (**Figure 8**) (Péli-Gulli et al., 2017). Lst4 contains a DENN (Differentially Expressed in Normal and Neoplastic cells) domain with an unfolded loop between residues 400 and 600 (Lst4$^{\mathrm{LOOP}}$) (Pacitto et al., 2015; Péli-Gulli et al., 2017). Upon TORC1 activation, TORC1 phosphorylates Lst4 at several sites within the Lst4$^{\mathrm{LOOP}}$, causing the complex to be released from the vacuolar membrane into the cytoplasm (Pacitto et al., 2015; Péli-Gulli et al., 2017). The creation of a phosphomimetic Lst4 variant (Lst4$^{\mathrm{5D}}$) and a phospho-null variant (Lst4$^{\mathrm{12A}}$) has enabled the analysis of these feedback inhibitory mechanisms (Péli-Gulli et al., 2017).

2.2.2. Pib2

In *S. cerevisiae*, another upstream branch that activates TORC1 is centered on the protein Pib2 (PhosphatidylInositol-3-phosphate Binding 2). Deleting either *PIB2* or *GTR1* results in defects in TORC1 activation and growth (Ukai et al., 2018), and causes the "EGO phenotype", characterized by the inability to recover after rapamycin treatment (Binda et al., 2009; Dubouloz et al., 2005). Additionally, their simultaneous deletion is lethal (Ukai et al., 2018). Pib2 operates through an independent activation pathway separate from the Rag

GTPases and does not associate with the EGO-TC (**Figure 8**) (Ukai et al., 2018). Pib2 features an N-terminal Inhibitory Domain (NID), a Kog1 Binding Domain (KBD), a FYVE (Fab 1, YOTB, Vac 1, and EEA1) domain, and a C-terminal Activatory Domain (CAD) (Hatakeyama, 2021). The FYVE domain enables Pib2 to bind to membranes containing PI3P (PhosphatidylInositol-3-Phosphate), such as signaling endosomes and vacuolar surfaces, which are crucial for regulating TORC1 activity (Ukai et al., 2018). The KBD facilitates the interaction between Kog1 and Pib2 (Hatakeyama, 2021; Michel et al., 2017). Pib2 is recognized as a sensor for glutamine (Tanigawa et al., 2021; Ukai et al., 2018) and cysteine (Tanigawa et al., 2021; Zeng et al., 2024), but, notably, Gtr1 can also be activated by glutamine (Zeng et al., 2024). Glutamine binds to Pib2 via its E motif, located before the FYVE domain (Tanigawa et al., 2021), while cysteine binds via the T motif, located after the FYVE domain (Zeng et al., 2024). The NID and CAD domains of Pib2 function independently of each other and the ECOC, each directly influencing TORC1 (**Figure 8**) (Michel et al., 2017). While the specific functions of these domains remain unclear beyond their general role in TORC1 activity (Hatakeyama, 2021), it is known that deletion of the CAD increases rapamycin sensitivity, similar to *pib2Δ* strains (Michel et al., 2017). Recently, a novel emerging role of Pib2 as a recruitment factor for TORC1 effectors has been identified (Cecil et al., 2023; Zeng et al., 2024).

2.2.3. TORC1 pools in yeast cells

TORC1 is located on the vacuolar surface, the yeast organelle responsible for nutrient storage (Binda et al., 2009; Powis & De Virgilio, 2016). Recently, TORC1, along with the EGOC, was also found at signaling endosomes (pre-vacuolar endosomes), which are the primary sites for PI[3,5]P_2 (PhosphatidylInositol-3,5 bisPhosphate) synthesis (Hatakeyama et al., 2019). Fab1 (Forms Aploid and Binucleate cells 1) is the only yeast lipid kinase known to convert PI3P into PI[3,5]P_2, a signaling lipid crucial for vacuolar trafficking (Duex et al., 2006; Lang et al., 2017). Under basal conditions, Fab1 activity is stimulated by its activators Vac7 (VACuolar segregation 7) and Vac14 (VACuolar segregation 14) (Duex et al., 2006). Yeast strains unable to synthesize PI[3,5]P_2 exhibit enlarged vacuoles and mislocalized proteins that should be transported to the vacuole (Duex et al., 2006). Interestingly, the active TORC1 pool at the endosomes phosphorylates the N-terminal FYVE domain of Fab1, relieving its autoinhibition and enhancing the binding of the FYVE domain to PI3P, thereby increasing PI[3,5]P_2 synthesis (Chen et al., 2021). Endosomes containing PI[3,5]P_2, Fab1, EGOC, and TORC1 fuse with the vacuole, and Fab1 is recycled back to the endosomes to synthesize more PI[3,5]P_2 (Chen et al., 2021).

2.3. Downstream signaling

Active TORC1 stimulates anabolic processes essential for cell growth while simultaneously downregulating cellular activities that are unnecessary when nitrogen and amino acid levels are high (De Virgilio & Loewith, 2006b). The primary anabolic pathway under TORC1 control is protein biosynthesis, which is regulated at multiple levels. This includes enhancing ribosome biogenesis and mRNA stability, stimulating translation initiation factors, and increasing the expression of high-affinity amino acid permeases (De Virgilio & Loewith, 2006b).

One key target of TORC1 in yeast is the protein kinase Sch9 (Scott Cameron HindIII library clone number 9) (Urban et al., 2007), which will be discussed in detail in **Paragraph 3** (*The Yeast Protein Kinase Sch9 Functions as a Central Nutrient-Responsive Hub That Calibrates Metabolic and Stress-Related Responses*).

2.3.1. Tap42 and protein phosphatases

To regulate amino acid metabolism, stress response, and autophagy, TORC1 controls the activity of PP2A and PP2A-like protein phosphatases through Tap42 (**Figure 9**) (Two A phosphatase Associated Protein 42) (Deprez et al., 2018; Di Como & Arndt, 1996; Duvel et al., 2003; Jiang & Broach, 1999). The heterotrimeric PP2A complex consists of a catalytic subunit (either Pph21 or Pph22), the scaffold subunit Tpd3 (tRNA Processing Deficient 3), and a regulatory subunit (either Cdc55 or Rts1) (Deprez et al., 2018; Lillo et al., 2014). The PP2A-like phosphatase in yeast, analogous to mammalian PP6, is a heterodimer composed of the catalytic subunit Sit4 and a regulatory subunit, which can be Sap4, Sap155, Sap185, or Sap190 (Sit4 Associated Protein 4/155/185/190) (Deprez et al., 2018; Jablonowski et al., 2009; Lillo et al., 2014). Active TORC1 phosphorylates Tap42 (**Figure 9**), promoting its interaction with the catalytic subunits of PP2A and PP2A-like phosphatases (Deprez et al., 2018; Di Como & Arndt, 1996; Jiang & Broach, 1999). This interaction prevents the association of catalytic and regulatory subunits, leading to the inactivation of the phosphatase complexes (Di Como & Arndt, 1996; Jiang & Broach, 1999). Interestingly, Tap42 recruits these protein phosphatases to the vacuolar membrane, preventing them from dephosphorylating TORC1 downstream targets (Di Como & Arndt, 1996; Jiang & Broach, 1999). During nitrogen starvation, Tap42 is dephosphorylated and dissociates from the PP2A and PP2A-like catalytic subunits, allowing their interaction with regulatory subunits and subsequent activity (Di Como & Arndt, 1996; Jiang & Broach, 1999). The release of Tap42 from the phosphatases depends on Tip41 (Tap42 Interacting Protein 41) (Di Como & Jiang, 2006; Jacinto et al., 2001). TORC1 phosphorylates also Tip41 (**Figure 9**), impairing its interaction with and inhibition of Tap42 (Di

Como & Jiang, 2006). Notably, active Sit4 can dephosphorylate Tip41, enabling its interaction with Tap42 and releasing Sit4 from Tap42 inhibition (Jacinto et al., 2001). Thus, TORC1 regulates PP2A and PP2A-like activity by directly phosphorylating Tip41 and preventing its dephosphorylation (Jacinto et al., 2001).

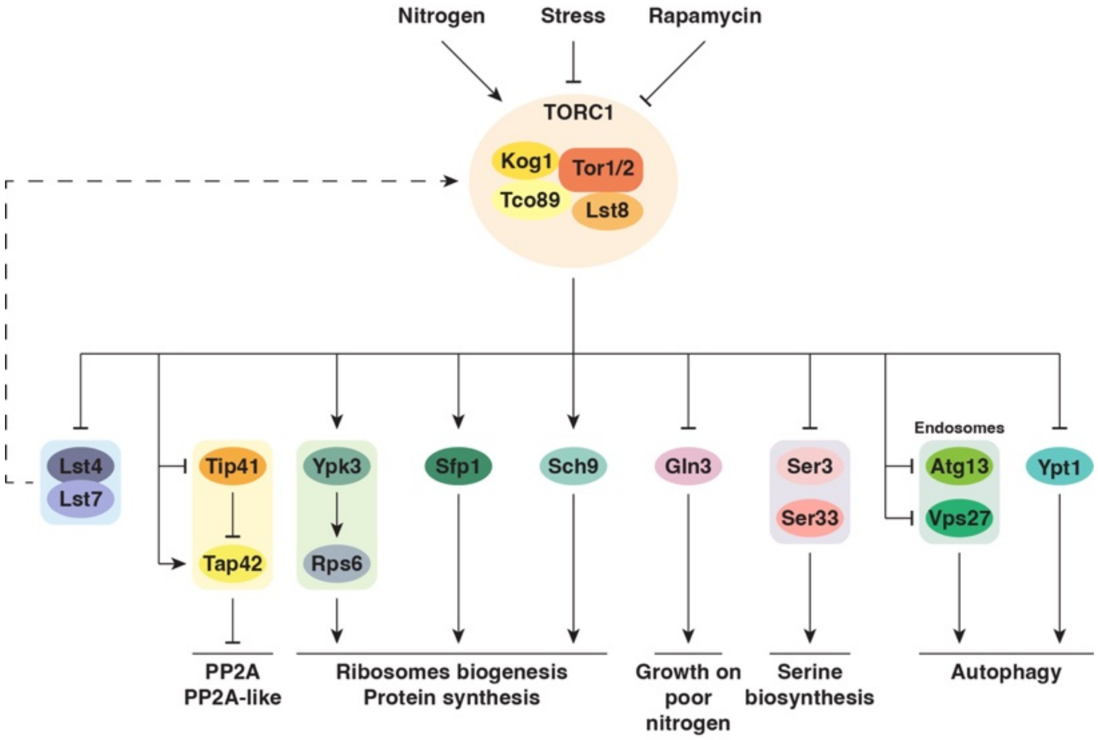
Nitrogen
Stress
Rapamycin
TORC1
Kog1
Tor1/2
Tco89
Lst8
Lst4
Lst7
Tip41
Tap42
Ypk3
Rps6
Sfp1
Sch9
Gln3
Ser3
Ser33
Endosomes
Atg13
Vps27
Ypt1
PP2A
PP2A-like
Ribosomes biogenesis
Protein synthesis
Growth on poor nitrogen
Serine biosynthesis
Autophagy

Figure 9. Scheme depicting the known direct TORC1 targets.

When nitrogen and amino acid levels are high, active TORC1 phosphorylates several proteins to promote cell growth and division, protein synthesis, ribosome biogenesis, and amino acid biosynthesis, and inhibits autophagy and stress responses. For more details, refer to the text.

PP2A activity is crucial for regulating the GAAC (General Amino Acid Control) signaling pathway, which coordinates amino acid availability with translation initiation (Gonzalez & Hall, 2017). During amino acid depletion, PP2A and PP2A-like phosphatases dephosphorylate Gcn2 (General Control Non-derepressible 2), rendering it more sensitive to uncharged tRNAs and become more active (Dokládal et al., 2021b; Hinnebusch, 2005). Active Gcn2 phosphorylates and inhibits eIF2α (Eukaryotic Initiation Factor 2α), promoting the translation of specific mRNAs, including *GCN4* (General Control Non-derepressible 4) (Dokládal et al., 2021b; Hinnebusch, 2005). Gcn4 is a transcriptional activator for amino acid transporters, amino acid metabolism enzymes, and autophagy-related factors (Hinnebusch, 2005). TORC1 inhibition of PP2A and PP2A-like phosphatases prevents Gcn2 dephosphorylation, rendering it less sensitive to uncharged tRNAs and hence promoting its inactive state (Hinnebusch, 2005). Consequently, during amino acid starvation, the translation of *GCN4* mRNA and the upregulation of the GAAC signaling pathway and macroautophagy depend on the presence of uncharged tRNAs and the activation status of TORC1 (Gonzalez & Hall, 2017; Hinnebusch, 2005).

The PP2A pathway also regulates the serine/threonine protein kinase Npr1 (Nitrogen Permease Reactivator 1) (Brito et al., 2019; Gander et al., 2008). In nitrogen-rich conditions, TORC1 downregulates PP2A and PP2A-like phosphatases, keeping Npr1 highly phosphorylated and inactive, partly through direct TORC1 phosphorylation of Npr1 at multiple sites (Boeckstaens et al., 2015; Hu et al., 2019; Schmidt et al., 1998). Under poor nitrogen conditions, Npr1 is dephosphorylated and activated, leading to the degradation of Tat2 (Tryptophan Amino acid Transporter 2), the high-affinity tryptophan transporter, via direct phosphorylation (Gander et al., 2008). Simultaneously, Npr1 facilitates the transport of the General Amino acid Permease (Gap1) to the plasma membrane by inhibiting its ubiquitination (Gander et al., 2008).

2.3.2. Other direct and indirect TORC1 targets

Active TORC1 phosphorylates Gln3 (**Figure 8**), enabling its interaction with the cytoplasmic repressor Ure2 (UREidosuccinate transport 2), which keeps Gln3 in the cytoplasm, preventing it from acting as a transcriptional activator (Bertram et al., 2000; De Virgilio & Loewith, 2006b; Tate et al., 2015). Through Gln3 phosphorylation, TORC1 inhibits the transcription of genes necessary for growth on non-preferential nitrogen sources (Bertram et al., 2000; De Virgilio & Loewith, 2006b; Tate et al., 2015).

Additionally, TORC1 affects macroautophagy by phosphorylating and inhibiting Atg13 (AuTophaGy related 13) (**Figure 9**), a subunit of the Atg1 kinase complex (Hatakeyama et al., 2019; Hu et al., 2019; Noda, 2017), on the surface of signaling endosomes (Hatakeyama et al., 2019). During nitrogen starvation, Atg13 is dephosphorylated due to TORC1 inactivation and subsequent activation of PP2A and PP2A-like phosphatases (Noda, 2017). Conversely, when nitrogen and amino acid levels are high, phosphorylated Atg13 cannot bind and activate the kinase Atg1, leading to the inhibition of macroautophagy (Noda, 2017).

At signaling endosomes, TORC1 also phosphorylates Vps27 (Vacuolar Protein Sorting 27) (**Figure 9**), involved in the sorting of multivesicular bodies, to downregulate microautophagy (Hatakeyama & De Virgilio, 2019; Hatakeyama et al., 2019; Henne et al., 2011; Morshed et al., 2020). TORC1 further inhibits autophagy by directly phosphorylating Ypt1 (Yeast Protein Two 1) (**Figure 9**) (Yao et al., 2023). Ypt1 is a GTPase that regulates membrane tethering events, including the formation of the PAS (Phagophore Assembly Site), a crucial step in autophagy (Lipatova et al., 2012; Papinski et al., 2014; J. Wang et al., 2015). Active Ypt1 recruits the Atg1 kinase complex to the PAS, promoting PAS maturation (Lipatova et al., 2012; Papinski et al., 2014; J. Wang et al., 2015). When nitrogen and amino acid levels are high, TORC1 phosphorylates Ypt1, inhibiting its binding to Atg1 and its recruitment to the PAS, thereby inhibiting autophagy (Yao et al., 2023).

To promote ribosomal protein synthesis, TORC1 indirectly regulates the phosphorylation of the ribosomal protein Rps6 (Ribosomal Protein of the Small subunit 6) (**Figure 9**) (Gonzalez et al., 2015; Yerlikaya et al., 2016). Although Sch9 can phosphorylate Rps6 *in vitro* (Urban et al., 2007), it does not do so *in vivo* (Gonzalez et al., 2015), suggesting that Sch9 is not the TORC1 effector for Rps6 activity. More recently, it has been observed that TORC1 directly phosphorylates and activates another AGC protein kinase, Ypk3 (Yeast Protein Kinase 3), by phosphorylating Ser^{513} in its hydrophobic motif (HM) (**Figure 9**) (Dokládal et al., 2021a; Gonzalez et al., 2015; Yerlikaya et al., 2016), similarly to Sch9 (Urban et al., 2007). Active Ypk3 phosphorylates Rps6 at $Ser^{232,233}$ *in vivo* and *in vitro* (Gonzalez et al., 2015; Yerlikaya et al., 2016), analogously to S6K in mammalian cells (Gonzalez et al., 2015). Interestingly, the protein phosphatase PP1 Glc7, associated with Shp1 (Suppressor of High-copy PP1), has been identified as responsible for dephosphorylating these residues after rapamycin treatment (Yerlikaya et al., 2016). In parallel, to promote ribosome biogenesis, TORC1 directly phosphorylates the transcription factor Sfp1 (Split Finger Protein 1) (**Figure 9**), thereby enhancing its nuclear localization and/or binding to RP and possibly RiBi gene promoters and stimulating their expression (Jorgensen et al., 2004; Lempiainen et al., 2009; Loewith & Hall, 2011).

Recently, two new TORC1 targets have been identified. Ser3 (SERine requiring 3) and Ser33 (SERine requiring 33) are directly phosphorylated by TORC1 in a Pib2-dependent manner, showing that TORC1 is directly involved in the regulation of amino acids biosynthesis (**Figure 9**) (Cecil et al., 2023; Zeng et al., 2024).

2.4. Molecules modulating TORC1 activity

TORC1 activation can be influenced by various molecules. The primary activators of TORC1 are amino acids, with glutamine, aspartate, asparagine, methionine, and cysteine having the most significant impact on TORC1 activity in yeast, as indicated by Sch9-Thr^{737} phosphorylation (De Virgilio & Loewith, 2006b; Péli-Gulli et al., 2015). In addition, elevated methionine levels lead to PP2A methylation and activation (Sutter et al., 2013), which leads to dephosphorylation and inactivation of SEACIT, with subsequent TORC1 activation (Nicastro et al., 2017; Sutter et al., 2013). Glutamine and cysteine also affect TORC1 activity through direct binding to the glutamine/cysteine sensor Pib2 (Tanigawa et al., 2021; Ukai et al., 2018; Zeng et al., 2024). Additionally, leucine plays a crucial role in TORC1 activation via LeuRS

(Bonfils et al., 2012; Powis & De Virgilio, 2016). The mechanisms by which amino acids impinge on the Rag GTPase in yeast are still poorly understood (De Virgilio & Loewith, 2006b; Péli-Gulli et al., 2015), however, more is known about their sensing mechanisms in mammalian cells (for more details see **Paragraph 2.5**).

Recently, Mn^{2+} has been identified as a novel TORC1 activator (Nicastro et al., 2022). Under normal conditions, Tor1 coordinates ATP with the divalent cation Mg^{2+} (Nicastro et al., 2022), which is more abundant than Mn^{2+} in yeast cells (McNaughton et al., 2010; van Eunen et al., 2010). Interestingly, Mn^{2+} competes with Mg^{2+} and more strongly activates TORC1 (Nicastro et al., 2022), indicating that Mn^{2+} homeostasis significantly impacts cell growth.

On the other hand, several molecules have been identified as TORC1 inhibitors. The most commonly used TORC1 inhibitor is the lipophilic macrolide rapamycin (De Virgilio & Loewith, 2006b; Wullschleger et al., 2006). Another inhibitor is wortmannin, a fungal metabolite that inhibits the PI3K kinase family (Ihara et al., 2020). Since Tor1/2 are part of the PIKKs family (De Virgilio & Loewith, 2006b; Wullschleger et al., 2006), they can also be inhibited by wortmannin (Cameroni et al., 2006; Yerlikaya et al., 2016), which is mainly used as an *in vitro* inhibitor (Chen et al., 2021; Nicastro et al., 2023; Nicastro et al., 2022). Additionally, ATP analogous molecules such as Torin2, caffeine, and indole-3-acetic acid have been shown to reduce TORC1 activity both *in vivo* and *in vitro* (Kumar et al., 2018; Nicastro et al., 2021; Wanke et al., 2008). More recently, malonyl-CoA has been identified as an ATP-competitive TORC1/mTORC1 inhibitor (Nicastro et al., 2023), due to its adenine group acting as an ATP analog. A model suggests that TORC1's low affinity for ATP (Dennis et al., 2001; Knight & Shokat, 2005) allows it to function as a homeostatic ATP sensor, responding to ATP level fluctuations and the presence of ATP analogs (Dennis et al., 2001). Evolutionarily, this characteristic enables TORC1 to quickly respond to ATP variations, immediately halting protein synthesis, ribosome biogenesis, and cell growth when ATP levels drop too low (Dennis et al., 2001).

2.5. Conservation of the TORC1 complex

2.5.1. Components of mTORC1

The mammalian equivalent of TORC1 is mTORC1 (Mechanistic Target Of Rapamycin Complex 1) (De Virgilio & Loewith, 2006a, 2006b; Gonzalez et al., 2020; Wullschleger et al., 2006). Unlike the *S. cerevisiae* genome, which encodes Tor1 and Tor2, higher eukaryotes have a single gene encoding the catalytic subunit for both mTORC1 and mTORC2, known as mTOR (**Table 2**) (De Virgilio & Loewith, 2006a, 2006b; Gonzalez et al., 2020; Wullschleger et al., 2006). The mammalian counterpart of Kog1 is Raptor, and the counterpart of Lst8 is mLST8 (**Table 2**) (De Virgilio & Loewith, 2006a, 2006b; Gonzalez et al., 2020; Wullschleger et al., 2006). The yeast Tco89 subunit of TORC1 is not conserved in mammals, but the protein PRAS40 (Proline-rich Akt substrate 40) is present in mTORC1 (**Table 2**) (Thedieck et al., 2007; Wang et al., 2007). PRAS40 inhibits the complex by competing with substrates binding to Raptor (Thedieck et al., 2007; Wang et al., 2007). An additional inhibitory component of the complex is Deptor (DEP-domain containing mTOR-interacting protein) (**Table 2**) (Catena & Fanciulli, 2017; Peterson et al., 2009).

TORC1 (*S. cerevisiae*)	mTORC1 (mammals)
Tor1, Tor2	mTOR
Lst8	mLST8
Kog1	Raptor
Tco89	-
-	PRAS40
-	Deptor

Table 2. TORC1 and mTORC1 components in *S. cerevisiae* and mammals, respectively.

2.5.2. Upstream regulation of mTORC1

2.5.2.1. Nutrient-mediated regulation of mTORC1

Similar to yeast TORC1, mTORC1 is regulated by Rag GTPases (Demetriades et al., 2014; Kim et al., 2008; Nicastro et al., 2017; Sekiguchi et al., 2001). RagA/B are the orthologs of Gtr1, while RagC/D are the orthologs of Gtr2 (Demetriades et al., 2014; Kim et al., 2008; Nicastro et al., 2017; Sekiguchi et al., 2001). For mTORC1 activation, RagA/B must be GTP-loaded and RagC/D GDP-loaded (active configuration) (Demetriades et al., 2014; Kim et al., 2008; Nicastro et al., 2017; Sekiguchi et al., 2001). In the presence of amino acids, RagA/B^{GTP}-RagC/D^{GDP} recruits mTORC1 to the lysosomal surface, an organelle that is functionally similar to yeast vacuoles, via direct interaction with Raptor (Sancak et al., 2008). The functional equivalent of the EGO-TC is the Ragulator complex, composed of LAMTOR1/p18, LAMTOR2/p14, LAMTOR3/pMP1, LAMTOR4/C7orf59, and LAMTOR5/HBXIP (Nicastro et al., 2017; Sancak et al., 2010). Like the EGO-TC, the Ragulator complex acts as a scaffold for the Rag GTPases and mTORC1 on the lysosomal surface (Nicastro et al., 2017; Sancak et al., 2010). It also exhibits GEF activity towards RagA/B (Bar-Peled et al., 2012; Jung et al., 2015; Nicastro et al., 2017).

The functional orthologs of SEACIT and SEACAT are GATOR1 (GAP Activity TOward Rags 1) and GATOR2 (GAP Activity TOward Rags 2), respectively, and they perform similar activities towards RagA/B (Gonzalez & Hall, 2017; Nicastro et al., 2017; Shen et al., 2019; Tafur et al., 2022; Valenstein et al., 2024; Valenstein et al., 2022; Wolfson et al., 2017). The GATOR1 complex is formed by DEPDC5, Nprl2, Nprl3, while the GATOR2 complex is composed of Mios, WDR24, WDR59, Seh1L, Sec13 (Peng et al., 2017; Shen et al., 2018). In line with this, the respective yeast and mammalian complexes appear to be structurally conserved (Tafur et al., 2022; Valenstein et al., 2022). In GATOR1, Nprl2, the ortholog of the yeast Npr2, has the catalytic residue Arg^{78}, which enhances the GTPase activity of RagA/B, favoring mTORC1 inhibition, similarly to yeast Npr2-Arg^{84} (Shen et al., 2019; Tafur et al., 2022; Valenstein et al., 2022).

By mass spectrometry analysis, four proteins (KPTN, ITFG2, C12orf66, and SZT2) have been identified as GATOR1 interactors (Wolfson et al., 2017). Together, they form the KICSTOR (KPTN, ITFG2, C12orf66, and SZT2-containing regulator of mTORC1) complex, which is not conserved in fungi (Wolfson et al., 2017). GATOR1, KICSTOR, and GATOR2 form the GATOR supercomplex (Valenstein et al., 2024). The role of KICSTOR is to localize GATOR1, but not GATOR2, to the lysosomal surface, where it can inhibit RagA/B (Wolfson et al., 2017). Indeed, knockout cell lines in the KICSTOR components show delocalized GATOR1 and hyperactive mTORC1 (Peng et al., 2017; Wolfson et al., 2017). More recently, a new model has been introduced, where GATOR1, similar to SEACIT in yeast (Tafur et al., 2022), is needed for the lysosomal localization of KICSTOR and GATOR2 (Valenstein et al., 2024). The Rag-Ragulator complex appears to anchor GATOR to the lysosome with RagA/B^{GDP} playing a critical role in recruiting GATOR (Valenstein et al., 2024). Therefore, a positive feedback regulation of RagA/B GDP and GATOR may explain this process, where GATOR1 promotes the RagA/B GDP-bound state, which in this conformation stabilizes GATOR1 on the lysosomal surface (Valenstein et al., 2024).

In yeast cells, Pib2 and LeuRS function as sensors for glutamine/cysteine and leucine, respectively, signaling their presence to TORC1 (Bonfils et al., 2012; Powis & De Virgilio, 2016; Tanigawa et al., 2021; Ukai et al., 2018; Zeng et al., 2024). In mammalian cells, different amino acid sensors are expressed. Notably, there are three isoforms of Sestrin proteins, with Sestrin2 identified as a key leucine sensor (Nicastro et al., 2017; Saxton et al., 2016; Wolfson et al., 2016). During amino acid starvation, Sestrin2 interacts with GATOR2, preventing GATOR2 from inhibiting GATOR1, thus allowing GATOR1's GAP activity on RagA/B, leading to mTORC1 inactivation (Lee et al., 2016; Nicastro et al., 2017; Saxton et al., 2016; Wolfson et al., 2016). When Sestrin2 binds to leucine, a conformational change prevents its interaction with GATOR2, allowing GATOR2 to inhibit GATOR1's GAP activity, resulting in mTORC1 activation (Lee et al., 2016; Nicastro et al., 2017; Saxton et al., 2016; Wolfson et al., 2016).

On the other hand, arginine is sensed by the cytosolic sensor CASTOR1, which functions as a homodimer or heterodimer with CASTOR2 (Chantranupong et al., 2016; Nicastro et al., 2017). The CASTOR dimer operates similarly to Sestrin2, leading to mTORC1 activation in the presence of arginine by preventing CASTOR from interacting with GATOR2, which can inhibit GATOR1's GAP activity (Chantranupong et al., 2016; Nicastro et al., 2017).

The protein SAMTOR (S-AdenosylMethionine sensor upstream of mTORC1) was also detected as an amino acid sensor and GATOR1-KICSTOR-specific interactor (Gu et al., 2017). SAMTOR is a negative regulator of mTORC1 by promoting the activity of GATOR1 (Gu et al., 2017). Similar to the mechanism of action of Sestrin and CASTOR towards GATOR2, in the presence of SAM (S-AdenosylMethionine), a product of methionine metabolism, SAMTOR dissociates from GATOR1-KICSTOR (Gu et al., 2017). In methionine-starved cells, the levels of SAM are reduced, and the interaction between SAMTOR and GATOR1-KICSTOR is strengthened (Gu et al., 2017). Conversely, the readdition of methionine weakens this interaction (Gu et al., 2017). In the absence of SAM, the N-terminal helical domain of SAMTOR is far from the SAM binding site, allowing the GATOR1-KICSTOR binding site to be available for interaction (Tang et al., 2022). Conversely, in the presence of SAM, the N-terminal helical domain is close to the SAM-binding site, a conformation stabilized by SAM itself (Tang et al., 2022). This conformational change blocks the GATOR1-KICSTOR binding site, leading to the activation of mTORC1 signaling (Tang et al., 2022).

Recently, the protein LYCHOS (LYsosomal CHOlesterol Signaling) has been identified as a cholesterol sensor and mTORC1 activator (Shin et al., 2022). At high cholesterol concentrations (*i.e.* in nutrient-rich conditions), the cholesterol present in the lysosomal membrane is sensed and bound by LYCHOS, which undergoes a conformational change that allows its interaction with GATOR1 (Shin et al., 2022). This event causes the dissociation of GATOR1 from KICSTOR, leading to its delocalization and inability to inhibit mTORC1 (Shin et al., 2022).

The GDP-loaded state of RagC/D is maintained by FLCN-FNIP1/2 (Folliculin Interacting Protein 1/2/Folliculin), the orthologs of Lst4-Lst7 (Gonzalez & Hall, 2017; Nicastro et al., 2017), with FLCN acting as the GAP through catalytic role of its its Arg^{164} (Lawrence et al., 2019). The binding of FLCN-FNIP1/2 to RagC/D increases upon amino acid deprivation (Jung et al., 2015). FLCN-FNIP1/2 stably interacts with the G domains of RagA^{GDP}-RagC^{GTP}-Ragulator, forming a complex known as the Lysosomal FLCN Complex (LFC) (Lawrence et al., 2019). In the LFC, FLCN-Arg^{164} is distant from the RagC nucleotide pocket, preventing it from performing its GAP activity and maintaining RagC in the GTP-bound state (Lawrence et al., 2019).

The sodium-coupled amino acid transporter SLC38A9 (SoLute Carrier family 38) is a lysosomal amino acid transporter that interacts with Ragulator and Rag GTPases via its N-terminal cytosolic tail (Jung et al., 2015). SLC38A9 has been shown to promote mTORC1 activation in the presence of glutamine, arginine, and leucine (Jung et al., 2015; Nicastro et al., 2017; Rebsamen et al., 2015; S. Wang et al., 2015). In SLC38A9 knockout cells, mTORC1 activity is abolished (Jung et al., 2015; Rebsamen et al., 2015; S. Wang et al., 2015), rendering it insensitive to amino acid changes (Jung et al., 2015), and impairing the lysosome-to-cytosol translocation upon amino acid deprivation (Jung et al., 2015; Rebsamen et al., 2015; S. Wang et al., 2015). Conversely, SLC38A9 overexpression causes mTORC1 hyperactivation, even under amino acid-scarce conditions (Jung et al., 2015; S. Wang et al., 2015).

More recently, it has been shown that SLC38A9 can signal amino acid availability to activate mTORC1 (Fromm et al., 2020). The latest regulation model of mTORC1 (**Figure 10**) suggests that, under amino acid-depleted conditions, FLCN-FNIP2 binds to inactive Rag GTPases, forming the LFC (**Figure 10**) (Fromm et al., 2020; Lawrence et al., 2019). During this phase, the cytosolic N-terminal tail of SLC38A9 occludes the amino acid binding site in the transmembrane domain and SLC38A9 cannot interact with inactive Rag GTPases (**Figure 10**) (Fromm et al., 2020). When amino acid levels rise, arginine, glutamine, and leucine outcompete the cytosolic N-terminal tail of SLC38A9 for binding in the transmembrane domain (Fromm et al., 2020). The N-terminal tail is then free to interact with the G domains of Rag GTPases, leading to LFC disassembly and activation of FLCN-FNIP2 GAP activity, which stimulates the hydrolysis of GTP to GDP in RagC/D (**Figure 10**) (Fromm et al., 2020). SLC38A9 acts as a Guanine nucleotide Dissociation Inhibitor (GDI) toward RagA/B (observed *in vitro*) stabilizing the RagA/B^{GDP}-RagC/D^{GDP} intermediate conformation (**Figure 10**) (Fromm et al., 2020; Valenstein et al., 2024). The dissociation of the SLC38A9 N-terminal tail enables the exchange of GDP for GTP in RagA (Fromm et al., 2020), generating the active conformation of Rag GTPases and allowing mTORC1 activation (**Figure 10**) (Fromm et al., 2020). Thus, the region formed by the G domains of the Rag GTPase heterodimer is considered a regulatory platform (Fromm et al., 2020). It can bind to FLCN-FNIP2 under amino acid-scarce conditions, to SLC38A9 after amino acid replenishment, and to mTORC1 via the Raptor subunit when they assume the active conformation (Fromm et al., 2020).

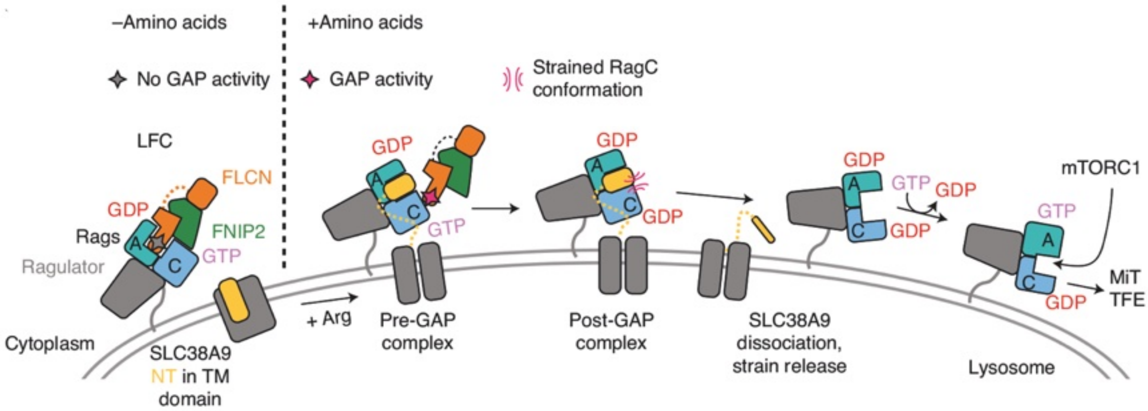
−Amino acids
+Amino acids
No GAP activity
GAP activity
Strained RagC conformation
LFC
FLCN
GDP
Rags
FNIP2
GTP
Ragulator
A
C
Cytoplasm
SLC38A9
NT in TM domain
+ Arg
GDP
GTP
Pre-GAP complex
GDP
GDP
Post-GAP complex
SLC38A9 dissociation, strain release
GDP
GTP
GDP
GDP
mTORC1
GTP
GDP
MiT
TFE
Lysosome

Figure 10. Model of the SLC38A9-mediated Rag GTPase activation of mTORC1 and its recruitment to the lysosome.

Image from (Fromm et al., 2020). NT (N-terminal domain); (TM, transmembrane domain). For more details, refer to the text.

Recently, it was observed that SLC38A9 is not needed for the response of mTORC1 to the presence of arginine (Valenstein et al., 2024), contradicting previous findings (S. Wang et al., 2015). Additionally, the overexpression of its N-terminal domain displaces GATOR from the lysosome, releasing RagA/B from inhibition by GATOR1, which explains why SLC38A9 positively regulates mTORC1 (Valenstein et al., 2024). Moreover, the conformation of the Rag GTPases seems to influence SLC38A9 transport activity, suggesting that it may act as an effector of the Rag GTPases rather than a regulator (Valenstein et al., 2024). Furthermore, the leucine efflux caused by SLC38A9 can positively regulate mTORC1 via the Sestrin1/2-GATOR2 axis (Valenstein et al., 2024). Consequently, SLC38A9 emerges as a positive regulator of mTORC1, however, further research is needed to fully elucidate its underlying mechanism of action.

2.5.2.2. Hormones-mediated regulation of mTORC1

mTORC1 regulation depends not only on nutrient availability but also on signaling induced by hormones and growth factors, such as insulin (Gonzalez & Hall, 2017; Gonzalez et al., 2020; Yoon, 2017). When blood glucose levels rise, insulin is released and binds to the insulin receptor (IR) (Gonzalez & Hall, 2017; Gonzalez et al., 2020; Yoon, 2017). This is a tyrosine kinase receptor that autophosphorylates its tyrosine residues in the intracellular β domain to activate its kinase activity (Gonzalez & Hall, 2017; Yoon, 2017). Once activated, the IR phosphorylates IRS (Insulin Receptor Substrates), specifically IRS1 and IRS2, which recruit PI3K to produce PIP3 (PhosphatidylInositol (3,4,5)-trisPhosphate) from PIP2 (PhosphatidylInositol (4,5)-bisPhosphate) (Gonzalez & Hall, 2017; Yoon, 2017). Conversely, PIP3 is hydrolyzed to PIP2 by the tumor suppressor protein PTEN (Phosphatase and TENsin homolog) (Georgescu, 2010). PIP3 serves as a docking site for PDK1 (3-Phosphoinositide-Dependent protein Kinase 1), which recruits and activates Akt/PKB by phosphorylation (Gonzalez & Hall, 2017; Yoon, 2017). Active Akt indirectly activates mTORC1 by phosphorylating and inhibiting TSC2 (Tuberous Sclerosis Complex 2) (Gonzalez & Hall, 2017; Inoki et al., 2003a; Yoon, 2017). TSC2, along with TSC1 (Tuberous Sclerosis Complex 1) and TBC1D7, forms the TSC complex or Rhebulator with GAP activity, which negatively regulates the TORC1 activator GTPase Rheb (RAS Homolog Enriched in the Brain) (Demetriades et al., 2014; Dibble et al., 2012; Gonzalez & Hall, 2017; Inoki et al., 2003a; Long et al., 2005; Sancak et al., 2007; Tee et al., 2003; Yang et al., 2017; Yoon, 2017). TSC2 is the subunit with GAP activity, TSC1 stabilizes TSC2 and enhances its GAP activity, and TBC1D7 stabilizes the interaction between TSC1 and TSC2 (Dibble et al., 2012; Garami et al., 2003; Inoki et al., 2003a; Zhang et al., 2003). Rheb, active in its GTP-bound state, triggers mTORC1 activation by allosterically realigning residues in the mTORC1 active site (Gonzalez & Hall, 2017; Inoki et al., 2003a; Yang et al., 2017; Yoon, 2017). Additionally, Akt phosphorylates and inhibits PRAS40, promoting mTORC1 activation (Wiza et al., 2012; Yoon, 2017). Interestingly, the mTORC1 direct target S6K phosphorylates IRS1, inducing its degradation and triggering a negative feedback to prevent mTORC1 hyperactivation, an effect that contributes to the development of type II diabetes (Gonzalez & Hall, 2017; Inoki et al., 2003a; Yoon, 2017). Growth factors, like insulin, also induce mTORC1 activation via similar signaling pathways (Yoon, 2017).

2.5.2.3. mTORC1 pools in mammalian cells

During growth in the presence of amino acids, mTORC1 is tethered to the lysosomal membrane via the Rag GTPases and Rheb (Betz & Hall, 2013; Demetriades et al., 2014; Sancak et al., 2010). There, Rheb can stimulate mTORC1 activity (Betz & Hall, 2013; Demetriades et al., 2014; Gonzalez & Hall, 2017; Inoki et al., 2003a; Long et al., 2005; Sancak et al., 2010; Yang et al., 2017; Yoon, 2017). Upon amino acid removal, these tethering mechanisms need to be reverted so that mTORC1 can be released from the lysosome (Demetriades et al., 2014). Both events are triggered by the Rag GTPases assuming an inactive conformation (Demetriades et al., 2014). Firstly, this causes a reduction in the binding of the Rag GTPases with mTORC1 (Demetriades et al., 2014) and their interaction with the lysosome (Malik et al., 2023). Secondly, it leads to the simultaneous recruitment of the TSC complex to the lysosome, which can better interact with the Rag GTPases in the inactive conformation (Demetriades et al., 2014; Yang et al., 2020). Here, the GAP activity of the TSC complex promotes the GDP-bound state of Rheb, causing the release of the second tethering mechanism of mTORC1 on the lysosome surface (Demetriades et al., 2014; Gonzalez & Hall, 2017; Inoki et al., 2003a; Yoon, 2017). Valenstein et al. (Valenstein et al., 2024) recently published findings that contradict the previous data from Demetriades et al. and Yang et al. (Demetriades et al., 2014; Yang et al., 2020), showing that Rag GTPases are not necessary for the lysosomal localization of the TSC complex. This finding keeps the area of mTORC1 regulation by TSC at the lysosome open for further exploration.

Interestingly, recent observations indicate that mTORC1 can also be localized and activated in the cytosol and potentially in other organelles (Fernandes et al., 2024), similar to findings in yeast cells (Hatakeyama et al., 2019). The localization and activation of the cytosolic mTORC1 pool is independent of Rag GTPases and is acitvated by exogenous amino acids (Fernandes et al., 2024). The study reveals that non-lysosomal mTORC1 retains its activity towards canonical substrates like S6K and 4E-BP1, but not towards lysosomal substrates like TFEB (Fernandes et al., 2024; Napolitano et al., 2018; Roczniak-Ferguson et al., 2012). In contrast, Valenstein et al. showed that the Rag GTPases are essential for mTORC1 activation, including towards cytosolic targets such as S6K1 (Valenstein et al., 2024). Additionally, Valenstein et al. reconstituted the Rag-Ragulator complexes to the mitochondria but failed to observe activation of mTORC1, arguing that amino acids cannot be sensed at the mitochondria (Valenstein et al., 2024). They concluded that mTORC1, as a nutrient-sensing pathway, functions specifically on the lysosomal surface (Valenstein et al., 2024).

2.5.3. mTORC1 downstream signaling

One of the main mTORC1 targets is the protein kinase S6K (S6 Kinase 1), which is phosphorylated in the hydrophobic motif (Fenton & Gout, 2011; Gonzalez et al., 2020; Hara et al., 1998; Magnuson et al., 2012; Wang et al., 1998), similar to yeast TORC1's phosphorylation and activation of Sch9 (Urban et al., 2007). When activated, S6K promotes protein synthesis by enhancing translation initiation and elongation, and by phosphorylating the ribosomal protein S6 (Gonzalez et al., 2020; Wu et al., 2022). Additionally, S6K phosphorylates other targets to promote cell proliferation, growth, survival, metabolism, and immune system activation (Wu et al., 2022). Another mTORC1 target is 4E-BP1 (eIF4E Binding Protein 1) (Hara et al., 1998; Ma & Blenis, 2009; Wang et al., 1998), whose phosphorylation leads to its inactivation, thereby promoting mRNA translation initiation (Gonzalez et al., 2020; Saxton & Sabatini, 2017).

Additionally, mTORC1 phosphorylates the transcription factor TFEB (Transcription Factor EB) (Cui et al., 2023; Napolitano et al., 2018; Roczniak-Ferguson et al., 2012).

Phosphorylation impairs TFEB's nuclear translocation, blocking the transcription of autophagy machinery and lysosomal clearance genes (Cui et al., 2023; Napolitano et al., 2018; Perera et al., 2019; Roczniak-Ferguson et al., 2012). On the contrary, AMPK promotes the expression of TFEB in nutrient-scarce conditions (Herzig & Shaw, 2018). mTORC1 can phosphorylate targets containing a TOS (TOR Signaling) motif, such as S6K or 4E-BP1, through its interaction with Raptor (Napolitano et al., 2022). Other targets, like TFEB or MiT-TFE, lack a TOS motif but possess an RBR (Rag Binding Region), enabling interaction with Rag GTPases only in their active configuration (Napolitano et al., 2022). This distinction categorizes mTORC1 substrates into two groups: those with an RBR, whose phosphorylation depends on the Rags configuration and responds to nutrient availability (non-canonical mTORC1); and those with TOS motifs, phosphorylated in response to mTORC1 activation status influenced by hormones and growth factors, downstream of Rheb (canonical mTORC1) (Napolitano et al., 2018; Roczniak-Ferguson et al., 2012).

Finally, mTORC1 downregulates autophagy, not only indirectly by inhibiting TFEB, but also directly by phosphorylating and inhibiting ULK1, the kinase essential for initiating autophagy in mammalian cells (Kim et al., 2011).

3. The Yeast Protein Kinase Sch9 Functions as a Central Nutrient-Responsive Hub That Calibrates Metabolic and Stress-Related Responses

3.1. Introduction

Effective coordination between nutrient availability and cell growth is essential for organisms to adapt successfully to environmental changes. In the budding yeast *Saccharomyces cerevisiae*, multiple signal transduction pathways are involved in nutrient sensing, cell growth regulation, and cell cycle progression. Among these, the TORC1 signaling pathway is crucial for nitrogen sensing and signaling (Péli-Gulli et al., 2015; Stracka et al., 2014; Ukai et al., 2018). TORC1 exerts its effects by phosphorylating its primary target, Sch9, which regulates ribosome biogenesis, translation initiation, protein synthesis, sphingolipid metabolism, cell cycle progression, cell size, stress response, and autophagy in response to nutrient availability (Huber et al., 2011; Swinnen et al., 2014; Urban et al., 2007). Sch9 is part of the AGC protein kinase family and is localized in both the cytosol and vacuolar membranes (Chen et al., 2021; Novarina et al., 2021). Sch9's full activation requires phosphorylation by various protein kinases, including Pkh1, Pkh2, and Pkh3, which phosphorylate Thr^{570} in the activation loop, and TORC1, which phosphorylates multiple residues in the C-terminal region (Liu et al., 2005; Roelants et al., 2004; Urban et al., 2007). Additionally, cyclin-dependent protein kinases Bur1 and Pho85 phosphorylate Thr^{723} and Ser^{726} (Deprez et al., 2023; Jin et al., 2022), while SNF1 inhibits Sch9 through phosphorylation of Ser^{288} under carbon starvation conditions (Caligaris et al., 2023a).

As a central signaling node, Sch9 regulates numerous downstream effectors, including the glucose-responsive protein kinase A (PKA) (Galello et al., 2010; Soulard et al., 2010). Sch9's target profile partially overlaps with that of PKA, and it plays a significant role in stress response regulation through its effects on various protein kinases and transcription factors (Roosen et al., 2005; Yorimitsu et al., 2007). Sch9 also influences proteasomal and autophagic degradation systems, and its loss extends the lifespan of yeast cells (Dokládal et al., 2021a; Fabrizio et al., 2001).

In this review, we summarize the functions of Sch9 as a hub integrating inputs from different pathways to modulate growth-related adaptations to nutrient changes, including stress response, autophagy, and longevity. We also focus on the regulation of Sch9 by other signaling pathways and lipid binding, and explore how regulatory events might affect Sch9's structure and function.

3.2. Contribution to this chapter:

- Introduction.
- Figure 2.
- Part of chapter 4. The Role of Sch9 in Metabolic Reprogramming and Stress Responses

Journal of *Fungi*

MDPI

Review

The Yeast Protein Kinase Sch9 Functions as a Central Nutrient-Responsive Hub That Calibrates Metabolic and Stress-Related Responses

Marco Caligaris [1], Belém Sampaio-Marques [2,3], Riko Hatakeyama [4], Benjamin Pillet [1], Paula Ludovico [2,3], Claudio De Virgilio [1], Joris Winderickx [5] and Raffaele Nicastro [1,*]

[1] Department of Biology, University of Fribourg, 1700 Fribourg, Switzerland; marco.caligaris@unifr.ch (M.C.); benjamin.pillet@unifr.ch (B.P.); claudio.devirgilio@unifr.ch (C.D.V.)
[2] Life and Health Sciences Research Institute (ICVS), School of Medicine, University of Minho, 4710-057 Braga, Portugal; mbmarques@med.uminho.pt (B.S.-M.); pludovico@med.uminho.pt (P.L.)
[3] ICVS/3B's-PT Government Associate Laboratory, 4806-909 Guimarães, Portugal
[4] Institute of Medical Sciences, University of Aberdeen, Aberdeen AB25 2ZD, UK; riko.hatakeyama@abdn.ac.uk
[5] Department of Biology, Functional Biology, KU Leuven, B-3001 Heverlee, Belgium; joris.winderickx@kuleuven.be
* Correspondence: raffaele.nicastro2@unifr.ch; Tel.: +41-26-300-8657

Abstract: Yeast cells are equipped with different nutrient signaling pathways that enable them to sense the availability of various nutrients and adjust metabolism and growth accordingly. These pathways are part of an intricate network since most of them are cross-regulated and subject to feedback regulation at different levels. In yeast, a central role is played by Sch9, a protein kinase that functions as a proximal effector of the conserved growth-regulatory TORC1 complex to mediate information on the availability of free amino acids. However, recent studies established that Sch9 is more than a TORC1-effector as its activity is tuned by several other kinases. This allows Sch9 to function as an integrator that aligns different input signals to achieve accuracy in metabolic responses and stress-related molecular adaptations. In this review, we highlight the latest findings on the structure and regulation of Sch9, as well as its role as a nutrient-responsive hub that impacts on growth and longevity of yeast cells. Given that most key players impinging on Sch9 are well-conserved, we also discuss how studies on Sch9 can be instrumental to further elucidate mechanisms underpinning healthy aging in mammalians.

Keywords: Sch9; TORC1; SNF1; Pkh1; Pkh2; Pkh3; Pho85; lipid; stress; longevity

check for updates

Citation: Caligaris, M.; Sampaio-Marques, B.; Hatakeyama, R.; Pillet, B.; Ludovico, P.; De Virgilio, C.; Winderickx, J.; Nicastro, R. The Yeast Protein Kinase Sch9 Functions as a Central Nutrient-Responsive Hub That Calibrates Metabolic and Stress-Related Responses. *J. Fungi* **2023**, *9*, 787. https://doi.org/10.3390/jof9080787

Academic Editors: Markus Proft and Amparo Pascual-Ahuir

Received: 30 May 2023
Revised: 20 July 2023
Accepted: 24 July 2023
Published: 26 July 2023

Copyright: © 2023 by the authors. Licensee MDPI, Basel, Switzerland. This article is an open access article distributed under the terms and conditions of the Creative Commons Attribution (CC BY) license (https://creativecommons.org/licenses/by/4.0/).

1. Introduction

Proper coordination between nutrient availability and cell growth is needed in all organisms to guarantee a successful adaptation to environmental changes. In the budding yeast *Saccharomyces cerevisiae*, several signal transduction pathways are involved in nutrient sensing, regulation of cell growth, and cell cycle progression. Among them, the TORC1 signaling pathway plays a key role in nitrogen sensing and signaling [1–5]. Responding to nutrient cues allows TORC1 to promote growth by regulating catabolic and anabolic processes [6]. The TORC1 structure is well-conserved in eukaryotes and in budding yeast. It consists of a multimeric complex that consists of the serine/threonine protein kinase catalytic subunit (Tor1 or Tor2) and three regulatory subunits (Kog1, Tco89, and Lst8) [7]. By phosphorylating its main target Sch9 [8], TORC1 regulates ribosome biogenesis, translation initiation, protein synthesis, sphingolipid metabolism, cell cycle progression, cell size, stress response, and autophagy in response to nutrient availability [9–14]. *SCH9* (for Scott Cameron *Hind*III library clone number 9; Takashi Toda; personal communication) has been initially identified as a multicopy suppressor of the growth defect caused by a temperature-sensitive *cdc25* allele [15], hinting at a connection with the Ras/PKA signaling pathway.

Sch9 belongs to the family of AGC protein kinases, and it is localized both in the cytosol and on vacuolar membranes [11,16,17], from where it is dispersed into the cytosol when cells are limited for carbon sources [18]. Full activation of Sch9 requires phosphorylation of different amino acid residues by various protein kinases (Figure 1a). These include the paralogous Pkh1, Pkh2, and Pkh3 kinases, which themselves are stimulated [19–21] or not [22] by phytosphingosine (PHS) (see [23] for a detailed discussion) and which phosphorylate Thr^{570} in the activation loop of Sch9 [8,19,24,25]. In addition, TORC1 phosphorylates multiple residues in the C-terminal region of Sch9 [8], and the cyclin-dependent protein kinases (CDKs) Bur1 and Pho85 phosphorylate Thr^{723} and Ser^{726}, both originally considered TORC1 target residues [26,27]. In contrast, Sch9 can also be inhibited through phosphorylation of Ser^{288} by SNF1 when cells are starved for carbon [28–30]. In line with its role as a central signaling node, Sch9 regulates a large number of downstream effectors, such as the glucose-responsive protein kinase A (PKA) [31], which is encoded by the paralogous *TPK1*, *TPK2*, and *TPK3* genes [32]. Interestingly, in this context, Sch9 exhibits a target profile that partially overlaps with the one of PKA [12,33]. In addition, Sch9 is important for stress response regulation through its effects on the activity of various protein kinases and transcription factors [34,35]. Moreover, Sch9 impacts the proteasomal and autophagic degradative systems, and loss of Sch9 causes an extension of lifespan in yeast cells [36–38].

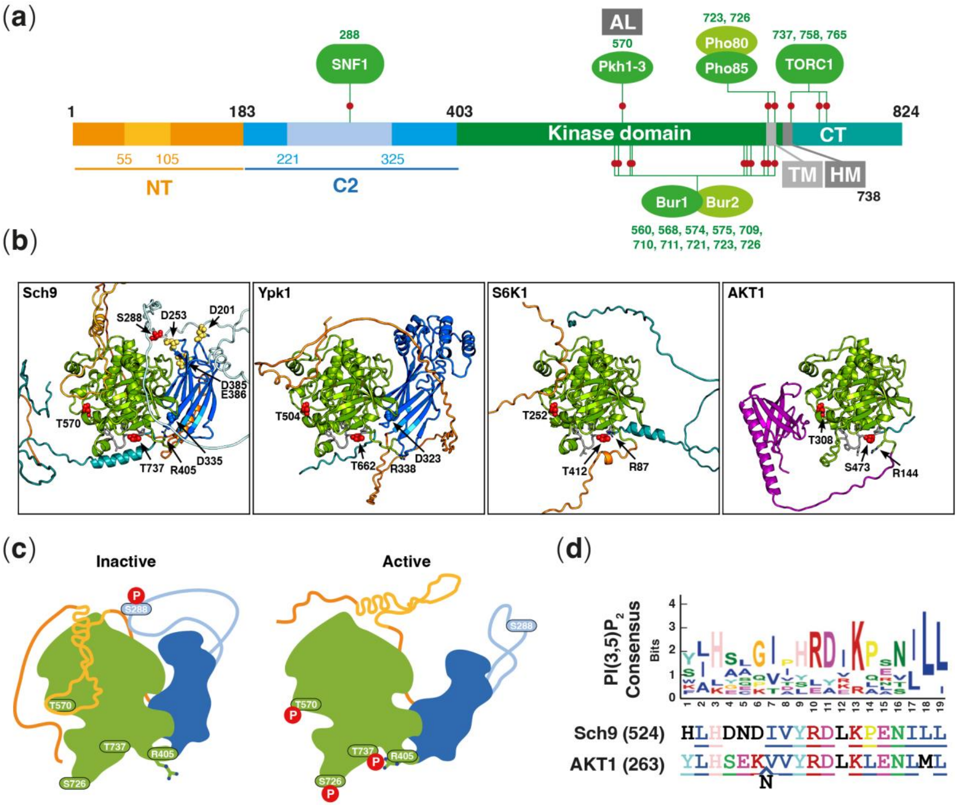
(a)
288
SNF1
AL
570
Pkh1-3
723, 726
Pho80
Pho85
737, 758, 765
TORC1
1
183
403
824
Kinase domain
CT
55
105
221
325
NT
C2
TM
HM
738
Bur1
Bur2
560, 568, 574, 575, 709, 710, 711, 721, 723, 726
(b)
Sch9
S288
D253
D201
D385
E386
T570
T737
R405
D335
Ypk1
T504
T662
R338
D323
S6K1
T252
T412
R87
AKT1
T308
S473
R144
(c)
Inactive
Active
P
S288
T570
T737
R405
S726
(d)
PI(3,5)P2 Consensus
Bits
Sch9 (524) HLHDNDIVYRDLKPENILL
AKT1 (263) YLHSEKVVYRDLKLENLML
N

Figure 1. Structural properties of Sch9. (**a**) Schematic domain architecture of Sch9. Red dots represent residues that are phosphorylated by the indicated protein kinases (green numbers refer to the phospho-residues within Sch9). NT, N-terminus; C2, C2 domain; AL, activation loop; TM, turn motif;

HM, hydrophobic motif; CT, C-terminus. (**b**) Side-by-side comparison of the Alphafold2 [39,40] predicted structures of Sch9 (AF-P11792-F1_v4.pdb), Ypk1 (AF-P12688-F1_v4.pdb), S6K1 (AF-P23443-F1_v4.pdb), and AKT1 (AF-P31749-F1_v4.pdb). The structural information is represented in cartoon style, and the domains (see Table 1) are colored as follows: N-terminus in orange; pleckstrin homology (PH) + linker in purple; C2 domain in blue; kinase domain in green; hydrophobic motif (HM) in grey (with side chains); and C-terminus in teal. The labeled phosphosites of the activation loop, the HM, and the C2 extended loop are displayed as balls and colored in red. The amino acids that could potentially coordinate Ca^{2+} on the top of the C2 domain of Sch9 are labeled, displayed as balls, and colored in yellow. The arginines corresponding to the Arg^{144} residue of AKT1 are labeled, and the side chains are represented as sticks. (**c**) Model depicting the spatial relationship of the kinase domain with the N-terminal region and the C2 domain and kinase domain of Sch9 in its inactive and active configuration, including the steric occlusion of the active site by the N-terminus in inactive Sch9 and the electrostatic interaction between Arg^{405} and $pThr^{737}$ in the active configuration. (**d**) Proposed consensus sequence for $PI(3,5)P_2$ binding [41] and the corresponding motifs upstream of the activation loop in Sch9 and AKT1.

Table 1. Structural domains of Sch9 and close homologues.

	Yeast		Mammalian	
Region	**Sch9**	**Ypk1**	**S6K1**	**AKT1**
N-terminus	1–183	1–117	1–83	See PH domain
PH + Linker	-	-	-	1–141
C2 domain	184–402	118–336	-	-
C2 extended loop	221–325	-	-	-
Kinase domain Activation loop Hydrophobic motif	403–738 570–574 (TFCGT) 733–738 (FAGFTF)	337–663 504–508 (TFCGT) 658–663 (FGGWTY)	84–413 252–256 (TFCGT) 408–413 (FLGFTY)	142–474 308–312 (TFCGT) 469–474 (FPQFSY)
C-terminus	739–824	664–680	414–525	475–480

In this review, we recapitulate the functions of the protein kinase Sch9, which serves as a hub that integrates inputs from different pathways, to modulate growth-related adaptations to nutrient changes, including stress response, autophagy, and longevity. We will additionally focus on the regulation of Sch9 by other signaling pathways and via lipid binding. Furthermore, a specific section will be devoted to exploring how regulatory events might affect Sch9 structure and function.

2. Structure of Sch9 and Confirmed Phosphosites

Although the experimental structure of Sch9 remains unresolved, the release of the Alphafold2 predicted protein structure database [39,40] provides high-accuracy models (Figure 1a) that, when combined with the known structural and functional characteristics of similar kinases, such as the yeast Ypk1 or the mammalian AKT1 and S6K1, can offer valuable insights (Figure 1b; Table 1). Based on these predicted structures and previous sequence analyses [8,42], Sch9 can be divided into four main regions: the disordered N-terminal region; the C2 domain; the kinase domain; and the C-terminal region.

The regions outlined in Table 1 and illustrated in Figure 1a–c have been defined based on the predicted structure of Sch9, Ypk1, S6K1, and AKT1. The N-terminal regions (PH + linker for AKT1) extend from the start of the protein to either the C2 domain (Sch9 and Ypk1) or the kinase domain (S6K1 and AKT1). The C2 domains were defined as starting with the first amino acid of the initial predicted β-strand (β1) and ending with the last amino acid of the final β-strand (β8), forming the β-sandwich. The kinase domains comprise the kinase core and the adjacent non-catalytic regions that are structurally aligned among the four analyzed kinases. These include the highly conserved activation loops and end with the hydrophobic motifs (HM) [43]. The C-terminal regions, consisting of all the amino acids following the HM, are predicted to have substantial structural variation among these kinases.

The N-terminus of Sch9 (amino acids: 1–183) is involved in membrane binding, and its structure is poorly predicted, indicating a predominantly disordered nature. In contrast, the N-terminus of AKT1 is well-folded and forms the PH (pleckstrin homology) domain (Figure 1b rightmost panel, purple) [44], which also engages in lipid binding [45–47]. Additionally, The PH domain of AKT1 fulfills an autoinhibitory role by binding to the kinase domain and shielding the activation loop [44]. Interestingly, although a part of the N-terminal region of Sch9 (spanning residues 55 to 105) exhibits a low average pLDDT (predicted Local Distance Difference Test) score, this region has a low Predicted Aligned Error (PAE) relative to the kinase domain, which indicates that it is likely positioned above the activation loop. This region of Sch9 could potentially play a role analogous to the PH domain of AKT1, keeping the activation loop buried while in its inactive form. Likewise, the N-terminal regions of Ypk1 and S6K are also predicted to be in proximity to the active site and may sterically occlude it as well (Figure 1a,c).

The first well-folded domain of Sch9 is a C2 domain of type II topology, which is characterized by the positioning of the N- and C-termini at the bottom of the β-barrel. Some C2 domains have been shown to coordinate Ca^{2+} on the loops between the β-sheets, which subsequently generates a binding surface that interacts with negatively charged lipids on the top of the C2 domain [48]. In contrast to Ypk1, which possesses α-helical structures in place of those loops, Sch9 has the potential to coordinate Ca^{2+} using the following amino acids: D201 (between β1 and β2), D353 (between β5 and β6); and D386/E387 (between β7 and β8). This mechanism could potentially stabilize the membrane tethering of Sch9 or enable Sch9 to bind to membranes with varying lipid compositions, although the membrane binding capacity of this particular C2 domain is so far questionable [16] (see also the next section). Unlike a typical C2 domain, Sch9 features an extended loop between β3 and β4. Importantly, this loop hosts Ser^{288}, which is phosphorylated by SNF1 to promote the inactivation of Sch9 [28]. In addition to the functionally relevant loops, the C2 domain was hypothesized to assist the N-terminus in inhibiting the kinase domain by imposing a conformational constraint due to its close proximity [49], which would explain the constitutive and TORC2-independent activity observed in Ypk1 (D242A) and Ypk2 (D239A) mutants [50–53]. These mutations are located at the interface between the C2 domain and the kinase domain, potentially weakening the interaction between the two domains. Consequently, the C2 domain could provide an additional autoinhibitory mechanism to the steric occlusion of the active site by the N-terminus.

The spatial relationship between the C2 domain and the kinase domain could be regulated by the phosphorylation of the kinase domain at amino acid Thr^{737}, which activates the Sch9 [8]. This phosphorylation has also been shown to reorder the hydrophobic motif [54]. Hypothetically, the negative charge of $pThr^{737}$ could electrostatically interact with Arg^{405}, bending the linker and connecting the C2 domain to the kinase domain. This would tilt the C2 domain away from the kinase domain, allowing for a catalytically competent conformation, as modeled in Figure 1c. The equivalent residue Arg^{144} of AKT1 was reported to drastically decrease its catalytic activity when mutated to alanine [55]. However, more recent research has challenged these findings, observing no effect resulting from the R144A mutation [44]. In the context of Sch9 and Ypk1, the linker between the two domains is shorter, suggesting that this mutation could have a more significant impact. Recently, the kinase domain was found to contain phosphorylation sites for the cyclin-dependent kinases Bur1 and Pho85 as well (Figure 1a), and especially the Pho85-mediated phosphorylation at Ser^{726} was shown to prime Sch9 for its subsequent activation by TORC1 [26,27]. Hence, it is tempting to speculate that this priming could also influence the spacing of the C2 domain and the kinase domain to relieve the occlusion by the N-terminus.

3. Lipid-Dependent Regulation of Sch9

Sch9 localizes throughout the cytoplasm, with a significant enrichment on the cytoplasmic surface of the vacuolar membrane [8,11]. The vacuolar localization is required for its activation through phosphorylation by TORC1, which resides on the same membrane [8,26,56]. The vacuolar targeting of Sch9 is mediated by the physical interaction between its N-terminal domain (1–183 amino acid residues; hereafter, Sch9$^{1-183}$) with the membrane lipid phosphatidylinositol 3,5-bisphosphate (PI(3,5)P$_2$) [16,17,57]. As mentioned, Sch9$^{1-183}$ is predicted to be largely disordered, unlike many other known phosphoinositide-binding domains that have defined configurations [58,59]. It is, therefore, unclear how exactly Sch9$^{1-183}$ interacts with PI(3,5)P$_2$.

Other domains of Sch9 also influence its membrane targeting. As mentioned in the previous section, Sch9 has a C2 domain (184–402 residues), a typical lipid-binding motif [60]. Surprisingly, however, the addition of this domain partially compromises the membrane recruitment of the Sch9$^{1-183}$ fragment, suggesting rather a negative role [16]. The underlying mechanism of this inhibitory effect is so far unknown. Another clue is provided by the comparison between the localization pattern of the full-length Sch9 and that of the Sch9$^{1-183}$ alone. While the full-length Sch9 exclusively localizes to the cytoplasm with enrichment at the vacuolar membrane, Sch9$^{1-183}$ alone is additionally found at signaling endosomes [16]. Since PI(3,5)P$_2$ is enriched on both vacuoles and signaling endosomes, this observation suggests that the non-N-terminal region of Sch9 biases the binding preference toward the vacuolar membrane. The underlying mechanism is again unknown but may involve the interaction of the 184–824 residues with other lipids or proteins residing uniquely on the vacuolar membrane. Alternatively, different physical properties of the two organelles, for example, the membrane curvature (as the vacuoles are significantly larger than signaling endosomes), may account for the altered preference. Of note, both Sch9 and AKT1 contain a motif upstream of the activation loop that closely resembles the proposed consensus sequence for the PI(3,5)P$_2$ binding [41]. However, the significance of this motif for the phosphoinositide interaction of Sch9 and AKT1 remains to be established.

Membrane targeting of Sch9 is dynamically regulated in response to environmental changes. For example, glucose starvation and oxidative stress cause Sch9 to detach from the vacuolar membrane [11,18,61]. The underlying mechanisms for the regulated (de)localization of Sch9 are not fully understood, but recent observations have shown that these also involve alterations in the amount or the subcellular distribution of PI(3,5)P$_2$. Indeed, evidence exists that PI(3,5)P$_2$ responds to various cellular stresses and nutrient availability. Osmotic stress, for instance, stimulates PI(3,5)P$_2$ production in a manner dependent on the cyclin-dependent kinase Pho85 [62,63]. Mechanistically, Pho85 activates, in association with the Pho80 cyclin, the lipid kinase complex that converts PI3P into PI(3,5)P$_2$ by direct phosphorylation of the catalytic phosphatidylinositol-3-phosphate 5-kinase subunit Fab1 and its regulatory subunit Vac7 [63]. Moreover, TORC1 phosphorylates Fab1 as well, thereby stimulating PI(3,5)P$_2$ production on signaling endosomes [16]. Upon fusion of the signaling endosome to the vacuole, PI(3,5)P$_2$ is delivered to the vacuolar membrane, which is required to recruit TORC1 and its substrate Sch9 [16,26,57]. Interestingly, TORC1 and Fab1 form a positive feedback loop [16]. These facts indicate that PI(3,5)P$_2$ acts as an important signaling lipid that links nutrient/stress-responsive pathways, such as Pho85 and TORC1 pathways, to downstream effectors, including Sch9 [26]. Notably, the research on PI(3,5)P$_2$ has been hampered by the lack of visualization tools. The use of GFP-fused Sch9$^{1-183}$ as a PI(3,5)P$_2$ biosensor may therefore be helpful in advancing the research in this area [16].

Another vacuolar membrane client that requires PI(3,5)P$_2$ and that influences the activation of Sch9 is the V-ATPase, the vacuolar proton pump, whose assembly and activity are dependent on glucose availability [64,65]. Initial studies suggested that the V-ATPase plays an important role in cellular stress responses by promoting the activities of the PKA and TORC1 pathways through an interaction with the Arf1 and Gtr1 GTPases, respectively [66,67]. The connection between V-ATPase and TORC1 activation was recently proposed to be mediated by the Ccr4-Not complex, which is a known downstream effector of TORC1 for ribosomal RNA biogenesis and transcription of stress-responsive genes [68,69], but which also acts upstream of TORC1 as a regulator of V-ATPase assembly and vacuolar acidification [70]. Interestingly, Sch9 is known to influence the activity of the V-ATPase as well since it facilitates V-ATPase disassembly upon glucose starvation, thus providing a possible feedback route [18]. How Ccr4-Not and Sch9 control the V-ATPase assembly/disassembly state is not known, but one suggested possibility involves the ubiquitylation and stability of one or more V-ATPase subunits [70,71]. In addition, the V-ATPase was proposed to act as a sensor of cytosolic pH [72]. This reconciles with data showing that also proton influx at the plasma membrane, which is catalyzed by amino-acid/H^+ symporters and driven by the H^+-ATPase Pma1, influences the TORC1 activation [73]. Since Sch9 is required to maintain normal Pma1 activity and extracellular acidification [18], it likely influences this plasma membrane symport of protons and amino acids as well.

Besides being recruited to the vacuolar membrane via phosphoinositide PI(3,5)P_2-binding, the Sch9 function is also fine-tuned by the long chain base (LCB) phytosphingosine (PHS), an intermediate of the sphingolipid metabolic pathway [19,74]. Here, a key role is played by protein kinases Pkh1, Pkh2, and Pkh3, the orthologues of the mammalian 3-phosphoinositide dependent kinase-1, PDK1, which are known to be involved in the maintenance of cell wall integrity and the control of eisosome dynamics [21,23,75]. These PDK1 orthologs phosphorylate the Sch9 activation loop at Thr^{570} (Figure 1a), an event that occurs independently of the C-terminal Sch9 phosphorylation by TORC1 and that is required to obtain a full Sch9 activity [8,25]. Interestingly, the Pkh-Sch9 axis appears to establish a feedback loop since, as depicted in Figure 2, sphingolipid metabolism is itself regulated by Sch9 at the level of the ceramide synthases Lac1 and Lag1, the ceramidases Ydc1 and Ypc1, as well as the inositol phosphosphingolipid phospholipase C, Isc1 [76]. The latter translocates from the endoplasmic reticulum to mitochondria during the diauxic shift and hydrolyzes the complex sphingolipids IPC, MIPC, and M(IP)$_2$C back into dihydro-/phytoceramides, which contribute to the normal functioning of mitochondria [77]. This Isc1 translocation to mitochondria is dependent on Sch9, explaining at least in part the requirement of Sch9 to properly traverse the diauxic shift [76,78].

Sphingolipids are important components of membranes that, beyond their structural role, also fulfill additional specific functions in several fundamental cellular processes. For instance, the dynamic balance between the different sphingolipid metabolites, especially LCBs, their phosphorylated derivatives (LCBPs), ceramides, and complex sphingolipids, have been shown to accompany stress responses, mitochondrial functioning and oxidative phosphorylation, cell wall synthesis and repair, autophagy, endocytosis, and actin cytoskeleton dynamics, thereby affecting the growth and longevity of yeast cells [74,79,80]. In general, LCBPs have been shown to act as pro-growth signals, while ceramides mainly act as antiproliferative signals [81]. The role of complex sphingolipids is less well-understood since they appear to be dispensable for yeast cell survival. Nonetheless, IPC has been associated with the regulation of cellular Ca^{2+} homeostasis [82,83] and autophagy [80]. As compared to wild-type cells, *sch9*Δ mutant cells display enhanced levels of the long-chain bases PHS and dihydrosphingosine (DHS) and their phosphorylated derivatives, decreased levels of several (phyto)ceramide species, and altered ratios of complex sphingolipids, a profile that is believed to contribute to the increased chronological lifespan of the mutant cells [76]. However, the relationship between sphingolipid metabolism and longevity is not straightforward, and other factors are at play as well. One such factor is Sit4, the catalytic subunit of a PP2A-type protein phosphatase that is down-regulated by TORC1 but up-regulated by ceramides [84,85]. Besides Sch9, there are also other kinases targeted by the yeast PDK1 orthologues to regulate sphingolipid metabolism. Indeed, Pkh1 and Pkh2 also control the activity of the protein kinases Ypk1 and Ypk2, which upon heat shock, boost the de novo biosynthesis of sphingoid bases by phosphorylating and relieving the inhibition exerted by the two ER-localized tetraspanins Orm1 and Orm2 [86]. In addition, Ypk1 promotes the production of complex sphingolipids through activation of the Lac1 and Lag1 ceramide synthases [87]. Hence, Sch9 and Ypk1/2 share common targets to regulate sphingolipid homeostasis. Full activation of Sch9 requires TORC1 at the vacuolar membrane to signal nutrient availability. Instead, the full activation of Ypk1 and Ypk2 depends on the phosphorylation in their hydrophobic motif by the TORC2 complex, which localizes at the plasma membrane and signals membrane perturbation and stress [23,51]. Thus, Sch9, Ypk1, and Ypk2 also share a similar mode of activation. Finally, Pho85 and SNF1 were also shown to be involved in the regulation of sphingolipid metabolism. Pho85, together with one of the redundant cyclins Pcl1 and Pcl2, phosphorylates the long-chain base kinase Lcb4 thereby marking this kinase for degradation [88]. Consistently, *pho85Δ* cells are characterized by reduced LCB levels and markedly increased LCBP levels [89]. An exact target for SNF1 has not been determined, but a strain lacking the catalytic subunit Snf1 was shown to display significantly increased IPC and MIPC levels but decreased $M(IP)_2C$ levels [90]. This would suggest that SNF1 could either directly or indirectly activate the inositol phosphotransferase Ipt1. Moreover, the constitutive active $snf1^{G53R}$ mutant was shown to rescue the nitrogen starvation-induced cell death of a strain lacking Csg2, an enzyme required for mannosylation of IPC to produce MIPC [91]. Given that both Pho85 and SNF1 phosphorylate and fine-tune the TORC1-dependent activation of Sch9, it would be interesting to further analyze their interplay with respect to the metabolism of sphingolipids.

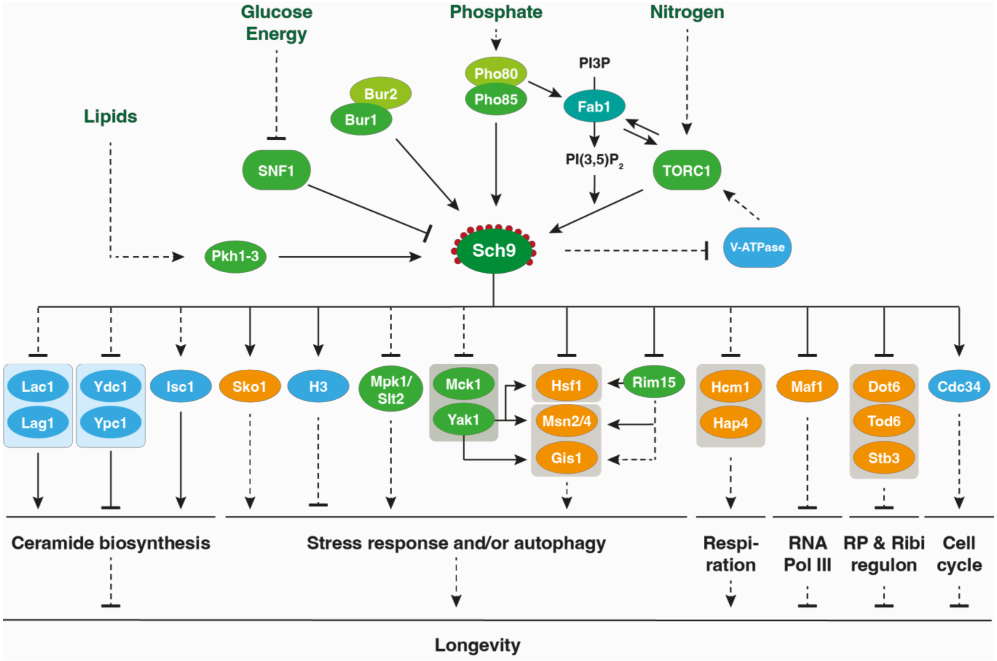
Glucose
Energy
Phosphate
Nitrogen
PI3P
Lipids
Bur2
Bur1
Pho80
Pho85
Fab1
SNF1
PI(3,5)P$_2$
TORC1
Pkh1-3
Sch9
V-ATPase
Lac1
Lag1
Ydc1
Ypc1
Isc1
Sko1
H3
Mpk1/
Slt2
Mck1
Yak1
Hsf1
Msn2/4
Gis1
Rim15
Hcm1
Hap4
Maf1
Dot6
Tod6
Stb3
Cdc34
Ceramide biosynthesis
Stress response and/or autophagy
Respi-
ration
RNA
Pol III
RP & Ribi
regulon
Cell
cycle
Longevity

Figure 2. Model of the Sch9 signaling network. Protein kinases, transcription factors, and various other proteins are colored green, orange, and blue, respectively. The lipid kinase Fab1 is colored turquoise. Arrows and bars refer to direct (full line) or indirect (dashed line) activating and inhibitory interactions, respectively. See main text for more details.

4. The Role of Sch9 in Metabolic Reprogramming and Stress Responses

As TORC1 and Sch9 are central players in the nutrient-controlled signaling network of yeast, it is not surprising that they have a crucial role in controlling growth, stress responses, and longevity (Figure 2). For instance, to support exponential fermentative growth, the TORC1-Sch9 pathway cooperates with the Ras-cAMP-PKA pathway to enhance protein synthesis by boosting the translation capacity of yeast cells. As such, both Sch9 and PKA stimulate ribosome biogenesis by hyperphosphorylating and influencing the subcellular localization of the transcription repressors Stb3, Dot6, and Tod6 [9,92,93] and the RNA polymerase III repressor Maf1 [94]. In addition, both kinases have a significant impact on cell cycle progression through the regulation of different downstream effectors, such as the ubiquitin-conjugating enzyme Cdc34, which controls the degradation of cyclins and cyclin-dependent kinase inhibitors [95]. Note that Sch9 was recently shown to be directly targeted by at least two cyclin-dependent kinases i.e., Pho85 and Bur1 [26,27], and these may provide cell cycle-dependent feedback given their roles in the elongation of telomeres [96,97].

TORC1 and Sch9 are intimately linked to the metabolic reprogramming during the diauxic shift transition and the proper entry of yeast cells into the non-dividing quiescent state (G_0) [98]. Here, the highly conserved energy sensor SNF1 plays an opposing role to TORC1 by promoting stress responses [99]. In order to guarantee energy homeostasis, SNF1 tunes down TORC1 activity, particularly during glucose starvation [100,101]. In our recent study [28], we performed a SNF1 phosphoproteomic analysis, which allowed us to identify direct SNF1 substrates. This demonstrated that SNF1 not only acts directly on the TORC1 complex itself, as previously shown [102], but that SNF1 also directly phosphorylates Sch9-Ser^{288}, thereby contributing to the inhibition of the TORC1 signaling pathway [28]. In addition, recent studies confirmed that reduced TORC1 activity drives cells into the quiescent state by unlocking signaling by several kinases, including Atg1, Gcn2, Npr1, Rim15, Yak1, and Mpk1/Slt2 [34,35,103]. In connection to the TORC1-Sch9 axis, previous data revealed that it cooperates with the Ras-cAMP-PKA pathway to control the cytoplasmic sequestration of the Greatwall protein kinase Rim15 via association with the 14-3-3 protein Bmh2, thereby preventing its activation when nutrients are plentifully available [12,104–106]. Importantly, the TORC1-Sch9 axis is itself a regulator of PKA activity as it prevents the phosphorylation and activation of Bcy1, the negative regulatory subunit of PKA, via the cell wall integrity MAPK Mpk1/Slt2 [31]. Moreover, Sch9 also indirectly controls, through Yak1 and the retention factor Zds1, the carbon source-dependent nucleocytoplasmic distribution of Bcy1, the stability and nucleocytoplasmic distribution of the PKA catalytic subunit Tpk2, and regulates the phosphorylation of the Ras GAP Cdc25 [107,108]. It is intriguing that Mpk1/Slt2 was also reported to inhibit TORC1 under conditions of ER stress [109] as it raises the possibility that Sch9 may also provide feedback to TORC1 via the MAPK. Once at the diauxic shift, the inhibitory actions of TORC1-Sch9 and PKA on Rim15 are relieved, and the kinase translocates into the nucleus to activate such transcription factors as Msn2/4 and Hsf1, thereby inducing the expression of genes that contain a stress-responsive or heat shock-responsive element in their promoter, respectively [12,104,110]. In addition, Rim15 indirectly controls the activity of the transcription factor Gis1 via the endosulfines Igo1/2 and PP2A-Cdc55 phosphatase and, as such, allows for the induction of genes containing the post-diauxic shift promoter element [111–114]. Interestingly, the nuclear retention of Rim15 is regulated by the Pho85-Pho80 CDK-cyclin pair, which phosphorylates Rim15 to dictate its nuclear export [115,116]. Hence, Pho85-Pho80 maintains a feed-forward system since, besides priming Sch9 for full activation by TORC1 [26], the CDK-cyclin pair directly controls the nucleocytoplasmic translocation of Rim15 to adjust the execution of the Rim15-dependent G_0 program response to phosphate availability. In parallel to Rim15, TORC1 and PKA signaling similarly maintain inactive Yak1 in the cytoplasm by tethering this kinase to the cytoplasmic 14-3-3 anchor proteins Bmh1/2 [117,118]. Once this inhibition is relieved at the diauxic shift, Yak1 becomes nuclear and impacts Msn2/4-, Hsf1-, and Gis1-mediated transcription as well [119,120]. Here, Sch9 plays a dual role since one study suggested that Sch9 not only phosphorylates Yak1 but that it also controls the stability of Yak1 during growth and stationary phase [108]. Notably, glucose starvation further stimulates Yak1 to phosphorylate the Ccr4-Not subunit

Pop2, which is essential to arrest the cell cycle at G_1 and to ensure proper entry into the stationary phase [121]. Yak1 also phosphorylates the transcriptional co-repressor Crf1, which inhibits the transcription of ribosomal genes [122]. Moreover, consistent with its role as a potential Sch9 substrate, Crf1 controls the nucleocytoplasmic distribution of Bcy1 as well [123]. Besides Rim15 and Yak1, there is a third kinase that has been proposed to act downstream of the TORC1-Sch9 axis for the entry into the quiescent state, namely, the GSK-3 homolog Mck1 [34,124]. Mck1 was originally identified as a downstream effector of the Pkc1-Mpk1/Slt2 cell wall integrity pathway that affects the subcellular redistribution of Bcy1 in response to heat stress [125,126]. Given the involvement of Mpk1/Slt2, it is not surprising that later studies confirmed Mck1 to be under negative control of the TORC1-Sch9 axis to coordinate reserve carbohydrates metabolism [127], the repression of ribosomes and tRNA synthesis [128], and the expression of different stress-induced and post-diauxic genes [129–131] in response to nutrient limitation. Moreover, this link between Mck1 and Sch9 is further corroborated by the observation that loss-of-function mutations or deletion of *MCK1* partially suppress the growth defects of *sch9*Δ cells under fermentative and respiratory conditions [132]. In line with these observations, our own phosphoproteomic analysis suggested that TORC1 inhibits the quiescence program in part via the Sch9-dependent inhibition of Mck1 [34].

Finally, SNF1 also has a profound impact on stress responses. Indeed, Msn2/4 and Gis1 were originally retrieved as multicopy suppressors of SNF1 defects [133,134], and although active SNF1 acts as an inhibitor of Sch9 [28], it also directly phosphorylates Msn2 and Hsf1, thereby constraining the nuclear localization of these factors and adapting the transcriptional stress response during glucose starvation [135–137]. Notably, SNF1 is also a negative regulator of PKA since it phosphorylates adenylate cyclase, thereby lowering cAMP levels [138].

5. The Involvement of Sch9 in Proteasomal Degradation and Autophagy

For optimal growth, the timely degradation of proteins to maintain proteostasis is essential. Different studies indicate that protein degradation is also used by yeast cells to adjust metabolic programming and fine-tune stress responses. For instance, TORC1 signaling is known to control the multivesicular body (MVB) pathway-driven degradation of plasma membrane proteins and lipids [139–142]. In addition, several transcription factors are known to be under the control of TORC1, such as Gcn4, Gln3, or Gat1, involved in amino acid biosynthesis and nitrogen catabolite repression, but also the stress-responsive factors Msn2/4, Gis1, and Hsf1, have all been shown to be subject of proteasomal degradation, thereby leading to the adjustment of their transcriptional responses [120,143–145]. In fact, one of these studies demonstrated that the proteasome is not only required to prevent activation of starvation-specific genes during exponential growth, but it is also essential for yeast cells to adapt to reduced TORC1 activity [120]. Interestingly, proteasome abundance and proteasome assembly are themselves regulated by TORC1 signaling [120,146–148]. It is likely that Sch9 is also involved since proteasome abundance is managed via the transcription of genes encoding proteasomal subunits through the transcription factor Rpn4, which itself is induced by the Hsf1 [149]. Furthermore, proteasome assembly is regulated by the translation of proteasome regulatory particle assembly chaperones (RPACs), which is under the control of Mpk1/Slt2 [147]. In cooperation with SNF1, Mpk1/Slt2 further controls the formation of proteasome storage granules upon the inhibition of mitochondrial function and the drop in ATP levels following carbon starvation [150,151]. These granules represent reversible cytosolic proteasome condensates that serve to protect cells against stress, as they are believed to shield the proteasome from autophagic degradation or proteophagy, which, besides SNF1 and Mpk1/Slt2, also involves TORC1 [152–154]. Upon exit from quiescence and resumption of cell proliferation, the proteasome storage granules rapidly resolve, and proteasomes reenter the nucleus [150].

As the master regulator controlling cell growth and metabolic activity, TORC1 plays a central role in the regulation of autophagy. Under nutrient-rich conditions, TORC1 is active, and general autophagy is inhibited. This inhibition is accomplished by the TORC1 pool localized at perivacuolar signaling endosomes and involves the phosphorylation of Atg13 to prevent its association with Atg1 and, thereby, the induction of macroautophagy [56,155,156]. In addition, TORC1 phosphorylates the Vps27 subunit of ESCRT-0 to antagonize cargo selection for microautophagy and the turnover of vacuolar membrane-resident and associated proteins through direct engulfment by the vacuolar membrane [56,157,158]. Interestingly, the trafficking of Vps27 to the vacuole and ESCRT-dependent microautophagy are also controlled by SNF1 under glucose-limiting conditions [159]. Whether Sch9 has a role in microautophagy is currently unknown. Nonetheless, Sch9 is clearly important for the inhibition of macroautophagy under nutrient-rich conditions, as the combined inactivation of Sch9 and PKA induces macroautophagy through a process that requires the Atg1-Atg13-Atg17 complex, Rim15, and Msn2/4 [14]. Consistent with this observation, Atg13 is also phosphorylated by PKA at residues that are distinct from those targeted by TORC1 [160]. A more recent study suggested that the induction of bulk autophagy at the diauxic shift occurs mainly via the inactivation of PKA and Sch9 and established that this is mediated by the cell wall integrity sensor Mtl1, which signals glucose limitation to Ras2 and Sch9 [161]. This pathway also controls the autophagic degradation of mitochondria when cells reach the stationary phase [161]. Indeed, most recent findings demonstrated that this type of glucose starvation-induced autophagy requires the recruitment of the DNA-damage sensor Mec1 to mitochondria, where it is phosphorylated by SNF1 and where it binds Atg1 and Atg13 to associate with the phagophore assembly site [162,163]. As for the roles of Rim15 and Msn2/4, several studies indicated that they control the transcription of several autophagy genes. Rim15 impacts on the expression of different *ATG* genes by relieving repression mediated by the histone demethylase protein Rph1 and the Ume6-Sin3-Rpd3 histone deacetylase complex [164–166]. Msn2/4, on the other hand, activates transcription of *ATG* genes, as shown, for instance, for *ATG8* [167] and *ATG39* [168]. Importantly, TORC1 signaling additionally controls the expression of *ATG* genes via the transcription factors Gln3, Gat1, and Gcn4 [166].

In contrast to SNF1, which inhibits both TORC1 and Sch9 once activated under nutrient-limiting conditions [28,102,169], the Pho85-Pho80 CDK-cyclin pair boosts Sch9 activity under nutrient-rich conditions by enhancing PI(3,5)P_2 production and by priming Sch9 for its subsequent activation by TORC1 [26]. In addition, Pho85-Pho80, either directly or indirectly, enhances Atg13 phosphorylation [26] and antagonizes the nuclear accumulation of Rim15 under glucose-limiting conditions [115,116]. Hence, it is not surprising that Pho85-pho80 has been reported to be a negative regulator of autophagy [170,171]. However, the role of Pho85 in autophagy is more complex. Accordingly, other cyclins are involved as well, and Pho80, Clg1, and Pcl1 combined also positively control autophagy by promoting the degradation of Sic1, a cyclin-dependent kinase inhibitor involved in cell cycle regulation that seemingly also acts as a negative regulator of autophagy by targeting Rim15 [171].

6. The Role of Sch9 on Longevity Modulation

Sch9, as part of the TORC1 pathway, is a prime determinant of cellular aging. Loss of Sch9 function increases the survival of stationary non-dividing cells, i.e., chronological lifespan (CLS) [36], and enhances replicative lifespan (RLS), i.e., the number of daughters that a single mother cell can produce asexually [172,173]. Interestingly, Sch9 has also been reported to play a major role in pro-longevity effects promoted by caloric and dietary restriction [174–178]. The role of Sch9 on longevity seems to be more complex and diverse than previously anticipated, being implicated in different stress responses, including the interplay between oxidative and metabolic stresses.

Caloric restriction (CR), characterized by a 10–30% reduction in calories compared to an *ad libitum* diet, is a potent modulator of longevity in several species. Although the longevity mechanisms of CR are not completely uncovered, it is clear that its benefits are related to alterations in the metabolic rate and the accumulation of reactive oxygen species (ROS). Initial studies have implicated inhibition of the TORC1-Sch9 axis as the longevity pathway through which CR modulates lifespan. In RLS, CR-induced longevity is mediated by reduced signaling through TORC1, Sch9, and PKA, which results in the downregulation of ribosome biogenesis. This proposed model for CR effects during RLS is independent of sirtuin 2 (Sir2) but likely links the signaling network from nutrients to ribosome assembly and protein synthesis [173]. Regarding CLS, it was found that CR still promotes CLS extension in cells lacking *SCH9*, suggesting that inhibition of the TORC1-Sch9 axis represents only one of the mechanisms through which CR modulates the lifespan [179]. Downregulation of Sch9, as well as downregulation of Ras2, delays aging through pathways that only partially overlap with the CR-mediated extension of the lifespan [180,181]. CR and Sch9-mediated longevity share the common downstream target Rim15 [36]. In the Sch9-mediated longevity pathway, Rim15 acts, in part, through the stress response transcription factor Gis1 [182], which binds post-diauxic shift elements found in the promoters of genes of the stress-resistance systems, such as *HSP26*, *HSP12*, and *SOD2* [183]. Consistent with this, the deletion of *SOD2* abolishes lifespan extension in *sch9*Δ mutant [184].

In natural scenarios, yeast and other organisms experience periods of nutritional stress, and an appropriate and efficient metabolic adaptation is, therefore, essential to ensure cell survival. Sch9 is a key player in this metabolic adaptation and in the assembled response to nutrient availability. Sch9 receives many different inputs and executes its function accordingly. As introduced above, one of the most important upstream kinases is the TORC1 kinase that targets Sch9 under favorable growth conditions [8,185], but Sch9 also has TORC1-independent functions under multiple stress conditions. In agreement with this notion, it has been shown that reducing Sch9 activity extends lifespan when yeast cells are pre-grown under nutrient-rich conditions, but it shortens the lifespan when pre-grown under nutrient-poor conditions [186]. This indicates that pre-adaptations to respiratory metabolism and oxidative stress play a central role in determining cellular longevity. As such, the deletion of both *TOR1* and *SCH9* results in the increased respiratory capacity associated with a higher ratio of mitochondrial respiratory-chain enzymes per mass during active growth [187,188]. Although the underlying mechanisms are still poorly understood, the transcription factors Hcm1 and Hap4 have been implicated in the nuclear regulation of mitochondrial respiration. While Sch9 directly phosphorylates Hcm1 to inhibit its nuclear import, it indirectly regulates Hap4 through sphingolipids signaling [76,189].

The elevated respiratory capacity of *tor1*Δ*sch9*Δ cells is, therefore, associated with increased ROS levels and increased longevity by a hormesis-like phenomenon [190]. The so-called hormesis effect mediates lifespan extension by an adaptative mitochondrial ROS signaling that, even under CR conditions, is independent of Rim15, which, as mentioned above, is a well-known target of Sch9 [191,191,192]. Nevertheless, when ROS levels are above a certain threshold, mitochondria can cause irreversible cellular damage, triggering regulated cell death and premature aging. This dichotomous function of mitochondria indicates that, as in other organisms, mitochondrial function is also a relevant hallmark of aging in yeast.

The TORC1-independent function of Sch9 on longevity seems to be mainly related to the activation of specific gene promoters and transcription factors. For example, as mentioned above, Sch9 regulates oxidative stress response by indirectly acting on the transcription factor Gis1 [182]. Sch9 can also crosstalk with the Hog1 MAP kinase via the Sko1 transcription factor, which activates stress gene expression upon a high osmolarity [8,185]. In addition to activating transcription factors, Sch9 can also affect gene expression through chromatin remodeling. Sch9 is required for the phosphorylation of the residue Thr^{11} of histone H3 under stress, and the loss of pThr^{11} prolongs CLS by altering the stress response at an early stage of the CLS [193]. Therefore, Sch9 also links nutritional stress to chromatin remodeling during aging.

Deletion of the *SCH9* also significantly decreases the overall mutation frequency and DNA damage during CLS [194], resulting in reduced genomic instability [179,195]. The increased *SOD2* expression and, consequently, reduced superoxide-induced DNA damage found in *sch9*Δ cells further contribute to the observed reduced genomic instability.

As previously referred, Sch9 acts on cell cycle regulation by promoting an efficient G1 arrest [196]. By inhibiting Rim15, Sch9 promotes the proteolysis of Sic1, a CDK inhibitor [95,196,197]. In accordance, the deletion of *SIC1* results in S phase entry and reduction in CLS by increased superoxide generation [198,199], and the constitutive activation of Sch9 shortens the CLS by a defect in proper G_1 arrest [95]. Importantly, the deletion of *SCH9*, but not CR, protects against the premature aging phenotype of yeast cells lacking the RecQ helicase Sgs1 (WRN and BLM homolog) by inhibiting error-prone recombination and preventing DNA damage and dedifferentiation [194]. It appears that enhanced cellular protection against stress, tighter G1 arrest, and reduced recombination errors are mechanisms by which the lack of Sch9 activity protects cells against genomic instability and dedifferentiation associated with accelerated aging when the Sgs1 is mutated [194].

Yeast aging is likely a suitable natural scenario to understand the role of Sch9 in the interplay between different stress responses and nutritional status, which can constitute, per se, a particular form of stress. Because of their differential participation in yeast longevity, the two main yeast aging models can provide valuable information regarding the signal transduction mediated by Sch9 in response to multiple inputs.

7. Conclusions and Future Directions

The investigation of the topology, regulation, and crosstalk of signaling pathways has proven invaluable in the dissection of the molecular mechanisms underlying pathophysiological processes [200–202]. During evolution, a rewiring of signaling cascades often occurred, reflecting the different environment of organisms, their uni- or multicellularity, and specialization. However, the use of regulation hubs, which integrate upstream inputs to conveniently control multiple downstream effectors at once, is a remarkably conserved system [203]. In this context, the yeast kinase Sch9 exemplifies the central node of a so-called bow-tie signaling network (Figure 2) [204].

In spite of the extensive studies which started to unravel the complex regulation and function of Sch9 and that are reviewed in depth above, recent findings hint at currently overlooked regulatory features. For instance, Sch9 was found to be phosphorylated by the CDK Bur1 at the Ser^{560}, Thr^{568}, Thr^{574}, Thr^{575}, Ser^{709}, Thr^{710}, Ser^{711}, and Thr^{721} residues, in addition to the more deeply studied Thr^{723} and Ser^{726} residues [27]. Furthermore, at least 12 lysine residues of Sch9 were reported to be ubiquitinated in high-throughput studies [205,206], but the regulation of the possible conditional Sch9 ubiquitination and degradation has not been investigated to date. Thus, future studies focused on these post-translational modifications could pinpoint new Sch9 regulatory mechanisms.

Sch9 does not have a readily identifiable orthologue in mammals. However, it shares functional similarities with the mammalian AGC kinase family member AKT (also known as protein kinase B or PKB), which exists in three different isoforms, AKT1, AKT2, and AKT3 [207], in what concerns its role in cellular signaling and regulation of growth-related processes [208]. Notably, Sch9 has also been suggested to be functionally related to the homologous mammalian S6K, although it appears that the cellular roles of yeast Ypk3 may more closely overlap with the ones of S6K in mammals [209,210]. Based on our current knowledge, we deem it possible that the functional similarities between Sch9 and AKT may also be extended to the role of these kinases in regulating longevity. In this context, the role of AKT in longevity is complex and multifaceted, ranging from promoting cell growth and survival, which can have beneficial effects on tissue repair and maintenance that are important for healthy aging, to detrimental effects that are related to increased cellular senescence or cancer promotion (when AKT is hyperactive) [200]. Studies on Sch9 could, thus, help elucidate the evolutionary functional origin of AKT and shed light on some of its most important functions. While the direct translation of findings from Sch9 in yeast to AKT in mammals may not be straightforward, studying the conserved functional aspects of these pathways can provide valuable information and generate hypotheses for further investigation in mammalian systems. Even though, as abovementioned and extensively presented in the current review, several features of the regulation and the regulators of Sch9 suggest some degree of functional homology to AKT in higher eukaryotes, remarkable differences also highlight the divergence between these two important signaling effectors. For instance, the lack of PI(3,4,5)P_3 in budding yeast [211] and the absence of a PH domain in Sch9 (Table 1) prevent its localization to the plasma membrane, the subcellular localization where AKT is activated and carries out its most studied functions [212].

Thus, it is important to consider the limitations and differences between yeast and mammalian biology, but utilizing Sch9 as a model can still contribute to our understanding of the broader principles and mechanisms involved in the regulation of pathophysiological processes. Specifically, investigation of the post-translational modifications and their impact on the structure and function of Sch9 may translate to equivalent findings regarding the biochemical regulation of AKT and related protein kinases. Moreover, as examined in depth in this review, Sch9 could serve as a case study for lipid-dependent regulation of signaling effectors, as well as a molecular tool to investigate the subcellular distribution of specific lipid species [16]. Finally, Sch9 shares upstream regulators with other AKT-like proteins [19,24,86], and it is thus likely that Sch9 regulation studies could help expand the understanding of signaling networks of cognate kinases.

Author Contributions: Conceptualization, M.C., B.S.-M., R.H., B.P., P.L., C.D.V., J.W. and R.N.; writing—original draft preparation, M.C., B.S.-M., R.H., B.P., P.L., C.D.V., J.W. and R.N.; writing—review and editing, M.C., B.S.-M., R.H., B.P., P.L., C.D.V., J.W. and R.N.; visualization, M.C., B.P., C.D.V. and J.W; funding acquisition, R.H., P.L., C.D.V. and J.W. All authors have read and agreed to the published version of the manuscript.

Funding: This research was funded by the Canton of Fribourg and the Swiss National Science Foundation (310030_166474/184671) to C.D.V., the Fonds Wetenschappelijk Onderzoek (FWO)-Vlaanderen (G069413, G0C7222N) and KU Leuven (C14/17/063, C14/21/095) to J.W., Biotechnology and Biological Sciences Research Council (BB/V016334/1) to RH, and Portuguese National funds, through the Foundation for Science and Technology (FCT)—project UIDB/50026/2020 and UIDP/50026/2020 for P.L. and B.S.-M. B.S.-M. was funded by FCT, grant number DL 57/2016.

Institutional Review Board Statement: Not applicable.

Informed Consent Statement: Not applicable.

Data Availability Statement: Data sharing is not applicable to this article as no datasets were generated or analyzed in the course of the current study.

Acknowledgments: We thank the editors Markus Proft and Amparo Pascual-Ahuir for their kind invitation to contribute this review to the special issue *'Yeast Response to Stress'*. We thank Marie-Pierre Péli-Gulli for critical reading of this manuscript. We would like to apologize to all the authors whose papers were not cited due to space constraints.

Conflicts of Interest: The authors declare no conflict of interest.

References

1. Kingsbury, J.M.; Sen, N.D.; Cardenas, M.E. Branched-Chain Aminotransferases Control TORC1 Signaling in *Saccharomyces cerevisiae*. *PLoS Genet.* **2015**, *11*, e1005714. [CrossRef] [PubMed]
2. Péli-Gulli, M.-P.; Sardu, A.; Panchaud, N.; Raucci, S.; De Virgilio, C. Amino Acids Stimulate TORC1 through Lst4-Lst7, a GTPase-Activating Protein Complex for the Rag Family GTPase Gtr2. *Cell Rep.* **2015**, *13*, 1–7. [CrossRef] [PubMed]
3. Stracka, D.; Jozefczuk, S.; Rudroff, F.; Sauer, U.; Hall, M.N. Nitrogen Source Activates TOR (Target of Rapamycin) Complex 1 via Glutamine and Independently of Gtr/Rag Proteins. *J. Biol. Chem.* **2014**, *289*, 25010–25020. [CrossRef]
4. Tanigawa, M.; Maeda, T. An in Vitro TORC1 Kinase Assay That Recapitulates the Gtr-Independent Glutamine-Responsive TORC1 Activation Mechanism on Yeast Vacuoles. *Mol. Cell. Biol.* **2017**, *37*, e00075-17. [CrossRef] [PubMed]
5. Ukai, H.; Araki, Y.; Kira, S.; Oikawa, Y.; May, A.I.; Noda, T. Gtr/Ego-Independent TORC1 Activation Is Achieved through a Glutamine-Sensitive Interaction with Pib2 on the Vacuolar Membrane. *PLoS Genet.* **2018**, *14*, e1007334. [CrossRef]
6. González, A.; Hall, M.N. Nutrient Sensing and TOR Signaling in Yeast and Mammals. *EMBO J.* **2017**, *36*, 397–408. [CrossRef]
7. Wullschleger, S.; Loewith, R.; Hall, M.N. TOR Signaling in Growth and Metabolism. *Cell* **2006**, *124*, 471–484. [CrossRef]

8. Urban, J.; Soulard, A.; Huber, A.; Lippman, S.; Mukhopadhyay, D.; Deloche, O.; Wanke, V.; Anrather, D.; Ammerer, G.; Riezman, H.; et al. Sch9 Is a Major Target of TORC1 in Saccharomyces Cerevisiae. *Mol. Cell* **2007**, *26*, 663–674. [CrossRef]
9. Huber, A.; French, S.L.; Tekotte, H.; Yerlikaya, S.; Stahl, M.; Perepelkina, M.P.; Tyers, M.; Rougemont, J.; Beyer, A.L.; Loewith, R. Sch9 Regulates Ribosome Biogenesis via Stb3, Dot6 and Tod6 and the Histone Deacetylase Complex RPD3L. *EMBO J.* **2011**, *30*, 3052–3064. [CrossRef]
10. Jin, Y.; Weisman, L.S. The Vacuole/Lysosome Is Required for Cell-Cycle Progression. *eLife* **2015**, *4*, e08160. [CrossRef]
11. Jorgensen, P.; Rupeš, I.; Sharom, J.R.; Schneper, L.; Broach, J.R.; Tyers, M. A Dynamic Transcriptional Network Communicates Growth Potential to Ribosome Synthesis and Critical Cell Size. *Genes Dev.* **2004**, *18*, 2491. [CrossRef]
12. Roosen, J.; Engelen, K.; Marchal, K.; Mathys, J.; Griffioen, G.; Cameroni, E.; Thevelein, J.M.; De Virgilio, C.; De Moor, B.; Winderickx, J. PKA and Sch9 Control a Molecular Switch Important for the Proper Adaptation to Nutrient Availability. *Mol. Microbiol.* **2005**, *55*, 862–880. [CrossRef]
13. Swinnen, E.; Ghillebert, R.; Wilms, T.; Winderickx, J. Molecular Mechanisms Linking the Evolutionary Conserved TORC1-Sch9 Nutrient Signalling Branch to Lifespan Regulation in Saccharomyces Cerevisiae. *FEMS Yeast Res.* **2014**, *14*, 17–32. [CrossRef] [PubMed]
14. Yorimitsu, T.; Zaman, S.; Broach, J.R.; Klionsky, D.J. Protein Kinase A and Sch9 Cooperatively Regulate Induction of Autophagy in Saccharomyces Cerevisiae. *Mol. Biol. Cell* **2007**, *18*, 4180–4189. [CrossRef] [PubMed]
15. Toda, T.; Cameron, S.; Sass, P.; Wigler, M. SCH9, a Gene of Saccharomyces Cerevisiae That Encodes a Protein Distinct from, but Functionally and Structurally Related to, CAMP-Dependent Protein Kinase Catalytic Subunits. *Genes Dev.* **1988**, *2*, 517–527. [CrossRef] [PubMed]
16. Chen, Z.; Malia, P.C.; Hatakeyama, R.; Nicastro, R.; Hu, Z.; Péli-Gulli, M.P.; Gao, J.; Nishimura, T.; Eskes, E.; Stefan, C.J.; et al. TORC1 Determines Fab1 Lipid Kinase Function at Signaling Endosomes and Vacuoles. *Curr. Biol.* **2021**, *31*, 297–309.e8. [CrossRef] [PubMed]
17. Novarina, D.; Guerra, P.; Milias-Argeitis, A. Vacuolar Localization via the N-Terminal Domain of Sch9 Is Required for TORC1-Dependent Phosphorylation and Downstream Signal Transduction. *J. Mol. Biol.* **2021**, *433*, 167326. [CrossRef] [PubMed]
18. Wilms, T.; Swinnen, E.; Eskes, E.; Dolz-Edo, L.; Uwineza, A.; Van Essche, R.; Rosseels, J.; Zabrocki, P.; Cameroni, E.; Franssens, V.; et al. The Yeast Protein Kinase Sch9 Adjusts V-ATPase Assembly/Disassembly to Control PH Homeostasis and Longevity in Response to Glucose Availability. *PLoS Genet.* **2017**, *13*, e1006835. [CrossRef]
19. Liu, K.; Zhang, X.; Lester, R.L.; Dickson, R.C. The Sphingoid Long Chain Base Phytosphingosine Activates AGC-Type Protein Kinases in Saccharomyces Cerevisiae Including Ypk1, Ypk2, and Sch9. *J. Biol. Chem.* **2005**, *280*, 22679–22687. [CrossRef]
20. Friant, S.; Lombardi, R.; Schmelzle, T.; Hall, M.N.; Riezman, H. Sphingoid Base Signaling via Pkh Kinases Is Required for Endocytosis in Yeast. *EMBO J.* **2001**, *20*, 6783–6792. [CrossRef]
21. Luo, G.; Gruhler, A.; Liu, Y.; Jensen, O.N.; Dickson, R.C. The Sphingolipid Long-Chain Base-Pkh1/2-Ypk1/2 Signaling Pathway Regulates Eisosome Assembly and Turnover. *J. Biol. Chem.* **2008**, *283*, 10433–10444. [CrossRef]
22. Roelants, F.M.; Baltz, A.G.; Trott, A.E.; Fereres, S.; Thorner, J. A Protein Kinase Network Regulates the Function of Aminophospholipid Flippases. *Proc. Natl. Acad. Sci. USA* **2010**, *107*, 34–39. [CrossRef] [PubMed]
23. Roelants, F.M.; Leskoske, K.L.; Martinez Marshall, M.N.; Locke, M.N.; Thorner, J. The TORC2-Dependent Signaling Network in the Yeast Saccharomyces Cerevisiae. *Biomolecules* **2017**, *7*, 66. [CrossRef] [PubMed]
24. Roelants, F.M.; Torrance, P.D.; Thorner, J. Differential Roles of PDK1- and PDK2-Phosphorylation Sites in the Yeast AGC Kinases Ypk1, Pkc1 and Sch9. *Microbiol. Read. Engl.* **2004**, *150*, 3289–3304. [CrossRef] [PubMed]
25. Voordeckers, K.; Kimpe, M.; Haesendonckx, S.; Louwet, W.; Versele, M.; Thevelein, J.M. Yeast 3-Phosphoinositide-Dependent Protein Kinase-1 (PDK1) Orthologs Pkh1-3 Differentially Regulate Phosphorylation of Protein Kinase A (PKA) and the Protein Kinase B (PKB)/S6K Ortholog Sch9. *J. Biol. Chem.* **2011**, *286*, 22017–22027. [CrossRef] [PubMed]
26. Deprez, M.-A.; Caligaris, M.; Rosseels, J.; Hatakeyama, R.; Ghillebert, R.; Sampaio-Marques, B.; Mudholkar, K.; Eskes, E.; Meert, E.; Ungermann, C.; et al. The Nutrient-Responsive CDK Pho85 Primes the Sch9 Kinase for Its Activation by TORC1. *PLoS Genet.* **2023**, *19*, e1010641. [CrossRef]
27. Jin, Y.; Jin, N.; Oikawa, Y.; Benyair, R.; Koizumi, M.; Wilson, T.E.; Ohsumi, Y.; Weisman, L.S. Bur1 Functions with TORC1 for Vacuole-Mediated Cell Cycle Progression. *EMBO Rep.* **2022**, *23*, e53477. [CrossRef]
28. Caligaris, M.; Nicastro, R.; Hu, Z.; Tripodi, F.; Hummel, J.E.; Pillet, B.; Deprez, M.-A.; Winderickx, J.; Rospert, S.; Coccetti, P.; et al. Snf1/AMPK Fine-Tunes TORC1 Signaling in Response to Glucose Starvation. *eLife* **2023**, *12*, e84319. [CrossRef]
29. Lu, J.-Y.; Lin, Y.-Y.; Sheu, J.-C.; Wu, J.-T.; Lee, F.-J.; Chen, Y.; Lin, M.-I.; Chiang, F.-T.; Tai, T.-Y.; Berger, S.L.; et al. Acetylation of Yeast AMPK Controls Intrinsic Aging Independently of Caloric Restriction. *Cell* **2011**, *146*, 969–979. [CrossRef] [PubMed]
30. Mudholkar, K.; Fitzke, E.; Prinz, C.; Mayer, M.P.; Rospert, S. The Hsp70 Homolog Ssb Affects Ribosome Biogenesis via the TORC1-Sch9 Signaling Pathway. *Nat. Commun.* **2017**, *8*, 937. [CrossRef]
31. Soulard, A.; Cremonesi, A.; Moes, S.; Schütz, F.; Jenö, P.; Hall, M.N. The Rapamycin-Sensitive Phosphoproteome Reveals That TOR Controls Protein Kinase A toward Some but Not All Substrates. *Mol. Biol. Cell* **2010**, *21*, 3475–3486. [CrossRef]
32. Galello, F.; Portela, P.; Moreno, S.; Rossi, S. Characterization of Substrates That Have a Differential Effect on Saccharomyces Cerevisiae Protein Kinase A Holoenzyme Activation. *J. Biol. Chem.* **2010**, *285*, 29770–29779. [CrossRef] [PubMed]
33. Plank, M. Interaction of TOR and PKA Signaling in S. Cerevisiae. *Biomolecules* **2022**, *12*, 210. [CrossRef]

34. Dokládal, L.; Stumpe, M.; Hu, Z.; Jaquenoud, M.; Dengjel, J.; De Virgilio, C. Phosphoproteomic Responses of TORC1 Target Kinases Reveal Discrete and Convergent Mechanisms That Orchestrate the Quiescence Program in Yeast. *Cell Rep.* **2021**, *37*, 110149. [CrossRef]
35. Smets, B.; Ghillebert, R.; De Snijder, P.; Binda, M.; Swinnen, E.; De Virgilio, C.; Winderickx, J. Life in the Midst of Scarcity: Adaptations to Nutrient Availability in Saccharomyces Cerevisiae. *Curr. Genet.* **2010**, *56*, 1–32. [CrossRef] [PubMed]
36. Fabrizio, P.; Pozza, F.; Pletcher, S.D.; Gendron, C.M.; Longo, V.D. Regulation of Longevity and Stress Resistance by Sch9 in Yeast. *Science* **2001**, *292*, 288–290. [CrossRef] [PubMed]
37. Sampaio-Marques, B.; Burhans, W.C.; Ludovico, P. Longevity Pathways and Maintenance of the Proteome: The Role of Autophagy and Mitophagy during Yeast Ageing. *Microb. Cell Graz Austria* **2014**, *1*, 118–127. [CrossRef]
38. Wei, M.; Fabrizio, P.; Hu, J.; Ge, H.; Cheng, C.; Li, L.; Longo, V.D. Life Span Extension by Calorie Restriction Depends on Rim15 and Transcription Factors Downstream of Ras/PKA, Tor, and Sch9. *PLoS Genet.* **2008**, *4*, e13. [CrossRef]
39. Jumper, J.; Evans, R.; Pritzel, A.; Green, T.; Figurnov, M.; Ronneberger, O.; Tunyasuvunakool, K.; Bates, R.; Žídek, A.; Potapenko, A.; et al. Highly Accurate Protein Structure Prediction with AlphaFold. *Nature* **2021**, *596*, 583–589. [CrossRef]
40. Varadi, M.; Anyango, S.; Deshpande, M.; Nair, S.; Natassia, C.; Yordanova, G.; Yuan, D.; Stroe, O.; Wood, G.; Laydon, A.; et al. AlphaFold Protein Structure Database: Massively Expanding the Structural Coverage of Protein-Sequence Space with High-Accuracy Models. *Nucleic Acids Res.* **2022**, *50*, D439–D444. [CrossRef]
41. Lu, K.-Y.; Tao, S.-C.; Yang, T.-C.; Ho, Y.-H.; Lee, C.-H.; Lin, C.-C.; Juan, H.-F.; Huang, H.-C.; Yang, C.-Y.; Chen, M.-S.; et al. Profiling Lipid-Protein Interactions Using Nonquenched Fluorescent Liposomal Nanovesicles and Proteome Microarrays. *Mol. Cell. Proteom. MCP* **2012**, *11*, 1177–1190. [CrossRef] [PubMed]
42. Sobko, A. Systems Biology of AGC Kinases in Fungi. *Sci. STKE Signal Transduct. Knowl. Environ.* **2006**, *2006*, re9. [CrossRef] [PubMed]
43. Pearce, L.R.; Komander, D.; Alessi, D.R. The Nuts and Bolts of AGC Protein Kinases. *Nat. Rev. Mol. Cell Biol.* **2010**, *11*, 9–22. [CrossRef] [PubMed]
44. Truebestein, L.; Hornegger, H.; Anrather, D.; Hartl, M.; Fleming, K.D.; Stariha, J.T.B.; Pardon, E.; Steyaert, J.; Burke, J.E.; Leonard, T.A. Structure of Autoinhibited Akt1 Reveals Mechanism of PIP3-Mediated Activation. *Proc. Natl. Acad. Sci. USA* **2021**, *118*, e2101496118. [CrossRef] [PubMed]
45. Frech, M.; Andjelkovic, M.; Ingley, E.; Reddy, K.K.; Falck, J.R.; Hemmings, B.A. High Affinity Binding of Inositol Phosphates and Phosphoinositides to the Pleckstrin Homology Domain of RAC/Protein Kinase B and Their Influence on Kinase Activity. *J. Biol. Chem.* **1997**, *272*, 8474–8481. [CrossRef]
46. James, S.R.; Downes, C.P.; Gigg, R.; Grove, S.J.; Holmes, A.B.; Alessi, D.R. Specific Binding of the Akt-1 Protein Kinase to Phosphatidylinositol 3,4,5-Trisphosphate without Subsequent Activation. *Biochem. J.* **1996**, *315 Pt 3*, 709–713. [CrossRef]
47. Thomas, C.C.; Deak, M.; Alessi, D.R.; van Aalten, D.M.F. High-Resolution Structure of the Pleckstrin Homology Domain of Protein Kinase b/Akt Bound to Phosphatidylinositol (3,4,5)-Trisphosphate. *Curr. Biol.* **2002**, *12*, 1256–1262. [CrossRef]
48. Corbalan-Garcia, S.; Gómez-Fernández, J.C. Signaling through C2 Domains: More than One Lipid Target. *Biochim. Biophys. Acta* **2014**, *1838*, 1536–1547. [CrossRef]
49. Thorner, J. TOR Complex 2 Is a Master Regulator of Plasma Membrane Homeostasis. *Biochem. J.* **2022**, *479*, 1917–1940. [CrossRef]
50. Kamada, Y.; Fujioka, Y.; Suzuki, N.N.; Inagaki, F.; Wullschleger, S.; Loewith, R.; Hall, M.N.; Ohsumi, Y. Tor2 Directly Phosphorylates the AGC Kinase Ypk2 to Regulate Actin Polarization. *Mol. Cell. Biol.* **2005**, *25*, 7239–7248. [CrossRef]
51. Leskoske, K.L.; Roelants, F.M.; Martinez Marshall, M.N.; Hill, J.M.; Thorner, J. The Stress-Sensing TORC2 Complex Activates Yeast AGC-Family Protein Kinase Ypk1 at Multiple Novel Sites. *Genetics* **2017**, *207*, 179–195. [CrossRef] [PubMed]
52. Martinez Marshall, M.N.; Emmerstorfer-Augustin, A.; Leskoske, K.L.; Zhang, L.H.; Li, B.; Thorner, J. Analysis of the Roles of Phosphatidylinositol-4,5-Bisphosphate and Individual Subunits in Assembly, Localization, and Function of Saccharomyces Cerevisiae Target of Rapamycin Complex 2. *Mol. Biol. Cell* **2019**, *30*, 1555–1574. [CrossRef] [PubMed]
53. Roelants, F.M.; Breslow, D.K.; Muir, A.; Weissman, J.S.; Thorner, J. Protein Kinase Ypk1 Phosphorylates Regulatory Proteins Orm1 and Orm2 to Control Sphingolipid Homeostasis in Saccharomyces Cerevisiae. *Proc. Natl. Acad. Sci. USA* **2011**, *108*, 19222–19227. [CrossRef] [PubMed]
54. Yang, J.; Cron, P.; Thompson, V.; Good, V.M.; Hess, D.; Hemmings, B.A.; Barford, D. Molecular Mechanism for the Regulation of Protein Kinase B/Akt by Hydrophobic Motif Phosphorylation. *Mol. Cell* **2002**, *9*, 1227–1240. [CrossRef]
55. Chu, N.; Salguero, A.L.; Liu, A.Z.; Chen, Z.; Dempsey, D.R.; Ficarro, S.B.; Alexander, W.M.; Marto, J.A.; Li, Y.; Amzel, L.M.; et al. Akt Kinase Activation Mechanisms Revealed Using Protein Semisynthesis. *Cell* **2018**, *174*, 897–907.e14. [CrossRef]
56. Hatakeyama, R.; Péli-Gulli, M.P.; Hu, Z.; Jaquenoud, M.; Garcia Osuna, G.M.; Sardu, A.; Dengjel, J.; De Virgilio, C. Spatially Distinct Pools of TORC1 Balance Protein Homeostasis. *Mol. Cell* **2019**, *73*, 325–338.e8. [CrossRef]
57. Jin, N.; Mao, K.; Jin, Y.; Tevzadze, G.; Kauffman, E.J.; Park, S.; Bridges, D.; Loewith, R.; Saltiel, A.R.; Klionsky, D.J.; et al. Roles for PI(3,5)P2 in Nutrient Sensing through TORC1. *Mol. Biol. Cell* **2014**, *25*, 1171–1185. [CrossRef]
58. Lemmon, M.A. Phosphoinositide Recognition Domains. *Traffic Cph. Den.* **2003**, *4*, 201–213. [CrossRef]
59. Posor, Y.; Jang, W.; Haucke, V. Phosphoinositides as Membrane Organizers. *Nat. Rev. Mol. Cell Biol.* **2022**, *23*, 797–816. [CrossRef]
60. Lemmon, M.A. Membrane Recognition by Phospholipid-Binding Domains. *Nat. Rev. Mol. Cell Biol.* **2008**, *9*, 99–111. [CrossRef]
61. Takeda, E.; Jin, N.; Itakura, E.; Kira, S.; Kamada, Y.; Weisman, L.S.; Noda, T.; Matsuura, A. Vacuole-Mediated Selective Regulation of TORC1-Sch9 Signaling Following Oxidative Stress. *Mol. Biol. Cell* **2018**, *29*, 510–522. [CrossRef] [PubMed]

62. Dove, S.K.; Cooke, F.T.; Douglas, M.R.; Sayers, L.G.; Parker, P.J.; Michell, R.H. Osmotic Stress Activates Phosphatidylinositol-3,5-Bisphosphate Synthesis. *Nature* **1997**, *390*, 187–192. [CrossRef]
63. Jin, N.; Jin, Y.; Weisman, L.S. Early Protection to Stress Mediated by CDK-Dependent PI3,5P2 Signaling from the Vacuole/Lysosome. *J. Cell Biol.* **2017**, *216*, 2075–2090. [CrossRef] [PubMed]
64. Banerjee, S.; Clapp, K.; Tarsio, M.; Kane, P.M. Interaction of the Late Endo-Lysosomal Lipid PI(3,5)P2 with the Vph1 Isoform of Yeast V-ATPase Increases Its Activity and Cellular Stress Tolerance. *J. Biol. Chem.* **2019**, *294*, 9161–9171. [CrossRef] [PubMed]
65. Banerjee, S.; Kane, P.M. Regulation of V-ATPase Activity and Organelle PH by Phosphatidylinositol Phosphate Lipids. *Front. Cell Dev. Biol.* **2020**, *8*, 510. [CrossRef] [PubMed]
66. Dechant, R.; Saad, S.; Ibáñez, A.J.; Peter, M. Cytosolic PH Regulates Cell Growth through Distinct Gtpases, Arf1 and Gtr1, to Promote Ras/PKA and TORC1 Activity. *Mol. Cell* **2014**, *55*, 409–421. [CrossRef] [PubMed]
67. Dechant, R.; Binda, M.; Lee, S.S.; Pelet, S.; Winderickx, J.; Peter, M. Cytosolic PH Is a Second Messenger for Glucose and Regulates the PKA Pathway through V-ATPase. *EMBO J.* **2010**, *29*, 2515–2526. [CrossRef] [PubMed]
68. Laribee, R.N.; Hosni-Ahmed, A.; Workman, J.J.; Chen, H. Ccr4-Not Regulates RNA Polymerase I Transcription and Couples Nutrient Signaling to the Control of Ribosomal RNA Biogenesis. *PLoS Genet.* **2015**, *11*, e1005113. [CrossRef]
69. Lenssen, E.; Oberholzer, U.; Labarre, J.; De Virgilio, C.; Collart, M.A. Saccharomyces Cerevisiae Ccr4-Not Complex Contributes to the Control of Msn2p-Dependent Transcription by the Ras/CAMP Pathway. *Mol. Microbiol.* **2002**, *43*, 1023–1037. [CrossRef]
70. Laribee, R.N. Ccr4-Not as a Mediator of Environmental Signaling: A Jack of All Trades and Master of All. *Curr. Genet.* **2021**, *67*, 707–713. [CrossRef]
71. Qie, B.; Lyu, Z.; Lyu, L.; Liu, J.; Gao, X.; Liu, Y.; Duan, W.; Zhang, N.; Du, L.; Liu, K. Sch9 Regulates Intracellular Protein Ubiquitination by Controlling Stress Responses. *Redox Biol.* **2015**, *5*, 290–300. [CrossRef] [PubMed]
72. Dechant, R.; Peter, M. The N-Terminal Domain of the V-ATPase Subunit "a" Is Regulated by PH In Vitro and In Vivo. *Channels* **2011**, *5*, 4–8. [CrossRef]
73. Saliba, E.; Evangelinos, M.; Gournas, C.; Corrillon, F.; Georis, I.; André, B. The Yeast H+-ATPase Pma1 Promotes Rag/Gtr-Dependent TORC1 Activation in Response to H+-Coupled Nutrient Uptake. *eLife* **2018**, *7*, e31981. [CrossRef]
74. Ren, J.; Hannun, Y.A. Metabolism and Roles of Sphingolipids in Yeast Saccharomyces Cerevisiae. In *Biogenesis of Fatty Acids, Lipids and Membranes*; Geiger, O., Ed.; Handbook of Hydrocarbon and Lipid Microbiology; Springer: Cham, Switzerland, 2019; pp. 341–361, ISBN 978-3-319-43676-0. [CrossRef]
75. Roelants, F.M.; Torrance, P.D.; Bezman, N.; Thorner, J. Pkh1 and Pkh2 Differentially Phosphorylate and Activate Ypk1 and Ykr2 and Define Protein Kinase Modules Required for Maintenance of Cell Wall Integrity. *Mol. Biol. Cell* **2002**, *13*, 3005–3028. [CrossRef]
76. Swinnen, E.; Wilms, T.; Idkowiak-Baldys, J.; Smets, B.; De Snijder, P.; Accardo, S.; Ghillebert, R.; Thevissen, K.; Cammue, B.; De Vos, D.; et al. The Protein Kinase Sch9 Is a Key Regulator of Sphingolipid Metabolism in Saccharomyces Cerevisiae. *Mol. Biol. Cell* **2014**, *25*, 196–211. [CrossRef]
77. Matmati, N.; Hannun, Y.A. Thematic Review Series: Sphingolipids. ISC1 (Inositol Phosphosphingolipid-Phospholipase C), the Yeast Homologue of Neutral Sphingomyelinases. *J. Lipid Res.* **2008**, *49*, 922–928. [CrossRef]
78. Rego, A.; Cooper, K.F.; Snider, J.; Hannun, Y.A.; Costa, V.; Côrte-Real, M.; Chaves, S.R. Acetic Acid Induces Sch9p-Dependent Translocation of Isc1p from the Endoplasmic Reticulum into Mitochondria. *Biochim. Biophys. Acta BBA-Mol. Cell Biol. Lipids* **2018**, *1863*, 576–583. [CrossRef] [PubMed]
79. Dickson, R.C.; Sumanasekera, C.; Lester, R.L. Functions and Metabolism of Sphingolipids in Saccharomyces Cerevisiae. *Prog. Lipid Res.* **2006**, *45*, 447–465. [CrossRef] [PubMed]
80. Yamagata, M.; Obara, K.; Kihara, A. Sphingolipid Synthesis Is Involved in Autophagy in Saccharomyces Cerevisiae. *Biochem. Biophys. Res. Commun.* **2011**, *410*, 786–791. [CrossRef]
81. Hannun, Y.A.; Obeid, L.M. Principles of Bioactive Lipid Signalling: Lessons from Sphingolipids. *Nat. Rev. Mol. Cell Biol.* **2008**, *9*, 139–150. [CrossRef]
82. Beeler, T.J.; Fu, D.; Rivera, J.; Monaghan, E.; Gable, K.; Dunn, T.M. SUR1 (CSG1/BCL21), a Gene Necessary for Growth of Saccharomyces Cerevisiae in the Presence of High Ca^{2+} Concentrations at 37 Degrees C, Is Required for Mannosylation of Inositolphosphorylceramide. *Mol. Gen. Genet. MGG* **1997**, *255*, 570–579. [CrossRef] [PubMed]
83. Uemura, S.; Kihara, A.; Iwaki, S.; Inokuchi, J.; Igarashi, Y. Regulation of the Transport and Protein Levels of the Inositol Phosphorylceramide Mannosyltransferases Csg1 and Csh1 by the Ca^{2+}-Binding Protein Csg2. *J. Biol. Chem.* **2007**, *282*, 8613–8621. [CrossRef] [PubMed]
84. Barbosa, A.D.; Osório, H.; Sims, K.J.; Almeida, T.; Alves, M.; Bielawski, J.; Amorim, M.A.; Moradas-Ferreira, P.; Hannun, Y.A.; Costa, V. Role for Sit4p-Dependent Mitochondrial Dysfunction in Mediating the Shortened Chronological Lifespan and Oxidative Stress Sensitivity of Isc1p-Deficient Cells. *Mol. Microbiol.* **2011**, *81*, 515–527. [CrossRef]
85. Teixeira, V.; Medeiros, T.C.; Vilaça, R.; Pereira, A.T.; Chaves, S.R.; Côrte-Real, M.; Moradas-Ferreira, P.; Costa, V. Ceramide Signalling Impinges on Sit4p and Hog1p to Promote Mitochondrial Fission and Mitophagy in Isc1p-Deficient Cells. *Cell. Signal.* **2015**, *27*, 1840–1849. [CrossRef]
86. Sun, Y.; Miao, Y.; Yamane, Y.; Zhang, C.; Shokat, K.M.; Takematsu, H.; Kozutsumi, Y.; Drubin, D.G. Orm Protein Phosphoregulation Mediates Transient Sphingolipid Biosynthesis Response to Heat Stress via the Pkh-Ypk and Cdc55-PP2A Pathways. *Mol. Biol. Cell* **2012**, *23*, 2388–2398. [CrossRef] [PubMed]

87. Muir, A.; Ramachandran, S.; Roelants, F.M.; Timmons, G.; Thorner, J. TORC2-Dependent Protein Kinase Ypk1 Phosphorylates Ceramide Synthase to Stimulate Synthesis of Complex Sphingolipids. *eLife* **2014**, *3*, e03779. [CrossRef]
88. Iwaki, S.; Kihara, A.; Sano, T.; Igarashi, Y. Phosphorylation by Pho85 Cyclin-Dependent Kinase Acts as a Signal for the down-Regulation of the Yeast Sphingoid Long-Chain Base Kinase Lcb4 during the Stationary Phase. *J. Biol. Chem.* **2005**, *280*, 6520–6527. [CrossRef] [PubMed]
89. Prieto, J.A.; Estruch, F.; Córcoles-Sáez, I.; Del Poeta, M.; Rieger, R.; Stenzel, I.; Randez-Gil, F. Pho85 and PI(4,5)P2 Regulate Different Lipid Metabolic Pathways in Response to Cold. *Biochim. Biophys. Acta BBA-Mol. Cell Biol. Lipids* **2020**, *1865*, 158557. [CrossRef] [PubMed]
90. Borklu Yucel, E.; Ulgen, K.O. Assessment of Crosstalks between the Snf1 Kinase Complex and Sphingolipid Metabolism in *S. cerevisiae* via Systems Biology Approaches. *Mol. Biosyst.* **2013**, *9*, 2914–2931. [CrossRef]
91. Knupp, J.; Martinez-Montañés, F.; Van Den Bergh, F.; Cottier, S.; Schneiter, R.; Beard, D.; Chang, A. Sphingolipid Accumulation Causes Mitochondrial Dysregulation and Cell Death. *Cell Death Differ.* **2017**, *24*, 2044–2053. [CrossRef]
92. Guerra, P.; Vuillemenot, L.-A.P.E.; van Oppen, Y.B.; Been, M.; Milias-Argeitis, A. TORC1 and PKA Activity towards Ribosome Biogenesis Oscillates in Synchrony with the Budding Yeast Cell Cycle. *J. Cell Sci.* **2022**, *135*, jcs260378. [CrossRef] [PubMed]
93. Lippman, S.I.; Broach, J.R. Protein Kinase A and TORC1 Activate Genes for Ribosomal Biogenesis by Inactivating Repressors Encoded by Dot6 and Its Homolog Tod6. *Proc. Natl. Acad. Sci. USA* **2009**, *106*, 19928–19933. [CrossRef] [PubMed]
94. Huber, A.; Bodenmiller, B.; Uotila, A.; Stahl, M.; Wanka, S.; Gerrits, B.; Aebersold, R.; Loewith, R. Characterization of the Rapamycin-Sensitive Phosphoproteome Reveals That Sch9 Is a Central Coordinator of Protein Synthesis. *Genes Dev.* **2009**, *23*, 1929–1943. [CrossRef] [PubMed]
95. Cocklin, R.; Goebl, M. Nutrient Sensing Kinases PKA and Sch9 Phosphorylate the Catalytic Domain of the Ubiquitin-Conjugating Enzyme Cdc34. *PLoS ONE* **2011**, *6*, e27099. [CrossRef]
96. Askree, S.H.; Yehuda, T.; Smolikov, S.; Gurevich, R.; Hawk, J.; Coker, C.; Krauskopf, A.; Kupiec, M.; McEachern, M.J. A Genome-Wide Screen for Saccharomyces Cerevisiae Deletion Mutants That Affect Telomere Length. *Proc. Natl. Acad. Sci. USA* **2004**, *101*, 8658–8663. [CrossRef]
97. Connelly, C.J.; Vidal-Cardenas, S.; Goldsmith, S.; Greider, C.W. The Bur1 Cyclin-Dependent Kinase Regulates Telomere Length in Saccharomyces Cerevisiae. *Yeast Chichester Engl.* **2022**, *39*, 177–192. [CrossRef]
98. Zaragoza, D.; Ghavidel, A.; Heitman, J.; Schultz, M.C. Rapamycin Induces the G0 Program of Transcriptional Repression in Yeast by Interfering with the TOR Signaling Pathway. *Mol. Cell. Biol.* **1998**, *18*, 4463–4470. [CrossRef]
99. Sanz, P. Snf1 Protein Kinase: A Key Player in the Response to Cellular Stress in Yeast. *Biochem. Soc. Trans.* **2003**, *31*, 178–181. [CrossRef]
100. Hughes Hallett, J.E.; Luo, X.; Capaldi, A.P. State Transitions in the TORC1 Signaling Pathway and Information Processing in *Saccharomyces cerevisiae*. *Genetics* **2014**, *198*, 773–786. [CrossRef]
101. Zhang, J.; Vaga, S.; Chumnanpuen, P.; Kumar, R.; Vemuri, G.N.; Aebersold, R.; Nielsen, J. Mapping the Interaction of Snf1 with TORC1 in Saccharomyces Cerevisiae. *Mol. Syst. Biol.* **2011**, *7*, 545. [CrossRef]
102. Hughes Hallett, J.E.; Luo, X.; Capaldi, A.P. Snf1/AMPK Promotes the Formation of Kog1/Raptor-Bodies to Increase the Activation Threshold of TORC1 in Budding Yeast. *eLife* **2015**, *4*, e09181. [CrossRef] [PubMed]
103. De Virgilio, C. The Essence of Yeast Quiescence. *FEMS Microbiol. Rev.* **2012**, *36*, 306–339. [CrossRef]
104. Cameroni, E.; Hulo, N.; Roosen, J.; Winderickx, J.; De Virgilio, C. The Novel Yeast PAS Kinase Rim 15 Orchestrates G0-Associated Antioxidant Defense Mechanisms. *Cell Cycle* **2004**, *3*, 462–468. [CrossRef] [PubMed]
105. Pedruzzi, I.; Dubouloz, F.; Cameroni, E.; Wanke, V.; Roosen, J.; Winderickx, J.; De Virgilio, C. TOR and PKA Signaling Pathways Converge on the Protein Kinase Rim15 to Control Entry into G0. *Mol. Cell* **2003**, *12*, 1607–1613. [CrossRef] [PubMed]
106. Reinders, A.; Bürckert, N.; Boller, T.; Wiemken, A.; De Virgilio, C. Saccharomyces Cerevisiae CAMP-Dependent Protein Kinase Controls Entry into Stationary Phase through the Rim15p Protein Kinase. *Genes Dev.* **1998**, *12*, 2943–2955. [CrossRef]
107. Zhang, A.; Shen, Y.; Gao, W.; Dong, J. Role of Sch9 in Regulating Ras-CAMP Signal Pathway in Saccharomyces Cerevisiae. *FEBS Lett.* **2011**, *585*, 3026–3032. [CrossRef]
108. Zhang, A.; Gao, W. Mechanisms of Protein Kinase Sch9 Regulating Bcy1 in Saccharomyces Cerevisiae. *FEMS Microbiol. Lett.* **2012**, *331*, 10–16. [CrossRef]
109. Sánchez-Adriá, I.E.; Sanmartín, G.; Prieto, J.A.; Estruch, F.; Randez-Gil, F. Slt2 Is Required to Activate ER-Stress-Protective Mechanisms through TORC1 Inhibition and Hexosamine Pathway Activation. *J. Fungi* **2022**, *8*, 92. [CrossRef]
110. Lee, P.; Kim, M.S.; Paik, S.-M.; Choi, S.-H.; Cho, B.-R.; Hahn, J.-S. Rim15-Dependent Activation of Hsf1 and Msn2/4 Transcription Factors by Direct Phosphorylation in Saccharomyces Cerevisiae. *FEBS Lett.* **2013**, *587*, 3648–3655. [CrossRef]
111. Bontron, S.; Jaquenoud, M.; Vaga, S.; Talarek, N.; Bodenmiller, B.; Aebersold, R.; De Virgilio, C. Yeast Endosulfines Control Entry into Quiescence and Chronological Life Span by Inhibiting Protein Phosphatase 2A. *Cell Rep.* **2013**, *3*, 16–22. [CrossRef]
112. Sarkar, S.; Dalgaard, J.Z.; Millar, J.B.A.; Arumugam, P. The Rim15-Endosulfine-PP2ACdc55 Signalling Module Regulates Entry into Gametogenesis and Quiescence via Distinct Mechanisms in Budding Yeast. *PLoS Genet.* **2014**, *10*, e1004456. [CrossRef] [PubMed]
113. Talarek, N.; Bontron, S.; De Virgilio, C. Quantification of MRNA Stability of Stress-Responsive Yeast Genes Following Conditional Excision of Open Reading Frames. *RNA Biol.* **2013**, *10*, 1299–1308. [CrossRef]

114. Talarek, N.; Cameroni, E.; Jaquenoud, M.; Luo, X.; Bontron, S.; Lippman, S.; Devgan, G.; Snyder, M.; Broach, J.R.; De Virgilio, C. Initiation of the TORC1-Regulated G0 Program Requires Igo1/2, Which License Specific MRNAs to Evade Degradation via the 5′-3′ MRNA Decay Pathway. *Mol. Cell* **2010**, *38*, 345–355. [CrossRef] [PubMed]
115. Swinnen, E.; Rosseels, J.; Winderickx, J. The Minimum Domain of Pho81 Is Not Sufficient to Control the Pho85-Rim15 Effector Branch Involved in Phosphate Starvation-Induced Stress Responses. *Curr. Genet.* **2005**, *48*, 18–33. [CrossRef] [PubMed]
116. Wanke, V.; Pedruzzi, I.; Cameroni, E.; Dubouloz, F.; De Virgilio, C. Regulation of G0 Entry by the Pho80-Pho85 Cyclin-CDK Complex. *EMBO J.* **2005**, *24*, 4271–4278. [CrossRef]
117. Lee, P.; Paik, S.-M.; Shin, C.-S.; Huh, W.-K.; Hahn, J.-S. Regulation of Yeast Yak1 Kinase by PKA and Autophosphorylation-Dependent 14-3-3 Binding. *Mol. Microbiol.* **2011**, *79*, 633–646. [CrossRef]
118. Schmelzle, T.; Beck, T.; Martin, D.E.; Hall, M.N. Activation of the RAS/Cyclic AMP Pathway Suppresses a TOR Deficiency in Yeast. *Mol. Cell. Biol.* **2004**, *24*, 338–351. [CrossRef]
119. Lee, P.; Cho, B.-R.; Joo, H.-S.; Hahn, J.-S. Yeast Yak1 Kinase, a Bridge between PKA and Stress-Responsive Transcription Factors, Hsf1 and Msn2/Msn4. *Mol. Microbiol.* **2008**, *70*, 882–895. [CrossRef]
120. Zhang, N.; Quan, Z.; Rash, B.; Oliver, S.G. Synergistic Effects of TOR and Proteasome Pathways on the Yeast Transcriptome and Cell Growth. *Open Biol.* **2013**, *3*, 120137. [CrossRef]
121. Moriya, H.; Shimizu-Yoshida, Y.; Omori, A.; Iwashita, S.; Katoh, M.; Sakai, A. Yak1p, a DYRK Family Kinase, Translocates to the Nucleus and Phosphorylates Yeast Pop2p in Response to a Glucose Signal. *Genes Dev.* **2001**, *15*, 1217–1228. [CrossRef]
122. Martin, D.E.; Soulard, A.; Hall, M.N. TOR Regulates Ribosomal Protein Gene Expression via PKA and the Forkhead Transcription Factor FHL1. *Cell* **2004**, *119*, 969–979. [CrossRef] [PubMed]
123. Griffioen, G.; Branduardi, P.; Ballarini, A.; Anghileri, P.; Norbeck, J.; Baroni, M.D.; Ruis, H. Nucleocytoplasmic Distribution of Budding Yeast Protein Kinase a Regulatory Subunit Bcy1 Requires Zds1 and Is Regulated by Yak1-Dependent Phosphorylation of Its Targeting Domain. *Mol. Cell. Biol.* **2001**, *21*, 511–523. [CrossRef] [PubMed]
124. Quan, Z.; Cao, L.; Tang, Y.; Yan, Y.; Oliver, S.G.; Zhang, N. The Yeast GSK-3 Homologue Mck1 Is a Key Controller of Quiescence Entry and Chronological Lifespan. *PLoS Genet.* **2015**, *11*, e1005282. [CrossRef] [PubMed]
125. Griffioen, G.; Swinnen, S.; Thevelein, J.M. Feedback Inhibition on Cell Wall Integrity Signaling by Zds1 Involves Gsk3 Phosphorylation of a CAMP-Dependent Protein Kinase Regulatory Subunit. *J. Biol. Chem.* **2003**, *278*, 23460–23471. [CrossRef]
126. Mizunuma, M.; Hirata, D.; Miyaoka, R.; Miyakawa, T. GSK-3 Kinase Mck1 and Calcineurin Coordinately Mediate Hsl1 down-Regulation by Ca^{2+} in Budding Yeast. *EMBO J.* **2001**, *20*, 1074–1085. [CrossRef]
127. Cao, L.; Tang, Y.; Quan, Z.; Zhang, Z.; Oliver, S.G.; Zhang, N. Chronological Lifespan in Yeast Is Dependent on the Accumulation of Storage Carbohydrates Mediated by Yak1, Mck1 and Rim15 Kinases. *PLoS Genet.* **2016**, *12*, e1006458. [CrossRef]
128. Hirata, Y.; Andoh, T.; Asahara, T.; Kikuchi, A. Yeast Glycogen Synthase Kinase-3 Activates Msn2p-Dependent Transcription of Stress Responsive Genes. *Mol. Biol. Cell* **2003**, *14*, 302–312. [CrossRef]
129. Gutin, J.; Joseph-Strauss, D.; Sadeh, A.; Shalom, E.; Friedman, N. Genetic Screen of the Yeast Environmental Stress Response Dynamics Uncovers Distinct Regulatory Phases. *Mol. Syst. Biol.* **2019**, *15*, e8939. [CrossRef]
130. Lee, J.; Moir, R.D.; McIntosh, K.B.; Willis, I.M. TOR Signaling Regulates Ribosome and TRNA Synthesis via LAMMER/Clk and GSK-3 Family Kinases. *Mol. Cell* **2012**, *45*, 836–843. [CrossRef]
131. Zhang, N.; Cao, L. Starvation Signals in Yeast Are Integrated to Coordinate Metabolic Reprogramming and Stress Response to Ensure Longevity. *Curr. Genet.* **2017**, *63*, 839–843. [CrossRef]
132. Peterson, P.P.; Liu, Z. Identification and Characterization of Rapidly Accumulating Sch9Δ Suppressor Mutations in Saccharomyces Cerevisiae. *G3 Genes* **2021**, *11*, jkab134. [CrossRef]
133. Balciunas, D.; Ronne, H. Yeast Genes GIS1-4: Multicopy Suppressors of the Gal- Phenotype of Snf1 Mig1 Srb8/10/11 Cells. *Mol. Gen. Genet. MGG* **1999**, *262*, 589–599. [CrossRef] [PubMed]
134. Estruch, F.; Carlson, M. Two Homologous Zinc Finger Genes Identified by Multicopy Suppression in a SNF1 Protein Kinase Mutant of Saccharomyces Cerevisiae. *Mol. Cell. Biol.* **1993**, *13*, 3872–3881. [CrossRef] [PubMed]
135. De Wever, V.; Reiter, W.; Ballarini, A.; Ammerer, G.; Brocard, C. A Dual Role for PP1 in Shaping the Msn2-Dependent Transcriptional Response to Glucose Starvation. *EMBO J.* **2005**, *24*, 4115–4123. [CrossRef] [PubMed]
136. Hahn, J.-S.; Thiele, D.J. Activation of the Saccharomyces Cerevisiae Heat Shock Transcription Factor under Glucose Starvation Conditions by Snf1 Protein Kinase. *J. Biol. Chem.* **2004**, *279*, 5169–5176. [CrossRef]
137. Mayordomo, I.; Estruch, F.; Sanz, P. Convergence of the Target of Rapamycin and the Snf1 Protein Kinase Pathways in the Regulation of the Subcellular Localization of Msn2, a Transcriptional Activator of STRE (Stress Response Element)-Regulated Genes. *J. Biol. Chem.* **2002**, *277*, 35650–35656. [CrossRef]
138. Nicastro, R.; Tripodi, F.; Gaggini, M.; Castoldi, A.; Reghellin, V.; Nonnis, S.; Tedeschi, G.; Coccetti, P. Snf1 Phosphorylates Adenylate Cyclase and Negatively Regulates Protein Kinase A-Dependent Transcription in Saccharomyces Cerevisiae. *J. Biol. Chem.* **2015**, *290*, 24715–24726. [CrossRef]
139. Dauner, K.; Eid, W.; Raghupathy, R.; Presley, J.F.; Zha, X. MTOR Complex 1 Activity Is Required to Maintain the Canonical Endocytic Recycling Pathway against Lysosomal Delivery. *J. Biol. Chem.* **2017**, *292*, 5737–5747. [CrossRef]
140. Dobzinski, N.; Chuartzman, S.G.; Kama, R.; Schuldiner, M.; Gerst, J.E. Starvation-Dependent Regulation of Golgi Quality Control Links the TOR Signaling and Vacuolar Protein Sorting Pathways. *Cell Rep.* **2015**, *12*, 1876–1886. [CrossRef]

141. Jones, C.B.; Ott, E.M.; Keener, J.M.; Curtiss, M.; Sandrin, V.; Babst, M. Regulation of Membrane Protein Degradation by Starvation-Response Pathways. *Traffic* **2012**, *13*, 468–482. [CrossRef]
142. MacGurn, J.A.; Hsu, P.-C.; Smolka, M.B.; Emr, S.D. TORC1 Regulates Endocytosis via Npr1-Mediated Phosphoinhibition of a Ubiquitin Ligase Adaptor. *Cell* **2011**, *147*, 1104–1117. [CrossRef]
143. Durchschlag, E.; Reiter, W.; Ammerer, G.; Schüller, C. Nuclear Localization Destabilizes the Stress-Regulated Transcription Factor Msn2. *J. Biol. Chem.* **2004**, *279*, 55425–55432. [CrossRef]
144. Irniger, S.; Braus, G.H. Controlling Transcription by Destruction: The Regulation of Yeast Gcn4p Stability. *Curr. Genet.* **2003**, *44*, 8–18. [CrossRef]
145. Zhang, N.; Oliver, S.G. The Transcription Activity of Gis1 Is Negatively Modulated by Proteasome-Mediated Limited Proteolysis. *J. Biol. Chem.* **2010**, *285*, 6465–6476. [CrossRef] [PubMed]
146. Rousseau, A.; Bertolotti, A. Regulation of Proteasome Assembly and Activity in Health and Disease. *Nat. Rev. Mol. Cell Biol.* **2018**, *19*, 697–712. [CrossRef] [PubMed]
147. Rousseau, A.; Bertolotti, A. An Evolutionarily Conserved Pathway Controls Proteasome Homeostasis. *Nature* **2016**, *536*, 184–189. [CrossRef]
148. Williams, T.D.; Cacioppo, R.; Agrotis, A.; Black, A.; Zhou, H.; Rousseau, A. Actin Remodelling Controls Proteasome Homeostasis upon Stress. *Nat. Cell Biol.* **2022**, *24*, 1077–1087. [CrossRef] [PubMed]
149. Hahn, J.-S.; Neef, D.W.; Thiele, D.J. A Stress Regulatory Network for Co-Ordinated Activation of Proteasome Expression Mediated by Yeast Heat Shock Transcription Factor. *Mol. Microbiol.* **2006**, *60*, 240–251. [CrossRef]
150. Laporte, D.; Salin, B.; Daignan-Fornier, B.; Sagot, I. Reversible Cytoplasmic Localization of the Proteasome in Quiescent Yeast Cells. *J. Cell Biol.* **2008**, *181*, 737–745. [CrossRef]
151. Waite, K.A.; Roelofs, J. Proteasome Granule Formation Is Regulated through Mitochondrial Respiration and Kinase Signaling. *J. Cell Sci.* **2022**, *135*, jcs259778. [CrossRef]
152. Karmon, O.; Ben Aroya, S. Spatial Organization of Proteasome Aggregates in the Regulation of Proteasome Homeostasis. *Front. Mol. Biosci.* **2019**, *6*, 150. [CrossRef] [PubMed]
153. Marshall, R.S.; McLoughlin, F.; Vierstra, R.D. Autophagic Turnover of Inactive 26S Proteasomes in Yeast Is Directed by the Ubiquitin Receptor Cue5 and the Hsp42 Chaperone. *Cell Rep.* **2016**, *16*, 1717–1732. [CrossRef] [PubMed]
154. Waite, K.A.; Burris, A.; Vontz, G.; Lang, A.; Roelofs, J. Proteaphagy Is Specifically Regulated and Requires Factors Dispensable for General Autophagy. *J. Biol. Chem.* **2022**, *298*, 101494. [CrossRef] [PubMed]
155. Hatakeyama, R.; De Virgilio, C. A Spatially and Functionally Distinct Pool of TORC1 Defines Signaling Endosomes in Yeast. *Autophagy* **2019**, *15*, 915–916. [CrossRef] [PubMed]
156. Kamada, Y.; Yoshino, K.-I.; Kondo, C.; Kawamata, T.; Oshiro, N.; Yonezawa, K.; Ohsumi, Y. Tor Directly Controls the Atg1 Kinase Complex to Regulate Autophagy. *Mol. Cell. Biol.* **2010**, *30*, 1049–1058. [CrossRef]
157. Hatakeyama, R.; De Virgilio, C. TORC1 Specifically Inhibits Microautophagy through ESCRT-0. *Curr. Genet.* **2019**, *65*, 1243–1249. [CrossRef]
158. Morshed, S.; Sharmin, T.; Ushimaru, T. TORC1 Regulates ESCRT-0 Complex Formation on the Vacuolar Membrane and Microautophagy Induction in Yeast. *Biochem. Biophys. Res. Commun.* **2020**, *522*, 88–94. [CrossRef]
159. Li, J.; Hochstrasser, M. Selective Microautophagy of Proteasomes Is Initiated by ESCRT-0 and Is Promoted by Proteasome Ubiquitylation. *J. Cell Sci.* **2022**, *135*, jcs259393. [CrossRef]
160. Stephan, J.S.; Yeh, Y.-Y.; Ramachandran, V.; Deminoff, S.J.; Herman, P.K. The Tor and PKA Signaling Pathways Independently Target the Atg1/Atg13 Protein Kinase Complex to Control Autophagy. *Proc. Natl. Acad. Sci. USA* **2009**, *106*, 17049–17054. [CrossRef]
161. Montella-Manuel, S.; Pujol-Carrion, N.; de la Torre-Ruiz, M.A. The Cell Wall Integrity Receptor Mtl1 Contributes to Articulate Autophagic Responses When Glucose Availability Is Compromised. *J. Fungi* **2021**, *7*, 903. [CrossRef]
162. Yao, W.; Li, Y.; Chen, Y.; Chen, Y.; Zhao, P.; Zhang, Y.; Jiang, Q.; Feng, Y.; Yang, F.; Wu, C.; et al. Mec1 Regulates PAS Recruitment of Atg13 via Direct Binding with Atg13 during Glucose Starvation-Induced Autophagy. *Proc. Natl. Acad. Sci. USA* **2023**, *120*, e2215126120. [CrossRef]
163. Yi, C.; Tong, J.; Lu, P.; Wang, Y.; Zhang, J.; Sun, C.; Yuan, K.; Xue, R.; Zou, B.; Li, N.; et al. Formation of a Snf1-Mec1-Atg1 Module on Mitochondria Governs Energy Deprivation-Induced Autophagy by Regulating Mitochondrial Respiration. *Dev. Cell* **2017**, *41*, 59–71.e4. [CrossRef] [PubMed]
164. Bartholomew, C.R.; Suzuki, T.; Du, Z.; Backues, S.K.; Jin, M.; Lynch-Day, M.A.; Umekawa, M.; Kamath, A.; Zhao, M.; Xie, Z.; et al. Ume6 Transcription Factor Is Part of a Signaling Cascade That Regulates Autophagy. *Proc. Natl. Acad. Sci. USA* **2012**, *109*, 11206–11210. [CrossRef] [PubMed]
165. Bernard, A.; Jin, M.; González-Rodríguez, P.; Füllgrabe, J.; Delorme-Axford, E.; Backues, S.K.; Joseph, B.; Klionsky, D.J. Rph1/KDM4 Mediates Nutrient-Limitation Signaling That Leads to the Transcriptional Induction of Autophagy. *Curr. Biol.* **2015**, *25*, 546–555. [CrossRef] [PubMed]
166. Lei, Y.; Huang, Y.; Wen, X.; Yin, Z.; Zhang, Z.; Klionsky, D.J. How Cells Deal with the Fluctuating Environment: Autophagy Regulation under Stress in Yeast and Mammalian Systems. *Antioxidants* **2022**, *11*, 304. [CrossRef] [PubMed]
167. Vlahakis, A.; Lopez Muniozguren, N.; Powers, T. Stress-Response Transcription Factors Msn2 and Msn4 Couple TORC2-Ypk1 Signaling and Mitochondrial Respiration to ATG8 Gene Expression and Autophagy. *Autophagy* **2017**, *13*, 1804–1812. [CrossRef]

168. Mizuno, T.; Irie, K. Msn2/4 Transcription Factors Positively Regulate Expression of Atg39 ER-Phagy Receptor. *Sci. Rep.* **2021**, *11*, 11919. [CrossRef]
169. DeMille, D.; Badal, B.D.; Evans, J.B.; Mathis, A.D.; Anderson, J.F.; Grose, J.H. PAS Kinase Is Activated by Direct SNF1-Dependent Phosphorylation and Mediates Inhibition of TORC1 through the Phosphorylation and Activation of Pbp1. *Mol. Biol. Cell* **2015**, *26*, 569–582. [CrossRef]
170. Ebrahimi, M.; Habernig, L.; Broeskamp, F.; Aufschnaiter, A.; Diessl, J.; Atienza, I.; Matz, S.; Ruiz, F.A.; Büttner, S. Phosphate Restriction Promotes Longevity via Activation of Autophagy and the Multivesicular Body Pathway. *Cells* **2021**, *10*, 3161. [CrossRef]
171. Yang, Z.; Geng, J.; Yen, W.-L.; Wang, K.; Klionsky, D.J. Positive or Negative Roles of Different Cyclin-Dependent Kinase Pho85-Cyclin Complexes Orchestrate Induction of Autophagy in Saccharomyces Cerevisiae. *Mol. Cell* **2010**, *38*, 250–264. [CrossRef]
172. Fabrizio, P.; Pletcher, S.D.; Minois, N.; Vaupel, J.W.; Longo, V.D. Chronological Aging-Independent Replicative Life Span Regulation by Msn2/Msn4 and Sod2 in Saccharomyces Cerevisiae. *FEBS Lett.* **2004**, *557*, 136–142. [CrossRef] [PubMed]
173. Kaeberlein, M.; Powers, R.W.; Steffen, K.K.; Westman, E.A.; Hu, D.; Dang, N.; Kerr, E.O.; Kirkland, K.T.; Fields, S.; Kennedy, B.K. Regulation of Yeast Replicative Life Span by TOR and Sch9 in Response to Nutrients. *Science* **2005**, *310*, 1193–1196. [CrossRef]
174. Mirisola, M.G.; Taormina, G.; Fabrizio, P.; Wei, M.; Hu, J.; Longo, V.D. Serine- and Threonine/Valine-Dependent Activation of PDK and Tor Orthologs Converge on Sch9 to Promote Aging. *PLoS Genet.* **2014**, *10*, e1004113. [CrossRef] [PubMed]
175. Lyu, Z.; Gao, X.; Wang, W.; Dang, J.; Yang, L.; Yan, M.; Ali, S.A.; Liu, Y.; Liu, B.; Yu, M.; et al. MTORC1-Sch9 Regulates Hydrogen Sulfide Production through the Transsulfuration Pathway. *Aging* **2019**, *11*, 8418–8432. [CrossRef] [PubMed]
176. Picazo, C.; Orozco, H.; Matallana, E.; Aranda, A. Interplay among Gcn5, Sch9 and Mitochondria during Chronological Aging of Wine Yeast Is Dependent on Growth Conditions. *PLoS ONE* **2015**, *10*, e0117267. [CrossRef]
177. Santos, J.; Leitão-Correia, F.; Sousa, M.J.; Leão, C. Ammonium Is a Key Determinant on the Dietary Restriction of Yeast Chronological Aging in Culture Medium. *Oncotarget* **2015**, *6*, 6511–6523. [CrossRef]
178. Wu, Z.; Liu, S.Q.; Huang, D. Dietary Restriction Depends on Nutrient Composition to Extend Chronological Lifespan in Budding Yeast Saccharomyces Cerevisiae. *PLoS ONE* **2013**, *8*, e64448. [CrossRef]
179. Fabrizio, P.; Gattazzo, C.; Battistella, L.; Wei, M.; Cheng, C.; McGrew, K.; Longo, V.D. Sir2 Blocks Extreme Life-Span Extension. *Cell* **2005**, *123*, 655–667. [CrossRef]
180. Kennedy, B.K.; Smith, E.D.; Kaeberlein, M. The Enigmatic Role of Sir2 in Aging. *Cell* **2005**, *123*, 548–550. [CrossRef]
181. Longo, V.D.; Finch, C.E. Evolutionary Medicine: From Dwarf Model Systems to Healthy Centenarians? *Science* **2003**, *299*, 1342–1346. [CrossRef]
182. Pedruzzi, I.; Bürckert, N.; Egger, P.; De Virgilio, C. Saccharomyces Cerevisiae Ras/CAMP Pathway Controls Post-Diauxic Shift Element-Dependent Transcription through the Zinc Finger Protein Gis1. *EMBO J.* **2000**, *19*, 2569–2579. [CrossRef] [PubMed]
183. Bitterman, K.J.; Medvedik, O.; Sinclair, D.A. Longevity Regulation in Saccharomyces Cerevisiae: Linking Metabolism, Genome Stability, and Heterochromatin. *Microbiol. Mol. Biol. Rev. MMBR* **2003**, *67*, 376–399. [CrossRef]
184. Fabrizio, P.; Liou, L.-L.; Moy, V.N.; Diaspro, A.; Valentine, J.S.; Gralla, E.B.; Longo, V.D. SOD2 Functions Downstream of Sch9 to Extend Longevity in Yeast. *Genetics* **2003**, *163*, 35–46. [CrossRef] [PubMed]
185. Pascual-Ahuir, A.; Proft, M. The Sch9 Kinase Is a Chromatin-Associated Transcriptional Activator of Osmostress-Responsive Genes. *EMBO J.* **2007**, *26*, 3098–3108. [CrossRef]
186. Piper, P.W.; Harris, N.L.; MacLean, M. Preadaptation to Efficient Respiratory Maintenance Is Essential Both for Maximal Longevity and the Retention of Replicative Potential in Chronologically Ageing Yeast. *Mech. Ageing Dev.* **2006**, *127*, 733–740. [CrossRef]
187. Bonawitz, N.D.; Chatenay-Lapointe, M.; Pan, Y.; Shadel, G.S. Reduced TOR Signaling Extends Chronological Life Span via Increased Respiration and Upregulation of Mitochondrial Gene Expression. *Cell Metab.* **2007**, *5*, 265–277. [CrossRef]
188. Lavoie, H.; Whiteway, M. Increased Respiration in the Sch9Delta Mutant Is Required for Increasing Chronological Life Span but Not Replicative Life Span. *Eukaryot. Cell* **2008**, *7*, 1127–1135. [CrossRef] [PubMed]
189. Cowart, L.A.; Shotwell, M.; Worley, M.L.; Richards, A.J.; Montefusco, D.J.; Hannun, Y.A.; Lu, X. Revealing a Signaling Role of Phytosphingosine-1-Phosphate in Yeast. *Mol. Syst. Biol.* **2010**, *6*, 349. [CrossRef] [PubMed]
190. Ludovico, P.; Burhans, W.C. Reactive Oxygen Species, Ageing and the Hormesis Police. *FEMS Yeast Res.* **2014**, *14*, 33–39. [CrossRef]
191. Mesquita, A.; Weinberger, M.; Silva, A.; Sampaio-Marques, B.; Almeida, B.; Leão, C.; Costa, V.; Rodrigues, F.; Burhans, W.C.; Ludovico, P. Caloric Restriction or Catalase Inactivation Extends Yeast Chronological Lifespan by Inducing H_2O_2 and Superoxide Dismutase Activity. *Proc. Natl. Acad. Sci. USA* **2010**, *107*, 15123–15128. [CrossRef]
192. Pan, Y. Mitochondria, Reactive Oxygen Species, and Chronological Aging: A Message from Yeast. *Exp. Gerontol.* **2011**, *46*, 847–852. [CrossRef] [PubMed]
193. Oh, S.; Suganuma, T.; Gogol, M.M.; Workman, J.L. Histone H3 Threonine 11 Phosphorylation by Sch9 and CK2 Regulates Chronological Lifespan by Controlling the Nutritional Stress Response. *eLife* **2018**, *7*, e36157. [CrossRef] [PubMed]
194. Madia, F.; Gattazzo, C.; Wei, M.; Fabrizio, P.; Burhans, W.C.; Weinberger, M.; Galbani, A.; Smith, J.R.; Nguyen, C.; Huey, S.; et al. Longevity Mutation in SCH9 Prevents Recombination Errors and Premature Genomic Instability in a Werner/Bloom Model System. *J. Cell Biol.* **2008**, *180*, 67–81. [CrossRef] [PubMed]
195. Fabrizio, P.; Battistella, L.; Vardavas, R.; Gattazzo, C.; Liou, L.-L.; Diaspro, A.; Dossen, J.W.; Gralla, E.B.; Longo, V.D. Superoxide Is a Mediator of an Altruistic Aging Program in Saccharomyces Cerevisiae. *J. Cell Biol.* **2004**, *166*, 1055–1067. [CrossRef]

196. Moreno-Torres, M.; Jaquenoud, M.; De Virgilio, C. TORC1 Controls G1-S Cell Cycle Transition in Yeast via Mpk1 and the Greatwall Kinase Pathway. *Nat. Commun.* **2015**, *6*, 8256. [CrossRef]
197. Moreno-Torres, M.; Jaquenoud, M.; Péli-Gulli, M.-P.; Nicastro, R.; De Virgilio, C. TORC1 Coordinates the Conversion of Sic1 from a Target to an Inhibitor of Cyclin-CDK-Cks1. *Cell Discov.* **2017**, *3*, 17012. [CrossRef]
198. Weinberger, M.; Mesquita, A.; Caroll, T.; Marks, L.; Yang, H.; Zhang, Z.; Ludovico, P.; Burhans, W.C. Growth Signaling Promotes Chronological Aging in Budding Yeast by Inducing Superoxide Anions That Inhibit Quiescence. *Aging* **2010**, *2*, 709–726. [CrossRef]
199. Zinzalla, V.; Graziola, M.; Mastriani, A.; Vanoni, M.; Alberghina, L. Rapamycin-Mediated G1 Arrest Involves Regulation of the Cdk Inhibitor Sic1 in Saccharomyces Cerevisiae. *Mol. Microbiol.* **2007**, *63*, 1482–1494. [CrossRef]
200. Hers, I.; Vincent, E.E.; Tavaré, J.M. Akt Signalling in Health and Disease. *Cell. Signal.* **2011**, *23*, 1515–1527. [CrossRef]
201. Liko, D.; Hall, M.N. MTOR in Health and in Sickness. *J. Mol. Med.* **2015**, *93*, 1061–1073. [CrossRef]
202. Carling, D. AMPK Signalling in Health and Disease. *Curr. Opin. Cell Biol.* **2017**, *45*, 31–37. [CrossRef] [PubMed]
203. Kitano, H. Biological Robustness. *Nat. Rev. Genet.* **2004**, *5*, 826–837. [CrossRef] [PubMed]
204. Friedlander, T.; Mayo, A.E.; Tlusty, T.; Alon, U. Evolution of Bow-Tie Architectures in Biology. *PLoS Comput. Biol.* **2015**, *11*, e1004055. [CrossRef] [PubMed]
205. Mayor, T.; Graumann, J.; Bryan, J.; MacCoss, M.J.; Deshaies, R.J. Quantitative Profiling of Ubiquitylated Proteins Reveals Proteasome Substrates and the Substrate Repertoire Influenced by the Rpn10 Receptor Pathway. *Mol. Cell. Proteom. MCP* **2007**, *6*, 1885–1895. [CrossRef]
206. Swaney, D.L.; Beltrao, P.; Starita, L.; Guo, A.; Rush, J.; Fields, S.; Krogan, N.J.; Villén, J. Global Analysis of Phosphorylation and Ubiquitylation Cross-Talk in Protein Degradation. *Nat. Methods* **2013**, *10*, 676–682. [CrossRef] [PubMed]
207. Gonzalez, E.; McGraw, T.E. The Akt Kinases: Isoform Specificity in Metabolism and Cancer. *Cell Cycle* **2009**, *8*, 2502–2508. [CrossRef]
208. Bos, J.L. *Molecular Mechanisms of Signal Transduction*; IOS Press: Amsterdam, The Netherlands, 2000; ISBN 978-1-58603-016-2.
209. González, A.; Shimobayashi, M.; Eisenberg, T.; Merle, D.A.; Pendl, T.; Hall, M.N.; Moustafa, T. TORC1 Promotes Phosphorylation of Ribosomal Protein S6 via the AGC Kinase Ypk3 in Saccharomyces Cerevisiae. *PLoS ONE* **2015**, *10*, e0120250. [CrossRef]
210. Yerlikaya, S.; Meusburger, M.; Kumari, R.; Huber, A.; Anrather, D.; Costanzo, M.; Boone, C.; Ammerer, G.; Baranov, P.V.; Loewith, R. TORC1 and TORC2 Work Together to Regulate Ribosomal Protein S6 Phosphorylation in Saccharomyces Cerevisiae. *Mol. Biol. Cell* **2016**, *27*, 397–409. [CrossRef]
211. Odorizzi, G.; Babst, M.; Emr, S.D. Phosphoinositide Signaling and the Regulation of Membrane Trafficking in Yeast. *Trends Biochem. Sci.* **2000**, *25*, 229–235. [CrossRef]
212. Fu, W.; Hall, M.N. Regulation of MTORC2 Signaling. *Genes* **2020**, *11*, 1045. [CrossRef]

Disclaimer/Publisher's Note: The statements, opinions and data contained in all publications are solely those of the individual author(s) and contributor(s) and not of MDPI and/or the editor(s). MDPI and/or the editor(s) disclaim responsibility for any injury to people or property resulting from any ideas, methods, instructions or products referred to in the content.

4. Crosstalk between the SNF1/AMPK and TORC1/mTORC1 signaling pathways

For the successful survival of cells, the activities of SNF1/AMPK and TORC1/mTORC1 must be well-coordinated. During stress conditions, such as nutrient depletion, the TORC1 signaling pathway needs to be inhibited to conserve energy, while SNF1 should be activated (Gonzalez et al., 2020). On the contrary, in nutrient-rich conditions, cell growth and proliferation should proceed rapidly, necessitating the activation of TORC1 and the repression of SNF1 to prevent catabolism and stress response activation (Gonzalez et al., 2020). Therefore, a finely tuned crosstalk between SNF1 and TORC1, at both upstream and downstream levels, is essential.

4.1. SNF1/AMPK regulation of TORC1/mTORC1

In human cells, AMPK inhibits mTORC1 through two distinct mechanisms (Gonzalez et al., 2020). First, AMPK directly phosphorylates Raptor on Ser^{722} and Ser^{792} (**Figure 10**), leading to the inhibition of the complex, by promoting Raptor association with 14-3-3 proteins and impairing the mTORC1 recruitment to the Rag GTPases (Gonzalez et al., 2020; Gwinn et al., 2008; Ramirez Reyes et al., 2021; Van Nostrand et al., 2020). Interestingly, Ser^{792} is highly conserved across eukaryotes, including *Drosophila melanogaster*, *Schizosaccharomyces pombe*, *Caenorhabditis elegans*, and *Saccharomyces cerevisiae* (Gonzalez et al., 2020; Gwinn et al., 2008). In budding yeast, Ser^{792} corresponds to Kog1-Ser^{959}, but phosphorylation at this site does not affect TORC1 activity (Gonzalez et al., 2020; Kawai et al., 2011). Second, AMPK phosphorylates TSC2 on Thr^{1271} and Ser^{1387}, thereby activating the TSC complex (**Figure 10**) (Gonzalez et al., 2020; Inoki et al., 2003b; Mihaylova & Shaw, 2011; Shaw et al., 2004; Van Nostrand et al., 2020). This activation inhibits Rheb and consequently prevents mTORC1 activation (**Figure 10**) (Gonzalez et al., 2020; Inoki et al., 2003b; Mihaylova & Shaw, 2011). Sestrin1/2 are involved in this process, as their expression is induced in response to genotoxic stress, forming a large protein complex with AMPK, TSC1, and TSC2, which facilitates AMPK-dependent TSC2 phosphorylation (**Figure 10**) (Budanov & Karin, 2008). Rheb and this pathway are primarily regulated by hormones and growth factors and are not conserved in yeast (Gonzalez et al., 2020). In yeast cells, a Rheb-like protein (Rhb1; RHeB homolog 1) is expressed, but it has not yet been shown to activate TORC1 (Tatebe & Shiozaki, 2017). Additionally, TSC1 and TSC2 do not have orthologs in *S. cerevisiae* (Tatebe & Shiozaki, 2017).

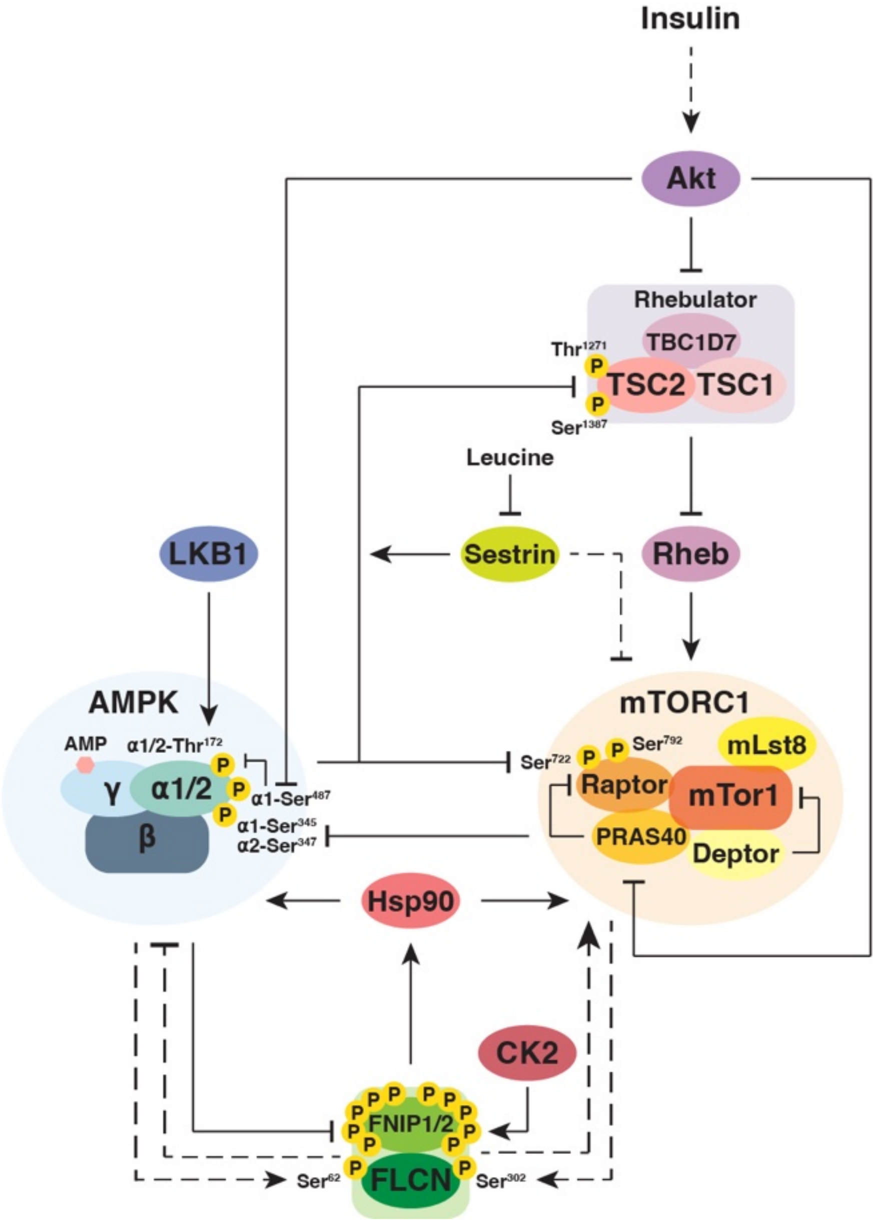
Insulin
Akt
Rhebulator
TBC1D7
Thr1271
P
TSC2
TSC1
P
Ser1387
Leucine
LKB1
Sestrin
Rheb
AMPK
AMP
α1/2-Thr172
P
γ
α1/2
P
α1-Ser487
P
α1-Ser345
α2-Ser347
β
mTORC1
Ser722
P
P
Ser792
mLst8
Raptor
mTor1
PRAS40
Deptor
Hsp90
CK2
P P P P
P P
FNIP1/2
P P
P P
P
FLCN
P
Ser62
Ser302

Figure 11. Scheme depicting the crosstalk between AMPK and mTORC1 in mammalian cells. The crosstalk between AMPK and mTORC1 happens at different layers, through reciprocal phosphorylation of members of the kinase complex or upstream regulators. For more details, refer to the text.

In mammalian cells, the scaffold protein AXIN1 acts as an adaptor that promotes LKB1 binding to AMPK and its phosphorylation (Gonzalez et al., 2020; Hindupur et al., 2015; Mallick & Gupta, 2021). AXIN1 interacts with and inhibits LAMTOR1 (Gonzalez et al., 2020; Hindupur et al., 2015; Mallick & Gupta, 2021). A proposed model suggests that AXIN1, localized at the lysosomal membrane via binding to the Ragulator complex, can recruit LKB1, promoting AMPK activation in this subcellular region and increasing the likelihood of mTORC1 inhibition (Gonzalez et al., 2020; Hindupur et al., 2015).

AMPK interacts with and phosphorylates FNIP1 at five sites (Ser^{220}, Ser^{230}, Ser^{232}, Ser^{261}, and Ser^{593}), inhibiting the activity of the FLCN-FNIP1 complex and promoting the GTP-bound state of RagC (Baba et al., 2006; Malik et al., 2023). This phosphorylation event leads to the dissociation of mTORC1 from the Rag GTPases (Betz & Hall, 2013; Demetriades et al., 2014; Sancak et al., 2010), preventing mTORC1 from phosphorylating TFEB (Cui et al., 2023; Malik et al., 2023; Napolitano et al., 2018; Roczniak-Ferguson et al., 2012). Consequently, AMPK phosphorylation of FNIP1 allows TFEB to promote lysosomal and mitochondrial biogenesis (Malik et al., 2023; Mihaylova & Shaw, 2011; Perera et al., 2019; Trefts & Shaw, 2021). When AMPK is active, TFEB is dephosphorylated and translocates to the nucleus (Malik et al., 2023). However, in cells with the 5 serine-to-alanine (SA5) mutations of the AMPK target residues in FNIP1, TFEB remains phosphorylated in an mTORC1-dependent manner (Malik et al., 2023; Napolitano et al., 2018; Roczniak-Ferguson et al., 2012). Although AMPK activation decreases mTORC1 signaling to S6K1 and 4E-BP1 in SA5-FNIP1 cells, TFEB remains constitutively phosphorylated due to mTORC1's continued association with TFEB (Malik et al., 2023; Napolitano et al., 2018; Roczniak-Ferguson et al., 2012). AMPK activation causes RagC and mTORC1 to dissociate from the lysosome but strengthens the interaction between TFEB and RagC (Malik et al., 2023). This suggests that RagC may help transport TFEB from the lysosome to the nucleus (Malik et al., 2023). Additionally, AMPK activation, through TFEB, upregulates PGC1α expression, thereby increasing the expression of genes involved in lysosomal and mitochondrial functions (Malik et al., 2023).

Although SNF1 does not phosphorylate Kog1 on the conserved residue Ser^{959} in yeast (Gonzalez et al., 2020; Kawai et al., 2011), it phosphorylates Kog1 on Ser^{491} and Ser^{494} during glucose or nitrogen starvation (Hughes Hallett et al., 2015). These phosphorylation events promote the formation of TORC1-bodies at the edge of the vacuole (Hughes Hallett et al., 2015; Sullivan et al., 2019). TORC1-body formation is a slow process but ensures TORC1 inhibition by increasing the reactivation threshold (Hughes Hallett et al., 2015; Sullivan et al., 2019). Since a *snf1Δ* strain shows a defect in Sch9 dephosphorylation after 5-10 minutes of starvation, while a *kog1*^{S491A,S494A} strain does not exhibit this phenotype, short-term TORC1 inhibition likely does not require Kog1 phosphorylation at Ser^{491} and Ser^{494}, as TORC1-body formation is a slow step in TORC1 inhibition (Hughes Hallett et al., 2015; Sullivan et al., 2019).

A different TORC1 structure, known as TOROIDs (TORC1 Organized in Inhibited Domains), forms during carbon starvation in a SNF1-independent manner (Prouteau et al., 2023; Prouteau et al., 2017). TOROIDs form within minutes of carbon starvation and disassemble 10 minutes after glucose readdition (Prouteau et al., 2017). TORC1 oligomerization in TOROIDs leads to allosteric obstruction of the active site and consequent

TORC1 inhibition (Prouteau et al., 2017). Additionally, the formation of these foci is promoted by the inactive conformation of the Rag GTPases (Gtr1^{GDP}/Gtr2^{GTP}), with the entire EGOC involved in TOROIDs formation (Prouteau et al., 2023; Prouteau et al., 2017).

Finally, phosphoproteomic analysis in *S. cerevisiae* indicated that SNF1 may influence the TORC1 signaling pathway at various levels (Braun et al., 2014; Kanshin et al., 2017). Although SNF1-dependent phosphorylation of TORC1-related proteins has been observed, further research is needed to elucidate the specific mechanisms triggering TORC1 inactivation upon SNF1 activation.

4.2. TORC1/mTORC1 regulation of SNF1/AMPK

In *S. pombe*, Ssp2, the ortholog of Snf1, is inhibited by direct TORC1 phosphorylation (Ling et al., 2020). Normally, after nutrient depletion, Ssp2 is phosphorylated on Thr^{189}, a residue functionally corresponding to Thr^{210} in *S. cerevisiae* Snf1 (Davie et al., 2015; Ling et al., 2020). This phosphorylation event is independent of the AMP/ATP ratio and occurs in response to stress and glucose or nitrogen starvation (Davie et al., 2015; Ling et al., 2020), similar to budding yeast (Crute et al., 1998; Hong & Carlson, 2007). Interestingly, active TORC1 phosphorylates Ssp2 at Ser^{367}, impairing Thr^{189} phosphorylation and consequently Ssp2 activity (Ling et al., 2020). On the contrary, the Ser^{367}-to-Ala mutant shows increased Thr^{189} phosphorylation (Ling et al., 2020). Ser^{367} is conserved across eukaryotes and corresponds to Snf1-Ser^{413} in *S. cerevisiae* and AMPKα1-Ser^{347} and AMPKα2-Ser^{345} in *H. sapiens* (Ling et al., 2020). Indeed, this direct mTORC1 inhibition of AMPK has been observed in mammalian cell lines (**Figure 11**) (Ling et al., 2020).

Insulin is a potent activator of the mTORC1 signaling pathway (Gonzalez & Hall, 2017; Gonzalez et al., 2020; Yoon, 2017). Interestingly, Akt activation in response to insulin leads to AMPK inactivation (**Figure 11**) (Hardie & Ashford, 2014). Active Akt phosphorylates and inhibits the AMPKα1 subunit on Ser^{487}, but not AMPKα2-Ser^{491} (**Figure 11**) (Hawley et al., 2014), which reduces Thr^{172} phosphorylation by LKB1 (Hardie & Ashford, 2014). Previously, AMPKα2-Ser^{491} was shown to be phosphorylated by S6K (Dagon et al., 2012), but rapamycin treatment did not cause differences in AMPKα1-Ser^{487} and AMPKα2-Ser^{491} phosphorylation, demonstrating that it cannot be caused by mTORC1 downstream effectors (Hardie & Ashford, 2014). This event prevents AMPK-dependent inhibition of mTORC1 (Hardie & Ashford, 2014).

In mammalian cells, the regulation of the AMPK pathway by mTORC1 involves the FLCN-FNIP1/2 complex (de Martin Garrido & Aylett, 2020; Ramirez Reyes et al., 2021). FNIP1 and FNIP2 C-terminal domains can interact with AMPK *in vitro* independently of FLCN (Baba et al., 2006; de Martin Garrido & Aylett, 2020; Ramirez Reyes et al., 2021). FLCN knockout results in constitutive AMPK activation, while mutations in FNIP1 increase AMPK activity (**Figure 11**) (de Martin Garrido & Aylett, 2020; Ramirez Reyes et al., 2021). Even though the FLCN-FNIP1/2 reglation mechanism of AMPK is not yet clear, a possible explanation is that, upon FLCN-FNIP1/2 loss, the reduction in mTORC1 activity causes increased AMPK activation (Ramirez Reyes et al., 2021). Moreover, AMPK and mTORC1 directly or indirectly phosphorylate FLCN at Ser^{62} and Ser^{302}, respectively (**Figure 11**) (Piao et al., 2009; Ramirez Reyes et al., 2021; Wang et al., 2010). The former phosphorylation causes increased FLCN binding to AMPK, while the latter has the opposite effect (Baba et al., 2006; Ramirez Reyes et al., 2021). Interestingly, CK2-dependent phosphorylation of FNIP1 enhances its interaction with the chaperone Hsp90 (de Martin Garrido & Aylett, 2020; Ramirez Reyes et al., 2021; Sager et al., 2018). Thus, FNIP1 acts as a co-chaperone, by recruiting Hsp90 which guarantees the correct folding of AMPK subunits, mTOR, and Raptor, suggesting an additional layer of regulation by FNIP1 (de Martin Garrido & Aylett, 2020; Ramirez Reyes et al., 2021; Sager et al., 2018).

4.3. SNF1 and TORC1 converge on common targets in budding yeast

The SNF1 and TORC1 signaling pathways intersect to regulate amino acid uptake, stress response, and autophagy.

The transcription factor Gln3's localization and activity are differentially controlled by SNF1 and TORC1 (**Figure 12**). SNF1 promotes Gln3's nuclear localization and activation through direct phosphorylation, enhancing the expression of genes necessary for growth on non-preferential nitrogen sources (Bertram et al., 2002; Hedbacker & Carlson, 2008). On the contrary, TORC1 phosphorylates Gln3, causing its retention in the cytosol and inhibition (De Virgilio & Loewith, 2006b).

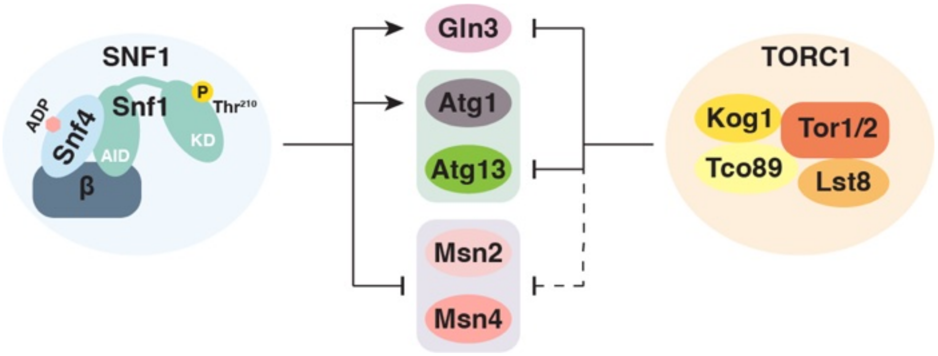

Figure 12. Scheme depicting the common effectors of SNF1 and TORC1.

SNF1 phosphorylates and activates Gln3 and Atg1, unlike TORC1, which inhibits Gln3 and Atg13. Both SNF1 and TORC1 converge on Msn2/4, leading to their inhibition. For more details, refer to the text.

SNF1 and TORC1 play opposing roles in autophagy regulation. SNF1 promotes autophagy by directly phosphorylating and activating Atg1 (**Figure 12**) (Adachi et al., 2017; Wang et al., 2001; Yi et al., 2017). In contrast, when nitrogen and amino acid levels are high, TORC1 phosphorylates Atg13, which inhibits the Atg1 kinase complex (Hatakeyama et al., 2019; Hu et al., 2019; Noda, 2017). Similarly, in mammalian cells, AMPK phosphorylates and activates ULK1, thereby inducing autophagy (Mihaylova & Shaw, 2011; Sadria et al., 2022). On the other hand, mTORC1 phosphorylates ULK1 at different sites, which leads to its inhibition and the downregulation of autophagy (Kim et al., 2011; Mihaylova & Shaw, 2011; Sadria et al., 2022).

Interestingly, SNF1 and TORC1 similarly regulate the stress response through the transcription factors Msn2/4 (**Figure 12**). Because the transcription of STRE-driven genes is not required during long-term adaptation to carbon starvation, SNF1-mediated phosphorylation promotes the cytosolic localization of Msn2/4 under these conditions (De Wever et al., 2005; Hedbacker & Carlson, 2008; Mayordomo et al., 2002; Petrenko et al., 2013). Similarly, in nutrient-rich conditions, TORC1 indirectly downregulates the stress response (Cameroni et al., 2004; Pedruzzi et al., 2003; Swinnen et al., 2014). TORC1 activates Sch9 (Urban et al., 2007), which phosphorylates and thereby promotes the cytosolic localization of the Rim15 protein kinase. Since Rim15 can only activate Msn2/4 when it is nuclear, the TORC1-Sch9 axis indirectly also downregulates the stress response (Cameroni et al., 2004; Pedruzzi et al., 2003; Swinnen et al., 2014).

CHAPTER 1:

Snf1/AMPK fine-tunes TORC1 signaling in response to glucose starvation

1. Introduction

The eukaryotic target of rapamycin complex 1 (TORC1/mTORC1) signaling pathway is a crucial regulator that integrates growth signals with metabolic pathways to control cell growth. TORC1 activity is positively influenced by intracellular nutrients, high energy levels, and extracellular growth factors such as insulin and IGF-1. This activation promotes cellular mass increase by stimulating lipid, nucleotide, and protein synthesis while inhibiting autophagy (Albert & Hall, 2015; Gonzalez & Hall, 2017; Laplante & Sabatini, 2012; Liu & Sabatini, 2020). TORC1 operates within complex feedback loops, and the disruption of its regulation is linked to altered lifespan in yeast and diseases like cancer, immunodeficiency, type 2 diabetes, and neurodegeneration in humans (Laplante and Sabatini, 2012).

AMPK, a key energy regulator, inactivates mTORC1 by phosphorylating TSC2, activating the Rheb GAP complex (Inoki et al., 2003a; Shaw et al., 2004). AMPK and its yeast counterpart SNF1 are activated by phosphorylation and regulate mTORC1/TORC1 through different mechanisms (Gonzalez et al., 2020; Hedbacker & Carlson, 2008). SNF1 also maintains TORC1 inactivity during glucose starvation through promoting the formation of TORC1-bodies during prolonged glucose starvation (Hughes Hallett et al., 2015; Sullivan et al., 2019).

To address how SNF1 contributes to TORC1 inhibition following glucose starvation, we used a yeast strain with an analog-sensitive (*snf1*^{as}) allele that can be conditionally inactivated Snf1 by the ATP-analog 2NM-PP1 and applied mass spectrometry-based phosphoproteomics strategies, both *in vivo* and *in vitro*. This approach identified numerous SNF1-dependent phosphorylation events and potential SNF1 targets within the TORC1 pathway. Genetic, biochemical, and physiological experiments revealed that SNF1 maintains TORC1 inactivity in glucose-starved cells primarily through the regulatory protein Pib2. Additionally, SNF1 phosphorylates the TORC1 effector kinase Sch9, counteracting its activation. These phosphorylation events by SNF1 are additive and crucial for the appropriate short-term response of TORC1 to acute glucose starvation.

2. Key contributions of this chapter

- **Figure 1**. Snf1 is required for proper downregulation of TORC1 in glucose-starved cells. Panels A to F.
- **Figure 1-figure supplement 1**. Specificity of 2NM-PP1and differential Snf1 activation upon nitrogen and carbon starvation. Panels A to C.
- **Figure 2**. Snf1 prevents transient TORC1 restimulation by glutamine in glucose- and glutamine-starved cells. Panels A to F.
- **Figure 3**. Quantitative phosphoproteomic analyses for the identification of potential Snf1 target sites. Panel A – OBIKA kinases and proteome purifications.
- **Figure 3-figure supplement 1**. Specific motif analyses of Snf1 phosphosites and role of Lst4 in TORC1 reactivation in glucose-starved, Snf1-inhibited cells. Panel C.
- **Figure 4**. Snf1 weakens the Pib2-Kog1 association by phosphorylating Pib2-Ser^{268,309}. Panels A to I.
- **Figure 5**. Snf1 phosphorylates Sch9-Ser^{288} to antagonize Sch9-Thr^{737} phosphorylation. Panels A to G.
- **Figure 5-figure supplement 1**. Snf1 *in* vitro kinase assays.
- **Figure 6**. Physiological effects of Sch9^{S288E} and Pib2^{S268E,S309E} are additive. Panels A to E.

Snf1/AMPK fine-tunes TORC1 signaling in response to glucose starvation

Marco Caligaris[1], Raffaele Nicastro[1]*, Zehan Hu[1], Farida Tripodi[2], Johannes Erwin Hummel[3], Benjamin Pillet[1], Marie-Anne Deprez[4], Joris Winderickx[4], Sabine Rospert[3,5], Paola Coccetti[2], Jörn Dengjel[1], Claudio De Virgilio[1]*

[1]Department of Biology, University of Fribourg, Fribourg, Switzerland; [2]Department of Biotechnology and Biosciences, University of Milano-Bicocca, Milano, Italy; [3]Institute of Biochemistry and Molecular Biology, Faculty of Medicine, University of Freiburg, Freiburg, Germany; [4]Functional Biology, KU Leuven, Heverlee, Belgium; [5]Signalling Research Centres BIOSS and CIBSS, University of Freiburg, Freiburg, Germany

Abstract The AMP-activated protein kinase (AMPK) and the target of rapamycin complex 1 (TORC1) are central kinase modules of two opposing signaling pathways that control eukaryotic cell growth and metabolism in response to the availability of energy and nutrients. Accordingly, energy depletion activates AMPK to inhibit growth, while nutrients and high energy levels activate TORC1 to promote growth. Both in mammals and lower eukaryotes such as yeast, the AMPK and TORC1 pathways are wired to each other at different levels, which ensures homeostatic control of growth and metabolism. In this context, a previous study (Hughes Hallett et al., 2015) reported that AMPK in yeast, that is Snf1, prevents the transient TORC1 reactivation during the early phase following acute glucose starvation, but the underlying mechanism has remained elusive. Using a combination of unbiased mass spectrometry (MS)-based phosphoproteomics, genetic, biochemical, and physiological experiments, we show here that Snf1 temporally maintains TORC1 inactive in glucose-starved cells primarily through the TORC1-regulatory protein Pib2. Our data, therefore, extend the function of Pib2 to a hub that integrates both glucose and, as reported earlier, glutamine signals to control TORC1. We further demonstrate that Snf1 phosphorylates the TORC1 effector kinase Sch9 within its N-terminal region and thereby antagonizes the phosphorylation of a C-terminal TORC1-target residue within Sch9 itself that is critical for its activity. The consequences of Snf1-mediated phosphorylation of Pib2 and Sch9 are physiologically additive and sufficient to explain the role of Snf1 in short-term inhibition of TORC1 in acutely glucose-starved cells.

Editor's evaluation

This rigorous and careful study provides some of the first mechanistic insights into the way that glucose starvation triggers inhibition of TORC1 (particularly in yeast) and will serve as an important resource for those interested in AMPK/Snf1 dependent regulation of a variety of other pathways and processes. The paper also provides the clearest picture yet of the regulation of Pib2, an important but poorly understood TORC1 regulator in yeast and likely beyond. The proposed mechanism is interesting and proposes multiple ways of interaction between the two signaling cascades, and will be of interest to researchers working on mechanisms of gene regulation by signaling pathways.

***For correspondence:** Raffaele.Nicastro2@unifr.ch (RN); Claudio.DeVirgilio@unifr.ch (CDV)

Competing interest: The authors declare that no competing interests exist.

Funding: See page 21

Preprinted: 18 October 2022
Received: 25 October 2022
Accepted: 06 February 2023
Published: 07 February 2023

Reviewing Editor: Kevin Struhl, Harvard Medical School, United States

© Copyright Caligaris *et al.* This article is distributed under the terms of the Creative Commons Attribution License, which permits unrestricted use and redistribution provided that the original author and source are credited.

Introduction

The eukaryotic target of rapamycin complex 1 (TORC1/mTORC1) signaling pathway serves as a central hub that couples growth signals with metabolic circuits that define cell growth. The TORC1 protein kinase activity is positively regulated by intracellular nutrients (*e.g.*, amino acids, glucose, and lipids), high energy levels, as well as extracellular growth factors (e.g. insulin and insulin-like growth factor 1 [IGF-1]). In response to these cues, it favors the increase of cellular mass by stimulating lipid, nucleotide, and protein synthesis and by inhibiting the autophagic recycling of macromolecules (***Albert and Hall, 2015***; ***González and Hall, 2017***; ***Laplante and Sabatini, 2012***; ***Liu and Sabatini, 2020***). TORC1 function is embedded in as yet incompletely understood feedback loops, allowing it to act as a metabolic rheostat. Uncoupling TORC1 from this regulatory network is associated with dramatically altered lifespan in unicellular organisms such as yeast and with diseases such as cancer, immunodeficiency, type 2 diabetes, and neurodegeneration in humans (***Laplante and Sabatini, 2012***).

The core structure of TORC1 is highly conserved among eukaryotes and consists of a dimer of a heterotrimeric complex that harbors a TOR serine/threonine protein kinase (Tor1 or Tor2 in the budding yeast *Saccharomyces cerevisiae* or mTOR in mammals) and two regulatory proteins (yeast Kog1 and Lst8, or the orthologous mammalian Raptor [regulatory-associated protein of mTOR] and LST8 [mLST8], respectively ***Wullschleger et al., 2006***). Additional non-conserved proteins, such as Tco89 in yeast or the proline-rich Akt substrate of 40 kDa (PRAS40) and the DEP domain-containing mTOR- interacting protein (DEPTOR) in mammals, associate with this core complex to adapt its function to species-specific requirements (***Loewith et al., 2002***; ***Peterson et al., 2009***; ***Reinke et al., 2004***; ***Sancak et al., 2007***). TORC1 mainly functions at the vacuolar/lysosomal surface both in lower eukaryotes like the yeast *S. cerevisiae* as well as in higher eukaryotes such as *Drosophila* and mammals. At this location, TORC1 binds to and/or is regulated by the conserved heterodimeric Rag GTPases (i.e. yeast Gtr1 bound to Gtr2, or mammalian RagA or B bound to RagC or D). These heterodimers associate with structurally conserved protein complexes coined the EGO (exit from rapamycin-induced growth arrest) ternary complex in yeast (EGO-TC; comprising Ego1/Mhe1, Ego2, and Ego3/Slm4) or the pentameric Ragulator complex in mammals (comprising p18, p14, MP1, C7orf59, and HBXIP) (***Bar-Peled et al., 2012***; ***Dubouloz et al., 2005***; ***Powis et al., 2015***; ***Sancak et al., 2010***). The complexes are anchored to vacuolar/lysosomal membranes through N-terminally lipidated Ego1 or p18, respectively (***Binda et al., 2009***; ***Nada et al., 2009***; ***Powis et al., 2015***; ***Sancak et al., 2010***). The Rag GTPases adopt one of two stable conformations, an active state in which Gtr1 or RagA/B is bound to GTP and Gtr2 or RagC/D to GDP, and an inactive state with the opposite GTP/GDP-loading configuration. The respective nucleotide-loading states are primarily preserved by crosstalk between the Rag GTPases and are regulated via a set of conserved GTPase activating (GAP) protein complexes (i.e. yeast SEACIT/mammalian GATOR1 and yeast Lst4-Lst7/mammalian FNIP-FLCN acting on Gtr1/RagA/B and Gtr2/RagC/D, respectively ***Bar-Peled et al., 2013***; ***Panchaud et al., 2013a***; ***Panchaud et al., 2013b***; ***Péli-Gulli et al., 2015***; ***Petit et al., 2013***; ***Shen et al., 2017***; ***Tsun et al., 2013***), which mediate cytosolic and/or vacuolar/lysosomal amino acid levels through different mechanisms (***González and Hall, 2017***; ***Liu and Sabatini, 2020***; ***Nicastro et al., 2017***). Notably, in flies and mammals, but likely not in yeast (***Powis and De Virgilio, 2016***), the Rag-GTPase tethered, lysosome-associated TORC1 pool is also allosterically activated by the small GTPase Rheb (Ras homolog enriched in brain) in its GTP-bound form (***Anandapadamanaban et al., 2019***; ***Buerger et al., 2006***; ***Long et al., 2005***; ***Rogala et al., 2019***). Rheb responds, among other factors, to energy levels that are mainly integrated by the Rheb GAP complex (comprising TSC1, TSC2, and TBC1D7), which is also known as Rhebulator (***Demetriades et al., 2014***; ***Dibble et al., 2012***; ***Inoki et al., 2003a***; ***Long et al., 2005***; ***Tee et al., 2003***; ***Yang et al., 2017***). This mechanism relies on the AMP-activated protein kinase (AMPK), a key regulator of cellular energy charge that inactivates mTORC1 indirectly by phosphorylating TSC2 and thereby activating the GAP activity of Rhebulator (***Inoki et al., 2003b***; ***Shaw et al., 2004***).

AMPK functions within a conserved heterotrimeric complex encompassing a catalytic α subunit (yeast Snf1 or mammalian α1/2), and one of each β- (yeast Gal83, Sip1, and Sip2 or mammalian β1/2) and γ- (yeast Snf4 or mammalian γ1/2/3) regulatory subunits (***Carling, 2004***; ***Ghillebert et al., 2011***; ***Hedbacker and Carlson, 2008***). In line with its denomination, mammalian AMPK is allosterically activated by AMP. This seems not to be the case for Snf1, since the latter is mainly activated by the absence of glucose in the medium and since regulatory sites have been characterized that preferably bind ADP instead of AMP (***Coccetti et al., 2018***; ***Herzig and Shaw, 2018***; ***Mayer et al.,***

2011; **Wilson et al., 1996**). Nonetheless, both mammalian AMPK and yeast Snf1 are similarly activated by phosphorylation of a conserved threonine (Thr) within their activation loop (yeast Thr^{210} or mammalian Thr^{172}) that is executed by specific upstream kinases (yeast Sak1, Tos3, and Elm1 or mammalian LKB1 and CaMKK2) (**González et al., 2020**; **Hedbacker and Carlson, 2008**). In yeast, this phosphorylation event is reversed by the type I protein phosphatase Glc7 (combined with the regulatory subunit Reg1) specifically when extracellular glucose is sufficiently available (**Ludin et al., 1998**; **McCartney and Schmidt, 2001**). Both AMPK and Snf1 are also wired to control mTORC1/TORC1 via Raptor and Kog1, respectively, albeit through different mechanisms. Accordingly, AMPK has been reported to inhibit mTORC1 through direct phosphorylation of Raptor (**Gwinn et al., 2008**). Although one of the respective AMPK target residues in Raptor is conserved in Kog1, Snf1 does not control TORC1 through this residue (Ser^{959}; **Kawai et al., 2011**), but rather through phosphorylation of Ser^{491} and Ser^{494}, thereby promoting the formation of TORC1-bodies during prolonged glucose starvation (**Hughes Hallett et al., 2015**; **Sullivan et al., 2019**). Notably, the latter process is also regulated by Pib2, a phosphatidylinositol-3-phosphate (PI3P) and Kog1-binding protein that senses glutamine levels and that can both activate and inhibit TORC1 through its C-terminal and N-terminal domains, respectively (**Hatakeyama, 2021**; **Kim and Cunningham, 2015**; **Michel et al., 2017**; **Sullivan et al., 2019**; **Tanigawa and Maeda, 2017**; **Tanigawa et al., 2021**; **Troutman et al., 2022**; **Ukai et al., 2018**; **Varlakhanova et al., 2017**). Finally, Snf1 also plays a role in maintaining TORC1 inactive during the early phase following acute glucose starvation, which is independent of TORC1-body formation, but the underlying mechanism is still elusive (**Hughes Hallett et al., 2015**).

To address the outstanding question of how Snf1 contributes to TORC1 inhibition following glucose starvation, we used a yeast strain in which Snf1 can be conditionally inactivated by addition of the ATP-analog 2NM-PP1 and applied a mass spectrometry (MS)-based phosphoproteomics strategy that combines in vivo proteomics with on-beads in vitro kinase assays (OBIKA) to identify direct Snf1 target residues on a global scale. This approach not only allowed us to uncover the currently largest set of Snf1-dependent phosphorylation events in *S. cerevisiae*, but also pinpointed several potential Snf1 targets within the TORC1 signaling pathway. Employing genetic, biochemical, and physiological experiments, we demonstrate that Snf1 temporally maintains TORC1 inactive in glucose-starved cells primarily through the regulatory protein Pib2. In addition, Snf1 specifically phosphorylates the TORC1 effector kinase Sch9 and thereby antagonizes the phosphorylation of a C-terminal TORC1-target residue within Sch9 that is critical for its activity. The consequences of Snf1-mediated phosphorylation of Pib2 and Sch9 are physiologically additive and sufficient to mediate an appropriate short-term response of TORC1 to acute glucose starvation.

Results

Snf1 prevents transient reactivation of TORC1 in glucose-starved cells

To study how Snf1 contributes to the inhibition of TORC1 in glucose-starved cells, we used a strain in which the *SNF1* locus expresses the *snf1*^{I132G} -allele (Snf1^{as}) that is sensitive to the ATP-analog 2-naphthylmethyl pyrazolopyrimidine 1 (2NM-PP1) and that supports normal growth on sucrose or low glucose-containing media (**Shirra et al., 2008**; **Zaman et al., 2009**). In our control experiments, the Snf1^{as} allele was appropriately activated by its upstream protein kinases, as assessed by the rapid increase in Thr^{210} phosphorylation that was comparable to wild-type Snf1, and it mediated the rapid phosphorylation of a synthetic AMPK activity reporter substrate (ACC1-GFP) in glucose-starved cells, albeit to a significantly lower extent than wild-type Snf1 (**Figure 1A and B**, and **Figure 1—figure supplement 1A**). Notably, nitrogen starvation also activates Snf1, but much less than glucose starvation (**Figure 1—figure supplement 1B, C**). As expected, the presence of 2NM-PP1 fully abrogated the activity of Snf1^{as}, but not that of wild-type Snf1 (**Figure 1—figure supplement 1A**), while its association with the Snf1^{as} kinase active site protected Snf1^{as}-pThr^{210} from dephosphorylation as reported earlier (**Chandrashekarappa et al., 2013**). Compared to DMSO-treated (control) *snf1*^{as} cells, 2NM-PP1-treated *snf1*^{as} cells were also significantly compromised in maintaining TORC1 inactive, as detected by measuring the phosphorylation of Thr^{737} in Sch9, a proxy for TORC1 activity (**Urban et al., 2007**), specifically during the time frame of 6–15 min following glucose starvation (**Figure 1A–D**). Because loss of Snf1 caused a comparable defect that was independent of the presence or absence of 2NM-PP1 (**Figure 1A**), our data corroborate the previous notion that Snf1 activity is required for

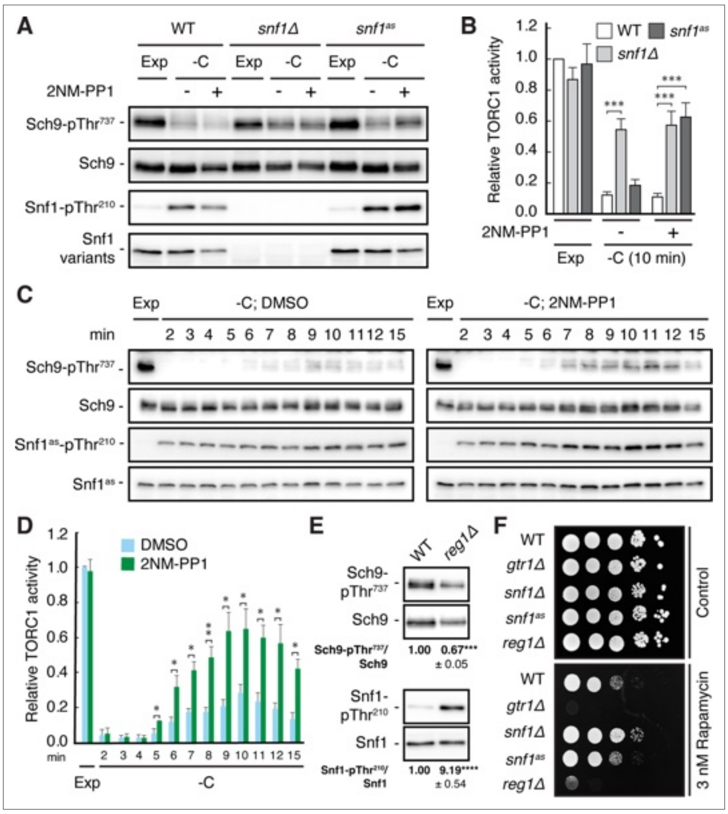

Figure 1. Snf1 is required for proper downregulation of TORC1 in glucose-starved cells. (**A, B**) Wild-type (WT), *snf1Δ*, and *snf1^{as}* (analog-sensitive) cells were grown exponentially (Exp) and starved for glucose for 10 min (-C) in the absence (-; DMSO vehicle control) or presence (+) of 2NM-PP1. Phosphorylation of the *bona fide* TORC1 target residue Thr^{737} in Sch9 and of Thr^{210} in Snf1 was detected by immunoblot analyses of whole cell extracts using phospho-specific antibodies against the respective phospho-residues. Anti-Sch9 and anti-His$_6$ antibodies served to detect the levels of Sch9 and Snf1, respectively (**A**). Notably, binding of 2NM-PP1 to the catalytic cleft of Snf1^{as} inhibits its kinase activity and, at the same time, prevents the dephosphorylation of phosphorylated Thr^{210} (pThr^{210}) in Snf1 (***Chandrashekarappa et al., 2013***). The mean TORC1 activities (*i.e.* Sch9-pThr^{737}/Sch9) were quantified, normalized relative to exponentially growing WT cells (set to 1.0), and shown in the bar diagram in (**B**) (n=6; + SEM; unpaired Student's t-test, ***≤0.0005). (**C, D**) Analog-sensitive *snf1^{as}* cells were treated as in (**A**), but harvested at the times indicated following glucose starvation (-C). The respective relative TORC1 activities were assessed as in (**B**), but cross-normalized (for each of the two sets of blots) to the same sample from exponentially growing cells (lane 1; Exp), and are shown in (**D**) (n=4; + SEM; unpaired Student's t-test, *p≤0.05, **p≤0.005). (**E**) WT and *reg1Δ* cells were grown exponentially and assayed for their mean relative TORC1 activities (Sch9-pThr^{737}/Sch9) and Snf1-Thr^{210} phosphorylation levels (Snf1-pThr^{210}/Snf1), each normalized to WT cells (set to 1.0; n=4; ± SEM). In unpaired Student's tests, both values in *reg1Δ* cells were significantly different from the ones in WT cells (***p≤0.0005, ****p≤0.00005). (**F**) Exponentially growing cells (of the indicated genotype) were 10-fold serially diluted, spotted on synthetic complete medium containing, or not (control), 3 nM rapamycin, and grown for 3 days at 30 °C (n=3). The online version of this article includes the following source data for ***Figure 1—source data 1***, quantification of blots for graphs shown in (**B, D and E**); ***Figure 1—source data 2***, uncropped blots shown in (**A, C and E**); Uncropped dropspots shown in (**F**); ***Figure 1—source data 3***, raw blots shown in (**A, C and E**) and raw dropspots shown in (**F**).

Figure 1 continued on next page

Figure 1 continued

The online version of this article includes the following source data and figure supplement(s) for figure 1:

Source data 1. Quantification of blots for graphs shown in B, D, E.

Source data 2. Uncropped blots shown in A, C, E and uncropped dropspots shown in F.

Source data 3. Raw blots shown in A, C, E and raw dropspots shown in F.

Figure supplement 1. Specificity of 2NM-PP1 and differential Snf1 activation upon nitrogen and carbon starvation.

Figure supplement 1—source data 1. Quantification of blots for graphs shown in C.

Figure supplement 1—source data 2. Uncropped blots shown in A, B.

Figure supplement 1—source data 3. Raw blots shown in A, B.

maintaining TORC1 inactive specifically during the early, but not at later, phases of glucose starvation (**Hughes Hallett et al., 2015**). Based on these observations, we reasoned that unscheduled hyperactivation of Snf1 might also inhibit TORC1 even in cells growing in a glucose-rich environment. This was indeed the case as loss of Reg1, the regulatory subunit that instructs the PP1 Glc7 to dephosphorylate pThr^{210} and thus inactivate Snf1 (**Ludin et al., 1998**; **Sanz et al., 2000**), resulted in hyperphosphorylation of Snf1-Thr^{210} that was accompanied by a significant reduction in TORC1 activity (**Figure 1E**). In line with these data, loss of Reg1, like loss of the TORC1-regulatory Rag GTPase Gtr1, rendered cells sensitive to sub-inhibitory levels of rapamycin (as also observed earlier; **Bertram et al., 2002**), while loss of Snf1 conferred slight resistance to rapamycin (**Figure 1F**).

It has previously been demonstrated that TORC1 activity can be transiently (on a short-time scale of 1–5 min) activated by the addition of a nitrogen source such as glutamine to nitrogen starved cells (**Stracka et al., 2014**). Based on our results above, we therefore assumed that the respective transient activation of TORC1 may be reduced in the absence of glucose, because we expected this to activate Snf1 and therefore (directly or indirectly) inhibit TORC1. Indeed, when *snf1^{as}* cells were starved for both glucose and glutamine at the same time, TORC1 was rapidly inactivated and could only be transiently reactivated when cells were refed with either glucose alone or with glucose and glutamine combined (**Figure 2A–D**), but not when refed with glutamine alone (**Figure 2E and F**). In the latter case, however, 2NM-PP1 treatment, and hence inactivation of Snf1^{as}, was able to partially restore the transient glutamine-mediated TORC1 activation (**Figure 2E and F**). From these experiments, we infer that Snf1 not only contributes to proper TORC1 inhibition in glucose-starved cells, but also helps to prevent the transient reactivation of TORC1 in glutamine refed, glucose-starved cells.

Global phosphoproteomics identifies potential Snf1 targets within the TORC1 signaling pathway

To dissect the mechanisms by which Snf1 impinges on TORC1 signaling, we decided to perform a set of stable isotope-labeling by amino acids in cell culture (SILAC)-based quantitative phosphoproteomic experiments, similarly as recently described (**Hu et al., 2021**). For in vivo analyses, *snf1^{as}* cells were grown in three different SILAC media supporting the comparison of three experimental conditions (**Figure 3A**). Cells grown in full medium (2% glucose, light label) served as control. The cellular response to glucose starvation was analyzed after 5 and 15 min (shift to 0.05% glucose, medium and heavy label, respectively). To discriminate potential Snf1 target sites from sites being regulated by other kinases, concomitantly to the glucose downshift, cells were treated, or not, with the selective ATP-competitive inhibitor 2NM-PP1. Snf1 target sites should be positively regulated in the control set and not, or significantly less, in the 2NM-PP1-treated set (**Figure 3A**; n=5 biological replicates per set). To further discriminate direct from indirect effects, we performed whole proteome on bead in vitro kinase assays (OBIKA) comparing the immobilized proteome of *snf1^{as}* cells (growing exponentially in the presence of 5% glucose and ATP analog) incubated with purified wild-type Snf1 to that incubated with a kinase-inactive Snf1^{T210A} mutant (**Figure 3A**; n=5 biological replicates) (**Hu et al., 2021**).

In vivo analyses led to the identification of 40’547 phosphosites, of which 34’747 could be quantified (**Figure 3B**). After stringent filtering, we used 21’223 sites, which clearly localized to a specific amino acid residue (localization probability >0.75) (**Olsen et al., 2006**; **Supplementary file 2A-B**), for statistical analyses to identify potential Snf1 target sites. Class I target sites had to fulfill two criteria: sites had to be significantly upregulated (i) when using a random effect model comparing starved

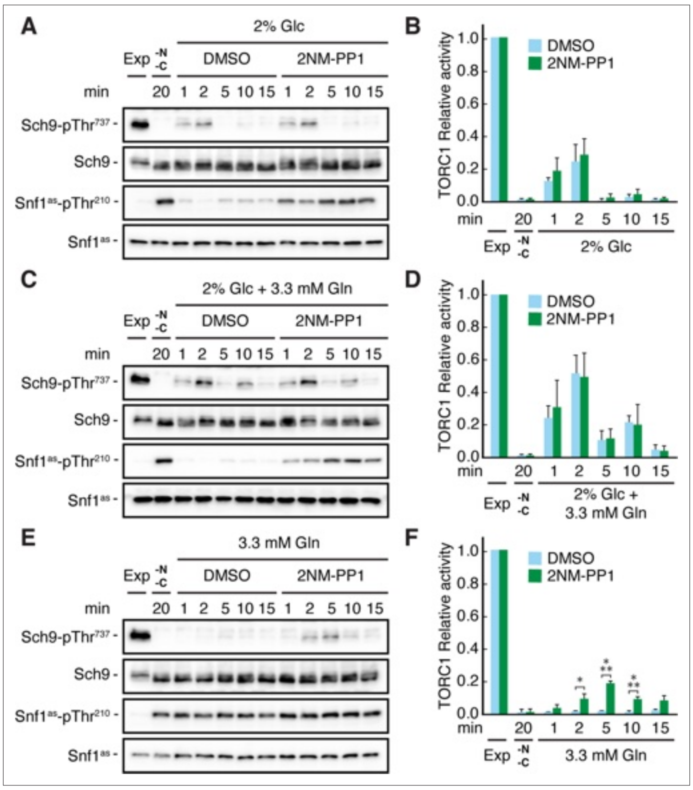

Figure 2. Snf1 prevents transient TORC1 restimulation by glutamine in glucose- and glutamine-starved cells. (**A–F**) Exponentially growing $snf1^{as}$ cells were starved for 20 min for nitrogen and glucose (-N, -C) and then restimulated for the times indicated, in the absence (DMSO) or presence of 2NM-PP1, with 2% glucose (Glc) (**A, B**), 2% glucose and 3.3 mM glutamine (Gln) (**C, D**), or 3.3 mM glutamine (**E, F**). Immunoblot analyses were performed as in ***Figure 1A*** and the relative TORC1 activities in (**A**), (**C**), and (**E**), were quantified as in ***Figure 1B*** and are shown in (**B**), (**D**), and (**F**), respectively (n=3; + SEM; unpaired Student's t-test, $*p \leq 0.05$, $***p \leq 0.0005$). The online version of this article includes the following source data for ***Figure 2—source data 1***, quantification of blots for graphs shown in (**B, D and F**); ***Figure 2—source data 2***, uncropped blots shown in (**A, C and E**); ***Figure 2—source data 3***, raw blots shown in (**A, C and E**).

The online version of this article includes the following source data for figure 2:

Source data 1. Quantification of blots for graphs shown in B, D and F.

Source data 2. Uncropped blots shown in A, C and E.

Source data 3. Raw blots shown in A, C and E.

(5 min and 15 min) to non-starved cells (p<0.05); and (ii) when comparing starved cells to cells treated additionally with the inhibitor 2NM-PP1 (Student's t-test, FDR<0.05). Class II target sites had only to fulfill the second criterium. Class II sites contained target residues such as Ser^{1157} in Acc1, the cytosolic acetyl-CoA carboxylase that is already phosphorylated by Snf1 in cells grown on 2% glucose, but dephosphorylated upon 2NM-PP1-mediated inhibition of Snf1^{as} (***Braun et al., 2014***). In total, this led to a shortlist of 1409 sites, divided into 984 class I sites and 425 class II sites (***Figure 3B*** and ***Supplementary file 2C***). Our shortlisted class I and class II sites cover between 26% and 53% of the

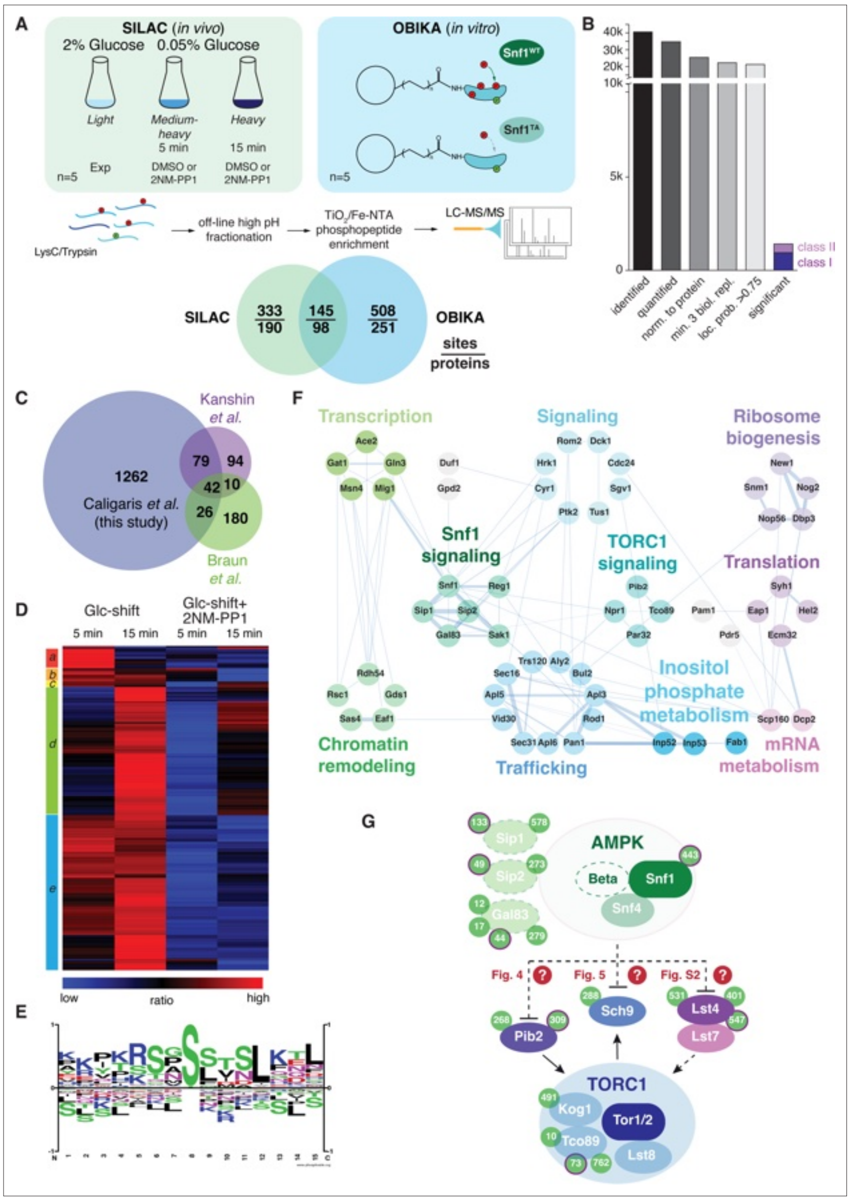
A
SILAC (in vivo)
2% Glucose 0.05% Glucose
Light
Medium-heavy 5 min
Heavy 15 min
Exp
DMSO or 2NM-PP1
DMSO or 2NM-PP1
n=5
OBIKA (in vitro)
Snf1WT
Snf1TA
n=5
LysC/Trypsin
off-line high pH fractionation
TiO2/Fe-NTA phosphopeptide enrichment
LC-MS/MS
SILAC
333/190
145/98
508/251
OBIKA
sites
proteins
B
40k
30k
20k
10k
5k
0
class II
class I
identified
quantified
norm. to protein
min. 3 biol. repl.
loc. prob. >0.75
significant
C
Kanshin et al.
79
94
1262
42
10
Caligaris et al. (this study)
26
180
Braun et al.
D
Glc-shift
Glc-shift+ 2NM-PP1
5 min 15 min 5 min 15 min
a b c d e
low ratio high
E
F
Transcription
Signaling
Ribosome biogenesis
Snf1 signaling
TORC1 signaling
Translation
Inositol phosphate metabolism
Chromatin remodeling
Trafficking
mRNA metabolism
G
AMPK
Sip1 Sip2 Gal83
Beta Snf1 Snf4
Fig. 4
Fig. 5
Fig. S2
Pib2 Sch9 Lst4 Lst7
TORC1
Kog1 Tor1/2 Tco89 Lst8

Figure 3. Quantitative phosphoproteomic analyses for the identification of potential Snf1 target sites. (**A**) Quantitative MS-based proteomics workflow (SILAC n=5, OBIKA n=5). (**B**) Histogram of the number of identified phosphosites in the SILAC analysis after each filtering step and the relative amount of phosphosites attributed to classes I and II among the significant ones. (**C**) Proportional Venn diagram highlighting the commonly identified phosphosites in the current and two recent Snf1 phosphoproteomic studies. (**D**) Heatmap of phosphosite kinetics. Normalized SILAC ratios (treated

Figure 3 continued on next page

Figure 3 continued

versus untreated) of class I and class II sites (highlighted in B) were log2 transformed and z normalized prior unsupervised hierarchical clustering of the rows tree using Euclidean distance as matrix. Five major clusters *a-e*, each highlighted by a different color, are observed. (**E**) Motif analyses of Snf1 phosphosites identified by in vivo SILAC and OBIKA experiments as outlined in (**A**). (**F**) Protein-protein interaction network comprising 57 interconnected proteins out of the 98 where at least one Snf1-dependent phosphosite was shortlisted by the intersection of the SILAC and OBIKA analyses. The network was generated with Cytoscape using the STRING plugin, setting the confidence (score) cut-off at 0.25. Edge thickness represents the score value of each interaction. (**G**) Schematic model representing components of the Snf1/AMPK and TORC1 signaling pathways that contain Snf1-regulated phosphosites. Phosphosites attributed to class II are highlighted with a bold-pink outline. The three Snf1 β-subunits are represented with a dashed outline on the left. Solid and dashed arrows refer to direct and indirect activating interactions, respectively. Dashed lines with bars refer to potential (question marks) inhibitory interactions that are experimentally addressed in the indicated figures in this study. Source data for this figure are provided in ***Supplementary file 2***.

The online version of this article includes the following source data and figure supplement(s) for figure 3:

Figure supplement 1. Specific motif analyses of Snf1 phosphosites and role of Lst4 in TORC1 reactivation in glucose-starved, Snf1-inhibited cells.

Figure supplement 1—source data 1. Quantification of blots for values shown in C.

Figure supplement 1—source data 2. Uncropped blots shown in C.

Figure supplement 1—source data 3. Raw blots shown in C.

---

previously published potential Snf1 target sites (***Braun et al., 2014***; ***Kanshin et al., 2017***; ***Supplementary file 2D***), overlapping to a larger extent with the respective studies than the studies with each other (***Figure 3***). In addition, we expand the potential Snf1 target repertoire by more than 1200 sites highlighting the resource character of the current study. We performed hierarchically clustering to characterize the kinetic behavior of sites and observed five major clusters (***Figure 3D***): cluster *a* contains sites that responded transiently after 5 min of stimulation; clusters *b*, *c*, and *e* contain sites that responded in a sustained manner after 5 min and 15 min; and cluster *d* contains responders that reacted only after 15 min. Source proteins of cluster *a* relate to 'regulation of growth', amongst them the Snf1 target Mig1, while those in clusters *b*, *c*, and *e* are linked to 'cell cycle, transcription, endocytosis, and proteins transport', such as the zinc-finger and Snf1 target protein Msn4, and those in cluster *d* are enriched in 'serine-threonine kinases', like Atg1 and Sch9 (***Supplementary file 2E***).

To discriminate potential indirect effects observed in vivo from direct Snf1 targets, we overlaid the significantly regulated sites from the SILAC and OBIKA datasets. Of the 986 commonly identified and quantified sites, 145 sites on 98 source proteins were significantly regulated by both approaches, characterizing them as *bona fide* Snf1 target sites (***Figure 3A*** and ***Supplementary file 2F***). The consensus motif of these sites corroborates the published AMPK and Snf1 motif with two basic amino acid residues in the –3 and –4 positions and a hydrophobic leucine residue in the +4 position (***Figure 3E***; ***Dale et al., 1995***; ***Gwinn et al., 2008***; ***Schaffer et al., 2015***; ***Scott et al., 2002***). As such, this further supports our interpretation that these sites are *bona fide* Snf1 target sites. Notably, of the 145 confirmed target sites, 81 (i.e. 72%) were significantly regulated after both 5 min and 15 min. Of the remaining 64 sites, 32 responded only after 5 min, while the other 32 responded only after 15 min. Some of the former residues are located within Snf1 itself, the β-subunit of the Snf1 complex (i.e. Sip1), the Snf1-targeting kinase Sak1, and Mig1, while some of the latter are located within the known Snf1-interacting proteins such as Gln3, Msn4, and Reg1. These observations indicate that Snf1-dependent phosphorylation initiates, as expected, within the Snf1 complex and then progresses to other effectors. Interestingly, based on the residues that responded exclusively after 5 min, we retrieved a perfect Snf1 consensus motif (i.e. an arginine residue in the –3 position and a leucine residue in the +4 position; ***Figure 3—figure supplement 1A***). The one retrieved for the residues that respond exclusively at 15 min, in contrast, significantly deviated from this consensus motif (***Figure 3—figure supplement 1B***). The temporal deferral of some Snf1 target phosphorylation events may therefore perhaps be in part be explained by reduced substrate affinity due to consensus motif divergence.

As a kinase generally regulates multiple proteins within a given pathway, we analyzed known protein-protein interactions of the 98 Snf1 target proteins in STRING DB, enabling us to generate a network of 57 proteins (***Figure 3F***; ***Szklarczyk et al., 2021***). In line with the significant overlap of our data with the ones published by ***Braun et al., 2014***, this network covers similar biological processes including intracellular trafficking, ribosome biogenesis, translation, mRNA metabolism, inositol phosphate metabolism, chromatin remodeling, and TORC1 signaling (***Figure 3F***). Gratifyingly, this network also includes most of the previously known proximal Snf1 targets including for instance Ccr4

(***Braun et al., 2014***), Cyr1/Cdc35 (***Nicastro et al., 2015***), Eap1 (***Braun et al., 2014***). Gat1 (***Kulkarni et al., 2006***), Gln3 (***Bertram et al., 2002***; ***Kulkarni et al., 2006***), Mig1 (***DeVit and Johnston, 1999***; ***Ostling and Ronne, 1998***; ***Smith et al., 1999***; ***Treitel et al., 1998***), Msn4 (***Estruch and Carlson, 1993***; ***Petrenko et al., 2013***), and Rod1 (***Alvaro et al., 2016***; ***Laussel et al., 2022***; ***O'Donnell and Schmidt, 2019***; ***Shinoda and Kikuchi, 2007***). In addition, the dataset also pinpoints potential Snf1 target residues in numerous proteins that have an assigned function as Snf1 effectors such as Aly2 and Bul2 (***Bowman et al., 2022***; ***O'Donnell and Schmidt, 2019***; ***Ptacek et al., 2005***), Glo3 (***Arakel et al., 2019***), Gpd2 (***Lee et al., 2012***), and Npr1 (***Brito et al., 2019***). Finally, Snf1-regulated residues were also identified in the Snf1-β-subunits Gal83 and Sip2 (***Carling, 2004***; ***Hedbacker and Carlson, 2008***), the Sak1 kinase that phosphorylates Snf1-Thr^{210} (***González et al., 2020***; ***Hedbacker and Carlson, 2008***), the PP1 phosphatase Glc7-regulatory subunit Reg1 and the protein phosphatase C Ptc1 that share an overlapping role in the dephosphorylation of Snf1-pThr^{210} (***Ludin et al., 1998***; ***McCartney and Schmidt, 2001***; ***Ruiz et al., 2013***), and Snf1 itself. These observations indicate that Snf1 is embedded and engaged in an elaborated feedback control network, which, based on our current data, can be experimentally addressed in the future.

As briefly mentioned above, our in vivo phosphoproteomic analyses also pinpointed several Snf1-regulated residues within proteins that act in the TORC1 signaling pathway, including Lst4 and Pib2 that function upstream of TORC1, the TORC1 subunits Kog1 and Tco89, and the proximal TORC1 effector Sch9 (***Urban et al., 2007***; ***Figure 3G***). From these 5 TORC1-related hits, we excluded Kog1 from further analyses because the potential Snf1 target residue in Kog1 that we identified was Ser^{491}, and mutation of this residue has previously been found not to affect the capacity of cells to maintain TORC1 inactive during the early phase of glucose starvation (***Hughes Hallett et al., 2015***; ***Sullivan et al., 2019***). We have also not given priority to the analysis of Tco89, since it is a heavily phosphorylated protein (>70 phosphorylated residues) that we intend to dissect separately in parallel studies. Finally, we also did not follow up on the TORC1-stimulating protein Lst4. The reason for this is that loss of Lst4 did not significantly change the transient reactivation of TORC1 in glucose-starved, 2NM-PP1-treated *snf1^{as}* cells (***Figure 3—figure supplement 1C***), even though it reduced the TORC1 activity in exponentially growing cells as reported (***Péli-Gulli et al., 2015***). Thus, we focused our subsequent experiments on the two remaining proteins, namely Pib2 and Sch9, and examined in more detail the consequences of their phosphorylation by Snf1 for signaling via the TORC1 pathway.

Snf1 phosphorylates Pib2-Ser^{268,309} to weaken its association with Kog1

Our phosphoproteomic approach identified two potential Snf1 target residues each within the Kog1-binding region of Pib2, Ser^{268} and Ser^{309}, of which the latter was also detected by OBIKA with Snf1 (***Figure 4A–C*** and ***Supplementary file 2C-F***). To further corroborate these data, we carried out an in vitro Snf1 kinase assay using an N-terminally truncated Pib2 fragment as substrate, which, unlike full-length Pib2, could be stably expressed in and purified from bacteria. Accordingly, wild-type Snf1 (purified from yeast), but not the kinase-inactive Snf1^{T210A}, was able to phosphorylate the Pib2 fragment. We also introduced mutations of Ser^{268} and Ser^{309} in the Pib2 fragment and replaced them with alanine (Ala) residues. The fragments carrying either one of these mutations were still phosphorylated by wild-type Snf1, though to a different extent, but when both mutations were combined, the phosphorylation level dropped significantly (***Figure 4D***). Together with our finding that the Snf1 complex was able to bind Pib2 in microscale thermophoresis assays (***Figure 4E***), our data therefore, led us to infer that Snf1 may control Pib2 function primarily through phosphorylation of the Ser^{268} and Ser^{309} residues.

To address the physiological role of Ser$^{268/309}$ phosphorylation in Pib2, we next studied the response to short-term glucose starvation of 2NM-PP1-treated and -untreated *snf1^{as}* strains that expressed either the phosphomutant Pib2^{S268A,S309A} or the phosphomimetic Pib2^{S268E,S309E}. The *snf1^{as}* strain in which *PIB2* was deleted served as control. Interestingly, expression of Pib2^{S268E,S309E} or loss of Pib2, but not the expression of Pib2^{S268A,S309A}, rendered TORC1 more sensitive to glucose-starvation in DMSO-treated control cells and largely suppressed the unscheduled reactivation of TORC1 in glucose-starved cells in which Snf1^{as} was inhibited by a 2NM-PP1-treatment (***Figure 4F and G***). The observation that loss of Pib2 and expression of the Pib2^{S268E,S309E} allele similarly affect TORC1 activity suggests that the latter allele may be compromised in a TORC1 activating mechanism. The Snf1-dependent phosphorylation of Pib2 may therefore possibly compromise the function of the C-terminal TORC1-activating domain

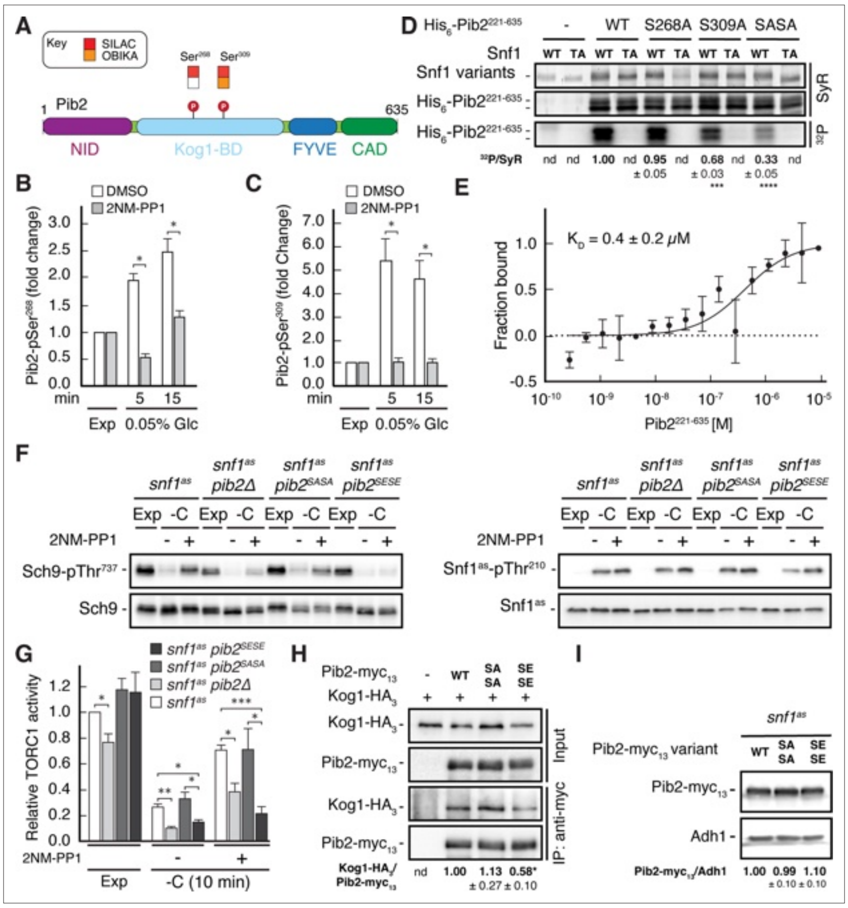

Figure 4. Snf1 weakens the Pib2-Kog1 association by phosphorylating Pib2-Ser^{268,309}. (**A**) Schematic representation of the structure of Pib2 with the N-terminal TORC1-inhibitory (NID), Kog1-binding (Kog1-BD), phosphatidylinositol-3-phosphate (PI3P) -binding Fab1-YOTB-Vac1-EEA1 (FYVE), and C-terminal TORC1-activatory (CAD) domains (***Hatakeyama, 2021***). The residues Ser^{268} and Ser^{309} in Pib2 were both identified as potential Snf1 targets (P) in vivo (SILAC), while only Ser^{309} was recovered in our highly multiplexed on-beads in vitro kinase assays (OBIKA) with Snf1. (**B, C**) Snf1 controls the phosphorylation of Ser^{268} and Ser^{309} in Pib2 in vivo. Phosphorylation levels of Pib2-Ser^{268} (**B**) and Pib2-Ser^{309} (**C**) in untreated (DMSO) and 2NM-PP1-treated *snf1^{as}* cells that were grown exponentially (Exp) and limited for glucose (0.05%) for the times indicated. Mean values were extracted from the SILAC experiment (***Supplementary file 2*** and ***Figure 3***) and normalized to the ones in exponentially growing cells (set to 1.0) (n=3; + SD; unpaired Student's t-test, *FDR ≤ 0.05). (**D**) Snf1 phosphorylates Ser^{268} and Ser^{309} in Pib2 in vitro. Snf1 (WT) and kinase-inactive Snf1^{T210A} (TA) were purified from yeast and used in protein kinase assays with [γ-^{32}P]-ATP and a bacterially-expressed fragment of Pib2 (Pib2$^{221\text{-}635}$) lacking the N-terminal 220 amino acids that, according to our in vivo proteomics analyses, did not contain a potential Snf1 target residue. In parallel protein kinase assays, we also used the respective Pib2^{S268A}, Pib2^{S309A}, and Pib2$^{S268A/S309A}$ (Pib2^{SASA}) mutant fragments as substrates. Substrate phosphorylation was detected by autoradiography (^{32}P, lower panel) and Sypro Ruby (SyR) staining is shown as loading control for the Snf1 variants (upper panel) and the His$_6$-tagged Pib2 fragments that were partially degraded and ran in more than 1 band (panel in the middle). The mean phosphorylation of Pib2^{S268A}, Pib2^{S309A}, and Pib2$^{S268A/S309A}$ (Pib2^{SASA}) fragments by wild-type Snf1 (i.e. ^{32}P signal/Sypro Ruby [SyR] substrate input level [including the indicated faster migrating proteolytic forms]; nd, not detected) was assessed relative to the one of the Pib2^{WT} fragment (set to 1.0; n=3; ± SEM; unpaired Student's t-test, ***p≤0.0005, ****p≤0.00005). (**E**) The Snf1 complex binds Pib2. The binding affinity between bacterially purified, titrated Pib2$^{221\text{-}635}$ and yeast purified Snf1 complex (containing the C-terminally GFP-tagged Snf4 γ-subunit) was assessed by microscale thermophoresis. The dissociation constant (K$_D$; 95% profile likelihood = 136–1098 nM,

Figure 4 continued on next page

Figure 4 continued

n=3; ± SEM) was calculated using a nonlinear asymmetric sigmoidal regression. (**F, G**) Expression of the phosphomimetic Pib2^{S268E,S309E} allele, like loss of Pib2, rescues the TORC1 inactivation defect in glucose-starved, Snf1-compromised cells. Exponentially growing *snf1*^{as}, *snf1*^{as} *pib2Δ*, *snf1*^{as} *pib2*^{S268A,S309A} (*pib2*^{SASA}), and *snf1*^{as} *pib2*^{S268E,S309E} (*pib2*^{SESE}) cells were grown exponentially (Exp) and then starved for 10 min for glucose (-C) in the absence (-; DMSO) or the presence (+) of 2NM-PP1. Immunoblot analyses of Sch9-pThr^{737} and Sch9 (left blots) and of Snf1^{as}-pThr^{210} and Snf1^{as} (right blots) were carried out as in ***Figure 1A*** (**F**). The mean relative TORC1 activities in the four strains were quantified as in ***Figure 1B*** and normalized to the values in exponentially growing *snf1*^{as} cells (set to 1.0; n=4; + SEM; unpaired Student's t-test, $^{*}p \leq 0.05$, $^{**}p \leq 0.005$, $^{***}p \leq 0.0005$) (**G**). (**H**) The phosphomimetic Pib2^{S268E,S309E} is compromised for TORC1-binding. Kog1-HA$_3$-expressing cells co-expressing Pib2-myc$_{13}$ (WT), Pib2^{S368A,S309A}-myc$_{13}$ (SASA), Pib2^{S368E,S309E}-myc$_{13}$ (SESE), or untagged Pib2 (-) were grown exponentially. Lysates (input) containing 60 mM glutamine and anti-myc immunoprecipitates (IP: anti-myc) were analyzed by immunoblotting with anti-HA and anti-myc antibodies, respectively. The mean relative amount of Kog1-HA$_3$ that was immunoprecipitated with Pib2-myc$_{13}$ and its variants was determined and normalized to the one between Kog1-HA$_3$ and Pib2-myc$_{13}$ (set to 1.0; n=4; + SEM; unpaired Student's t-test, $^{*}p \leq 0.05$; nd, not detected). (**I**) Pib2-myc$_{13}$ alleles are adequately expressed. Expression of Pib2-myc$_{13}$ variants (as in F) was probed by immunoblot analysis in extracts of exponentially growing cells using anti-myc antibodies. Values were quantified relative to Adh1 levels (detected with anti-Adh1 antibodies) and normalized to the respective Pib2-myc$_{13}$/Adh1 ratio in cells expressing the WT Pib2-myc$_{13}$ (n=3; ± SEM; unpaired Student's t-test; nd, not detected). The online version of this article includes the following source data for ***Figure 4—source data 1***, data for the graph shown in (**B, C and E**) and quantifications of the blots in (**D, H and I**) and for the graph shown in (**G**); ***Figure 4—source data 2***, uncropped blots, gels and autoradiographies shown in (**D, F, H and I**); ***Figure 4—source data 3***, raw blots, gels and autoradiographies shown in (**D, F, H and I**).

The online version of this article includes the following source data for figure 4:

Source data 1. Data for the graph shown in B, C and E and quantifications of the blots in D, H and I and for the graph shown in G.

Source data 2. Uncropped blots, gels and autoradiographies shown in D, F, H and I.

Source data 3. Raw blots, gels and autoradiographies shown in D, F, H and I.

(CAD) rather than the N-terminal TORC1-inhibitory domain (NID). Consequently, loss of Snf1, would allow the Pib2-CAD to transiently activate TORC1 in glucose-starved cells.

Notably, as a readout for TORC1 activity, we monitored the phosphorylation of the downstream effector kinase Sch9, which as mentioned above and further explained below, is itself a potential direct Snf1 substrate. Therefore, we sought to understand how Pib2 phosphorylation may affect TORC1 signaling. We noticed that the Ser^{268} and Ser^{309} Snf1 target sites reside within the Kog1-binding domains of Pib2 (***Michel et al., 2017***; ***Sullivan et al., 2019***; ***Troutman et al., 2022***), which led us to speculate that the phosphorylation state of these residues could affect the Pib2-Kog1 association. To this end, we performed co-immunoprecipitation assays and found that this was indeed the case, as we observed that the Pib2^{S268E,S309E} variant exhibited significantly reduced affinity for Kog1 when compared to wild-type Pib2 or Pib2^{S268A,S309A} (***Figure 4H***). Importantly, immunoblot analyses of the myc-tagged phosphomutant and phosphomimetic Pib2 variants showed that the introduction of the respective mutations in Pib2 did not affect the stability of the proteins (***Figure 4I***). Thus, the combined data led us to conclude that Snf1 activation in glucose-starved cells mediates temporal TORC1 inhibition primarily through phosphorylation of Pib2 at Ser$^{268/309}$, which serves to weaken the association between Pib2 and Kog1 and prevent it from activating TORC1 under these conditions.

Snf1 constrains Sch9-Thr^{737} phosphorylation by targeting Sch9-Ser^{288}

Our phosphoproteomic approach also identified one potential Snf1 target residue, namely Ser^{288}, that lies within the C2 domain of Sch9 (***Figure 5A and B***, and ***Supplementary file 2C, F***). Like for Pib2, we tried to corroborate these data using in vitro Snf1 kinase assays and an N-terminal fragment of Sch9 as substrate, which, unlike full-length Sch9, could be stably expressed in and purified from bacteria. Here too, wild-type Snf1, but not the kinase-inactive Snf1^{T210A} mutant, was able to phosphorylate this Sch9 fragment, and mutation of Ser^{288} to alanine in the Sch9 fragment significantly reduced the respective phosphorylation level, indicating that this residue is likely the primary Snf1 target in the N-terminal part of Sch9 (***Figure 5—figure supplement 1***). To further study the dynamics of Ser^{288} phosphorylation in vivo, we raised antibodies that specifically recognize phosphorylated Ser^{288} in Sch9 (Sch9-pSer^{288}). Using these antibodies, we observed that the Sch9-pSer^{288} levels were barely detectable in *snf1*^{as} cells growing exponentially on 2% glucose, but then rapidly and strongly increased in a Snf1-dependent manner following glucose starvation in DMSO-treated cells but not in 2NM-PP1 treated, Snf1-inhibited cells (***Figure 5D***; upper panels, left side). In addition, the Sch9-pSer^{288} levels were quite elevated in cells growing exponentially on very low glucose levels (i.e. 0.05%), but rapidly declined in cells where Snf1^{as} was inactivated by 2NM-PP1 treatment (***Figure 5D***; upper panels, right

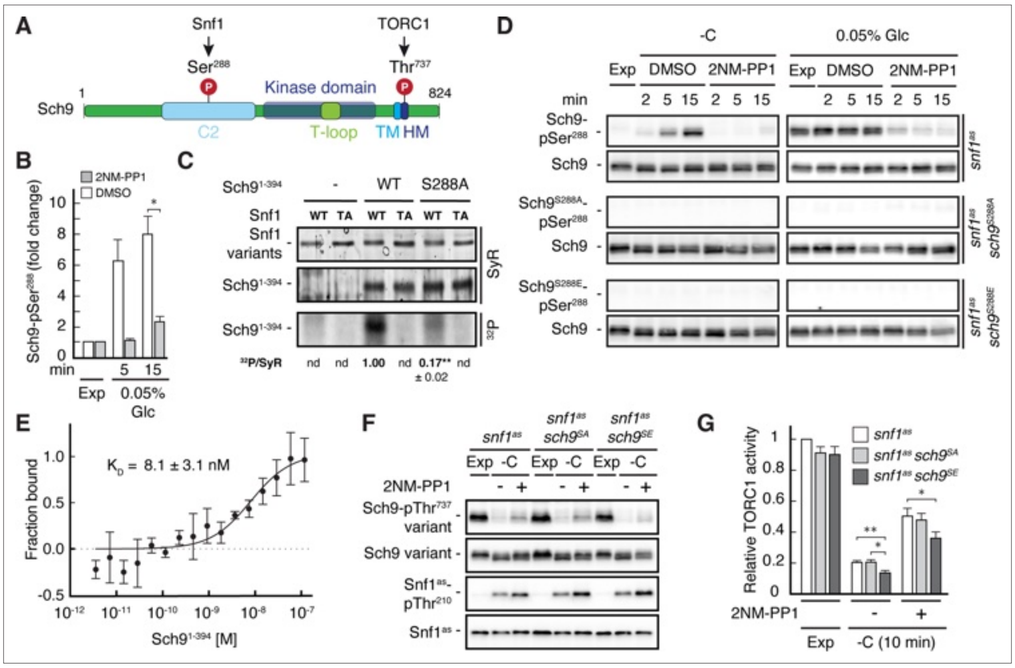

Figure 5. Snf1 phosphorylates Sch9-Ser^{288} to antagonize Sch9-Thr^{737} phosphorylation. (**A**) Schematic representation of the structure of Sch9 with the C2 domain, the kinase domain including the T-loop, the turn motif, and the hydrophobic motif (HM). The position of the potential Snf1 target residue (*i.e.* phosphorylated [P] Ser^{288}) and one of the 5 C-terminal TORC1 target residues (***Urban et al., 2007***; i.e. phosphorylated [P] Thr^{737} in the HM motif that is used to probe TORC1 activity here) are indicated. (**B**) Phosphoproteomic analyses identify Sch9-Ser^{288} as a potential Snf1 target. Mean phosphorylation levels of Sch9-Ser^{288} in untreated (DMSO) and 2NM-PP1-treated *snf1^{as}* cells, grown exponentially (Exp) and limited for glucose (0.05% Glc) for the times indicated, were extracted from the SILAC experiment (***Supplementary file 2*** and ***Figure 3***) and normalized to the ones in exponentially growing cells (set to 1.0; n=3; + SD; unpaired Student's t-test, *FDR ≤0.05). (**C**) Snf1 phosphorylates Ser^{288} in Sch9 in vitro. Snf1 (WT) and kinase-inactive Snf1^{T210A} (TA) were purified from yeast and used in protein kinase assays with [γ-^{32}P]-ATP and the N-terminal fragment of Sch9 (encompassing the N-terminal 394 amino acids; Sch9$^{1-394}$) as substrate (WT). In parallel protein kinase assays, we also used the respective Sch9$^{1-394}$ fragment harboring the Ser^{288}-to-Ala mutation as substrate (S288A). Substrate phosphorylation was detected by autoradiography (^{32}P, lower panel) and Sypro Ruby (SyR) staining is shown as loading control for the Snf1 variants (upper panel) and the Sch9 fragments (panel in the middle). The mean phosphorylation of the Sch9^{S288A} mutant fragment by wild-type Snf1 (i.e. ^{32}P signal/Sypro Ruby [SyR] substrate input level; nd, not detected) was assessed relative to the one of the Sch9^{WT} fragment (set to 1.0, n=3; ± SEM; unpaired Student's t-test, **p≤0.05; nd, not detected). (**D**) Snf1 controls Sch9-Ser^{288} phosphorylation in vivo. Cells (*i.e. snf1^{as}*, *snf1^{as} sch9^{S288A}*, and *snf1^{as} sch9^{S288E}*) were grown exponentially on 2% glucose (Exp) and then starved for glucose (-C) in the absence (DMSO) or presence of 2NM-PP1 for the times indicated (panels on the left). In parallel, cells were grown exponentially (Exp) on low glucose media (0.05%; panels on the right) and then treated with vehicle (DMSO) or 2-NMPP1 for the times indicated. The levels of Ser^{288} phosphorylation in Sch9 (Sch9-pSer^{288}) and total levels of Sch9 were assayed by immunoblot analyses using anti-Sch9-pSer^{288} and anti-Sch9 antibodies, respectively (n=3). (**E**) Snf1 binds Sch9. The binding affinity between Sch9$^{1-394}$ (purified from yeast) titrated against the Snf1 complex (also purified from yeast and containing the C-terminally GFP-tagged Snf4 γ-subunit) was assessed by microscale thermophoresis. The dissociation constant (K_D; 95% profile likelihood = 3.2–19.1 nM; n=3; ± SEM) was calculated using a nonlinear asymmetric sigmoidal regression. (**F, G**) The phosphomimetic Sch9^{S288E} allele compromises proper phosphorylation of the C-terminal Thr^{737} residue in Sch9. *snf1^{as}*, *snf1^{as} sch9^{S288A}* (*sch9^{SA}*), and *snf1^{as} sch9^{S288E}* (*sch9^{SE}*) cells were grown exponentially (Exp) and then starved for 10 min for glucose (-C) in the absence (-; DMSO) or the presence (+) of 2NM-PP1. Immunoblot analyses of Sch9-pThr^{737}, Sch9, Snf1-pThr^{210}, and Snf1 were carried out as in ***Figure 1A*** (**F**). The mean relative TORC1 activities in the three strains were quantified as in ***Figure 1B*** and normalized to the values in exponentially growing *snf1^{as}* cells (set to 1.0; n=6; + SEM; unpaired Student's t-test, *p≤0.05, **p≤0.005) (**G**). The online version of this article includes the following source data for ***Figure 5—source data 1***, data for the graph shown in (**B and E**) and quantifications of the blots in (**C**) and for the graph shown in (**G**); ***Figure 5—source data 2***, uncropped blots, gels and autoradiographies shown in (**C, D and F**); ***Figure 5—source data 3***, raw blots, gels and autoradiographies shown in (**C, D and F**).

The online version of this article includes the following source data and figure supplement(s) for figure 5:

Figure 5 continued on next page

Figure 5 continued

Source data 1. Data for the graph shown in B and E and quantifications of the blots in C and for the graph shown in G.

Source data 2. Uncropped blots, gels and autoradiographies shown in C, D and F.

Source data 3. Raw blots, gels and autoradiographies shown in C, D and F.

Figure supplement 1. Snf1 in vitro kinase assays.

Figure supplement 1—source data 1. Uncropped blots.

Figure supplement 1—source data 2. Raw blots.

side). As expected, in control experiments performed with strains expressing Sch9^{S288A} or Sch9^{S288E} mutant versions, no Sch9-pSer^{288} signal was detected (middle and lower panels). Together with our finding that the Snf1 complex was also able to bind the N-terminal Sch9 fragment in microscale thermophoresis assays (***Figure 5E***), our data therefore indicate that Ser^{288} in Sch9 is a bona fide Snf1 target residue.

To address the physiological role of Ser^{288} phosphorylation in Sch9, we next studied the relative TORC1 activity upon short-term glucose starvation in 2NM-PP1-treated and -untreated *snf1^{as}* strains that expressed either wild-type Sch9, the phosphomutant Sch9^{S288A}, or the phosphomimetic Sch9^{S288E} using Sch9-pThr^{737} levels as a proxy. Interestingly, expression of Sch9^{S288E}, but not expression of wild-type Sch9 or Sch9^{S288A}, slightly but significantly suppressed the unscheduled reactivation of TORC1 in 2NM-PP1-treated Snf1^{as}-inhibited glucose-starved cells (***Figure 5F and G***). Thus, our data suggest that Snf1-mediated phosphorylation of Ser^{288} negatively impacts on the capacity of TORC1 to phosphorylate the C-terminal Thr^{737} in Sch9.

Physiological effects of Sch9^{S288E} and Pib2^{S268E,S309E} are additive

Our data so far indicated that Snf1 controls TORC1 signaling both upstream (Pib2) and downstream (Sch9) of TORC1. To address the question of whether these effects are additive concerning the TORC1-controlled phosphorylation of Thr^{737} in Sch9, we studied *snf1^{as}* strains in which the phosphomutant and phosphomimetic variants of Sch9 and Pib2 were expressed separately or combined. In line with our data above, the separate expression of Sch9^{S288E} in Snf1^{as}-inhibited (2NM-PP1-treated), glucose-starved cells only weakly suppressed the unscheduled reactivation of TORC1 (i.e. relative Sch9-Thr^{737} phosphorylation), while this effect was already strong in case of the separate expression of Pib2^{S268E,S309E} and even stronger when the expression of Sch9^{S288E} and Pib2^{S268E,S309E} were combined (***Figure 6A and B***). In contrast, the separate and combined expression of Sch9^{S288A} and Pib2^{S268A,S309A} showed, as predicted, no significant effect in the same experiment. Unexpectedly, however, the latter combination did not result in transient reactivation of TORC1, like we observed in glucose-starved, Snf1-compromised cells. This may be explained if TORC1 reactivation would rely on specific biophysical properties of the non-phosphorylated serine residues within Sch9 and Pib2 that are not mimicked by respective serine-to-alanine substitutions. Alternatively, Snf1 may employ additional parallel mechanisms (perhaps through phosphorylation of Tco89, Kog1, and/or other factors; see above) to prevent TORC1 reactivation even when Pib2 and Sch9 cannot be appropriately phosphorylated. While such models warrant future studies, our current data still suggest that Snf1-mediated phosphorylation of Pib2 and Sch9 may be both additive and together sufficient to appropriately maintain TORC1 inactive in glucose-starved cells. Corroborating this conclusion, we found the combined expression of Pib2^{S268E,S309E} and Sch9^{S288E}, but not their individual expression, nor individual or combined expression of Pib2^{S268A,S309A} and Sch9^{S288A}, to significantly reduce the relative Sch9-Thr^{737} phosphorylation when cells were grown exponentially on low-nitrogen-containing media where TORC1 activity is intrinsically low and Snf1 activity somewhat elevated (***Figure 6C and D***). In line with these data, the *snf1^{as} pib2^{SESE} sch9^{SE}* strain also exhibited a slightly higher doubling time than the *snf1^{as}* strain that was statistically significant on both low-nitrogen-containing media (i.e. 3.28±0.04 h versus 3.06±0.03 h, respectively; n=3; ± SEM; $p<0.05$) and standard synthetic complete media (i.e. 1.44±0.02 h versus 1.38±0.01 h, respectively; n=3; ± SEM; $p<0.05$). Finally, cells that combined the expression of Pib2^{S268E,S309E} and Sch9^{S288E} were also more sensitive to sub-inhibitory concentrations of rapamycin than cells expressing only one of these alleles (***Figure 6E***). Thus, Snf1-mediated fine-tuning of TORC1 activity relies on the proper phosphorylation of both Pib2 and Sch9.

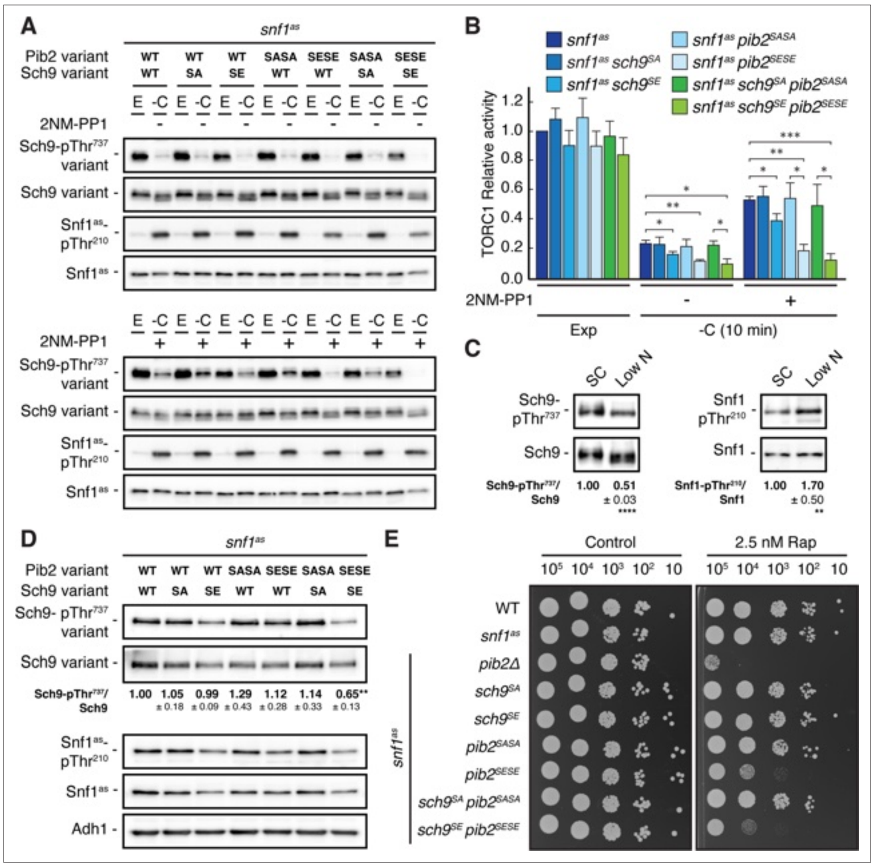

Figure 6. Physiological effects of Sch9^{S288E} and Pib2^{S268E,S309E} are additive. (**A, B**) Exponentially growing (E) *snf1*^{as} cells expressing the indicated combinations of wild type Pib2 (Pib2 variant: WT), Pib2^{S268A,S309A} (Pib2 variant: SASA), and Pib2^{S268E,S309E} (Pib2 variant: SESE) and wild type Sch9 (Sch9 variant: WT), Sch9^{288A} (Sch9 variant: SA), and Sch9^{S288E} (Sch9 variant: SE) were starved for glucose (10 min; -C) in the absence (-; DMSO; upper panels) and presence of 2NM-PP1 (+; lower panels). Immunoblot analyses were performed as in ***Figure 1A*** and the mean relative TORC1 activities (i.e. Sch9-pThr^{737}/Sch9) were quantified, normalized relative to exponentially growing *snf1*^{as} cells (set to 1.0), and shown in the bar diagram in (**B**) (n=4; + SEM; unpaired Student's t-test, *$p \leq 0.05$, **$p \leq 0.005$, ***$p \leq 0.0005$). (**C**) Growth on media containing low nitrogen levels activates Snf1-Thr^{210} phosphorylation and decreases TORC1 activity. WT cells were grown exponentially on SC or low nitrogen medium and assayed for their mean relative TORC1 activities (Sch9-pThr^{737}/Sch9) and Snf1-Thr^{210} phosphorylation levels (Snf1-pThr^{210}/Snf1), each normalized to the values of cells grown on SC (set to 1.0; n=10; ± SEM). In unpaired Student's tests, both values in cells growing on low nitrogen medium were significantly different form the ones growing on SC (**$p \leq 0.005$, ****$p \leq 0.005$). (**D, E**) Combined expression of Sch9^{S288E} and Pib2^{S268E,S309E} causes reduced Sch9-Thr^{737} phosphorylation (**D**) and enhanced rapamycin sensitivity (**E**). In (**D**), indicated strains were grown exponentially on low nitrogen medium and assayed for their mean TORC1 activities as in (**C**), which were normalized to the value of WT cells (set to 1.0; n=4; ± SEM; unpaired Student's t-test, **$p \leq 0.005$). In (**E**), cells with the indicated genotypes were grown exponentially in SD, then 10-fold serially diluted, spotted on control plates (SD) or 2.5 nM rapamycin-containing plates, and grown for 3 days at 30 °C (n=4). The online version of this article includes the following source data for ***Figure 6—source data 1***, quantifications of the blots in (**C and D**) and for graph shown in (**B**); ***Figure 6—source data 2***, uncropped blots shown in (**A, C and D**); uncropped dropspots shown in (**E**); ***Figure 6—source data 3***, raw blots shown in (**A, C and D**); raw dropspots shown in (**E**).

The online version of this article includes the following source data for figure 6:

Source data 1. Quantifications of the blots in C and D and for graph shown in B.

Figure 6 continued on next page

Figure 6 continued

Source data 2. Uncropped blots shown in A, C and D; uncropped dropspots shown in E.

Source data 3. Raw blots shown in A and C.

Source data 4. Raw blots shown in D; raw dropspots shown in E.

Discussion

Snf1/AMPK and TORC1 are conserved central kinase modules of two opposing signaling pathways that control cell growth and metabolism in response to the availability of nutrients and energy. Accordingly, energy depletion activates Snf1/AMPK, which helps to maintain energy homeostasis by favoring catabolic and inhibiting anabolic processes that generate and consume ATP, respectively (***Hardie et al., 2012***). In contrast, intracellular nutrients and high energy levels activate TORC1, which favors anabolic processes such as lipid, nucleotide, and protein synthesis and inhibits the catabolic autophagic recycling of macromolecules (***Albert and Hall, 2015***; ***González and Hall, 2017***; ***Laplante and Sabatini, 2012***; ***Liu and Sabatini, 2020***). Given the reciprocal cellular roles of Snf1/AMPK and TORC1, it is not surprising that their signaling pathways are wired to each other at different levels to coordinate the establishment of cellular homeostasis. TORC1, for instance, phosphorylates and thereby inhibits the catalytic subunit of AMPK in both mammals and the fission yeast *Schizosaccharomyces pombe* (***Ling et al., 2020***). Conversely, AMPK inhibits mTORC1 through phosphorylation of TSC2 and Raptor (***Gwinn et al., 2008***; ***Inoki et al., 2003b***), while Snf1 contributes to TORC1-body formation through phosphorylation of Kog1, although this does not seem to be required for rapid TORC1 inactivation, nor for maintaining TORC1 inactive following acute glucose starvation (***Hughes Hallett et al., 2015***; ***Sullivan et al., 2019***). In this context, the heterodimeric Gtr1-Gtr2 Rag GTPase complex has been mechanistically linked to the rapid glucose-starvation induced inactivation of TORC1 and its assembly into oligomeric structures coined TOROIDs (TORC1 organized in inhibited domains) (***Prouteau et al., 2017***), but these processes occur independently of Snf1 and rely on still elusive mechanisms that link glucose signals to the nucleotide-loading state of the Rag GTPases. Despite these findings, Snf1 may be more intimately linked to TORC1 than current knowledge suggests, because both our current and previous proteomics approaches identified several additional potential Snf1 target residues within TORC1 and some of its upstream regulators (***Braun et al., 2014***; ***Kanshin et al., 2017***). Here, we followed up on one of these leads, that is Pib2, and demonstrated that the Snf1-mediated phosphorylation of Pib2 is critical to maintain TORC1 inactive during the early phase of acute glucose starvation. Thus, our data extend the function of Pib2 to a hub that integrates both glutamine, as reported earlier (***Tanigawa and Maeda, 2017***; ***Tanigawa et al., 2021***; ***Ukai et al., 2018***), and glucose signals to control TORC1. Our current data favor a model according to which Snf1-mediated phosphorylation of the Kog1-binding domain in Pib2 weakens its affinity to Kog1 and thereby reduces the TORC1-activating influence of Pib2 that is mediated by the C-terminal TORC1-activating (CAD) domain via a mechanism that is still largely elusive. Interestingly, Pib2 has also been involved in the formation of TORC1-bodies, which seem not to be required for TORC1 inactivation per se but rather serve to increase the threshold for TORC1 reactivation after long-term glucose starvation (***Sullivan et al., 2019***). The latter process is primarily driven by phosphorylation of Kog1 and, albeit dependent on Pib2, may also require loosening of the Kog1-Pib2 association, because deletion of the N-terminal TORC1-inhibitory domain (NID) in Pib2 has been found to induce TORC1-body formation (***Sullivan et al., 2019***). Here too, the mechanistic details remain to be deciphered and will likely require detailed structural information on the interactions between Pib2, Kog1, and the EGOC that also plays a role in TORC1-body formation (***Sullivan et al., 2019***). Curiously, human phafin/LAPF, which is structurally most closely related to Pib2 and with which it shares the FYVE and CAD domains (***Kim and Cunningham, 2015***), also regulates mTORC1-controlled processes, but it remains currently unknown whether these effects are executed through regulation of mTORC1 (***Hatakeyama, 2021***).

The activities of the Snf1 and TORC1 pathways are also wired to each other through a set of directly or indirectly controlled common effectors that, given the opposite roles of Snf1 and TORC1 in cell metabolism, are generally inversely regulated by these pathways (***De Virgilio, 2012***). For instance, Snf1 and TORC1 converge on the transcription factor Gln3 and the eukaryotic translation initiation factor 2α (eIF2α) to oppositely regulate their function (***Beck and Hall, 1999***; ***Bertram et al., 2002***; ***Cherkasova et al., 2010***; ***Cherkasova and Hinnebusch, 2003***). Interestingly, Snf1 and TORC1 have already previously been reported to directly converge on different residues within Sch9 (**Lu et al., 2011**), a key controller of protein synthesis and aging in yeast (**Loewith and Hall, 2011**). Accordingly, both kinases phosphorylate Sch9, but, while the TORC1 target residues in Sch9 have been functionally well-defined and located in the C-terminus of Sch9 (**Urban et al., 2007**), the respective Snf1 target residue(s) remained unidentified (**Lu et al., 2011**). Here, we show that Snf1 phosphorylates Ser^{288} in Sch9, which is not only supported by our current and previous phosphoproteomic approaches (**Braun et al., 2014**), but also by our extended biochemical in vitro and in vivo studies of wild-type and Sch9^{S288A} alleles. In line with the opposite conceptual roles of Snf1 and TORC1 within cells, our physiological experiments posit a model in which Snf1-mediated phosphorylation of Ser^{288} in Sch9 antagonizes the TORC1-mediated phosphorylation (at Thr^{737}) and hence activation of Sch9. Notably, such a model also provides an elegant explanation for the reciprocal role of Snf1 and Sch9 in controlling chronological life span (**Maqani et al., 2018**; **Wei et al., 2008**; **Wierman et al., 2017**), although it is difficult to reconcile with the idea that Snf1 activates Sch9 (in parallel to TORC1) to inhibit replicative lifespan (**Lu et al., 2011**). The latter assumption, however, appears to depend in part on the phosphorylation of a threonine(s) in Sch9, specifically in cells lacking the regulatory Snf1 subunit Sip2, and may therefore not be related to the Sch9-Ser^{288} phosphorylation studied here. Of note, the question of how Ser^{288} phosphorylation restrains TORC1-mediated phosphorylation of Sch9-Thr^{737} also warrants further experimental efforts. The Ser^{288} residue lies within the C2 domain that has been suggested to mediate the vacuolar recruitment of Sch9 (**Jin et al., 2014**). However, recent studies have elaborated that the membrane-localization of Sch9 is primarily defined by its N-terminal 184 amino acids, but not the C2 domain (**Chen et al., 2021**; **Novarina et al., 2021**). We therefore assume that the phosphorylation of Ser^{288} within the C2 domain, rather than controlling the subcellular localization, may either favor the recruitment of a pThr^{737}-targeting phosphatase to Sch9 or interfere with appropriate TORC1 docking. The latter could for instance be achieved if the phosphorylated C2 domain would act as an auto-inhibitory domain that folds back to the C-terminal part of Sch9 to impose specific conformational constraints. Intriguingly, a similar regulatory mechanism has been suggested for the protein kinase Ypk1, a TORC2 target that is very closely related to Sch9 (**Thorner, 2022**). In this case, structural predictions suggested that a critical aspartate (D242) located in a N-terminal C2-like domain is packed tightly against the upper lobe of the kinase domain in Ypk1 to favor its inactive state (**van Dam et al., 2011**). For Sch9, as for Pib2, the resolution of these issues will likely require more detailed structural information on Sch9 that is currently not available.

In this study, we focused on the mechanisms through which Snf1 regulates TORC1 during the early phase of acute glucose starvation. Our phosphoproteome data, however, indicate that Snf1 may also control TORC1 through processes that are relevant during later phases of prolonged glucose starvation. For instance, we identified the lipid kinase Fab1, which generates phosphatidylinositol-3,5-bisphosphate (PI(3,5)P$_2$) from PI3P, as a potential Snf1 target (**Figure 3F**). Fab1 is not only a TORC1 effector, but it also defines the activity and subcellular distribution (between vacuolar membranes and signaling endosomes) of TORC1 (**Chen et al., 2021**). Snf1 may therefore modulate the feedback control loop between Fab1 and TORC1 in response to glucose limitation. This function is likely executed by Snf1 complexes containing the β-subunit Sip1, which, in addition to being potentially feedback-controlled by Snf1, tethers Snf1 complexes to vacuolar membranes in response to carbon stress (**Hedbacker et al., 2004**). We also identified Snf1-regulated phospho-residues in Apl6, a subunit of the adaptor protein 3 (AP-3) complex that functions in cargo-selective protein transport from the TGN to the vacuole (**Cowles et al., 1997**). In this case, Snf1 may control the flux of Ego1 towards (and hence assembly of the TORC1-regulatory EGOC at) vacuolar membranes, which requires proper AP-3 function (**Hatakeyama et al., 2019**). Our mass spectrometry approaches further highlighted several phospho-residues in α-arrestins including Aly2, Bul1, and Bul2 that appeared to be regulated by Snf1. These arrestins drive Rsp5-mediated ubiquitination of specific nutrient transporters such as the amino acid permeases Gap1, Dip5, and others to orchestrate their endocytosis in response to nutrients (**Kahlhofer et al., 2021**; **Zbieralski and Wawrzycka, 2022**). Because amino acid permeases control TORC1 either via their role in distributing amino acids across cellular membrane compartments or through their proposed role as transceptors (**Melick and Jewell, 2020**; **Wolfson and Sabatini, 2017**; **Zheng et al., 2016**), it is conceivable that Snf1 also controls TORC1 indirectly via phosphorylation of α-arrestins. In a similar vein, Snf1 may also reduce ammonium uptake by impinging on the Npr1-regulated Par32, which inhibits the ammonium transporters Mep1 and Mep3 and thereby indirectly reduces TORC1 activity (**Boeckstaens et al., 2015**; **Varlakhanova et al., 2018**). Finally, two protein kinases, namely Ptk2 and Hkr1, which activate the plasma membrane H^+-ATPase Pma1 in response to glucose (**Eraso et al., 2006**; **Goossens et al., 2000**), were also among the presumed Snf1 targets in our data set (**Figure 3F**). Through Ptk2 and Hkr1, Snf1 may conceivably adjust TORC1 activation that is related to Pma1 and H^+-coupled nutrient uptake (**Saliba et al., 2018**). In sum, our proteomics study provides a wealth of new leads for future studies on how Snf1 may be wired to TORC1 to ensure cellular homeostasis under long-term glucose limitation.

Materials and methods

Yeast strains, plasmids, and growth conditions

Saccharomyces cerevisiae strains and plasmids are listed in **Supplementary file 1A** and **Supplementary file 1B**. Point mutations were introduced in the genome by CRISPR-Cas9, as described (**Generoso et al., 2016**), while gene deletion and tagging were performed using the pFA6a system-based PCR-toolbox (**Janke et al., 2004**). The oligos used to generate the CRISPR-Cas9 plasmids are listed in **Supplementary file 1C**. Plasmids were created as described earlier (**Generoso et al., 2016**). Strains were rendered prototrophic, unless stated otherwise, by transforming them with the empty centromeric plasmids listed in **Supplementary file 1B**. In order to maintain the plasmids, cells were pregrown in a synthetic dropout (SD; 0.17% yeast nitrogen base, 0.5% ammonium sulfate [AS], 0.2% dropout mix [USBiological], and 2% glucose) medium. Then, synthetic complete (SC; SD with all amino acids) medium was used for the dilution of the cells the following day. The same procedure was adopted for experiments where cells were grown in media containing low glucose (i.e. 0.05% instead of 2% glucose) or low nitrogen (with a reduced amount of AS [0.0625%] and devoid of amino acids). Starvation experiments were performed by cell filtration and transfer to carbon starvation medium (SC without glucose), nitrogen starvation medium (2% glucose, 0.17% yeast nitrogen base) or nitrogen and carbon starvation medium (0.17% yeast nitrogen base), for the times indicated. For re-addition experiments, 2% final glucose and/or 3.3 mM glutamine was/were added to the culture. When indicated, 10 µM 2NM-PP1 dissolved in DMSO was added to the culture. As a control, the same volume of DMSO was added. Strains and plasmids are available upon request. Cell growth was monitored by measuring the concentration (OD_{600nm}/mL) with a spectrophotometer.

Growth tests on plates

Cells were pregrown over-day in SD or SC until OD_{600nm} above 1.0. Cells were washed two times with water and starting from the concentration of 1.0 OD_{600nm}/mL, 10-fold serial dilutions were prepared in water. Cells were spotted on SD or SC plates with or without rapamycin, at the indicated concentrations, and further grown for 3 days at 30 °C.

SILAC conditions and cell lysis

Yeast strains were grown in SC medium containing either non-labeled or labeled lysine and arginine variants ('medium-heavy' L-arginine-$^{13}C_6$ (Arg6) and L-lysine-$^{2}H_4$ (Lys4), or 'heavy' L-arginine-$^{13}C_6$-$^{15}N_4$ (Arg10) and L-lysine-$^{13}C_6$-$^{15}N_2$ (Lys8) amino acids (Sigma-Aldrich)), until reaching an OD_{600nm} of approximatively 1.0. Then, cultures grown in the presence of 'medium-heavy' and 'heavy' arginine and lysine were filtered and resuspended in carbon starvation medium for 5 and 15 min, respectively, in the presence of the vehicle (DMSO) or 2NM-PP1. All cultures were ultimately collected by filtration. The nitrocellulose filter was dipped in tubes containing 40 mL of the cell culture medium plus TCA, 6% final concentration. Cells were pelleted and washed with 40 mL acetone and subsequently dried overnight in a freeze-dryer (ZIRBUS). Dried differentially labeled cells (30 mg) of each sample were mixed. Cells were lysed in 50 mL tubes with 6 mL urea buffer (8 M urea, 50 mM Tris HCl pH 8.0) and acid-washed glass beads using a Precellys machine (6x30 s, with 60 s pause after each cycle). Debris were pelleted and the supernatants containing cellular proteins were collected, followed by MS sample preparation.

On beads in vitro kinase assay (OBIKA)

Cell pellets were obtained by five different cultures of exponentially growing *snf1^{as}* cells. Cells were pre-grown overnight in 5% glucose YP (yeast extract-peptone) and the following day, they were diluted at the concentration of 0.2 OD_{600nm}/mL in 2 L 5% glucose YP (yeast extract-peptone). Cells were grown until late exponential phase, when they were treated with 10 μM 1NM-PP1 for 20 min. Cells were then collected by filtration, frozen in liquid nitrogen, and cryogenically disrupted by using a Precellys homogenizer in 10 mL of primary amine-free lysis buffer (50 mM HEPES pH 7.5, 1% NP-40, 150 mM NaCl, 1 mM EDTA pH 8.0, 1 mM EGTA pH 8.0 and Roche complete protease inhibitor EDTA-free) and acid-washed glass beads using a Precellys machine (6x30 s, with 60 s pause after each cycle). Lysates were collected by centrifugation at 4000 rpm at 4 °C. The lysates were dialyzed using dialysis buffer (50 mM HEPES pH 7.5, 0.1% NP-40, 150 mM NaCl, 1 mM EDTA pH 8.0, 1 mM EGTA pH 8.0, and 1 mM PMSF) and a molecular-porous membrane tubing (14 kDa, Sigma-Aldrich) to remove primary amine containing metabolites. After 2 h at 4 °C, the buffer was refreshed for overnight dialysis. N-hydroxy-succinimide (NHS) -activated Sepharose beads (5 mL) were washed three times with 10 mL of ice-cold 1 mM HCl and two times with 10 mL of lysis buffer before incubating with 60 mg protein to saturate the beads. The coupling was performed on a rotating mixer at 4 °C overnight. Next, the beads were spun down to remove the supernatant. Beads were then washed three times with 10 mL of phosphatase buffer (50 mM HEPES, 100 mM NaCl, 0.1% NP-40). Phosphatase buffer (1 mL) containing 5’000–10’000 units of lambda phosphatase with 1 mM $MnCl_2$ was added and incubated for 4 h at room temperature or overnight at 4 °C on a rotating mixer to dephosphorylate endogenous proteins. Beads were washed two times with 10 mL of kinase buffer (50 mM Tris-HCl pH 7.6, 10 mM $MgCl_2$, 150 mM NaCl, and 1 x PhosSTOP). Endogenous kinases bound to beads were inhibited by incubation with 1 mM FSBA in 1 mL of kinase buffer at RT on the rotor for 2 h. In addition, staurosporine was added to a final concentration of 100 μM to inhibit the remaining active kinases for 1 h. The beads were washed three times with 10 mL of kinase buffer to remove non-bound kinase inhibitors. The supernatant was removed completely by gel loading tips. Kinase buffer was added to a volume of 860 μL for both kinase inactive and wild-type Snf1 samples. Subsequently, 100 μl of 10 mM ATP, 10 μL of 100 mM DTT, and 30 μl of purified kinase variants were added into each tube. Kinase assays were performed on a rotor at 30 °C for 4 h. Finally, reactions were quenched by snap freezing in liquid nitrogen and samples were lyophilized overnight. Urea buffer (250 μL) was added to the dry beads, followed by MS sample preparation (***Hu et al., 2021***).

MS sample preparation

For in vivo phosphoproteome and OBIKA samples, lysates or proteins on beads were reduced with 1 mM DTT, alkylated with 5 mM iodoacetamide, and digested with endoproteinase Lys-C for 4 h. The concentration of urea was diluted to 1 M before overnight trypsin digestion. The peptides were purified and fractionated as described previously (***Hu et al., 2019***). Briefly, peptides were purified by SPE using HR-X columns in combination with C18 cartridges. The purified peptides were frozen, lyophilized, and fractionated by HpH reversed-phase chromatography (***Batth et al., 2014***). A total of 96 fractions were mixed with an interval of 12 to yield 8 final fractions. The peptides were acidified, frozen in liquid nitrogen, and lyophilized before phosphopeptide enrichment.

For manual phosphopeptide enrichment, samples were incubated with 2 mg TiO_2 slurry, which was pre-incubated with 300 mg/mL lactic acid in 80% acetonitrile/1% trifluoroacetic acid (TFA) before enrichment for 30 min at room temperature (***Zarei et al., 2016***). For peptide elution, TiO_2 beads were transferred to 200 μL pipette tips, which were blocked by C8 discs. Tips were sequentially washed with 200 μL of 10% acetonitrile/1% TFA, twice with 200 μL of 80% acetonitrile/1% TFA, and 100 μL of LC-MS grade water. Phosphopeptides were eluted into single tubes with 50 μL of 1.25% ammonia in 20% acetonitrile and 50 μL of 1.25% ammonia in 80% acetonitrile. Eluates were acidified with 5 μL of formic acid. Samples were concentrated by vacuum concentration and resuspended in 20 μL of 0.1% formic acid for LC-MS/MS analysis. The tip flow-through was desalted by STAGE tips for non-phosphopeptide analysis.

Automated phosphopeptide enrichment was performed on an Automated Liquid Handling Platform (Bravo, Agilent) (***Post et al., 2017***). The Fe (III)-NTA cartridges (5 μL) were primed with 0.1% TFA in acetonitrile and equilibrated with 0.1% TFA in 80% acetonitrile (equilibration/washing buffer). Peptides were resuspended in 200 μL of equilibration buffer and loaded on the cartridges with a flow rate of 5 μL/min. Cartridges were washed twice with 200 μL of washing buffer with a flow rate of 10 μL/min. Phosphopeptides were eluted with 100 μL of 1% ammonia in 80% acetonitrile with a flow rate of 5 μL/min. Eluates were acidified with 5 μL of formic acid. Samples were concentrated by lyophilizer and resuspended in 20 μL of 0.1% formic acid for LC-MS/MS analysis.

LC-MS/MS

LC-MS/MS measurements were performed on a QExactive (QE) Plus, HF-X, and Exploris480 mass spectrometer coupled to an EasyLC 1000 and EasyLC 1200 nanoflow-HPLC, respectively (all Thermo Scientific). Peptides were fractionated on a fused silica HPLC-column tip (I.D. 75 μm, New Objective, self-packed with ReproSil-Pur 120 C18-AQ, 1.9 μm (Dr. Maisch) to a length of 20 cm) using a gradient of A (0.1% formic acid in water) and B (0.1% formic acid in 80% acetonitrile in water): samples were loaded with 0% B with a max. pressure of 800 Bar; peptides were separated by 5–30% B within 85 min with a flow rate of 250 nL/min. The spray voltage was set to 2.3 kV and the ion-transfer tube temperature to 250 °C; no sheath and auxiliary gas were used. Mass spectrometers were operated in the data-dependent mode; after each MS scan (mass range m/z=370–1750; resolution: 70’000 for QE Plus and 120’000 for HF-X and Exploris480) a maximum of ten scans for QE Plus, 12 scans HF-X and 20 scans for Exploris480 were performed using a normalized collision energy of 25%, a target value of 10’000 (QE Plus and HF-X)/5000 (Exploris480) and a resolution of 17’500 for QE Plus, 30’000 for HF-X and 60’000 for Exploris480. MS raw files were analyzed using MaxQuant (version 1.6.2.10; **Cox and Mann, 2008**) using a Uniprot full-length *S. cerevisiae* database plus common contaminants such as keratins and enzymes used for in-gel digestion as reference. Carbamidomethylcysteine was set as fixed modification and protein amino-terminal acetylation, serine-, threonine-, and tyrosine- phosphorylation, and oxidation of methionine were set as variable modifications. The MS/MS tolerance was set to 20 ppm and three missed cleavages were allowed using trypsin/P as enzyme specificity. Peptide, site, and protein FDR based on a forward-reverse database were set to 0.01, the minimum peptide length was set to 7, the minimum score for modified peptides was 40, and the minimum number of peptides for identification of proteins was set to one, which must be unique. The ‘match-between-run’ option was used with a time window of 0.7 min. MaxQuant results were analyzed using Perseus (**Tyanova et al., 2016**).

MS data analyses

The in vivo phosphoproteome data were analyzed as described (**Hu et al., 2019**). Briefly, measurements of the log2 fold changes on each site were combined into a random effect model, considering a priori the sites as a random effect, and including the variability among replicates by also considering the replicates as a random effect. The model assigns an average effect size and its corresponding 95% confidence interval to each site. If the confidence interval includes values of zeros, then there is no statistically significant log2 fold change, whereas if the confidence interval is above (below) zero, there is statistical evidence for upregulation (downregulation). Additionally, imputation processes were applied on both protein and phosphosite levels. Proteins that were quantified in at least two biological replicates were kept and missing values were replaced by random values of a normal distribution to mimic low abundance measurements. Both width and down shift were applied according to Perseus default settings. Phosphosites were further normalized to the protein levels. Only sites which were quantified in at least three replicates in either DMSO 5 min or 15 min were kept. Missing values in 2NM-PP1-treated samples were then replaced by the maximum likelihood estimators (MLE) imputation method (**Messer and Natarajan, 2008**). Finally, a t-test (FDR≤0.05) was performed between DMSO and 2NM-PP1-treated samples to determine significantly changing phosphosites.

OBIKA data were analyzed using Perseus. Phosphosites which were quantified in at least three replicates in WT samples were kept. Missing values in kinase-inactive samples were replaced by either random values of a normal distribution to mimic low abundance measurements, both width and down shift were applied according to default settings, when none of five replicates was quantified, or MLE, when at least 1 of five replicates was quantified. T-tests (FDR≤0.05) were performed between WT and kinase-inactive samples to identify significantly changing sites.

Protein purification and in vitro kinase assays

The Snf1 complex was purified from a Snf1-TEV-TAP-expressing yeast strain grown in YPD. To induce Snf1 activation, cells were washed on a filter. The same procedure was adopted to purify the catalytically inactive Snf1 complex containing the *snf1*^{T210A} α-subunit and the Snf1 complex, containing the C-terminally GFP-tagged Snf4 γ-subunit. Yeast cells carrying the plasmids for Sch9$^{1-394}$-TEV-TAP or Sch9-TEV-TAP expression were grown overnight in SRafinose-Ura medium supplemented with 0.01% sucrose. The next day, in order to induce Sch9$^{1-394}$-TEV-TAP and Sch9-TEV-TAP expression, 2% (final concentration) galactose was added to the cells when they reached OD_{600nm}/mL of 0.2. The induction with galactose was carried out for 6 h.

For all the protein purification from yeast, cells were then collected by filtration, frozen in liquid nitrogen, and cryogenically disrupted by using a Precellys homogenizer in 10 mL of lysis buffer (50 mM Tris-HCl pH 7.5, 150 mM NaCl, 0.1% NP-40, 10% glycerol, 400 mM Pefabloc, and Roche complete protease inhibitor EDTA-free). The cleared lysates were incubated for 2 h at 4 °C with IgG-coupled Dynabeads (Dynabeads M-270 Epoxy; Invitrogen, Thermo Fisher Scientific, Basel, Switzerland). The beads were washed five times with lysis buffer and proteins were eluted in TEV buffer (50 mM Tris-HCl pH 7.5, 0.5 mM EDTA,) with 2% TEV protease and stored at –80 °C after the addition of 10% glycerol.

His_6-$Pib2^{221-635}$ variants were purified from *E. coli* as described in ***Péli-Gulli et al., 2015*** using Ni-charged agarose beads (QIAGEN, product number 30210). Proteins were eluted in elution buffer (50 mM NaH_2PO_4 pH 8.0, and 200 mM imidazole) and stored at –80 °C after the addition of 10% glycerol.

In vitro radioactive kinase reactions were carried out in Snf1 kinase buffer (20 mM HEPES pH 7.5, 100 mM NaCl, 0.5 mM EDTA, 0.5 mM DTT, and 5 mM MgAc), with 60 ng Snf1 (quantified with respect to the Snf1 subunit), 1 µg Pib2, or 80 ng Sch9 in 20 µL total volume, and started by adding the ATP Mix (3 µL [γ–32P]-ATP [Hartmann Analytic, SRP-501], 6 µL 200 µM ATP, and 1 µL Kinase Buffer 1 X) and stopped by adding SDS-PAGE sample buffer. Reactions were carried out at 30 °C and for 10 min or 30 min for Pib2 or Sch9, respectively. Proteins were separated by SDS-PAGE, stained with SYPRO Ruby (Sigma) to assess loading, and analysed using a phosphoimager (Typhoon FLA 9500; GE Healthcare). In vitro kinase assays probed by immunoblot analysis was carried out similarly as described above. The reaction was performed in 40 µL volume for 30 min at 30 °C. In the ATP mix, [γ-^{32}P]-ATP was substituted with H_2O. Finally, the reaction was probed using the following antibodies: custom-made rabbit anti-Sch9-$pSer^{288}$ (Eurogentec, 1:4000), and goat anti-Sch9 (GenScript, 1:1000). To assess the loading, the gel was stained with SYPRO Ruby (Sigma).

Co-immunoprecipitation

Yeast cells expressing the indicated fusion proteins were harvested by filtration, frozen in liquid nitrogen, and cryogenically disrupted using the Precellys homogenizer in 4 mL of lysis buffer (50 mM Tris-HCl pH 7.5, 150 mM NaCl, 0.1% NP-40, 10% glycerol, 400 mM Pefabloc, and Roche complete protease inhibitor EDTA-free) with the addition of 60 mM glutamine as in ***Ukai et al., 2018***. Cleared lysates were equilibrated in the same lysis buffer. For input samples, aliquots of cleared lysates were collected and denatured in presence of SDS-PAGE sample buffer. For co-immunoprecipitations, the cleared lysates were incubated for 2 h at 4 °C with prewashed anti-c-myc MagBeads (Pierce Thermo Fisher Scientific, product number 88843). After five washes with lysis buffer, beads were resuspended in 20 µL lysis buffer and denatured in presence of SDS-PAGE sample buffer. Inputs and pull-down samples were analyzed by SDS-PAGE immunoblot with mouse anti-myc (Santa Cruz, 1:10,000) and mouse anti-HA (ENZO, 1:1000) antibodies.

Microscale thermophoresis

Microscale thermophoresis (MST) experiments were performed using a Monolith NT.115 (Nanotemper Technologies). Labeled purified Snf1 complex (0.144 µM), containing the C-terminally GFP-tagged Snf4 γ-subunit, was mixed with a twofold serial dilution (a total of 16 samples) of unlabeled 18.1 µM His_6-$Pib2^{221-635}$ in elution buffer (50 mM NaH_2PO_4 pH 8.0, 200 mM imidazole, and 10% glycerol) or with unlabeled 0.118 µM $Sch9^{1-394}$ in elution buffer (50 mM Tris-HCl pH 8.0, 0.5 mM EDTA, and 10% glycerol). Samples were loaded into Monolith NT.115 Capillaries and MST measurements were performed using 20% laser power setting at 30 °C. Experiments were performed in triplicates and data were fitted using the K_d model of the MO.Affinity Analysis software (Nanotemper Technologies). The dissociation constant K_d was obtained by plotting the bound fraction against the logarithm of ligand concentration.

Cell lysate preparation and immunoblot analyses

Cell lysates were prepared similarly as described in ***Hatakeyama et al., 2019***. After denaturation at 98 °C for 5 min, samples were loaded on SDS-PAGE and transferred onto nitrocellulose membranes. After 1 h blocking with blocking buffer (5% milk powder in tris-buffered saline), membranes were immunoblotted with the following primary antibodies: rabbit anti-Adh1 (Calbiochem, product number 126745; 1:200,000 dilution), rabbit anti-Sch9-pThr^{737} (De Virgilio lab, 1:10,000 dilution), rabbit anti-Sch9-pSer^{288} (Rospert lab, 1:4000 dilution), goat anti-Sch9 (De Virgilio lab, 1:1000 dilution), rabbit anti-AMPK-pThr^{172} (Cell Signal, product number 2535 S, 1:1000 dilution) to detect the phosphorylation of Snf1-Thr^{210}, mouse anti-His$_6$ (Sigma, product number H1029, 1:1000 dilution) to detect total levels of Snf1, anti-ACC1-pSer^{79} (Thermo Fisher Scientific, product number PA5-17564, 1:500 dilution), and mouse anti-GFP (Roche, product number 11814460001, 1:3000 dilution). After 3 washes, the membranes were incubated with anti-mouse (BIO-RAD, product number 170–6516; 1:3000 dilution), rabbit (BIO-RAD, product number 170–6515; 1:3000 dilution), or goat (BIO-RAD, product number 5160–2104; 1:3000 dilution) secondary antibodies conjugated with horseradish peroxidase, washed again for three times, and developed with ECL (GE Healthcare).

Statistical analyses

Statistical significance was determined by three or more independent biological replicates, by using Student's t-test analysis, performed with GraphPad Prism 9.0. Unpaired Student's t-test was used for the comparison of normalized data. Values with a p-value (or FDR where indicated) lower than 0.05 were considered significantly different. In the figure legends, the number of independent replicas, method used to express the variability, specific statistical tests, and significance are indicated.

Figures 2–6

Acknowledgements

We thank Riko Hatakeyama and Dieter Kressler for plasmids, Malika Jaquenoud for technical assistance, Marie-Pierre Péli-Gulli for carefully reading the manuscript and guidance with microscopy, Roberto Pagliarin for the kind gift of the 2NM-PP1 inhibitor, Sebastien Leon and Andrew Capaldi for constructive criticism based on the preprint version of this article, and Jeremy Thorner for pointing out the mechanistic aspects of Ypk1 regulation. This work was supported by the Canton of Fribourg (to J D and C D V), the Swiss National Science Foundation (310030_166474/184671 to CDV, 310030_184781 to JD, and 316030_177088 to JD and CDV), FWO-Vlaanderen (G069413, G0C7222N) and KU Leuven (C14/17/063, C14/21/095) to JW. We also acknowledge financial support from the Italian Ministry of University and Research (MUR) through grants 2020-ATE-0329 and Dipartimenti di Eccellenza 2017 to the University of Milano-Bicocca, Department of Biotechnology and Biosciences (to FT and PC) and from the Deutsche Forschungsgemeinschaft (DFG, German Research Foundation) through Project-ID 403222702 - SFB 1381, TP B08 (to SR) and RO 1028/5–2 (to SR).

Additional information

Funding

Funder	Grant reference number	Author
Canton of Fribourg		Jörn Dengjel Claudio De Virgilio
Schweizerischer Nationalfonds zur Förderung der Wissenschaftlichen Forschung	310030_166474/184671	Claudio De Virgilio
Schweizerischer Nationalfonds zur Förderung der Wissenschaftlichen Forschung	310030_184781	Jörn Dengjel

Funder	Grant reference number	Author
Schweizerischer Nationalfonds zur Förderung der Wissenschaftlichen Forschung	316030_177088	Jörn Dengjel Claudio De Virgilio
Fonds Wetenschappelijk Onderzoek	G069413	Joris Winderickx
Fonds Wetenschappelijk Onderzoek	G0C7222N	Joris Winderickx
Katholieke Universiteit Leuven	C14/17/063	Joris Winderickx
Katholieke Universiteit Leuven	C14/21/095	Joris Winderickx
Ministero dell'Università e della Ricerca	2020-ATE-0329	Farida Tripodi Paola Coccetti
Deutsche Forschungsgemeinschaft	Project-ID 403222702 - SFB 1381	Sabine Rospert
Deutsche Forschungsgemeinschaft	RO 1028/5-2	Sabine Rospert
Deutsche Forschungsgemeinschaft	TP B08	Sabine Rospert

The funders had no role in study design, data collection and interpretation, or the decision to submit the work for publication.

Author contributions

Marco Caligaris, Conceptualization, Formal analysis, Validation, Investigation, Visualization, Methodology, Writing – review and editing; Raffaele Nicastro, Conceptualization, Formal analysis, Supervision, Validation, Investigation, Visualization, Methodology, Project administration, Writing – review and editing; Zehan Hu, Conceptualization, Data curation, Formal analysis, Validation, Investigation, Visualization, Methodology, Writing – review and editing; Farida Tripodi, Joris Winderickx, Sabine Rospert, Paola Coccetti, Conceptualization, Validation, Writing – review and editing; Johannes Erwin Hummel, Validation, Investigation, Methodology, Writing – review and editing; Benjamin Pillet, Conceptualization, Formal analysis; Marie-Anne Deprez, Validation, Writing – review and editing; Jörn Dengjel, Conceptualization, Resources, Formal analysis, Validation, Methodology, Writing - original draft, Writing – review and editing; Claudio De Virgilio, Conceptualization, Resources, Data curation, Supervision, Funding acquisition, Validation, Methodology, Writing - original draft, Writing – review and editing

Author ORCIDs

Marco Caligaris http://orcid.org/0000-0003-1732-7694
Raffaele Nicastro http://orcid.org/0000-0002-5420-2228
Farida Tripodi http://orcid.org/0000-0003-1246-979X
Benjamin Pillet http://orcid.org/0000-0002-7313-4304
Joris Winderickx http://orcid.org/0000-0003-3133-7733
Sabine Rospert http://orcid.org/0000-0002-3089-9614
Paola Coccetti http://orcid.org/0000-0001-5898-5883
Jörn Dengjel http://orcid.org/0000-0002-9453-4614
Claudio De Virgilio http://orcid.org/0000-0001-8826-4323

Decision letter and Author response

Decision letter https://doi.org/10.7554/eLife.84319.sa1
Author response https://doi.org/10.7554/eLife.84319.sa2

Additional files

Supplementary files

- Supplementary file 1. Strains, plasmids and oligonucleotides used in this study.
- Supplementary file 2. Significantly in vivo and in vitro regulated phosphosites.
- MDAR checklist

Data availability

All data generated or analyzed during this study are included in the manuscript and supporting files. Source data files have been provided for Figures 1-6 and figure supplements. The mass spectrometry proteomics data have been deposited to the ProteomeXchange Consortium via the PRIDE partner repository with the dataset identifier PXD037381.

The following dataset was generated:

Author(s)	Year	Dataset title	Dataset URL	Database and Identifier
Dengjel J	2022	Snf1/AMPK fine-tunes TORC1 signaling in response to glucose starvation	https://www.ebi.ac.uk/pride/archive/projects/PXD037381	PRIDE, PXD037381

References

Albert V, Hall MN. 2015. Mtor signaling in cellular and organismal energetics. *Current Opinion in Cell Biology* **33**:55–66. DOI: https://doi.org/10.1016/j.ceb.2014.12.001, PMID: 25554914

Alvaro CG, Aindow A, Thorner J. 2016. Differential phosphorylation provides a switch to control how α-arrestin Rod1 down-regulates mating pheromone response in *Saccharomyces cerevisiae*. *Genetics* **203**:299–317. DOI: https://doi.org/10.1534/genetics.115.186122, PMID: 26920760

Anandapadamanaban M, Masson GR, Perisic O, Berndt A, Kaufman J, Johnson CM, Santhanam B, Rogala KB, Sabatini DM, Williams RL. 2019. Architecture of human RAG GTPase heterodimers and their complex with mTORC1. Science **366**:203–210. DOI: https://doi.org/10.1126/science.aax3939, PMID: 31601764

Arakel EC, Huranova M, Estrada AF, Rau EM, Spang A, Schwappach B. 2019. Dissection of GTPase-activating proteins reveals functional asymmetry in the COPI coat of budding yeast. *Journal of Cell Science* **132**:jcs232124. DOI: https://doi.org/10.1242/jcs.232124, PMID: 31331965

Bar-Peled L, Schweitzer LD, Zoncu R, Sabatini DM. 2012. Ragulator is a GEF for the RAG GTPases that signal amino acid levels to mTORC1. *Cell* **150**:1196–1208. DOI: https://doi.org/10.1016/j.cell.2012.07.032, PMID: 22980980

Bar-Peled L, Chantranupong L, Cherniack AD, Chen WW, Ottina KA, Grabiner BC, Spear ED, Carter SL, Meyerson M, Sabatini DM. 2013. A tumor suppressor complex with gap activity for the RAG GTPases that signal amino acid sufficiency to mTORC1. Science **340**:1100–1106. DOI: https://doi.org/10.1126/science.1232044, PMID: 23723238

Batth TS, Francavilla C, Olsen JV. 2014. Off-line high-pH reversed-phase fractionation for in-depth phosphoproteomics. *Journal of Proteome Research* **13**:6176–6186. DOI: https://doi.org/10.1021/pr500893m, PMID: 25338131

Beck T, Hall MN. 1999. The TOR signalling pathway controls nuclear localization of nutrient-regulated transcription factors. *Nature* **402**:689–692. DOI: https://doi.org/10.1038/45287, PMID: 10604478

Bertram PG, Choi JH, Carvalho J, Chan T-F, Ai W, Zheng XFS. 2002. Convergence of TOR-nitrogen and Snf1-glucose signaling pathways onto Gln3. *Molecular and Cellular Biology* **22**:1246–1252. DOI: https://doi.org/10.1128/MCB.22.4.1246-1252.2002, PMID: 11809814

Binda M, Péli-Gulli MP, Bonfils G, Panchaud N, Urban J, Sturgill TW, Loewith R, De Virgilio C. 2009. The vam6 GEF controls TORC1 by activating the ego complex. *Molecular Cell* **35**:563–573. DOI: https://doi.org/10.1016/j.molcel.2009.06.033, PMID: 19748353

Boeckstaens M, Merhi A, Llinares E, Van Vooren P, Springael JY, Wintjens R, Marini AM. 2015. Identification of a novel regulatory mechanism of nutrient transport controlled by TORC1-npr1-amu1/par32. *PLOS Genetics* **11**:e1005382. DOI: https://doi.org/10.1371/journal.pgen.1005382, PMID: 26172854

Bowman RW, Jordahl EM, Davis S, Hedayati S, Barsouk H, Ozbaki-Yagan N, Chiang A, Li Y, O'Donnell AF. 2022. Torc1 signaling controls the stability and function of α-arrestins aly1 and aly2. *Biomolecules* **12**:533. DOI: https://doi.org/10.3390/biom12040533

Braun KA, Vaga S, Dombek KM, Fang F, Palmisano S, Aebersold R, Young ET. 2014. Phosphoproteomic analysis identifies proteins involved in transcription-coupled mRNA decay as targets of Snf1 signaling. *Science Signaling* **7**:ra64. DOI: https://doi.org/10.1126/scisignal.2005000, PMID: 25005228

Brito AS, Soto Diaz S, Van Vooren P, Godard P, Marini AM, Boeckstaens M. 2019. Pib2-dependent feedback control of the TORC1 signaling network by the Npr1 kinase. *IScience* **20**:415–433. DOI: https://doi.org/10.1016/j.isci.2019.09.025, PMID: 31622882

Buerger C, DeVries B, Stambolic V. 2006. Localization of Rheb to the endomembrane is critical for its signaling function. *Biochemical and Biophysical Research Communications* **344**:869–880. DOI: https://doi.org/10.1016/j.bbrc.2006.03.220, PMID: 16631613

Carling D. 2004. The AMP-activated protein kinase cascade -- a unifying system for energy control. *Trends in Biochemical Sciences* **29**:18–24. DOI: https://doi.org/10.1016/j.tibs.2003.11.005, PMID: 14729328

Chandrashekarappa DG, McCartney RR, Schmidt MC. 2013. Ligand binding to the AMP-activated protein kinase active site mediates protection of the activation loop from dephosphorylation. *The Journal of Biological Chemistry* **288**:89–98. DOI: https://doi.org/10.1074/jbc.M112.422659, PMID: 23184934

Chen Z, Malia PC, Hatakeyama R, Nicastro R, Hu Z, Péli-Gulli M-P, Gao J, Nishimura T, Eskes E, Stefan CJ, Winderickx J, Dengjel J, De Virgilio C, Ungermann C. 2021. Torc1 determines fab1 lipid kinase function at signaling endosomes and vacuoles. *Current Biology* **31**:297–309.. DOI: https://doi.org/10.1016/j.cub.2020.10.026, PMID: 33157024

Cherkasova VA, Hinnebusch AG. 2003. Translational control by TOR and Tap42 through dephosphorylation of eIF2alpha kinase GCN2. *Genes & Development* **17**:859–872. DOI: https://doi.org/10.1101/gad.1069003, PMID: 12654728

Cherkasova V, Qiu H, Hinnebusch AG. 2010. Snf1 promotes phosphorylation of the alpha subunit of eukaryotic translation initiation factor 2 by activating GCN2 and inhibiting phosphatases Glc7 and Sit4. *Molecular and Cellular Biology* **30**:2862–2873. DOI: https://doi.org/10.1128/MCB.00183-10, PMID: 20404097

Coccetti P, Nicastro R, Tripodi F. 2018. Conventional and emerging roles of the energy sensor snf1/AMPK in *Saccharomyces cerevisiae*. *Microbial Cell* **5**:482–494. DOI: https://doi.org/10.15698/mic2018.11.655, PMID: 30483520

Cowles CR, Odorizzi G, Payne GS, Emr SD. 1997. The AP-3 adaptor complex is essential for cargo-selective transport to the yeast vacuole. *Cell* **91**:109–118. DOI: https://doi.org/10.1016/s0092-8674(01)80013-1, PMID: 9335339

Cox J, Mann M. 2008. MaxQuant enables high peptide identification rates, individualized p.p.b.-range mass accuracies and proteome-wide protein quantification. *Nature Biotechnology* **26**:1367–1372. DOI: https://doi.org/10.1038/nbt.1511, PMID: 19029910

Dale S, Wilson WA, Edelman AM, Hardie DG. 1995. Similar substrate recognition motifs for mammalian AMP-activated protein kinase, higher plant HMG-CoA reductase kinase-A, yeast Snf1, and mammalian calmodulin-dependent protein kinase I. *FEBS Letters* **361**:191–195. DOI: https://doi.org/10.1016/0014-5793(95)00172-6, PMID: 7698321

Deroover S, Ghillebert R, Broeckx T, Winderickx J, Rolland F. 2016. Trehalose-6-phosphate synthesis controls yeast gluconeogenesis downstream and independent of SNF1. *FEMS Yeast Research* **16**:fow036. DOI: https://doi.org/10.1093/femsyr/fow036, PMID: 27189362

De Virgilio C. 2012. The essence of yeast quiescence. *FEMS Microbiology Reviews* **36**:306–339. DOI: https://doi.org/10.1111/j.1574-6976.2011.00287.x, PMID: 21658086

Demetriades C, Doumpas N, Teleman AA. 2014. Regulation of TORC1 in response to amino acid starvation via lysosomal recruitment of TSC2. *Cell* **156**:786–799. DOI: https://doi.org/10.1016/j.cell.2014.01.024, PMID: 24529380

DeVit MJ, Johnston M. 1999. The nuclear exportin Msn5 is required for nuclear export of the Mig1 glucose repressor of *Saccharomyces cerevisiae*. *Current Biology* **9**:1231–1241. DOI: https://doi.org/10.1016/s0960-9822(99)80503-x, PMID: 10556086

Dibble CC, Elis W, Menon S, Qin W, Klekota J, Asara JM, Finan PM, Kwiatkowski DJ, Murphy LO, Manning BD. 2012. Tbc1D7 is a third subunit of the TSC1-TSC2 complex upstream of mTORC1. *Molecular Cell* **47**:535–546. DOI: https://doi.org/10.1016/j.molcel.2012.06.009, PMID: 22795129

Dubouloz F, Deloche O, Wanke V, Cameroni E, De Virgilio C. 2005. The TOR and ego protein complexes orchestrate microautophagy in yeast. *Molecular Cell* **19**:15–26. DOI: https://doi.org/10.1016/j.molcel.2005.05.020, PMID: 15989961

Eraso P, Mazón MJ, Portillo F. 2006. Yeast protein kinase Ptk2 localizes at the plasma membrane and phosphorylates in vitro the C-terminal peptide of the H+-ATPase. *Biochimica et Biophysica Acta* **1758**:164–170. DOI: https://doi.org/10.1016/j.bbamem.2006.01.010, PMID: 16510118

Estruch F, Carlson M. 1993. Two homologous zinc finger genes identified by multicopy suppression in a Snf1 protein kinase mutant of *Saccharomyces cerevisiae*. *Molecular and Cellular Biology* **13**:3872–3881. DOI: https://doi.org/10.1128/mcb.13.7.3872-3881.1993, PMID: 8321194

Generoso WC, Gottardi M, Oreb M, Boles E. 2016. Simplified CRISPR-Cas genome editing for *Saccharomyces cerevisiae*. *Journal of Microbiological Methods* **127**:203–205. DOI: https://doi.org/10.1016/j.mimet.2016.06.020, PMID: 27327211

Ghillebert R, Swinnen E, Wen J, Vandesteene L, Ramon M, Norga K, Rolland F, Winderickx J. 2011. The AMPK/SNF1/snrk1 fuel gauge and energy regulator: structure, function and regulation. *The FEBS Journal* **278**:3978–3990. DOI: https://doi.org/10.1111/j.1742-4658.2011.08315.x, PMID: 21883929

González A, Hall MN. 2017. Nutrient sensing and TOR signaling in yeast and mammals. *The EMBO Journal* **36**:397–408. DOI: https://doi.org/10.15252/embj.201696010, PMID: 28096180

González A, Hall MN, Lin SC, Hardie DG. 2020. Ampk and TOR: the yin and yang of cellular nutrient sensing and growth control. *Cell Metabolism* **31**:472–492. DOI: https://doi.org/10.1016/j.cmet.2020.01.015, PMID: 32130880

Goossens A, de La Fuente N, Forment J, Serrano R, Portillo F. 2000. Regulation of yeast H (+) -ATPase by protein kinases belonging to a family dedicated to activation of plasma membrane transporters. *Molecular and Cellular Biology* **20**:7654–7661. DOI: https://doi.org/10.1128/MCB.20.20.7654-7661.2000, PMID: 11003661

Gwinn DM, Shackelford DB, Egan DF, Mihaylova MM, Mery A, Vasquez DS, Turk BE, Shaw RJ. 2008. Ampk phosphorylation of raptor mediates a metabolic checkpoint. *Molecular Cell* **30**:214–226. DOI: https://doi.org/10.1016/j.molcel.2008.03.003, PMID: 18439900

Hardie DG, Ross FA, Hawley SA. 2012. Ampk: a nutrient and energy sensor that maintains energy homeostasis. *Nature Reviews. Molecular Cell Biology* **13**:251–262. DOI: https://doi.org/10.1038/nrm3311, PMID: 22436748

Hatakeyama R, Péli-Gulli MP, Hu Z, Jaquenoud M, Garcia Osuna GM, Sardu A, Dengjel J, De Virgilio C. 2019. Spatially distinct pools of TORC1 balance protein homeostasis. *Molecular Cell* **73**:325–338.. DOI: https://doi.org/10.1016/j.molcel.2018.10.040

Hatakeyama R. 2021. Pib2 as an emerging master regulator of yeast TORC1. *Biomolecules* **11**:1489. DOI: https://doi.org/10.3390/biom11101489, PMID: 34680122

Hedbacker K, Townley R, Carlson M. 2004. Cyclic AMP-dependent protein kinase regulates the subcellular localization of Snf1-Sip1 protein kinase. *Molecular and Cellular Biology* **24**:1836–1843. DOI: https://doi.org/10.1128/MCB.24.5.1836-1843.2004, PMID: 14966266

Hedbacker K, Carlson M. 2008. Snf1/Ampk pathways in yeast. *Frontiers in Bioscience* **13**:2408–2420. DOI: https://doi.org/10.2741/2854, PMID: 17981722

Herzig S, Shaw RJ. 2018. Ampk: guardian of metabolism and mitochondrial homeostasis. *Nature Reviews. Molecular Cell Biology* **19**:121–135. DOI: https://doi.org/10.1038/nrm.2017.95, PMID: 28974774

Hu Z, Raucci S, Jaquenoud M, Hatakeyama R, Stumpe M, Rohr R, Reggiori F, De Virgilio C, Dengjel J. 2019. Multilayered control of protein turnover by TORC1 and Atg1. *Cell Reports* **28**:3486–3496.. DOI: https://doi.org/10.1016/j.celrep.2019.08.069, PMID: 31553916

Hu Z, Sankar DS, Vu B, Leytens A, Vionnet C, Wu W, Stumpe M, Martínez-Martínez E, Stork B, Dengjel J. 2021. Ulk1 phosphorylation of striatin activates protein phosphatase 2A and autophagy. *Cell Reports* **36**:109762. DOI: https://doi.org/10.1016/j.celrep.2021.109762, PMID: 34592149

Hughes Hallett JE, Luo X, Capaldi AP. 2015. Snf1/Ampk promotes the formation of Kog1/Raptor-bodies to increase the activation threshold of TORC1 in budding yeast. *eLife* **4**:e09181. DOI: https://doi.org/10.7554/eLife.09181, PMID: 26439012

Inoki K, Li Y, Xu T, Guan KL. 2003a. Rheb gtpase is a direct target of TSC2 GAP activity and regulates mtor signaling. *Genes Dev* **17**:1829–1834. DOI: https://doi.org/10.1101/gad.1110003

Inoki K, Zhu T, Guan KL. 2003b. TSC2 mediates cellular energy response to control cell growth and survival. *Cell* **115**:577. DOI: https://doi.org/10.1016/s0092-8674(03)00929-2

Janke C, Magiera MM, Rathfelder N, Taxis C, Reber S, Maekawa H, Moreno-Borchart A, Doenges G, Schwob E, Schiebel E, Knop M. 2004. A versatile toolbox for PCR-based tagging of yeast genes: new fluorescent proteins, more markers and promoter substitution cassettes. *Yeast* **21**:947–962. DOI: https://doi.org/10.1002/yea.1142

Jin N, Mao K, Jin Y, Tevzadze G, Kauffman EJ, Park S, Bridges D, Loewith R, Saltiel AR, Klionsky DJ, Weisman LS. 2014. Roles for PI(3,5)P$_2$ in nutrient sensing through TORC1. *Mol. Biol. Cell* **25**:1171–1185. DOI: https://doi.org/10.1091/mbc.E14-01-0021

Kahlhofer J, Leon S, Teis D, Schmidt O. 2021. The α-arrestin family of ubiquitin ligase adaptors links metabolism with selective endocytosis. *Biol. Cell* **113**:183–219. DOI: https://doi.org/10.1111/boc.202000137

Kanshin E, Giguère S, Jing C, Tyers M, Thibault P. 2017. Machine learning of global phosphoproteomic profiles enables discrimination of direct versus indirect kinase substrates. *Molecular & Cellular Proteomics* **16**:786–798. DOI: https://doi.org/10.1074/mcp.M116.066233, PMID: 28265048

Kawai S, Urban J, Piccolis M, Panchaud N, De Virgilio C, Loewith R. 2011. Mitochondrial genomic dysfunction causes dephosphorylation of Sch9 in the yeast *Saccharomyces cerevisiae*. *Eukaryotic Cell* **10**:1367–1369. DOI: https://doi.org/10.1128/EC.05157-11, PMID: 21841122

Kim A, Cunningham KW. 2015. A LAPF/phafin1-like protein regulates TORC1 and lysosomal membrane permeabilization in response to endoplasmic reticulum membrane stress. *Molecular Biology of the Cell* **26**:4631–4645. DOI: https://doi.org/10.1091/mbc.E15-08-0581, PMID: 26510498

Kulkarni A, Buford TD, Rai R, Cooper TG. 2006. Differing responses of GAT1 and Gln3 phosphorylation and localization to rapamycin and methionine sulfoximine treatment in *Saccharomyces cerevisiae*. *FEMS Yeast Research* **6**:218–229. DOI: https://doi.org/10.1111/j.1567-1364.2006.00031.x, PMID: 16487345

Laplante M, Sabatini DM. 2012. Mtor signaling in growth control and disease. *Cell* **149**:274–293. DOI: https://doi.org/10.1016/j.cell.2012.03.017, PMID: 22500797

Laussel C, Albanèse V, García-Rodríguez FJ, Ballin A, Defenouillère Q, Léon S. 2022. 2-Deoxyglucose transiently inhibits yeast AMPK signaling and triggers glucose transporter endocytosis, potentiating the drug toxicity. *PLOS Genetics* **18**:e1010169. DOI: https://doi.org/10.1371/journal.pgen.1010169, PMID: 35951639

Lee YJ, Jeschke GR, Roelants FM, Thorner J, Turk BE. 2012. Reciprocal phosphorylation of yeast glycerol-3-phosphate dehydrogenases in adaptation to distinct types of stress. *Molecular and Cellular Biology* **32**:4705–4717. DOI: https://doi.org/10.1128/MCB.00897-12, PMID: 22988299

Ling NXY, Kaczmarek A, Hoque A, Davie E, Ngoei KRW, Morrison KR, Smiles WJ, Forte GM, Wang T, Lie S, Dite TA, Langendorf CG, Scott JW, Oakhill JS, Petersen J. 2020. Mtorc1 directly inhibits AMPK to promote cell proliferation under nutrient stress. *Nature Metabolism* **2**:41–49. DOI: https://doi.org/10.1038/s42255-019-0157-1, PMID: 31993556

Liu GY, Sabatini DM. 2020. Mtor at the nexus of nutrition, growth, ageing and disease. *Nature Reviews Molecular Cell Biology* **21**:183–203. DOI: https://doi.org/10.1038/s41580-019-0199-y

Loewith R, Jacinto E, Wullschleger S, Lorberg A, Crespo JL, Bonenfant D, Oppliger W, Jenoe P, Hall MN. 2002. Two TOR complexes, only one of which is rapamycin sensitive, have distinct roles in cell growth control. *Molecular Cell* **10**:457–468. DOI: https://doi.org/10.1016/s1097-2765(02)00636-6, PMID: 12408816

Loewith R, Hall MN. 2011. Target of rapamycin (TOR) in nutrient signaling and growth control. *Genetics* **189**:1177–1201. DOI: https://doi.org/10.1534/genetics.111.133363, PMID: 22174183

Long X, Lin Y, Ortiz-Vega S, Yonezawa K, Avruch J. 2005. Rheb binds and regulates the mTOR kinase. *Current Biology* **15**:702–713. DOI: https://doi.org/10.1016/j.cub.2005.02.053, PMID: 15854902

Lu J-Y, Lin Y-Y, Sheu J-C, Wu J-T, Lee F-J, Chen Y, Lin M-I, Chiang F-T, Tai T-Y, Berger SL, Zhao Y, Tsai K-S, Zhu H, Chuang L-M, Boeke JD. 2011. Acetylation of yeast AMPK controls intrinsic aging independently of caloric restriction. *Cell* **146**:969–979. DOI: https://doi.org/10.1016/j.cell.2011.07.044, PMID: 21906795

Ludin K, Jiang R, Carlson M. 1998. Glucose-regulated interaction of a regulatory subunit of protein phosphatase 1 with the snf1 protein kinase in *Saccharomyces cerevisiae*. *PNAS* **95**:6245–6250. DOI: https://doi.org/10.1073/pnas.95.11.6245, PMID: 9600950

Maqani N, Fine RD, Shahid M, Li M, Enriquez-Hesles E, Smith JS. 2018. Spontaneous mutations in cyc8 and mig1 suppress the short chronological lifespan of budding yeast lacking snf1/AMPK. *Microbial Cell* **5**:233–248. DOI: https://doi.org/10.15698/mic2018.05.630, PMID: 29796388

Mayer FV, Heath R, Underwood E, Sanders MJ, Carmena D, McCartney RR, Leiper FC, Xiao B, Jing C, Walker PA, Haire LF, Ogrodowicz R, Martin SR, Schmidt MC, Gamblin SJ, Carling D. 2011. Adp regulates Snf1, the *Saccharomyces cerevisiae* homolog of AMP-activated protein kinase. *Cell Metabolism* **14**:707–714. DOI: https://doi.org/10.1016/j.cmet.2011.09.009, PMID: 22019086

McCartney RR, Schmidt MC. 2001. Regulation of snf1 kinase activation requires phosphorylation of threonine 210 by an upstream kinase as well as a distinct step mediated by the snf4 subunit. *The Journal of Biological Chemistry* **276**:36460–36466. DOI: https://doi.org/10.1074/jbc.M104418200, PMID: 11486005

Melick CH, Jewell JL. 2020. Regulation of mTORC1 by upstream stimuli. *Genes* **11**:989. DOI: https://doi.org/10.3390/genes11090989, PMID: 32854217

Messer K, Natarajan L. 2008. Maximum likelihood, multiple imputation and regression calibration for measurement error adjustment. *Statistics in Medicine* **27**:6332–6350. DOI: https://doi.org/10.1002/sim.3458, PMID: 18937275

Michel AH, Hatakeyama R, Kimmig P, Arter M, Peter M, Matos J, De Virgilio C, Kornmann B. 2017. Functional mapping of yeast genomes by saturated transposition. *eLife* **6**:e23570. DOI: https://doi.org/10.7554/eLife.23570, PMID: 28481201

Nada S, Hondo A, Kasai A, Koike M, Saito K, Uchiyama Y, Okada M. 2009. The novel lipid raft adaptor p18 controls endosome dynamics by anchoring the MEK-ERK pathway to late endosomes. *The EMBO Journal* **28**:477–489. DOI: https://doi.org/10.1038/emboj.2008.308, PMID: 19177150

Nicastro R, Tripodi F, Gaggini M, Castoldi A, Reghellin V, Nonnis S, Tedeschi G, Coccetti P. 2015. Snf1 phosphorylates adenylate cyclase and negatively regulates protein kinase A-dependent transcription in *Saccharomyces cerevisiae*. *The Journal of Biological Chemistry* **290**:24715–24726. DOI: https://doi.org/10.1074/jbc.M115.658005, PMID: 26309257

Nicastro R, Sardu A, Panchaud N, De Virgilio C. 2017. The architecture of the RAG GTPase signaling network. *Biomolecules* **7**:48. DOI: https://doi.org/10.3390/biom7030048, PMID: 28788436

Novarina D, Guerra P, Milias-Argeitis A. 2021. Vacuolar localization via the N-terminal domain of sch9 is required for TORC1-dependent phosphorylation and downstream signal transduction. *Journal of Molecular Biology* **433**:167326. DOI: https://doi.org/10.1016/j.jmb.2021.167326, PMID: 34695378

O'Donnell AF, Schmidt MC. 2019. Ampk-Mediated regulation of alpha-arrestins and protein trafficking. *International Journal of Molecular Sciences* **20**:515. DOI: https://doi.org/10.3390/ijms20030515, PMID: 30691068

Olsen JV, Blagoev B, Gnad F, Macek B, Kumar C, Mortensen P, Mann M. 2006. Global, in vivo, and site-specific phosphorylation dynamics in signaling networks. *Cell* **127**:635–648. DOI: https://doi.org/10.1016/j.cell.2006.09.026, PMID: 17081983

Ostling J, Ronne H. 1998. Negative control of the Mig1p repressor by snf1p-dependent phosphorylation in the absence of glucose. *European Journal of Biochemistry* **252**:162–168. DOI: https://doi.org/10.1046/j.1432-1327.1998.2520162.x, PMID: 9523726

Panchaud N, Péli-Gulli MP, De Virgilio C. 2013a. Amino acid deprivation inhibits TORC1 through a gtpase-activating protein complex for the RAG family gtpase gtr1. *Science Signaling* **6**:ra42. DOI: https://doi.org/10.1126/scisignal.2004112, PMID: 23716719

Panchaud N, Péli-Gulli MP, De Virgilio C. 2013b. SEACing the gap that negociates TORC1 activation: evolutionary conservation of RAG gtpase regulation. *Cell Cycle* **12**:2948–2952. DOI: https://doi.org/10.4161/cc.26000, PMID: 23974112

Péli-Gulli MP, Sardu A, Panchaud N, Raucci S, De Virgilio C. 2015. Amino acids stimulate TORC1 through lst4-lst7, a GTPase-activating protein complex for the RAG family GTPase gtr2. *Cell Reports* **13**:1–7. DOI: https://doi.org/10.1016/j.celrep.2015.08.059, PMID: 26387955

Peterson TR, Laplante M, Thoreen CC, Sancak Y, Kang SA, Kuehl WM, Gray NS, Sabatini DM. 2009. Deptor is an mTOR inhibitor frequently overexpressed in multiple myeloma cells and required for their survival. *Cell* **137**:873–886. DOI: https://doi.org/10.1016/j.cell.2009.03.046, PMID: 19446321

Petit CS, Roczniak-Ferguson A, Ferguson SM. 2013. Recruitment of folliculin to lysosomes supports the amino acid-dependent activation of RAG GTPases. *The Journal of Cell Biology* **202**:1107–1122. DOI: https://doi.org/10.1083/jcb.201307084, PMID: 24081491

Petrenko N, Chereji RV, McClean MN, Morozov AV, Broach JR. 2013. Noise and interlocking signaling pathways promote distinct transcription factor dynamics in response to different stresses. *Molecular Biology of the Cell* **24**:2045–2057. DOI: https://doi.org/10.1091/mbc.E12-12-0870, PMID: 23615444

Post H, Penning R, Fitzpatrick MA, Garrigues LB, Wu W, MacGillavry HD, Hoogenraad CC, Heck AJR, Altelaar AFM. 2017. Robust, sensitive, and automated phosphopeptide enrichment optimized for low sample amounts applied to primary hippocampal neurons. *Journal of Proteome Research* **16**:728–737. DOI: https://doi.org/10.1021/acs.jproteome.6b00753, PMID: 28107008

Powis K, Zhang T, Panchaud N, Wang R, De Virgilio C, Ding J. 2015. Crystal structure of the ego1-ego2-ego3 complex and its role in promoting RAG GTPase-dependent TORC1 signaling. *Cell Research* **25**:1043–1059. DOI: https://doi.org/10.1038/cr.2015.86, PMID: 26206314

Powis K, De Virgilio C. 2016. Conserved regulators of RAG gtpases orchestrate amino acid-dependent TORC1 signaling. *Cell Discovery* **2**:15049. DOI: https://doi.org/10.1038/celldisc.2015.49, PMID: 27462445

Prouteau M, Desfosses A, Sieben C, Bourgoint C, Lydia Mozaffari N, Demurtas D, Mitra AK, Guichard P, Manley S, Loewith R. 2017. Torc1 organized in inhibited domains (toroids) regulate TORC1 activity. *Nature* **550**:265–269. DOI: https://doi.org/10.1038/nature24021, PMID: 28976958

Ptacek J, Devgan G, Michaud G, Zhu H, Zhu X, Fasolo J, Guo H, Jona G, Breitkreutz A, Sopko R, McCartney RR, Schmidt MC, Rachidi N, Lee S-J, Mah AS, Meng L, Stark MJR, Stern DF, De Virgilio C, Tyers M, et al. 2005. Global analysis of protein phosphorylation in yeast. *Nature* **438**:679–684. DOI: https://doi.org/10.1038/nature04187, PMID: 16319894

Reinke A, Anderson S, McCaffery JM, Yates J, Aronova S, Chu S, Fairclough S, Iverson C, Wedaman KP, Powers T. 2004. Tor complex 1 includes a novel component, tco89p (ypl180w), and cooperates with ssd1p to maintain cellular integrity in *Saccharomyces cerevisiae*. *The Journal of Biological Chemistry* **279**:14752–14762. DOI: https://doi.org/10.1074/jbc.M313062200, PMID: 14736892

Rogala KB, Gu X, Kedir JF, Abu-Remaileh M, Bianchi LF, Bottino AMS, Dueholm R, Niehaus A, Overwijn D, Fils A-CP, Zhou SX, Leary D, Laqtom NN, Brignole EJ, Sabatini DM. 2019. Structural basis for the docking of mTORC1 on the lysosomal surface. Science **366**:468–475. DOI: https://doi.org/10.1126/science.aay0166, PMID: 31601708

Ruiz A, Xu X, Carlson M. 2013. Ptc1 protein phosphatase 2C contributes to glucose regulation of SNF1/AMP-activated protein kinase (AMPK) in *Saccharomyces cerevisiae*. *The Journal of Biological Chemistry* **288**:31052–31058. DOI: https://doi.org/10.1074/jbc.M113.503763, PMID: 24019512

Saliba E, Evangelinos M, Gournas C, Corrillon F, Georis I, Andre B. 2018. The yeast H^+-atpase pma1 promotes rag/gtr-dependent TORC1 activation in response to H^+-coupled nutrient uptake. *eLife* **7**:e31981. DOI: https://doi.org/10.7554/eLife.31981

Sancak Y, Thoreen CC, Peterson TR, Lindquist RA, Kang SA, Spooner E, Carr SA, Sabatini DM. 2007. Pras40 is an insulin-regulated inhibitor of the mTORC1 protein kinase. *Molecular Cell* **25**:903–915. DOI: https://doi.org/10.1016/j.molcel.2007.03.003, PMID: 17386266

Sancak Y, Bar-Peled L, Zoncu R, Markhard AL, Nada S, Sabatini DM. 2010. Ragulator-rag complex targets mTORC1 to the lysosomal surface and is necessary for its activation by amino acids. *Cell* **141**:290–303. DOI: https://doi.org/10.1016/j.cell.2010.02.024, PMID: 20381137

Sanz P, Alms GR, Haystead TA, Carlson M. 2000. Regulatory interactions between the Reg1-Glc7 protein phosphatase and the Snf1 protein kinase. *Molecular and Cellular Biology* **20**:1321–1328. DOI: https://doi.org/10.1128/MCB.20.4.1321-1328.2000, PMID: 10648618

Schaffer BE, Levin RS, Hertz NT, Maures TJ, Schoof ML, Hollstein PE, Benayoun BA, Banko MR, Shaw RJ, Shokat KM, Brunet A. 2015. Identification of AMPK phosphorylation sites reveals a network of proteins involved in cell invasion and facilitates large-scale substrate prediction. *Cell Metabolism* **22**:907–921. DOI: https://doi.org/10.1016/j.cmet.2015.09.009, PMID: 26456332

Scott JW, Norman DG, Hawley SA, Kontogiannis L, Hardie DG. 2002. Protein kinase substrate recognition studied using the recombinant catalytic domain of AMP-activated protein kinase and a model substrate. *Journal of Molecular Biology* **317**:309–323. DOI: https://doi.org/10.1006/jmbi.2001.5316, PMID: 11902845

Shaw RJ, Bardeesy N, Manning BD, Lopez L, Kosmatka M, DePinho RA, Cantley LC. 2004. The LKB1 tumor suppressor negatively regulates mTOR signaling. *Cancer Cell* **6**:91–99. DOI: https://doi.org/10.1016/j.ccr.2004.06.007, PMID: 15261145

Shen K, Choe A, Sabatini DM. 2017. Intersubunit crosstalk in the RAG GTPase heterodimer enables mTORC1 to respond rapidly to amino acid availability. *Molecular Cell* **68**:552–565.. DOI: https://doi.org/10.1016/j.molcel.2017.09.026, PMID: 29056322

Shinoda J, Kikuchi Y. 2007. Rod1, an arrestin-related protein, is phosphorylated by Snf1-kinase in *Saccharomyces cerevisiae*. *Biochemical and Biophysical Research Communications* **364**:258–263. DOI: https://doi.org/10.1016/j.bbrc.2007.09.134, PMID: 17949685

Shirra MK, McCartney RR, Zhang C, Shokat KM, Schmidt MC, Arndt KM. 2008. A chemical genomics study identifies Snf1 as a repressor of GCN4 translation. *The Journal of Biological Chemistry* **283**:35889–35898. DOI: https://doi.org/10.1074/jbc.M805325200, PMID: 18955495

Smith FC, Davies SP, Wilson WA, Carling D, Hardie DG. 1999. The Snf1 kinase complex from *Saccharomyces cerevisiae* phosphorylates the transcriptional repressor protein Mig1p in vitro at four sites within or near regulatory domain 1. *FEBS Letters* **453**:219–223. DOI: https://doi.org/10.1016/s0014-5793(99)00725-5, PMID: 10403407

Stracka D, Jozefczuk S, Rudroff F, Sauer U, Hall MN. 2014. Nitrogen source activates TOR (target of rapamycin) complex 1 via glutamine and independently of Gtr/Rag proteins. *The Journal of Biological Chemistry* **289**:25010–25020. DOI: https://doi.org/10.1074/jbc.M114.574335, PMID: 25063813

Sullivan A, Wallace RL, Wellington R, Luo X, Capaldi AP. 2019. Multilayered regulation of TORC1-body formation in budding yeast. *Molecular Biology of the Cell* **30**:400–410. DOI: https://doi.org/10.1091/mbc.E18-05-0297, PMID: 30485160

Szklarczyk D, Gable AL, Nastou KC, Lyon D, Kirsch R, Pyysalo S, Doncheva NT, Legeay M, Fang T, Bork P, Jensen LJ, von Mering C. 2021. The string database in 2021: customizable protein-protein networks, and functional characterization of user-uploaded gene/measurement sets. *Nucleic Acids Research* **49**:D605–D612. DOI: https://doi.org/10.1093/nar/gkaa1074, PMID: 33237311

Tanigawa M, Maeda T. 2017. An in vitro TORC1 kinase assay that recapitulates the gtr-independent glutamine-responsive TORC1 activation mechanism on yeast vacuoles. *Molecular and Cellular Biology* **37**:e00075-17. DOI: https://doi.org/10.1128/MCB.00075-17, PMID: 28483912

Tanigawa M, Yamamoto K, Nagatoishi S, Nagata K, Noshiro D, Noda NN, Tsumoto K, Maeda T. 2021. A glutamine sensor that directly activates TORC1. *Communications Biology* **4**:1093. DOI: https://doi.org/10.1038/s42003-021-02625-w, PMID: 34535752

Tee AR, Manning BD, Roux PP, Cantley LC, Blenis J. 2003. Tuberous sclerosis complex gene products, tuberin and hamartin, control mTOR signaling by acting as a GTPase-activating protein complex toward Rheb. *Current Biology* **13**:1259–1268. DOI: https://doi.org/10.1016/s0960-9822(03)00506-2, PMID: 12906785

Thorner J. 2022. Tor complex 2 is a master regulator of plasma membrane homeostasis. *The Biochemical Journal* **479**:1917–1940. DOI: https://doi.org/10.1042/BCJ20220388, PMID: 36149412

Treitel MA, Kuchin S, Carlson M. 1998. Snf1 protein kinase regulates phosphorylation of the Mig1 repressor in *Saccharomyces cerevisiae*. *Molecular and Cellular Biology* **18**:6273–6280. DOI: https://doi.org/10.1128/MCB.18.11.6273, PMID: 9774644

Troutman KK, Varlakhanova NV, Tornabene BA, Ramachandran R, Ford MGJ. 2022. Conserved pib2 regions have distinct roles in TORC1 regulation at the vacuole. *Journal of Cell Science* **135**:jcs259994. DOI: https://doi.org/10.1242/jcs.259994, PMID: 36000409

Tsun ZY, Bar-Peled L, Chantranupong L, Zoncu R, Wang T, Kim C, Spooner E, Sabatini DM. 2013. The folliculin tumor suppressor is a gap for the ragc/D GTPases that signal amino acid levels to mTORC1. *Molecular Cell* **52**:495–505. DOI: https://doi.org/10.1016/j.molcel.2013.09.016, PMID: 24095279

Tyanova S, Temu T, Cox J. 2016. The maxquant computational platform for mass spectrometry-based shotgun proteomics. *Nature Protocols* **11**:2301–2319. DOI: https://doi.org/10.1038/nprot.2016.136, PMID: 27809316

Ukai H, Araki Y, Kira S, Oikawa Y, May AI, Noda T. 2018. Gtr/ego-independent TORC1 activation is achieved through a glutamine-sensitive interaction with pib2 on the vacuolar membrane. *PLOS Genetics* **14**:e1007334. DOI: https://doi.org/10.1371/journal.pgen.1007334, PMID: 29698392

Urban J, Soulard A, Huber A, Lippman S, Mukhopadhyay D, Deloche O, Wanke V, Anrather D, Ammerer G, Riezman H, Broach JR, De Virgilio C, Hall MN, Loewith R. 2007. Sch9 is a major target of TORC1 in *Saccharomyces cerevisiae*. *Molecular Cell* **26**:663–674. DOI: https://doi.org/10.1016/j.molcel.2007.04.020, PMID: 17560372

van Dam TJP, Zwartkruis FJT, Bos JL, Snel B. 2011. Evolution of the TOR pathway. *Journal of Molecular Evolution* **73**:209–220. DOI: https://doi.org/10.1007/s00239-011-9469-9, PMID: 22057117

Varlakhanova NV, Mihalevic MJ, Bernstein KA, Ford MGJ. 2017. Pib2 and the ego complex are both required for activation of TORC1. *Journal of Cell Science* **130**:3878–3890. DOI: https://doi.org/10.1242/jcs.207910, PMID: 28993463

Varlakhanova NV, Tornabene BA, Ford MGJ. 2018. Feedback regulation of TORC1 by its downstream effectors Npr1 and par32. *Molecular Biology of the Cell* **29**:2751–2765. DOI: https://doi.org/10.1091/mbc.E18-03-0158, PMID: 30156471

Wei M, Fabrizio P, Hu J, Ge H, Cheng C, Li L, Longo VD. 2008. Life span extension by calorie restriction depends on Rim15 and transcription factors downstream of Ras/PKA, TOR, and Sch9. *PLOS Genetics* **4**:e13. DOI: https://doi.org/10.1371/journal.pgen.0040013, PMID: 18225956

Wierman MB, Maqani N, Strickler E, Li M, Smith JS. 2017. Caloric restriction extends yeast chronological life span by optimizing the Snf1 (AMPK) signaling pathway. *Molecular and Cellular Biology* **37**:e00562-16. DOI: https://doi.org/10.1128/MCB.00562-16, PMID: 28373292

Wilson WA, Hawley SA, Hardie DG. 1996. Glucose repression/derepression in budding yeast: Snf1 protein kinase is activated by phosphorylation under derepressing conditions, and this correlates with a high AMP: ATP ratio. *Current Biology* **6**:1426–1434. DOI: https://doi.org/10.1016/s0960-9822(96)00747-6, PMID: 8939604

Wolfson RL, Sabatini DM. 2017. The dawn of the age of amino acid sensors for the mTORC1 pathway. *Cell Metabolism* **26**:301–309. DOI: https://doi.org/10.1016/j.cmet.2017.07.001, PMID: 28768171

Wullschleger S, Loewith R, Hall MN. 2006. Tor signaling in growth and metabolism. *Cell* **124**:471–484. DOI: https://doi.org/10.1016/j.cell.2006.01.016, PMID: 16469695

Yang H, Jiang X, Li B, Yang HJ, Miller M, Yang A, Dhar A, Pavletich NP. 2017. Mechanisms of mTORC1 activation by Rheb and inhibition by PRAS40. *Nature* **552**:368–373. DOI: https://doi.org/10.1038/nature25023, PMID: 29236692

Zaman S, Lippman SI, Schneper L, Slonim N, Broach JR. 2009. Glucose regulates transcription in yeast through a network of signaling pathways. *Molecular Systems Biology* **5**:245. DOI: https://doi.org/10.1038/msb.2009.2, PMID: 19225458

Zarei M, Sprenger A, Rackiewicz M, Dengjel J. 2016. Fast and easy phosphopeptide fractionation by combinatorial ERLIC-SCX solid-phase extraction for in-depth phosphoproteome analysis. *Nature Protocols* **11**:37–45. DOI: https://doi.org/10.1038/nprot.2015.134, PMID: 26633130

Zbieralski K, Wawrzycka D. 2022. Α-Arrestins and their functions: from yeast to human health. *International Journal of Molecular Sciences* **23**:4988. DOI: https://doi.org/10.3390/ijms23094988, PMID: 35563378

Zheng L, Zhang W, Zhou Y, Li F, Wei H, Peng J. 2016. Recent advances in understanding amino acid sensing mechanisms that regulate mTORC1. *International Journal of Molecular Sciences* **17**:1636. DOI: https://doi.org/10.3390/ijms17101636, PMID: 27690010

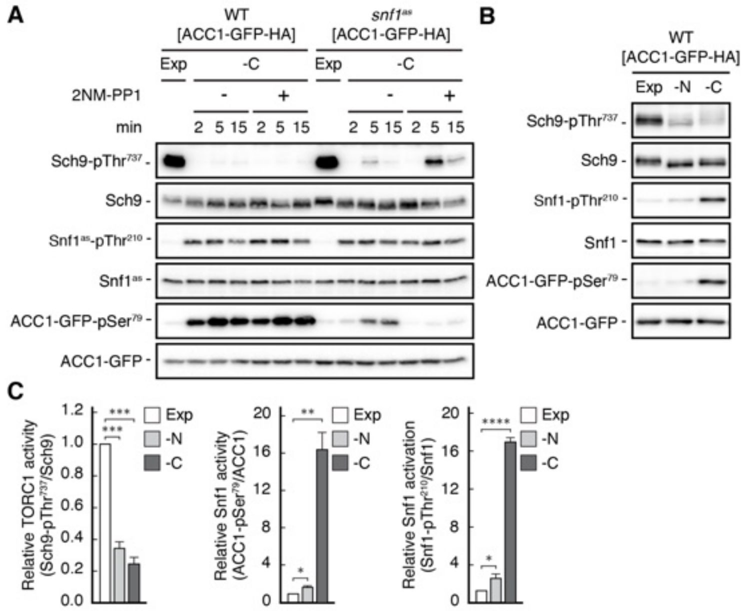

Figure 1-Figure Supplement 1. Specificity of 2NM-PP1 and differential Snf1 activation upon nitrogen and carbon starvation.

(**A**) 2NM-PP1 treatment inhibits Snf1^{as} activity *in vivo*. WT and ATP-analogue-sensitive *snf1^{as}* cells expressing a plasmid-encoded synthetic reporter of Snf1 activity that is based on a rat ACC1 peptide (ACC1-GFP; Deroover et al., 2016) were grown exponentially (Exp) and then starved for 2, 5, and 15 min for glucose (-C) and treated with vehicle (-; DMSO) or 2NM-PP1 (+). Immunoblot analyses were performed as in Figure 1A, except that anti-GFP and anti-ACC1-pSer^{79} were additionally used to detect the levels of ACC1-GFP and the phosphorylation state of the Snf1/AMPK target residue in ACC1-GFP that corresponds to Ser^{79} in rat ACC1 (n=3). (**B, C**) Activation of Snf1 following glucose or nitrogen starvation. Wild-type cells (as in (**A**)) were grown exponentially (Exp), or starved for nitrogen (-N; 10 min), or glucose (-C; 10 min) and subjected to immunoblot analyses (**B**). The mean relative TORC1 (Sch9-pThr^{737}/Sch9) and Snf1 activities (*i.e.* Snf1-pThr^{210}/Snf1 and ACC1-GFP-pSer^{79}/ACC1-GFP) were quantified, normalized relative to exponentially growing WT cells (set to 1.0), and shown in the bar diagrams in (**C**) (n=3; + SEM; unpaired Student's t-test, $*\leq0.05$, $**p\leq0.005$, $***p\leq0.0005$, $****p\leq0.00005$). The online version of this article includes the following source data for Figure 1—figure supplement 1—source data 1, quantification of blots for graphs shown in (**C**); in Figure 1—figure supplement 1—source data 2, uncropped blots shown in (**A and B**); Figure 1—figure supplement 1—source data 3, raw blots shown in (**A and B**).

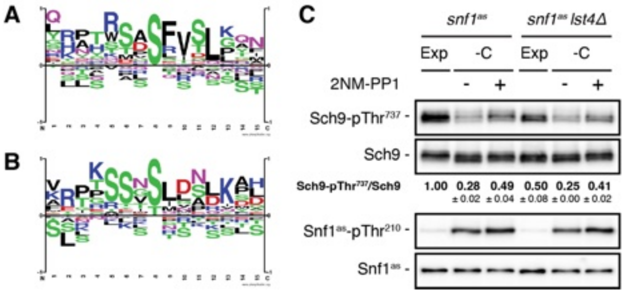

Figure 3-Figure Supplement 1. Specific motif analyses of Snf1 phosphosites and role of Lst4 in TORC1 reactivation in glucose-starved, Snf1-inhibited cells.

(**A, B**) Motif analyses of Snf1 phosphosites identified by both *in vivo* SILAC and OBIKA experiments and only responding after 5 min (**A**) and 15 min (**B**). (**C**) Lst4 does not mediate TORC1 reactivation in glucose-starved, Snf1-inhibited cells. Exponentially growing *snf1*^{as} or *snf1*^{as} *lst4Δ* cells (Exp) were starved for glucose (-C; 10 min) in the presence of vehicle (-; DMSO) or 2NM-PP1 (+), and analyzed as in Figure 1A. The mean TORC1 activities (*i.e.* Sch9-pThr^{737}/Sch9) were quantified, normalized relative to exponentially growing snf1as cells (set to 1.0), and shown below the Sch9 input blot (n=3; ± SEM). The online version of this article includes the following source data for Figure 3—figure supplement 1—source data 1, quantification of blots for values shown in (**C**); Figure 3—figure supplement 1—source data 2, uncropped blots shown in (**C**); Figure 3—figure supplement 1—source data 3, raw blots shown in (**C**).

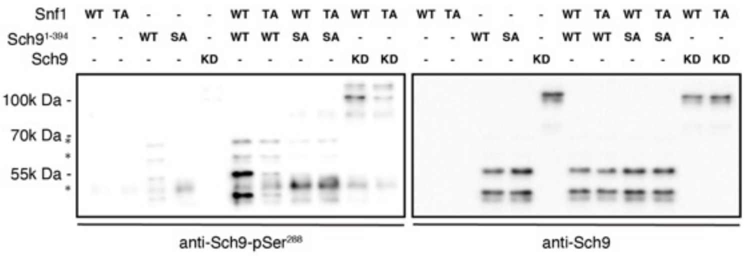
Snf1 WT TA - - - WT TA WT TA WT TA WT TA - - - WT TA WT TA WT TA
Sch9¹⁻³⁹⁴ - - WT SA - WT WT SA SA - - - - WT SA - WT WT SA SA - -
Sch9 - - - - KD - - - - KD KD - - - - KD - - - - KD KD
100k Da -
70k Da
55k Da -
*
*
*
*
anti-Sch9-pSer288
anti-Sch9

Figure 5-Figure Supplement 1. Specificity of 2NM-PP1 and differential Snf1 activation upon nitrogen and carbon starvation.

The assays were performed as in Figure 5C, except for the use of cold ATP and the inclusion of a full-length kinase-dead Sch9 variant (Sch9^{KD}: KD) as substrate. In addition, phosphorylation of Sch9-Ser^{288} and the levels of Sch9^{KD} or Sch9$^{1-394}$ variants were assayed by immunoblot analyses using specific anti-Sch9-pSer^{288} (left blot) and anti-Sch9 (right blot) antibodies, respectively (n=2). Nomenclature: wild-type Snf1 complex: WT; kinase-inactive Snf1^{T210A} complex: TA; N-terminal wild-type fragment of Sch9 encompassing the N-terminal 394 amino acids (Sch9$^{1-394}$): WT; and Sch9$^{1-394}$ harboring the Ser^{288}-to-Ala mutation: SA. The online version of this article includes the following source data for Figure 5—figure supplement 1—source data 1, uncropped blots; Figure 5—figure supplement 1—source data 2, raw blots.

CHAPTER 2:

The nutrient-responsive CDK Pho85 primes the Sch9 kinase for its activation by TORC1

1. Introduction

In yeast, nutritional responses are governed by a network of interconnected and conserved nutrient-sensing pathways that enable cells to adapt their metabolism according to nutrient availability, thereby influencing their growth potential and survival. A pivotal component in the nutrient-responsive network of *Saccharomyces cerevisiae* is the protein kinase Sch9, which is proposed to integrate the functions of the mammalian S6-kinase (S6K) and protein kinase B (PKB)/Akt (Caligaris et al., 2023b; Urban et al., 2007). Sch9 regulates various processes, including transcription and translation, cellular stress responses, sphingolipid metabolism, pH homeostasis, and both chronological and replicative lifespan (Caligaris et al., 2023b; Cameroni et al., 2004; Fabrizio et al., 2001; Huber et al., 2009; Jorgensen et al., 2004; Pan & Shadel, 2009). Sch9 activity is modulated by multiple upstream signals, including the target of rapamycin complex 1 (TORC1), phytosphingosine-dependent kinases Pkh1, Pkh2, and Pkh3 (Caligaris et al., 2023b; Liu et al., 2005; Roelants et al., 2004; Urban et al., 2007), and the cellular energy sensor Snf1 (Caligaris et al., 2023a; Lu et al., 2011). Additionally, Sch9 is recruited to the vacuolar membrane via phosphatidylinositol-3,5-bisphosphate (PI[3,5]P_2), a process essential for its TORC1-dependent activation (Jin et al., 2014).

Previous studies have shown that the deletion of *SCH9* in combination with either *PHO81* or *PHO85* results in synthetic lethality (Wilms et al., 2017), highlighting the critical balance required between Pho85 and the TORC1-Sch9 axis. Pho81 and Pho85 are crucial in the phosphate-responsive signaling pathway (PHO) that regulates gene expression for phosphate homeostasis (Jimenez et al., 2016; Menoyo et al., 2013; Mouillon & Persson, 2006; Nishizawa, 2015; Wanke et al., 2005). Pho81 inhibits the CDK-cyclin pair Pho85-Pho80 when phosphate is limited, allowing transcription factor Pho4 to localize in the nucleus and induce gene expression for extracellular phosphate foraging, import, and storage, and intracellular phosphate recycling (Lee et al., 2007; Lenburg & O'Shea, 1996; Mouillon & Persson, 2006). Pho81 also controls the activity of the Pho85-Pcl7 CDK-cyclin pair, which is involved in phosphate sensing (Lee et al., 2000). Pho85 regulates various aspects of cell cycle control and environmental signaling (Wanke et al., 2005). Deletion of Pho85 leads to defects such as altered phosphate metabolism, slow growth, cell cycle defects, abnormal cell morphology, enhanced sensitivity to stress, altered lipid metabolism, compromised reserve carbohydrate accumulation, reduced autophagy, and longevity (Huang et al., 2002; Jimenez et al., 2016; Lee et al., 2007; Lenburg & O'Shea, 1996; Mouillon & Persson, 2006). These defects can be linked to the function of specific Pho85-cyclins directing the Pho85 kinase to specific substrates. The cyclins are divided into two groups based on sequence similarity: the Pho80-

like subfamily and the Pcl1,2-like subfamily (Measday et al., 1997). Pho80-like cyclins and Pcl5 regulate metabolism in response to environmental changes, while Pcl1,2-like cyclins are mainly connected to cell cycle control and morphogenesis (Measday et al., 1997). The Pho85-Pho80 CDK-cyclin complex can phosphorylate and boost Fab1 activity under hyperosmotic stress conditions (Jin et al., 2017), suggesting Fab1 could act as a possible convergence point with the TORC1 signaling cascade

Our study investigates the synthetic lethality caused by the combined deletion of *SCH9* and either *PHO85* or *PHO81*, revealing that these lethalities arise from conflicting signals in the crosstalk between Pho85, TORC1, and Sch9. We demonstrate that Pho85-Pho80 directly phosphorylates Sch9, priming it for subsequent phosphorylation by TORC1, and that Pho85-Pho80 influences Fab1 activity. Furthermore, we provide evidence that Pho85-Pcl6 and Pho85-Pcl7 are involved in regulating cellular PI[3,5]P_2 levels, as indicated by the vacuolar recruitment of Sch9. Finally, we show that the transcription factor Pho4 is a downstream target of both Pho85 and TORC1-Sch9 signaling.

2. Key contributions of this chapter

- **Figure 2**. Pho85-Pho80 is involved in the recruitment of Fab1 to the vacuolar membrane. Panels B to E.
- **Figure 4**. Tor1 localization and TORC1 activity in WT, *pho85Δ*, and *pho80Δ* strains. Panels B and C.
- **Figure 5**. Pho85-Pho80-mediated phosphorylation of Ser^{726} primes Sch9 for its subsequent activation by TORC1. Panels B, C, and E to G.
- **Figure 6**. The Pho85-cyclins Pcl6 and Pcl7 contribute to the regulation of Fab1 and the vacuolar recruitment of Sch9. Panel D.
- **Figure 8**. Crosstalk between the PHO pathway and TORC1-Sch9 signaling and conservation of the turn motif priming principle. Panel A.
- **Figure S3**. Sch9 phosphorylation in cells eith enhanced Fab1 activity and GFP-Sch9 abundance at the vacuolar membrane. Panel A
- **Figure S4**. Pho85-Pho80-mediated phosphorylation of Ser^{726} primes Sch9 for its subsequent activation by TORC1. Panel B.
- **Figure S5**. The Pho85-cyclins Pcl6 and Pcl7 contribute to the regulation of Sch9. Panels D and E.

PLOS GENETICS

RESEARCH ARTICLE

The nutrient-responsive CDK Pho85 primes the Sch9 kinase for its activation by TORC1

Marie-Anne Deprez[1☯], Marco Caligaris[2☯], Joëlle Rosseels[1☯], Riko Hatakeyama[2,3], Ruben Ghillebert[1], Belém Sampaio-Marques[4,5], Kaivalya Mudholkar[6], Elja Eskes[1], Els Meert[1], Christian Ungermann[7], Paula Ludovico[4,5], Sabine Rospert[6], Claudio De Virgilio[2]*, Joris Winderickx[1]*

1 Department of Biology, Functional Biology, KU Leuven, Heverlee, Belgium, **2** Department of Biology, University of Fribourg, Fribourg, Switzerland, **3** Institute of Medical Sciences, University of Aberdeen, Aberdeen, Scotland, United Kingdom, **4** Life and Health Sciences Research Institute (ICVS), School of Health Sciences, University of Minho, Braga, Portugal, **5** ICVS/3B's—PT Government Associate Laboratory, Braga/Guimarães, Braga, Portugal, **6** Institute of Biochemistry and Molecular Biology, ZBMZ, Faculty of Medicine, University of Freiburg, Freiburg, Germany, **7** Department of Biology/Chemistry & Center of Cellular Nanoanalytics (CellNanOs), University of Osnabrück, Osnabrück, Germany

☯ These authors contributed equally to this work.
* claudio.devirgilio@unifr.ch (CDV); joris.winderickx@kuleuven.be (JW)

OPEN ACCESS

Citation: Deprez M-A, Caligaris M, Rosseels J, Hatakeyama R, Ghillebert R, Sampaio-Marques B, et al. (2023) The nutrient-responsive CDK Pho85 primes the Sch9 kinase for its activation by TORC1. PLoS Genet 19(2): e1010641. https://doi.org/10.1371/journal.pgen.1010641

Editor: Geraldine Butler, University College Dublin, IRELAND

Received: August 15, 2022

Accepted: January 27, 2023

Published: February 15, 2023

Copyright: © 2023 Deprez et al. This is an open access article distributed under the terms of the Creative Commons Attribution License, which permits unrestricted use, distribution, and reproduction in any medium, provided the original author and source are credited.

Data Availability Statement: All relevant data are within the manuscript and its Supporting Information files. All numerical data are included in the supplementary table: S4 Table.

Funding: Research was funded by fellowships of FWO-Vlaanderen (Fonds Wetenschappelijk Onderzoek) to RG and EE, a grant of the Biotechnology and Biological Sciences Research Council (BB/V016334/1) to RH, grants of the Deutsche Forschungsgemeinschaft (DFG, German Research Foundation) through Project-ID

Abstract

Yeast cells maintain an intricate network of nutrient signaling pathways enabling them to integrate information on the availability of different nutrients and adjust their metabolism and growth accordingly. Cells that are no longer capable of integrating this information, or that are unable to make the necessary adaptations, will cease growth and eventually die. Here, we studied the molecular basis underlying the synthetic lethality caused by loss of the protein kinase Sch9, a key player in amino acid signaling and proximal effector of the conserved growth-regulatory TORC1 complex, when combined with either loss of the cyclin-dependent kinase (CDK) Pho85 or loss of its inhibitor Pho81, which both have pivotal roles in phosphate sensing and cell cycle regulation. We demonstrate that it is specifically the CDK-cyclin pair Pho85-Pho80 or the partially redundant CDK-cyclin pairs Pho85-Pcl6/Pcl7 that become essential for growth when Sch9 is absent. Interestingly, the respective three CDK-cyclin pairs regulate the activity and distribution of the phosphatidylinositol-3 phosphate 5-kinase Fab1 on endosomes and vacuoles, where it generates phosphatidylinositol-3,5 bisphosphate that serves to recruit both TORC1 and its substrate Sch9. In addition, Pho85-Pho80 directly phosphorylates Sch9 at Ser^{726}, and to a lesser extent at Thr^{723}, thereby priming Sch9 for its subsequent phosphorylation and activation by TORC1. The TORC1-Sch9 signaling branch therefore integrates Pho85-mediated information at different levels. In this context, we also discovered that loss of the transcription factor Pho4 rescued the synthetic lethality caused by loss of Pho85 and Sch9, indicating that both signaling pathways also converge on Pho4, which appears to be wired to a feedback loop involving the high-affinity phosphate transporter Pho84 that fine-tunes Sch9-mediated responses.

403222702, SFB 1381, TP B08 to SR and RO 1028/5-2 to SR, the Germany's Excellence Strategy, (BIOSS) EXC 949 and CIBSS (EXC 2189) to SR, the DFG projects UN111/10-2 and SFB 1557, TP14 to CU, the Swiss National Science Foundation (310030_166474/184671) to CDV, FWO-Vlaanderen (G069413, G0C7222N) to JW and KU Leuven (C14/17/063, C14/21/095) to JW. The funders had no role in study design, data collection and analysis, decision to publish, or preparation of the manuscript.

Competing interests: The authors have declared that no competing interests exist.

Author summary

Cells possess different signaling pathways that sense and signal the availability of nutrients. Crosstalk between these pathways is essential to integrate the incoming signals and allow cells to make appropriate adaptations to sustain their metabolism and proliferation. In this study, we deciphered the crosstalk between two well-known nutrient-responsive pathways in yeast, namely the PHO pathway that signals the availability of phosphate via the cyclin-dependent protein kinase Pho85, and the TORC1 signaling pathway that communicates information on the availability of free amino acids via its downstream effector kinase Sch9. We show that Pho85 facilitates the TORC1-dependent activation of Sch9 through two different mechanisms. By interfering with the biosynthesis of the lipid phosphatidylinositol-3,5 bisphosphate, Pho85 controls the recruitment of Sch9 at the vacuolar membrane, thereby bringing this effector in close proximity to TORC1. In addition, Pho85 also directly phosphorylates Sch9, which primes the latter for its subsequent phosphorylation and activation by TORC1. Conversely, we provide evidence that the TORC1-Sch9 axis gives feedback to the PHO pathway by restraining the nuclear translocation of the transcription factor Pho4 that controls the expression of genes encoding proteins required to maintain phosphate homeostasis.

Introduction

During the past decades, significant progress has been made in unravelling the dynamic and tightly regulated nutritional responses in yeast. These responses are controlled by a network of interconnected and conserved nutrient sensing routes that allow cells to adapt their metabolism in function of nutrient availability, thereby determining the growth potential and survival of cells.

A central role in the nutrient-responsive network of the yeast *Saccharomyces cerevisiae* is played by the protein kinase Sch9, which was suggested to combine the functions of the mammalian S6-kinase (S6K) [1] and protein kinase B (PKB)/Akt [2]. Sch9 controls several processes, including the regulation of transcription and translation [3–5], cellular stress responses [6–9], sphingolipid metabolism [10], pH homeostasis [11], and chronological as well as replicative lifespan [12,13]. Sch9 receives input from several upstream players. A first input is provided by the target of rapamycin complex 1 (TORC1), which signals nitrogen and amino acid availability and activates Sch9 by phosphorylation of at least 5 residues in the C-terminus [1]. Secondly, to gain full activity, Sch9 has to be phosphorylated in the activation loop by either one of the three phytosphingosine-dependent kinases, *i.e.* Pkh1, Pkh2, or Pkh3, the yeast orthologues of mammalian PDK1 [1,14,15]. Thirdly, the cellular energy sensor Snf1, the yeast AMPK orthologue, modulates Sch9 activity by phosphorylating residues that are distinct from those phosphorylated by TORC1 and Pkh1-3 [16–19]. Finally, the activity of Sch9 is also controlled by its recruitment to the vacuolar membrane where the kinase binds to phosphatidylinositol-3,5-bisphosphate (PI[3,5]P_2), generated by the phosphatidylinositol-3-phosphate (PI3P) 5-kinase Fab1, the orthologue of the mammalian PIKfyve [20,21]. This recruitment is dependent on the N-terminal domain of Sch9 [22] and is essential for the TORC1-dependent activation of Sch9 [21,22]. Intriguingly, Fab1 is a substrate of TORC1, and its TORC1-dependent phosphorylation seems to control the distribution and shuttling of Fab1 between the vacuole and a subpopulation of prevacuolar endosomes, termed signaling endosomes [22–24]. At these signaling endosomes, Fab1 generates the main pool of PI[3,5]P_2, which is subsequently delivered to the vacuole [22,24].

In a previous study, we reported on the genome-wide synthetic genetic array (SGA) analysis of *sch9Δ*. We noted that the combined deletion of *SCH9* with either the cyclin-dependent kinase (CDK) inhibitor *PHO81* or the CDK *PHO85* resulted in a synthetic lethal phenotype [11]. Pho81 and Pho85 are key players in the phosphate-responsive signaling pathway, known as the PHO pathway, that regulates the expression of genes required to maintain proper phosphate homeostasis. In this pathway, the CDK inhibitor (CKI) Pho81 becomes active when phosphate is limiting and inhibits the activity of the CDK–cyclin pair Pho85–Pho80, thereby enabling the transcription factor Pho4 to localize in the nucleus and induce the expression of genes required for the foraging, import, and storage of extracellular phosphate and the recycling of intracellular phosphate [25–27]. Notably, Pho81 also controls the activity of the Pho85-Pcl7 CDK-cyclin pair, which is suggested to be involved in phosphate sensing as well given its ability to phosphorylate Pho4 *in vitro* [28,29]. Our observation of a synthetic lethality between *pho81Δ* or *pho85Δ* and *sch9Δ* indicates that both hyperactivation and disruption of Pho85 is detrimental for cell survival in the absence of Sch9 activity and is in line with multiple observations linking phosphate sensing to other nutrient-responsive pathways [30]. Hence, the activities of Pho85 and the TORC1-Sch9 axis are required to be critically balanced and coordinated.

Pho85 is involved in the regulation of many different aspects of cell cycle control and environmental signaling [31–37]. Its deletion results in numerous defects, which besides altered phosphate metabolism, also includes slow growth, inability to grow on non-fermentable carbon sources, cell cycle defects, abnormal cell morphology and cell wall integrity, enhanced sensitivity to several types of stress, altered lipid metabolism, compromised reserve carbohydrate accumulation, as well as reduced autophagy and longevity [31,38–44]. Each of these defects can be linked to the function of specific Pho85-cyclins directing the Pho85 kinase to specific substrates [45–48]. The cyclins have been divided into two groups based on their sequence similarity: the Pho80-like subfamily, which besides Pho80 and Pcl7 also includes Pcl6, Pcl8 and Pcl10, and the Pcl1,2-like subfamily, which contains Pcl1, Pcl2, Pcl5, Pcl9, and Clg1 [46]. The Pho80-like cyclins and Pcl5 are involved in the regulation of metabolism in response to environmental changes, while the Pcl1,2-like cyclins are mainly connected to cell cycle control and morphogenesis [29,46,49]. Interestingly, the Pho85-Pho80 CDK-cyclin complex can phosphorylate and boost the activity of Fab1 under hyperosmotic stress conditions [50], suggesting that Fab1 could act as a possible point of convergence with the TORC1 signaling cascade.

In this study, we explored the synthetic lethality caused by the combined deletion of *SCH9* and either *PHO85* or *PHO81*. We demonstrate that these synthetic lethalities are due to conflicting signals in the crosstalk between Pho85, TORC1, and Sch9. We provide evidence that the CDK-cyclin pair Pho85-Pho80 directly phosphorylates Sch9 to prime this kinase for subsequent phosphorylation by TORC1. In addition, we confirm that Pho85-Pho80 affects Fab1 activity and provide evidence that also Pho85-Pcl6 and Pho85-Pcl7 are likely involved in the regulation of the cellular PI[3,5]P_2 levels as judged from the vacuolar recruitment of Sch9. Finally, we show that the transcription factor Pho4 is not only a downstream target of Pho85 signaling but of TORC1-Sch9 signaling as well.

Results

Crosstalk between Pho85 and the TORC1-Sch9 axis involves the cyclins Pho80, Pcl6, and Pcl7

To confirm the previously reported genetic interactions between Sch9, Pho81, and Pho85, and to identify which Pho85 cyclins contribute to the observed effects, we crossed the *sch9Δ* strain with isogenic strains lacking *PHO81*, *PHO85*, or either one of the known cyclins, and

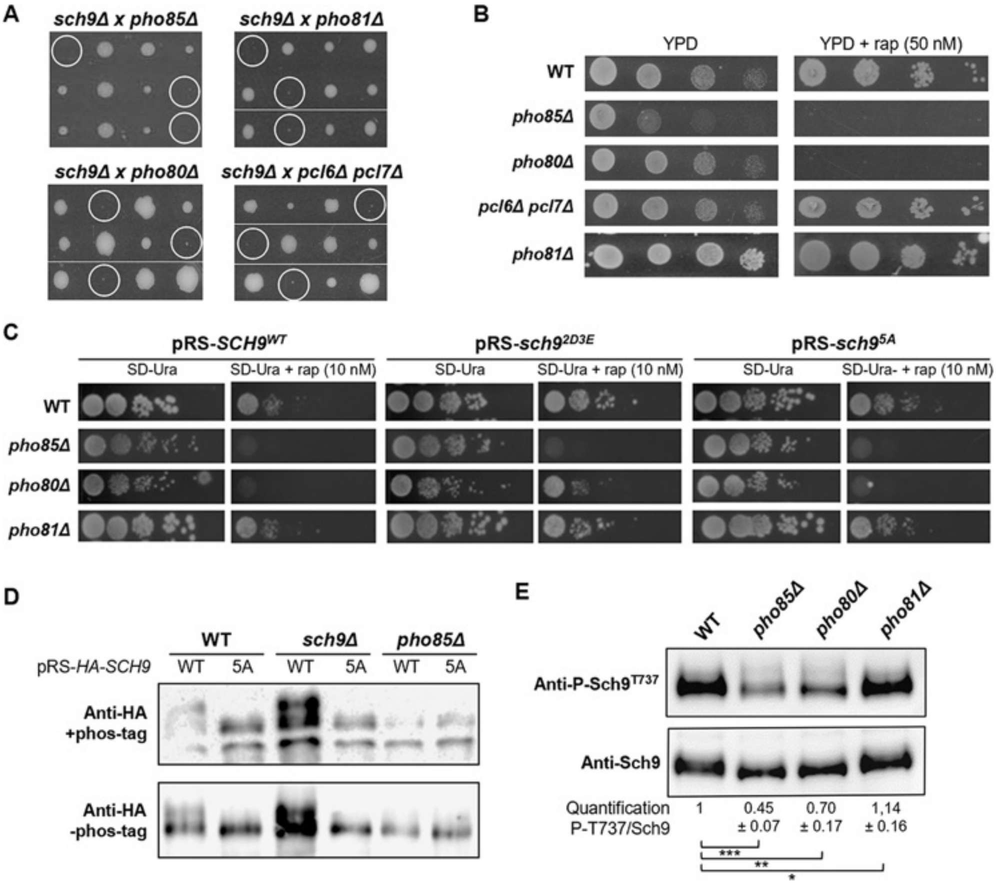

Fig 1. Genetic interaction between the Pho85 and Sch9 signaling pathways. (A) Tetrad analysis on YPD plates of a cross between the *sch9Δ* mutant and mutant strains lacking either Pho81, Pho85, Pho80, or the combination of Pcl6 and Pcl7. The spores that combine the deletions of the parental mutant strains and define the synthetic lethal or synthetic sick phenotype are indicated by the white circles. Pictures were taken 3 to 5 days after dissection. See S1 Fig for the complete genotypic analysis of all cyclin mutants. (B) Rapamycin sensitivity analysis of the WT (BY4741), *pho85Δ*, *pho80Δ*, *pcl6Δ pcl7Δ*, and *pho81Δ* strains. The strains were grown to exponential growth phase on YPD medium, diluted to an OD_{600nm} of 0.1 and serial 10-fold dilutions were then spotted on YPD plates without or with 50 nM rapamycin (rap) and grown at 30˚C. See S2 Fig for the rapamycin sensitivity test of all cyclin mutants. (C) Rapamycin sensitivity analysis of the WT, *pho85Δ*, *pho80Δ*, and *pho81Δ* strains transformed with centromere plasmids allowing for expression of either $Sch9^{WT}$, $Sch9^{2D3E}$, or $Sch9^{5A}$, and assessed by growth on SD medium lacking uracil (SD-ura) without or with 10 nM rapamycin. (D) Phos-tag immunoblot analysis to assess Sch9 phosphorylation levels in protein extracts obtained from exponentially growing WT, *sch9Δ*, and *pho85Δ* cells expressing either HA-$Sch9^{WT}$ or HA-$Sch9^{5A}$. The protein extracts were resolved on phos-tag gels and subsequently analyzed via immunoblotting with anti-HA antibodies. (E) Immunoblot analysis of protein extracts obtained from exponentially growing WT, *pho85Δ*, *pho80Δ*, and *pho81Δ* cells using the anti-P-$Sch9^{T737}$ and anti-Sch9 antibodies. The quantifications show the ratio of phosphorylated to total Sch9 as normalized to the ratio obtained for the WT cells. A two-tailed student's T test was used to calculate significances (*, $P < 0.1$; **, $P < 0.01$; ***, $P < 0.001$).

https://doi.org/10.1371/journal.pgen.1010641.g001

performed a systematic tetrad analysis. As shown in Fig 1A, the synthetic lethal phenotype of the *sch9Δ pho81Δ* and *sch9Δ pho85Δ* strains was mimicked by the combined deletion of *SCH9* and *PHO80*. The *sch9Δ pho80Δ* spores were still able to germinate but showed a very severe synthetic growth defect. For all other cyclins, the combined deletion with *SCH9* yielded viable spores that did not exhibit significant growth differences in comparison to the *sch9Δ* strain (S1 Fig). However, since the cyclins Pcl1 and Pcl2, Pcl6 and Pcl7, or Pcl8 and Pcl10 have partially redundant functions [28,47,51], we also tested their combined deletions. While the combined deletion of *PCL1* and *PCL2*, or of *PCL8* and *PCL10* in the *sch9Δ* background did not further exacerbate the slow growth phenotype of the *sch9Δ* mutant, a pronounced synthetic growth defect was noticed in case of the combined *PLC6* and *PLC7* deletion (Fig 1A, S1 Fig). Hence, we can conclude that loss of the cyclin functions of Pho80 and a combination of Pcl6 and Pcl7 contribute to the synthetic lethal phenotype of the *sch9Δ pho85Δ* strain.

Because Sch9 activity is dependent on its phosphorylation by TORC1 [1], the growth of the *pho81Δ*, *pho85Δ*, and cyclin deletion strains was also monitored in the presence of sub-lethal levels of rapamycin, a specific inhibitor of TORC1. As shown in Fig 1B, both the *pho85Δ* and *pho80Δ* cells were unable to grow on rich medium supplemented with 50 nM rapamycin, which is consistent with previously made observations [40,43]. In contrast, wild-type cells (BY4741; WT) and the other strains carrying either single or double cyclin deletions or a *PHO81* deletion did not display rapamycin-sensitive growth (S2A and S2B Fig). This is an intriguing observation, because it suggests that under these sub-lethal conditions there is still sufficient Sch9 activity to maintain growth of the *pho81Δ* and *pcl6Δ pcl7Δ* strains.

Next, we investigated whether the rapamycin-induced growth defect of the *pho85Δ* and *pho80Δ* strains could be restored by transforming the strains with a centromere plasmid expressing the constitutive active TORC1 phosphomimetic Sch9^{2D3E} mutant [1]. As a control, strains were also transformed with plasmids expressing wild-type Sch9^{WT} or the Sch9^{5A} mutant that cannot be activated by TORC1. As shown in Fig 1C, neither the expression of Sch9^{WT} nor Sch9^{5A} could restore the rapamycin-induced growth defect of the strains, while overexpression of Sch9^{2D3E} clearly improved growth in the presence of rapamycin in case of the *pho80Δ* strain, but not in case of the *pho85Δ* strain. For comparison, we also included the WT and the *pho81Δ* strain in this experiment and, as expected, their growth on rapamycin-containing medium was slightly improved by the expression of the Sch9^{2D3E} allele (Fig 1C). Thus, the observation that Sch9^{2D3E} expression rescues the rapamycin sensitivity of the *pho80Δ* strain suggests that the Pho85-Pho80 CDK-cyclin pair may be specifically required for TORC1-mediated phosphorylation and activation of Sch9. To address this possibility, we performed a Phos-tag mobility shift analysis using protein extracts of WT, *sch9Δ*, and *pho85Δ* cells expressing HA-tagged constructs of either Sch9^{WT} or the Sch9^{5A} mutant that served as control (Fig 1D). This clearly demonstrated that the phosphorylation of Sch9 was compromised in the *pho85Δ* strain because only in this strain the slowly migrating band corresponding to fully phosphorylated Sch9^{WT} was absent, resulting in a similar mobility pattern for Sch9^{WT} as that seen for Sch9^{5A}. Consistently, immunodetection of native Sch9 and of its phosphorylation state at the TORC1 residue Thr^{737} (using anti-Sch9 and anti-phospho-Sch9^{T737} antibodies, respectively), demonstrated that Sch9 phosphorylation was significantly reduced in the *pho85Δ* and the *pho80Δ* strain, while being enhanced in the *pho81Δ* (Figs 1E and S2C).

Pho85-Pho80 is required for vacuolar recruitment of Fab1 and Sch9

Previous studies indicated that Sch9 is recruited to the vacuolar membrane during fermentative growth where it binds PI[3,5]P$_2$ via its N-terminal domain and then becomes phosphorylated by TORC1 [1,21,22,52]. PI[3,5]P$_2$ is generated from PI3P by the PIKfyve-like kinase Fab1, whose activity is tightly regulated by intramolecular inhibitory interactions and by different regulatory proteins that form a complex with Fab1 [53–57]. Both TORC1 and Pho85-Pho80 impact on the Fab1 activity [22, 50]. Previous research demonstrated signaling endosomes to be the main site for PI[3,5]P_2 production [22]. These signaling endosomes contain the EGO complex and TORC1, which phosphorylates Fab1 in the N-terminal half close to the FYVE (Fab1, YOTB, Vac1 and EEA1) domain, thereby enhancing the PI3P binding of Fab1 and promoting the PI[3,5]P_2 generation. According to the current working model, PI [3,5]P_2 is delivered to the vacuolar membrane upon fusion of the signaling endosome with the vacuole, and the EGO complex, TORC1, and Fab1 become dispersed over the vacuolar membrane. Fab1 is then recycled back to the signaling endosome in order to restart PI[3,5]P_2 production [22]. Pho85-Pho80 is known to boost the activity of Fab1 by phosphorylation in the C-terminal region close to the catalytic kinase domain, thereby enhancing PI[3,5]P_2 production upon stress [50]. In addition, Pho85-Pho80 also phosphorylates Vac7, a positive regulator of Fab1 [50]. Thus, to address the possibility that Pho85-Pho80 affects the TORC1-dependent phosphorylation of Sch9 indirectly through the regulation of Fab1, we wondered whether overactivation of Fab1 would restore the rapamycin-induced growth defect of the *pho85Δ* and *pho80Δ* strains. To make the comparison with the aforementioned growth assay (Fig 1C), we again transformed the WT, *pho85Δ*, *pho80Δ*, and *pho81Δ* strains with the centromere plasmid encoding Sch9^{WT} but this time together with a centromere plasmid providing either additional copies of wild-type Fab1 or the hyperactive Fab1^{VLA} mutant that was reported to yield more than 10-fold increased basal PI[3,5]P_2 levels [55]. As shown in Fig 2A, neither wild-type Fab1, nor the Fab1^{VLA} mutant allowed the *pho85Δ* or the *pho80Δ* strains to grow on medium supplemented with 10 nM rapamycin. In fact, we noticed that the Fab1^{VLA} mutant even caused rapamycin sensitivity in the WT and *pho81Δ* strain. Both observations incited us to monitor the expression of the Fab1 and Fab1^{VLA} proteins in more detail. Since currently no Fab1 antibody is available, we transformed the different strains with centromere plasmids allowing the expression of both Fab1 proteins as C-terminally tagged GFP fusion under control of the *FAB1* promotor. When assayed for growth in the presence of 10 nM rapamycin, similar results were obtained as before, *i.e.* no growth in case of the *pho85Δ* and *pho80Δ* strains and enhanced sensitivity for the WT and *pho81Δ* strain when expressing the Fab1^{VLA}-GFP fusion (Fig 2B). We further noted that the *pho85Δ* strain was slightly less sensitive to rapamycin than the *pho80Δ* strain when grown on lower levels (*i.e.* 4.5 nM) of rapamycin (Fig 2B). Next, we used an anti-GFP antibody to estimate the expression levels of the Fab1-GFP and Fab1^{VLA}-GFP fusions in the different strains using Adh2 as loading control. When compared to genomically expressed Fab1-GFP levels in WT cells, centromere plasmid-expressed Fab1-GFP levels appeared to be roughly 5-fold higher in WT, 4-fold higher in *pho81Δ*, and 1.5-fold higher in *pho85Δ* and *pho80Δ* cells (Fig 2C). In WT and *pho81Δ* cells, the plasmid-expressed Fab1^{VLA}-GFP levels were even slightly higher than the ones observed for plasmid-expressed Fab1-GFP, but they were somewhat lower than the respective plasmid-expressed Fab1-GFP levels in both *pho85Δ* and *pho80Δ* cells (Fig 2C). Thus, even though *pho85Δ* and *pho80Δ* cells exhibit plasmid-expressed Fab1-/Fab1^{VLA}-GFP levels that are in a comparable range to the ones of genomically expressed Fab1-GFP in WT cells, they appear, unlike WT and *pho81Δ* cells, unable to support (plasmid-driven) expression of much higher Fab1-/Fab1^{VLA}-GFP levels. We then monitored the intracellular localization of the Fab1-GFP and Fab1^{VLA}-GFP fusions in the different WT and mutant strains (Fig 2D and 2E). In line with the measured expression levels, Fab1-GFP was present on vacuolar membranes in all strains, but the staining was on average less intense in *pho85Δ* and *pho80Δ* cells as compared to WT and *pho81Δ* cells. Furthermore, in *pho85Δ* cells and *pho80Δ* cells, Fab1-GFP mainly localized at small vacuoles as well as in foci close to, or at the vacuolar membrane. These foci probably correspond to the previously reported signaling endosomes [22,24]. If confirmed, we deem it reasonable to assume that the lack of Pho85 or Pho80 impedes the fusion of these perivacuolar endosomes and as such the distribution or stabilization of Fab1 at vacuolar membranes. As expected, and consistent with

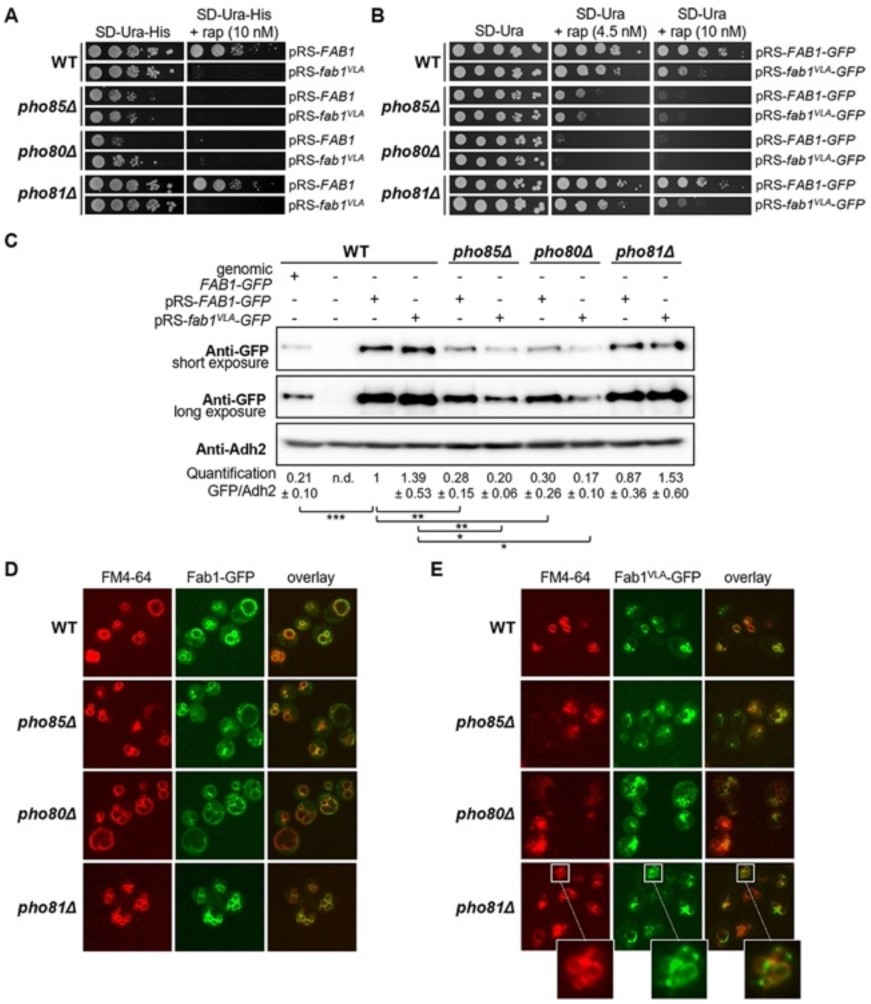
A
SD-Ura-His
SD-Ura-His + rap (10 nM)
WT
pho85Δ
pho80Δ
pho81Δ
pRS-FAB1
pRS-fab1VLA
B
SD-Ura
SD-Ura + rap (4.5 nM)
SD-Ura + rap (10 nM)
pRS-FAB1-GFP
pRS-fab1VLA-GFP
C
genomic FAB1-GFP
pRS-FAB1-GFP
pRS-fab1VLA-GFP
Anti-GFP short exposure
Anti-GFP long exposure
Anti-Adh2
Quantification GFP/Adh2
0.21 ± 0.10
n.d.
1
1.39 ± 0.53
0.28 ± 0.15
0.20 ± 0.06
0.30 ± 0.26
0.17 ± 0.10
0.87 ± 0.36
1.53 ± 0.60
***
**
**
*
*
D
FM4-64
Fab1-GFP
overlay
E
Fab1VLA-GFP

Fig 2. Pho85-Pho80 is involved in the recruitment of Fab1 to the vacuolar membrane. (A) Rapamycin sensitivity analysis of the WT, *pho85Δ*, *pho80Δ*, and *pho81Δ* strains expressing Sch9^{WT} and Fab1 alleles from centromere plasmids. Growth was assessed on selective synthetic medium without or with 10 nM rapamycin (rap). (B) Rapamycin sensitivity analysis in the presence of 4.5 nM or 10 nM rapamycin of the WT, *pho85Δ*, *pho80Δ*, and *pho81Δ* strains expressing either the GFP-tagged wild-type Fab1 or the GFP-tagged Fab1^{VLA} allele from a centromere plasmid as indicated. (C) Immunoblot analysis of the WT, *pho85Δ*, *pho80Δ*, and *pho81Δ* strains to compare the expression levels of the Fab1-GFP and Fab1^{VLA}-GFP fusions when introduced on centromere plasmids with the expression level of a genomically tagged Fab1-GFP present in the WT strain. Expression levels were calculated based on the ratios obtained for GFP and the loading control Adh2. A two-tailed student's T test was used to calculate significances (*, $P < 0.1$; **, $P < 0.01$; ***, $P < 0.001$). (D) Microscopic analysis of Fab1-GFP and Fab1^{VLA}-GFP localization in the WT, *pho85Δ*, *pho80Δ*, and *pho81Δ* strains. The strains were grown to mid-log phase on selective synthetic medium. The lipophilic dye FM4-64 was used to visualize the vacuolar membrane. The indents in the pictures of Fab1^{VLA}-GFP expressing *pho81Δ* cells are magnifications to clarify that this hyperactive Fab1 mutant largely fails to stain vacuolar membranes and is mainly localized in foci close to, or at the vacuole.

https://doi.org/10.1371/journal.pgen.1010641.g002

previous observations [50,55], cells expressing the hyperactive Fab1^{VLA}-GFP version displayed small and tiny, almost vesicle-like, vacuoles. Interestingly, Fab1^{VLA}-GFP was to a large extent absent from membranes of the discernible vacuoles and almost exclusively present in foci, and this independently of the presence or absence of Pho85, Pho80, or Pho81. This defect is unlikely caused by the GFP tag because wild-type Fab1-GFP properly localized to vacuolar membranes and, because both GFP-tagged and untagged Fab1^{VLA} caused rapamycin-sensitivity to a similar extent in all strains studied. However, we noted that the mutations in the Fab1^{VLA} allele (E1822V, F1833L, T2250A; [55]) are located within the reported cluster of potential Pho85-Pho80 target residues (T1569, T1583, T1594, T1691, S1924, T1953, T1963, and S2166; [50]). It is therefore possible that the mutations in this Fab1 variant mimic the phosphorylation by Pho85-Pho80 and that this prevents the stabilization of Fab1 at the vacuolar membrane resulting in a continuous recycling back to the perivacuolar signaling endosome to generate more PI[3,5]P$_2$, a model that remains to be addressed in future studies. If true, then the phosphorylation of Fab1 by Pho85-Pho80 not only stimulates the fusion of signaling endosomes to the vacuole but also promotes the localization of Fab1 at perivacuolar signaling endosomes. Such a model would also elegantly explain why cells with hyperactive Pho85 (e.g., due to the lack of the CKI Pho81) mostly display smaller and fragmented vacuoles (Fig 2D and 2E). Thus, our combined data suggest that the equilibrium of endosomal and vacuolar Fab1 is critically controlled by both TORC1, as previously reported [22], and Pho85-Pho80.

Finally, the enhanced rapamycin sensitivity observed for the WT strain when expressing Fab1^{VLA} led us to monitor the Sch9^{T737} phosphorylation levels. We found these to be slightly lower in cells expressing Fab1^{VLA} as compared to cells with the empty vector control or cells expressing Fab1, suggesting that hyperactivation of Fab1 is associated with reduced TORC1 activity (S3A Fig). A similar but more pronounced effect was previously observed for cells expressing the Fab1^{6D} mutant that also displays enhanced Fab1 activity [22].

In line with our data on Fab1-GFP localization and a model in which Pho85-Pho80 is an upstream activator of Fab1 that boosts the PI[3,5]P$_2$ content of the vacuolar membrane, thereby determining vacuolar size and morphology [50,58,59], we noticed that in comparison to the WT or *pho81Δ* strains, the *pho85Δ* strain and especially the *pho80Δ* strain had many cells with enlarged vacuoles. In contrast to cells displaying small and fragmented vacuoles, the cells with these enlarged vacuoles appeared to be hampered for the vacuolar recruitment of a genomically tagged GFP-Sch9^{WT} (Figs 3A and S3B). Likewise, we also found lower GFP-Sch9 levels at the membranes of vacuoles when these were isolated from cells lacking Pho85 (S3C and S3D Fig). Given that Sch9 normally needs to bind PI[3,5]P$_2$ at the vacuolar membrane, we wondered whether forced anchoring of Sch9 to the vacuolar membrane would be sufficient to correct the reduced Sch9 phosphorylation by TORC1 as seen in the *pho85Δ* and *pho80Δ* strains and thereby resolve their rapamycin sensitivity. To address this, a genomically tagged GFP-FYVE-Sch9^{WT} was introduced in the WT, *pho85Δ*, *pho80Δ*, and *pho81Δ* strains. As described previously, fusing the FYVE domain from mammalian EEA1 to the N-terminus of Sch9, artificially tethers the kinase to PI3P in the vacuolar membranes of yeast cells [60]. As such, we indeed observed a strong vacuolar enrichment of GFP-FYVE-Sch9^{WT}, even in *pho85Δ* and *pho80Δ* cells with enlarged vacuoles, which now displayed fluorescence over the entire vacuolar membrane (Figs 3A and S3B). The artificial tethering came along with dramatically enhanced phosphorylation levels of GFP-FYVE-Sch9^{WT} at the Thr^{737} residue in all the strains, but still, this was significantly lower in the *pho80Δ* and *pho85Δ* strains as compared to the WT strain (Fig 3B). Furthermore, despite the enhanced phosphorylation, GFP-FYVE-Sch9^{WT} did not alleviate the rapamycin sensitivity of the *pho85Δ* and *pho80Δ* strain (Fig 3C), suggesting that the Pho85-Pho80 CDK-cyclin pair could also (directly or indirectly) target Sch9, besides Fab1. This possibility is further supported by our initial observation that expression of the

TORC1 phosphomimetic Sch9^{2D3E} mutant rescues the rapamycin sensitivity of the *pho80Δ* strain (Fig 1C).

Pho85-Pho80 primes Sch9 for phosphorylation by TORC1 at the vacuolar membrane

To further support that Sch9 is a substrate for Pho85-Pho80, we first wanted to rule out the possibility that the observed decreased phosphorylation of Sch9 in the *pho85Δ* and *pho80Δ*

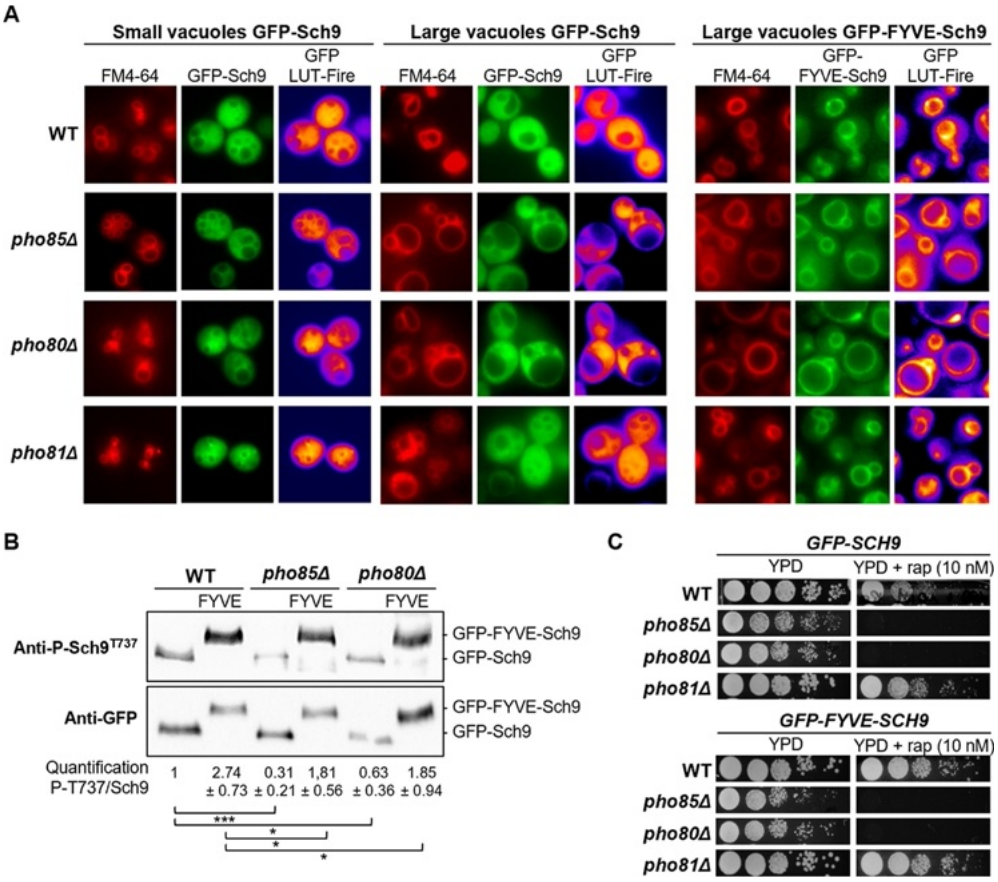
A
Small vacuoles GFP-Sch9
Large vacuoles GFP-Sch9
Large vacuoles GFP-FYVE-Sch9
FM4-64
GFP-Sch9
GFP LUT-Fire
FM4-64
GFP-Sch9
GFP LUT-Fire
FM4-64
GFP-FYVE-Sch9
GFP LUT-Fire
WT
pho85Δ
pho80Δ
pho81Δ
B
WT
pho85Δ
pho80Δ
FYVE
FYVE
FYVE
Anti-P-Sch9T737
Anti-GFP
GFP-FYVE-Sch9
GFP-Sch9
GFP-FYVE-Sch9
GFP-Sch9
Quantification P-T737/Sch9
1
2.74 ± 0.73
0.31 ± 0.21
1,81 ± 0.56
0.63 ± 0.36
1.85 ± 0.94
***
*
*
*
C
GFP-SCH9
YPD
YPD + rap (10 nM)
WT
pho85Δ
pho80Δ
pho81Δ
GFP-FYVE-SCH9
YPD
YPD + rap (10 nM)
WT
pho85Δ
pho80Δ
pho81Δ

Fig 3. Pho85-Pho80 is required for the vacuolar recruitment of Sch9. (A) Microscopic analysis of Sch9 localization in the WT, *pho85Δ*, *pho80Δ*, and *pho81Δ* strains expressing genomically tagged GFP-Sch9 or GFP-FYVE-Sch9 fusion proteins. Strains were grown to mid-log phase on complete synthetic medium. The lipophilic dye FM4-64 was used to visualize the vacuolar membrane and a LUT Fire was applied using ImageJ to show the levels of the GFP signal. (B) Immunoblot analysis to compare the Sch9 phosphorylation levels in WT, *pho85Δ*, and *pho80Δ* cells expressing either GFP-Sch9 or GFP-FYVE-Sch9 when grown to mid-log phase on complete synthetic medium. The Sch9-Thr^{737} phosphorylation levels were quantified based on the ratio of the signals obtained with the anti-P-Sch9^{T737} and anti-Sch9 antibodies and normalized to WT cells. A two-tailed student's T test was used to calculate significances (*, $P < 0.1$; **, $P < 0.01$; ***, $P < 0.001$). (C) Rapamycin sensitivity analysis of the WT (BY4741), *pho85Δ*, *pho80Δ*, and *pho81Δ* strains expressing genomically tagged GFP-Sch9 or GFP-FYVE-Sch9 as assessed by growth on YPD plates without or with 10 nM rapamycin (rap).

https://doi.org/10.1371/journal.pgen.1010641.g003

strains would simply be due to a reduced TORC1 activity at the vacuolar membrane. As mentioned above, the EGO complex and TORC1 are mainly present in different pools. In prevacuolar endosomes, both complexes have been described to decorate signaling endosomes, and the HOPS-mediated fusion of these endosomes with the vacuole determines the pool of the latter [22–24]. We first monitored the intracellular localization of a genomically tagged GFP-Tor1 in WT, *pho85Δ*, and *pho80Δ* strains. In WT cells, the GFP-Tor1 fusion nicely stained the membranes of all vacuoles. In the *pho85Δ* and the *pho80Δ* cells, however, the staining was more confined to small vacuoles and in those cells with large vacuoles, the signal on the vacuolar membrane was only weak or even absent and staining was restricted to prevacuolar endosomes, especially in the *pho80Δ* strain (Fig 4A). This again suggests that the Pho85-Pho80 CDK-cyclin pair is required for an optimal fusion of endosomes with the vacuole.

Next, we evaluated the phosphorylation of two additional TORC1 clients to compare this with the phosphorylation of Sch9. The first client is Atg13, a regulatory subunit of the Atg1 complex involved in macroautophagy that was previously found to be phosphorylated at Ser^{554} by TORC1 localized on signaling endosomes [61,62]. We genomically expressed Atg13 as C-terminal triple HA-tagged fusion and quantified the phosphorylation-dependent band shift when using the anti-HA antibody. This demonstrated a consistent and significantly reduced phosphorylation of Atg13-HA$_3$ in the *pho85Δ* and *pho80Δ* strains as compared to the WT strain (Fig 4B). Thus, similar as for Sch9, the Pho85-Pho80 CDK-cyclin pair has a direct or indirect effect on Atg13 phosphorylation, which may not be surprising because Pho85--Pho80 was shown to contribute to the complex regulation of autophagy when cells suffer nutrient starvation [44,63]. Of note, Atg13 was shown to recruit the phosphatidylinositol 3-kinase complex subunit Atg14 to the pre-autophagosomal structure in a phospho-dependent manner [64], and thereby Atg13 likely sets the conditions for the recruitment of Fab1 as well.

The second additional TORC1 client tested is Lst4, which in complex with Lst7 functions as GAP for the Rag family GTPase Gtr2 of the EGO complex [65]. At the vacuole, Lst4 ensures a rapid amino acid-dependent activation of TORC1, but once activated, TORC1 in turn phosphorylates Lst4 at several residues thereby triggering displacement of Lst4 from the vacuole. This feedback cycle prevents hyperactivation of TORC1 and safeguards the dynamic adjustment of TORC1 activity in response to amino acid availability [66]. We genomically expressed Lst4 as C-terminal V5-tagged fusion in the WT, *pho85Δ*, and *pho80Δ* strains and monitored the TORC1-dependent phosphorylation of Ser^{523}. However, neither immunodetection with the anti-phospho-Lst4^{S523} antibody, nor the band shift seen when using the anti-V5 antibody, pointed to a significant difference in Lst4 phosphorylation between the strains (Fig 4C). Thus, even the *pho85Δ* and *pho80Δ* strains maintain sufficient vacuolar TORC1 activity to provide homeostatic control of Lst4. As such, it is unlikely that the reduced phosphorylation of Sch9 seen in these two deletion strains would solely be the consequence of a hampered vacuolar TORC1 recruitment, which raises again the possibility that Sch9 could be a specific substrate of the Pho85-Pho80 CDK-cyclin pair.

Like the mammalian CDK counterparts, Pho85 is a proline-directed Ser/Thr protein kinase [35,67]. The previously reported TORC1 phospho-epitope mapping of Sch9 identified two Ser/Thr-Pro sites, *i.e.* Thr^{723} and Ser^{726} upstream of the hydrophobic motif (HM; amino acids 733–738) and, interestingly, this study suggested that the phosphorylation of Ser^{726} primed the kinase for Thr^{723} phosphorylation [1]. To confirm this and to address whether such a priming role would extend to other Sch9 phosphosites as well, we again turned to Phos-tag mobility shift assays, this time using Flag-tagged Sch9 constructs in which Thr^{723} and Ser^{726} were replaced by Ala, either separately or in combination. As shown in Fig 5A, only when Ser^{726} was replaced by Ala, the corresponding Sch9 mutants fail to become fully phosphorylated by TORC1, yielding a migration profile comparable to that seen for Sch9^{WT} and Sch9^{5A} in the

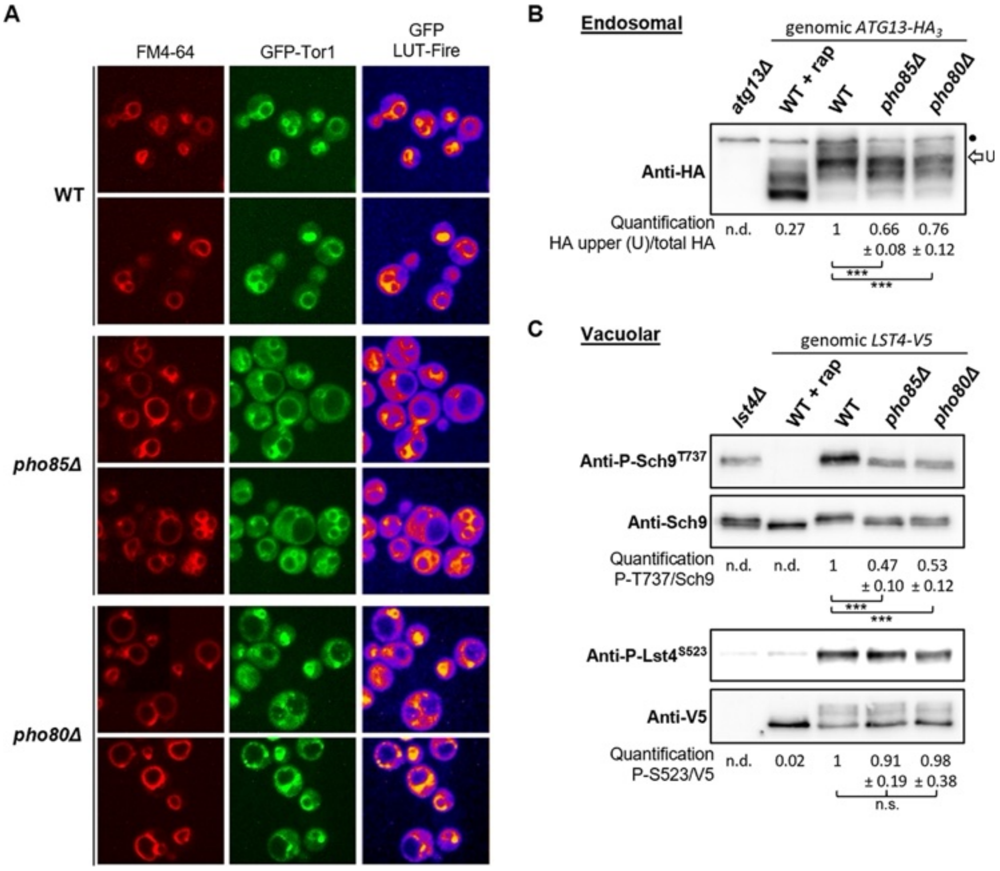
A
FM4-64
GFP-Tor1
GFP LUT-Fire
WT
pho85Δ
pho80Δ
B
Endosomal
genomic ATG13-HA3
atg13Δ
WT + rap
WT
pho85Δ
pho80Δ
Anti-HA
U
Quantification HA upper (U)/total HA
n.d.
0.27
1
0.66 ± 0.08
0.76 ± 0.12
***
***
C
Vacuolar
genomic LST4-V5
lst4Δ
WT + rap
WT
pho85Δ
pho80Δ
Anti-P-Sch9T737
Anti-Sch9
Quantification P-T737/Sch9
n.d.
n.d.
1
0.47 ± 0.10
0.53 ± 0.12
***
***
Anti-P-Lst4S523
Anti-V5
Quantification P-S523/V5
n.d.
0.02
1
0.91 ± 0.19
0.98 ± 0.38
n.s.

Fig 4. Tor1 localization and TORC1 activity in WT, *pho85Δ*, and *pho80Δ* strains. (A) Microscopic analysis of Tor1 localization in the WT, *pho85Δ*, and *pho80Δ* strains expressing a genomically tagged GFP-Tor1 fusion. Strains were grown to mid-log phase on complete synthetic medium. The lipophilic dye FM4-64 was used to visualize the vacuolar membrane and a LUT Fire was applied using ImageJ to visualize the levels of the GFP signal. (B, C) Immunoblot analyses to compare the Atg13 (B), or Sch9 and Lst4 (C) phosphorylation levels in WT, *pho85Δ*, and *pho80Δ* cells expressing either a genomically introduced Atg13-HA$_3$ or Lst4-V5 fusion when grown to mid-log phase on complete synthetic medium. The dot in the Atg13-HA$_3$ blots indicate a non-specific cross-reacting band, the arrow 'U' points to the bands corresponding to the most phosphorylated Atg13-HA$_3$ isoforms that was quantified and used to calculate the ratio relative to the total HA signal. For Sch9 and Lst4, the phosphorylation levels were quantified based on the ratio of the signals obtained with the anti-P-Sch9^{T737} or anti-P-Lst4^{S523}, and the anti-Sch9 or anti-V5 antibodies, respectively, and normalized to the one in WT cells. As indicated, the *atg13Δ* strain, the *lst4Δ* strain, and the WT strain expressing either genomic Atg13-HA$_3$ or Lst4-V5, but treated with 200 nM rapamycin (rap) for 30 min, served as controls. A two-tailed student's T test was used to calculate significances (*, $P < 0.1$; **, $P < 0.01$; ***, $P < 0.001$, n.s.: not significant).

https://doi.org/10.1371/journal.pgen.1010641.g004

pho85Δ strain (Fig 1D). We also tested other Sch9 phosphomutants, but only the Sch9^{S726A} was compromised in priming for subsequent TORC1-mediated phosphorylation (S4A Fig). To confirm this priming effect, we independently created genomic Sch9-Ser^{726}-to-Ala and phosphomimetic Sch9-Ser^{726}-to-Asp mutations and then tested the expressed proteins (*i.e.* Sch9^{S726A} and Sch9^{S726D}) for their phosphorylation of Thr^{737} *in vivo*. Consistent with a

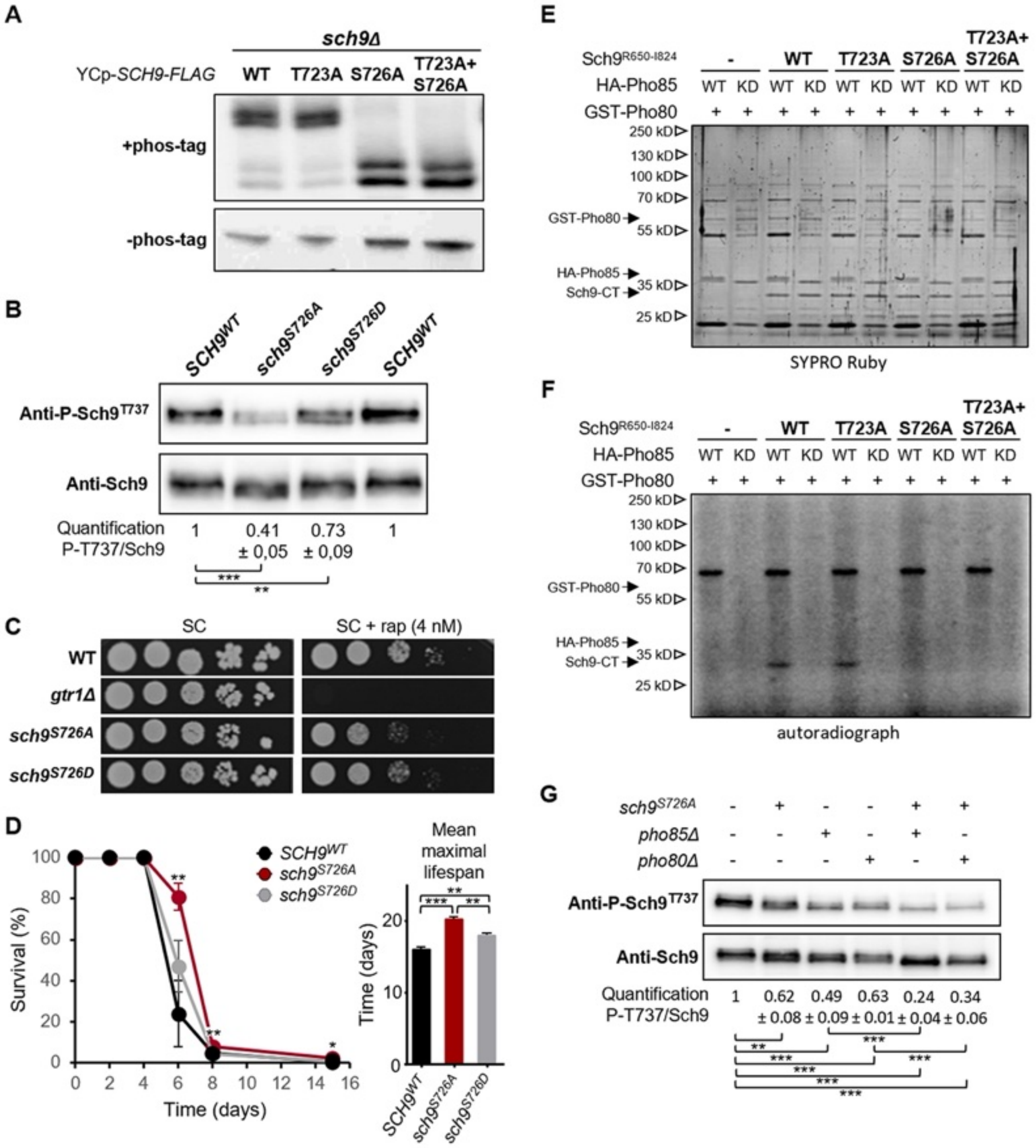

Fig 5. Pho85-Pho80-mediated phosphorylation of Ser^{726} primes Sch9 for its subsequent activation by TORC1. (A) Phos-tag immunoblot analysis of protein extracts obtained from exponentially growing *sch9Δ* cells transformed with a centromere plasmid driving the expression of C-terminally FLAG-tagged Sch9^{WT}, Sch9^{T723A}, Sch9^{S726A}, or Sch9$^{T723A/S726A}$ as indicated. Total protein extracts were resolved on phos-tag gels and were subsequently analyzed via immunoblotting with anti-FLAG

antibodies. (B) Immunoblot analysis to assess the Sch9-Thr^{737} phosphorylation levels in protein extracts obtained from exponentially growing BY4741 cells expressing endogenous Sch9^{WT} or the mutant versions Sch9^{S726A} or Sch9^{S726D}. The Thr^{737} phosphorylation levels were quantified based on the ratio of the signals obtained with the anti-P-Sch9^{T737} and anti-Sch9 antibodies and normalized to the ratio obtained for Sch9^{WT}. (C) Rapamycin sensitivity analysis of BY4741 cells expressing endogenous Sch9^{WT} or the mutant versions Sch9^{S726A} or Sch9^{S726D} as assessed by growth on complete synthetic medium without or with 5 nM rapamycin. (D) Chronological lifespan assay showing the survival of BY4741 cells expressing endogenous Sch9^{WT} or the mutant versions Sch9^{S726A} or Sch9^{S726D} when starved for phosphate for several days as indicated. The bar diagram depicts the mean maximal lifespan. (E, F) Pho85-Pho80 phosphorylates Ser^{726} in the Sch9 C-terminus (CT). Purified recombinant Sch9$^{R650-I824}$-TAP fragments corresponding to Sch9^{WT}, Sch9^{T723A}, Sch9^{S726A}, or Sch9$^{T723A/S726A}$ were subjected to *in vitro* phosphorylation by the Pho85-Pho80 CDK-cyclin pair purified from yeast. The assay was performed using wild-type Pho85 (WT) or the kinase dead Pho85^{E53A} mutant (KD), which was included as control. Representative SYPRO Ruby staining (E) and autoradiography (^{32}P) blots (F) are shown. (G) Western blot analysis to assess the Sch9 Thr^{737} phosphorylation levels in protein extracts obtained from exponentially growing WT, *pho85Δ*, or *pho80Δ* cells expressing endogenous Sch9^{WT} or the mutant version Sch9^{S726A}. The Thr^{737} phosphorylation levels were quantified based on the ratio of the signals obtained with the anti-P-Sch9^{T737} and anti-Sch9 antibodies and normalized to the ratio obtained for Sch9^{WT} in the WT strain. A two-tailed student's T test was used to calculate significances (*, $P < 0.1$; **, $P < 0.01$; ***, $P < 0.001$).

https://doi.org/10.1371/journal.pgen.1010641.g005

priming effect, Thr^{737} phosphorylation was strongly reduced on Sch9^{S726A} when compared to the respective phosphorylation on Sch9^{WT} (Fig 5B). Notably, Thr^{737} was also slightly reduced on Sch9^{S726D}, which indicates that the phosphomimetic Ser^{726}-to-Asp mutation does not completely reproduce the changes seen by protein phosphorylation. We corroborated these data with growth assays where Sch9^{S726A}-expressing cells were clearly rapamycin-sensitive, while Sch9^{S726D}-expressing cells, although exhibiting a higher sensitivity to rapamycin than WT cells, were still coping better with rapamycin than Sch9^{S726A}-expressing cells (Fig 5C). A similar picture was seen when we determined longevity, which is inversely correlated with Sch9 activity [68]. Accordingly, under phosphate starvation conditions, cells expressing the phosphomutant Sch9^{S726A} displayed a longer lifespan than those expressing Sch9^{WT}, with cells expressing Sch9^{S726D} exhibiting a lifespan that was between the ones of Sch9^{WT} and Sch9^{S726A} expressing cells (Fig 5D). No significant difference in lifespan was seen between these cells when starved for nitrogen or carbon (S4D Fig), which was to be expected since both conditions abrogate the TORC1-dependent phosphorylation of Sch9 [69].

To test whether the Pho85-Pho80 CDK-cyclin pair directly phosphorylates Sch9, we next performed an *in vitro* protein kinase assay. To this end, HA-Pho85, the kinase-inactive HA-Pho85^{E53A}, and GST-Pho80 were purified from yeast lysates and peptides covering the C-termini of Sch9^{WT}, Sch9^{T723A}, Sch9^{S726A}, or Sch9^{T723A,S726A} were used as substrates. As shown, phosphorylation was obtained with the peptides corresponding to Sch9^{WT} and Sch9^{T723A}, but not with those corresponding to Sch9^{S726A} or Sch9^{T723A,S726A}, thus confirming that Ser^{726} is indeed the predominant epitope phosphorylated by Pho85-Pho80 (Figs 5E, 5F and S4B). When combined, our data thus corroborate that phosphorylation of Sch9 on Ser^{726} by Pho85-Pho80 primes Sch9 for its phosphorylation by TORC1.

As shown above, both Tor1 and Sch9 are still present at membranes of emerging small vacuoles in the *pho85Δ* and *pho80Δ* strains, but this localization is hampered as vacuoles become larger, especially in the *pho80Δ* strain. In consequence, these small vacuoles must be the primary site where TORC1-mediated Sch9 activation occurs in both deletion strains. Since vacuolar size is inversely correlated to Fab1 activity [59], our data also infer a low PI[3,5]P2 content in the membranes of the enlarged vacuoles, which is consistent with our observation that the Pho85-Pho80 CDK-cyclin pair plays a role to properly shift Fab1 from signaling endosomes to vacuoles. To get an estimate on the relative contributions to Sch9-Thr^{737} phosphorylation through both the Fab1-mediated TORC1 control and the Pho85-Pho80-mediated Sch9-Ser^{726} priming phosphorylation, we first sought to rule out that the phosphorylation of Sch9 at Ser^{726} itself affects the vacuolar recruitment of Sch9. In a previous report it was already shown that the GFP-Sch9^{5A} and GFP-Sch9^{2D3E} mutants, which both include the Ser^{726}mutation, normally localize to the vacuolar membranes when expressed in WT cells [1]. To elaborate on this, we examined the intracellular localization of GFP-Sch9^{S726A} and GFP-Sch9^{S726D} and found, as expected, both fusion proteins to normally localize at the vacuole as well (S4C Fig). Next, we studied whether the reduced phosphorylation level of Thr^{737} on the priming site mutant Sch9^{726A} would be further reduced by loss of Pho85 or Pho80. This was indeed the case as the partially compromised Sch9-Thr^{737} phosphorylation levels in *pho85Δ* and *pho80Δ* cells were further reduced by roughly 50% when combined with the Sch9^{S726A} mutation (Fig 5G). These data combined not only indicate that priming of Sch9 at Ser^{726} and proper regulation of Fab1 are almost equally important for optimal activation of Sch9 by TORC1, but also that Ser^{726} can be targeted by other kinases as well. The latter fits well with another recent report in which Sch9-Ser^{726} has been suggested to be phosphorylated by the CDK9 homologue Bur1 [70].

Pho85-Pcl6 and Pho85-Pcl7 differentially impact on Sch9 phosphorylation

The observation that episomal expression of Sch9^{2D3E} partially alleviated the rapamycin sensitivity of the *pho80Δ* strain, but not that of the *pho85Δ* strain, suggested that additional cyclins are involved in mediating a normal activation of Sch9 by TORC1. The best-placed candidates to make such a contribution would be Pcl6 and Pcl7, because loss of both proteins together led to a severe synthetic growth defect when combined with loss of Sch9 (Figs 1A and S1). It is well established that both Pho85-Pcl6 and Pho85-Pcl7 contribute to the regulation of the type1 protein phosphatase Glc7 via control of its regulatory subunit Glc8, but, while Pho85-Pcl7 is the best performing kinase *in vitro*, Pho85-Pcl6 is the main Glc8 kinase *in vivo* [71]. We examined the possibility that Glc7 may dephosphorylate Sch9 by monitoring Sch9-Thr^{737} phosphorylation in the *pcl6Δ*, *pcl7Δ*, and *pcl6Δ pcl7Δ* strains during exponential growth. We noted that the Sch9 phosphorylation level was not affected in the *pcl6Δ* strain but reduced in the *pcl7Δ* strain as compared to the WT strain (S5A Fig). In addition, we also examined strains lacking Glc8, or other non-essential Glc7-interacting proteins, using the approach previously described that identified Glc7-Shp1 as a protein phosphatase for Rps6 [72]. Although we observed some variation among the strains, none of them maintained significant Sch9 phosphorylation levels after rapamycin treatment (S5B Fig), suggesting that the Glc7 phosphatase does not play a major role in controlling the Sch9 phosphorylation status under the conditions tested.

This led us to use another strategy and to combine the *PHO80* deletion with combinations of the *PCL6* and *PCL7* deletions. We also created the quintuple *pho80Δ pcl6Δ pcl7Δ pcl8Δ pcl10Δ* deletion mutant that lacks all Pho80-like cyclin subfamily members to serve as an additional control. The strains were again tested for their rapamycin sensitivity when expressing Sch9^{WT} or Sch9^{2D3E} from centromere plasmids and this revealed an intricate interplay of the cyclins. Indeed, when compared to the *pho80Δ* strain, the additional deletion of *PCL6* prevented Sch9^{2D3E} from rescuing the rapamycin-induced growth defect, while the deletion of *PCL7* improved growth both of the Sch9^{WT} and Sch9^{2D3E} transformants and under conditions with or without rapamycin addition. However, it sufficed to introduce the *PCL6* deletion in the *pho80Δ pcl7Δ* strain to abrogate its improved growth (Fig 6A). The quintuple control strain behaved like the *pho80Δ pcl6Δ* and the *pho80Δ pcl6Δ pcl7Δ* strains, confirming that Pcl8 and Pcl10 did not contribute to the observed phenotype. Consistently, a similar phenomenon was seen when monitoring the vacuolar size and vacuolar membrane recruitment of GFP-tagged Sch9^{WT}. In contrast to the loss of Pcl6, the loss of Pcl7 prevented the formation of enlarged vacuoles with reduced Sch9 decoration that typifies the *pho80Δ* strain, but again this phenotype was reverted when the *pho80Δ* strain lacked both Pcl6 and Pcl7 (Figs 6B and S5C). Furthermore, we observed a significantly increased Sch9-Thr^{737} phosphorylation in the *pho80Δ pcl7Δ* strain as compared to the single *pho80Δ* strain and the WT strain. However, in the *pho80Δ pcl6Δ pcl7Δ* and the control strain the degree of Sch9-Thr^{737} phosphorylation was again markedly reduced (Fig 6C). This suggests that Pho85-Pcl6 and Pho85-Pcl7 may

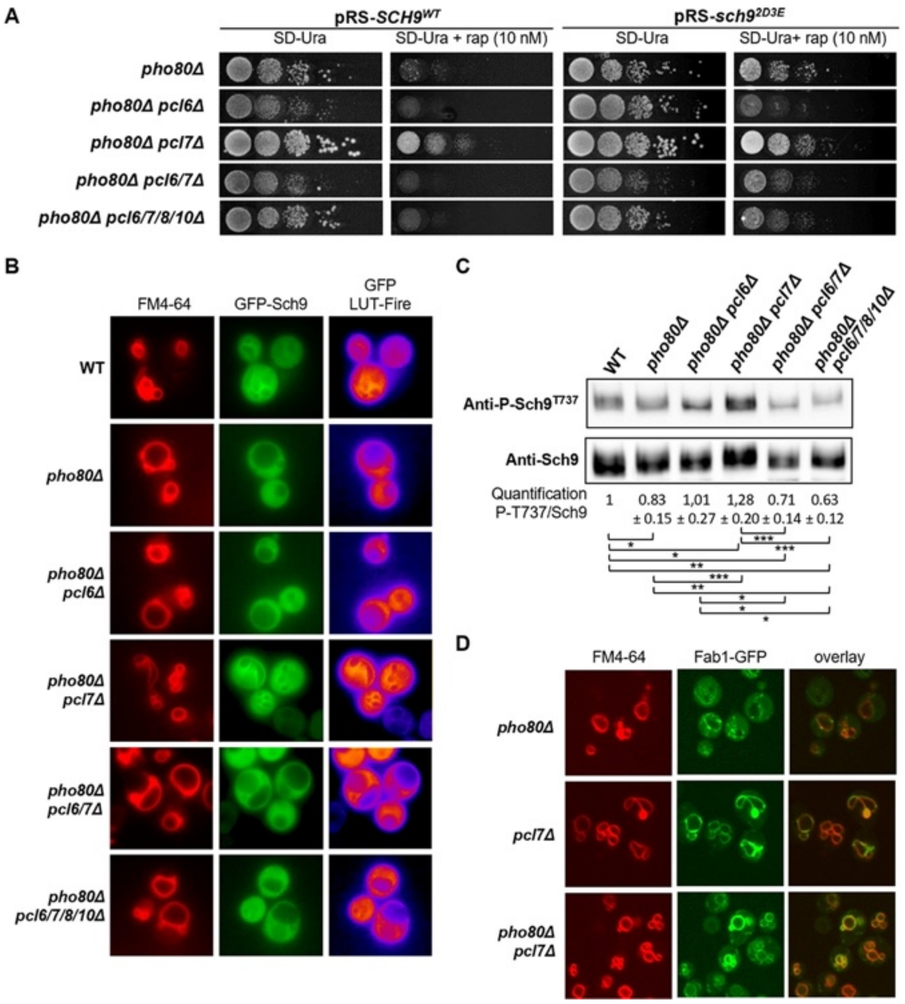
A
pRS-SCH9WT
SD-Ura
SD-Ura + rap (10 nM)
pRS-sch92D3E
SD-Ura
SD-Ura+ rap (10 nM)
pho80Δ
pho80Δ pcl6Δ
pho80Δ pcl7Δ
pho80Δ pcl6/7Δ
pho80Δ pcl6/7/8/10Δ
B
FM4-64
GFP-Sch9
GFP LUT-Fire
WT
pho80Δ
pho80Δ pcl6Δ
pho80Δ pcl7Δ
pho80Δ pcl6/7Δ
pho80Δ pcl6/7/8/10Δ
C
WT
pho80Δ
pho80Δ pcl6Δ
pho80Δ pcl7Δ
pho80Δ pcl6/7Δ
pho80Δ pcl6/7/8/10Δ
Anti-P-Sch9T737
Anti-Sch9
Quantification P-T737/Sch9
1
0.83 ± 0.15
1,01 ± 0.27
1,28 ± 0.20
0.71 ± 0.14
0.63 ± 0.12
*
*
**
***
**
***
***
*
*
*
D
FM4-64
Fab1-GFP
overlay
pho80Δ
pcl7Δ
pho80Δ pcl7Δ

Fig 6. The Pho85-cyclins Pcl6 and Pcl7 contribute to the regulation Fab1 and the vacuolar recruitment of Sch9. (A) Rapamycin sensitivity analysis of the *pho80Δ*, *pho80Δ pcl6Δ*, *pho80Δ pcl7Δ*, *pho80Δ pcl6Δ pcl7Δ*, and *pho80Δ pcl6Δ pcl7Δ pcl8Δ pcl10Δ* strains expressing either Sch9^{WT} or Sch9^{2D3E} from a centromere plasmid. The strains were spotted on selective synthetic medium without and with 10 nM rapamycin. (B) Microscopic analysis of the strains mentioned in (A) but expressing GFP-Sch9^{WT}. The strains were grown to mid-log phase on selective synthetic medium. The lipophilic dye FM4-64 was used to visualize the vacuolar membrane. (C) Immunoblot analysis of protein extracts from the strains mentioned in (A) and exponentially grown on complete synthetic medium to assess changes in Sch9 phosphorylation. The Sch9-Thr^{737}-phoshorylation levels were quantified based on based on the ratio of the anti-P-Sch9^{T737} and anti-Sch9 signals, and normalized to the ratio obtained for the WT cells. A two-tailed student's T test was used to calculate significances (*, $P < 0.1$; **, $P < 0.01$; ***, $P < 0.001$). (D) Microscopic analysis of Fab1-GFP localization in the *pho80Δ*, *pcl7Δ*, and *pho80Δ pcl7Δ* strains. The strains were grown to mid-log phase on selective synthetic medium. The lipophilic dye FM4-64 was used to visualize the vacuolar membrane.

https://doi.org/10.1371/journal.pgen.1010641.g006

oppositely impact on the activity of the Fab1 complex, either on Fab1 itself or on one of its regulatory subunits, *i.e.* Fig4, Vac14, Vac7, or Atg18 [20].

Since both vacuolar size and vacuolar recruitment of Sch9 are linked to PI[3,5]P_2 production, and given that vacuolar recruitment is a prerequisite for the phosphorylation of Sch9 by TORC1, we wondered whether Fab1 would localize again at the vacuolar membrane in the *pho80Δ pcl7Δ* strain. To this end, we transformed the *pcl7Δ* and *pho80Δ pcl7Δ* strains with the aforementioned centromere *FAB1-GFP* or *fab1*^{VLA}*-GFP* plasmids and compared the expression levels and localization of both fusion proteins with that seen in the *pho80Δ* strain. The additional deletion of *PCL7* in the *pho80Δ* cells partially restored the expression levels of both fusions (S5D Fig). Furthermore, Fab1-GFP nicely stained the vacuolar membranes in both the *pcl7Δ* strain and the *pho80Δ pcl7Δ* strain, indicative that the additional deletion of *PCL7* in the *pho80Δ* strain also restored the shift of Fab1 from endosomes to the vacuolar membrane (Fig 6D). The Fab1^{VLA}-GFP expression, however, came along with tiny vesicle-like vacuoles and, similar as seen for all other strains tested (Fig 2E), Fab1^{VLA}-GFP still localized in perivacuolar foci in the *pcl7Δ* and *pho80Δ pcl7Δ* cells, which we believe to correspond to endosomes (S5E Fig). As such, these data indicate that even in the *pho80Δ pcl7Δ* strain the hyperactive Fab1 mutant inherently fails to properly translocate from endosomes to vacuoles and to feed vacuolar membrane biogenesis.

Of note, the phenotypes observed for the *pho80Δ pcl7Δ* strain most closely resembled those described above for the *pho81Δ* mutant (Figs 1B, 1E, 2D and 2E)). This is not surprising given that Pcl7 and Pho80 are the only known members of the Pho80-like cyclin family that physically interact with Pho81 [25,28,29,73]. Furthermore, similarly as for the *pho81Δ* strain (Fig 1A), tetrad analysis confirmed that also in case of the *pho80Δ pcl7Δ* strain the presence of Sch9 is essential to maintain growth (S1 Fig).

Identification of Pho4 as effector for Pho85 and TORC1-Sch9 crosstalk

To further clarify the mechanisms by which dysfunction of Pho85 signaling is leading to a synthetic lethality in the *sch9Δ* background, we next tested the contribution of three well-known downstream targets of the Pho85-Pho80 CDK-cyclin pair, *i.e.* the protein kinase Rim15 and the transcription factors Crz1 and Pho4 [31,34,43,67,74]. To this end, we crossed the *RIM15*, *CRZ1*, or *PHO4* deletion into the *pho85Δ* and *pho80Δ* strains and then mated these with the *sch9Δ* strain. Tetrad analysis showed that the deletion of *PHO4*, but not the deletion of *RIM15 or CRZ1*, allowed outgrowth of the triple deletion spores, but, while the loss of Pho4 alleviated the synthetic lethality of the combined *SCH9* and *PHO80* deletion, the germinated *sch9Δ pho85Δ pho4Δ* spores were still severely sick as the strains grew very poorly and lost viability after storage (Figs 7A and S6A, S6B). Interestingly, loss of Pho4 also rescued the rapamycin-induced growth inhibition of the *pho80Δ* mutant (Fig 7B). These data suggest that inappropriate Pho4-mediated transcription could be the cause for the observed synthetic lethality when signaling through Pho85-Pho80 and the TORC1-Sch9 axis is deregulated.

Pho4 controls the transcription of genes in response to phosphate starvation but in phosphate-rich medium it is phosphorylated by Pho85-Pho80 and excluded from the nucleus [67,75] (Fig 7C). We analyzed whether TORC1 and Sch9 would affect the intracellular localization of Pho4 by expression of a C-terminally tagged Pho4-GFP version. As shown, the Pho4-GFP fusion protein localized in the cytoplasm in exponentially growing WT cells, but it translocated into the nucleus when the WT cells were subjected to phosphate starvation. Interestingly, Pho4-GFP also localized in the nucleus when WT cells were treated with rapamycin as well as in exponentially growing *sch9Δ* cells, which suggests that the TORC1-Sch9 axis controls the nuclear import of the transcription factor. Yet, Pho4-GFP remained cytoplasmic in rapamycin-treated *pho81Δ* cells, indicative that the rapamycin treatment did not overrule the

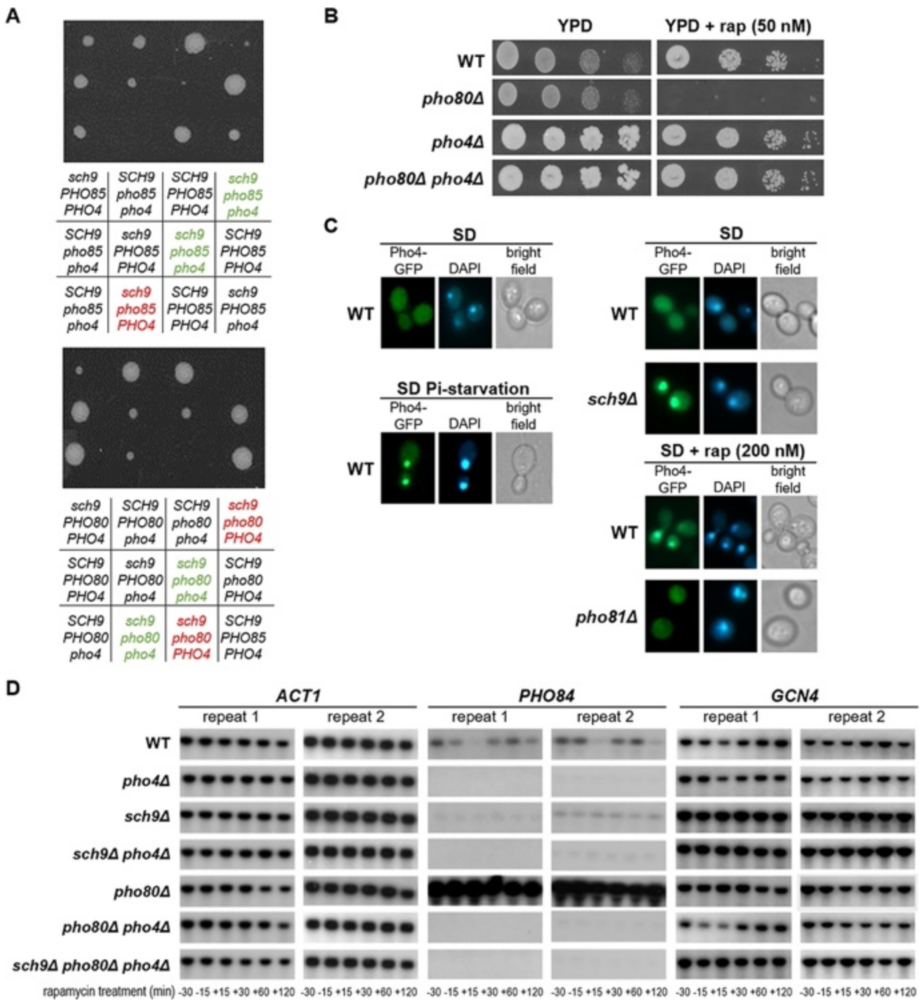
A
sch9 PHO85 PHO4
SCH9 pho85 pho4
SCH9 PHO85 PHO4
sch9 pho85 pho4
SCH9 pho85 pho4
sch9 PHO85 PHO4
sch9 pho85 pho4
SCH9 PHO85 PHO4
SCH9 pho85 pho4
sch9 pho85 PHO4
SCH9 PHO85 PHO4
sch9 PHO85 pho4
sch9 PHO80 PHO4
SCH9 PHO80 pho4
SCH9 pho80 pho4
sch9 pho80 PHO4
SCH9 PHO80 PHO4
sch9 PHO80 pho4
sch9 pho80 pho4
SCH9 pho80 PHO4
SCH9 PHO80 pho4
sch9 pho80 pho4
sch9 pho80 PHO4
SCH9 PHO85 PHO4
B
YPD
YPD + rap (50 nM)
WT
pho80Δ
pho4Δ
pho80Δ pho4Δ
C
SD
Pho4-GFP
DAPI
bright field
WT
SD Pi-starvation
Pho4-GFP
DAPI
bright field
WT
SD
Pho4-GFP
DAPI
bright field
WT
sch9Δ
SD + rap (200 nM)
Pho4-GFP
DAPI
bright field
WT
pho81Δ
D
ACT1
PHO84
GCN4
repeat 1
repeat 2
WT
pho4Δ
sch9Δ
sch9Δ pho4Δ
pho80Δ
pho80Δ pho4Δ
sch9Δ pho80Δ pho4Δ
rapamycin treatment (min) -30 -15 +15 +30 +60 +120

Fig 7. The transcription factor Pho4 is a mutual target Pho85 and Sch9. (A) Tetrad analysis demonstrated that the additional deletion of *PHO4* rescues the synthetic lethality of the *pho85Δ sch9Δ* and *pho80Δ sch9Δ* strains (see genotypes indicated in green and red, respectively). (B) Rapamycin sensitivity analysis of the WT, *pho80Δ*, *pho4Δ*, and *pho80Δ pho4Δ* strains spotted on YPD plates without and with 50 nM rapamycin (rap). (C) Microscopic analysis of Pho4-GFP localization in WT, *sch9Δ*, and *pho81Δ* cells. Cells were grown to mid-log phase in selective synthetic medium. As indicated, part of the WT and *pho81Δ* cultures were then either washed and transferred to phosphate starvation medium or subjected to 200 nM rapamycin treatment for 2 hours. The cells were stained with DAPI to visualize the nucleus. (D) Northern blot analysis to monitor the expression of *PHO84*, *GCN4*, or the *ACT1* control in the WT, *pho4Δ*, *sch9Δ*, *sch9 pho4Δ*, *pho80Δ*, *pho80Δ pho4Δ*, and *sch9Δ pho80Δ pho4Δ* strains before or after treatment with 200 nM rapamycin for the time indicated.

https://doi.org/10.1371/journal.pgen.1010641.g007

regulation of Pho4 by Pho85-Pho80 (Fig 7C). In addition, we performed Northern blot analysis to monitor the expression of *PHO84*, encoding the high-affinity phosphate transporter. As expected, the transcription of *PHO84* was clearly upregulated in the *pho80Δ* strain in a Pho4-dependent manner but despite the nuclear translocation of Pho4 upon rapamycin treatment, or the deletion of *SCH9*, no induction of *PHO84* was observed under these conditions (Fig 7D). On the contrary, the addition of rapamycin triggered *PHO84* repression with a transient recovery up to 60 min, while the deletion of *SCH9* resulted in a constitutive low basal expression of *PHO84*. Similar results were obtained when we used RT-PCR to monitor the expression of *PHO5*, another Pho4-dependent gene encoding an acid phosphatase (S6C Fig). Thus, even though Pho4 resides in the nucleus in rapamycin-treated WT and *sch9Δ* cells, neither *PHO84* nor *PHO5* were induced. Whether this is due to a deregulation of Pho4 or one of the auxiliary transcription factors required for expression of the PHO regulon [76], remains to be clarified. Another process that should be considered is chromatin remodeling as this is known to be controlled by the TORC1-Sch9 axis via Ino80 and required for opening the chromatin at the promotors of several metabolic genes, including *PHO5* [77,78].

Since Pho4 has been shown to fine-tune the timely transcription of post-diauxic genes that are also responsive to amino acid starvation [79], we additionally monitored the expression of a known Sch9 target, *i.e.* the transcription activator of the general amino acid control pathway encoded by *GCN4* [5]. We have chosen *GCN4* because it controls a major number of amino acid biosynthesis and nitrogen responsive genes [80] and because the stability of this transcription factor under amino acid starvation conditions is stringently controlled Pho85 signaling [29], thus providing an interesting point of crosstalk with TORC1-Sch9 signaling. Consistent with our previously published data [5], the *sch9Δ* strain already displayed an enhanced expression of *GCN4* during exponential growth and this level was maintained during the rapamycin treatment (Fig 7D). Enhanced *GCN4* expression was also observed in the *pho80Δ* strain, which was expected given that Pho85-Pho80 phosphorylation primes Sch9 for full TORC1-mediated activation. However, while the derepression in the *sch9Δ* mutant appeared to be Pho4 independent, that of the *pho80Δ* mutant was clearly mediated by Pho4 as the *GCN4* expression profile in the *pho80Δ pho4Δ* strain was more comparable to that of the WT strain. Yet, the additional deletion of *SCH9* in the *pho80Δ pho4Δ* strain rendered *GCN4* derepression again Pho4-independent (Fig 7D). These data indicate that the loss of Sch9 overrules the Pho4 requirement thereby defining Sch9 as direct regulator of *GCN4* expression and suggesting that the role of Pho4 is restricted to fine-tuning via the PHO pathway. As such, it would be interesting to analyze whether this Pho4-dependent fine-tuning of *GCN4* is mediated by the enhanced expression of Pho84 and signaling via Pho81.

Discussion

In this paper, we aimed to understand how two distinct kinases, Pho85 and TORC1, control nutrient signaling [11,43]. That both loss of Pho85 or its inhibitor Pho81 result in a synthetic growth defect when combined with Sch9 deletions not only indicates a close link to phosphate sensing, but it shows that growth is depending on a tight balance between Pho85 and TORC1-Sch9 signaling. We found this relation between Pho85 and TORC1-Sch9 in supporting growth to be multifaceted, involving Pho80 and the partially redundant cyclins Pcl6 and Pcl7.

Events occurring at the vacuole and signaling endosomes

It is well known that TORC1 phosphorylates and activates Sch9 at the vacuolar membrane [1,22,52]. We now provide evidence that Pho85-Pho80 directly phosphorylates Sch9 at Ser^{726} and that this primes Sch9 for further activation by TORC1. The priming effect of phospho-Ser^{726} has previously been noticed for the nearby epitope Thr^{723} when studying

TORC1-dependent Sch9 phosphorylation [1], but now we extend these data by showing that Ser^{726} is targeted by Pho85-Pho80 and that its priming effect also applies to other TORC1-dependent epitopes, such as Thr^{737}. Intriguingly, Ser^{726} is located immediately adjacent to the C-terminal hydrophobic motif (HM; that contains Thr^{737}), and a similar priming site for subsequent mTORC1-mediated HM phosphorylation has been described for mammalian S6K1 (Fig 8A). In this case, the S6K1-Ser^{371}, like the Sch9-Ser^{726}, is also followed by a proline and phosphorylated by proline-directed kinases including Cdc2-cyclin B and GSK-3 [81–84]. Notably, the Ser^{371}-Pro-^{372} motif in S6K1 has been coined turn motif (TM), which occurs in some AGC kinases where it stabilizes the kinase and/or promotes the phosphorylation state within the HM motif when it is phosphorylated at the Ser position [85,86]. Based on the functional analogy and structurally similar positioning of S6K1-Ser^{371} and Sch9-Ser^{726} just upstream of the HM, we therefore infer that the Ser^{726}-Pro^{727} motif in Sch9 corresponds to the TM and that TM priming sites represent an evolutionary conserved principle that allows S6K1 and Sch9 to integrate additional signals (Fig 8A).

The fact that Pho85-Pho80 phosphorylate Ser^{726} implies that the full activation of Sch9 requires phosphate uptake and phosphate sensing via the CDK-inhibitor Pho81, which is consistent with the observed increased Sch9 phosphorylation in the *pho81Δ* strain. It is also consistent with the observation that, particularly under phosphate starvation conditions, cells expressing the phosphomutant Sch9^{S726A} display a longer lifespan as compared to cells expressing the phosphomimetic variant Sch9^{S726D} or the Sch9^{WT} allele. We were not the first to notice a connection to phosphate signaling. A recent study demonstrated a link between phosphate acquisition via the high-affinity transporter Pho84 and TORC1 activity as assayed by Sch9 phosphorylation [89]. The authors proposed the Gtr1 Rag-GTPase of the EGO complex as the main phosphate signal receiver upstream of TORC1, thus acting in parallel to Pho85-Pho80. Given that Sch9 is an orthologue of PKB/Akt1, it is interesting to note that a similar role of phosphate has been noticed in mice where a high phosphate diet activates the Akt-mTORC1-S6K pathway thereby accelerating aging [90].

Pho85 signaling also elicits a second important effect that equally contributes to the regulation of the TORC1-Sch9 signaling axis. Just like TORC1 [22], Pho85 signaling controls the distribution of Fab1 between endosomal and vacuolar membranes as well. As such, Pho85 and its cyclins impact on the PI[3,5]P$_2$ content in the vacuolar membrane, which in turn is required for the recruitment of Sch9 and essential for its TORC1-dependent phosphorylation [21]. We show that mainly the Pho80 and Pcl7 cyclins are at play here. Albeit control of PI[3,5]P$_2$ synthesis by Pho85 signaling has been described as a stress response [50], it is clear that it is also required to maintain an optimal PI[3,5]P$_2$ synthesis under non-stressed conditions as evidenced by the observation that a significant fraction of *pho85Δ* and *pho80Δ* cells display enlarged vacuoles while *pho81Δ* and *pcl7Δ* cells appear to have more fragmented small vacuoles during exponential growth. The question is thus how the Pho85 signaling interferes with the endosomal and vacuolar distribution of Fab1. Our data on Fab1-GFP and Fab1^{VLA}-GFP suggest that besides controlling the activity of Fab1 itself [50], Pho85-Pho80 also ensures an optimal fusion of signaling endosomes and an optimal recycling of Fab1 from the vacuolar membrane. To understand these actions, one must look at the Fab1 complex. Apart from its N-terminal FYVE domain and the C-terminal lipid kinase domain, the central region of the Fab1 subunit harbors two additional conserved domains, *i.e.* the CCT-like domain that shares homology with 'chaperonin-containing TCP-1' chaperonins and the cysteine-rich domain. These domains allow binding of Fab1 to the Vac14 and Fig4 subunits. Vac14 is a scaffold that coordinates the activities of Fab1 and Fig4, the latter being a PI[3,5]P$_2$-5-phosphatase, which in addition has protein phosphatase activity that counteracts a repressive autophosphorylation in the kinase activation loop of Fab1 [20,87]. The scaffold Vac14 also interacts with the

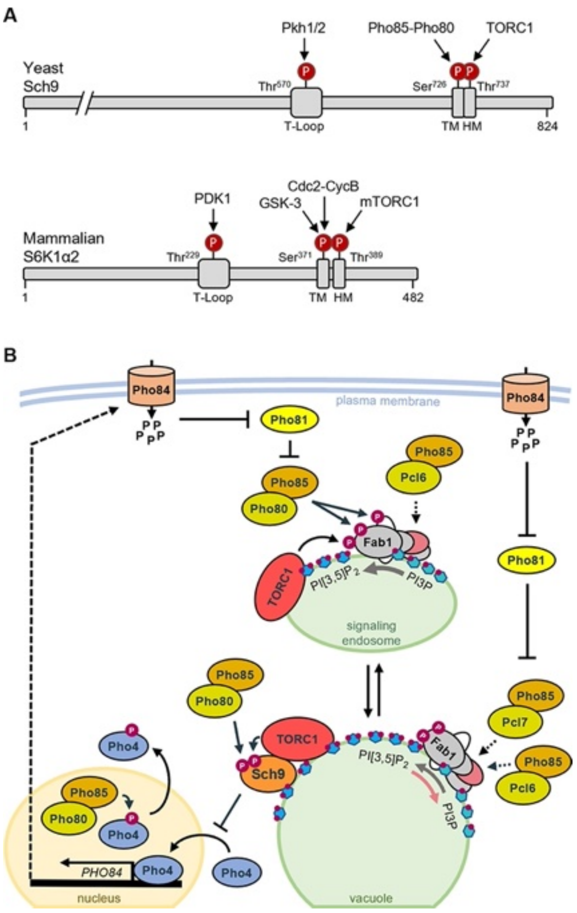
A
Yeast Sch9
Pkh1/2
Pho85-Pho80
TORC1
P
Thr570
Ser726
Thr737
T-Loop
TM HM
1
824
Mammalian S6K1α2
PDK1
Cdc2-CycB
GSK-3
mTORC1
Thr229
Ser371
Thr389
T-Loop
TM HM
1
482
B
Pho84
plasma membrane
P P P P
Pho81
Pho85
Pho80
Pcl6
Fab1
TORC1
PI[3,5]P2
PI3P
signaling endosome
Pho85
Pho80
TORC1
Sch9
Pho4
Pcl7
Pcl6
PHO84
nucleus
vacuole

Fig 8. Crosstalk between the PHO pathway and TORC1-Sch9 signaling and conservation of the turn motif priming principle. (A) Schematic representation of yeast Sch9 and mammalian S6K1 to highlight the evolutionary conservation of the TM priming principle. Indicated are the phosphorylation sites within the T-loop, which is targeted by Pkh1/2 in Sch9 and PDK1 in S6K1, and within the turn motif (TM) that is targeted by Pho85-Pho80 in Sch9 and by GSK3 and Cdc2-CycB in S6K1 as well as the phosphorylation site in the C-terminal hydrophobic motif that is targeted by TORC1 in Sch9 and mTORC1 in S6K1. (B) Shown is a hypothetical model based on previously reported data and observations made in our current study to depict the possible different connections for the interplay between the PHO pathway and the TORC1-Sch9 axis. At the endosome, TORC1 and Pho85-Pho80 phosphorylate and stimulate the Fab1 lipid kinase subunit to convert PI3P into PI[3,5]P_2 (grey arrow) [22,50]. Pho85-Pho80 also phosphorylates Vac7 (white subunit) [50], thereby probably enhancing endosomal fusion. Pho85-Pcl6 could act on the Vac14-Fig4 subcomplex to induce the protein phosphatase activity of Fig4 (pink subunit) required to relieve an inhibitory autophosphorylation of the Fab1 subunit [87]. At the vacuole, Sch9 is recruited by binding PI[3,5]P_2 where it is phosphorylated by Pho85-Pho80, which primes Sch9 for its subsequent phosphorylation and activation by TORC1. In the Fab1 complex, Pho85-Pcl7 may act on the Vac14-Fig4 subcomplex to control the lipid phosphatase activity of Fig4, which allows to recycle PI3P from PI[3,5]P_2 (pink arrow) [57,58] Active Sch9 prevents nuclear entry of the Pho4 transcription factor, while phosphorylation of Pho4 by Pho85-Pho80 triggers its export from the nucleus [34,67], thereby preventing transcription of *PHO84*, which encodes a high-affinity phosphate transporter [88]. Phosphate uptake by Pho84 inhibits Pho81, which in turn acts as inhibitor for Pho85-Pho80 and Pho85-Pcl7 [28,73].

https://doi.org/10.1371/journal.pgen.1010641.g008

regulatory subunits Atg18 and Vac7. Both these subunits are particularly important. Atg18, also known as Svp1, binds PI3P at the pre-autophagosomal structure and endosomes but PI[3,5]P_2 at the vacuole where it fulfils an important role in membrane recycling from the vacuole to late endosomes [20,56,91,92]. Consistently, we have previously shown by using a fluorescent PI[3,5]P_2-reporter that deletion of *ATG18* shifts this reporter from the signaling endosome to the vacuole, which indeed suggests that Atg18 is involved in the recycling of Fab1 complex from the vacuole to the signaling endosome [22]. Atg18 requires Vac7 for its recruitment at the vacuolar membrane [20,56]. Vac7 is a transmembrane protein and positive regulator of the Fab1 complex that is phosphorylated by Pho85-Pho80 [20,50]. Recently, it was shown that Vac7 shares a late embryogenesis abundant-2 (LEA) domain with Tag1, a protein named after its role to terminate autophagy, which predicts that both Vac7 and Tag1 are important for lipid transfer [93]. This raises the possibility that phosphorylation of Vac7 by Pho85-Pho80 facilitates endosomal fusion to deliver PI[3,5]P2 and the Fab1 complex to the vacuole as depicted in Fig 8B. Concerning the role of Pho85-Pcl7, our data suggest that it mainly impacts on the vacuolar PI[3,5]P_2 content and vacuolar fission. Hence, a possible scenario would be that Pho85-Pcl7 reduces the PI[3,5]P_2 levels by placing the Fab1 complex in a configuration that favors the Fig4 lipid phosphatase activity to convert PI[3,5]P_2 back to PI3P at the vacuole [57,58]. As such, Pho85-Pcl7 would either target Fig4 or Vac14, because Fig4 not only needs to be recruited by Vac14 to the Fab1 complex, but it also must interact with the Vac14 scaffold to be active [57,87]. Finally, our data also strongly suggest that the Pho85-Pcl6 CDK-cyclin pair opposes the role of Pho85-Pcl7 in controlling the Fab1 complex. This became most obvious by the observation that the loss of Pcl7 no longer prevented the formation of enlarged vacuoles in the *pho80Δ pcl6Δ* mutant, while this was readily the case in the *pho80Δ* strain. Furthermore, the additional deletion of *PCL6* also hampered Sch9^{2D3E} to rescue the growth of the *pho80Δ* strain on rapamycin-containing medium, which is probably due to a further reduction of the PI[3,5]P_2 levels and the vacuolar recruitment of Sch9^{2D3E} in the *pho80Δ pcl6Δ* strain. Thus, it may well be that Pho85-Pcl6 also impacts on the Vac14-Fig4 subcomplex, for instance, to enhance the protein phosphatase activity of Fig4 required to counteract the autophosphorylation of Fab1 at Ser^{48} and Ser^{2053}, which repress the basal activity of the Fab1 subunit [87]. While at the moment this is only speculative, it is important to realize that the opposing roles of Pcl6 and Pcl7 were only observed in the *pho80Δ* background in which the phosphorylation of the Fab1 kinase and its regulator Vac7 are compromised [50]. Importantly, there are many other players involved in vacuolar fission/fusion, such as Env7 [94], the HOPS subunit Vps41 [95] or the I-BAR signature protein Ivy1 that seems to control the availability of PI3P for Fab1 at signaling endosomes [24,96]. Hence, further research is needed to fully understand the roles of Pho85 and the aforementioned cyclins in controlling the endosome-vacuole dynamics.

The fact that loss of Pcl7 counteracts the loss of Pho80 in controlling the vacuolar PI[3,5]P_2 content and the recruitment of Sch9 is interesting since these are the two cyclins that interact with the CDK-inhibitor Pho81. It indicates that Pho81 fulfills a balancing role by adjusting the cellular PI[3,5]P_2 content in function of phosphate availability. At least for Pho85-Pho80, the inhibitory action of Pho81 depends on myo-d-inositol heptakisphosphate or IP7 [25], underscoring the importance of inositol polyphosphate signaling to maintain the proper balance of PI[3,5]P_2 levels and phosphate availability. Kcs1 is the main IP6 kinase in yeast and, not surprisingly, its deletion is synthetic lethal when combined with loss of Sch9 [11]. In line with this, we observed that a proper equilibration of the PI[3,5]P_2 levels is not only essential for Pho85 signaling, but for TORC1 signaling as well, and that the activities of Fab1 and Sch9 must be aligned in order to support growth on rapamycin. This is consistent with the previously made observation that strains harboring a deletion of *FAB1* or the TORC1 phosphomimetic *fab1*^{6D} allele, both characterized by reduced Sch9 phosphorylation, are more rapamycin sensitive, this in contrast to a strain expressing the phosphomutant Fab1^{6A} in which the Sch9 phosphorylation level is similar as that in WT cells [22].

Another interesting aspect is that the expression of Pcl7 is cell cycle dependent and peaks in S-phase, while the expression of Pcl6 is constitutive [28]. This makes Pcl7 a prime candidate to control the PI[3,5]P_2 levels during the course of the cell cycle. Indeed, the PI[3,5]P_2-mediated process of vacuolar fission and fusion not only allows to adjust the vacuolar surface-to-volume ratio and the retrograde traffic from the vacuole to the Golgi upon environmental changes, but during the cell cycle vacuolar membrane fission is important for the transmission of the organelle to the growing daughter cell [97]. Obviously, also Pho85-Pho80 and TORC1 play their part in orchestrating the vacuolar fission/fusion equilibrium and cell cycle [22,31,50,51,97–99]. In connection to Sch9, it was shown that this kinase is only recruited to newly formed vacuoles at a late stage in their maturation process and that the TORC1-dependent phosphorylation of Sch9 then signals the vacuolar maturity to the cell cycle machinery, thereby dictating cell cycle progression [52]. Most recently, this link between vacuole maturation and cell cycle progression was further strengthened by showing that not only TORC1 is at play, but that in parallel Sch9 becomes phosphorylated by the CDK9 homologue Bur1. Based on mass spectrometry, the authors identified eleven Bur1-sensitive epitopes, including the Pkh1/2 phosphoepitope Thr^{570} as well as canonical CDK sites Thr^{723} and Ser^{726}, the latter being the residues we associated with Pho85-Pho80 priming [70]. Bur1, also known as Sgv1, is an essential protein that was proposed to act in the same pathway as the G1 cyclin Cln3 [100]. It is mainly, but not exclusively, localized in the nucleus where it acts together with its cyclin Bur2 to modify histones, to control transcription, and to regulate telomere length [101]. The latter is of particular interest since telomere length is also known to be affected by the loss of Pho85-Pho80, Gtr1, or the catalytic (Vps34) and regulatory (Vps15) subunits of the PI3-kinase [102]. As such, it is tempting to speculate that especially telomere length may serve as additional checkpoint that is signaled to the cell cycle machinery by the phosphorylation of Sch9. An issue might be the nuclear localization of Bur1/Bur2. However, note that Pho80 can drag other proteins into the nucleus as shown for Pho81 and Fab1 [50,103]. Whether this is also the case for Sch9 is currently unknown as we did not observe a nuclear accumulation of GFP-Sch9 in our studies, but at least under hyperosmotic shock, which induces a temporary arrest of cell-cycle progression, Sch9 was reported to be nuclear and to act as chromatin-associated transcription activator of stress responsive genes [104,105].

To end, the role of Pho85 signaling in simultaneously controlling PI[3,5]P_2 synthesis and priming Sch9 for activation by TORC1 may be conceptually conserved in higher eukaryotes. Accordingly, in neuronal cells, the Pho85-Pho80 orthologous CDK5-p35 complex directly phosphorylates S6K1 at Ser^{411} located within the autoinhibitory domain, thereby controlling dendritic spine morphogenesis, a process in which metabolic turnover and compartmentalization of phosphoinositides play an important role and where the CDK5-p39 complex controls the endosomal adaptor protein WD repeat and FYVE domain-containing 1 (WDFY1) [106–108]. Interestingly, here also Ser^{411} phosphorylation primes S6K1 for its subsequent rapamycin-sensitive phosphorylation of Thr^{389} and activation [109]. In insulin-stimulated adipocytes, Cdk5-dependent phosphorylation is not only observed for Ser^{411} but for Ser^{424} and Ser^{429} as well, and the latter appears to dictate altered S6K1 substrate specificity towards enzymes involved in lipid metabolism [110]. In addition, CDK5–p35 also phosphorylates mammalian Fab1/PIKfyve to positively regulate PI[3,5]P_2 production [50] and in adipocytes enhanced PI [3,5]P_2 levels are associated with the mTORC1-mediated stimulation of S6K1 [111]. Finally, CDK5 also shows significant crosstalk with the PI3K-Akt cascade in prostate cancer cell proliferation since CDK5 seems to physically interact with Akt to control Akt membrane sequestration and androgen receptor-mediated activation [112].

Events happening in the nucleus

Apart from the processes occurring at the vacuole, we show that the synthetic lethality caused by an imbalanced Pho85 and TORC1 signaling is also associated with Pho4. This transcription factor is excluded from the nucleus due to its phosphorylation by Pho85-Pho80 when cells are growing in nutrient-rich medium with plentiful phosphate [34,113]. We now show that Pho4 is retained in the cytoplasm if Sch9 is active and that it translocates to the nucleus upon rapamycin treatment or loss of Sch9. This nucleocytoplasmic regulation is reminiscent to the control of Rim15, which is also excluded from the nucleus by phosphorylation via Pho85-Pho80 and is anchored to the 14-3-3 proteins in the cytoplasm when phosphorylated by TORC1-Sch9 [31,43]. Interestingly, a previous study reported that deletion of the 14-3-3 encoding genes *BMH1* or *BMH2* leads to heterogeneity in the expression of Pho4-regulated genes [114]. However, the nuclear localization of Pho4 triggered by loss of Sch9 activity is not sufficient to induce transcription of *PHO84* nor *PHO5*, both typical representatives of the PHO regulon. According to the *Saccharomyces* Genome Database Sch9 and Pho4 physically interact and based on a comprehensive mass spectrometry analysis of the rapamycin-sensitive phosphoproteome Pho4 has a perfect RRxS* consensus site for Sch9-mediated phosphorylation [62]. Hence, it is well possible that Sch9 directly targets Pho4 to control its activity. It is known that Pho4 is phosphorylated at different residues that control nuclear import or export and determine its transcriptional activity [67,113,115,116]. Export of Pho4 requires Msn5 [117] and, interestingly, as judged by our previously reported SGA analysis the combined deletion of *SCH9* and *MSN5* may result in a synthetic sick phenotype [11]. Alternatively, or in parallel, the lack of transcriptional induction by nuclear localized Pho4 in rapamycin-treated WT and *sch9Δ* cells can be due to an incompatible chromatin structure preventing Pho4 from having access to the promotors of *PHO84* and *PHO5*. It is known that the TORC1-Sch9 axis signals chromatin remodeling at many target genes via Ino80 and this appears to include at least *PHO5* [77,78].

For the expression of *GCN4*, our data confirm the previously reported results on its derepression during exponential growth upon loss of Sch9. Consistent with the priming by Pho85-Pho80 for subsequent TORC1-mediated activation of Sch9, a similar derepression is seen in the *pho80Δ* strain but in contrast to the *sch9Δ* strain, the derepression of *GCN4* in the *pho80Δ* is dependent on Pho4. Even so, the requirement of Pho4 was overruled by the additional deletion of *SCH9* in the *pho80Δ pho4Δ* strain, suggesting that Sch9 is the downstream target directly controlling *GCN4* expression and confining the role of Pho4 to fine-tuning via the PHO pathway. Given that Pho4 mediates a massive expression of the *PHO84* high-affinity phosphate transporter in the *pho80Δ* strain, we believe this fine-tuning can be explained by a model in which Pho84 phosphate uptake inhibits Pho81 in *pho80Δ* cells, leading to an active Pho85-Pcl7 kinase complex that in turn would lower the PI[3,5]P_2 levels and thereby reduce the vacuolar recruitment and activation of Sch9 (Fig 8B). If true, then the reasons why loss of Pho4 rescues the synthetic lethality seen upon the combined deletion of *SCH9* and *PHO80* is to prevent the aberrant expression of Pho84, which otherwise results in failure to adjust PI[3,5]P_2 levels in function of the TORC1-Sch9 output. It implies that phosphate uptake is normally strictly calibrated to the availability of other nutrient sources, including amino acids and nitrogen. That Gcn4 plays an important role here is underscored by the fact that also the stability of this short-lived transcription factor is under strict control of the phosphate sensing machinery as Pho85-Pcl5 triggers its nuclear degradation, while Pho81 and Pho85-Pcl7 are required to maintain its stability [29]. The calibration of phosphate uptake apparently also relates to the availability of fermentable carbon sources since Pho84 was shown to act as a transceptor that signals to PKA [118] and because enhanced PKA influences the downregulation and internalization of Pho84 from the plasma membrane [119]. The important role of Pho84 is reflected in another way as well. It is the main player connecting the retrograde response to replicative lifespan extension [120], the latter being equally dependent on PKA, Pho85-Pho80, TORC1, and Sch9 [121,122] and, obviously, also determined by telomere length [123]. Furthermore, it was shown that the additional deletion of *PHO4* partially restores the short-lived phenotype of the *pho85Δ* and *pho80Δ* strains [122], which is in line with our data.

Concluding remark

This study started with the observation of synthetic lethality when the deletions of *SCH9* and *PHO85* or *PHO81* are combined [11]. Our data now provide a first glimpse of the crosstalk between these key players in nutrient signaling showing that this crosstalk is a complex but ingenious matter, dedicated to calibrating the responses triggered by a variety of nutritional signals through an interplay of processes at different levels. Our data demonstrate the importance of phosphatidylinositol metabolism to dictate the recruitment of Sch9 at vacuolar membrane, the consequence of Sch9 phosphorylation by Pho85 to prime for the subsequent phosphorylation and activation of Sch9 by TORC1, and the cooperation of Pho85 and TORC1-Sch9 signaling to control the nucleocytoplasmic translocation of Pho4 in a similar manner as previously described for Rim15 [31,43]. As such, it becomes evident that Sch9 functions as central integrator that allows to align different input signals and achieve accuracy in the responses. Given that Sch9 is also a substrate for the phytosphingosine-dependent kinases Pkh1, Pkh2, and Pkh3 [1,14,15] and the cellular energy sensor Snf1 [16–18], it will be interesting to elucidate how these inputs interfere with the Pho85-dependent processes described above.

Materials and methods

Yeast strains, plasmids, and growth conditions

The *Saccharomyces cerevisiae* strains used in this study for phenotypical analysis are listed in S1 Table. Deletion strains created for this study were generated using either polymerase chain reaction-based disruption cassettes, as previously described [124], or mating of haploid deletion strains of opposite mating types, followed by sporulation and tetrad analysis. Only deletion mutants with a BY4741 genotype (*his3Δ1 leu2Δ0 met15Δ0 ura3Δ0*) were used in subsequent experiments. The strains with the Sch9^{S726A} and Sch9^{S726D} point mutations were obtained by CRISPR/Cas9 [125]. For the creation of the Cas9 plasmid (pMC019; see S2 Table), the 'SCH9-S726 Proto F' and 'SCH9-S726 Proto R' primers were used (S3 Table). We co-transformed with both the plasmid and the corresponding single-stranded DNA donor sequences templates (S3 Table) for homology-directed repair. The point mutations in *SCH9* in plasmids pMC027, pMC028 and pMC029 were introduced by QuikChange kit (Agilent, Basel, Switzerland) by using plasmid pMC014 as template and the oligonucleotides 'SCH9 mut T723A', 'SCH9 mut S726A' and 'SCH9 mut T723A-S726A' (S3 Table). Yeast cells were transformed using the Gietz method [126]. Yeast cells were grown in YPD medium overnight and then diluted to 0.1 OD_{600nm} in the morning. Cells were grown to exponential phase, washed with sterile water, and then with 1 mL of 0.1 M LiAc. The corresponding μL of 10 OD_{600nm} of cells were used for transformation. The transformation mix contained 240 μL 50% PEG, 36 μL 1M LiAc, 2 μL of pRCC-K and 20 μL of donor sequence. Cells were incubated at 42˚C for 40 min. After the transformation, the cells were re-suspended in YPD and grown at 30˚C for 3 h and then plated onto YPD plates containing G418. To identify the clones containing the correct mutations in the *SCH9* region of interest was sequenced.

Many plasmids used in this study were a generous gift from other research groups (S2 Table). The centromere plasmids pRS413-Fab1 and pRS413-Fab1^{VLA} plasmids were subcloned from pRS416-*FAB1* and pRS416-*fab1-14* (kindly provided by L. Weisman, [55]). The plasmid for the expression of Fab1^{VLA}-GFP under the control of its own promoter was created by PCR. Starting from a plasmid for the expression of Fab1-GFP, the backbone of the pRS416 plasmid, *FAB1* promoter, GFP, and *FAB1* terminator, were amplified by PCR. With a separate PCR, *FAB1-VLA* was amplified using pRS416-fab1-14 (provided by L. Weisman, [55]) as a template. The two PCR products were ligated with the Gibson Assembly Master Mix (New England Biolabs, Ipswich, USA) [127]. The ligation product was used for *E. coli* transformation and the plasmid was confirmed by sequencing. The construction of C-terminally FLAG-tagged (DYKDDDDK) versions of Sch9 (Sch9-FLAG) including Sch9^{WT}, Sch9^{T723A}, Sch9^{S726A}, Sch9$^{T723A/S726A,}$ Sch9^{T737A}, Sch9^{S758A}, and Sch9^{S765A} and cloning into the centromere plasmid pYCPlac33 has been described previously [18].

Yeast cells were grown in standard rich medium containing 2% bacto peptone, 1% yeast extract and 2% glucose (YPD) or in minimal medium containing 0.5% $(NH_4)_2SO_4$, 1.9 g/l yeast nitrogen base without amino acids (Formedium, Norfolk, UK), supplemented with either synthetic selective drop-out mixtures (SD) or a complete synthetic mixture (SC) (Formedium, Norfolk, UK) as required, and 2% glucose. Solid medium contained an additional 1,5% agar. For phosphate starvation, the cells were grown to mid-log phase on SC medium and then transferred to yeast nitrogen base with ammonium sulphate and without phosphates (Formedium, Norfolk, UK) supplemented with 0.5% ammonium sulfate, the complete synthetic amino acid mixture and 4% glucose. For nitrogen starvation, the cells were transferred to yeast nitrogen base without amino acids and without ammonium sulfate (Formedium, Norfolk, UK) supplemented with 4% glucose. For carbon source starvation, the cells were transferred to SC medium without glucose.

Rapamycin sensitivity analysis

Cells were grown to mid-log phase in either YPD, SD or SC medium, diluted to an optical density 600 nm (OD_{600nm}) of 0.1. and serial dilutions (1:10) were spotted onto YPD, SD or SC plates with or without different concentrations of rapamycin as indicated and imaged after 3 to 5 days of growth at 30˚C.

Tetrad analysis

The diploids to assess genetic interaction of Sch9 with the Pho85-cyclins were generated by crossing either *sch9*::*HIS3* (BY4741, JW 01 306) or *sch9*::*LEU2* (BY4741, JW 01 307*)* with single cyclin deletion mutants form the Yeast Knock-Out Collection (YKO; EUROSCARF, BY4742). Similarly, the deletion strains of the genes identified as possible mutual targets of Pho85 and TORC1-Sch9 were obtained from the YKO Collection (EUROSCARF, BY4742), and crossed with either *pho85*::*KANMX4* (BY4741, JW 03 595) or *pho80*::*HIS3* (BY4741, JW 03 721). Sporulation was induced by spotting and incubating diploid cells on sporulation plates containing 1% potassium acetate, 0.1% $KHCO_3$, pH 6.0 for 5–6 days at 25˚C. Tetrads were treated with 0.02 mg/ml lyticase for 10 min at room temperature and were dissected on a YPD plate using a micromanipulator (Singer Instruments). After 3–5 days, the germinated spores were genotyped by plating them on the specific selective media and/or by PCR analysis. At least 6 tetrads were analyzed, and representative spores are shown in the pictures.

Phos-tag and Western blot analysis

To analyze differential phosphorylation of Sch9 with Phos-tag SDS-PAGE, cells expressing either HA-Sch9 or Sch9-FLAG were grown on synthetic medium to mid-log phase. For the experiments with HA-tagged Sch9, cells were collected and washed with ice cold PBS and subsequently snap frozen in liquid nitrogen. A bead beating based lysis technique was used for protein extraction using a Triton-Deoxycholate buffer (50 mM HEPES pH7.4; 13.5 mM NaCl; 1% Triton X-100; 0.05% sodium deoxycholate), complemented with a protease and phosphatase inhibitor cocktail (Thermo Fisher Scientific, Merelbeke, Belgium). The cell lysates were cleared by a couple of subsequent centrifugation steps. Protein concentration was measured with the Bradford method (Bio-Rad, Temse, Belgium) and the samples were diluted to the same protein concentration in lysis buffer supplemented with Laemmli loading buffer. Samples were run on a 6,5% SDS-PAGE gel containing 25 μM Phos-tag (Fujifilm Wako Chemicals, Neuss, Germany). Full length HA-Sch9 was detected using an anti-HA-antibody (Roche, Merck, Hoeilaart, Belgium). For the experiments with FLAG-tagged Sch9, cells were heat-inactivated prior to collection and the preparation of protein extracts followed a protocol described previously [18]. Detection was done using an anti-FLAG antibody (Agilent, Basel, Switzerland). Both methods yielded comparable results.

For the analysis of Sch9 phosphorylation levels, cells expressing GFP-Sch9, GFP-FYVE-Sch9 or only endogenous Sch9 were grown to mid-log phase on synthetic medium. Cell lysate preparation was done as previously described, using bead beating in urea lysis buffer [61]. The phosphospecific anti-Sch9-P-Thr^{737} and anti-Sch9 antibodies [61,128], and the anti-GFP antibody (Roche, Merck, Hoeilaart, Belgium) were used to detect phosphorylated, endogenous Sch9, and GFP-Sch9 respectively after running the samples on an SDS-PAGE gel. Densitometry measurements were done with ImageJ to quantify the phosphorylation levels. The anti-GFP antibody was also used to determine the expression levels of the Fab1-GFP and Fab1^{VLA}-GFP constructs as compared to the loading control Adh2 (anti-Adh2 antibody, Millipore, Merck, Hoeilaart, Belgium). For the detection of Atg13 and Lst4 phosphorylation levels, the strains were transformed with plasmids expressing the tagged constructs Atg13-HA$_3$ or Lst4-V5, respectively. Sample preparations, detection using the anti-HA or anti-Lst4-P-Ser^{523} antibodies and quantifications were done as previously described [62,66].

Protein purification

HA$_2$-Pho85, HA$_2$-Pho85^{E53A} (kinase-dead), and Pho80-GST were purified based on the description in [31]. The *pho85Δ* strain was transformed with plasmids pVW883, pVW884, and p946 (S2 Table). Cells were grown overnight in SD -Ura liquid medium. In the morning cells were diluted at 0.2 OD$_{600nm}$ in 2 L SD -Ura. To induce Pho80-GST expression, cells were treated with 500 μM CuSO$_4$ for 1 h, before harvesting the cells. Cells were collected by filtration, frozen in liquid nitrogen, and cryogenically disrupted by using a Precellys homogenizer in 10 ml of lysis buffer (50 mM Tris-HCl pH 7.5, 150 mM NaCl, 0.5 mM EDTA, 0.1% NP-40, 10% glycerol, 1 mM PMSF, 1 mM DTT, 400 mM Pefabloc, Roche complete protease inhibitor EDTA-free) in the presence of acid-washed glass beads. The cleared lysate was incubated for 2 h at 4˚C with anti-HA magnetic beads (Fisher Scientific AG, Basel, Switzerland) for HA$_2$-Pho85 and HA$_2$-Pho85^{E53A} purifications and glutathione magnetic agarose beads (Fisher Scientific AG, Basel, Switzerland) for Pho80-GST purification. After 5 washes with lysis buffer, HA-beads coupled with Pho85 or Pho85^{E53A} were resuspended in 250 μL of elution buffer (50 mM Tris-HCl pH 7.5, 150 mM NaCl) and stored at 80˚C after addition of 10% glycerol. GST-coupled beads with Pho80 were eluted at room temperature in 250 μL of elution buffer (50 mM Tris-HCl pH 7.5, 150 mM NaCl, 10 mM L-glutathione reduced) for 2h.

Yeast cells bearing the plasmids for Sch9$^{R650-I824}$-TAP expression were grown overnight in SRaffinose-Ura supplemented with 0.01% sucrose. The day after, at 0.2 OD$_{600nm}$, 2% final galactose was added to the cells for 6 h, to induce Sch9$^{R650-I824}$-TAP expression. Cells were collected by filtration, frozen in liquid nitrogen, and cryogenically disrupted by using Precellys homogenizer in 10 mL of lysis buffer (50 mM Tris-HCl pH 7.5, 150 mM NaCl, 0.5 mM EDTA, 0.1% NP-40, 10% glycerol, 400 mM Pefabloc, Roche complete protease inhibitor EDTA-free). The cleared lysate was incubated with IgG-coupled Dynabeads M-270 (Thermo Fisher Scientific, Basel, Switzerland) for 2h at 4˚C. After 5 washes with lysis buffer, Sch9$^{R650-I824}$ was eluted in 150 μL TEV buffer (50mM Tris-HCl pH 7.5, 0.5mM EDTA,) with 2% TEV protease and stored at 80˚C after the addition of 10% glycerol. Purified proteins were separated by SDS-PAGE, and stained with Sypro Ruby (Invitrogen, Thermo Fisher Scientific, Basel, Switzerland) to perform a quantification.

Kinase assay

Kinase assays were performed with HA$_2$-Pho85- and HA$_2$- Pho85^{E53A} -bound beads, as described in [31]. The reaction was performed in kinase buffer (50 mM Tris-HCl pH 7.5, 20 mM MgCl$_2$, 1 mM DTT). The reaction was carried out with 50 ng of kinase and Pho80 and 40 ng of the substrate. By adding the ATP mix (final concentration in reaction: 1mM ATP, 10 μCi γ-[32^P]-ATP) the reaction was started and performed for 30 min at 30˚C. By adding 2X SDS-PAGE sample buffer, the reaction was stopped. Samples were denatured at 65˚C for 10 min, proteins were separated by SDS-PAGE, stained with Sypro Ruby (Invitrogen, Thermo Fisher Scientific, Basel, Switzerland) to assess loading, and analyzed using a phospho-imager (Typhoon FLA 9500; GE Healthcare, Opfikon, Switzerland), as described in [22].

Fluorescence microscopy

Localization of Sch9 was determined in cells either expressing GFP-Sch9 from a plasmid [1] or genomically. The genomically tagged *pho85Δ*, *pho80Δ*, and *pho81Δ* strains were generated by crossing the *SCH9*::*GFP-SCH9* and *SCH9*::*GFP-FYVE-SCH9* strains (generously provided by A. Matsuura) with the respective deletion strains. Pho4 localization was monitored in cells containing the p*PHO4pr-PHO4-GFP* plasmid [129]. To assess vacuolar morphology, cells were stained with the lipid interacting dye FM4-64 (Invitrogen, Thermo Fisher Scientific, Merelbeke, Belgium) for 1 h. For all these assays, cells were grown to mid-log phase (OD$_{600nm}$ 1–2) in glucose-containing synthetic medium. In case a glucose starvation condition was included, cells were washed twice and starved for 1 h on medium lacking glucose.

Most images were generated using either a Leica DMi8 S platform fluorescence microscope equipped with a Leica DFC9000 camera or a Leica DM 4000B fluorescence microscope equipped with a Leica DFC 300G camera (Leica Microsystems, Diegem, Belgium). A LUT Fire was applied using ImageJ to compare the intensities of the GFP signal. When indicated pictures were deconvoluted using the Huygens software (version 18.10; Scientific Volume Imaging B.V., Hilversum, The Netherlands). Confocal images of the Fab1-GFP and Fab1^{VLA}-GFP constructs were captured with an inverted Spinning Disk Confocal Microscope (Nikon Ti-E inverted microscope, VisiScope CSU-W1, Amstelveen, The Netherlands) equipped with a PCO.edge 4.2 sCMOS camera and a 100x 1.3 NA oil immersion Nikon CFI series objective.

RNA extraction, RT-PCR and Northern analysis

Northern blot analysis was performed as described previously [5]. In short, yeast cultures were grown overnight on YPD. Cultures were then diluted and allowed to grow till an OD$_{600nm}$ of 1.5. Then control samples were taken (-30 and -15 min). Next, rapamycin was added to a final concentration of 200 nM and samples were taken after 15, 30, 60, and 120 min. RNA extraction and Northern blotting were performed as described previously [43]. The filters were hybridized with ^{32}P-dCTP-labelled probes, generated with the High Prime kit (Roche, Merck, Hoeilaart, Belgium). Primers used for generation of the probes are listed in S3 Table. After washing, the filters were exposed to X-ray films (AGFA, Mortsel, Belgium).

For RT-PCR for *PHO5* expression analysis, 300 ng of the total RNA was retro-transcribed using the first-strand cDNA Synthesis kit (Nzytech, Lissabon, Portugal). NZYSpeedy qPCR Green Master Mix SYBR green Master Mix (Nzytech, Lisssabon, Portugal) was used to perform quantitative PCR in an Applied Biosystems 7500 fast qPCR system (Merck Life Sciences, Algés, Portugal). Data were analyzed with the Δ2CT method and normalized to the expression of *ACT1*, *PDA1* and *TDH2* genes in the same sample. The primer pairs used are listed in S3 Table.

GFP-Sch9 quantification at isolated vacuoles

Vacuoles of GFP-Sch9 expressing WT, *pho85Δ*, and *fab1Δ* cells were isolated as described before [130], with the exception of some minor changes. Yeast cultures were grown in YPD to approximately OD_{600nm} 1. Cells were harvested, washed once, and resuspended in 0,03 M Tris-HCl pH 8,9 containing 10 mM DTT. After a 10 min incubation at 30˚C, cells were incubated at 30˚C in spheroplasting buffer (YP 0.2% glucose; 0.6 M sorbitol; 50 mM KP_i; 0.1 mM pefabloc; 6U zymolyase/OD_{600nm} unit) for at least 30 min. The collected spheroplastes are resuspended in 15% ficoll buffer (15% ficoll; 10 mM PIPES/KOH pH 6.8; 0.2 M sorbitol; 0.1 mM pefabloc, 0.1 μg/ml leupeptin, 10 μg/ml o-phenantrolin, 0.5 μg/ml pepstatin A), to which 50 μl of 0.4 mg/ml diethylaminoethyl (DEAE) dextran was added per 100 OD_{600nm} units of cells. After 2 min incubation on ice, followed by 2 min at 30˚C, the spheroplast suspension was transferred to a transparent SW41 tube (Beckman Coulter, Suarlée, Belgium). 8% ficoll buffer, 4% ficoll buffer and 0% ficoll buffer were pipetted carefully on top to create a discontinuous ficoll gradient. The samples were centrifuged for 90 min at 30'000 rpm in a SW41 rotor, at 4˚C (Beckman Coulter, Suarlée, Belgium). After collecting the vacuolar fraction from the 0% - 4% ficoll interphase, vacuolar vesicles were further concentrated by diluting ½ in 10 mM PIPES/KOH pH 6.8 and centrifugation for 10 min at 5200g, 4˚C. The purity of the isolated vacuolar vesicles was monitored by Western analysis, using Anti-Vph1 (Abcam, Cambridge, UK), anti-ATP6V1A (Abcam, Cambridge, UK), anti-Porin (Invitrogen, Thermo Fisher Scientific, Merelbeke, Belgium), anti-Pma1 (kindly provided by B. André), anti-Dpm1 (Invitrogen, Thermo Fisher Scientific, Merelbeke, Belgium). Total protein concentrations were measured with the Bradford method (Bio-Rad, Temse, Belgium). The obtained vacuolar vesicles were diluted to 0.1 μg/μl in 10 mM PIPES/KOH pH 6.8 and stained with 8 μM FM4-64 (Invitrogen, Thermo Fisher Scientific, Merelbeke, Belgium). GFP and FM4-64 signal intensity was measured with the Fluoroskan Ascent FL Microplate Fluorometer (Thermo Fisher Scientific, Merelbeke, Belgium), using a 485/518 filter pair and 530/645 filter pair respectively. The GFP ratio's relative to FM4-64 or protein content in each sample was determined to serve as a measure of GFP-Sch9 abundance at the vacuolar membrane.

Supporting information

S1 Fig. Genetic interaction of SCH9 with different players of the Pho85 signaling pathway. Diploids were generated by crossing the haploid *SCH9* deletion strain with haploid strains carrying either a *PHO85*, *PHO81*, a single cyclin deletion or double cyclin deletion. Tetrad analysis only revealed a genetic interaction between *SCH9* and *PHO85*, *PHO81*, *PHO80*, *PCL6 PCL7* and *PHO80 PCL7* as indicated in red. The dissected spores were grown on YPD plates and pictures were taken after 3 to 5 days at 30˚C.
(TIF)

S2 Fig. Interaction between the TORC1- and Pho85-signaling pathways. (A, B) The WT strain or mutant strains lacking Pho85, Pho80, Pho81, a single cyclin (A) or two partially redundant cyclins (B) were grown exponentially on YPD, diluted to an OD_{600nm} of 0.1 and tenfold serial dilutions were spotted on YPD plates without or with 50 nM rapamycin. The strains were grown for 2 to 4 days at 30˚C. (C) Immunoblot analysis of exponentially growing WT, *pho85Δ*, *pho80Δ*, and *pho81Δ* cells expressing GFP-$Sch9^{WT}$ from an episomal plasmid in addition to endogenous Sch9. The Sch9-Thr^{737} phosphorylation level of GFP-Sch9 and endogenous Sch9 was quantified based on densitometry of the anti-P-$Sch9^{T737}$ and anti-Sch9 signals, and normalized to WT cells. The data are represented as mean ± standard deviation. Paired two-tailed student's T tests were used to calculate significances (*, $P < 0.1$; **, $P < 0.01$; ***, $P < 0.001$).
(TIF)

S3 Fig. Phosphorylation of GFP-Sch9 in cells with enhanced Fab1 activity and GFP-Sch9 abundance at the vacuolar membrane. (A) Immunoblot analysis of exponentially growing WT cells expressing either Fab1 or $Fab1^{VLA}$ from a centromere plasmid. The Sch9-Thr^{737} phosphorylation was quantified based on densitometry of the anti-P-$Sch9^{T737}$ and anti-Sch9 signals, and normalized to WT cells transformed with an empty vector. (B) Microscopic analysis of Sch9 localization in the WT, *pho85Δ*, *pho80Δ*, and *pho81Δ* strains expressing the genomically tagged GFP-Sch9 or GFP-FYVE-Sch9 fusion protein. Strains were grown to mid-log phase on complete synthetic medium. The lipophilic dye FM4-64 was used to visualize the vacuolar membrane. Pictures were deconvoluted using the Huygens software (version 18.10). A LUT Fire was applied using ImageJ in order to show the levels of the GFP signal. (C) Western blot analysis to assess purity of the isolated vacuolar vesicles. Vacuoles were purified from spheroplasted cells using a density gradient centrifugation method as described in the materials and methods section. The high abundance of 2 typical vacuolar membrane proteins (Vma1 and Vph1) in the isolated vacuolar fraction in comparison to the whole cell protein extract (= Input) confirmed the strong enrichment of vacuolar proteins in this fraction. The presence of ER (Dpm1), mitochondrial (Por1) and plasma membrane (Pma1) markers, on the other hand, was very low in the isolated vacuolar fraction. (D) Fluorescence microscopic pictures of the purified vacuoles of GFP-$Sch9^{WT}$-expressing cells, confirming the presence of GFP-Sch9 at the membranes of purified vacuoles. Staining with the lipophilic FM4-64 dye confirms the integrity of the isolated vacuolar vesicles. The intensity of the GFP-signal was quantified with a Fluoroskan plate reader as explained in the materials and methods section and expressed relative to the FM4-64 signal as well as the total protein content. The data are represented as mean ± standard deviation. Paired two-tailed student's T tests were used to calculate significances (*, $P < 0.1$; **, $P < 0.01$; ***, $P < 0.001$).
(TIF)

S4 Fig. Pho85-Pho80-mediated phosphorylation of Ser^{726} primes Sch9 for its subsequent activation by TORC1. (A) Phos-tag immunoblot analysis of protein extracts obtained from exponentially growing *sch9Δ* cells transformed with a centromere plasmid allowing for expressing C-terminally FLAG-tagged $Sch9^{T723A}$, $Sch9^{S726A}$, $Sch9^{T737A}$, $Sch9^{S758A}$, $Sch9^{S765A}$, or $Sch9^{WT}$ (WT) as indicated. Total protein extracts were resolved on phos-tag gels and were subsequently analyzed via immunoblotting with an anti-FLAG antibody. (B) Setup for the *in vitro* kinase assay to demonstrate phosphorylation of Sch9 by Pho85-Pho80. Various mixtures of purified HA-tagged Pho85 or the kinase dead (KD) $Pho85^{E53A}$ mutant, GST-tagged Pho80, and a TAP-tag purified fragment corresponding to the C-terminus (CT) of Sch9 (Arg^{650} to Ile^{824}) were used. The SYPRO Ruby staining and ^{32}P autoradiograph are shown. (C) Microscopic analysis of WT (BY4741) cells expressing genomically tagged GFP-$Sch9^{WT}$ or the

mutant versions GFP-Sch9^{S726A} or GFP-Sch9^{S726D} showing the recruitment at the vacuolar membrane of wild-type Sch9 as well as both Sch9 variants. The strains were grown to mid-log phase on complete synthetic medium. The lipophilic dye FM4-64 was used to visualize the vacuolar membrane. (D) Survival profiles of cells expressing either SCH9^{WT}, Sch9^{S726A} or Sch9^{S726D} when maintained on complete synthetic medium or starved for carbon (C), nitrogen (N) or phosphate (P).
(TIF)

S5 Fig. The Pho85-cyclins Pcl6 and Pcl7 contribute the regulation of Sch9. (A) Immunoblot analysis of protein extracts from the WT, *pcl6Δ*, *pcl7Δ*, and *pcl6Δ pcl7Δ* strains exponentially growing on complete synthetic medium to assess changes in Sch9 phosphorylation. The Sch9-Thr^{737} phosphorylation levels were quantified based on the ratio of the anti-P-Sch9^{T737} and anti-Sch9 signals, and normalized to the ratio obtained for the WT cells. Paired two-tailed student's T tests were used to calculate significances (*, $P < 0.1$; **, $P < 0.01$; ***, $P < 0.001$). (B) Immunoblot analysis of protein extracts of the WT strain and strains lacking non-essential Glc7-interacting proteins. The strains were grown to mid-log phase and were then treated with 200 nM rapamycin. Samples were taken before and after rapamycin treatment for 1 hour. The anti-Sch9 and anti-P-Sch9^{T737} antibodies were used for detection. The difference in mobility of the phosphorylated (P-Sch9) and non-phosphorylated (Sch9) isoforms as detected with the anti-Sch9 antibodies are indicated. (C) FM4-64 staining of the vacuolar membrane to show the difference in vacuolar size between WT cells and cells lacking Pho81, Pho85, or different combinations of Pho85 cyclins. Strains were grown to mid-log phase on complete synthetic medium containing 2% glucose. (D) Immunoblot analysis of the WT, *pho80Δ*, *pcl7Δ*, and *pho80Δ pcl7Δ* strains to compare the expression levels of the Fab1-GFP and Fab1^{VLA}-GFP fusions when introduced on centromere plasmids as based on the ratio of the anti-GFP and anti-Adh2 signals. (E) Microscopic analysis of Fab1^{VLA}-GFP localization in the WT, *pho80Δ*, *pcl7Δ*, and *pho80Δ pcl7Δ* strains. Strains were grown to mid-log phase on selective synthetic medium. The lipophilic dye FM4-64 was used to visualize the vacuolar membrane. The indents are magnifications showing that Fab1^{VLA} mainly localizes in foci at the periphery of small emerging vacuoles.
(TIF)

S6 Fig. Analysis of downstream Pho85 effectors for the interplay with TORC1 signaling. (A) Diploids were generated by crossing the haploid *sch9Δ* strain with the *pho85Δ rim15Δ*, or the *pho85Δ crz1Δ* strain followed by genotype analysis of the dissected germinated spores. (B) Rapamycin sensitivity analysis of cells lacking Rim15 or Crz1 in a WT, *pho85Δ*, or *pho80Δ* background as determined by spot assays on YPD plates without or with 50 nM rapamycin. (C) Expression of *PHO5* as determined by RT-PCR in WT, *pho85Δ*, *pho80Δ*, and *sch9Δ* cells carrying an empty vector, or *sch9Δ* cells transformed with a centromere plasmid encoding Sch9^{WT} when grown to mid-logarithmic phase in SD-Ura medium before or after treatment with 200 nM rapamycin for 30 min. The data are represented as mean ± standard deviation. Paired two-tailed student's T tests were used to calculate significances (*, $P < 0.1$; **, $P < 0.01$; ***, $P < 0.001$).
(TIF)

S1 Table. *S. cerevisiae* strains used in this study.
(DOCX)

S2 Table. Plasmids used in this study.
(DOCX)

S3 Table. Oligonucleotides used in this study.
(DOCX)

S4 Table. Data statistics.
(XLSX)

Acknowledgments

We thank R. Loewith, L. Weisman, J. Heitman, M. Cardenas, E. Boles, A. Matsuura, M. Peter, and B. André for providing plasmids, strains, or antibodies. We also thank Marie-Pierre Péli-Gulli and Ladislav Doklàdal for guidance with microscopy.

Author Contributions

Conceptualization: Marie-Anne Deprez, Marco Caligaris, Riko Hatakeyama, Belém Sampaio-Marques, Christian Ungermann, Paula Ludovico, Sabine Rospert, Claudio De Virgilio, Joris Winderickx.

Data curation: Marie-Anne Deprez, Marco Caligaris, Riko Hatakeyama, Christian Ungermann, Paula Ludovico, Sabine Rospert, Claudio De Virgilio, Joris Winderickx.

Formal analysis: Marie-Anne Deprez, Marco Caligaris, Joëlle Rosseels, Riko Hatakeyama, Ruben Ghillebert, Belém Sampaio-Marques, Kaivalya Mudholkar, Elja Eskes, Els Meert.

Funding acquisition: Riko Hatakeyama, Christian Ungermann, Sabine Rospert, Claudio De Virgilio, Joris Winderickx.

Investigation: Marie-Anne Deprez, Marco Caligaris, Joëlle Rosseels, Riko Hatakeyama, Ruben Ghillebert, Kaivalya Mudholkar, Elja Eskes, Els Meert.

Methodology: Marie-Anne Deprez, Marco Caligaris, Joëlle Rosseels, Riko Hatakeyama, Ruben Ghillebert, Belém Sampaio-Marques, Kaivalya Mudholkar, Elja Eskes, Els Meert, Christian Ungermann, Paula Ludovico, Sabine Rospert, Claudio De Virgilio, Joris Winderickx.

Resources: Christian Ungermann, Sabine Rospert, Claudio De Virgilio, Joris Winderickx.

Supervision: Sabine Rospert, Claudio De Virgilio, Joris Winderickx.

Validation: Marie-Anne Deprez, Marco Caligaris, Joëlle Rosseels, Riko Hatakeyama, Ruben Ghillebert, Belém Sampaio-Marques, Elja Eskes, Els Meert.

Visualization: Marie-Anne Deprez, Marco Caligaris, Belém Sampaio-Marques, Claudio De Virgilio, Joris Winderickx.

Writing – original draft: Marie-Anne Deprez, Joris Winderickx.

Writing – review & editing: Marie-Anne Deprez, Marco Caligaris, Joëlle Rosseels, Riko Hatakeyama, Ruben Ghillebert, Belém Sampaio-Marques, Kaivalya Mudholkar, Elja Eskes, Els Meert, Christian Ungermann, Paula Ludovico, Sabine Rospert, Claudio De Virgilio, Joris Winderickx.

References

1. Urban J, Soulard A, Huber A, Lippman S, Mukhopadhyay D, Deloche O, et al. Sch9 is a major target of TORC1 in Saccharomyces cerevisiae. Mol Cell. 2007; 26(5):663–74. https://doi.org/10.1016/j.molcel.2007.04.020 WOS:000247378000006. PMID: 17560372

2. Geyskens I, Kumara SHMC, Donaton MCV, Bergsma JCT, Thevelein JM, Wera S. Expression of mammalian PKB partially complements deletion of the yeast protein kinase Sch9. Nato Sci S a Lif Sci. 2000; 316:117–26. WOS:000167298000016.

3. Jorgensen P, Rupes I, Sharom JR, Schneper L, Broach JR, Tyers M. A dynamic transcriptional network communicates growth potential to ribosome synthesis and critical cell size. Genes Dev. 2004; 18 (20):2491–505. https://doi.org/10.1101/gad.1228804 PMID: 15466158; PubMed Central PMCID: PMC529537.

4. Huber A, Bodenmiller B, Uotila A, Stahl M, Wanka S, Gerrits B, et al. Characterization of the rapamycin-sensitive phosphoproteome reveals that Sch9 is a central coordinator of protein synthesis. Genes Dev. 2009; 23(16):1929–43. https://doi.org/10.1101/gad.532109 PMID: 19684113; PubMed Central PMCID: PMC2725941.

5. Smets B, De Snijder P, Engelen K, Joossens E, Ghillebert R, Thevissen K, et al. Genome-wide expression analysis reveals TORC1-dependent and -independent functions of Sch9. FEMS Yeast Res. 2008; 8(8):1276–88. Epub 2008/09/02. https://doi.org/10.1111/j.1567-1364.2008.00432.x [pii] PMID: 18759743.

6. Pedruzzi I, Burckert N, Egger P, De Virgilio C. Saccharomyces cerevisiae Ras/cAMP pathway controls post-diauxic shift element-dependent transcription through the zinc finger protein Gis1. EMBO J. 2000; 19(11):2569–79. https://doi.org/10.1093/emboj/19.11.2569 PMID: 10835355; PubMed Central PMCID: PMC212766.

7. Cameroni E, Hulo N, Roosen J, Winderickx J, De Virgilio C. The novel yeast PAS kinase Rim 15 orchestrates G0-associated antioxidant defense mechanisms. Cell Cycle. 2004; 3(4):462–8. PMID: 15300954.

8. Bonawitz ND, Chatenay-Lapointe M, Pan Y, Shadel GS. Reduced TOR signaling extends chronological life span via increased respiration and upregulation of mitochondrial gene expression. Cell Metab. 2007; 5(4):265–77. https://doi.org/10.1016/j.cmet.2007.02.009 PMID: 17403371; PubMed Central PMCID: PMC3460550.

9. Pan Y, Shadel GS. Extension of chronological life span by reduced TOR signaling requires down-regulation of Sch9p and involves increased mitochondrial OXPHOS complex density. Aging (Albany NY). 2009; 1(1):131–45. https://doi.org/10.18632/aging.100016 PMID: 20157595; PubMed Central PMCID: PMC2815770.

10. Swinnen E, Wilms T, Idkowiak-Baldys J, Smets B, De Snijder P, Accardo S, et al. The protein kinase Sch9 is a key regulator of sphingolipid metabolism in Saccharomyces cerevisiae. Mol Biol Cell. 2014; 25(1):196–211. https://doi.org/10.1091/mbc.E13-06-0340 PMID: 24196832; PubMed Central PMCID: PMC3873890.

11. Wilms T, Swinnen E, Eskes E, Dolz-Edo L, Uwineza A, Van Essche R, et al. The yeast protein kinase Sch9 adjusts V- ATPase assembly/ disassembly to control pH homeostasis and longevity in response to glucose availability. PLOS Genetics. 2017; 13(6):e1006835. https://doi.org/10.1371/journal.pgen.1006835 PMID: 28604780

12. Fabrizio P, Pozza F, Pletcher SD, Gendron CM, Longo VD. Regulation of longevity and stress resistance by Sch9 in yeast. Science. 2001; 292(5515):288–90. https://doi.org/10.1126/science.1059497 PMID: 11292860.

13. Kaeberlein M, Kirkland KT, Fields S, Kennedy BK. Genes determining yeast replicative life span in a long-lived genetic background. Mech Ageing Dev. 2005; 126(4):491–504. https://doi.org/10.1016/j.mad.2004.10.007 PMID: 15722108.

14. Liu K, Zhang X, Lester RL, Dickson RC. The sphingoid long chain base phytosphingosine activates AGC-type protein kinases in Saccharomyces cerevisiae including Ypk1, Ypk2, and Sch9. J Biol Chem. 2005; 280(24):22679–87. https://doi.org/10.1074/jbc.M502972200 PMID: 15840588.

15. Roelants FM, Torrance PD, Thorner J. Differential roles of PDK1- and PDK2-phosphorylation sites in the yeast AGC kinases Ypk1, Pkc1 and Sch9. Microbiology. 2004; 150(Pt 10):3289–304. https://doi.org/10.1099/mic.0.27286-0 PMID: 15470109.

16. Lu JY, Lin YY, Sheu JC, Wu JT, Lee FJ, Chen Y, et al. Acetylation of yeast AMPK controls intrinsic aging independently of caloric restriction. Cell. 2011; 146(6):969–79. https://doi.org/10.1016/j.cell.2011.07.044 PMID: 21906795; PubMed Central PMCID: PMC3176974.

17. Braun KA, Vaga S, Dombek KM, Fang F, Palmisano S, Aebersold R, et al. Phosphoproteomic analysis identifies proteins involved in transcription-coupled mRNA decay as targets of Snf1 signaling. Sci Signal. 2014; 7(333):ra64. https://doi.org/10.1126/scisignal.2005000 PMID: 25005228.

18. Mudholkar K, Fitzke E, Prinz C, Mayer MP, Rospert S. The Hsp70 homolog Ssb affects ribosome biogenesis via the TORC1-Sch9 signaling pathway. Nat Commun. 2017; 8(1):937. https://doi.org/10.1038/s41467-017-00635-z PMID: 29038496; PubMed Central PMCID: PMC5643326.

19. Voordeckers K, Kimpe M, Haesendonckx S, Louwet W, Versele M, Thevelein JM. Yeast 3-Phosphoinositide-dependent Protein Kinase-1 (PDK1) Orthologs Pkh1-3 Differentially Regulate Phosphorylation of Protein Kinase A (PKA) and the Protein Kinase B (PKB)/S6K Ortholog Sch9. J Biol Chem. 2011; 286(25):22017–27. https://doi.org/10.1074/jbc.M110.200071 WOS:000291719900008. PMID: 21531713

20. Ho CY, Alghamdi TA, Botelho RJ. Phosphatidylinositol-3,5-bisphosphate: no longer the poor PIP2. Traffic. 2012; 13(1):1–8. https://doi.org/10.1111/j.1600-0854.2011.01246.x PMID: 21736686.

21. Jin N, Mao K, Jin Y, Tevzadze G, Kauffman EJ, Park S, et al. Roles for PI(3,5)P-2 in nutrient sensing through TORC1. Mol Biol Cell. 2014; 25(7):1171–85. https://doi.org/10.1091/mbc.E14-01-0021 WOS:000339629900016.

22. Chen Z, Malia PC, Hatakeyama R, Nicastro R, Hu Z, Peli-Gulli MP, et al. TORC1 Determines Fab1 Lipid Kinase Function at Signaling Endosomes and Vacuoles. Curr Biol. 2021. https://doi.org/10.1016/j.cub.2020.10.026 PMID: 33157024.

23. Hatakeyama R, De Virgilio C. A spatially and functionally distinct pool of TORC1 defines signaling endosomes in yeast. Autophagy. 2019; 15(5):915–6. https://doi.org/10.1080/15548627.2019.1580107 PMID: 30732525; PubMed Central PMCID: PMC6526828.

24. Gao J, Nicastro R, Peli-Gulli MP, Grziwa S, Chen Z, Kurre R, et al. The HOPS tethering complex is required to maintain signaling endosome identity and TORC1 activity. J Cell Biol. 2022; 221(5). https://doi.org/10.1083/jcb.202109084 PMID: 35404387; PubMed Central PMCID: PMC9011323.

25. Lee YS, Mulugu S, York JD, O'Shea EK. Regulation of a cyclin-CDK-CDK inhibitor complex by inositol pyrophosphates. Science. 2007; 316(5821):109–12. https://doi.org/10.1126/science.1139080 PMID: 17412959; PubMed Central PMCID: PMC2211727.

26. Lenburg ME O'Shea EK. Signaling phosphate starvation. Trends Biochem Sci. 1996; 21(10):383–7. PMID: 8918192.

27. Mouillon JM, Persson BL. New aspects on phosphate sensing and signalling in Saccharomyces cerevisiae. FEMS Yeast Res. 2006; 6(2):171–6. https://doi.org/10.1111/j.1567-1364.2006.00036.x PMID: 16487340.

28. Lee M O'Regan S, Moreau JL, Johnson AL, Johnston LH, Goding CR. Regulation of the Pcl7-Pho85 cyclin-cdk complex by Pho81. Mol Microbiol. 2000; 38(2):411–22. https://doi.org/10.1046/j.1365-2958.2000.02140.x PMID: 11069666.

29. Bomeke K, Pries R, Korte V, Scholz E, Herzog B, Schulze F, et al. Yeast Gcn4p stabilization is initiated by the dissociation of the nuclear Pho85p/Pcl5p complex. Mol Biol Cell. 2006; 17(7):2952–62. https://doi.org/10.1091/mbc.e05-10-0975 PMID: 16611745; PubMed Central PMCID: PMC1483032.

30. Eskes E, Deprez MA, Wilms T, Winderickx J. pH homeostasis in yeast; the phosphate perspective. Curr Genet. 2018; 64(1):155–61. https://doi.org/10.1007/s00294-017-0743-2 PMID: 28856407; PubMed Central PMCID: PMC5778149.

31. Wanke V, Pedruzzi I, Cameroni E, Dubouloz F, De Virgilio C. Regulation of G0 entry by the Pho80-Pho85 cyclin-CDK complex. EMBO J. 2005; 24(24):4271–8. https://doi.org/10.1038/sj.emboj.7600889 PMID: 16308562; PubMed Central PMCID: PMC1356330.

32. Nishizawa M. The regulators of yeast PHO system participate in the transcriptional regulation of G1 cyclin under alkaline stress conditions. Yeast. 2015; 32(3):367–78. https://doi.org/10.1002/yea.3064 PMID: 25582350.

33. Nishizawa M, Tanigawa M, Hayashi M, Maeda T, Yazaki Y, Saeki Y, et al. Pho85 kinase, a cyclin-dependent kinase, regulates nuclear accumulation of the Rim101 transcription factor in the stress response of Saccharomyces cerevisiae. Eukaryot Cell. 2010; 9(6):943–51. https://doi.org/10.1128/EC.00247-09 PMID: 20382759; PubMed Central PMCID: PMC2901641.

34. Kaffman A, Herskowitz I, Tjian R, O'Shea EK. Phosphorylation of the transcription factor PHO4 by a cyclin-CDK complex, PHO80-PHO85. Science. 1994; 263(5150):1153–6. https://doi.org/10.1126/science.8108735 PMID: 8108735.

35. Menoyo S, Ricco N, Bru S, Hernandez-Ortega S, Escote X, Aldea M, et al. Phosphate-activated cyclin-dependent kinase stabilizes G1 cyclin to trigger cell cycle entry. Mol Cell Biol. 2013; 33(7):1273–84. https://doi.org/10.1128/MCB.01556-12 PMID: 23339867; PubMed Central PMCID: PMC3624280.

36. Shemer R, Meimoun A, Holtzman T, Kornitzer D. Regulation of the transcription factor Gcn4 by Pho85 cyclin PCL5. Mol Cell Biol. 2002; 22(15):5395–404. https://doi.org/10.1128/MCB.22.15.5395-5404.2002 PMID: 12101234; PubMed Central PMCID: PMC133946.

37. Ghillebert R, Swinnen E, De Snijder P, Smets B, Winderickx J. Differential roles for the low-affinity phosphate transporters Pho87 and Pho90 in Saccharomyces cerevisiae. Biochem J. 2011; 434(2):243–51. https://doi.org/10.1042/BJ20101118 PMID: 21143198.

38. Timblin BK, Tatchell K, Bergman LW. Deletion of the gene encoding the cyclin-dependent protein kinase Pho85 alters glycogen metabolism in Saccharomyces cerevisiae. Genetics. 1996; 143(1):57–66. https://doi.org/10.1093/genetics/143.1.57 PMID: 8722762; PubMed Central PMCID: PMC1207288.

39. Uesono Y, Tanaka K, Toh-e A. Negative regulators of the PHO system in Saccharomyces cerevisiae: isolation and structural characterization of PHO85. Nucleic Acids Res. 1987; 15(24):10299–309. https://doi.org/10.1093/nar/15.24.10299 PMID: 3320965; PubMed Central PMCID: PMC339945.

40. Huang D, Moffat J, Andrews B. Dissection of a complex phenotype by functional genomics reveals roles for the yeast cyclin-dependent protein kinase Pho85 in stress adaptation and cell integrity. Mol Cell Biol. 2002; 22(14):5076–88. https://doi.org/10.1128/MCB.22.14.5076-5088.2002 PMID: 12077337; PubMed Central PMCID: PMC139770.

41. Lee J, Colwill K, Aneliunas V, Tennyson C, Moore L, Ho Y, et al. Interaction of yeast Rvs167 and Pho85 cyclin-dependent kinase complexes may link the cell cycle to the actin cytoskeleton. Curr Biol. 1998; 8(24):1310–21. https://doi.org/10.1016/s0960-9822(07)00561-1 PMID: 9843683.

42. Prieto JA, Estruch F, Corcoles-Saez I, Del Poeta M, Rieger R, Stenzel I, et al. Pho85 and PI(4,5)P2 regulate different lipid metabolic pathways in response to cold. Biochim Biophys Acta Mol Cell Biol Lipids. 2020; 1865(2):158557. https://doi.org/10.1016/j.bbalip.2019.158557; PubMed Central PMCID: PMC7254492.

43. Swinnen E, Rosseels J, Winderickx J. The minimum domain of Pho81 is not sufficient to control the Pho85-Rim15 effector branch involved in phosphate starvation-induced stress responses. Curr Genet. 2005; 48(1):18–33. https://doi.org/10.1007/s00294-005-0583-3 PMID: 15926040.

44. Ebrahimi M, Habernig L, Broeskamp F, Aufschnaiter A, Diessl J, Atienza I, et al. Phosphate Restriction Promotes Longevity via Activation of Autophagy and the Multivesicular Body Pathway. Cells. 2021; 10(11). https://doi.org/10.3390/cells10113161 PMID: 34831384; PubMed Central PMCID: PMC8620443.

45. Wilson WA, Mahrenholz AM, Roach PJ. Substrate targeting of the yeast cyclin-dependent kinase Pho85p by the cyclin Pcl10p. Mol Cell Biol. 1999; 19(10):7020–30. https://doi.org/10.1128/MCB.19.10.7020 PMID: 10490639; PubMed Central PMCID: PMC84697.

46. Measday V, Moore L, Retnakaran R, Lee J, Donoviel M, Neiman AM, et al. A family of cyclin-like proteins that interact with the Pho85 cyclin-dependent kinase. Mol Cell Biol. 1997; 17(3):1212–23. https://doi.org/10.1128/MCB.17.3.1212 PMID: 9032248; PubMed Central PMCID: PMC231846.

47. Huang D, Moffat J, Wilson WA, Moore L, Cheng C, Roach PJ, et al. Cyclin partners determine Pho85 protein kinase substrate specificity in vitro and in vivo: control of glycogen biosynthesis by Pcl8 and Pcl10. Mol Cell Biol. 1998; 18(6):3289–99. https://doi.org/10.1128/MCB.18.6.3289 PMID: 9584169; PubMed Central PMCID: PMC108910.

48. Ptacek J, Devgan G, Michaud G, Zhu H, Zhu X, Fasolo J, et al. Global analysis of protein phosphorylation in yeast. Nature. 2005; 438(7068):679–84. https://doi.org/10.1038/nature04187 PMID: 16319894.

49. Carroll AS, O'Shea EK. Pho85 and signaling environmental conditions. Trends Biochem Sci. 2002; 27(2):87–93. https://doi.org/10.1016/s0968-0004(01)02040-0 PMID: 11852246.

50. Jin N, Jin Y, Weisman LS. Early protection to stress mediated by CDK-dependent PI3,5P2 signaling from the vacuole/lysosome. J Cell Biol. 2017; 216(7):2075–90. https://doi.org/10.1083/jcb.201611144 PMID: 28637746; PubMed Central PMCID: PMC5496620.

51. Huang D, Friesen H, Andrews B. Pho85, a multifunctional cyclin-dependent protein kinase in budding yeast. Mol Microbiol. 2007; 66(2):303–14. https://doi.org/10.1111/j.1365-2958.2007.05914.x PMID: 17850263.

52. Jin Y, Weisman LS. The vacuole/lysosome is required for cell-cycle progression. Elife. 2015; 4. https://doi.org/10.7554/eLife.08160 PMID: 26322385; PubMed Central PMCID: PMC4586482.

53. Lang MJ, Strunk BS, Azad N, Petersen JL, Weisman LS. An intramolecular interaction within the lipid kinase Fab1 regulates cellular phosphatidylinositol 3,5-bisphosphate lipid levels. Mol Biol Cell. 2017; 28(7):858–64. https://doi.org/10.1091/mbc.E16-06-0390 PMID: 28148651; PubMed Central PMCID: PMC5385934.

54. Alghamdi TA, Ho CY, Mrakovic A, Taylor D, Mao D, Botelho RJ. Vac14 protein multimerization is a prerequisite step for Fab1 protein complex assembly and function. J Biol Chem. 2013; 288(13):9363–72. https://doi.org/10.1074/jbc.M113.453712 PMID: 23389034; PubMed Central PMCID: PMC3611006.

55. Duex JE, Tang F, Weisman LS. The Vac14p-Fig 4p complex acts independently of Vac7p and couples PI3,5P2 synthesis and turnover. J Cell Biol. 2006; 172(5):693–704. https://doi.org/10.1083/jcb.200512105 PMID: 16492811; PubMed Central PMCID: PMC2063702.

56. Efe JA, Botelho RJ, Emr SD. Atg18 regulates organelle morphology and Fab1 kinase activity independent of its membrane recruitment by phosphatidylinositol 3,5-bisphosphate. Mol Biol Cell. 2007; 18

(11):4232–44. https://doi.org/10.1091/mbc.e07-04-0301 PMID: 17699591; PubMed Central PMCID: PMC2043547.

57. Rudge SA, Anderson DM, Emr SD. Vacuole size control: regulation of PtdIns(3,5)P2 levels by the vacuole-associated Vac14-Fig 4 complex, a PtdIns(3,5)P2-specific phosphatase. Mol Biol Cell. 2004; 15 (1):24–36. https://doi.org/10.1091/mbc.e03-05-0297 PMID: 14528018; PubMed Central PMCID: PMC307524.

58. Gary JD, Sato TK, Stefan CJ, Bonangelino CJ, Weisman LS, Emr SD. Regulation of Fab1 phosphatidylinositol 3-phosphate 5-kinase pathway by Vac7 protein and Fig 4, a polyphosphoinositide phosphatase family member. Mol Biol Cell. 2002; 13(4):1238–51. https://doi.org/10.1091/mbc.01-10-0498 PMID: 11950935; PubMed Central PMCID: PMC102265.

59. Gary JD, Wurmser AE, Bonangelino CJ, Weisman LS, Emr SD. Fab1p is essential for PtdIns(3)P 5-kinase activity and the maintenance of vacuolar size and membrane homeostasis. J Cell Biol. 1998; 143(1):65–79. https://doi.org/10.1083/jcb.143.1.65 PMID: 9763421; PubMed Central PMCID: PMC2132800.

60. Takeda E, Jin N, Itakura E, Kira S, Kamada Y, Weisman LS, et al. Vacuole-mediated selective regulation of TORC1-Sch9 signaling following oxidative stress. Mol Biol Cell. 2018; 29(4):510–22. https://doi.org/10.1091/mbc.E17-09-0553 PMID: 29237820; PubMed Central PMCID: PMC6014174.

61. Hatakeyama R, Peli-Gulli MP, Hu Z, Jaquenoud M, Garcia Osuna GM, Sardu A, et al. Spatially Distinct Pools of TORC1 Balance Protein Homeostasis. Mol Cell. 2019; 73(2):325–38 e8. https://doi.org/10.1016/j.molcel.2018.10.040 PMID: 30527664.

62. Hu Z, Raucci S, Jaquenoud M, Hatakeyama R, Stumpe M, Rohr R, et al. Multilayered Control of Protein Turnover by TORC1 and Atg1. Cell Rep. 2019; 28(13):3486–96 e6. https://doi.org/10.1016/j.celrep.2019.08.069 PMID: 31553916.

63. Yang Z, Geng J, Yen WL, Wang K, Klionsky DJ. Positive or negative roles of different cyclin-dependent kinase Pho85-cyclin complexes orchestrate induction of autophagy in Saccharomyces cerevisiae. Mol Cell. 2010; 38(2):250–64. https://doi.org/10.1016/j.molcel.2010.02.033 PMID: 20417603; PubMed Central PMCID: PMC2861662.

64. Jao CC, Ragusa MJ, Stanley RE, Hurley JH. A HORMA domain in Atg13 mediates PI 3-kinase recruitment in autophagy. Proc Natl Acad Sci U S A. 2013; 110(14):5486–91. https://doi.org/10.1073/pnas.1220306110 PMID: 23509291; PubMed Central PMCID: PMC3619307.

65. Peli-Gulli MP, Sardu A, Panchaud N, Raucci S, De Virgilio C. Amino Acids Stimulate TORC1 through Lst4-Lst7, a GTPase-Activating Protein Complex for the Rag Family GTPase Gtr2. Cell Rep. 2015; 13 (1):1–7. https://doi.org/10.1016/j.celrep.2015.08.059 PMID: 26387955.

66. Peli-Gulli MP, Raucci S, Hu Z, Dengjel J, De Virgilio C. Feedback Inhibition of the Rag GTPase GAP Complex Lst4-Lst7 Safeguards TORC1 from Hyperactivation by Amino Acid Signals. Cell Rep. 2017; 20(2):281–8. https://doi.org/10.1016/j.celrep.2017.06.058 PMID: 28700931.

67. O'Neill EM, Kaffman A, Jolly ER, O'Shea EK. Regulation of PHO4 nuclear localization by the PHO80-PHO85 cyclin-CDK complex. Science. 1996; 271(5246):209–12. https://doi.org/10.1126/science.271.5246.209 PMID: 8539622.

68. Longo VD, Shadel GS, Kaeberlein M, Kennedy B. Replicative and chronological aging in Saccharomyces cerevisiae. Cell Metab. 2012; 16(1):18–31. https://doi.org/10.1016/j.cmet.2012.06.002 PMID: 22768836; PubMed Central PMCID: PMC3392685.

69. Deprez MA, Eskes E, Winderickx J, Wilms T. The TORC1-Sch9 pathway as a crucial mediator of chronological lifespan in the yeast Saccharomyces cerevisiae. FEMS Yeast Res. 2018; 18(5). https://doi.org/10.1093/femsyr/foy048 PMID: 29788208.

70. Jin Y, Jin N, Oikawa Y, Benyair R, Koizumi M, Wilson TE, et al. Bur1 functions with TORC1 for vacuole-mediated cell cycle progression. EMBO Rep. 2022; 23(4):e53477. https://doi.org/10.15252/embr.202153477 PMID: 35166010; PubMed Central PMCID: PMC8982600.

71. Tan YS, Morcos PA, Cannon JF. Pho85 phosphorylates the Glc7 protein phosphatase regulator Glc8 in vivo. J Biol Chem. 2003; 278(1):147–53. https://doi.org/10.1074/jbc.M208058200 PMID: 12407105.

72. Yerlikaya S, Meusburger M, Kumari R, Huber A, Anrather D, Costanzo M, et al. TORC1 and TORC2 work together to regulate ribosomal protein S6 phosphorylation in Saccharomyces cerevisiae. Mol Biol Cell. 2016; 27(2):397–409. https://doi.org/10.1091/mbc.E15-08-0594 PMID: 26582391; PubMed Central PMCID: PMC4713140.

73. Schneider KR, Smith RL, O'Shea EK. Phosphate-regulated inactivation of the kinase PHO80-PHO85 by the CDK inhibitor PHO81. Science. 1994; 266(5182):122–6. https://doi.org/10.1126/science.7939631 PMID: 7939631.

74. Sopko R, Huang D, Preston N, Chua G, Papp B, Kafadar K, et al. Mapping pathways and phenotypes by systematic gene overexpression. Mol Cell. 2006; 21(3):319–30. https://doi.org/10.1016/j.molcel.2005.12.011 PMID: 16455487.

75. Ogawa N, DeRisi J, Brown PO. New components of a system for phosphate accumulation and polyphosphate metabolism in Saccharomyces cerevisiae revealed by genomic expression analysis. Mol Biol Cell. 2000; 11(12):4309–21. https://doi.org/10.1091/mbc.11.12.4309 PMID: 11102525; PubMed Central PMCID: PMC15074.

76. Persson BL, Lagerstedt JO, Pratt JR, Pattison-Granberg J, Lundh K, Shokrollahzadeh S, et al. Regulation of phosphate acquisition in Saccharomyces cerevisiae. Curr Genet. 2003; 43(4):225–44. https://doi.org/10.1007/s00294-003-0400-9 PMID: 12740714.

77. Barbaric S, Luckenbach T, Schmid A, Blaschke D, Horz W, Korber P. Redundancy of chromatin remodeling pathways for the induction of the yeast PHO5 promoter in vivo. J Biol Chem. 2007; 282 (38):27610–21. https://doi.org/10.1074/jbc.M700623200 PMID: 17631505.

78. Morrison AJ. Chromatin-remodeling links metabolic signaling to gene expression. Mol Metab. 2020; 38:100973. https://doi.org/10.1016/j.molmet.2020.100973 PMID: 32251664; PubMed Central PMCID: PMC7300377.

79. Nishizawa M, Komai T, Morohashi N, Shimizu M, Toh-e A. Transcriptional repression by the Pho4 transcription factor controls the timing of SNZ1 expression. Eukaryot Cell. 2008; 7(6):949–57. https://doi.org/10.1128/EC.00366-07 PMID: 18408055; PubMed Central PMCID: PMC2446651.

80. Staschke KA, Dey S, Zaborske JM, Palam LR, McClintick JN, Pan T, et al. Integration of general amino acid control and target of rapamycin (TOR) regulatory pathways in nitrogen assimilation in yeast. J Biol Chem. 2010; 285(22):16893–911. https://doi.org/10.1074/jbc.M110.121947 PMID: 20233714; PubMed Central PMCID: PMC2878067.

81. Moser BA, Dennis PB, Pullen N, Pearson RB, Williamson NA, Wettenhall RE, et al. Dual requirement for a newly identified phosphorylation site in p70s6k. Mol Cell Biol. 1997; 17(9):5648–55. https://doi.org/10.1128/MCB.17.9.5648 PMID: 9271440; PubMed Central PMCID: PMC232413.

82. Saitoh M, Pullen N, Brennan P, Cantrell D, Dennis PB, Thomas G. Regulation of an activated S6 kinase 1 variant reveals a novel mammalian target of rapamycin phosphorylation site. J Biol Chem. 2002; 277(22):20104–12. https://doi.org/10.1074/jbc.M201745200 PMID: 11914378.

83. Shah OJ, Ghosh S, Hunter T. Mitotic regulation of ribosomal S6 kinase 1 involves Ser/Thr, Pro phosphorylation of consensus and non-consensus sites by Cdc2. J Biol Chem. 2003; 278(18):16433–42. https://doi.org/10.1074/jbc.M300435200 PMID: 12586835.

84. Shin S, Wolgamott L, Yu Y, Blenis J, Yoon SO. Glycogen synthase kinase (GSK)-3 promotes p70 ribosomal protein S6 kinase (p70S6K) activity and cell proliferation. Proc Natl Acad Sci U S A. 2011; 108 (47):E1204–13. https://doi.org/10.1073/pnas.1110195108 PMID: 22065737; PubMed Central PMCID: PMC3223461.

85. Newton AC. Protein kinase C: structural and spatial regulation by phosphorylation, cofactors, and macromolecular interactions. Chem Rev. 2001; 101(8):2353–64. https://doi.org/10.1021/cr0002801 PMID: 11749377.

86. Pearce LR, Komander D, Alessi DR. The nuts and bolts of AGC protein kinases. Nat Rev Mol Cell Biol. 2010; 11(1):9–22. https://doi.org/10.1038/nrm2822 PMID: 20027184.

87. Lees JA, Li P, Kumar N, Weisman LS, Reinisch KM. Insights into Lysosomal PI(3,5)P2 Homeostasis from a Structural-Biochemical Analysis of the PIKfyve Lipid Kinase Complex. Mol Cell. 2020; 80 (4):736–43 e4. https://doi.org/10.1016/j.molcel.2020.10.003 PMID: 33098764; PubMed Central PMCID: PMC7962480.

88. Bun-Ya M, Nishimura M, Harashima S, Oshima Y. The PHO84 gene of Saccharomyces cerevisiae encodes an inorganic phosphate transporter. Mol Cell Biol. 1991; 11(6):3229–38. https://doi.org/10.1128/mcb.11.6.3229-3238.1991 PMID: 2038328; PubMed Central PMCID: PMC360175.

89. Liu NN, Flanagan PR, Zeng J, Jani NM, Cardenas ME, Moran GP, et al. Phosphate is the third nutrient monitored by TOR in Candida albicans and provides a target for fungal-specific indirect TOR inhibition. Proc Natl Acad Sci U S A. 2017; 114(24):6346–51. https://doi.org/10.1073/pnas.1617799114 PMID: 28566496; PubMed Central PMCID: PMC5474788.

90. Kawai M, Kinoshita S, Ozono K, Michigami T. Inorganic Phosphate Activates the AKT/mTORC1 Pathway and Shortens the Life Span of an alphaKlotho-Deficient Model. J Am Soc Nephrol. 2016; 27 (9):2810–24. https://doi.org/10.1681/ASN.2015040446 PMID: 26872488; PubMed Central PMCID: PMC5004643.

91. Dove SK, Piper RC, McEwen RK, Yu JW, King MC, Hughes DC, et al. Svp1p defines a family of phosphatidylinositol 3,5-bisphosphate effectors. EMBO J. 2004; 23(9):1922–33. https://doi.org/10.1038/sj.emboj.7600203 PMID: 15103325; PubMed Central PMCID: PMC404323.

92. Baskaran S, Ragusa MJ, Boura E, Hurley JH. Two-site recognition of phosphatidylinositol 3-phosphate by PROPPINs in autophagy. Mol Cell. 2012; 47(3):339–48. https://doi.org/10.1016/j.molcel.2012.05.027 PMID: 22704557; PubMed Central PMCID: PMC3595537.

93. Levine TP. TMEM106B in humans and Vac7 and Tag1 in yeast are predicted to be lipid transfer proteins. Proteins. 2022; 90(1):164–75. https://doi.org/10.1002/prot.26201 PMID: 34347309.

94. Manandhar SP, Siddiqah IM, Cocca SM, Gharakhanian E. A kinase cascade on the yeast lysosomal vacuole regulates its membrane dynamics: conserved kinase Env7 is phosphorylated by casein kinase Yck3. J Biol Chem. 2020; 295(34):12262–78. https://doi.org/10.1074/jbc.RA119.012346 PMID: 32647006; PubMed Central PMCID: PMC7443493.

95. LaGrassa TJ, Ungermann C. The vacuolar kinase Yck3 maintains organelle fragmentation by regulating the HOPS tethering complex. J Cell Biol. 2005; 168(3):401–14. https://doi.org/10.1083/jcb.200407141 PMID: 15684030; PubMed Central PMCID: PMC2171739.

96. Malia PC, Numrich J, Nishimura T, Gonzalez Montoro A, Stefan CJ, Ungermann C. Control of vacuole membrane homeostasis by a resident PI-3,5-kinase inhibitor. Proc Natl Acad Sci U S A. 2018; 115 (18):4684–9. https://doi.org/10.1073/pnas.1722517115 PMID: 29674454; PubMed Central PMCID: PMC5939101.

97. Weisman LS. Yeast vacuole inheritance and dynamics. Annu Rev Genet. 2003; 37:435–60. https://doi.org/10.1146/annurev.genet.37.050203.103207 PMID: 14616069.

98. Nicolson TA, Weisman LS, Payne GS, Wickner WT. A truncated form of the Pho80 cyclin redirects the Pho85 kinase to disrupt vacuole inheritance in S. cerevisiae. J Cell Biol. 1995; 130(4):835–45. https://doi.org/10.1083/jcb.130.4.835 PMID: 7642701; PubMed Central PMCID: PMC2199970.

99. Stauffer B, Powers T. Target of rapamycin signaling mediates vacuolar fission caused by endoplasmic reticulum stress in Saccharomyces cerevisiae. Mol Biol Cell. 2015; 26(25):4618–30. https://doi.org/10.1091/mbc.E15-06-0344 PMID: 26466677; PubMed Central PMCID: PMC4678019.

100. Irie K, Nomoto S, Miyajima I, Matsumoto K. SGV1 encodes a CDC28/cdc2-related kinase required for a G alpha subunit-mediated adaptive response to pheromone in S. cerevisiae. Cell. 1991; 65(5):785–95. https://doi.org/10.1016/0092-8674(91)90386-d PMID: 1828190.

101. Connelly CJ, Vidal-Cardenas S, Goldsmith S, Greider CW. The Bur1 cyclin-dependent kinase regulates telomere length in Saccharomyces cerevisiae. Yeast. 2022; 39(3):177–92. https://doi.org/10.1002/yea.3680 PMID: 34781413.

102. Askree SH, Yehuda T, Smolikov S, Gurevich R, Hawk J, Coker C, et al. A genome-wide screen for Saccharomyces cerevisiae deletion mutants that affect telomere length. Proc Natl Acad Sci U S A. 2004; 101(23):8658–63. https://doi.org/10.1073/pnas.0401263101 PMID: 15161972; PubMed Central PMCID: PMC423251.

103. Huang S, Jeffery DA, Anthony MD, O'Shea EK. Functional analysis of the cyclin-dependent kinase inhibitor Pho81 identifies a novel inhibitory domain. Mol Cell Biol. 2001; 21(19):6695–705. https://doi.org/10.1128/MCB.21.19.6695-6705.2001 PMID: 11533256; PubMed Central PMCID: PMC99814.

104. Pascual-Ahuir A, Proft M. Control of stress-regulated gene expression and longevity by the Sch9 protein kinase. Cell Cycle. 2007; 6(20):2445–7. https://doi.org/10.4161/cc.6.20.4792 PMID: 17726371.

105. Pascual-Ahuir A, Proft M. The Sch9 kinase is a chromatin-associated transcriptional activator of osmostress-responsive genes. EMBO J. 2007; 26(13):3098–108. https://doi.org/10.1038/sj.emboj.7601756 PMID: 17568771; PubMed Central PMCID: PMC1914104.

106. Lai KO, Liang Z, Fei E, Huang H, Ip NY. Cyclin-dependent Kinase 5 (Cdk5)-dependent Phosphorylation of p70 Ribosomal S6 Kinase 1 (S6K) Is Required for Dendritic Spine Morphogenesis. J Biol Chem. 2015; 290(23):14637–46. https://doi.org/10.1074/jbc.M114.627117 PMID: 25903132; PubMed Central PMCID: PMC4505530.

107. Dotti CG, Esteban JA, Ledesma MD. Lipid dynamics at dendritic spines. Front Neuroanat. 2014; 8:76. https://doi.org/10.3389/fnana.2014.00076 PMID: 25152717; PubMed Central PMCID: PMC4126552.

108. Ouyang L, Chen Y, Wang Y, Chen Y, Fu AKY, Fu WY, et al. p39-associated Cdk5 activity regulates dendritic morphogenesis. Sci Rep. 2020; 10(1):18746. https://doi.org/10.1038/s41598-020-75264-6 PMID: 33127972; PubMed Central PMCID: PMC7603351.

109. Hou Z, He L, Qi RZ. Regulation of s6 kinase 1 activation by phosphorylation at ser-411. J Biol Chem. 2007; 282(10):6922–8. https://doi.org/10.1074/jbc.M607836200 PMID: 17220300.

110. Arif A, Jia J, Willard B, Li X, Fox PL. Multisite Phosphorylation of S6K1 Directs a Kinase Phospho-code that Determines Substrate Selection. Mol Cell. 2019; 73(3):446–57 e6. https://doi.org/10.1016/j.molcel.2018.11.017 PMID: 30612880; PubMed Central PMCID: PMC6415305.

111. Bridges D, Ma JT, Park S, Inoki K, Weisman LS, Saltiel AR. Phosphatidylinositol 3,5-bisphosphate plays a role in the activation and subcellular localization of mechanistic target of rapamycin 1. Mol Biol Cell. 2012; 23(15):2955–62. https://doi.org/10.1091/mbc.E11-12-1034 PMID: 22696681; PubMed Central PMCID: PMC3408421.

112. Lindqvist J, Imanishi SY, Torvaldson E, Malinen M, Remes M, Orn F, et al. Cyclin-dependent kinase 5 acts as a critical determinant of AKT-dependent proliferation and regulates differential gene expression by the androgen receptor in prostate cancer cells. Mol Biol Cell. 2015; 26(11):1971–84. https://doi.org/10.1091/mbc.E14-12-1634 PMID: 25851605; PubMed Central PMCID: PMC4472009.

113. Komeili A, O'Shea EK. Roles of phosphorylation sites in regulating activity of the transcription factor Pho4. Science. 1999; 284(5416):977–80. https://doi.org/10.1126/science.284.5416.977 PMID: 10320381.

114. Teunissen JHM, Crooijmans ME, Teunisse PPP, van Heusden GPH. Lack of 14-3-3 proteins in Saccharomyces cerevisiae results in cell-to-cell heterogeneity in the expression of Pho4-regulated genes SPL2 and PHO84. BMC Genomics. 2017; 18(1):701. https://doi.org/10.1186/s12864-017-4105-8 PMID: 28877665

115. Jeffery DA, Springer M, King DS, O'Shea EK. Multi-site phosphorylation of Pho4 by the cyclin-CDK Pho80-Pho85 is semi-processive with site preference. J Mol Biol. 2001; 306(5):997–1010. https://doi.org/10.1006/jmbi.2000.4417 PMID: 11237614.

116. Springer M, Wykoff DD, Miller N, O'Shea EK. Partially phosphorylated Pho4 activates transcription of a subset of phosphate-responsive genes. PLoS Biol. 2003; 1(2):E28. https://doi.org/10.1371/journal.pbio.0000028 PMID: 14624238; PubMed Central PMCID: PMC261874.

117. Kaffman A, Rank NM, O'Neill EM, Huang LS, O'Shea EK. The receptor Msn5 exports the phosphorylated transcription factor Pho4 out of the nucleus. Nature. 1998; 396(6710):482–6. https://doi.org/10.1038/24898 PMID: 9853758.

118. Samyn DR, Ruiz-Pavon L, Andersson MR, Popova Y, Thevelein JM, Persson BL. Mutational analysis of putative phosphate- and proton-binding sites in the Saccharomyces cerevisiae Pho84 phosphate:H (+) transceptor and its effect on signalling to the PKA and PHO pathways. Biochem J. 2012; 445 (3):413–22. https://doi.org/10.1042/BJ20112086 PMID: 22587366.

119. Lundh F, Mouillon JM, Samyn D, Stadler K, Popova Y, Lagerstedt JO, et al. Molecular mechanisms controlling phosphate-induced downregulation of the yeast Pho84 phosphate transporter. Biochemistry. 2009; 48(21):4497–505. https://doi.org/10.1021/bi9001198 PMID: 19348508.

120. Jiang JC, Stumpferl SW, Tiwari A, Qin Q, Rodriguez-Quinones JF, Jazwinski SM. Identification of the Target of the Retrograde Response that Mediates Replicative Lifespan Extension in Saccharomyces cerevisiae. Genetics. 2016; 204(2):659–73. https://doi.org/10.1534/genetics.116.188086 PMID: 27474729; PubMed Central PMCID: PMC5068853.

121. Wasko BM, Kaeberlein M. Yeast replicative aging: a paradigm for defining conserved longevity interventions. FEMS Yeast Res. 2014; 14(1):148–59. https://doi.org/10.1111/1567-1364.12104 PMID: 24119093; PubMed Central PMCID: PMC4134429.

122. Nakajima T, Maruhashi T, Morimatsu T, Mukai Y. Cyclin-dependent kinase Pho85p and its cyclins are involved in replicative lifespan through multiple pathways in yeast. FEBS Lett. 2020; 594(7):1166–75. https://doi.org/10.1002/1873-3468.13707 PMID: 31797348.

123. Kupiec M. Biology of telomeres: lessons from budding yeast. FEMS Microbiol Rev. 2014; 38(2):144–71. https://doi.org/10.1111/1574-6976.12054 PMID: 24754043.

124. Brachmann CB, Davies A, Cost GJ, Caputo E, Li J, Hieter P, et al. Designer deletion strains derived from Saccharomyces cerevisiae S288C: a useful set of strains and plasmids for PCR-mediated gene disruption and other applications. Yeast. 1998; 14(2):115–32. Epub 1998/03/04. https://doi.org/10.1002/(SICI)1097-0061(19980130)14:2<115::AID-YEA204>3.0.CO;2-2 PMID: 9483801.

125. Generoso WC, Gottardi M, Oreb M, Boles E. Simplified CRISPR-Cas genome editing for Saccharomyces cerevisiae. J Microbiol Methods. 2016; 127:203–5. https://doi.org/10.1016/j.mimet.2016.06.020 PMID: 27327211.

126. Gietz RD, Schiestl RH, Willems AR, Woods RA. Studies on the transformation of intact yeast cells by the LiAc/SS-DNA/PEG procedure. Yeast. 1995; 11(4):355–60. Epub 1995/04/15. https://doi.org/10.1002/yea.320110408 PMID: 7785336.

127. Gibson DG, Young L, Chuang RY, Venter JC, Hutchison CA 3rd, Smith HO. Enzymatic assembly of DNA molecules up to several hundred kilobases. Nat Methods. 2009; 6(5):343–5. https://doi.org/10.1038/nmeth.1318 PMID: 19363495.

128. Kingsbury JM, Sen ND, Maeda T, Heitman J, Cardenas ME. Endolysosomal membrane trafficking complexes drive nutrient-dependent TORC1 signaling to control cell growth in Saccharomyces cerevisiae. Genetics. 2014; 196(4):1077–89. https://doi.org/10.1534/genetics.114.161646 PMID: 24514902; PubMed Central PMCID: PMC3982701.

129. Kaffman A, Rank NM, O'Shea EK. Phosphorylation regulates association of the transcription factor Pho4 with its import receptor Pse1/Kap121. Genes Dev. 1998; 12(17):2673–83. https://doi.org/10.1101/gad.12.17.2673 PMID: 9732266; PubMed Central PMCID: PMC317126.

130. Conradt B, Shaw J, Vida T, Emr S, Wickner W. In vitro reactions of vacuole inheritance in Saccharomyces cerevisiae. J Cell Biol. 1992; 119(6):1469–79. https://doi.org/10.1083/jcb.119.6.1469 PMID: 1334958; PubMed Central PMCID: PMC2289757.

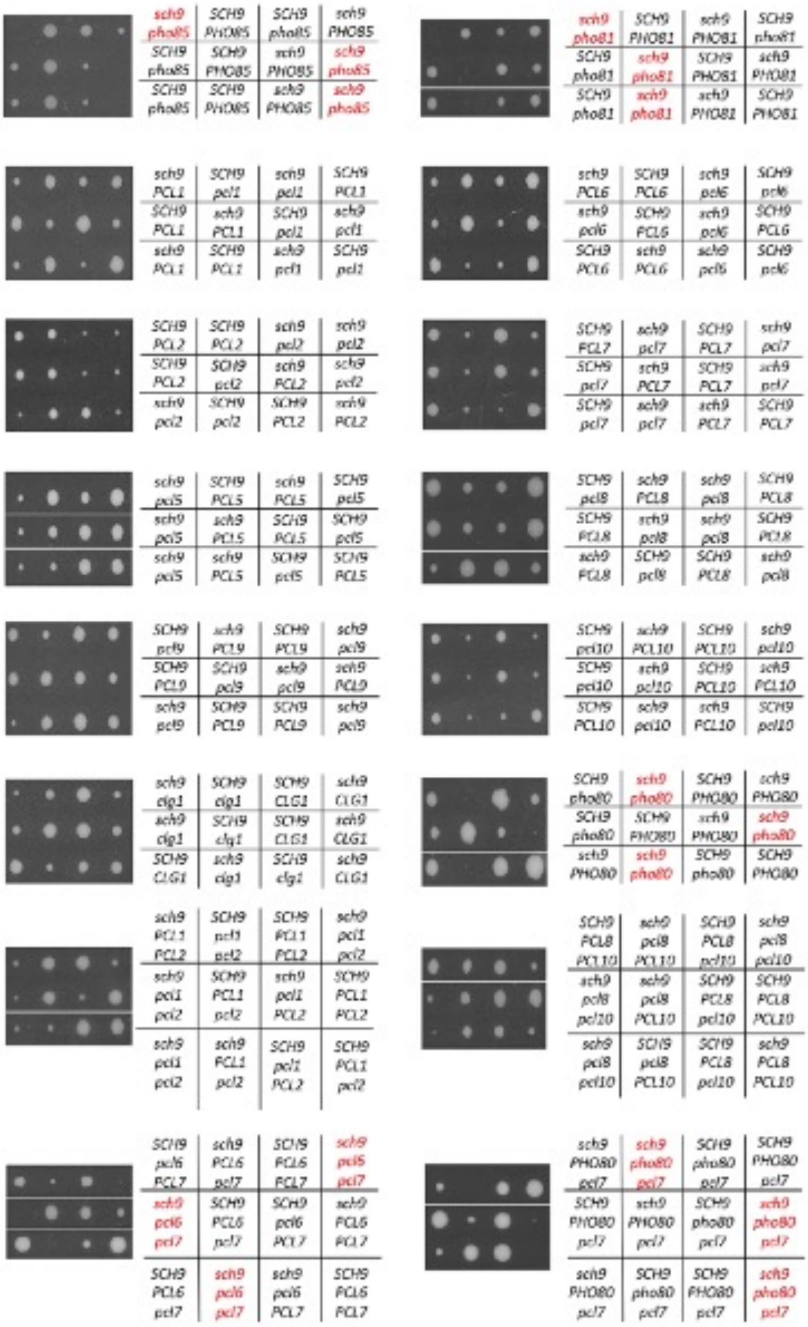
sch9 phο85 | SCH9 PHO85 | SCH9 pho85 | sch9 PHO85
SCH9 pho85 | SCH9 PHO85 | sch9 PHO85 | sch9 pho85
SCH9 pho85 | SCH9 PHO85 | sch9 PHO85 | sch9 pho85
sch9 pho81 | SCH9 PHO81 | sch9 PHO81 | SCH9 pho81
SCH9 pho81 | sch9 pho81 | SCH9 PHO81 | sch9 PHO81
SCH9 pho81 | sch9 pho81 | sch9 PHO81 | SCH9 PHO81
sch9 PCL1 | SCH9 pcl1 | sch9 pcl1 | SCH9 PCL1
SCH9 PCL1 | sch9 PCL1 | SCH9 pcl1 | sch9 pcl1
sch9 PCL1 | SCH9 PCL1 | sch9 pcl1 | SCH9 pcl1
sch9 PCL6 | SCH9 PCL6 | sch9 pcl6 | SCH9 pcl6
sch9 pcl6 | SCH9 PCL6 | sch9 pcl6 | SCH9 PCL6
SCH9 PCL6 | sch9 PCL6 | sch9 pcl6 | SCH9 pcl6
SCH9 PCL2 | SCH9 PCL2 | sch9 pcl2 | sch9 pcl2
SCH9 PCL2 | SCH9 pcl2 | sch9 PCL2 | sch9 pcl2
sch9 pcl2 | SCH9 pcl2 | SCH9 PCL2 | sch9 PCL2
SCH9 PCL7 | sch9 pcl7 | SCH9 PCL7 | sch9 pcl7
SCH9 pcl7 | sch9 PCL7 | SCH9 PCL7 | sch9 pcl7
SCH9 pcl7 | sch9 pcl7 | sch9 PCL7 | SCH9 PCL7
sch9 pcl5 | SCH9 PCL5 | sch9 PCL5 | SCH9 pcl5
sch9 pcl5 | sch9 PCL5 | SCH9 PCL5 | SCH9 pcl5
sch9 pcl5 | sch9 PCL5 | SCH9 pcl5 | SCH9 PCL5
SCH9 pcl8 | sch9 PCL8 | sch9 pcl8 | SCH9 PCL8
SCH9 PCL8 | sch9 pcl8 | sch9 pcl8 | SCH9 PCL8
sch9 PCL8 | SCH9 pcl8 | SCH9 PCL8 | sch9 pcl8
SCH9 pcl9 | sch9 PCL9 | SCH9 PCL9 | sch9 pcl9
SCH9 PCL9 | SCH9 pcl9 | sch9 pcl9 | sch9 PCL9
sch9 pcl9 | SCH9 PCL9 | SCH9 PCL9 | sch9 pcl9
SCH9 pcl10 | sch9 PCL10 | SCH9 PCL10 | sch9 pcl10
SCH9 pcl10 | sch9 pcl10 | SCH9 PCL10 | sch9 PCL10
SCH9 PCL10 | sch9 pcl10 | sch9 PCL10 | SCH9 pcl10
sch9 clg1 | SCH9 clg1 | SCH9 CLG1 | sch9 CLG1
sch9 clg1 | SCH9 clg1 | SCH9 CLG1 | sch9 CLG1
SCH9 CLG1 | sch9 clg1 | SCH9 clg1 | sch9 CLG1
SCH9 pho80 | sch9 pho80 | SCH9 PHO80 | sch9 PHO80
SCH9 pho80 | SCH9 PHO80 | sch9 PHO80 | sch9 pho80
sch9 PHO80 | sch9 pho80 | SCH9 pho80 | SCH9 PHO80
sch9 PCL1 PCL2 | SCH9 pcl1 pcl2 | SCH9 PCL1 PCL2 | sch9 pcl1 pcl2
sch9 pcl1 pcl2 | SCH9 PCL1 pcl2 | sch9 pcl1 PCL2 | SCH9 PCL1 PCL2
sch9 pcl1 pcl2 | sch9 PCL1 pcl2 | SCH9 pcl1 PCL2 | SCH9 PCL1 pcl2
SCH9 PCL8 PCL10 | sch9 pcl8 PCL10 | SCH9 PCL8 pcl10 | sch9 pcl8 pcl10
sch9 pcl8 pcl10 | sch9 pcl8 PCL10 | SCH9 PCL8 pcl10 | SCH9 PCL8 PCL10
sch9 pcl8 pcl10 | SCH9 pcl8 PCL10 | SCH9 PCL8 pcl10 | sch9 PCL8 PCL10
SCH9 pcl6 PCL7 | sch9 PCL6 pcl7 | SCH9 PCL6 PCL7 | sch9 pcl6 pcl7
sch9 pcl6 pcl7 | SCH9 PCL6 pcl7 | SCH9 pcl6 PCL7 | sch9 PCL6 PCL7
SCH9 PCL6 pcl7 | sch9 pcl6 pcl7 | sch9 pcl6 PCL7 | SCH9 PCL6 PCL7
sch9 PHO80 pcl7 | sch9 pho80 pcl7 | SCH9 pho80 pcl7 | SCH9 PHO80 pcl7
SCH9 PHO80 pcl7 | sch9 PHO80 pcl7 | SCH9 pho80 pcl7 | sch9 pho80 pcl7
sch9 PHO80 pcl7 | SCH9 pho80 pcl7 | SCH9 PHO80 pcl7 | sch9 pho80 pcl7

S1 Fig: Genetic interaction of SCH9 with different players of the Pho85 signaling pathway. Diploids were generated by crossing the haploid *SCH9* deletion strain with haploid strains carrying either a *PHO85*, *PHO81*, a single cyclin deletion or double cyclin deletion. Tetrad analysis only revealed a genetic interaction between *SCH9* and *PHO85*, *PHO81*, *PHO80*, *PCL6 PCL7* and *PHO80 PCL7* as indicated in red. The dissected spores were grown on YPD plates and pictures were taken after 3 to 5 days at 30°C.

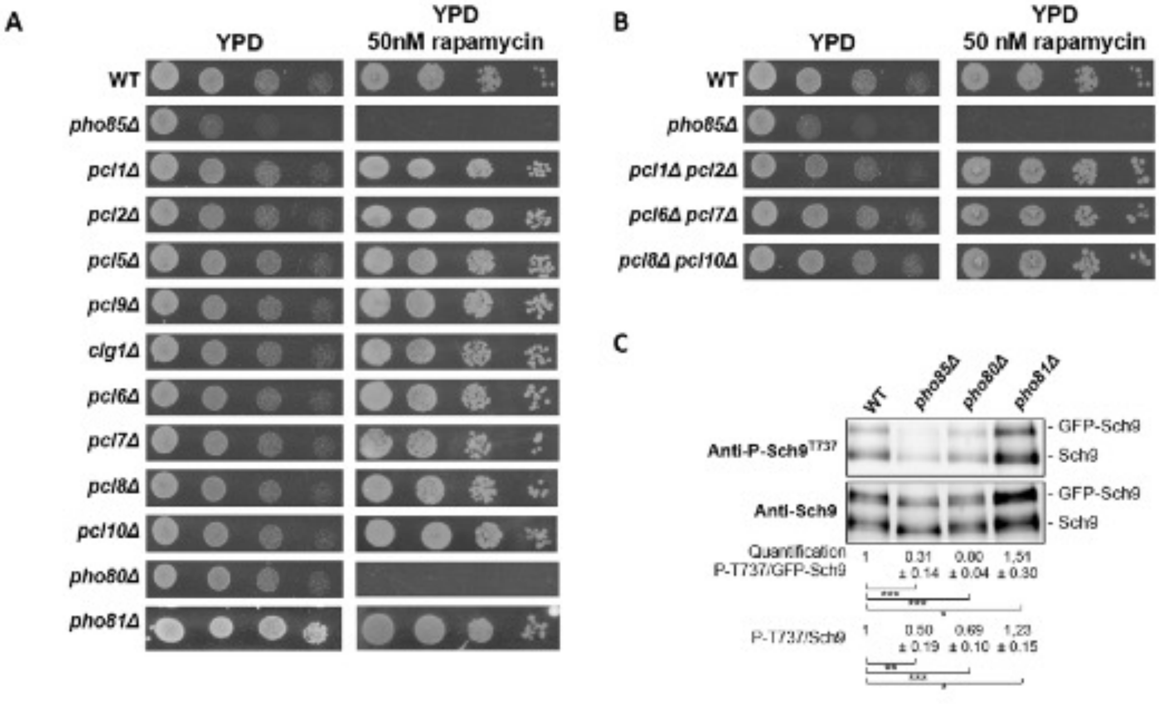
A
YPD
YPD
50nM rapamycin
WT
pho85Δ
pcl1Δ
pcl2Δ
pcl5Δ
pcl9Δ
clg1Δ
pcl6Δ
pcl7Δ
pcl8Δ
pcl10Δ
pho80Δ
pho81Δ
B
YPD
YPD
50 nM rapamycin
WT
pho85Δ
pcl1Δ pcl2Δ
pcl6Δ pcl7Δ
pcl8Δ pcl10Δ
C
WT
pho85Δ
pho80Δ
pho81Δ
Anti-P-Sch9T737
Anti-Sch9
- GFP-Sch9
- Sch9
- GFP-Sch9
- Sch9
Quantification
P-T737/GFP-Sch9
1
0.31 ± 0.14
0.00 ± 0.04
1.51 ± 0.30
***
***
*
P-T737/Sch9
1
0.50 ± 0.19
0.69 ± 0.10
1.23 ± 0.15
**
***
*

S2 Fig: Interaction between the TORC1- and Pho85-signaling pathways. (A, B) The WT strain or mutant strains lacking Pho85, Pho80, Pho81, a single cyclin (A) or two partially redundant cyclins (B) were grown exponentially on YPD, diluted to an OD_{600nm} of 0.1 and tenfold serial dilutions were spotted on YPD plates without or with 50 nM rapamycin. The strains were grown for 2 to 4 days at 30°C. (C) Immunoblot analysis of exponentially growing WT, *pho85Δ*, *pho80Δ*, and *pho81Δ* cells expressing GFP-$Sch9^{WT}$ from an episomal plasmid in addition to endogenous Sch9. The Sch9-Thr^{737} phosphorylation level of GFP-Sch9 and endogenous Sch9 was quantified based on densitometry of the anti-P-$Sch9^{T737}$ and anti-Sch9 signals, and normalized to WT cells. The data are represented as mean ± standard deviation. Paired two-tailed student's T tests were used to calculate significances (*, $P < 0.1$; **, $P < 0.01$; ***, $P < 0.001$).

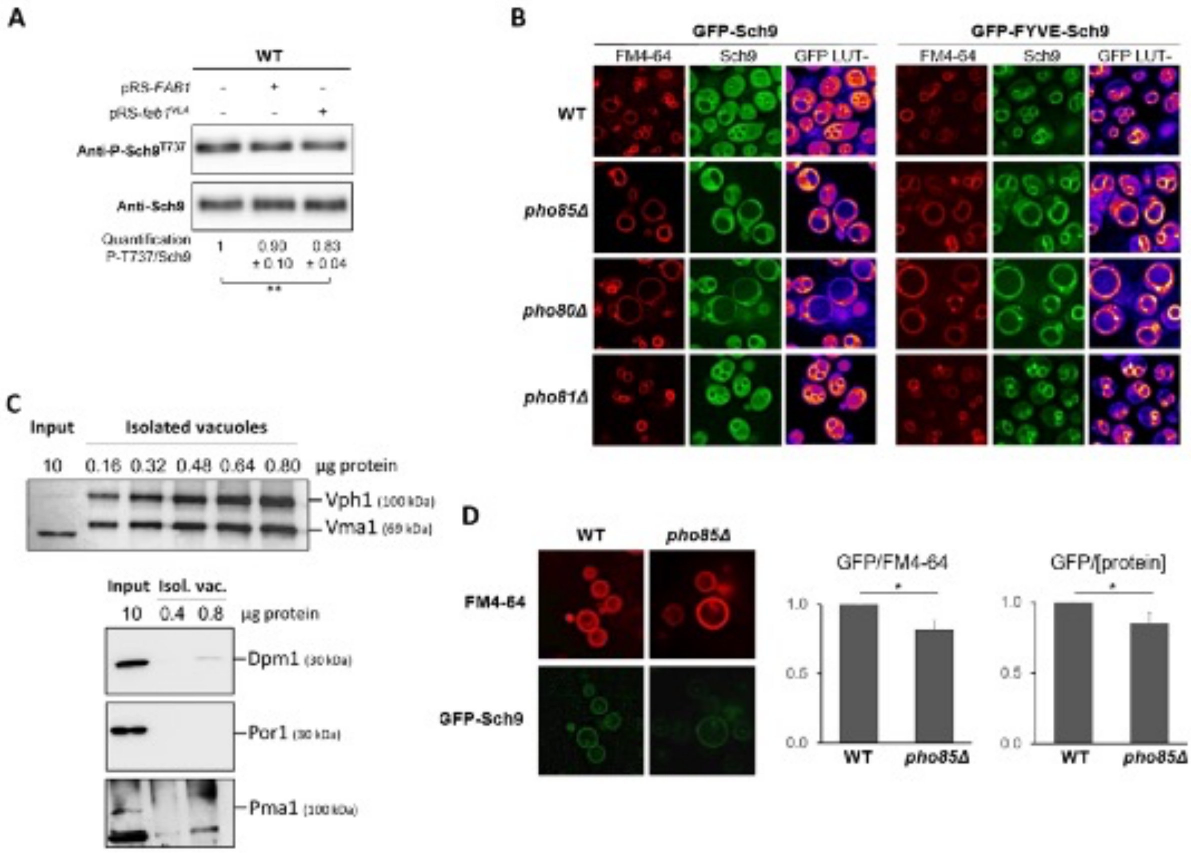
A
WT
pRS-FAB1
pRS-fab1^{VL4}
- + -
- - +
Anti-P-Sch9^{T737}
Anti-Sch9
Quantification P-T737/Sch9
1
0.90 + 0.10
0.83 + 0.04
**
B
GFP-Sch9
GFP-FYVE-Sch9
FM4-64
Sch9
GFP LUT-
WT
pho85Δ
pho80Δ
pho81Δ
C
Input
Isolated vacuoles
10
0.16
0.32
0.48
0.64
0.80
µg protein
Vph1 (100 kDa)
Vma1 (69 kDa)
Input
Isol. vac.
10
0.4
0.8
µg protein
Dpm1 (30 kDa)
Por1 (30 kDa)
Pma1 (100 kDa)
D
WT
pho85Δ
FM4-64
GFP-Sch9
GFP/FM4-64
GFP/[protein]
1.0
0.5
0.0
*
WT
pho85Δ

S3 Fig: Sch9 phosphorylation in cells with enhanced Fab1 activity and GFP-Sch9 abundance at the vacuolar membrane. (A) Immunoblot analysis of exponentially growing WT cells expressing either Fab1 or Fab1^{VLA} from a centromere plasmid. The Sch9-Thr^{737} phosphorylation was quantified based on densitometry of the anti-P-Sch9^{T737} and anti-Sch9 signals, and normalized to WT cells transformed with an empty vector. (B) Microscopic analysis of Sch9 localization in the WT, *pho85Δ*, *pho80Δ*, and *pho81Δ* strains expressing the genomically tagged GFP-Sch9 or GFP-FYVE-Sch9 fusion protein. Strains were grown to mid-log phase on complete synthetic medium. The lipophilic dye FM4-64 was used to visualize the vacuolar membrane. Pictures were deconvoluted using the Huygens software (version 18.10). A LUT Fire was applied using ImageJ in order to show the levels of the GFP signal. (C) Western blot analysis to assess purity of the isolated vacuolar vesicles. Vacuoles were purified from spheroplasted cells using a density gradient centrifugation method as described in the materials and methods section. The high abundance of 2 typical vacuolar membrane proteins (Vma1 and Vph1) in the isolated vacuolar fraction in comparison to the whole cell protein extract (=Input) confirmed the strong enrichment of vacuolar proteins in this fraction. The presence of ER (Dpm1), mitochondrial (Por1) and plasma membrane (Pma1) markers, on the other hand, was very low in the isolated vacuolar fraction. (D) Fluorescence microscopic pictures of the purified vacuoles of GFP-Sch9^{WT}-expressing cells, confirming the presence of GFP-Sch9 at the membranes of purified vacuoles. Staining with the lipophilic FM4-64 dye confirms the integrity of the isolated vacuolar vesicles. The intensity of the GFP-signal was quantified with a Fluoroskan plate reader as explained in the materials and methods section and expressed relative to the FM4-64 signal as well as the total protein content. The data are represented as mean ± standard deviation. Paired two-tailed student's T tests were used to calculate significances (*, $P < 0.1$; **, $P < 0.01$; ***, $P < 0.001$).

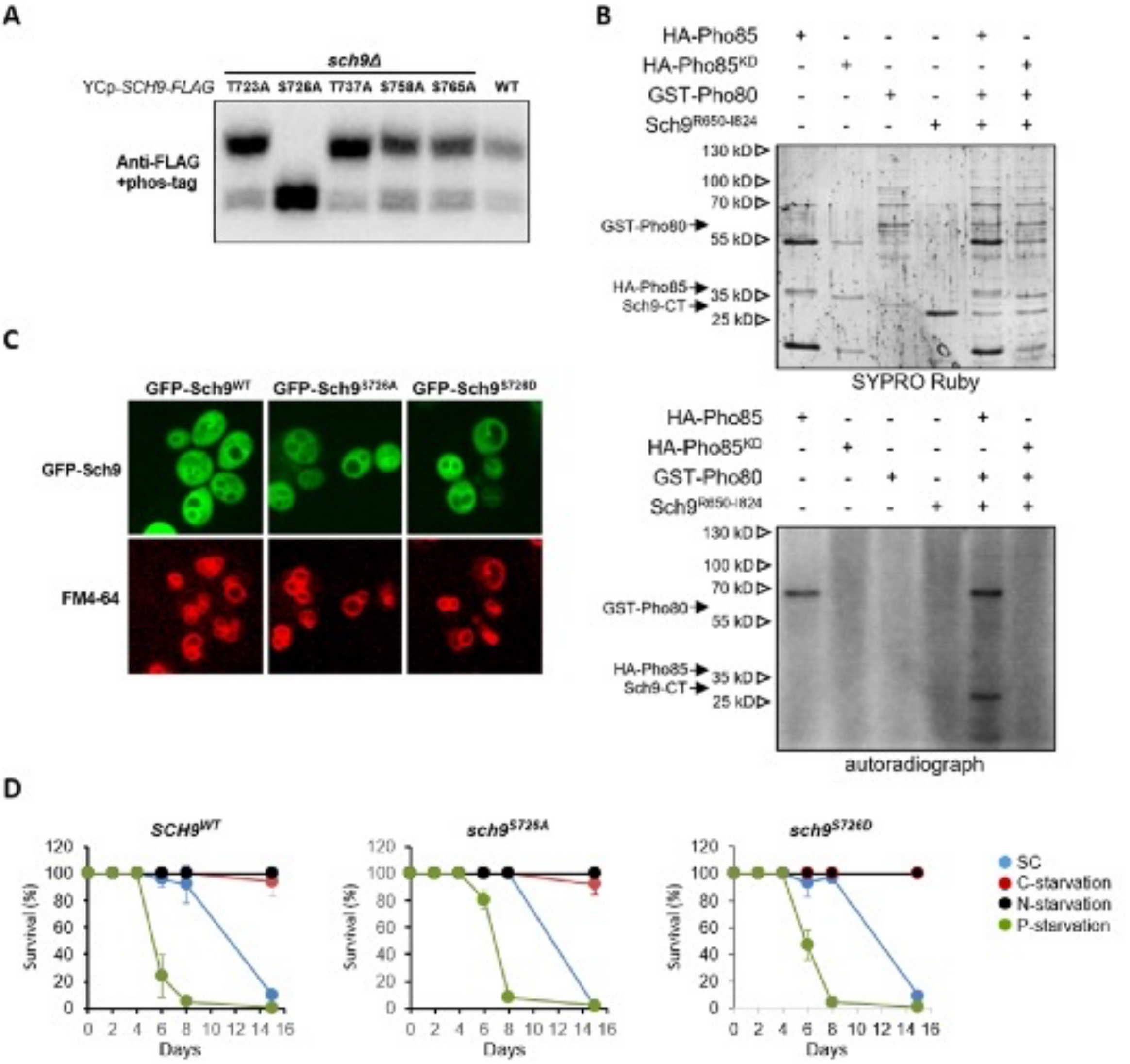

S4 Fig: Pho85-Pho80-mediated phosphorylation of Ser^{726} primes Sch9 for its subsequent activation by TORC1. (A) Phos-tag immunoblot analysis of protein extracts obtained from exponentially growing *sch9Δ* cells transformed with a centromere plasmid allowing for expressing C-terminally FLAG-tagged Sch9^{T723A}, Sch9^{S726A}, Sch9^{T737A}, Sch9^{S758A}, Sch9^{S765A}, or Sch9^{WT} (WT) as indicated. Total protein extracts were resolved on phos-tag gels and were subsequently analyzed via immunoblotting with an anti-FLAG antibody. (B) Setup for the *in vitro* kinase assay to demonstrate phosphorylation of Sch9 by Pho85-Pho80. Various mixtures of purified HA-tagged Pho85 or the kinase dead (KD) Pho85^{E53A} mutant, GST-tagged Pho80, and a TAP-tag purified fragment corresponding to the C-terminus (CT) of Sch9 (Arg^{650} to Ile^{824}) were used. The SYPRO Ruby staining and ^{32}P autoradiograph are shown. (C) Microscopic analysis of WT (BY4741) cells expressing genomically tagged GFP-Sch9^{WT} or the mutant versions GFP-Sch9^{S726A} or GFP-Sch9^{S726D} showing the recruitment at the vacuolar membrane of wild-type Sch9 as well as both Sch9 variants. The strains were grown to mid-log phase on complete synthetic medium. The lipophilic dye FM4-64 was used to visualize the vacuolar membrane. (D) Survival profiles of cells expressing either SCH9^{WT}, Sch9^{S726A} or Sch9^{S726D} when maintained on complete synthetic medium or starved for carbon (C), nitrogen (N) or phosphate (P).

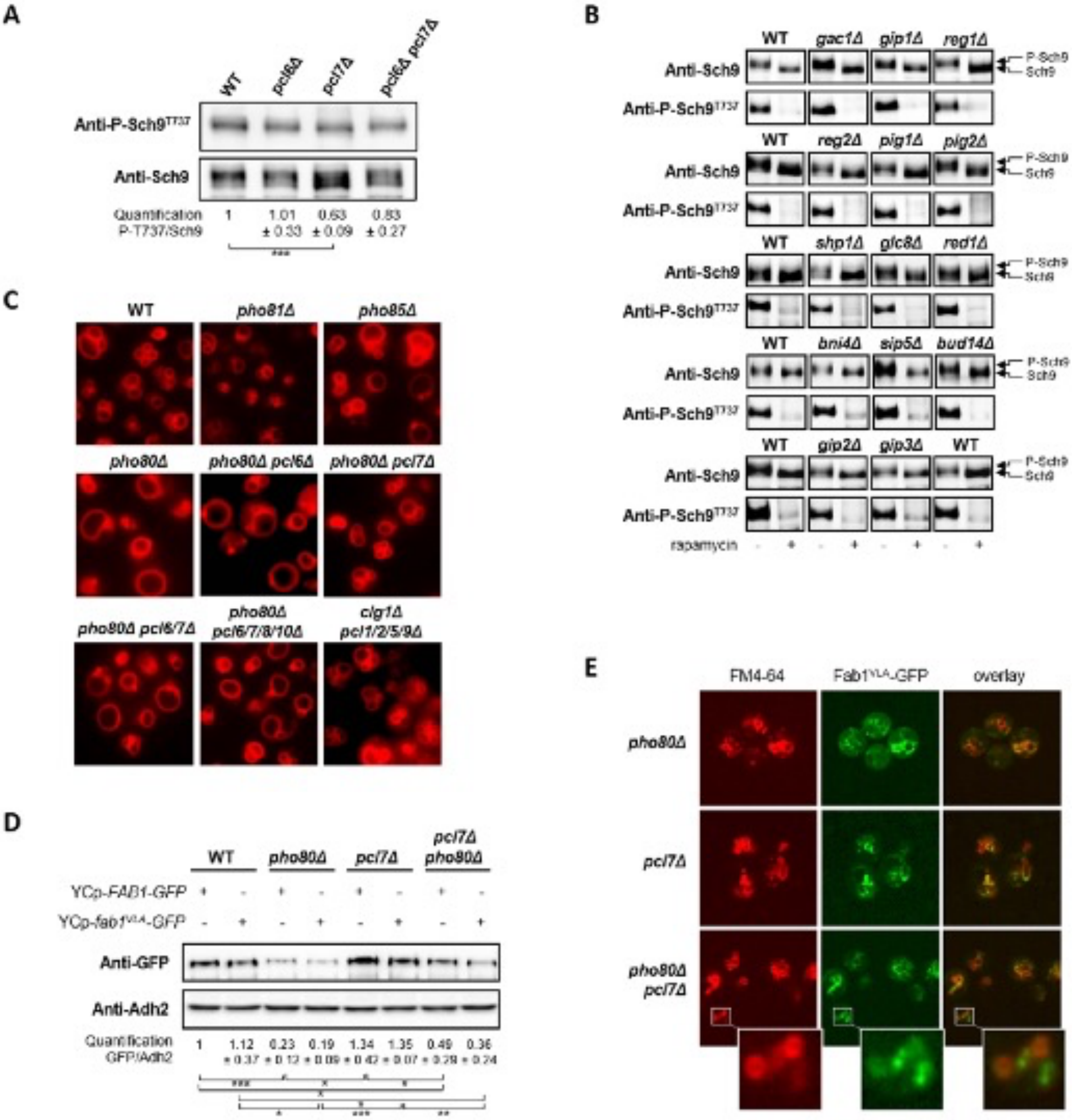
A
WT
pcl6Δ
pcl7Δ
pcl6Δ pcl7Δ
Anti-P-Sch9T737
Anti-Sch9
Quantification P-T737/Sch9
1
1.01 ± 0.33
0.63 ± 0.09
0.83 ± 0.27
***
B
WT
gac1Δ
gip1Δ
reg1Δ
reg2Δ
pig1Δ
pig2Δ
shp1Δ
glc8Δ
red1Δ
bni4Δ
sip5Δ
bud14Δ
gip2Δ
gip3Δ
Anti-Sch9
Anti-P-Sch9T737
P-Sch9
Sch9
rapamycin
C
WT
pho81Δ
pho85Δ
pho80Δ
pho80Δ pcl6Δ
pho80Δ pcl7Δ
pho80Δ pcl6/7Δ
pho80Δ pcl6/7/8/10Δ
clg1Δ pcl1/2/5/9Δ
D
WT
pho80Δ
pcl7Δ
pcl7Δ pho80Δ
YCp-FAB1-GFP
YCp-fab1VLA-GFP
Anti-GFP
Anti-Adh2
Quantification GFP/Adh2
1
1.12 ± 0.37
0.23 ± 0.12
0.19 ± 0.09
1.34 ± 0.42
1.35 ± 0.07
0.49 ± 0.28
0.36 ± 0.24
***
*
**
E
FM4-64
Fab1VLA-GFP
overlay
pho80Δ
pcl7Δ
pho80Δ pcl7Δ

S5 Fig: The Pho85-cyclins Pcl6 and Pcl7 contribute the regulation of Sch9. (A) Immunoblot analysis of protein extracts from the WT, *pcl6Δ*, *pcl7Δ*, and *pcl6Δ pcl7Δ* strains exponentially growing on complete synthetic medium to assess changes in Sch9 phosphorylation. The Sch9-Thr^{737} phosphorylation levels were quantified based on the ratio of the anti-P-Sch9^{T737} and anti-Sch9 signals, and normalized to the ratio obtained for the WT cells. Paired two-tailed student's T tests were used to calculate significances (*, $P < 0.1$; **, $P < 0.01$; ***, $P < 0.001$). (B) Immunoblot analysis of protein extracts of the WT strain and strains lacking non-essential Glc7-interacting proteins. The strains were grown to mid-log phase and were then treated with 200 nM rapamycin. Samples were taken before and after rapamycin treatment for 1 hour. The anti-Sch9 and anti-P-Sch9^{T737} antibodies were used for detection. The difference in mobility of the phosphorylated (P-Sch9) and non-phosphorylated (Sch9) isoforms as detected with the anti-Sch9 antibodies are indicated. (C) FM4-64 staining of the vacuolar membrane to show the difference in vacuolar size between WT cells and cells lacking Pho81, Pho85, or different combinations of Pho85 cyclins. Strains were grown to mid-log phase on complete synthetic medium containing 2% glucose. (D) Immunoblot analysis of the WT, *pho80Δ*, *pcl7Δ*, and *pho80Δ pcl7Δ* strains to compare the expression levels of the Fab1-GFP and Fab1^{VLA}-GFP fusions when introduced on centromere plasmids as based on the ratio of the anti-GFP and anti-Adh2 signals. (E) Microscopic analysis of Fab1^{VLA}-GFP localization in the WT, *pho80Δ*, *pcl7Δ*, and *pho80Δ pcl7Δ* strains. Strains were grown to mid-log phase on selective synthetic medium. The lipophilic dye FM4-64 was used to visualize the vacuolar membrane. The indents are magnifications showing that Fab1^{VLA} mainly localizes in foci at the periphery of small emerging vacuoles.

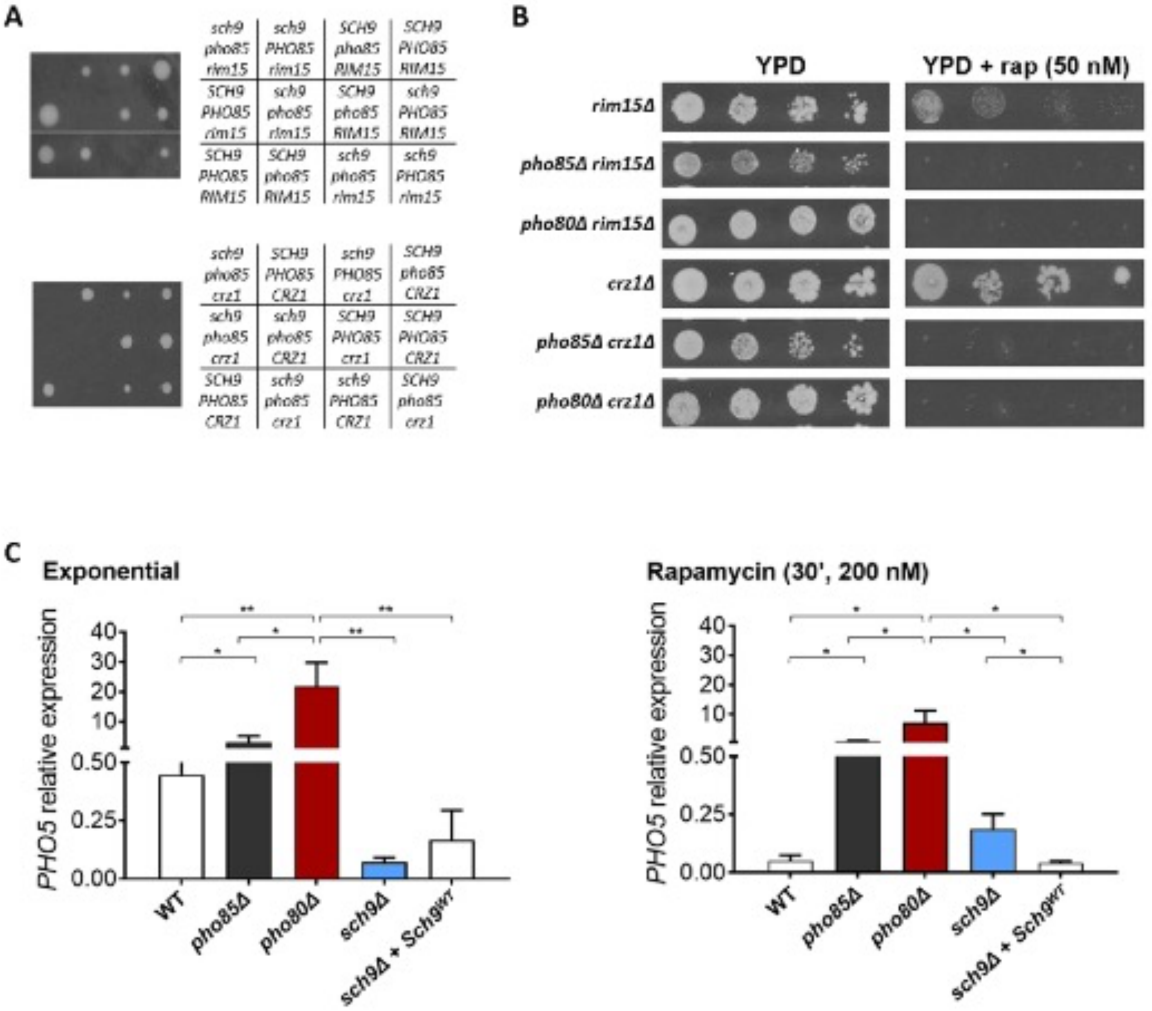

S6 Fig: Analysis of downstream Pho85 effectors for the interplay with TORC1 signaling. (A) Diploids were generated by crossing the haploid *sch9Δ* strain with the *pho85Δ rim15Δ*, or the *pho85Δ crz1Δ* strain followed by genotype analysis of the dissected germinated spores. (B) Rapamycin sensitivity analysis of cells lacking Rim15 or Crz1 in a WT, *pho85Δ*, or *pho80Δ* background as determined by spot assays on YPD plates without or with 50 nM rapamycin. (C) Expression of *PHO5* as determined by RT-PCR in WT, *pho85Δ*, *pho80Δ*, and *sch9Δ* cells carrying an empty vector, or *sch9Δ* cells transformed with a centromere plasmid encoding Sch9^{WT} when grown to mid-logarithmic phase in SD-Ura medium before or after treatment with 200 nM rapamycin for 30 min. The data are represented as mean ± standard deviation. Paired two-tailed student's T tests were used to calculate significances (*, $P < 0.1$; **, $P < 0.01$; ***, $P < 0.001$).

CHAPTER 3:
Identification of spatially distinct pools of SNF1/AMPK and their targets in yeast

3.1. INTRODUCTION

3.1.1. The SNF1 β-subunits

In the budding yeast *Saccharomyces cerevisiae*, Snf1 can associate with three different β-subunits: Gal83 (GALactose metabolism 83), Sip1 (SNF1-Interacting Protein 1), and Sip2 (SNF1-Interacting Protein 2) (Hedbacker & Carlson, 2008). These subunits serve as scaffolds for the interaction between Snf1 and Snf4, regulate the localization of the complex, and are involved in substrate recognition (Sanz et al., 2016). Gal83 plays a crucial role in regulating growth on non-fermentable carbon sources and in invasive growth, Sip1 is involved in meiosis and nitrogen metabolism, and Sip2 is implicated in aging by promoting lifespan (Ashrafi et al., 2000; Hedbacker & Carlson, 2008; Sanz et al., 2016). The β-subunits are essential for *in vivo* Snf1 activity, as the *gal83Δ sip1Δ sip2Δ* mutant exhibits growth defects in media containing galactose, glycerol, raffinose, or ethanol as sole carbon sources (Schmidt & McCartney, 2000). Conversely, strains expressing at least one β-subunit do not show significant growth defects, except for strains expressing only *SIP1*, which display a growth defect on ethanol-glycerol (Schmidt & McCartney, 2000; Zhang et al., 2010).

Gal83, which is considered to be the subunit that is responsible for the majority of the SNF1 activity (Hedbacker et al., 2004a), is the most abundant of the β-subunits (Breker et al., 2013; Chandrashekarappa et al., 2016; Elbing et al., 2006b; Mangat et al., 2010; Vincent et al., 2001) and was initially identified as a protein involved in the regulation of the GAL genes (Hedbacker & Carlson, 2008). Sip1, the least abundant of the β-subunits (Chandrashekarappa et al., 2016), and Sip2, of intermediate abundance (Chandrashekarappa et al., 2016), were identified as Snf1 interactors in yeast two-hybrid screens (Hedbacker & Carlson, 2008). Interestingly, Sip2 levels increase during shifts to non-fermentable carbon sources (Vincent et al., 2001). Gal83 and Sip2 share 55% identity and have similar sizes, with 415 and 417 residues, respectively (Mangat et al., 2010). In contrast, Sip1 is composed of 815 amino acids and has a lower identity percentage (Hedbacker et al., 2004b; Mangat et al., 2010). Its non-conserved N-terminal region is responsible for its low expression level (Hedbacker et al., 2004b; Mangat et al., 2010). Accordingly, in a *sip1*$^{\Delta N}$ mutant, Sip1 is more expressed compared to wild-type levels (Mangat et al., 2010).

The interaction regions between the β-subunits and the α- and γ-subunits have been mapped by Y2H (Yeast Two-Hybrid) analysis, which corroborated their role as scaffolds of the complex (Jiang & Carlson, 1997; Woods et al., 1996). A region named KIS (Kinase Interacting Sequence) has been identified that mediates the interaction with Snf1, while an ASC (Associated with SNF1 Complex domain) domain has been identified for interaction with Snf4

(**Figure 1**) (Hedbacker & Carlson, 2008; Sanz et al., 2016). More recently, the β-subunits have also been shown to contain a Glycogen Binding Domain (GBD), otherwise also known as the Carbohydrate-Binding Module (CBM) (**Figure 1**) (Crozet et al., 2014; Hedbacker & Carlson, 2008; Mangat et al., 2010; Sanz et al., 2016). The KIS domain is located between the GBD and ASC domains (Crozet et al., 2014). The GBD in the yeast β-subunits contains consensus residues that are conserved in AMPKβ1 and that facilitate carbohydrate binding (Hedbacker & Carlson, 2008; Mangat et al., 2010; Sanz et al., 2016): Gal83 can bind glycogen strongly *in vitro*, whereas Sip2 binds it weakly (Hedbacker & Carlson, 2008; Mangat et al., 2010). Evidence also suggests that the GBD negatively regulates the SNF1 complex. For instance, Snf1-Thr^{210} is phosphorylated even under high glucose conditions in strains where the GBD was deleted from *GAL83* (in *sip1Δ sip2Δ*) and hence independently of glycogen binding could not take place (Hedbacker & Carlson, 2008; Sanz et al., 2016). Furthermore, GBD appears crucial for recruiting and binding Glc7-Reg1, which would then dephosphorylate and deactivate Snf1 (Sanz et al., 2016).

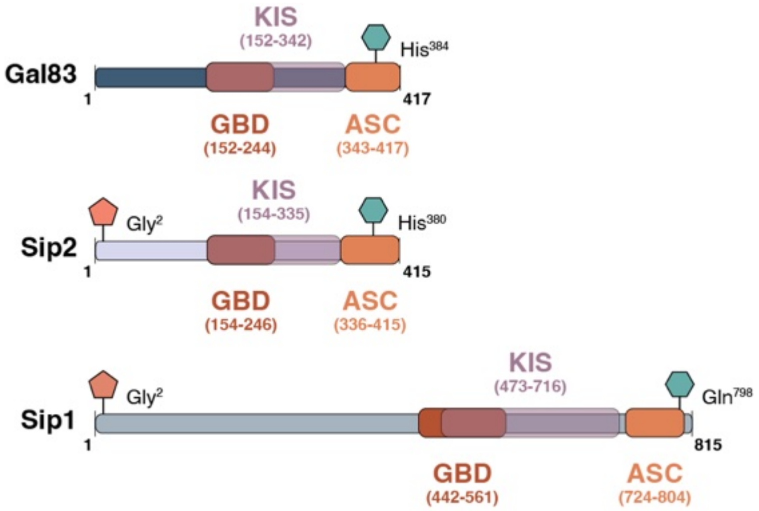

Figure 1. Schematic representation of the structure of the SNF1 β-type subunits.
Scheme depicting the structure of the β-subunits Gal83, Sip1, and Sip2, and their main domains: GBD (Glycogen Binding Domain), KIS (Kinase Interacting Sequence), and ASC (Associated with SNF1 Complex domain). The green hexagons represent the residues that can be modified to alanine to induce the inactivation of the subunit; the orange pentagons indicate the residues that can be myristoylated.

Both Sip1 and Sip2 have been reported to undergo myristoylation (**Figure 1**) (Hedbacker et al., 2004b; Lin et al., 2003). Sip1 is N-myristoylated at Gly^2, enabling its interaction with the vacuolar surface during carbon starvation (Hedbacker et al., 2004b). Interestingly, Sip2 can also be N-myristoylated at Gly^2, but this post-translational modification does not affect its localization during carbon starvation (Lin et al., 2003). In fact, myristoylated Sip2 can associate with the plasma membrane in young cells, while it remains cytosolically enriched in aged cells (Lin et al., 2003). Overall, these myristoylation events are not the sole cause of the β-subunits' localization during carbon starvation (Hedbacker et al., 2004b).

3.1.1.1. The role of the β-subunits in regulating SNF1 localization

The most divergent region among the β-type subunits is the N-terminal portion, which plays a role in regulating the localization of the complex (Vincent et al., 2001) and in substrate recognition (Crozet et al., 2014; Hedbacker & Carlson, 2008). The localization of each β-subunit is independent of their association with Snf1 (Hedbacker et al., 2004b). The SNF1 complex is found in the cytosol during growth in high glucose but relocates to different cellular compartments within 15 minutes after shifting to low glucose (Vincent et al., 2001). Gal83-containing complexes become enriched in the nucleus, Sip1-containing complexes accumulate on the vacuolar surface, and Sip2-containing complexes remain cytosolic (**Figure 2**) (Chandrashekarappa et al., 2016; Hedbacker et al., 2004b; Mangat et al., 2010; Vincent et al., 2001). The enrichment of Snf1-Sip1-Snf4 on the vacuolar membrane was confirmed through both microscopy and vacuole purification followed by proteomics, which also verified the absence of Gal83- and Sip2-containing complexes (Klossel et al., 2024). Additionally, the significance of the N-terminal region for Sip1 localization was demonstrated by fusing the N-terminus of Sip1 with GFP (Hedbacker et al., 2004b). This construct exhibited a localization pattern similar to that of full-length Sip1 (Hedbacker et al., 2004b). Furthermore, in cells expressing only Sip1 (*gal83Δ sip2Δ*) Snf1-GFP localizes to the vacuole during carbon starvation (Hedbacker et al., 2004b).

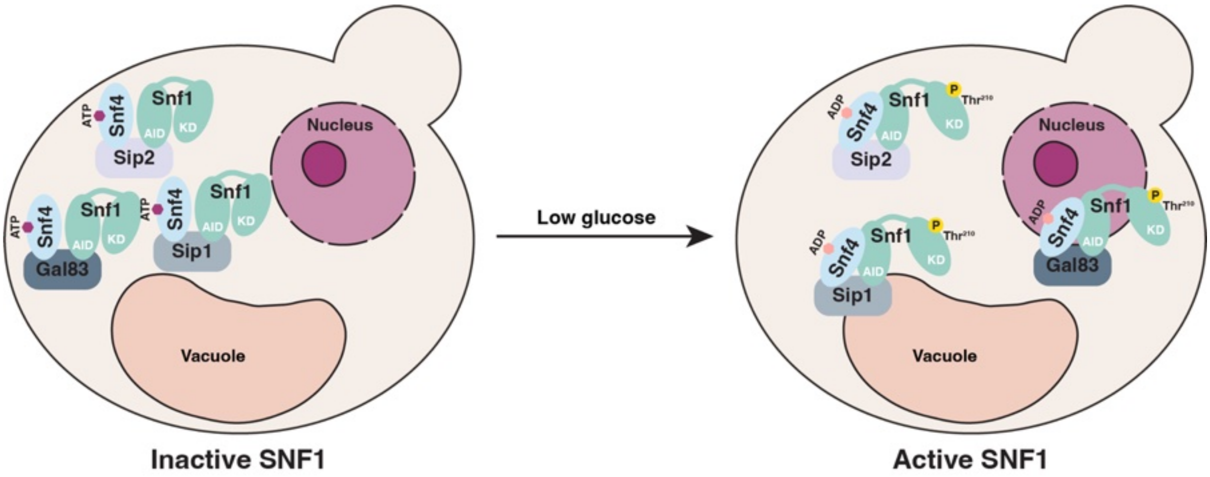

Figure 2. Scheme depicting the localization of the SNF1 complex after glucose depletion.
The SNF1 complex, regardless of the associated β-type subunit, is localized in the cytosol during growth in high glucose (Chandrashekarappa et al., 2016; Hedbacker et al., 2004b; Mangat et al., 2010; Vincent et al., 2001). After carbon starvation, SNF1 relocalizes to the nucleus when associated with Gal83, to the vacuolar surface when associated with Sip1, and remains cytosolic when associated with Sip2 (Chandrashekarappa et al., 2016; Hedbacker et al., 2004b; Mangat et al., 2010; Vincent et al., 2001).

The β-subunit Gal83 is the most extensively studied, likely due to its significant relevance. It was observed that when Snf1 is inactivated through *SAK1* deletion or T210A or K84R mutations, Snf1 could not properly relocalize to the nucleus during carbon starvation (Hedbacker et al., 2004a). Conversely, the localization of Gal83 remained correctly localized in a *sak1Δ snf1Δ* strain grown under the same conditions (Hedbacker et al., 2004a). This suggests that the nuclear enrichment of Snf1 depends on its activity and the presence of Gal83, while the nuclear enrichment of Gal83 appears to be independent of Snf1 and Sak1 activities (Hedbacker et al., 2004a). The N-terminus of Gal83 contains a Nuclear Export Signal (NES), which is also conserved in Sip2 (Vincent et al., 2001). This NES is required for Gal83 export from the nucleus during growth in high glucose, which is mediated by the nuclear export receptor (exportin) Crm1 (Chromosome Region Maintenance 1) (Hedbacker & Carlson, 2006). Additionally, Gal83 seems to contain a Nuclear Localization Signal (NLS), the mutation of which impairs only the localization of C-terminally truncated versions of Gal83, but not the full-length protein (Hedbacker & Carlson, 2006). Thus, Gal83 may either contain a nonclassical NLS or its nuclear import may depend on other unidentified interactors containing an NLS (Hedbacker & Carlson, 2006).

The cytosolic localization of the Snf1-Sip1-Snf4 complex is promoted by PKA, either through direct phosphorylation of Sip1 or via an intermediate protein that may influence its localization (Hedbacker et al., 2004b). Additionally, similar to what was observed for Gal83, Snf1 is not required to induce the relocalization of Sip1 to the vacuolar surface during the shift to low glucose (Hedbacker et al., 2004b).

3.1.1.2. Localization and regulation of AMPK complexes in mammalian cells

In mammalian cells, AMPK is predominantly found in the cytosol, with significant enrichment at mitochondria, lysosomes, and the ER (Gonzalez et al., 2020; Trefts & Shaw, 2021). Growth conditions influence AMPK's interaction with two key regulators of anabolic processes: SREBP1c, which is tethered to the ER and lysosomal membranes, and RAPTOR, a subunit of the mTORC1 complex (Zong et al., 2019). This interaction between AMPK and RAPTOR is also observed in yeast, where Snf1 phosphorylates Kog1 on the vacuolar surface (Hughes Hallett et al., 2015; Sullivan et al., 2019). Additionally, the scaffold and adaptor protein AXIN1 can recruit LKB1 and AMPK to the lysosomal membrane (Gonzalez et al., 2020; Hindupur et al., 2015; Mallick & Gupta, 2021).

Although spatially distinct pools of AMPK are recognized, it is not well understood whether these complexes are differentially regulated or how they might locally influence specific effectors. For instance, AMPKα2 has been observed to be enriched in the nucleus of muscle cells upon exercise (Herzig & Shaw, 2018; Salt et al., 1998; Schmitt et al., 2022), while AMPKβ subunits have been identified as enriched at autophagosomes and mitochondria upon N-myristoylation (Herzig & Shaw, 2018; Liang et al., 2015). Thus, there is still limited data on the localization of the complex and its various isoforms (Steinberg & Hardie, 2023). Nevertheless, it was observed that the different AMPK pools are activated by different stimuli (Zong et al., 2019). For instance, the lysosomal AMPK pool is activated under glucose starvation without changes in AMP:ATP or ADP:ATP ratios, the cytosolic AMPK pool is activated with moderate increases in AMP, independent of the lysosomal pathway but dependent on AXIN1, and the mitochondrial AMPK pool is activated only under severe nutrient stress with high AMP levels, independent of AXIN1 (Zong et al., 2019). In contrast, in yeast cells, there is no evidence of differential activation of the SNF1 pools in response to different stimuli. Conversely, it is known that they exhibit substrate specificity and distinct regulatory roles (Ashrafi et al., 2000; Hedbacker & Carlson, 2008; Sanz et al., 2016).

Notably, it is known that specific AMPK subunit combinations are expressed in particular tissues. For example, in muscles, combinations such as α1β2γ1, α2β2γ1, and α2β2γ3 have been detected, with only the α2β2γ3 variant appearing to be phosphorylated on Thr^{172} upon muscle contraction (Herzig & Shaw, 2018). Thus, different compositions of AMPK subunits allow the various AMPK complexes to respond to different stress stimuli (Herzig & Shaw, 2018).

3.1.1.3. Modulation of SNF1 activity via the β-subunits

In the ASC domain of the β-subunits, two antiparallel β-sheets are preceded by a conserved motif (NHVXNHL) found in all organisms ranging from yeast to mammals (**Figure 3A**) (Chandrashekarappa et al., 2016). These histidine residues interact with the activation loop when Snf1 is phosphorylated on the residue Thr^{210}, stabilizing the kinase's active conformation (Chandrashekarappa et al., 2016). Mutations of the second histidine residues in this conserved motif lead to reduced SNF1 and AMPK activity (Chandrashekarappa et al., 2016; Mayer et al., 2011) and have been reported to inactivate the SNF1 complexes without affecting their assembly (Chandrashekarappa et al., 2016). This phenotype is observed in *gal83*^{H384A} and *sip2*^{H380A} (Chandrashekarappa et al., 2016). For Sip1, mutagenesis of these histidine residues did not cause any phenotype, but a similar effect was seen when a premature stop codon was introduced at position Gln^{798} (**Figure 3B**) (Chandrashekarappa et al., 2016).

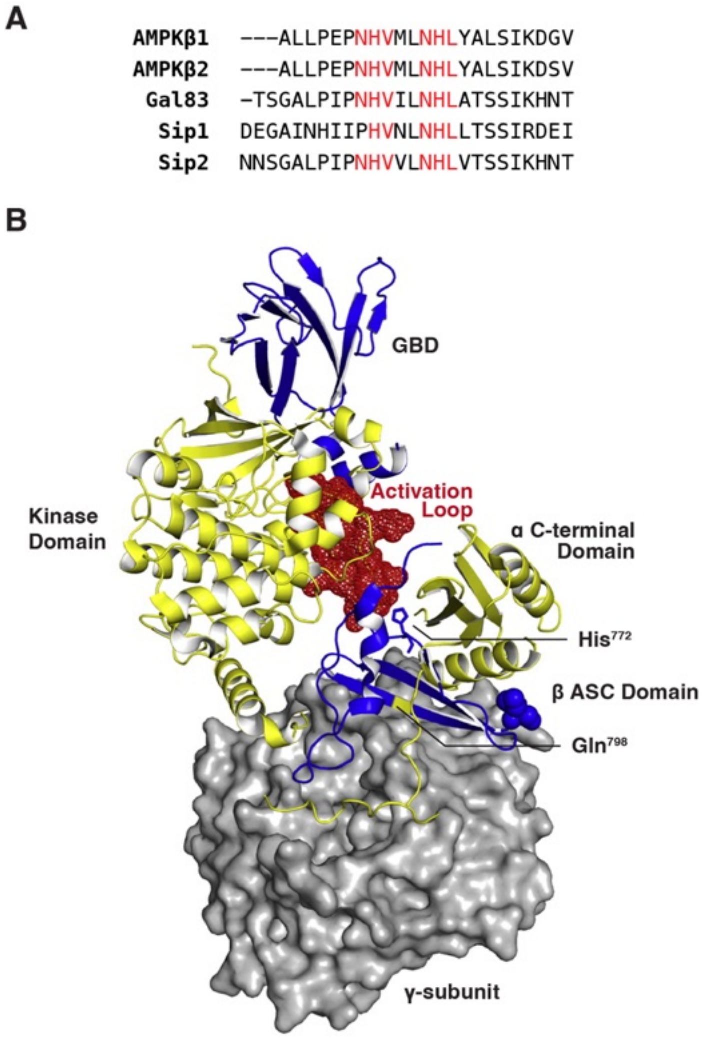

```
AMPKβ1   ---ALLPEPNHVMLNHLYALSIKDGV
AMPKβ2   ---ALLPEPNHVMLNHLYALSIKDSV
 Gal83   -TSGALPIPNHVILNHLATSSIKHNT
  Sip1   DEGAINHIIPHVNLNHLLTSSIRDEI
  Sip2   NNSGALPIPNHVVLNHLVTSSIKHNT
```

Figure 3. Structural model of the SNF1 complex based on the mammalian AMPK.

(**A**) Sequence alignment of the *H. sapiens* (AMPKβ1 and AMPKβ2) and *S. cerevisiae* (Gal83, Sip1, and Sip2) β-subunits. Highlighted in red is the conserved NHVXNHL motif. (**B**) The α-subunit Snf1 and the β-subunit Sip1 are displayed in the cartoon representation in yellow and blue, respectively. The γ-subunit Snf4 is displayed in surface representation in gray. The kinase domain, the C-terminal domain, and the activation loop (in red spheres) of Snf1, and the C-terminus and Glycogen Binding Domain (GBD) of Sip1 are indicated. The position of the residues His772 and Gln798 in Sip1 are accentuated in the structure. (Image adapted from (Chandrashekarappa et al., 2016)).

3.2. RESULTS

3.2.1. Targeted mutagenesis and functional analysis of SNF1 pools in yeast

To identify the specific targets and separately study the activities of the three SNF1 pools (*i.e.* nuclear, vacuolar, and cytosolic), combinations of amino acid substitutions were introduced by CRISPR/Cas9 (Generoso et al., 2016) in the conserved NHVXNHL motif in Gal83 and Sip2, while a premature stop codon was introduced in Sip1 (**Figure 4**) (Chandrashekarappa et al., 2016). Thereby, we generated three independent yeast strains: *sip1*^{Q798*} *sip2*^{H380A}, *gal83*^{H384A} *sip2*^{H380A}, and *gal83*^{H384A} *sip1*^{Q798*}, in which only one β-subunit, and hence one local pool of SNF1, is active and functional.

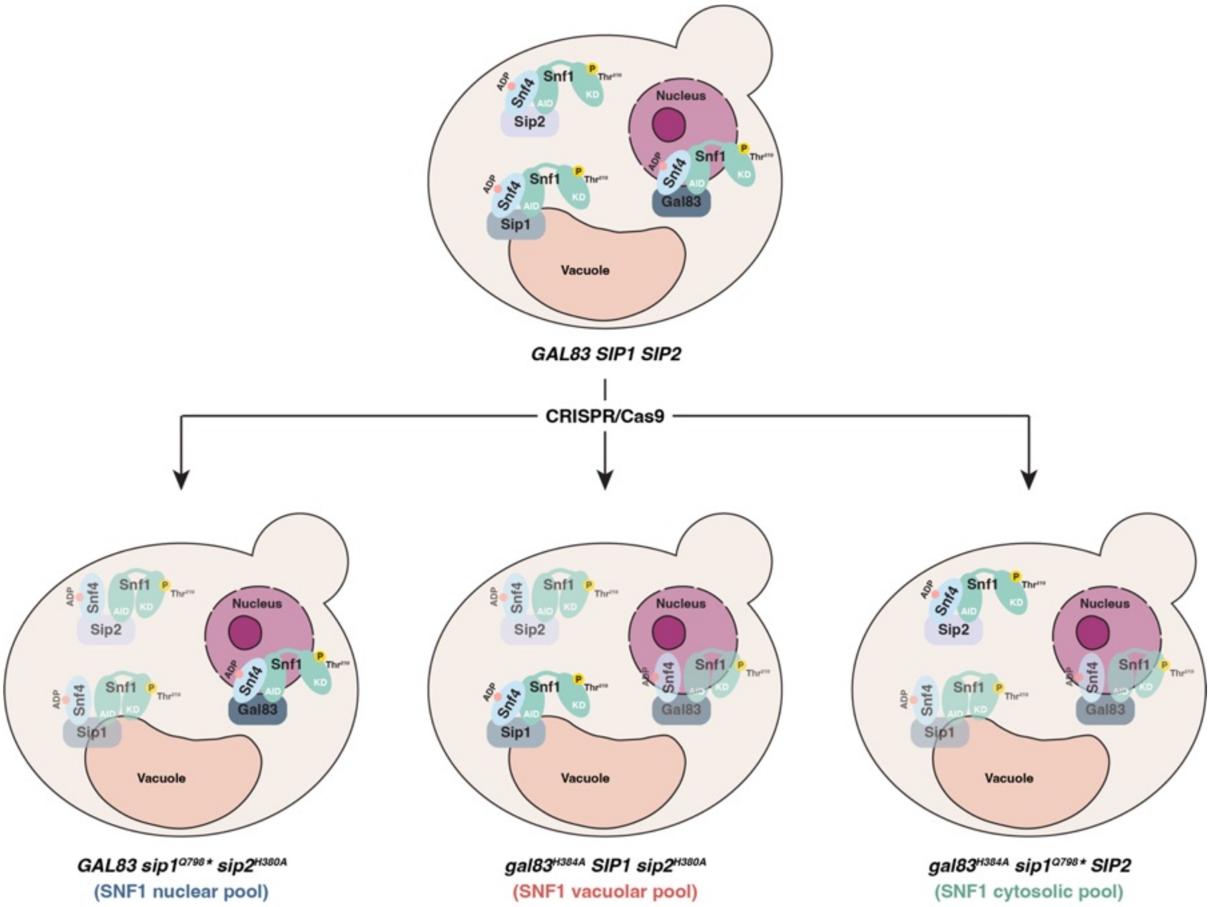
ADP
Snf4
Snf1
P
Thr210
AID
KD
Sip2
Nucleus
Sip1
Gal83
Vacuole
GAL83 SIP1 SIP2
CRISPR/Cas9
GAL83 sip1Q798* sip2H380A
(SNF1 nuclear pool)
gal83H384A SIP1 sip2H380A
(SNF1 vacuolar pool)
gal83H384A sip1Q798* SIP2
(SNF1 cytosolic pool)

Figure 4. Scheme depicting the generation of the SNF1 pool mutants by CRISPR/Cas9.
To study the activity of each SNF1 pool separately, we simultaneously introduced point mutations in two subunits using CRISPR/Cas9, while keeping the third subunit wild-type. This approach allowed us to generate yeast strains in which we could specifically monitor the activity of SNF1 in the nucleus, at the vacuole, or in the cytosol.

SNF1-deficient strains are known to exhibit growth defects on alternative and non-fermentable carbon sources (Ashrafi et al., 2000; Hedbacker & Carlson, 2008; Mayer et al., 2011; Sanz et al., 2016; Zhang et al., 2010). To determine if point mutations in the β-subunits cause aberrant phenotypes, we grew yeast strains with only one functional SNF1 pool, achieved by either deleting two subunits or by rendering two subunits non-functional through point mutations, under restrictive conditions. As expected, strains expressing Gal83 as the sole active β-subunit did not show any growth defects (**Figure 5**), which can be explained by its predominant role in promoting growth on alternative and non-fermentable carbon sources (Chandrashekarappa et al., 2016; Mangat et al., 2010; Vincent et al., 2001). Strains with Sip1 as the only remaining functional subunit exhibited a growth defect on ethanol-glycerol, as previously described (Mayer et al., 2011; Zhang et al., 2010), and a mild defect on 2% sorbitol (**Figure 5**). Additionally, point mutations in *GAL83* and *SIP2* resulted in a mild growth defect on ethanol-glycerol and sorbitol compared to the deletion strains. Finally, strains expressing Sip2 as the only functional subunit showed growth impairment on 2% raffinose (**Figure 6**).

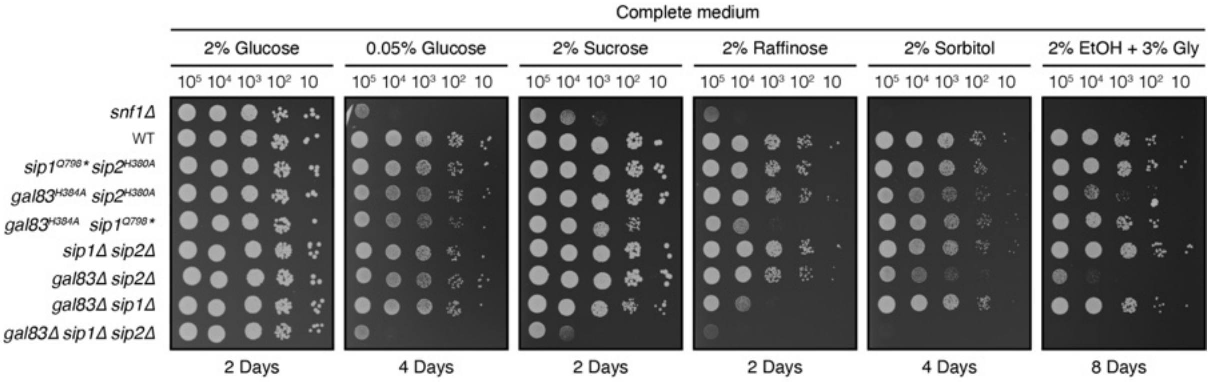
Complete medium
2% Glucose
0.05% Glucose
2% Sucrose
2% Raffinose
2% Sorbitol
2% EtOH + 3% Gly
10⁵ 10⁴ 10³ 10² 10
snf1Δ
WT
sip1^Q798* sip2^H380A
gal83^H384A sip2^H380A
gal83^H384A sip1^Q798*
sip1Δ sip2Δ
gal83Δ sip2Δ
gal83Δ sip1Δ
gal83Δ sip1Δ sip2Δ
2 Days
4 Days
2 Days
2 Days
4 Days
8 Days

Figure 5. The β-subunits have different roles in promoting the growth on alternative or non-fermentable carbon sources.

Exponentially growing cells of the indicated genotype were 10-fold serially diluted and spotted on complete media supplemented with different carbon sources for the number of days indicated at 30 °C (n=2).

Given that these strains behaved as expected, we investigated whether the remaining functional β-subunit properly localized after the shift to a carbon-depleted medium. To test this, we created yeast strains with either Snf1 or each β-subunit genomically tagged with GFP and combined these with the deletion or inactivation of the two remaining β-subunits. These strains also expressed genomically tagged *VPH1-mCherry*, serving as a vacuolar marker, or a single copy of integrated *SV40-NLS-3xmScarlet*, serving as a nuclear marker. The GFP-tagged proteins were properly expressed, with Gal83 being the most abundant of the β-subunits, as previously described (**Figures 6A-6D**) (Breker et al., 2013; Chandrashekarappa et al., 2016). Furthermore, the levels of the tagged β-subunits did not change when the other two β-subunits were deleted or mutated (**Figures 6A-6D**). Additionally, the co-expression of *VPH1-mCherry* (**Figures 6A and 6B**) or *SV40-NLS-3xmScarlet* (**Figures 6C and 6D**) did not affect the relative levels of the β-subunits. Finally, we also confirmed that Snf1 is more abundant than the β-subunits, consistent with previous observations (Breker et al., 2013).

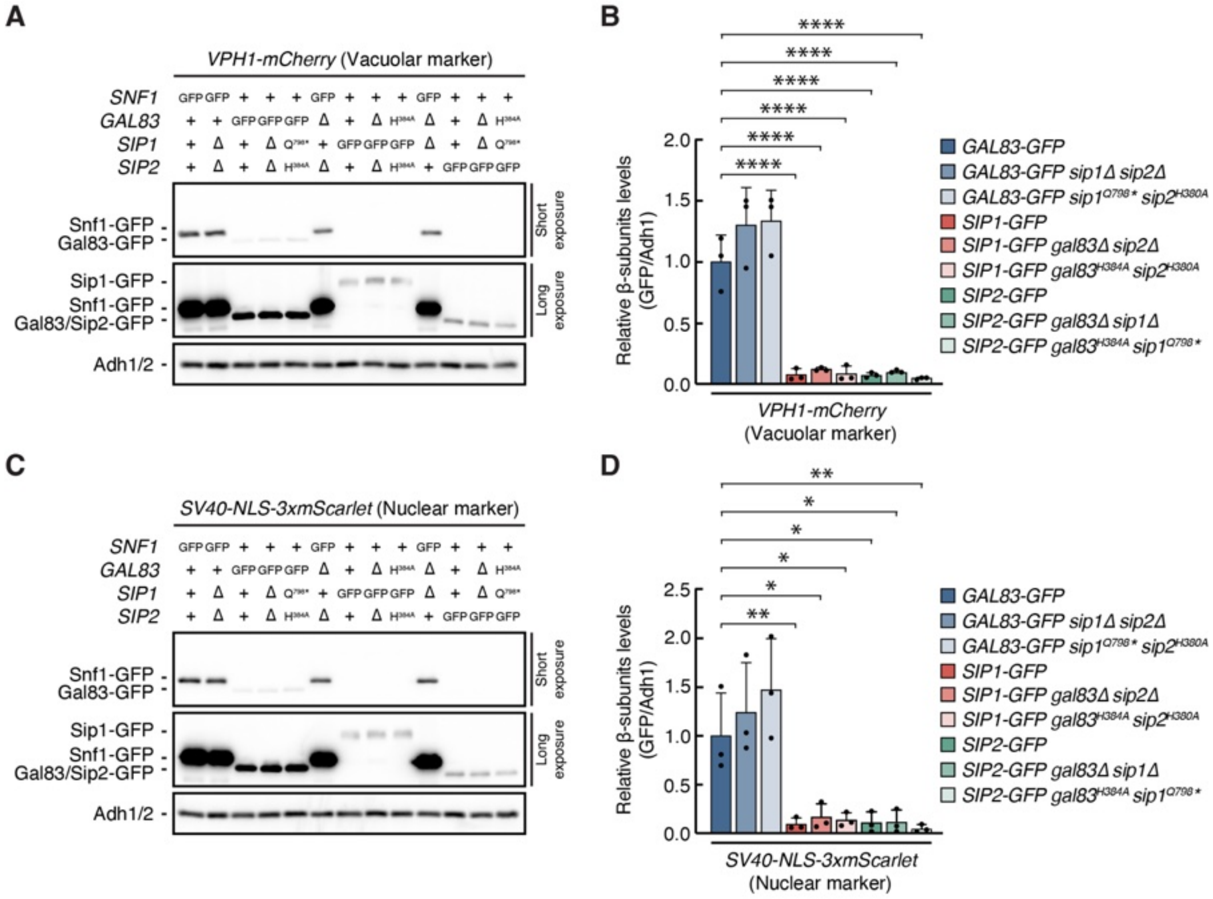

Figure 6. The levels of GFP-tagged β-subunits are not affected by the deletion or mutation of the other two β-subunits.

α- and β-subunits were GFP genomically tagged in yeast strains expressing genomically m-Cherry tagged Vph1 (**A** and **B**) or *SV40-NLS-3xmScarlet* expressed from a single-copy integrative plasmid (**C** and **D**). Cells were grown exponentially in SC medium. Snf1-GFP, Gal83-GFP, Sip1-GFP, and Sip2-GFP levels were detected by immunoblot analyses of whole cell extracts using anti-GFP antibodies. Anti-ADH antibodies were used to detect Adh1/2 as a loading control. (**A**) Immunoblots of cells co-expressing Vph1-mCherry. (**B**) The mean relative β-subunit levels (GFP/Adh1) were quantified, normalized relative to Gal83-GFP expressing WT cells, and shown in the bar diagrams (n=3; + SD; paired Student's t-test, ****$p \leq 0.00005$). (**C**) Immunoblots of cells co-expressing *SV40-NLS-3xmScarlet*. (**D**) The mean relative β-subunit levels (GFP/Adh1) were quantified, normalized relative to Gal83-GFP expressing WT cells, and shown in the bar diagrams (n=3; + SD; paired Student's t-test, *$p \leq 0.05$, **$p \leq 0.005$).

We initially confirmed that Snf1 is cytosolic during growth in high glucose and becomes enriched in the nucleus after the shift to a carbon-depleted medium, as evidenced by its colocalization with the nuclear marker SV40-NLS-3xmScarlet (**Figures 7A and 7B**) (Vincent et al., 2001).

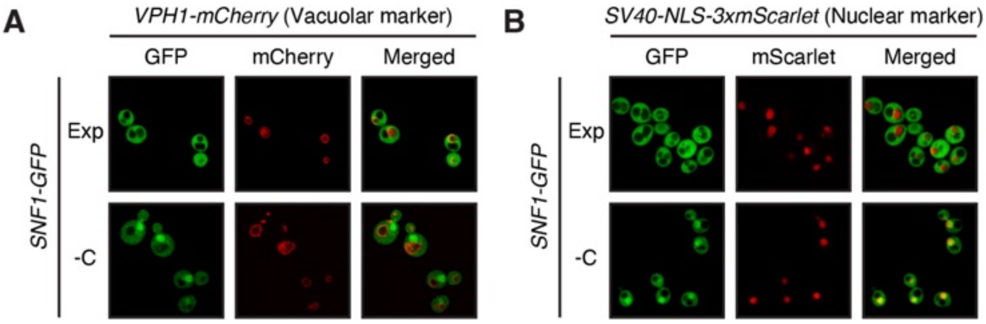
A
VPH1-mCherry (Vacuolar marker)
GFP
mCherry
Merged
SNF1-GFP
Exp
-C
B
SV40-NLS-3xmScarlet (Nuclear marker)
GFP
mScarlet
Merged
SNF1-GFP
Exp
-C

Figure 7. Nuclear enrichment of Snf1 in carbon-starved cells.
Microscopic analysis of Snf1-GFP localization. Strains were grown to exponential phase (Exp) in SC medium and then starved for glucose (-C) for 15 minutes. Vph1-mCherry served as a vacuolar marker (**A**), while SV40-NLS-3xmScarlet was used as a nuclear marker (**B**).

We then monitored the localization of Gal83, Sip1, and Sip2 in glucose-rich conditions and after glucose starvation. As previously described (Chandrashekarappa et al., 2016; Hedbacker et al., 2004b; Vincent et al., 2001), Gal83 relocated to the nucleus after carbon starvation, independently of the presence or mutation of Sip1 and Sip2 (**Figures 8A and 9A**). Snf1, in cells expressing only Gal83, also became enriched in the nucleus (**Figures 8A and 9A**). Sip1 relocated to the vacuolar surface, independently of the presence or mutation of Gal83 and Sip2 (**Figures 8B and 9B**). Interestingly, Snf1, when in complex only with Sip1, also became enriched on the vacuolar surface (**Figures 8A and 9A**). Notably, due to the low levels of Sip1, and Snf1-Sip1 complexes in wild-type cells, it may be difficult to appreciate the enrichment of Snf1 on the vacuole. However, this enrichment is clearly observable in cells where Snf1 can associate exclusively with Sip1, as previously noted (Hedbacker et al., 2004b). The absence of Gal83, which normally directs Snf1 to the nucleus, likely allows for this vacuolar enrichment to be observed. Finally, Sip2 shows proper localization, being constitutively cytosolic, independently of the presence or mutation of Gal83 and Sip1 (**Figures 8C and 9C**). Also in this case, Snf1, in cells expressing only Sip2, behaves similarly to the remaining subunit, staying in the cytosol after the shift to a carbon-depleted medium (**Figures 8C and 9C**).

Although we observed the enrichment of β-subunits in specific subcellular compartments, it is important to note that significant fractions of Gal83- and Sip1-containing SNF1 complexes remain cytosolic during acute carbon starvation, consistent with previous findings (Chandrashekarappa et al., 2016; Hedbacker et al., 2004b; Vincent et al., 2001).

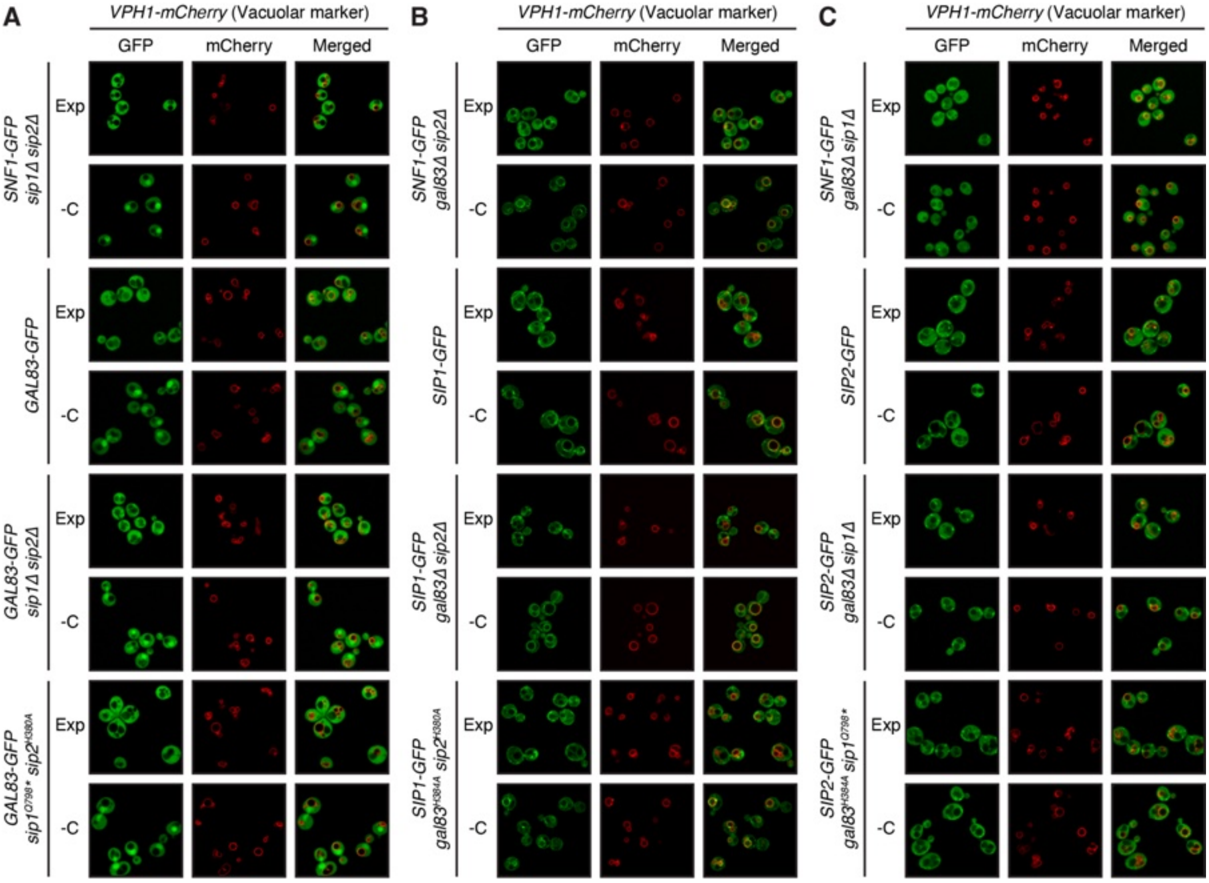
A
B
C
VPH1-mCherry (Vacuolar marker)
GFP
mCherry
Merged
Exp
-C
SNF1-GFP sip1Δ sip2Δ
GAL83-GFP
GAL83-GFP sip1Δ sip2Δ
GAL83-GFP sip1Q798* sip2H380A
SNF1-GFP gal83Δ sip2Δ
SIP1-GFP
SIP1-GFP gal83Δ sip2Δ
SIP1-GFP gal83H384A sip2H380A
SNF1-GFP gal83Δ sip1Δ
SIP2-GFP
SIP2-GFP gal83Δ sip1Δ
SIP2-GFP gal83H384A sip1Q798*

Figure 8. Localization of β-subunits in carbon-starved cells, using Vph1-mCherry as a vacuolar marker.

(**A**) Microscopic analysis of the Gal83-containing SNF1 complex. Snf1-GFP and Gal83-GFP localization was observed in strains where the other two β-subunits were either wild-type (WT), deleted (*sip1Δ sip2Δ*), or inactivated by point mutation (*sip1*^{Q798*} *sip2*^{H380A}). Strains were grown to exponential phase (Exp) in SC medium and starved for glucose (-C) for 15 minutes. Genomically tagged Vph1-mCherry served as a vacuolar marker. (**B**) Microscopic analysis of the Sip1-containing SNF1 complex. Snf1-GFP and Sip1-GFP localization was observed in strains where the other two β-subunits were either WT, deleted (*gal83Δ sip2Δ*), or inactivated by point mutation (*gal83*^{H384A} *sip2*^{H380A}). Strains were grown to exponential phase (Exp) in SC medium and starved for glucose (-C) for 15 minutes. Genomically tagged Vph1-mCherry served as a vacuolar marker. (**C**) Microscopic analysis of the Sip2-containing SNF1 complex. Snf1-GFP and Sip2-GFP localization was observed in strains where the other two β-subunits were either WT, deleted (*gal83Δ sip1Δ*), or inactivated by point mutation (*gal83*^{H384A} *sip1*^{Q798*}). Strains were grown to exponential phase (Exp) in SC medium and starved for glucose (-C) for 15 minutes. Genomically tagged Vph1-mCherry served as a vacuolar marker.

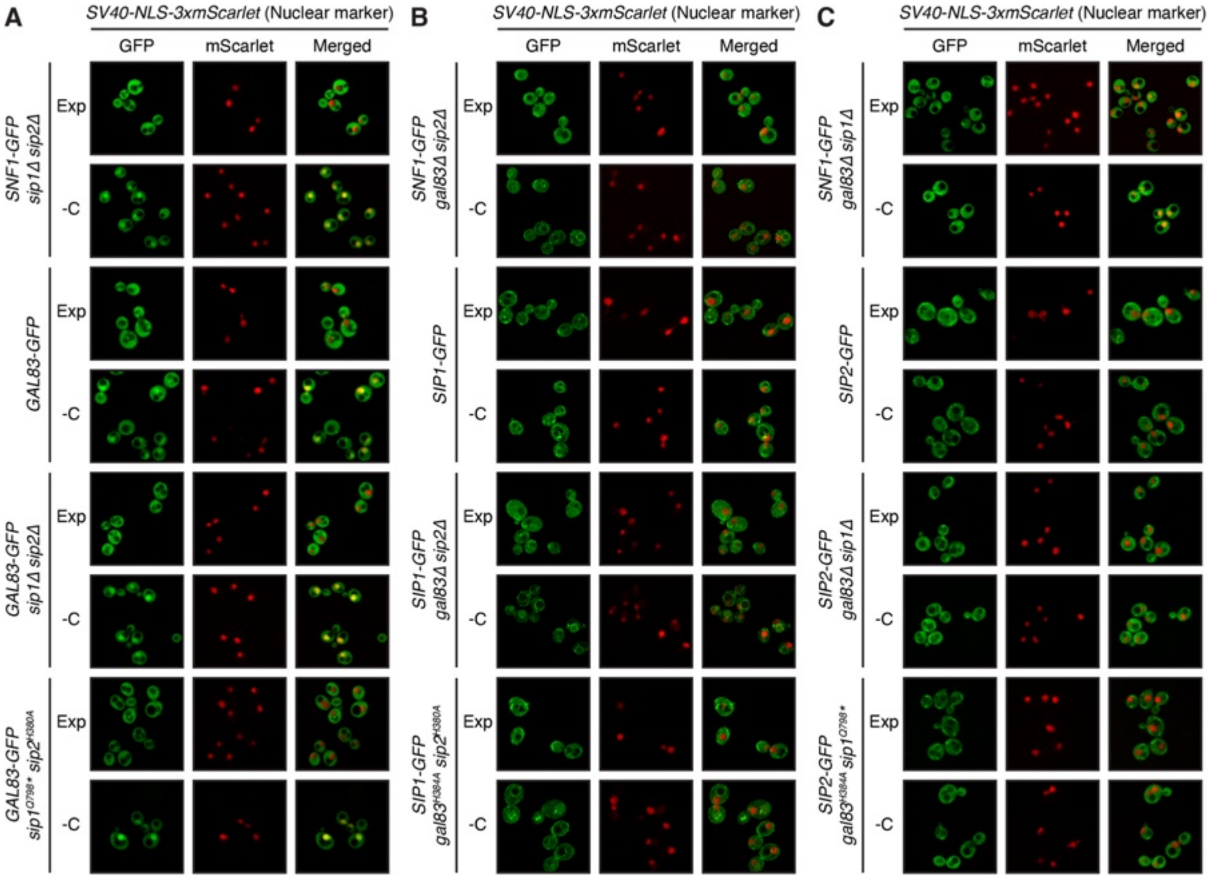
A
SV40-NLS-3xmScarlet (Nuclear marker)
GFP
mScarlet
Merged
SNF1-GFP sip1Δ sip2Δ
Exp
-C
GAL83-GFP
GAL83-GFP sip1Δ sip2Δ
GAL83-GFP sip1Q798* sip2H380A
B
SV40-NLS-3xmScarlet (Nuclear marker)
GFP
mScarlet
Merged
SNF1-GFP gal83Δ sip2Δ
SIP1-GFP
SIP1-GFP gal83Δ sip2Δ
SIP1-GFP gal83H384A sip2H380A
C
SV40-NLS-3xmScarlet (Nuclear marker)
GFP
mScarlet
Merged
SNF1-GFP gal83Δ sip1Δ
SIP2-GFP
SIP2-GFP gal83Δ sip1Δ
SIP2-GFP gal83H384A sip1Q798*

Figure 9. Localization of β-subunits in carbon-starved cells, using SV40-NLS-3xmScarlet as a nuclear marker.

(**A**) Microscopic analysis of the Gal83-containing SNF1 complex. Snf1-GFP and Gal83-GFP localization was observed in strains where the other two β-subunits were either wild-type (WT), deleted (*sip1Δ sip2Δ*), or inactivated by point mutation (*sip1*^{Q798*} *sip2*^{H380A}). Strains were grown to exponential phase (Exp) in SC medium and starved for glucose (-C) for 15 minutes. *SV40-NLS-3xmScarlet* expressed from a single-copy integrative plasmid served as a nuclear marker. (**B**) Microscopic analysis of the Sip1-containing SNF1 complex. Snf1-GFP and Sip1-GFP localization was observed in strains where the other two β-subunits were either WT, deleted (*gal83Δ sip2Δ*), or inactivated by point mutation (*gal83*^{H384A} *sip2*^{H380A}). Strains were grown to exponential phase (Exp) in SC medium and starved for glucose (-C) for 15 minutes. *SV40-NLS-3xmScarlet* expressed from a single-copy integrative plasmid served as a nuclear marker. (**C**) Microscopic analysis of the Sip2-containing SNF1 complex. Snf1-GFP and Sip2-GFP localization was observed in strains where the other two β-subunits were either WT, deleted (*gal83Δ sip1Δ*), or inactivated by point mutation (*gal83*^{H384A} *sip1*^{Q798*}). Strains were grown to exponential phase (Exp) in SC medium and starved for glucose (-C) for 15 minutes. *SV40-NLS-3xmScarlet* expressed from a single-copy integrative plasmid served as a nuclear marker.

Overall, we observed that inactivating the β-subunits through point mutations mimics the effects of the respective full gene deletions, and that the remaining active β-subunit continues to perform its functions, localizes correctly, and does not compensate for the loss of the other subunits.

3.2.2. Targeted localization and activity of SNF1-specific probes in yeast cellular compartments

To ensure that the newly created strains, in which only one β-type subunit remains wild-type, are active in specific cellular compartments, we generated SNF1-specific probes for various subcellular localizations, similarly to what has been recently done in human cells (Schmitt et al., 2022). We utilized the extensively used ACC1-GFP-HA reporter of SNF1 activity, which consists of 13 amino acids from rat ACC1 expressed in tandem, followed by GFP and HA to monitor its levels (Deroover et al., 2016). This probe can be phosphorylated in yeast by SNF1, and its phosphorylation can be detected by immunoblot using an anti-ACC1-pSer^{79} specific antibody. Originally expressed from a multicopy plasmid, we cloned it into a single-copy integrative plasmid (referred to as ACC1^{Probe}) (**Figure 10A**) to avoid fluctuations in expression within cell populations. Fluorescence microscopy revealed that this probe localizes to both the nucleus and the cytosol (**Figure 10B**), making it difficult to distinguish its phosphorylation by different SNF1 pools. However, we demonstrated that this reporter, expressed from a genomic locus, is still specifically phosphorylated by SNF1 (**Figures 10C and 10D**), similar to the previous version expressed from multicopy plasmids (Caligaris et al., 2023a; Deroover et al., 2016).

To further refine this construct, we added different localization sequences at its C-terminus: a nuclear export signal (ACC1^{Probe}-NES) to localize it primarily outside the nucleus in the cytosol (**Figure 10E and 10F**), the N-terminal domain (Met^{1}-Ser^{63}) of the Pho8 protein (ACC1^{Probe}-Pho8^{N}) to localize it to the vacuolar surface (**Figure 10I and 10J**), and a nuclear localization sequence (ACC1-GFP-HA-NLS) to localize it mainly within the nucleus (**Figure 10M and 10N**). The latter version of the probe was enriched in the nucleus but still showed a significant cytosolic fraction, perhaps due to diffusion outside the nucleus because of its small size (~31 kDa). Therefore, we modified it by adding two more GFPs, creating a stably nuclear-localized version of the probe (ACC1-3xGFP-HA-NLS, referred to as ACC1^{Probe}-NLS) (**Figure 10N**).

These probes (*i.e.* ACC1^{Probe}-NES, ACC1^{Probe}-Pho8^{N}, and ACC1^{Probe}-NLS) were expressed in wild-type and *snf1Δ* cells to probe their phosphorylation upon shift to carbon-depleted medium. We observed a complete lack of phosphorylation at Ser^{79} in the absence of

SNF1 (**Figures 10G-H, 10K-L, and 10O-P**). Interestingly, the vacuolar probe showed prephosphorylation during exponential phase in both strains, suggesting that another vacuolar kinase, active under glucose- and amino acid-rich conditions, can recognize and phosphorylate this short amino acid stretch (**Figures 10K and 10L**). Nevertheless, we observed an increase in its phosphorylation upon carbon starvation, with a significant defect in *snf1Δ* strains, allowing us to use it to probe SNF1 activity at the vacuole.

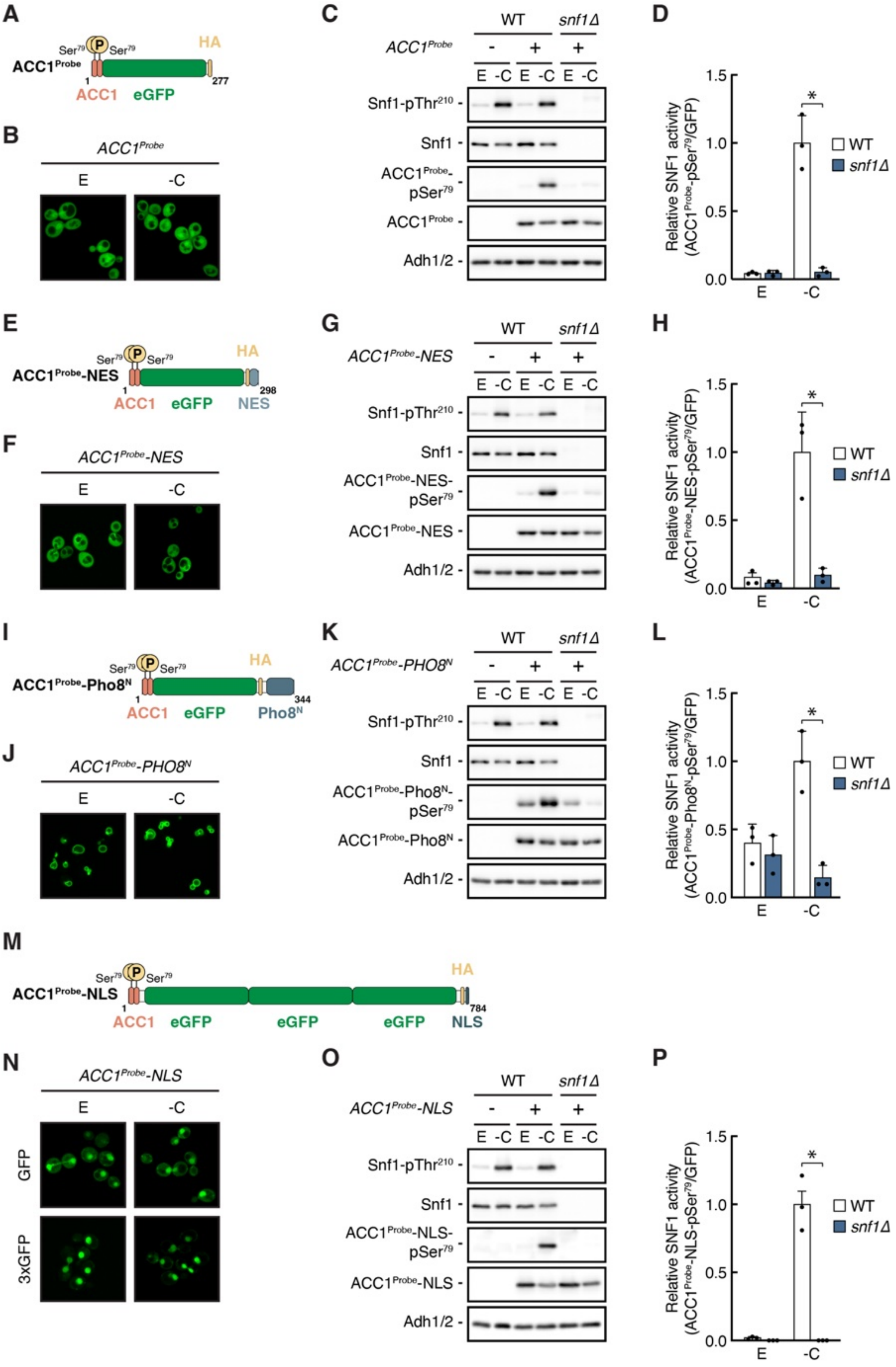
A
Ser79 P Ser79
HA
ACC1Probe
1
277
ACC1 eGFP
B
ACC1Probe
E -C
C
WT snf1Δ
ACC1Probe - + +
E -C E -C E -C
Snf1-pThr210
Snf1
ACC1Probe-pSer79
ACC1Probe
Adh1/2
D
Relative SNF1 activity (ACC1Probe-pSer79/GFP)
1.5 1.0 0.5 0.0
*
WT
snf1Δ
E -C
E
ACC1Probe-NES
298
ACC1 eGFP NES
F
ACC1Probe-NES
G
ACC1Probe-NES
ACC1Probe-NES-pSer79
H
Relative SNF1 activity (ACC1Probe-NES-pSer79/GFP)
I
ACC1Probe-Pho8N
344
ACC1 eGFP Pho8N
J
ACC1Probe-PHO8N
K
ACC1Probe-PHO8N
ACC1Probe-Pho8N-pSer79
ACC1Probe-Pho8N
L
Relative SNF1 activity (ACC1Probe-Pho8N-pSer79/GFP)
M
ACC1Probe-NLS
784
ACC1 eGFP eGFP eGFP NLS
N
ACC1Probe-NLS
GFP
3xGFP
O
ACC1Probe-NLS
ACC1Probe-NLS-pSer79
P
Relative SNF1 activity (ACC1Probe-NLS-pSer79/GFP)

Figure 10. Specific phosphorylation of ACC1^{Probes} by SNF1.

ACC1^{Probe} versions (*ACC1*^{Probe}, *ACC1*^{Probe}*-NES*, *ACC1*^{Probe}*-PHO8*^{N}, *ACC1-GFP-HA-NLS*, and *ACC1*^{Probe}*-NLS*) were expressed from a single-copy integrative plasmid in WT and *snf1Δ* strains. Cells were grown to exponential phase (E) in SC medium and starved for glucose (-C) for 15 minutes. Correct localization of the ACC1^{Probes} was observed by fluorescence microscopy. The residue Thr^{210} in Snf1 and the SNF1 target residue Ser^{79} in ACC1^{Probes} were detected by immunoblot analyses of whole cell extracts using phospho-specific antibodies against the respective phospho-residues. Anti-His$_6$ and anti-GFP antibodies were used to detect the levels of Snf1 and ACC1^{Probe}, respectively. Anti-ADH antibodies were used to detect Adh1/2 as a loading control. (**A**) Scheme depicting the structure of the ACC1^{Probe} and its domains: ACC1 (portion of rat ACC1 repeated in tandem), eGFP, and HA. The yellow circle represents the phosphorylated residue Ser^{79} in ACC1. (**B**) Microscopic analysis of the ACC1^{Probe} localization. (**C**) Immunoblots of cells expressing ACC1^{Probe}. (**D**) The mean relative SNF1 activity (ACC1-pSer^{79}/GFP) was quantified, normalized relative to WT cells in -C, and shown in bar diagrams (n=3; + SD; paired Student's t-test, *$p \leq 0.05$). (**E**) Scheme depicting the structure of the ACC1^{Probe}-NES and its domains: ACC1 (portion of rat ACC1 repeated in tandem), eGFP, and HA. The yellow circle represents the phosphorylated residue Ser^{79} in ACC1. (**F**) Microscopic analysis of the ACC1^{Probe}-NES localization. (**G**) Immunoblots of cells expressing the ACC1^{Probe}-NES. (**H**) The mean relative SNF1 activity (ACC1-pSer^{79}/GFP) was quantified, normalized relative to WT cells in -C, and shown in bar diagrams (n=3; + SD; paired Student's t-test, *$p \leq 0.05$). (**I**) Scheme depicting the structure of the ACC1^{Probe}-Pho8^{N} and its domains: ACC1 (portion of rat ACC1 repeated in tandem), eGFP, and HA. The yellow circle represents the phosphorylated residue Ser^{79} in ACC1. (**J**) Microscopic analysis of the ACC1^{Probe}-Pho8^{N} localization. (**K**) Immunoblots of cells expressing the ACC1^{Probe}-PHO8^{N}. (**L**) The mean relative SNF1 activity (ACC1-pSer^{79}/GFP) was quantified, normalized relative to WT cells in -C, and shown in bar diagrams (n=3; + SD; paired Student's t-test, *$p \leq 0.05$). (**M**) Scheme depicting the structure of the ACC1^{Probe}-NLS and its domains: ACC1 (portion of rat ACC1 repeated in tandem), eGFP, and HA. The yellow circle represents the phosphorylated residue Ser^{79} in ACC1. (**N**) Microscopic analysis of the ACC1-GFP-HA-NLS and the ACC1^{Probe}-NLS localization. (**O**) Immunoblots of cells expressing the ACC1^{Probe}-NLS. (**P**) The mean relative SNF1 activity (ACC1-pSer^{79}/GFP) was quantified, normalized relative to WT cells in -C, and shown in bar diagrams (n=3; + SD; paired Student's t-test, *$p \leq 0.05$).

3.2.3. Functional analysis of SNF1 pools in yeast via monitoring ACC1^{Probes}

We proceeded to express the newly generated ACC1^{Probes} (*i.e.* ACC1^{Probe}-NES, ACC1^{Probe}-Pho8^{N}, and ACC1^{Probe}-NLS) in yeast strains containing only one functional SNF1 pool, accomplished by either deleting or mutating two β-subunits as above. This approach allows us to monitor the activity of each SNF1 pool within different cellular compartments and observe any differential activity between strains with deleted or mutated β-subunits.

Upon carbon starvation, the cytosolic probe did not show a significant difference in phosphorylation in mutants expressing only SNF1 pools with Gal83, regardless of the method used to inactivate the other two remaining subunits (**Figures 11A and 11B**). Conversely, cells expressing only SNF1 pools with Sip1 or Sip2 exhibited significantly lower phosphorylation of the ACC1^{Probe}-NES compared to Gal83-positive strains (**Figures 11A and 11B**). This is likely because Sip1 and Sip2 are present in only a lower fraction of SNF1 complexes due to their low abundance, leading to an overall reduction in the total number of active SNF1 complexes in these strains. Additionally, the capability of all the pools to be able to phosphorylate the cytosolic probe is not surprising, considering that a significant fraction of each SNF1 pool remains cytosolic upon carbon starvation, allowing them to encounter and phosphorylate the ACC1^{Probe}-NES (**Figures 8A-C and 9A-C**).

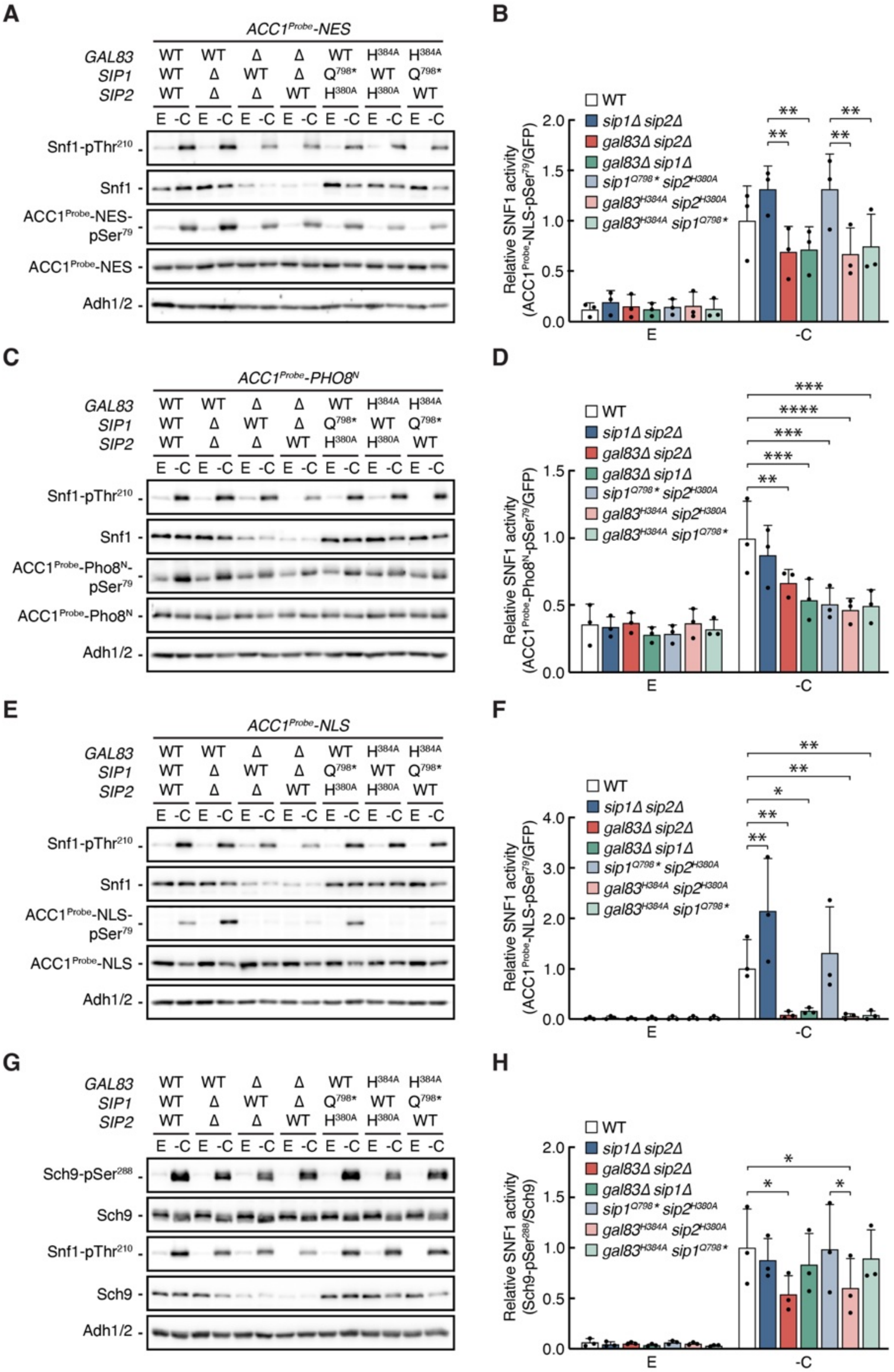
A
ACC1Probe-NES
GAL83 WT WT Δ Δ WT H384A H384A
SIP1 WT Δ WT Δ Q798* WT Q798*
SIP2 WT Δ Δ WT H380A H380A WT
E -C E -C E -C E -C E -C E -C E -C
Snf1-pThr210
Snf1
ACC1Probe-NES-pSer79
ACC1Probe-NES
Adh1/2
B
WT
sip1Δ sip2Δ
gal83Δ sip2Δ
gal83Δ sip1Δ
sip1Q798* sip2H380A
gal83H384A sip2H380A
gal83H384A sip1Q798*
Relative SNF1 activity (ACC1Probe-NLS-pSer79/GFP)
0.0 0.5 1.0 1.5 2.0
E -C
** ** ** **
C
ACC1Probe-PHO8N
GAL83 WT WT Δ Δ WT H384A H384A
SIP1 WT Δ WT Δ Q798* WT Q798*
SIP2 WT Δ Δ WT H380A H380A WT
E -C E -C E -C E -C E -C E -C E -C
Snf1-pThr210
Snf1
ACC1Probe-Pho8N-pSer79
ACC1Probe-Pho8N
Adh1/2
D
WT
sip1Δ sip2Δ
gal83Δ sip2Δ
gal83Δ sip1Δ
sip1Q798* sip2H380A
gal83H384A sip2H380A
gal83H384A sip1Q798*
Relative SNF1 activity (ACC1Probe-Pho8N-pSer79/GFP)
0.0 0.5 1.0 1.5
E -C
*** **** *** *** **
E
ACC1Probe-NLS
GAL83 WT WT Δ Δ WT H384A H384A
SIP1 WT Δ WT Δ Q798* WT Q798*
SIP2 WT Δ Δ WT H380A H380A WT
E -C E -C E -C E -C E -C E -C E -C
Snf1-pThr210
Snf1
ACC1Probe-NLS-pSer79
ACC1Probe-NLS
Adh1/2
F
WT
sip1Δ sip2Δ
gal83Δ sip2Δ
gal83Δ sip1Δ
sip1Q798* sip2H380A
gal83H384A sip2H380A
gal83H384A sip1Q798*
Relative SNF1 activity (ACC1Probe-NLS-pSer79/GFP)
0.0 1.0 2.0 3.0 4.0
E -C
** ** * ** **
G
GAL83 WT WT Δ Δ WT H384A H384A
SIP1 WT Δ WT Δ Q798* WT Q798*
SIP2 WT Δ Δ WT H380A H380A WT
E -C E -C E -C E -C E -C E -C E -C
Sch9-pSer288
Sch9
Snf1-pThr210
Sch9
Adh1/2
H
WT
sip1Δ sip2Δ
gal83Δ sip2Δ
gal83Δ sip1Δ
sip1Q798* sip2H380A
gal83H384A sip2H380A
gal83H384A sip1Q798*
Relative SNF1 activity (Sch9-pSer288/Sch9)
0.0 0.5 1.0 1.5 2.0
E -C
* * *

Figure 11. Differential phosphorylation of ACC1^{Probes} by various SNF1 complexes.

(**A-E**) ACC1^{Probe} versions (*ACC1^{Probe}-NES*, *ACC1^{Probe}-PHO8^{N}*, and *ACC1^{Probe}-NLS*) were expressed from a single-copy integrative plasmid in WT cells and yeast strains where two β-subunits were either deleted (Δ) or inactivated by point mutation. Cells were grown to exponential phase (E) in SC medium and starved for glucose (-C) for 15 minutes. The residue Thr^{210} in Snf1 and the SNF1 target residue Ser^{79} in ACC1^{Probes} were detected by immunoblot analyses of whole cell extracts using phospho-specific antibodies against the respective phospho-residues. Anti-His$_6$ and anti-GFP antibodies were used to detect the levels of Snf1 and ACC1Probe, respectively. Anti-ADH antibodies were used to detect Adh1/2 as a loading control. (**A**) Immunoblots of cells expressing the ACC1^{Probe}-NES. (**B**) The mean relative SNF1 activity (ACC1-pSer^{79}/GFP) was quantified, normalized relative to WT cells in -C, and shown in bar diagrams (n=3; + SD; paired Student's t-test, *$p \leq 0.05$, **$p \leq 0.005$). (**C**) Immunoblots of cells expressing the ACC1^{Probe}-PHO8^{N}. (**D**) The mean relative SNF1 activity (ACC1-pSer^{79}/GFP) was quantified, normalized relative to WT cells in -C, and shown in bar diagrams (n=3; + SD; paired Student's t-test, **$p \leq 0.005$, ***$p \leq 0.0005$, ****$p \leq 0.00005$). (**E**) Immunoblots of cells expressing the ACC1^{Probe}-NLS. (**F**) The mean relative SNF1 activity (ACC1-pSer^{79}/GFP) was quantified, normalized relative to WT cells in -C, and shown in bar diagrams (n=3; + SD; paired Student's t-test, *$p \leq 0.05$, **$p \leq 0.005$). (**G**) WT cells and yeast strains in which two β-subunits were either deleted or inactivated by point mutation were grown to exponential phase (E) in SC medium and starved for glucose (-C) for 15 minutes. The residue Thr^{210} in Snf1 and the SNF1 target residue Ser^{288} in Sch9 were detected by immunoblot analyses of whole cell extracts using phospho-specific antibodies against the respective phospho-residues. Anti-His$_6$ and anti-Sch9 antibodies were used to detect the levels of Snf1 and Sch9, respectively. (**H**) The mean relative SNF1 activity (Sch9-pSer^{288}/Sch9) was quantified, normalized relative to WT cells in -C, and shown in bar diagrams (n=3; + SD; paired Student's t-test, *$p \leq 0.05$).

The vacuolar probe was significantly less phosphorylated by SNF1 pools containing only functional Sip1 and Sip2, regardless of the method used to inactivate the other two subunits (**Figures 11C and 11D**). Similarly, cells expressing only active Gal83 due to point inactivation of Sip1 and Sip2 exhibited the same effect (**Figures 11C and 11D**). This defect is not observable in *sip1Δ sip2Δ* strains, possibly due to compensatory activity by Gal83, which is not evident in *sip1^{Q798*} sip2^{H380A}* strains where the other two subunits are still expressed but non-functional. Unexpectedly, we did not observe prominent phosphorylation of this probe by Sip1-containing SNF1 complexes, likely because Sip1 is present in only a fraction of SNF1 complexes due to its low abundance (**Figures 6A-D**) (Chandrashekarappa et al., 2016). Consequently, these complexes alone cannot account for the activity observed in wild-type strains, where Gal83- and Sip2-containing complexes can also interact with and phosphorylate this probe. Indeed, despite being localized on the vacuolar surface, the probe remains exposed to the cytosol and cytosolic proteins.

The nuclear probe demonstrated the highest specificity for Gal83-containing SNF1 complexes (**Figures 11E and 11F**). Notably, phosphorylation of this probe was almost absent in SNF1 pools containing only the active subunits Sip1 and Sip2, regardless of the method used to inactivate the other two subunits (**Figures 11E and 11F**). Furthermore, in the *sip1Δ sip2Δ* strain, its phosphorylation was significantly higher than in wild-type cells, which was not observed in the *sip1*^{Q798*} *sip2*^{H380A} strains (**Figures 11E and 11F**), possibly due to compensatory activity by Gal83. These results confirm that Gal83 is the sole subunit responsible for SNF1 activity in the nucleus (Chandrashekarappa et al., 2016; Hedbacker et al., 2004b; Mangat et al., 2010; Vincent et al., 2001), as the ACC1$^{\text{Probe}}$-NLS could not be phosphorylated in its absence. Additionally, strains expressing functional Sip1 and Sip2 cannot phosphorylate the ACC1$^{\text{Probe}}$-NLS, confirming the lack of a compensatory effect.

The ACC1$^{\text{Probes}}$ are exogenous reporters of SNF1 activity and lack physiological relevance. Therefore, we investigated the phosphorylation of the endogenous SNF1 target Sch9-Ser^{288} (**Figures 11G and 11H**) (Caligaris et al., 2023a; Caligaris et al., 2023b; Lu et al., 2011), which can be assessed by immunoblotting. As previously described, we observed an increase in Sch9-Ser^{288} phosphorylation following carbon starvation in wild-type cells (Caligaris et al., 2023a). A similar trend was observed for complexes containing only active Gal83 and Sip2. However, in cells expressing only functional Sip1, this phosphorylation event was defective. Although Sch9 is considered as a vacuolar resident protein and is expected to be primarily phosphorylated by the vacuolar Sip1-containing SNF1 pool, it has been shown that a significant fraction of Sch9 relocates from the vacuolar surface to the cytosol after carbon starvation (Jorgensen et al., 2004; Takeda et al., 2018; Wilms et al., 2017). This relocation may explain the reduction in phosphorylation by Snf1-Sip1 complexes, which cannot interact with Sch9. Additionally, a significant fraction of Gal83 remains cytosolic during carbon starvation (**Figures 8A and 9A**), allowing it to encounter and phosphorylate Sch9.

Overall, we observed that (i) due to the promiscuous cytosolic localization of all SNF1 pools (**Figures 8A-C and 9A-C**), it is more challenging to differentiate them with respect to the phosphorylation of the cytosolic and vacuolar probes and Sch9, and (ii) the point mutations recapitulate the same phenotypes as deletion mutants, with the advantage of a reduced compensatory effect by Gal83 towards the vacuolar and nuclear probes, which was mainly observed when *SIP1* and *SIP2* genes were deleted rather than rendered non-functional by point mutation.

3.2.4. Phosphoproteomic profiling of SNF1 complexes

To identify the specific targets phosphorylated by each SNF1 pool within cellular compartments, we next performed a quantitative SILAC-based phosphoproteomic analysis in five independent replicates, as recently described (Caligaris et al., 2023a; Hu et al., 2019). This approach aimed to detect which targets are phosphorylated based on the β-subunit associated with Snf1 and are specifically phosphorylated by SNF1 in the nucleus, at the vacuole, or in the cytosol.

We compared wild-type cells with strains expressing only one functional β-subunit, where the other two were inactivated by CRISPR/Cas9 point mutation (**Figure 4**). Wild-type cells were grown exponentially in high glucose light-labeled medium, which served as a control, while β-subunit mutant strains were grown exponentially in high glucose medium-heavy-labeled medium (**Figure 12A**). The response of SNF1 pools to glucose starvation was analyzed 15 minutes after the shift to a glucose-deprived heavy-labeled medium (**Figure 12A**). Correct activation of SNF1 was observed by immunoblot probing the phosphorylation of Snf1-Thr^{210} and Sch9-Ser^{288} (Caligaris et al., 2023a) (**Figure 12B**).

To identify differentially phosphorylated sites, we employed a multi-step filtering process. Initially, we focused on sites that were upregulated in the wild-type during glucose starvation. Each site had to meet several criteria: at least two valid values, statistical significance based on our model (confidence interval), and a minimum two-fold increase during glucose starvation. This method allowed us to identify 2272 phosphosites that increased during carbon starvation and were potentially SNF1-dependent in wild-type cells. We then compared this dataset to our recently published SNF1 phosphoproteome (**Figure 12C**) (Caligaris et al., 2023a). In the previous dataset, we identified 1029 SNF1-dependent phosphosites after 15 minutes of carbon starvation, with an overlap of 346 phosphosites between the two datasets (**Figure 12C**).

In the second filtering step, we ensured that there were no significant differences between the mutants and the wild-type during the exponential phase. For each mutant, we excluded any sites showing significant changes. In the final step, we identified sites that were upregulated during carbon starvation compared to exponential growth for each mutant, analyzing them separately. This process led to the identification of 1394 Gal83-, 911 Sip1-, and 737 Sip2-dependent phosphosites (**Figure 12D**). Among these, 451 phosphosites were common across all datasets, indicating a high degree of promiscuity within the SNF1 pools (**Figure 12D**).

To highlight the differences between the mutants, we applied an additional filter to exclude any sites phosphorylated by more than one SNF1 pool. This led to the identification of 459 Gal83-, 66 Sip1-, and 31 Sip2-specific phosphosites. GO term enrichment analysis of the cellular components revealed an enrichment of nuclear targets dependent on Gal83 for phosphorylation (**Figure 12E**). In contrast, Sip1 and Sip2 showed similar enrichment of GO terms for cellular compartments associated with their targets (**Figures 12F and 12G**). Consensus motif analysis confirmed the previously identified SNF1 consensus motif (Caligaris et al., 2023a; Dale et al., 1995) (**Figure 2**) for Gal83, with an enrichment of basic residues at -3 and leucine at +4 (**Figure 12H**). Sip2 favored sites with basic residues at -3 (**Figure 12J**). Conversely, Sip1 did not exhibit any specific consensus enrichment and did not match the previously published data (**Figure 12I**).

We then analyzed known protein-protein interactions of the SNF1 targets to identify pathways regulated by each SNF1 pool. Using the STRING database, we generated a network of 101 proteins phosphorylated in a Gal83-dependent manner (**Figure 13**), and 28 and 18 proteins for Sip1 and Sip2, respectively (**Figures 14A and 14B**). We identified SNF1 targets in biological processes, consistent with previously published SNF1 phosphoproteomes (Braun et al., 2014; Caligaris et al., 2023a; Kanshin et al., 2017). Specifically, Gal83-containing SNF1 complexes targeted proteins involved in processes ranging from DNA stability and repair, transcription, translation, and mRNA regulation, to stress response, cell cycle, and TORC1 signaling pathway (**Figure 13**). Conversely, Snf1-Sip1 appeared to control responses to environmental changes, multidrug resistance, DNA repair, receptor internalization, translation initiation, Golgi to plasma membrane transport, actin and cytoskeleton organization, and TORC1 signaling (**Figure 14A**). Meanwhile, Sip2-containing complexes regulated nitrogen and carbohydrate metabolism, protein modification and ubiquitination, membrane trafficking, and cell polarity (**Figure 14B**).

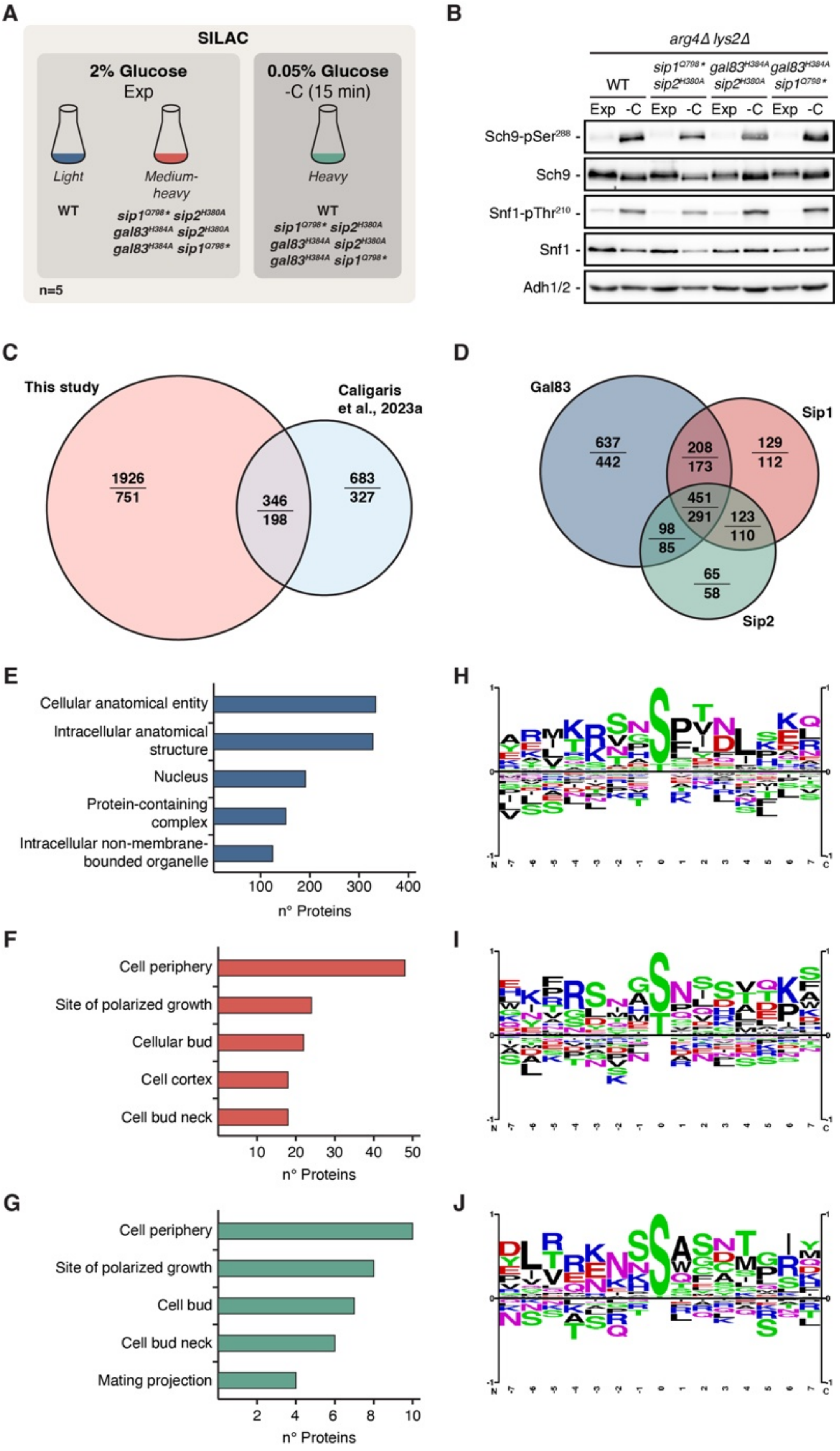
A
SILAC
2% Glucose
Exp
0.05% Glucose
-C (15 min)
Light
Medium-heavy
Heavy
WT
sip1Q798* sip2H380A
gal83H384A sip2H380A
gal83H384A sip1Q798*
WT
sip1Q798* sip2H380A
gal83H384A sip2H380A
gal83H384A sip1Q798*
n=5
B
arg4Δ lys2Δ
WT
sip1Q798* sip2H380A
gal83H384A sip2H380A
gal83H384A sip1Q798*
Exp -C Exp -C Exp -C Exp -C
Sch9-pSer288
Sch9
Snf1-pThr210
Snf1
Adh1/2
C
This study
Caligaris et al., 2023a
1926/751
346/198
683/327
D
Gal83
Sip1
Sip2
637/442
208/173
129/112
451/291
98/85
123/110
65/58
E
Cellular anatomical entity
Intracellular anatomical structure
Nucleus
Protein-containing complex
Intracellular non-membrane-bounded organelle
100 200 300 400
n° Proteins
F
Cell periphery
Site of polarized growth
Cellular bud
Cell cortex
Cell bud neck
10 20 30 40 50
n° Proteins
G
Cell periphery
Site of polarized growth
Cell bud
Cell bud neck
Mating projection
2 4 6 8 10
n° Proteins
H
I
J
N -7 -6 -5 -4 -3 -2 -1 0 1 2 3 4 5 6 7 C

Figure 12. Quantitative phosphoproteomics analysis to identify SNF1 targets across cellular compartments.

(**A**) Quantitative SILAC-based phosphoproteomics workflow (n=5). Wild-type (WT) or strains with β-subunits inactivated by point mutation (i.e., *sip1*^{Q798*} *sip2*^{H830A}, *gal83*^{H384A} *sip2*^{H830A}, and *gal83*^{H384A} *sip1*^{Q798*}) were grown exponentially (Exp) in 2% glucose-containing medium with non-labeled or labeled lysine and arginine variants ("medium-heavy" L-arginine-$^{13}C_6$ (Arg6) and L-lysine-$^{2}H_4$ (Lys4), or "heavy" L-arginine-$^{13}C_6$-$^{15}N_4$ (Arg10) and L-lysine-$^{13}C_6$-$^{15}N_2$ (Lys8) amino acids). Cells were then starved for 15 minutes for carbon (-C) in the presence of non-labeled or labeled lysine and arginine variants. (**B**) Immunoblot analysis of the samples used in the phosphoproteomics analysis to confirm proper induction of SNF1 activity upon carbon starvation. The residue Thr^{210} in Snf1 and the SNF1 target residue Ser^{288} in Sch9 were detected by immunoblot analyses of whole cell extracts using phospho-specific antibodies against the respective phospho-residues. Anti-His$_6$ and anti-Sch9 antibodies were used to detect the levels of Snf1 and Sch9, respectively. Anti-ADH antibodies were used to detect Adh1/2 as a loading control. (**C**) Proportional Venn diagram highlighting the commonly identified phosphosites (phosphosites on total proteins) in the current and previous SNF1 phosphoproteomic analyses (Caligaris et al., 2023a). (**D**) Proportional Venn diagram highlighting the commonly identified phosphosites (phosphosites on total proteins) in a Gal83-, Sip1-, and Sip2-dependent manner. (**E**) GO terms enrichment analysis of the most enriched and statistically significant ($p \leq 0.05$) cellular components in the Gal83-specific substrates. (**F**) GO terms enrichment analysis of the most enriched and statistically significant ($p \leq 0.05$) cellular components in the Sip1-specific substrates. (**G**) GO terms enrichment analysis of the most enriched and statistically significant ($p \leq 0.05$) cellular components in the Sip2-specific substrates. (**H**) Motif analysis of the Gal83-dependent phosphosites identified by the *in vivo* SILAC phosphoproteomic analysis. (**I**) Motif analysis of the Sip1-dependent phosphosites identified by the *in vivo* SILAC phosphoproteomic analysis. (**J**) Motif analysis of the Sip2-dependent phosphosites identified by the *in vivo* SILAC phosphoproteomic analysis.

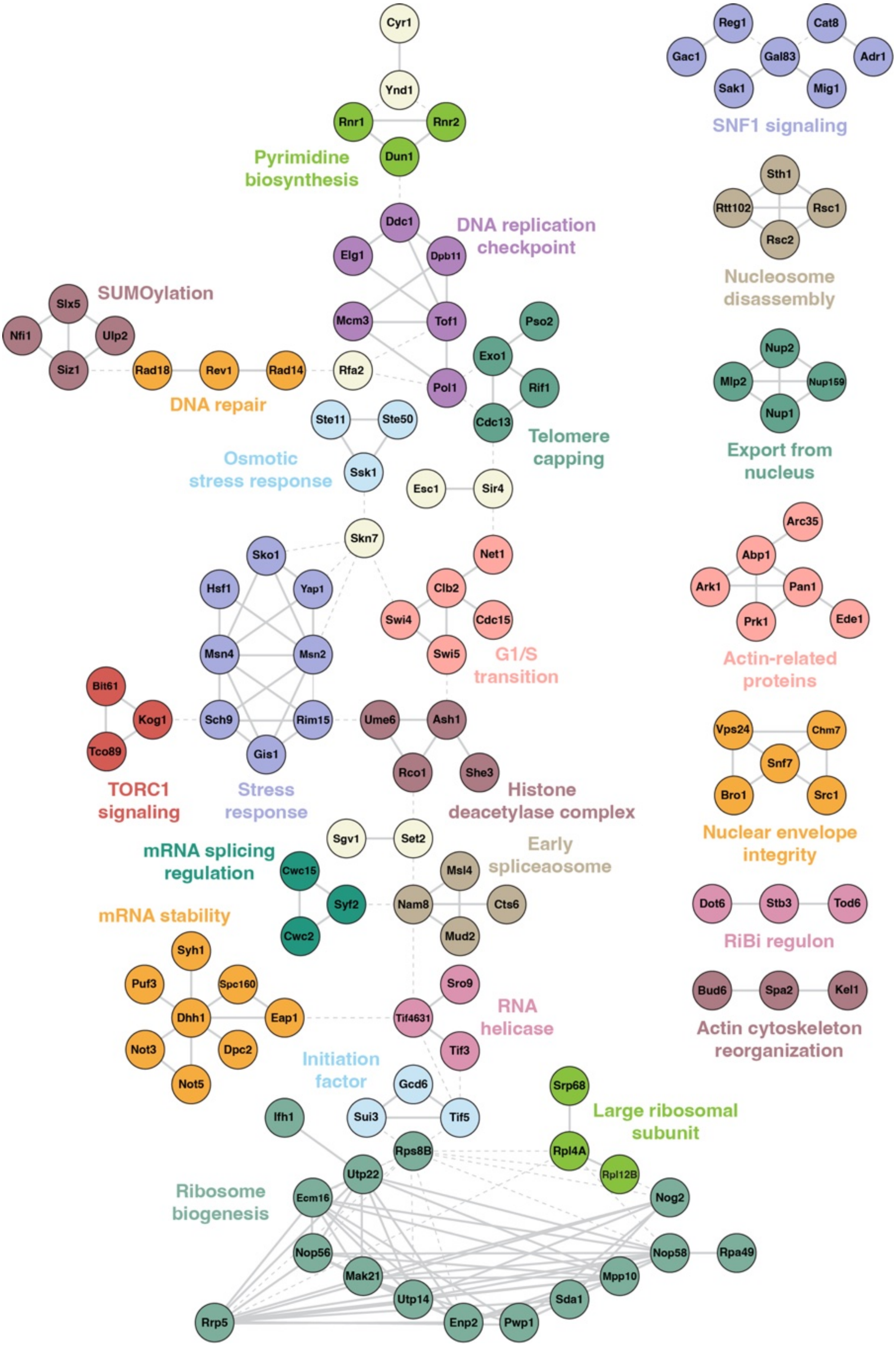
Cyr1
Ynd1
Rnr1
Rnr2
Dun1
Pyrimidine biosynthesis
Reg1
Cat8
Gac1
Gal83
Adr1
Sak1
Mig1
SNF1 signaling
Ddc1
Elg1
Dpb11
DNA replication checkpoint
Sth1
Rtt102
Rsc1
Rsc2
Nucleosome disassembly
Slx5
Nfi1
Ulp2
Siz1
SUMOylation
Mcm3
Tof1
Pso2
Exo1
Rif1
Rad18
Rev1
Rad14
Rfa2
Pol1
DNA repair
Nup2
Mlp2
Nup159
Nup1
Export from nucleus
Ste11
Ste50
Cdc13
Telomere capping
Osmotic stress response
Ssk1
Esc1
Sir4
Skn7
Sko1
Hsf1
Yap1
Net1
Clb2
Swi4
Cdc15
Swi5
G1/S transition
Msn4
Msn2
Arc35
Abp1
Ark1
Pan1
Prk1
Ede1
Actin-related proteins
Bit61
Kog1
Tco89
TORC1 signaling
Sch9
Rim15
Gis1
Stress response
Ume6
Ash1
Rco1
She3
Histone deacetylase complex
Vps24
Chm7
Snf7
Bro1
Src1
Nuclear envelope integrity
Sgv1
Set2
mRNA splicing regulation
Cwc15
Syf2
Cwc2
Msl4
Nam8
Cts6
Mud2
Early spliceaosome
Dot6
Stb3
Tod6
RiBi regulon
mRNA stability
Syh1
Puf3
Spc160
Dhh1
Eap1
Not3
Dpc2
Not5
Bud6
Spa2
Kel1
Actin cytoskeleton reorganization
Sro9
Tif4631
Tif3
RNA helicase
Initiation factor
Gcd6
Sui3
Tif5
Ifh1
Srp68
Large ribosomal subunit
Rps8B
Rpl4A
Rpl12B
Utp22
Ribosome biogenesis
Ecm16
Nog2
Nop56
Nop58
Rpa49
Mak21
Mpp10
Utp14
Sda1
Rrp5
Enp2
Pwp1

Figure 13. Gal83-dependent substrate protein-protein interaction network.

Network illustrating the interactions among 101 proteins, selected from a total of 347 that are phosphorylated in a Gal83-dependent manner. The network was constructed using the STRING plugin for Cytoscape, with a confidence score threshold of 0.900, and clustered using the MCL algorithm. The thickness of the edges indicates the confidence score of each interaction.

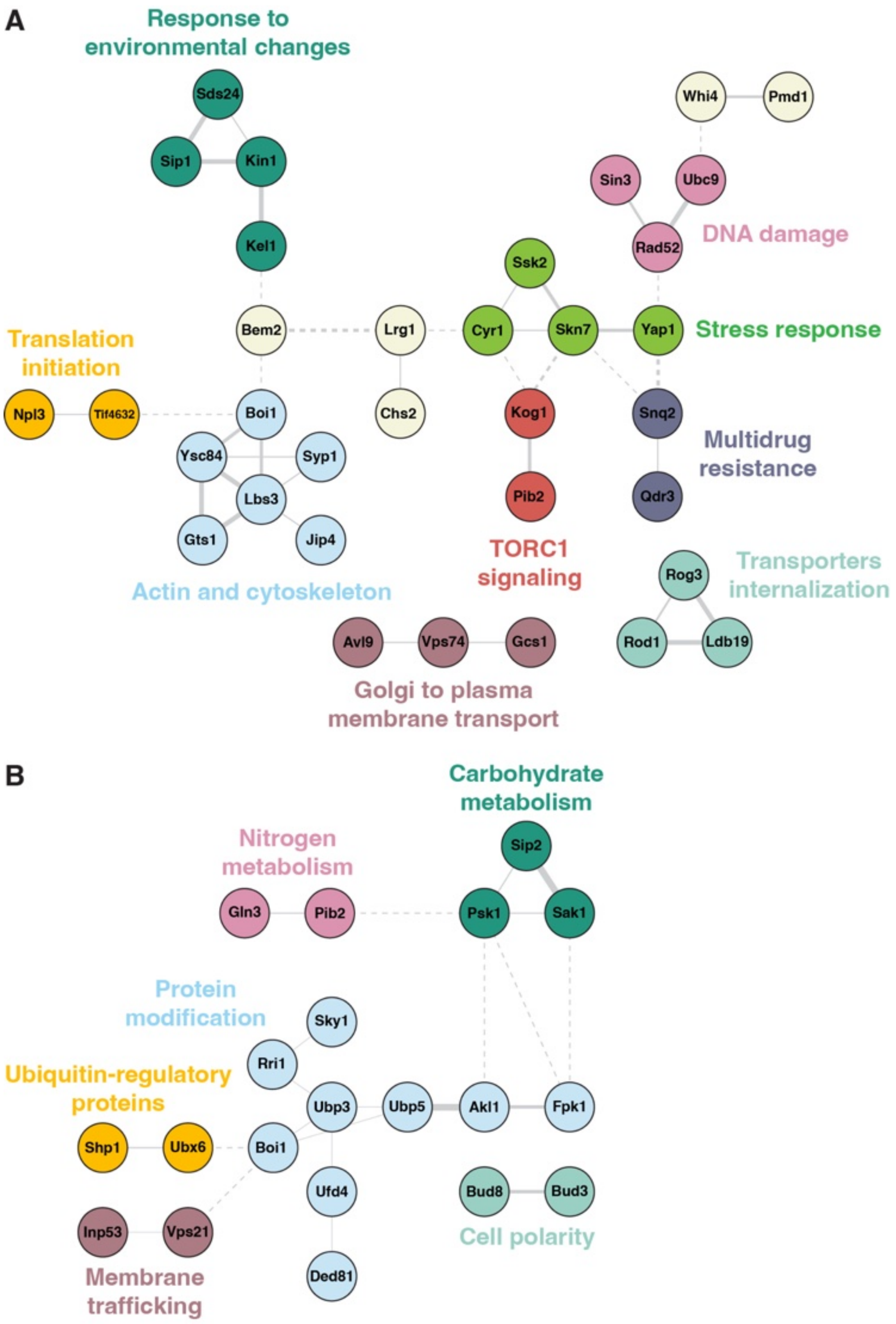

A
Response to environmental changes
Sds24
Sip1
Kin1
Kel1
Whi4
Pmd1
Sin3
Ubc9
Rad52
DNA damage
Ssk2
Translation initiation
Bem2
Lrg1
Cyr1
Skn7
Yap1
Stress response
Npl3
Tif4632
Boi1
Chs2
Kog1
Snq2
Ysc84
Syp1
Multidrug resistance
Lbs3
Pib2
Qdr3
Gts1
Jip4
TORC1 signaling
Rog3
Transporters internalization
Actin and cytoskeleton
Avl9
Vps74
Gcs1
Rod1
Ldb19
Golgi to plasma membrane transport
B
Carbohydrate metabolism
Nitrogen metabolism
Sip2
Gln3
Pib2
Psk1
Sak1
Protein modification
Sky1
Rri1
Ubiquitin-regulatory proteins
Ubp3
Ubp5
Akl1
Fpk1
Shp1
Ubx6
Boi1
Ufd4
Bud8
Bud3
Inp53
Vps21
Cell polarity
Membrane trafficking
Ded81

Figure 14. Sip1- and Sip2-dependent substrate protein-protein interaction networks.
(**A**) Network illustrating the interactions among 28 proteins, selected from a total of 59 that are phosphorylated in a Sip1-dependent manner. The network was constructed using the STRING plugin for Cytoscape, with a confidence score threshold of 0.400, and clustered using the MCL algorithm. The thickness of the edges indicates the confidence score of each interaction. (**B**) Network illustrating the interactions among 18 proteins, selected from a total of 28 that are phosphorylated in a Sip2-dependent manner. The network was constructed using the STRING plugin for Cytoscape, with a confidence score

threshold of 0.250, and clustered using the MCL algorithm. The thickness of the edges indicates the confidence score of each interaction.

As shown in the networks (**Figures 13 and 14**), the phosphoproteomic analysis identified targets for each SNF1 pool within their specific compartments. Among these, we confirmed previously published and characterized targets of SNF1. Additionally, we have been able to determine which SNF1 pool is involved in their *in vivo* phosphorylation. For instance, Gal83 is the β-subunit required for the SNF1-dependent phosphorylation of Adr1 (Ratnakumar et al., 2009; Sanz et al., 2016; Young et al., 2003), Cat8 (Roth et al., 2004; Sanz et al., 2016; Vincent & Carlson, 1999; Young et al., 2003), Dhh1 (Braun et al., 2014), Eap1 (Braun et al., 2014; Caligaris et al., 2023a), Glo3 (Arakel et al., 2019; Braun et al., 2014), Mig1 (Coccetti et al., 2018; DeVit & Johnston, 1999; Ostling & Ronne, 1998; Papamichos-Chronakis et al., 2004; Smith et al., 1999; Treitel et al., 1998), Msn2 (De Wever et al., 2005; Gorner et al., 2002; Mayordomo et al., 2002), Msn4 (Caligaris et al., 2023a; De Wever et al., 2005; Hedbacker & Carlson, 2008; Mayordomo et al., 2002; Petrenko et al., 2013), Puf3 (Braun et al., 2014), Reg1 (Caligaris et al., 2023a), Sch9 (Braun et al., 2014; Caligaris et al., 2023a; Lu et al., 2011), and Scp160 (Braun et al., 2014). Interestingly, we identified Gal83-dependent sites on Atg13 and Atg31, which are involved in autophagosome formation (Feng et al., 2015), and on Atg33, which is involved in mitophagy (Kanki et al., 2010). Atg31 requires phosphorylation at Ser^{174} for its activity (Feng et al., 2015), and we observed a significant increase in its phosphorylation upon carbon starvation. Previously, SNF1's role in regulating autophagy was shown to be through Atg1 phosphorylation (Wang et al., 2001; Yao et al., 2020), but our data suggest a new possible layer of regulation via Atg31. Additionally, we detected the phosphorylation of Eaf1, a member of the NuA4 complex, which is involved in regulating chromatin remodeling and gene transcription through histone acetylation (Dacquay et al., 2017). We also identified the phosphorylation of the transcriptional repressors Dot6, Tod6, and Stb3, as well as the transcriptional coactivator Ifh1. All of these proteins play roles in regulating the transcription of ribosomal proteins and ribosome biogenesis genes (Huber et al., 2009; Huber et al., 2011; Lippman & Broach, 2009; Loewith & Hall, 2011). The dataset also suggested the involvement of SNF1 in promoting entry into the G0 phase by direct phosphorylation of Gis1. Gis1 is a transcriptional activator whose activity is tightly regulated by phosphorylation. The protein phosphatase PP2A dephosphorylates Gis1, inhibiting its activity and preventing it from binding to certain gene promoters. The Rim15 kinase and Igo1/2 proteins inhibit PP2A, keeping Gis1 active. Yak1 kinase also phosphorylates Gis1 at Ser^{425}, which is crucial for its activity (Dokládal et al., 2021a). Additionally, Rim15 was significantly more phosphorylated in a Gal83-dependent manner upon glucose depletion, suggesting a new nutrient-sensing pathway impinging on Rim15. Indeed, Rim15 integrates signals from nutrient-dependent protein kinases, such as PKA, TORC1, and Pho85-Pho80 (Sampaio-Marques et al., 2014; Swinnen et al., 2014). Gal83-Snf1 complexes may also regulate the CDK Pho85 via direct phosphorylation of its upstream inhibitor Pho81 (Jimenez et al., 2016; Menoyo et al., 2013; Mouillon & Persson, 2006; Nishizawa, 2015; Wanke et al., 2005). Gal83-containing complexes may also regulate Pkh2 and Pkh3, kinases involved in sphingolipid-mediated signaling and upstream activators of Sch9 (Caligaris et al., 2023b; Liu et al., 2005; Roelants et al., 2004; Urban et al., 2007; Voordeckers et al., 2011). SNF1 may also regulate the multidrug response by phosphorylating Pdr1, the transcription factor that induces the transcription of the multidrug transporter Pdr5 (Balzi et al., 1994). Finally, we revealed Gal83-depdendent sites on nucleolar (Nop56 and Nop58) and nucleoporin (Nup1, Nup2, and Nup159) proteins.

Conversely, Sip1 appears to be the β-subunit required for the SNF1-dependent phosphorylation of Rod1 (Alvaro et al., 2016; Becuwe et al., 2012; Laussel et al., 2022; O'Donnell & Schmidt, 2019; Shinoda & Kikuchi, 2007) and other previously unexplored targets such as Atg16, Muk1, Rad52, and Pep3. Atg16 is a conserved protein involved in autophagy and necessary for autophagosome formation (Popelka et al., 2021). Thus, in addition to the possible role of Gal83-containing complexes in the regulation of autophagy via Atg13, Atg31, and Atg33, Sip1-Snf1 complexes may also contribute to inducing autophagy via Atg16 phosphorylation. Muk1 is a GEF that activates Rab5 family GTPases, which are molecular switches regulating early endocytosis, membrane tethering and fusion, and endosomal motility (Paulsel et al., 2013). Its phosphorylation in a Sip1-dependent manner may play a role in controlling intracellular trafficking by ensuring proper sorting and transport within the cell during carbon starvation. Pep3 is a member of the CORVET membrane tethering complex, involved in the formation and maintenance of vacuoles (Ding et al., 2015). Additionally, Pep3 is implicated in stress response and tolerance to acetic acid stress by enhancing vacuolar surface area and V-ATPase activity, which helps in proton sequestration and pH homeostasis (Ding et al., 2015). Rad52 plays a crucial role in the repair of DNA double-strand breaks through homologous recombination (Deveryshetty et al., 2023), supporting the role of SNF1 in regulating the DNA damage response (Lucca et al., 2024).

On the other hand, Sip2-containing complexes appear to be involved in the phosphorylation of Gln3 (Bertram et al., 2002; Hedbacker & Carlson, 2008; Kulkarni et al., 2006; Perez-Sampietro et al., 2013; K. J. Simpson-Lavy & M. Kupiec, 2023) as well as Ubp3, Ubp5, and Bud3. Ubp3 and Ubp5 are ubiquitin-specific proteases involved in the removel of ubiquiting from ubiqutylated proteins (Baker et al., 1992; Xiao et al., 1994), with Ubp5 being localized at the bud neck (Xiao et al., 1994). Indeed, Snf1 has been reported to localize at the bud neck, where it plays a role in mitosis by promoting proper spindle alignment and cell cycle progression (Tripodi et al., 2018b). At this location, Snf1-Sip2 complexes may phosphorylate Ubp5 and Bud3.

Interestingly, as previously reported (Braun et al., 2014; Caligaris et al., 2023a), we identified phosphosites on Gal83 (Caligaris et al., 2023a; Mangat et al., 2010), Sip1 (Caligaris et al., 2023a; Yang et al., 1992), and Sip2 (Caligaris et al., 2023a). The phosphosites on Gal83 were Gal83-dependent, while those on Sip1 and Sip2 were identified in a Sip1- and Sip2-dependent manner, respectively. Interestingly, SNF1 was reported to form homodimers *in vivo* and *in vitro* (Nayak et al., 2006; Rudolph et al., 2005), fitting with our phosphoproteomics data which support the fact that the different SNF1 complexes do not cross-phosphorylate each other.

Certain known SNF1 targets appeared in two out of three datasets, indicating that different SNF1 pools phosphorylate the same protein on different residues. Among these, we identified sites on Cyr1 (Caligaris et al., 2023a; Nicastro et al., 2015a) and Kog1 (Caligaris et al., 2023a; Hughes Hallett et al., 2015; Kanshin et al., 2017). While other previously hinted as putative or new possible targets showed shared sites among two β-subunits, such as Rog3 (Laussel et al., 2022; O'Donnell et al., 2015), Tco89 (Caligaris et al., 2023a), and Tda1. Interestingly, Tda1 is the yeast ortholog of NUAK1, an AMPK-related kinase overexpressed in various cancers and associated with tumor malignancy and invasiveness (Oh et al., 2020), plays crucial roles in responding to nutrient stress by regulating histone phosphorylation and gene transcription (Oh et al., 2020).

Finally, we identified only two proteins that show increased phosphorylation upon carbon starvation and may be phosphorylated by all the complexes: Pib2 and Boi1. Pib2 was previously reported as a SNF1 target (Caligaris et al., 2023a). In this study, we identified the phosphorylation of Ser^{79} (by Gal83), Ser^{434} (by Sip1), and Ser^{267} (by Sip2), although it was previously reported to be phosphorylated on Ser^{268} and Ser^{309} (Caligaris et al., 2023a). If Ser^{267} and Ser^{268} correspond to the same site, the difference may arise from mass spectrometry analysis, while the other sites may be newly detected. This cannot be excluded, as in the previous analysis, the serine-to-alanine mutant of Pib2 at Ser^{268} and Ser^{309} still showed low remaining phosphorylation in *in vitro* kinase assay (**Chapter 1 - Figure 4D**). Alternatively, the sites detected here, which increased upon carbon starvation, may be phosphorylated by other kinases that become active under these conditions.

Ultimately, this phosphoproteomic analysis enabled us to confirm known SNF1 effectors and identify new potential ones. However, there remains a degree of overlap in their activity, making the complete identification of their specific targets challenging.

3.2.5. Impact of β-subunit deletions on Snf1 levels and stability

While comparing the activity of the SNF1 complexes where two β-subunits were either deleted or inactivated by point mutations, we noticed variations in the total levels of the α-subunit Snf1 (**Figures 11A, 11C, 11E, and 11G**). Specifically, in the case of the deletions of two β-subunits, the total levels of Snf1 were notably reduced, an effect that was not present in the strains where the two β-subunits were inactivated by point mutations. This effect was particularly prominent when the remaining expressed subunit was either Sip1 or Sip2.

We hypothesized that Snf1 might undergo degradation when not associated with the β-subunits, and possibly also when not associated with the Snf4 γ-subunit due to the scaffolding role of the β-subunits (Hedbacker & Carlson, 2008; Sanz et al., 2016). To investigate this, we engineered yeast strains with different deletions: two β-subunits, all β-subunits, only the γ-subunit (*SNF4*), or both β- and γ-subunits together. Our measurements indicated that the levels of Snf1 correlated with the abundance of the β-subunits. Due to the high abundance of Gal83, when it was expressed, we did not observe a significant reduction in Snf1 levels (**Figures 15A and 15B**). Conversely, when only Sip1 and Sip2 were expressed, we observed a significant reduction in Snf1 levels (**Figures 15A and 15B**), consistent with previous publications (Hedbacker et al., 2004a). In triple deletion strains (*gal83Δ sip1Δ sip2Δ*), the levels of Snf1 were even lower (**Figures 15A and 15B**). This contrasts with a previous publication, where such changes were not observed (Elbing et al., 2006b). However, this discrepancy could be due to a different tagging method, as Elbing et al. expressed Snf1 from a centromeric plasmid (Elbing et al., 2006b), which is known to be present in more copies than the single genomic allele (Karim et al., 2013). Additionally, the deletion of *SNF4* causes a reduction in Snf1 levels and a dysregulation of its phosphorylation on Thr^{210} (**Figures 15A and 15B**), as previously observed (Elbing et al., 2006b). In the quadruple deletion strain (*gal83Δ sip1Δ sip2Δ snf4Δ*), Snf1 levels were like those in the triple deletion strain (*gal83Δ sip1Δ sip2Δ*), indicating that *SNF4* deletion does not cause an additive effect (**Figures 15A and 15B**).

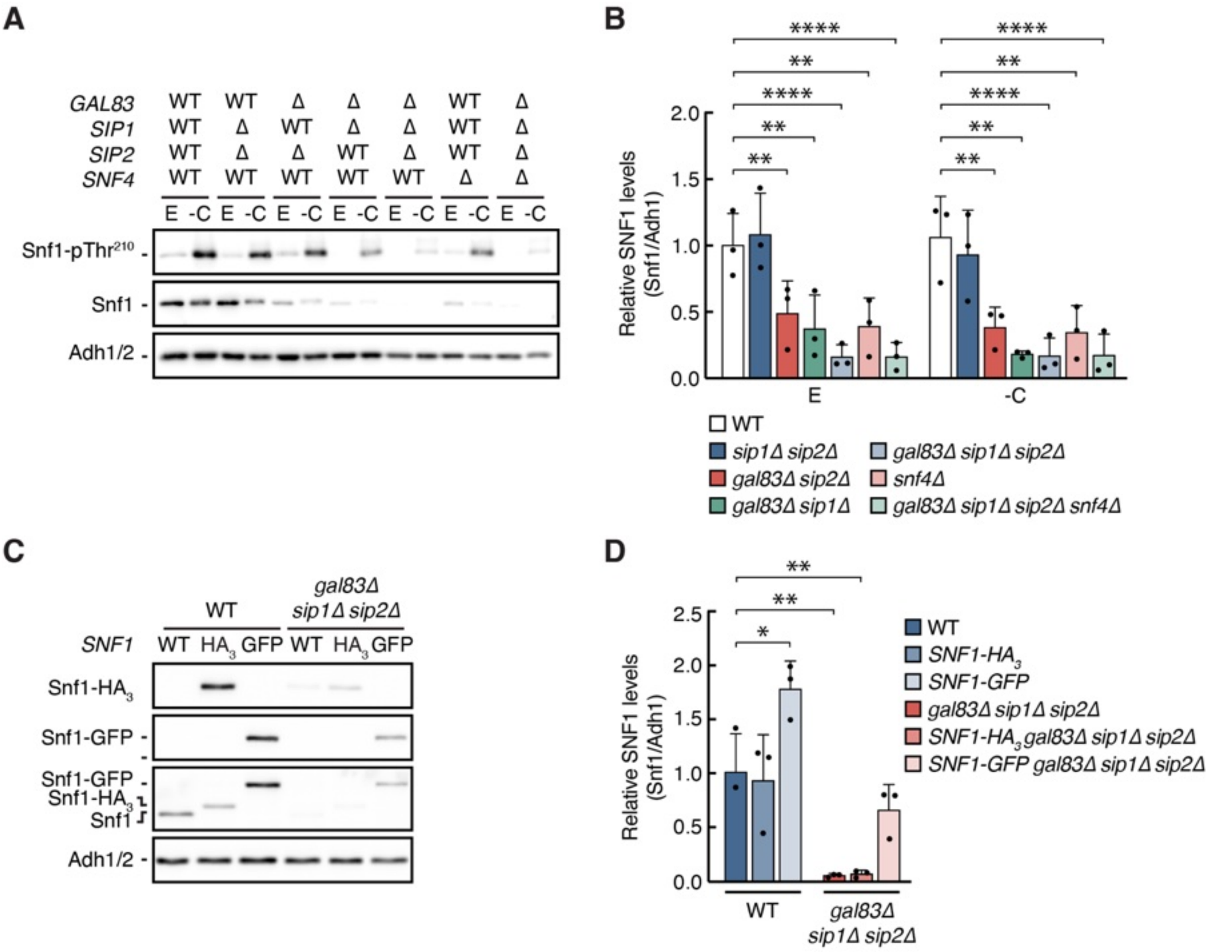

Figure 15. Stabilization of Snf1 by association with β-subunits.

(**A**) Immunoblot analysis of WT, *sip1Δ sip2Δ*, *gal83Δ sip2Δ*, *gal83Δ sip1Δ*, *gal83Δ sip1Δ sip2Δ*, *snf4Δ*, and *gal83Δ sip1Δ sip2Δ snf4Δ* cells grown to exponential phase (E) in SC medium and starved for glucose (-C) for 15 minutes. The residue Thr^{210} in Snf1 was detected by immunoblot analyses of whole cell extracts using a phospho-specific antibody against the phospho-residues. Anti-His$_6$ antibodies were used to detect the levels of Snf1. Anti-ADH antibodies were used to detect Adh1/2 as a loading control. (**B**) The mean relative Snf1 levels (Snf1/Adh1) were quantified, normalized relative to WT cells, and shown in bar diagrams (n=3; + SD; paired Student's t-test, **$p \leq 0.005$, ****$p \leq 0.00005$). (**C**) Immunoblot analysis of WT or *gal83Δ sip1Δ sip2Δ* cells expressing Snf1 genomically tagged with HA$_3$ or GFP, grown to exponential phase. Snf1, Snf1-HA$_3$, and Snf1-GFP levels were detected by immunoblot analyses of whole cell extracts using anti-His$_6$, anti-HA, and anti-GFP antibodies, respectively. Anti-ADH antibodies were used to detect Adh1/2 as a loading control. (**D**) The mean relative Snf1 levels (Snf1/Adh1) were quantified, normalized relative to WT cells, and shown in bar diagrams (n=3; + SD; paired Student's t-test, *$p \leq 0.05$, **$p \leq 0.005$).

We hypothesized that the binding of the β-subunit to the C-terminal portion of Snf1 stabilizes Snf1 and possibly protects it from SUMOylation, an event occurring in the region identified to interact with the β-subunits (**General introduction - Figure 2A**) (Simpson-Lavy

& Johnston, 2013). Indeed, when Snf1 is genomically tagged at its C-terminus, we observed an increase in its levels (**Figures 15C and 15D**). This was the case for a large tag, like GFP (27 kDa), but not for smaller ones, like HA_3 (3.5 kDa) (**Figures 15C and 15D**). Additionally, the GFP C-terminal tag could restore Snf1 levels in *gal83Δ sip1Δ sip2Δ* strains to wild-type levels (**Figures 15C and 15D**), indicating that the C-terminal portion of Snf1 is involved in the regulation of its levels.

Overall, we speculate that the binding of the β-subunits to the C-terminal portion of Snf1, like the presence of a large tag, can protect Snf1 from being SUMOylated and degraded (Simpson-Lavy & Johnston, 2013). However, we cannot exclude a transcriptional effect caused by the deletion of the β-subunits at this point and further studies will be required to address this issue.

3.3. DISCUSSION

In this chapter, we explored the role of SNF1 β-type subunits and how the compartmentalization of SNF1 enables specificity toward downstream effectors. Understanding the role of SNF1/AMPK in different cellular compartments has been an open question for many years (Chandrashekarappa et al., 2016; Hedbacker et al., 2004b; Mangat et al., 2010; Vincent et al., 2001), attracting significant and growing interest in the field (Gonzalez et al., 2020; Herzig & Shaw, 2018; Liang et al., 2015; Salt et al., 1998; Schmitt et al., 2022; Steinberg & Hardie, 2023; Trefts & Shaw, 2021; Zong et al., 2019).

It is well established that in yeast, SNF1 localizes to various cellular compartments (*i.e.* nucleus, vacuole, and cytosol) upon carbon starvation in a β-subunit-dependent manner (Chandrashekarappa et al., 2016; Hedbacker et al., 2004b; Vincent et al., 2001). β-subunits are also involved in substrate recognition; however, to date, only a few substrates have been identified as being specific for each SNF1 pool (Hedbacker & Carlson, 2008; Sanz et al., 2016). This research project aimed to identify the SNF1 targets specifically phosphorylated in each cellular compartment, a mechanism that should be dependent on and facilitated by the specific association with distinct β-subunits.

To selectively study each SNF1 pool, we generated yeast strains using CRISPR/Cas9 that bear point mutations rendering two out of three β-subunits non-functional (Chandrashekarappa et al., 2016). This approach should prevent any compensatory effects at the transcriptional or protein stability level that might arise from the simultaneous deletion of two other β-subunit genes (Chandrashekarappa et al., 2016). The activity of SNF1 complexes expressing only one β-subunit was assessed by comparing cell growth on alternative or non-fermentable carbon sources. In these cases, inactivation by point mutation or deletion of the β-subunits caused growth phenotypes consistent with previous publications (Mayer et al., 2011; Zhang et al., 2010). The only exception was observed in cells expressing non functional Gal83 and Sip2. These cells showed milder but improved growth compared to the double deletion strains on ethanol glycerol plates, although their growth was still not at wild-type levels.

Additionally, we observed that upon glucose depletion, the β-subunits properly localized to their expected cellular location, indicating that they were functioning correctly despite the mutation of the other β-subunits. We also confirmed that the β-subunits have different abundances, with Gal83 being the most prevalent (Breker et al., 2013; Chandrashekarappa et al., 2016; Elbing et al., 2006b; Mangat et al., 2010; Vincent et al., 2001), and, most importantly, their relative levels were not affected by the inactivation or deletion of the other two subunits.

These findings support the notion that inactivating two β-subunits does not lead to compensatory effects. To observe this at the molecular level, we probed the activity of SNF1 *in vivo*. Over the decades, various tools and methods have been developed for this purpose. One possible readout is the measurement of invertase expression (*i.e. SUC2*), which is negatively regulated by Mig1, a protein inhibited by phosphorylation via SNF1 (Coccetti et al., 2018; DeVit & Johnston, 1999; Ostling & Ronne, 1998; Papamichos-Chronakis et al., 2004; Smith et al., 1999; Treitel et al., 1998). Alternatively, we recently demonstrated that phosphorylation of the protein kinase Sch9 at residue Ser^{288} can serve as a readout of SNF1 activity (Caligaris et al., 2023a). However, these methods have limitations due to the intrinsic localization of these targets: in high glucose Mig1 is enriched in the nucleus and Sch9 is on the vacuolar surface, then released to the cytosol upon carbon depletion (Jorgensen et al., 2004; Takeda et al., 2018; Wilms et al., 2017). Previous studies have shown that all SNF1 pools are involved in Mig1 phosphorylation upon carbon starvation, whereas the Gal83-containing pool is responsible for the phosphorylation and inactivation of Mig2 upon alkaline stress activation of the complex (Chandrashekarappa et al., 2016; Mayordomo et al., 2002). Additionally, we demonstrated that all SNF1 pools can phosphorylate Sch9 at Ser^{288}. This is not surprising, given that the localization of SNF1 pools is not an all-or-nothing effect. Indeed, a significant fraction of the pools remains cytosolic, where they can encounter and phosphorylate Sch9.

Recently, a reporter for *in vivo* AMPK activity in human cells, named ExRai AMPKAR, was developed (Schmitt et al., 2022). This reporter consists of an AMPK substrate, GFP, and FHA1 (phosphoamino acid-binding ForkHead-Associated domain 1) (Schmitt et al., 2022). The ExRai AMPKAR reporter was also targeted to different organelles, such as mitochondria and lysosomes, to evaluate spatial AMPK activity (Schmitt et al., 2022). Additionally, Schmitt et al. proposed a mechanistic model where nuclear AMPK activity (AMPKα2-dependent) in response to 2-DeoxyGlucose (2-DG) is initiated in the cytoplasm in an upstream kinases-dependent manner (Schmitt et al., 2022). Subsequently, AMPK translocates into the nucleus to phosphorylate nuclear targets (Schmitt et al., 2022). However, the specific mechanisms that allow AMPK to shuttle in and out of the nucleus remain unclear (Schmitt et al., 2022). This model aligns with the known localization model of the Snf1-Gal83-Snf4 complex, which gets phosphorylated by Sak1 in the cytosol and then translocates into the nucleus (Chandrashekarappa et al., 2016; Hedbacker et al., 2004b; Vincent et al., 2001) while the upstream kinase remains cytosolic (Liu et al., 2011).

In line with this, we generated an *in vivo* SNF1 probe targeted at each cellular compartment that could be phosphorylated by the local SNF1 pools. Instead of a microscopy-based reporter, we opted for an immunoblot probing method. We modified the widely used ACC1$^{\mathrm{Probe}}$ (Caligaris et al., 2023a; Deroover et al., 2016; Tripodi et al., 2018a). Given that it consists of only a short stretch of the rat ACC1 (13 amino acids) and serves as an exogenous reporter of SNF1 activity with no physiological role in yeast cells, we proposed that this could be an unbiased reporter, phosphorylatable by each SNF1 pool. By fusing it with an NES, the Pho8 N-terminal domain (Pho8$^{\mathrm{N}}$), and an NLS, we enriched the ACC1$^{\mathrm{Probe}}$ in the cytosol, on the vacuolar surface, and in the nucleus, respectively. We demonstrated that these probes, as well as the original one, were phosphorylated in an SNF1-dependent manner. Despite the high enrichment of these probes at the desired cell compartments, and most likely due to the promiscuous cytosolic localization of the SNF1 complexes, all of them were able to phosphorylate the cytosolic (ACC1$^{\mathrm{Probe}}$-NES) and vacuolar (ACC1$^{\mathrm{Probe}}$-Pho8$^{\mathrm{N}}$) probes. Conversely, the nuclear probe (ACC1$^{\mathrm{Probe}}$-NLS) was solely phosphorylated by the Gal83-containing complex, as it is the only one capable of entering the nucleus and encountering this probe. Thus, we show that while rendering two β-subunits non-functional, the remaining one still performs its activity and does not compensate for the others.

To advance our understanding of the specificity of SNF1 pools, we conducted a SILAC-based phosphoproteomic analysis. While several SNF1 phosphoproteome analyses have been performed to date (Braun et al., 2014; Caligaris et al., 2023a; Kanshin et al., 2017), they differ in the conditions under which SNF1 activity was induced and probed. However, none of these studies focused on the activity of the SNF1 pools; instead, they examined the overall SNF1 phosphoproteome. Our study is the first to provide a comprehensive understanding of the compartmentalized SNF1 targets phosphorylated by different SNF1 pools. We identified sites specifically phosphorylated by each SNF1 pool, indicating which β-subunit is involved in the phosphorylation of previously identified targets, such as Mig1, Msn2/4, Gln3, and Rod1 (Alvaro et al., 2016; Becuwe et al., 2012; Bertram et al., 2002; Caligaris et al., 2023a; Coccetti et al., 2018; De Wever et al., 2005; DeVit & Johnston, 1999; Gorner et al., 2002; Hedbacker & Carlson, 2008; Kulkarni et al., 2006; Laussel et al., 2022; Mayordomo et al., 2002; O'Donnell & Schmidt, 2019; Ostling & Ronne, 1998; Papamichos-Chronakis et al., 2004; Perez-Sampietro et al., 2013; Petrenko et al., 2013; Shinoda & Kikuchi, 2007; K. J. Simpson-Lavy & M. Kupiec, 2023; Smith et al., 1999; Treitel et al., 1998). Nevertheless, some targets have been shown to be phosphorylated by more than one SNF1 pool, albeit at different sites, such as Kog1, Pib2, and Cyr1. Additionally, we identified new putative SNF1 targets, phosphorylated in different cellular compartments, which will require more detailed investigation (for details, refer to the **General Discussion**).

An interesting observation consistently appearing in our results was that when two subunits, specifically the most abundant Gal83, were deleted, but not when they were inactivated by mutation, the total levels of the α-subunit Snf1 decreased. This may relate to the additional role of the β-subunits as scaffolds for the SNF1 complex (Hedbacker & Carlson, 2008; Sanz et al., 2016). At the C-terminal region of Snf1, within the β-subunit binding region (Hedbacker & Carlson, 2008; Sanz et al., 2016), there is a site for SUMOylation at residue Lys^{549}, an event that promotes its ubiquitination and degradation (Crozet et al., 2014; Simpson-Lavy & Johnston, 2013). We propose a model in which the binding of the β-subunit protects Snf1 from being SUMOylated. To test this, we measured the total levels of Snf1 in strains where the composition of the SNF1 complex was affected by the deletion of the β-subunits. We observed that in *gal83Δ sip1Δ sip2Δ* strains, the levels of Snf1 were significantly reduced. Previously, controversial findings were published regarding the total levels of Snf1 in the same deletion background strain, with some studies showing reduced levels (Hedbacker et al., 2004a; Liu et al., 2011), and others showing unchanged levels (Elbing et al., 2006b). It should be noted that the findings by Elbing et al., 2006 could be affected by increased expression of Snf1 due to expression from centromeric plasmids, which are known to cause increased allele expression (Karim et al., 2013). This could have led to discrepancies in Snf1 measurements. Conversely, the C-terminal tagging of Snf1 with a relatively large tag (*e.g.*, GFP) may mimic the interaction with the β-type subunit and protect Snf1 from interacting with the E3 SUMO ligase Mms21, thereby preventing its SUMOylation and degradation (Crozet et al., 2014; Simpson-Lavy & Johnston, 2013). It was reported that the K549R mutant of Snf1, which cannot be SUMOylated, showed higher levels and stability of Snf1 (Simpson-Lavy & Johnston, 2013). Therefore, we aim in the future to combine β-subunit deletions with CRISPR/Cas9-

mediated mutation of lysine-to-arginine to potentially revert this phenotype. Nevertheless, we cannot yet exclude the possibility that this regulatory effect occurs at the transcriptional level.

Additionally, the deletion of *SNF4*, which is known to reduce the interaction of Snf1 with the β-subunits, also led to a reduction in Snf1 levels (Elbing et al., 2006b; Hedbacker & Carlson, 2008; Hedbacker et al., 2004a; Leech et al., 2003; Liu et al., 2011). Consistent with previous studies, this deletion led to the deregulation of Snf1-Thr^{210} phosphorylation (Elbing et al., 2006b).

Ultimately, this study validated the use of β-subunit point mutants, demonstrating that when two β-subunits were rendered non-functional, the remaining one did not exhibit compensatory effects and remained catalytically active. Using these strains, we performed a phosphoproteomics analysis that enabled us to distinguish the specificity of SNF1 pools and identify their specific targets. We confirmed previously published targets and identified new, intriguing targets that may reveal unexplored roles of SNF1. Additional omic analyses and *in vivo* experiments will further elucidate the specific roles of each SNF1 pool. This study serves as a starting point for better understanding the role of SNF1/AMPK isoforms across all eukaryotes.

CHAPTER 4:
Proxies introduce bias in decoding TORC1 activity

1. Introduction

The eukaryotic target of rapamycin complex 1 (TORC1) kinase is a crucial integrator of nutritional, energy, and hormonal signals that link metabolic cues to cell growth and homeostasis. Genetically inherited or acquired deregulation of TORC1 uncouples growth and homeostasis from the respective signals, thereby establishing conditions that drive the emergence of human diseases such as neurodegeneration, epilepsy, immunodeficiencies, cancer, and metabolic syndrome (Albert & Hall, 2015; Gonzalez & Hall, 2017; Laplante & Sabatini, 2012; Liu & Sabatini, 2020). Research in this field relies on accurate quantification of TORC1 activities in various genetic settings and under defined physiological conditions (Ma & Blenis, 2009).

In mammalian cells, TORC1 activity is typically assessed via the phosphorylation levels of direct TORC1 target residues in the eukaryotic initiation factor 4E-binding protein 1 (4E-BP1) (Ma & Blenis, 2009) and the ribosomal protein S6 (rpS6) kinase 1 (S6K1) (Fenton & Gout, 2011; Magnuson et al., 2012), or on the direct target of the latter kinase, rpS6 (Meyuhas & Dreazen, 2009). The most commonly used proxies for TORC1 activities in yeast are phosphorylation of the *bona fide* TORC1 residue Thr^{737} in the protein kinase Sch9 (Caligaris et al., 2023b; Urban et al., 2007) and phosphorylation of Ser^{232,233} in Rps6, carried out by the Sch9-related TORC1 effector kinase Ypk3 (Gonzalez et al., 2015; Yerlikaya et al., 2016). However, whether Sch9 and Rps6 phosphorylation can be used interchangeably to report TORC1 activity in yeast under these conditions is currently not known.

To address this question, we compared the dynamics of Sch9-pThr^{737} and Rps6-Ser^{232,233} dephosphorylation in rapamycin-treated and nitrogen-starved cells, as well as their rephosphorylation kinetics upon amino acid readdition. Additionally, we investigated which protein phosphatases might be involved in the dephosphorylation process of Rps6-Ser^{232,233} following TORC1 inactivation.

2. Key contributions of this chapter

- **Figure 1**. Distinct phosphorylation patterns of Sch9 and Rps6 in response to dynamic TORC1 regulation. Panels A to K.

microPublication BIOLOGY

3/27/2024 - *Open Access*

Proxies introduce bias in decoding TORC1 activity

Marco Caligaris[1], Claudio De Virgilio[1§]

[1]Department of Biology, University of Fribourg, Fribourg, Fribourg, Switzerland

[§]To whom correspondence should be addressed: claudio.devirgilio@unifr.ch

Abstract

The eukaryotic TORC1 kinase integrates and links nutritional, energy, and hormonal signals to cell growth and homeostasis, and its deregulation is associated with human diseases including neurodegeneration, cancer, and metabolic syndrome. Quantification of TORC1 activities in various genetic settings and defined physiological conditions generally relies on the assessment of the phosphorylation level of residues in TORC1 targets. Here we show that two commonly used TORC1 effectors in yeast, namely Sch9 and Rps6, exhibit distinct phosphorylation patterns in response to rapamycin treatment or changes in nitrogen availability, indicating that the choice of TORC1 proxies introduces a bias in decoding TORC1 activity.

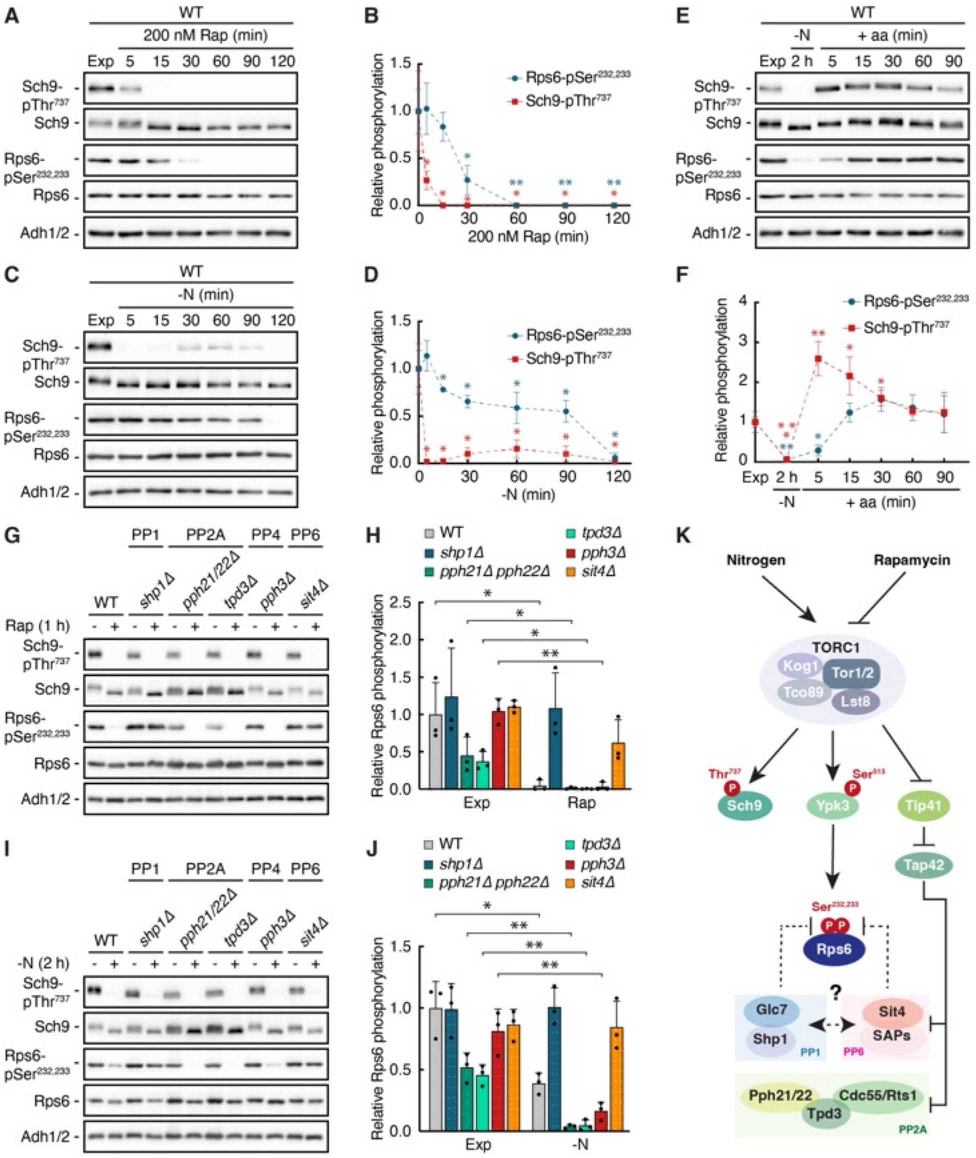

Figure 1. Distinct phosphorylation patterns of Sch9 and Rps6 in response to dynamic TORC1 regulation:

(**A, B**) Prototrophic wild-type (WT) cells were grown exponentially (Exp) and treated with 200 nM rapamycin (Rap) for 5, 15, 30, 60, 90, and 120 min. Phosphorylations of the *bona fide* TORC1 target residue Sch9-Thr^{737} and the Ypk3 target residues Rps6-Ser^{232,233} were probed by immunoblot analyses of whole cell extracts using phospho-specific antibodies against the respective phospho-residues. Anti-Sch9 and anti-Rps6 antibodies served to detect the levels of Sch9 and Rps6, respectively.

Adh1/2 levels probed with specific antibodies served as a loading control. (A). The mean TORC1 (*i.e.* Sch9-pThr^{737}/Sch9) and Ypk3 activities (*i.e.* Rps6-pSer^{232,233}/Rps6) were then quantified, normalized relative to the mean values of exponentially growing WT cells, and shown in (B) (n=3; ± SD; unpaired Student's t-test, *p≤0.05, **p≤0.005, ***p≤0.0005). (**C, D**) Prototrophic wild-type (WT) cells were grown exponentially (Exp), starved for nitrogen (-N) for 5, 15, 30, 60, 90, and 120 min, and analyzed (C) and quantified (D) as in (A) and (B), respectively. (**E**) Prototrophic wild-type (WT) cells were grown exponentially (Exp), starved for nitrogen (-N) for 2h, and then restimulated with a mix of all amino acids (+ aa) for 5, 15, 30, 60, and 90 min. Analyses (E) and quantifications (F) were performed as in (A) and (B), respectively. (**G, H**) Auxotrophic wild-type (WT), *shp1*Δ, *pph21*Δ *pph22*Δ, *tpd3*Δ, *pph3*Δ, and *sit4*Δ cells were grown exponentially (Exp) and treated with 200 nM rapamycin (Rap) for 1 h (G) and analyzed as in (A). The mean Ypk3 activities were quantified, normalized relative to the mean value of exponentially growing WT cells, and shown in the bar diagram (H) (n=3; + SD; unpaired Student's t-test, *p≤0.05, **p≤0.005). (**I, J**) Auxotrophic wild-type (WT), *shp1*Δ, *pph21*Δ *pph22*Δ, *tpd3*Δ, *pph3*Δ, and *sit4*Δ cells were grown exponentially (Exp), starved for nitrogen (-N) for 2 h (I), and analyzed as in (A). The mean Ypk3 activities (J) were quantified as in (H). (**K**) Model illustrating the key effector kinases and phosphatases emanating from TORC1 in budding yeast. TORC1 directly phosphorylates and activates Sch9 and Ypk3. A bona fide TORC1 target residue in Sch9 is Thr^{737} in the hydrophobic motif (HM) (Urban et al., 2007), which is equivalent to Ser^{513} in Ypk3 (González et al., 2015; Yerlikaya et al., 2016). Active Ypk3 phosphorylates Rps6 on Ser^{232,233} (González et al., 2015; Yerlikaya et al., 2016). In parallel, TORC1 inhibits Tip41, an inhibitor of Tap42, which allows the latter to interact with and inhibit PP2A (Pph21/Pph22-Tpd3-Cdc55/Rts1) and PP6 (Sit4-SAPs). Dephosphorylation of Ser^{232,233} in Rps6 in rapamycin-treated and nitrogen-starved cells requires both PP1 (Glc7-Shp1; (Yerlikaya *et al.*, 2016)) and, as shown here, PP6 (Sit4-SAPs). Arrows and bars refer to direct (full line) or indirect (dashed line) activating and inhibitory interactions, respectively. For details, see text.

Description

The eukaryotic target of rapamycin complex 1 (TORC1) kinase is a central integrator of nutritional, energy, and hormonal signals that links these metabolic cues to cell growth and homeostasis. Genetically inherited or acquired deregulation of TORC1 uncouples growth and homeostasis from the respective signals, thereby establishing conditions that drive the emergence of human diseases such as neurodegeneration, epilepsy, immunodeficiencies, cancer, and metabolic syndrome (Albert and Hall, 2015; González and Hall, 2017; Laplante and Sabatini, 2012; Liu and Sabatini, 2020). Research in this field critically depends on the accurate quantification of TORC1 activities in various genetic settings and under defined physiological conditions. In mammalian cells, TORC1 activity is typically assessed via the phosphorylation levels of direct TORC1 target residues in the eukaryotic initiation factor 4E-binding protein 1 (4E-BP1; (Ma and Blenis, 2009)) and the ribosomal protein S6 (rpS6) kinase 1 (S6K1) (Fenton and Gout, 2011; Magnuson et al., 2012), or the ones in rpS6, the effector of the latter kinase (Meyuhas and Dreazen, 2009). The most commonly used proxies for TORC1 activities in the budding yeast *Saccharomyces cerevisiae* include, similar to S6K phosphorylation in mammalian cells, phosphorylation of the *bona fide* TORC1 residue Thr^{737} in the protein kinase Sch9 (Caligaris et al., 2023; Urban *et al.*, 2007) and, analogous to mammalian rpS6, phosphorylation of Ser^{232,233} in Rps6, which is carried out by the Sch9-related TORC1 effector kinase Ypk3 (González *et al.*, 2015; Yerlikaya *et al.*, 2016). Accordingly, phospho-specific antibodies against Sch9-pThr^{737} and Rps6-pSer^{232,233} (that only recognize doubly phosphorylated Rps6) have been used to assess TORC1 activities under various physiological conditions such as limitation and starvation for amino acids or nitrogen and refeeding of amino acids or high-quality nitrogen sources to previously starved cells (Brito et al., 2019; Cecil et al., 2023; Chen et al., 2017; Chen et al., 2018; Hatakeyama et al., 2019; Liang et al., 2023; Péli-Gulli et al., 2015; Picazo et al., 2018; Takahara and Maeda, 2012; Vallejo et al., 2020). In these studies, both TORC1 proxies were used over highly disparate time lapses of treatment conditions ranging from minutes up to 6 hours (sometimes with intervals of minutes to hours). However, whether Sch9 and Rps6 phosphorylation can be used interchangeably to report TORC1 activity in yeast under these conditions is currently not known.

To address this question, we first compared the dynamics of Sch9-pThr^{737} and Rps6-Ser^{232,233} dephosphorylation in rapamycin-treated and nitrogen-starved cells. Following rapamycin treatment, Sch9-pThr^{737} was very quickly dephosphorylated with a $t_{1/2}$ of 2.6 min (95% CI = [1.34, 4.41] min), while Rps6-pSer^{232,233} was dephosphorylated with much slower kinetics ($t_{1/2}$ = 22.11 min; 95% CI [13.82, 41.08] min) (Fig. 1A, B). Interestingly, dephosphorylation of Sch9-pThr^{737} was similarly swift upon nitrogen-starvation of cells, while Rps6-pSer^{232,233} dephosphorylation did not even reach 50% after 90 min and only approached 0% after 2 h of nitrogen starvation (Fig. 1C, D). We speculate that the significantly delayed dephosphorylation of Rps6-pSer^{232,233} may perhaps be due to limiting phosphatase activity as Rps6 is approximately 100-fold more abundant than Sch9 (SGD; (Breker et al., 2013; Chong et al., 2015; Ghaemmaghami et al., 2003)). Alternatively, the different dephosphorylation kinetics of Sch9-pThr^{737} and Rps6-pSer^{232,233} may be explained by contrasting activities or substrate affinities of the respective phosphatases targeting these residues. Finally, it has also been proposed that TORC2 may in part phosphorylate Rps6-pSer^{232,233} via the Ypk3-paralogs TORC2 effector kinases Ypk1/2, which may counteract the dephosphorylation of these residues when TORC2 remains active (Yerlikaya *et al.*, 2016). In sum, it appears that Rps6-pSer^{232,233} dephosphorylation is a poor predictor of TORC1 inactivation when compared to Sch9-pThr^{737} dephosphorylation specifically in cells that are starved for nitrogen for less than 90 min.

In parallel to the studies above, we have also compared the utility of Sch9 and Rps6 phosphorylation to detect TORC1 reactivation following addition of amino acids to nitrogen-starved cells. The phosphorylation of Sch9-Thr^{737} was maximal after 5 min following amino acid re-addition, while the respective peak of Rps6-Ser^{232,233} was delayed by about 15 min (Fig. 1E, F). Hence, both reporters can reveal TORC1 activation, but do so with different kinetics. The time lag in Rps6-Ser^{232,233} phosphorylation may result from the fact that TORC1 favors Rps6 phosphorylation indirectly via Ypk3, or, again, be due to the high abundance of Rps6 or more effective counteracting phosphatase(s). Regarding the latter, we confirmed the previously published role of the type 1 protein phosphatase (PP1; Glc7) regulatory subunit Shp1 in the dephosphorylation of Rps6-pSer^{232,233} in both rapamycin-treated and nitrogen-starved cells (Fig. 1G-J) (Yerlikaya *et al.*, 2016; Zhang et al., 1995). Interestingly, however, we also discovered that the catalytic type 6 protein phosphatase (PP6) subunit Sit4 is equally important for this process, while the catalytic (Pph21 and Pph22) and scaffolding (Tpd3) subunits of the type 2A protein phosphatase (PP2A) and the catalytic (Pph3) subunit of the type 4 protein phosphatase (PP4) were not required for the dephosphorylation of Rps6-pSer^{232,233} (Fig.1G-J) (Arino et al., 2019; Lillo et al., 2014). This suggests that either Glc7-Shp1 acts upstream of Sit4 (and the Sit4-associated [SAP] regulatory proteins) or *vice versa*. Alternatively, Glc7-Shp1 and Sit4-SAPs may each target only either pSer^{232} or pSer^{233} in Rps6 in a mutually exclusive, but partially cooperative way (Fig. 1K). Under the same conditions, dephosphorylation of pThr^{737} in Sch9 remained unaffected by loss of the PP1 regulator Shp1, or by loss of PP2A (in *pph21*Δ *pph22*Δ or *tpd3*Δ cells), PP4 (in *pph3*Δ cells), or PP6 (in *sit4*Δ cells).

In conclusion, our data show that the assessment of TORC1 activity is strongly biased by the choice of the TORC1 target residues (direct such as Thr^{737} in Sch9 or indirect such as Ser^{232,233} in Rps6) that are probed for their phosphorylation levels. Accordingly, the relative affinities and activities of TORC1 and the counteracting protein phosphatases for a particular target residue, just as they are influenced by the relative abundance of these proteins, inevitably yield substrate-specific responses. Our data therefore align well with a more general paradigm shift in the TORC1 signaling field according to which TORC1 activity is not simply a uniform entity within a given cell, but an activity that can be locally (Betz and Hall, 2013; Hatakeyama *et al.*, 2019), temporally, and quantitatively harnessed for the phosphorylation of specific targets in response to discrete physiological cues (Cecil *et al.*, 2023; Nicastro et al., 2017; Powis and De Virgilio, 2016; Zeng et al., 2024).

Methods

Yeast strains and plasmids

Saccharomyces cerevisiae strains and plasmids are listed in **Table 1** and **Table 2**, respectively. Gene deletions were performed using the pFA6a system-based PCR-toolbox (Janke et al., 2004), and the primers listed in **Table 3**. Yeast cells were transformed via standard methods (Gietz and Woods, 2001), as previously described (Deprez et al., 2023). The transformation mix contained 240 µL 50% PEG, 36 µL 1 M LiAc, 5.3 µL of ssDNA (salmon sperm DNA solution), 15 µL of deletion cassette, and 54 µL of sterile H_2O. After the transformation, cells were washed 2 times with 1 mL of sterile H_2O and then plated on SD-Leu (synthetic dropout; 0.17% yeast nitrogen base, 0.5% ammonium sulfate [AS], 0.2% dropout mix without leucine [USBiological], and 2% glucose) plates. To identify the clones containing the correct deletion, colony PCR using the primers listed in **Table 3** was performed. Strains were rendered prototrophic, unless stated otherwise, by transforming them with the empty centromeric plasmids listed in **Table 2**. All strains and plasmids are available upon request.

Growth conditions

To maintain the plasmids, prototrophic cells were pre-grown in a synthetic dropout (SD; 0.17% yeast nitrogen base, 0.5% ammonium sulfate [AS], 0.2% dropout mix [USBiological], and 2% glucose) medium. Auxotrophic strains were pre-grown in a synthetic complete medium (SC; SD with all amino acids) medium. Subsequently, SC medium was used for the dilution of the cells the following day. When indicated, 200 nM rapamycin was added to the culture. Starvation experiments were performed by filtration and transfer of cells to a nitrogen starvation medium (0.17% yeast nitrogen base, 2% glucose, 0.01% adenine, and 0.005% uracil) for the indicated times. For amino acid re-addition experiments, a 25 times concentrated amino acid mix (25X dropout mix without histidine [USBiological] and 0.125% histidine) was added to the cultures, to reach the same concentration present in the SC medium. Cell growth was monitored by measuring the concentration (OD_{600nm}/mL) with a spectrophotometer.

Cell lysate preparation and immunoblot analysis

Cell lysates were prepared as described in (Hatakeyama *et al.*, 2019). Samples were denatured at 98°C for 5 minutes, loaded on SDS-PAGE, and transferred onto nitrocellulose membranes. Blocking with blocking buffer (5% milk powder in Tris-buffered saline) was performed for 1 h at room temperature. Membranes were immunoblotted with the primary antibodies listed in **Table 4**. After 3 washes, the membranes were incubated with the secondary antibodies conjugated with horseradish peroxidase listed in **Table 4**. Membranes were washed again 3 times and developed with ECL (GE Healthcare).

Statistical analyses

Three independent biological replicates of each experiment were performed. To determine the statistical significance, unpaired Student's t-test analysis was made with GraphPad Prism 10. Values with a p-value lower than 0.05 were considered significantly different. To express the variability, the standard deviation was calculated with GraphPad Prism 10 and shown in the graphs. In the figure legend, the number of independent replicas, the method used to express the variability, specific statistical tests, and significance are indicated.

Reagents

Table 1. Strains used in this study

Strain	Genotype	Source	Panel
BY4741	*MATa; ura3Δ0, leu2Δ0, his3Δ1, met15Δ0*	Euroscarf	G-J
YL515	[BY4741] *his3Δ1, leu2Δ0, ura3Δ0*	(Binda et al., 2009)	A-F
MC380	[BY4741] *shp1Δ::LEU2*	This study	G-J
YSB165-144-1C	[BY4741] *pph21Δ::kanMX, pph22Δ::kanMX*	CDV lab strain	G-J
YAL016w	[BY4741] *tpd3Δ::kanMX*	Euroscarf	G-J
YDR075w	[BY4741] *pph3Δ::kanMX*	Euroscarf	G-J
YDL047w	[BY4741] *sit4Δ::kanMX*	Euroscarf	G-J

Table 2. Plasmids used in this study

Plasmid	Genotype	Source	Panel
pRS413	*CEN, ARS, amp^R, HIS3*	(Brachmann et al., 1998)	A-F
pRS415	*CEN, ARS, amp^R, LEU2*	(Brachmann *et al.*, 1998)	A-F
pRS416	*CEN, ARS, amp^R, URA3*	(Brachmann *et al.*, 1998)	A-F
pFA-LEU2	*amp^R, LEU2p-LEU2*	This study	

Table 3. Primers used in this study

Name	Orientation	Sequence

SHP1 pFA del For	Forward	TTTAAATATATAAGAAACGTCGGTAGCACAACAATTAACTCATTATTTAGGTATGCGGATCCCCGGGTTAATTAA
SHP1 pFA del Rev	Reverse	TTTATATATTAAGTTGAAGTCTTTTCCCGTTTCTGTTTTTGTATATTTATGCTCAGAATTCGAGCTCGTTTAAAC
SHP1 -253 For	Forward	AAGAAGCCAGCAAGTAGTGG
SHP1 +1483 Rev	Reverse	ATCACTTGGGGTGAATGCAG

Table 4. Antibodies used in this study

Name	**Dilution**	**Source; product number**
Rabbit anti-ADH	1 :200000	Calbiochem; 126745
Rabbit anti-Sch9-phospho-Thr^{737}	1:10000	CDV lab
Goat anti-Sch9	1:1000	CDV lab
Rabbit anti-human-phospho-S6 ribosomal protein Ser^{235,236}	1:1000	Proteintech; 29223-1-AP
Guinea pig anti-Rps6	1:1000	(Yerlikaya *et al.*, 2016)
Goat anti-rabbit HRP conjugated	1:3000	BIO-RAD; 170-6515
Rabbit anti-goat HRP conjugated	1:3000	BIO-RAD; 5160-2104
Goat anti-guinea pig HRP conjugated	1:5000	Invitrogen; A18769

Acknowledgements:

We thank Robbie Loewith and Jörn Dengjel for providing anti-Rps6 antibodies, Pauline Six, Susanne Stumpe, and Olga Sudan for technical assistance, Marie-Pierre Péli-Gulli for carefully reading the manuscript.

References

Albert V, Hall MN. 2015. mTOR signaling in cellular and organismal energetics. Curr Opin Cell Biol 33: 55-66. PubMed ID: 25554914

Ariño J, Velázquez D, Casamayor A. 2019. Ser/Thr protein phosphatases in fungi: structure, regulation and function. Microb Cell 6(5): 217-256. PubMed ID: 31114794

Betz C, Hall MN. 2013. Where is mTOR and what is it doing there? J Cell Biol 203(4): 563-74. PubMed ID: 24385483

Binda M, Péli-Gulli MP, Bonfils G, Panchaud N, Urban J, Sturgill TW, Loewith R, De Virgilio C. 2009. The Vam6 GEF controls TORC1 by activating the EGO complex. Mol Cell 35(5): 563-73. PubMed ID: 19748353

Brachmann CB, Davies A, Cost GJ, Caputo E, Li J, Hieter P, Boeke JD. 1998. Designer deletion strains derived from Saccharomyces cerevisiae S288C: a useful set of strains and plasmids for PCR-mediated gene disruption and other applications. Yeast 14(2): 115-32. PubMed ID: 9483801

Breker M, Gymrek M, Schuldiner M. 2013. A novel single-cell screening platform reveals proteome plasticity during yeast stress responses. J Cell Biol 200(6): 839-50. PubMed ID: 23509072

Brito AS, Soto Diaz S, Van Vooren P, Godard P, Marini AM, Boeckstaens M. 2019. Pib2-Dependent Feedback Control of the TORC1 Signaling Network by the Npr1 Kinase. iScience 20: 415-433. PubMed ID: 31622882

Caligaris M, Sampaio-Marques B, Hatakeyama R, Pillet B, Ludovico P, De Virgilio C, Winderickx J, Nicastro R. 2023. The Yeast Protein Kinase Sch9 Functions as a Central Nutrient-Responsive Hub That Calibrates Metabolic and Stress-Related Responses. J Fungi (Basel) 9(8). PubMed ID: 37623558

Cecil JH, Padilla CM, Lipinski AA, Langlais PR, Luo X, Capaldi AP. 2023. The Molecular Logic of Gtr1/2 and Pib2 Dependent TORC1 Regulation in Budding Yeast. bioRxiv. PubMed ID: 38106135

Chen J, Sutter BM, Shi L, Tu BP. 2017. GATOR1 regulates nitrogenic cataplerotic reactions of the mitochondrial TCA cycle. Nat Chem Biol 13(11): 1179-1186. PubMed ID: 28920930

Chong YT, Koh JL, Friesen H, Duffy SK, Cox MJ, Moses A, et al., Andrews BJ. 2015. Yeast Proteome Dynamics from Single Cell Imaging and Automated Analysis. Cell 161(6): 1413-24. PubMed ID: 26046442

Deprez MA, Caligaris M, Rosseels J, Hatakeyama R, Ghillebert R, Sampaio-Marques B, et al., Winderickx J. 2023. The nutrient-responsive CDK Pho85 primes the Sch9 kinase for its activation by TORC1. PLoS Genet 19(2): e1010641. PubMed ID: 36791155

Fenton TR, Gout IT. 2011. Functions and regulation of the 70kDa ribosomal S6 kinases. Int J Biochem Cell Biol 43(1): 47-59. PubMed ID: 20932932

Ghaemmaghami S, Huh WK, Bower K, Howson RW, Belle A, Dephoure N, O'Shea EK, Weissman JS. 2003. Global analysis of protein expression in yeast. Nature 425(6959): 737-41. PubMed ID: 14562106

Gietz RD, Woods RA. 2001. Genetic transformation of yeast. Biotechniques 30(4): 816-20, 822-6, 828 passim. PubMed ID: 11314265

González A, Hall MN. 2017. Nutrient sensing and TOR signaling in yeast and mammals. EMBO J 36(4): 397-408. PubMed ID: 28096180

González A, Shimobayashi M, Eisenberg T, Merle DA, Pendl T, Hall MN, Moustafa T. 2015. TORC1 promotes phosphorylation of ribosomal protein S6 via the AGC kinase Ypk3 in Saccharomyces cerevisiae. PLoS One 10(3): e0120250. PubMed ID: 25767889

Hatakeyama R, Péli-Gulli MP, Hu Z, Jaquenoud M, Garcia Osuna GM, Sardu A, Dengjel J, De Virgilio C. 2019. Spatially Distinct Pools of TORC1 Balance Protein Homeostasis. Mol Cell 73(2): 325-338.e8. PubMed ID: 30527664

Janke C, Magiera MM, Rathfelder N, Taxis C, Reber S, Maekawa H, et al., Knop M. 2004. A versatile toolbox for PCR-based tagging of yeast genes: new fluorescent proteins, more markers and promoter substitution cassettes. Yeast 21(11): 947-62. PubMed ID: 15334558

Laplante M, Sabatini DM. 2012. mTOR signaling in growth control and disease. Cell 149(2): 274-93. PubMed ID: 22500797

Liang J, Tang H, Snyder LF, Youngstrom CE, He BZ. 2023. Divergence of TORC1-mediated stress response leads to novel acquired stress resistance in a pathogenic yeast. PLoS Pathog 19(10): e1011748. PubMed ID: 37871123

Lillo C, Kataya AR, Heidari B, Creighton MT, Nemie-Feyissa D, Ginbot Z, Jonassen EM. 2014. Protein phosphatases PP2A, PP4 and PP6: mediators and regulators in development and responses to environmental cues. Plant Cell Environ 37(12): 2631-48. PubMed ID: 24810976

Liu GY, Sabatini DM. 2020. mTOR at the nexus of nutrition, growth, ageing and disease. Nat Rev Mol Cell Biol 21(4): 183-203. PubMed ID: 31937935

Ma XM, Blenis J. 2009. Molecular mechanisms of mTOR-mediated translational control. Nat Rev Mol Cell Biol 10(5): 307-18. PubMed ID: 19339977

Magnuson B, Ekim B, Fingar DC. 2012. Regulation and function of ribosomal protein S6 kinase (S6K) within mTOR signalling networks. Biochem J 441(1): 1-21. PubMed ID: 22168436

Meyuhas O, Dreazen A. 2009. Ribosomal protein S6 kinase from TOP mRNAs to cell size. Prog Mol Biol Transl Sci 90: 109-53. PubMed ID: 20374740

Nicastro R, Sardu A, Panchaud N, De Virgilio C. 2017. The Architecture of the Rag GTPase Signaling Network. Biomolecules 7(3). PubMed ID: 28788436

Péli-Gulli MP, Sardu A, Panchaud N, Raucci S, De Virgilio C. 2015. Amino Acids Stimulate TORC1 through Lst4-Lst7, a GTPase-Activating Protein Complex for the Rag Family GTPase Gtr2. Cell Rep 13(1): 1-7. PubMed ID: 26387955

Picazo C, Matallana E, Aranda A. 2018. Yeast thioredoxin reductase Trr1p controls TORC1-regulated processes. Sci Rep 8(1): 16500. PubMed ID: 30405153

Powis K, De Virgilio C. 2016. Conserved regulators of Rag GTPases orchestrate amino acid-dependent TORC1 signaling. Cell Discov 2: 15049. PubMed ID: 27462445

Takahara T, Maeda T. 2012. Transient sequestration of TORC1 into stress granules during heat stress. Mol Cell 47(2): 242-52. PubMed ID: 22727621

Urban J, Soulard A, Huber A, Lippman S, Mukhopadhyay D, Deloche O, et al., Loewith R. 2007. Sch9 is a major target of TORC1 in Saccharomyces cerevisiae. Mol Cell 26(5): 663-74. PubMed ID: 17560372

Vallejo B, Matallana E, Aranda A. 2020. Saccharomyces cerevisiae nutrient signaling pathways show an unexpected early activation pattern during winemaking. Microb Cell Fact 19(1): 124. PubMed ID: 32505207

Yerlikaya S, Meusburger M, Kumari R, Huber A, Anrather D, Costanzo M, et al., Loewith R. 2016. TORC1 and TORC2 work together to regulate ribosomal protein S6 phosphorylation in Saccharomyces cerevisiae. Mol Biol Cell 27(2): 397-409. PubMed ID: 26582391

Zeng Q, Araki Y, Noda T. 2024. Pib2 is a cysteine sensor involved in TORC1 activation in Saccharomyces cerevisiae. Cell Rep 43(1): 113599. PubMed ID: 38127619

Zhang S, Guha S, Volkert FC. 1995. The Saccharomyces SHP1 gene, which encodes a regulator of phosphoprotein phosphatase 1 with differential effects on glycogen metabolism, meiotic differentiation, and mitotic cell cycle progression. Mol Cell Biol 15(4): 2037-50. PubMed ID: 7891699

Funding:

This work was supported by the Canton of Fribourg and the Swiss National Science Foundation (310030_214824 to CDV).

Author Contributions: Marco Caligaris: conceptualization, data curation, formal analysis, investigation, validation, visualization, methodology, writing - original draft, writing - review editing. Claudio De Virgilio: conceptualization, resources, supervision, funding acquisition, validation, methodology, project administration, writing - original draft, writing - review editing, visualization.

Reviewed By: Anonymous

History: Received February 29, 2024 **Revision Received** March 22, 2024 **Accepted** March 25, 2024 **Published Online** March 27, 2024 **Indexed** April 10, 2024

Copyright: © 2024 by the authors. This is an open-access article distributed under the terms of the Creative Commons Attribution 4.0 International (CC BY 4.0) License, which permits unrestricted use, distribution, and reproduction in any medium, provided the original author and source are credited.

Citation: Caligaris, M; De Virgilio, C (2024). Proxies introduce bias in decoding TORC1 activity. microPublication Biology. 10.17912/micropub.biology.001170

GENERAL DISCUSSION

Mechanistic insights on SNF1 regulation of TORC1 activity

The highly conserved SNF1/AMPK kinase complex is a key regulator of eukaryotic cellular energy levels (Coccetti et al., 2018; Crozet et al., 2014; Hardie & Ashford, 2014; Hedbacker & Carlson, 2008; Polge & Thomas, 2007; Sanz et al., 2016). Its function is essential for adaptation to changes in environmental conditions, and, particularly in yeast, SNF1 responds to carbon source availability (Hedbacker & Carlson, 2008; Hong & Carlson, 2007; Sanz et al., 2016; K. J. Simpson-Lavy & M. Kupiec, 2023). Conversely, TORC1/mTORC1 is considered the master regulator of cell growth and proliferation, being active in nutrient- and amino acid-rich conditions (De Virgilio & Loewith, 2006a, 2006b; Hu et al., 2019; Wullschleger et al., 2006). The crosstalk between these two antagonistic signaling pathways is crucial for wiring cellular processes such as metabolism, stress response, protein synthesis, and autophagy in response to nutrient availability.

In human cells, multiple layers of regulation of the mTORC1 pathway by AMPK have been characterized. The primary mechanisms involve the direct phosphorylation of the mTORC1 subunit Raptor and the upstream regulator TSC2 (**Figure 1**) (Gonzalez et al., 2020; Gwinn et al., 2008; Hindupur et al., 2015; Inoki et al., 2003b; Malik et al., 2023; Mallick & Gupta, 2021; Mihaylova & Shaw, 2011; Shaw et al., 2004; Smiles et al., 2024). Through these mechanisms, AMPK can tune down mTORC1 activtiy, inhibiting cell growth and by inducing genes needed for stress reponse and adaptaion (Gonzalez et al., 2020).

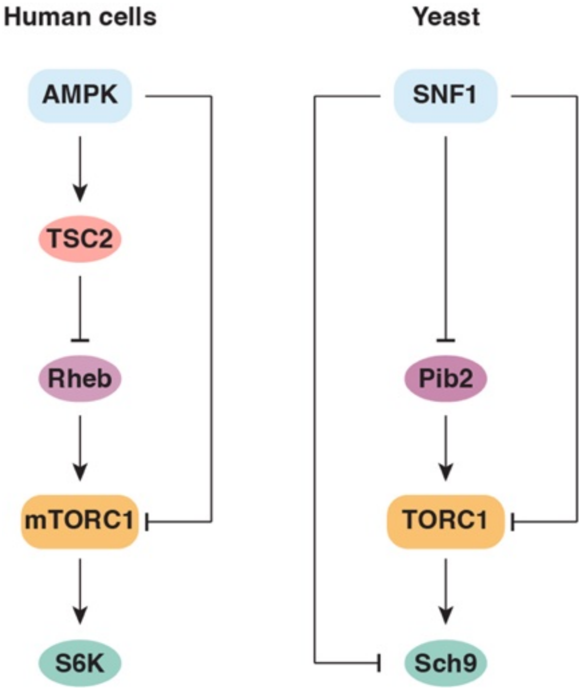

Figure 1. Comparative mechanisms of SNF1/AMPK-mediated inhibition of TORC1/mTORC1. Left Panel: schematic representation of the mechanism by which AMPK inhibits mTORC1 in human cells. AMPK phosphorylates and activates TSC2, which, through its GAP activity, inhibits the mTORC1

activator Rheb. Additionally, AMPK directly phosphorylates the mTORC1 subunit Raptor, leading to the inactivation of the complex. Right Panel: schematic representation of the mechanism by which SNF1 inhibits TORC1 in yeast. SNF1 phosphorylates and inhibits the upstream TORC1 regulator Pib2. Similarly to human cells, SNF1 phosphorylates the TORC1 subunit Kog1, resulting in the formation of TORC1-bodies. SNF1 also phosphorylates and inhibits the primary TORC1 target, Sch9.

In yeast, it was recently observed that SNF1 phosphorylates the TORC1 subunit Kog1 to induce TORC1 inhibition via the formation of TORC1-bodies (**Figure 1**) (Hughes Hallett et al., 2015; Sullivan et al., 2019). Additionally, and independently of SNF1, TORC1 assembles into TOROID structures after long carbon starvation, which is necessary for its inactivation (Prouteau et al., 2023; Prouteau et al., 2017). However, these long-term inhibitory mechanisms (Hughes Hallett et al., 2015) do not explain the rapid inhibition of TORC1 observed within the first minutes of acute carbon starvation (Caligaris et al., 2023a; Hughes Hallett et al., 2015; Prouteau et al., 2023; Prouteau et al., 2017). Here, we provide a more comprehensive understanding of the mechanisms by which SNF1 rapidly modulates TORC1 activity. Using SILAC-based phosphoproteomic analysis and *in vitro* kinase assays, we identified and confirmed the direct phosphorylation of the TORC1 upstream regulator Pib2 and the downstream effector Sch9 by SNF1 (**Figure 1**). The combination of these mutants increased the inhibitory effect of SNF1 on the TORC1 pathway. However, we could not achieve complete inhibition of TORC1, hinting that SNF1 may also target other TORC1 regulators.

In the same dataset, we identified putative SNF1 phosphorylation sites on other proteins connected to the TORC1 signaling pathway, such as Lst4, Apl6, and Sea2/Rtc1, all upstream regulators of TORC1, that act through different mechanisms (Hatakeyama et al., 2019; Nicastro et al., 2017; Panchaud et al., 2013a; Péli-Gulli et al., 2017; Péli-Gulli et al., 2015). To date, we cannot yet exclude the possibility that their additional phosphorylation and modulation by SNF1 is required to completely inhibit TORC1 within the first minutes after carbon depletion. Further investigations into the role of SNF1 phosphorylation of Lst4, Apl6, and Sea2 is needed to decipher the additional regulatory layers between SNF1 and TORC1.

Given their well-established involvement in different cellular processes and functions, it can be tested whether SNF1-dependent phosphorylation of Lst4, Apl6, and Sea2 affects their function. Indeed, *in vivo* mutants could be generated using CRISPR/Cas9 to monitor their activity. One might expect, for instance , weakened GAP activity of Lst4 towards Gtr2 (Nicastro et al., 2017; Péli-Gulli et al., 2017; Péli-Gulli et al., 2015). Similar to nitrogen starvation, Lst4 is enriched on the vacuolar surface during carbon depletion (Pacitto et al., 2015; Péli-Gulli et al., 2017). Based on the mammalian model illustrated by Fromm et al., it could be tested whether the Lst4-Lst7 dimer, when phosphorylated by SNF1, localizes to the vacuole and interact with Gtr1-Gtr2 (Fromm et al., 2020). A functional model could predict that upon glucose readdition, Lst4 could become dephosphorylated on the SNF1-dependent residues, leading to a stimulation of its GAP activity, and thereby promoting the hydrolysis of GTP to GDP in Gtr2. This would lead to TORC1 activation, and phosphorylation of the Lst4 intra-DENN loop, resulting in Lst4 being released from the vacuole and translocated into the cytosol (Péli-Gulli et al., 2017). Interestingly, our newly identified sites on Lst4, and the TORC1-dependent phosphosites (Péli-Gulli et al., 2017; Péli-Gulli et al., 2015), are both localized in the intra-DENN loop.

The function of Apl6, which is involved in the proper distribution of the EGOC on the vacuole (Hatakeyama et al., 2019), may also be impaired by SNF1. Therefore, the localization of the EGOC can be monitored under carbon starvation and be analyzed for its dependency on SNF1 and in serine-to-alanine and serine-to-glutamate mutants of Apl6. However, even if SNF1 would limit the translocation of EGOC from the Golgi to the vacuole, the effect on TORC1 activity would likely be delayed. This delay occurs because the initial vacuolar pool of EGOC would need to be turned over and displaced from the vacuole before any observable effect on TORC1.

In human cells, AMPK phosphorylates the ortholog of Sea2, namely WDR24 (Dai et al., 2023; Tafur et al., 2022). Dai et al. suggest a model where the WD40 domain of WDR24 provides a site for AMPK-mediated phosphorylation at Ser^{155}, which facilitates interaction with the 14-3-3γ protein (Dai et al., 2023). This interaction likely induces conformational changes in the GATOR2 complex, impacting its integrity and subsequently regulating mTORC1 signaling under glucose starvation conditions (Dai et al., 2023). Even though the putative phosphorylated sites on Sea2 do not correspond to the AMPK-phosphosites on WDR24 (by BLAST protein sequence alignment), SNF1 could still affect the SEACAT complex via phosphorylating Sea2 (Nicastro et al., 2017; Panchaud et al., 2013a). Indeed, SNF1 may decrease the interaction between SEACAT and SEACIT, which could be monitored by measuring the interaction of Sea2 with members of the SEAC using standard CoIPs, as well as probing its localization via microscopic analysis. Recent observations by Tafur et al. suggest that SEACAT is the core complex of SEAC and likely functions as a sensor to regulate the activity of SEACIT (Tafur et al., 2022). Therefore, by targeting the subunit Sea2, SNF1 may indirectly signal the absence of glucose to the SEAC, and control the GTP/GDP loading status of Gtr1.

After verifying the involvement of SNF1 in the regulation of the aforementioned proteins, a challenging but informative analysis would be to create a yeast strain bearing serine-to-alanine or serine-to-glutamate mutations of the presumably SNF1-regulated residues in all the proteins that could impact the TORC1 pathway. This approach would help to recapitulate all the mechanisms employed by SNF1 to inhibit TORC1.

Phosphorylation and functional modulation of Sch9 by nutrient-sensing pathways

The AGC protein kinase Sch9 is a central regulator of cellular processes essential for cell growth, ribosome biogenesis, and protein synthesis, and is the most well-characterized TORC1 effector in yeast (Caligaris & De Virgilio, 2024; Caligaris et al., 2023b; Deprez et al., 2023; Jorgensen et al., 2004; Urban et al., 2007). Although Sch9 does not have a direct human ortholog, it shares functional similarities with AKT due to their common role in promoting growth (Gonzalez et al., 2015; Yerlikaya et al., 2016). Conversely, while S6K and Sch9 are similarly regulated and activated by C-terminal phosphorylation in the hydrophobic motif by mTORC1 and TORC1 respectively, the function of S6K in yeast cells is performed by Ypk3 (Gonzalez et al., 2015; Urban et al., 2007; Yerlikaya et al., 2016).

Sch9 is phosphorylated in response to the presence of nutrients by Pkh1-3, TORC1, and Pho85-Pho80, in absence of glucose by SNF1, and to promote cell cycle by Bur1-Bur2, making it a central hub for nutrient sensing in yeast (**Figure 2**) (Caligaris et al., 2023a; Caligaris et al., 2023b; Deprez et al., 2023; Jin et al., 2022; Urban et al., 2007). Here, we demonstrated that SNF1 phosphorylates Sch9 on Ser^{288} (Caligaris et al., 2023a) and a recent study has shown that SNF1 also phosphorylates Sch9 at Ser^{160} and Ser^{163} in response to DNA damage in aged cells (Lucca et al., 2024). We also proved that Pho85 phosphorylates Sch9 on Ser^{726} (Deprez et al., 2023). Additionally, a recent preprint by Jin et al. proposed that Pho85-Pho80 phosphorylates Sch9 on Thr^{570}, a site previously attributed to Pkh1-3, upon reactivation after hyperosmotic stress to restart the cell cycle (Jin et al., 2024). Based on their findings, not only does Pho85-Pho80 prime Sch9 for subsequent TORC1 phosphorylation (Deprez et al., 2023), but it also appears to be required for its full activation by phosphorylating the T-loop (Jin et al., 2024).

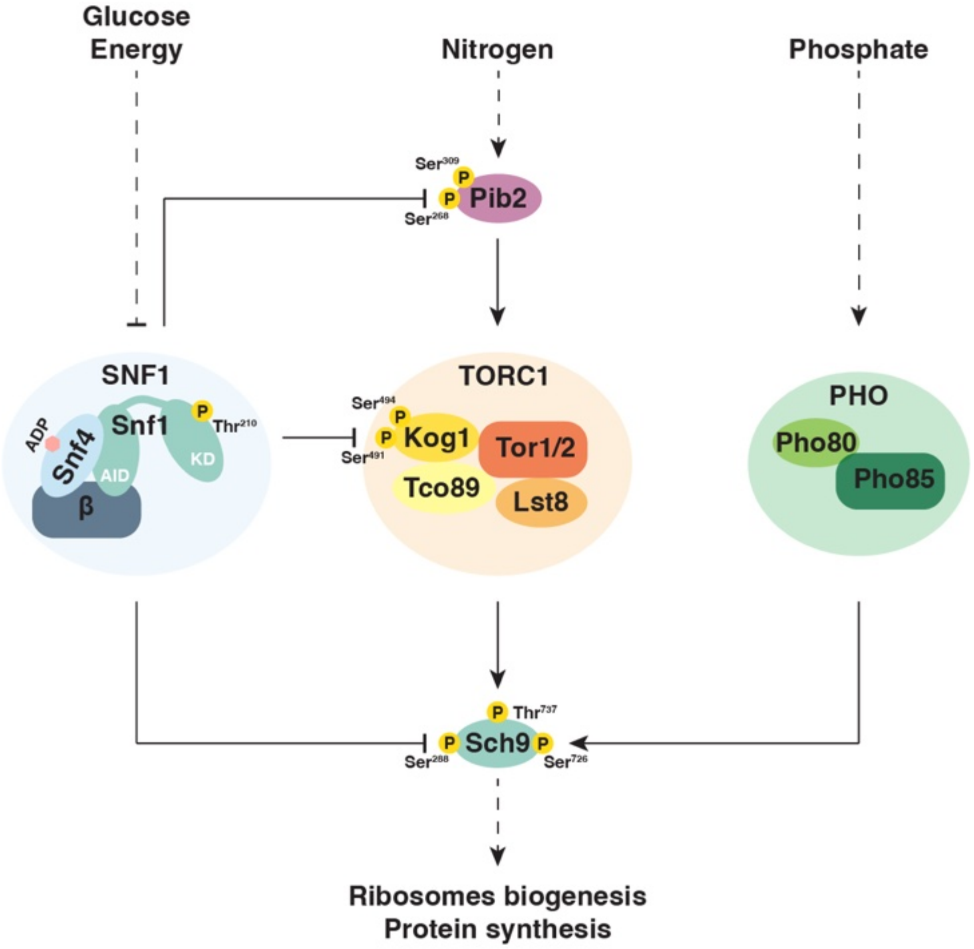
Glucose
Energy
Nitrogen
Phosphate
Ser309
P
P
Pib2
Ser268
SNF1
ADP
Snf4
Snf1
P
Thr210
KD
AID
β
TORC1
Ser494
P
P
Kog1
Tor1/2
Ser491
Tco89
Lst8
PHO
Pho80
Pho85
P
Thr737
P
Sch9
P
Ser288
Ser726
Ribosomes biogenesis
Protein synthesis

Figure 2. SNF1, TORC1, and PHO nutrient sensing pathways converge on Sch9.
The nutrient sensing pathways analyzed in this thesis (*i.e.* SNF1, TORC1, and PHO) impinge on Sch9. In the presence of amino acids, TORC1 phosphorylates the residue Thr^{737} of Sch9. In the presence of phosphate, Pho85-Pho80 phosphorylate the residue Ser^{726}. In the absence of glucose, SNF1 phosphorylates the residue Ser^{288}. Additionally, SNF1 inhibits TORC1 via direct phosphorylation of Kog1 on Ser^{491} and Ser^{494}, and of Pib2 on Ser^{268} and Ser^{309}.

In this study, we demonstrated that Pho85 primes Sch9 for TORC1 phosphorylation of Thr^{737} and that the serine-to-alanine mutation at residue Ser^{726} on Sch9 resulted in a mild but significant increase in cell survival under phosphate starvation (Deprez et al., 2023). To further clarify the role of Pho85-dependent phosphorylation of Sch9, it would be beneficial to investigate whether the phosphomimetic mutant (serine-to-glutamate) can support growth in the complete absence of phosphate. This condition is challenging to achieve due to the extensive phosphate reservoirs in yeast vacuoles. Additionally, considering recent findings, this investigation could be combined with thereonine-to-alanine and threonine-to-glutamate mutants of Thr^{570} (Jin et al., 2024). Sch9 functionality could be monitored not only through growth assays but also by assessing the gel mobility of its targets Maf1, however this approach might yield misleading results due to Maf1's dual phosphorylation by PKA (Huber et al., 2009;

Moir et al., 2006), and Rim15 on residue Ser^{1061} (Wanke et al., 2008). Concurrently, phosphorylation of Thr^{1075} on Rim15 could serve as a control for Pho85 activtiy under these conditions (Wanke et al., 2005).

Similarly to Sch9, S6K is targeted by various kinases, including PDK1, GSK-3, Cdc2-CycB, and mTORC1, which converge their signals onto it (Deprez et al., 2023; Moser et al., 1997; Saitoh et al., 2002; Shah et al., 2003; Shin et al., 2011). As S6K is dysregulated in diseases such as cancer, diabetes, and obesity (Tavares et al., 2015), it is gaining interest as a therapeutic target (Antoniou et al., 2022; Tavares et al., 2015). Since targeting upstream regulators may also affect other downstream effectors (Tavares et al., 2015), understanding that specific dysregulated pathways impact S6K and that S6K is the cause of the disease can be advantageous for treatment. Therefore, increasing our knowledge of Sch9/S6K and their regulation can be beneficial for developing treatments.

Spatial regulation and target specificity of SNF1 in yeast

It is well established that in yeast the protein kinase complex SNF1 localizes to different cellular compartments upon activation (Chandrashekarappa et al., 2016; Hedbacker et al., 2004b; Mangat et al., 2010; Vincent et al., 2001). This localization is dependent on the β-subunits Gal83, Sip1, and Sip2, which have divergent N-terminal regions that facilitate their spatial separation (Chandrashekarappa et al., 2016; Hedbacker et al., 2004b; Mangat et al., 2010; Vincent et al., 2001). SNF1 compartmentalization confers substrate specificity to the kinase, allowing it to modulate different signaling pathways and processes within specific cellular regions. Our study aims to provide a more detailed understanding of the specific targets recognized by each spatially separated SNF1 pool.

Using SILAC-based phosphoproteomic analysis, we have been able to confirm previously identified SNF1 targets and determine which SNF1 pool is involved in their phosphorylation. Additionally, we identified new putative targets, which are specifically phosphorylated by spatially distinct SNF1 pools, such as Atg13, Atg31, Atg33, Dot6, Tod6, Stb3, Ifh1, Rim15, Pho81, Pkh2, and Pkh3, phosphorylated by the Gal83-Snf1 complex; Atg16, Muk1, Rad52, and Pep3, phosphorylated by the Sip1-Snf1 complex; and Ubp3, Ubp5, and Bud3, phosphorylated by the Sip2-Snf1 complex. By combining this dataset with other omic analyses, such as interactomics and TurboID proximity labeling (**Figure 3**), we aim to increase the resolution of the identification of SNF1 pool targets. Specifically, for the proxisome analysis, we propose to genomically tag the β-subunits with TurboID to monitor their proxisome localization under high and low glucose conditions (Larochelle et al., 2019). As a control, we aim to express the sole TurboID and force its targeting to the nucleus, vacuole, or cytosol. Additionally, to ensure comparable expression levels to the β-subunits, they will be expressed under the control of the β-subunits' promoters. Ideally, this approach will allow us to discriminate between nonspecifically biotinylated proteins and those in proximity to the specific SNF1 pools.

Once new putative targets are identified via omic analyses, we aim to validate them through *in vivo* mutagenesis and phenotype studies. Our final goal is to address the role of SNF1 in the nucleus, vacuole, and cytosol, and to determine which specific pathways are regulated in these compartments.

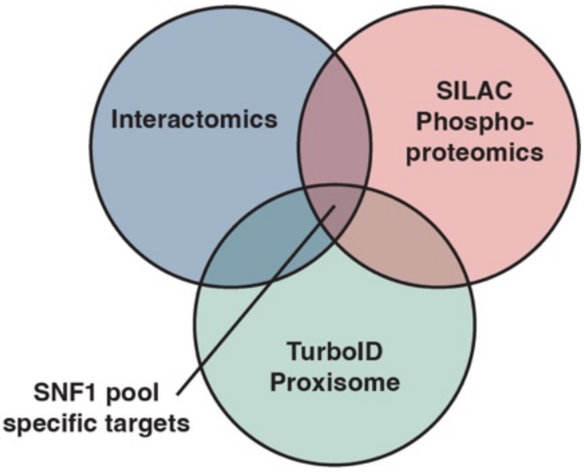

Figure 3. Schematic representation of the experimental approach to identify SNF1 targets in different cellular compartments.

The Venn diagrams illustrate the overlap between three datasets: SILAC-based phosphoproteomics (red), interactomics (blue), and TurboID proximity labeling (green). The intersections of these datasets highlight the specific targets of SNF1 in each cellular compartment, providing higher resolution and deeper insights into its compartment-specific functions.

One particularly interesting role of SNF1, which warrants further investigation, is its function on the vacuolar surface. Here, SNF1 may directly regulate the TORC1 signaling pathway by phosphorylating both upstream and downstream TORC1 regulators (Caligaris et al., 2023a). An intriguing and unexplored hypothesis is that Sip1 may function as a functional ortholog of AXIN1 in human cells (Gonzalez et al., 2020; Hindupur et al., 2015; Mallick & Gupta, 2021). AXIN1 bridges Ragulator with LKB1 and AMPK, allowing AMPK to come into closer contact with mTORC1 (**Figure 4**) (Gonzalez et al., 2020; Hindupur et al., 2015; Mallick & Gupta, 2021). Similarly, it can be hypothesized that Sip1, not only via myristoylation, is enriched on the vacuolar surface (Hedbacker et al., 2004b), but it may also interact with subunits of the EGOC to bring SNF1 and TORC1 into close proximity and function as a functional ortholog of AXIN1 (**Figure 4**). Ultimately, this would also facilitate a possible regulation of SNF1 by TORC1 in nutrient- and amino acid-rich conditions.

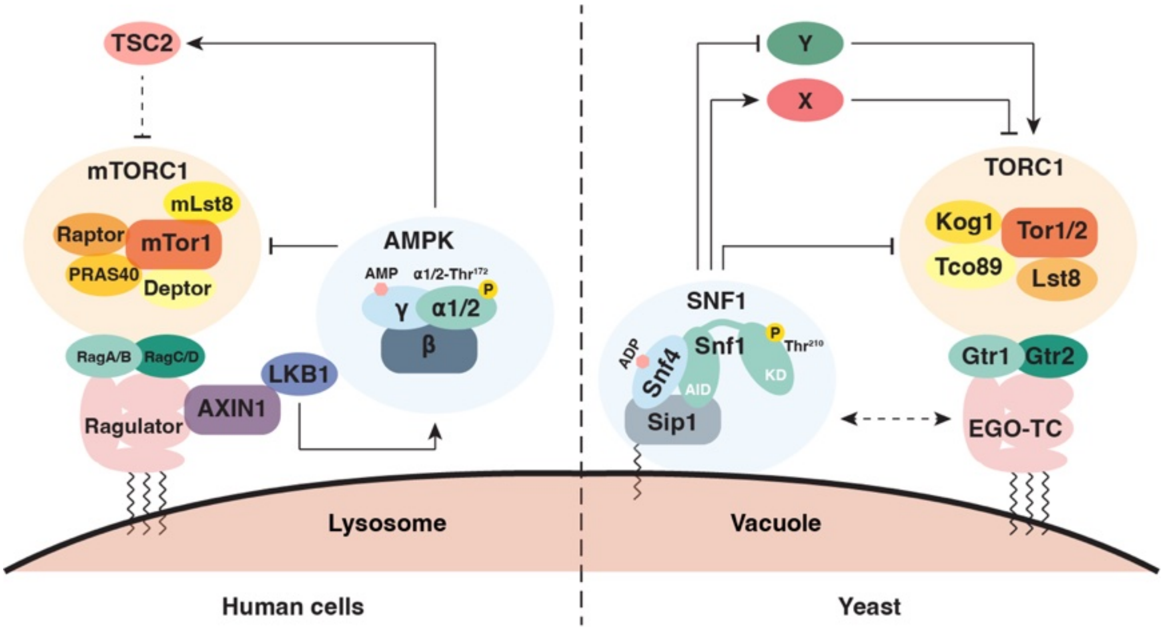
TSC2
mTORC1
mLst8
Raptor
mTor1
PRAS40
Deptor
AMPK
AMP
α1/2-Thr^{172}
P
γ
α1/2
β
RagA/B
RagC/D
LKB1
AXIN1
Ragulator
Lysosome
Human cells
Y
X
TORC1
Kog1
Tor1/2
Tco89
Lst8
SNF1
ADP
Snf4
Snf1
P
Thr^{210}
AID
KD
Sip1
Gtr1
Gtr2
EGO-TC
Vacuole
Yeast

Figure 4. Lysosomal and vacuolar targeting of SNF1/AMPK in TORC1/mTORC1 inhibition. In mammalian systems, AMPK is recruited to the lysosomal surface via the Ragulator-AXIN1-LKB1 complex, where it can inhibit mTORC1 through various mechanisms. In yeast, SNF1 is tethered to the vacuolar surface via Sip1. We aim to identify upstream regulators of TORC1 that mediate the Snf1-Sip1-dependent inhibition of TORC1. For more details, refer to the text.

The spatial compartmentalization of SNF1 and the target specificity of its pools are significant topics of interest in the field. Recent efforts have focused on identifying similar mechanisms in human cells (Gonzalez et al., 2020; Herzig & Shaw, 2018; Liang et al., 2015; Salt et al., 1998; Schmitt et al., 2022; Steinberg & Hardie, 2023; Trefts & Shaw, 2021; Zong et al., 2019). In our laboratory, through an ongoing collaborative project, we aim to explore the evolutionarily conserved mechanisms of energy regulation by AMPK and its orthologs in human cells, animal models, and plants (*A. thaliana*). Our focus is on their functional roles and the importance of spatially distinct pools within cells. Dysregulation of AMPK is linked to various human diseases, including metabolic syndrome and diabetes, making this research highly relevant for understanding disease mechanisms and developing potential therapies (Hardie, 2013; Hardie et al., 2016).

MATERIAL AND METHODS

Material and Methods

Yeast strains and plasmid

The *Saccharomyces cerevisiae* strains and plasmids used in this thesis are listed in **Tables 1 to 8** in the next section. Gene deletions and tagging were introduced using the pFA6a (Janke et al., 2004) and the pGT (Wosika et al., 2016) system-based PCR toolboxes. Point mutants were generated by CRISPR/Cas9 mutagenesis (Generoso et al., 2016). For the creation of the Cas9-expressing plasmids, oligos containing the variable part of the gRNA were used to amplify the entire plasmids (pRCC-K; (Generoso et al., 2016)) by PCR. The PCR products were ligated for 30 min at 50 °C with the Gibson Assembly Master Mix (New England Biolabs; M5510), and the ligation products were used to transform competent *E. coli* cells. Plasmids were confirmed by sequencing.

Unless stated otherwise, yeast strains were rendered prototrophic by transforming them with empty centromeric plasmids listed in the **Tables 2, 4, 6, and 8** in the next section.

Yeast transformation

Yeast cells were transformed using the Gietz method (Gietz et al., 1995). Cells were pre-grown in YPD medium overnight and then diluted in fresh YPD to 0.1 OD_{600nm}/mL in the morning. Cells were grown to exponential phase, washed with sterile water, and then with 1 mL of 0.1 M LiAc. The corresponding volume of cells at 10 OD_{600nm} was used for transformation. The transformation mix contained 240 µL of 50% PEG, 36 µL of 1 M LiAc, 5.3 µL of ssDNA (Salmon Sperm DNA), and a total of 69 µL of sterile H_2O and exogenous DNA.

For site-directed mutagenesis by CRISPR/Cas9 method, 5 µL of plasmid and 20 µL of donor sequence were used. For gene deletion or tagging, 15 µL of DNA cassettes were used. For plasmid expression, 1 to 3 µL of plasmids were used. Cells were incubated at 42 °C for 40 min. After the heat shock, cells were washed twice with sterile water. If the exogenous DNA contained a metabolic marker, cells were directly plated on selective media. If the exogenous DNA contained a dominant marker, cells were re-suspended in 5 mL of YPD and grown at 30 °C for 3 h. Afterward, they were washed with sterile water and then plated onto YPD plates containing the selection drug.

Clones containing the correct mutations were verified by colony PCR for gene deletions, western blot for gene tagging, and colony PCR and sequencing for CRISPR/Cas9 mutagenesis.

Growth conditions

To maintain plasmids for gene expression or which render the strains prototrophic, cells were pre-grown overnight in synthetic dropout (SD) medium (0.17% yeast nitrogen base, 0.5% ammonium sulfate [AS], 0.2% dropout mix [USBiological], and 2% glucose). In the morning, cells were diluted in synthetic complete (SC) medium (SD with all amino acids). A similar procedure was adopted for experiments where cells were grown in media containing low glucose (0.05% instead of 2% glucose) or low nitrogen (0.0625% AS instead of 0.5% and devoid of amino acids). Starvation experiments were conducted by filtering cells and transferring them to carbon starvation medium (SC without glucose), nitrogen starvation medium (2% glucose, 0.17% yeast nitrogen base, 0.1 g/L adenine, and 0.05 g/L uracil), or nitrogen and carbon starvation medium (0.17% yeast nitrogen base, 0.1 g/L adenine, and 0.05 g/L uracil) for the times indicated. In nutrient readdition experiments, 2% final glucose, 3.3 mM glutamine, or 1X final all amino acids mix were added to the culture. Solid media contained an additional 2% agar.

When indicated, cells were treated with the following drugs: 10 µM 2NM-PP1 dissolved in DMSO (DiMethylSulfOxide), with the same volume of DMSO added to the culture as a control; and 200 nM final rapamycin (dissolved in 90% ethanol and 10% Tween).

Cell growth was assessed by measuring the concentration (expressed as OD_{600nm}/mL) using a spectrophotometer.

Growth assay on plate

Yeast cell cultures were pre-grown overnight in either SD or SC media until reaching an OD_{600nm} above 1.0. After pelleting, cells were washed twice with sterile H_2O. 10-fold serial dilutions, starting from an initial concentration of 1.0 OD_{600nm}/mL, were prepared in sterile water. Subsequently, cells were spotted onto plates containing various carbon or nitrogen sources, or in the presence of rapamycin at specified concentrations. Cells were then incubated for 3 days at 30 °C.

Cell lysate preparation

Cell lysates were prepared similarly to the method previously described (Hatakeyama et al., 2019). Specifically, 10 mL of exponentially growing cells (with an OD_{600nm} ranging from 0.5 to 0.8) were harvested in a pre-cooled tube containing 100% TCA (trichloroacetic acid), resulting in a final TCA concentration of 6%. In cases of exponential growth in restrictive media (such as low glucose or low nitrogen conditions), a larger volume of cells (14 mL) was harvested. The harvested samples were cooled on ice for 10 min. Next, the cells were pelleted at 4 °C, and the TCA was almost completely removed. Cell pellets were then transferred to 1.5 mL Eppendorf tubes. After pelleting the cells again at 4 °C, they were washed with 1 mL of pre-cooled 100% acetone. Subsequently, the acetone was removed, and the pellets were dried using a Savant SpeedVac. To the dried pellets, urea buffer (6 M urea, 50 mM Tris-HCl pH 7.5, 5 mM EDTA, and 1% SDS) was added in proportion to 100 μL of buffer per 8.0 OD_{600nm} of cells. Additionally, an equal volume of acid-washed glass beads was added. The cells were then lysed by beating in a Precellys machine (using 2 cycles of 3 rounds of 30 seconds each, followed by a 60-second pause) at 4 °C. Finally, 2X Laemmli buffer (350 mM Tris-HCl pH 6.8, 10% SDS, 30% glycerol, 0.0002% bromophenol blue, and 600 mM DTT) was added, and the samples were denatured at 98 °C for 5 min.

SDS-PAGE and Western blotting

Protein separation was performed on polyacrylamide gels. Stacking gels were made at a concentration of 4.5% polyacrylamide (125 mM Tris-HCl pH 6.8, 1% SDS, 1% APS, and 0.2% TEMED) while running gels were made at a concentration of polyacrylamide between 7.5% and 12% (375 mM Tris-HCl pH 8.8, 1% SDS, 0.5% APS, and 0.16% TEMED). The run inside the stacking gel was performed at a constant voltage of 60 V, while inside the running gel at 15 mAh for each gel in the running apparatus, at constant amperage. The running apparatus was immersed in the running buffer (25 mM Tris, 192 mM glycine, and 0.1% SDS).

After separation, proteins were transferred to a nitrocellulose membrane using the wet transfer blot system. The transfer was performed using transfer buffer (20% methanol, 25 mM Tris-HCl pH 8.3, and 192 mM glycine) for 90 min. The correct transfer was checked by staining the membrane with Ponceau S (1% acetic acid and 0.1% Ponceau powder). The stain was removed by washing the membrane with TBS 1X (20 mM Tris-HCl pH 7.4, 150 mM NaCl, and 2.7 mM KCl).

Blocking was performed using TBS supplemented with 5% milk for 1 h at room temperature. The filters were incubated overnight at 4 °C with the primary antibody listed in **Table 9**, with slow but continuous mixing. The following day, the membrane was washed 3 times for 5 min with TBS or PBS (2.7 mM KCl, 150 mM NaCl, 7.4 mM $Na_2HPO_4 \cdot 2H_2O$, and 1.5 mM KH_2PO_4) solutions containing Tween. The membranes were incubated with the secondary antibodies (**Table 9**) for 1 h at room temperature and then washed 3 times for 5 min with TBS or PBS solutions containing Tween.

Signals were detected using ECL (Enhanced Chemiluminescence) solutions with different sensitivities, depending on the intensity of the expected signal, and using the FUSION FX machine (VILBER).

Co-immunoprecipitation

Yeast cells expressing the indicated fusion proteins were grown overnight in 500 mL SC medium and harvested by filtration when they reached a concentration of 1.0 OD_{600nm}/mL. Cells were frozen in liquid nitrogen and cryogenically disrupted using the Precellys homogenizer in 4 mL of lysis buffer (50 mM Tris-HCl pH 7.5, 150 mM NaCl, 0.1% NP-40, 10% glycerol, Roche PhoSTOP phosphatase inhibitor, and Roche complete protease inhibitor EDTA-free) in the presence of acid-washed glass beads using 2 cycles of 3 rounds of 30 seconds each, followed by a 60-second pause. In the case of Pib2 co-immunoprecipitation, 60 mM glutamine was added to the lysis buffer as in (Ukai et al., 2018). Protein concentration was measured with the Bradford method (Bradford, 1976). Cleared lysates were equilibrated in the same lysis buffer. For input samples, aliquots of cleared lysates were collected and denatured in the presence of 2X Laemmli buffer. For co-immunoprecipitations, the cleared lysates were incubated for 4 hours at 4 °C with prewashed anti-c-myc MagBeads (Pierce Thermo Fisher Scientific, product number 88843). After 5 washes with lysis buffer, beads were resuspended in 20 µL lysis buffer and denatured in the presence of 2X Laemmli buffer. Inputs and pull-down samples were analyzed by SDS-PAGE immunoblot and immunodecorated with the antibody listed in **Table 9**.

Protein purification from yeast

For the purification of the SNF1 complex, yeast strains expressing Snf1-TEV-TAP variants were pre-grown overnight in YPD medium. The following day, cells were diluted in 2 L of YPD to 0.2 OD_{600nm}/mL. Once the cells reached approximately the concentration of 2.0 OD_{600nm}/mL, they were harvested by filtration. To purify an active and phosphorylated SNF1 complex, the cells were washed on the filter with 1 L of H_2O. Cells expressing the catalytically inactive SNF1 complex (containing the Snf1^{T210A} α-subunit) were treated similarly. The same procedure was used for the purified SNF1 complex employed in MicroScale Thermophoresis (MST), which contained the C-terminally GFP-tagged Snf4 γ-subunit.

Yeast cells bearing plasmids for the expression of Sch9$^{1\text{-}394}$-TEV-TAP (Sch9$^{N\text{-}Term}$), Sch9$^{R650\text{-}I824}$-TEV-TAP (Sch9$^{C\text{-}Term}$), or Sch9^{K441A}-TEV-TAP (Sch9$^{KD\text{-}Full\ Length}$) under the control of the *GAL1* promoter (**Tables 2 and 4**) were pre-grown during the day in SRafinose-Ura medium supplemented with 0.1% sucrose (0.17% yeast nitrogen base, 0.5% ammonium sulfate [AS], 0.2% dropout mix without uracil [USBiological], 2% raffinose, and 0.1% sucrose). In the evening, cells were diluted in 2 L of SRafinose-Ura medium supplemented with 0.1% sucrose to 0.0004 OD_{600nm}/mL. To induce gene expression, 2% galactose was added when the cells reached a concentration of approximately 0.2 OD_{600nm}/mL. The induction with galactose was carried out for 6 h, after which the cells were harvested by filtration.

For the protein purification of SNF1 complex variants or Sch9 variants, cells were collected by filtration, frozen in liquid nitrogen, and cryogenically disrupted using a Precellys homogenizer in 10 mL of lysis buffer (50 mM Tris-HCl pH 7.5, 150 mM NaCl, 0.1% NP-40, 10% glycerol, Roche PhoSTOP phosphatase inhibitor, and Roche complete protease inhibitor EDTA-free) in the presence of acid-washed glass beads, using 2 cycles of 3 rounds of 30 seconds each, followed by a 60-second pause. The cleared lysates were incubated for 4 h at 4 °C with IgG-coupled Dynabeads (Dynabeads M-270 Epoxy; Invitrogen, Thermo Fisher Scientific, Basel, Switzerland). The beads were washed 5 times with lysis buffer, and proteins were eluted in TEV buffer (50 mM Tris-HCl pH 7.5 and 0.5 mM EDTA) with 2% TEV protease for 1 h at 18 °C. Finally, 10% glycerol was added to the purified proteins, which were then stored at -80 °C.

pho85Δ yeast cells bearing plasmids for the expression of HA_2-Pho85, HA_2-Pho85^{E53A} (kinase-dead), and Pho80-GST (**Table 4**) were pre-grown overnight in SD-Ura medium (0.17% yeast nitrogen base, 0.5% ammonium sulfate [AS], 0.2% dropout mix without uracil [USBiological], and 2% glucose). In the morning, cells were diluted to 0.2 OD_{600nm}/mL in 2 L of SD-Ura. When the cells reached a concentration of approximately 2.0 OD_{600nm}/mL, they were harvested by filtration. To induce Pho80-GST expression, 500 µM $CuSO_4$ was added to the culture for 1 h (Wanke et al., 2005).

For the protein purification of Pho85 variants and Pho80, cells were collected by filtration, frozen in liquid nitrogen, and cryogenically disrupted using a Precellys homogenizer in 10 mL of lysis buffer (50 mM Tris-HCl pH 7.5, 150 mM NaCl, 0.5 mM EDTA, 0.1% NP-40, 10% glycerol, 1 mM PMSF, 1 mM DTT, Roche PhoSTOP phosphatase inhibitor, and Roche complete protease inhibitor EDTA-free) (Wanke et al., 2005) in the presence of acid-washed glass beads, using 2 cycles of 3 rounds of 30 seconds each, followed by a 60-second pause. The cleared lysate was incubated for 2 h at 4 °C with anti-HA magnetic beads (Fisher Scientific AG, Basel, Switzerland) for HA_2-Pho85 and HA_2-Pho85^{E53A} purifications, and glutathione magnetic agarose beads (Fisher Scientific AG, Basel, Switzerland) for Pho80-GST purification. The beads were washed 5 times with lysis buffer. HA-beads coupled with Pho85 or Pho85^{E53A} were resuspended in elution buffer (50 mM Tris-HCl pH 7.5 and 150 mM NaCl) and stored at -80 °C after the addition of 10% glycerol. GST-coupled beads with Pho80 were eluted at room temperature in elution buffer (50 mM Tris-HCl pH 7.5, 150 mM NaCl, and 10 mM L-glutathione reduced) for 2 h.

Purified proteins were separated by SDS-PAGE and stained with SYPRO Ruby (S4942, Sigma-Aldrich) for quantification.

Protein purification from *E. coli*

Proteins were purified from *E. coli* as described in (Péli-Gulli et al., 2015). *E. coli* cells bearing plasmids for the expression of His$_6$-Pib2$^{221\text{-}635}$ variants (**Table 2**) were pre-grown overnight in LB (Luria-Bertani; 20 g LB [USBiological]) medium containing 25 μg/mL kanamycin and 34 μg/mL chloramphenicol at 37 °C. The following day, cells were diluted to 0.05 OD$_{600nm}$/mL in 1 L LB containing 25 μg/mL kanamycin and 34 μg/mL chloramphenicol, and grown at 37 °C until they reached 0.6 OD$_{600nm}$/mL. Cells were then transferred to a pre-cooled incubator at 16 °C. When they reached 0.8 OD$_{600nm}$/mL, protein expression was induced overnight by adding 1 mM IPTG (Isopropyl β-D-1-thiogalactopyranoside).

Cells were harvested by centrifugation at 4000 rpm for 10 min at 4 °C and resuspended in 20 mL lysis buffer (50 mM NaH_2PO_4 pH 8.0, 300 mM NaCl, 0.1% NP-40, and Roche complete protease inhibitor EDTA-free). Cells were disrupted by sonication, and the clear lysate was incubated with Ni-charged agarose beads (QIAGEN, product number 30210) for 2 h at 4 °C. Beads were washed 5 times with washing buffer (50 mM NaH_2PO_4 pH 8.0, 300 mM NaCl, and 10 mM imidazole). Finally, proteins were eluted with elution buffer (50 mM NaH_2PO_4 pH 8.0 and 200 mM imidazole) and stored at -80 °C after the addition of 10% glycerol.

Purified proteins were separated by SDS-PAGE and stained with Coomassie Blue (0.25% Coomassie Brilliant Blue R-250, 40% ethanol, and 10% acetic acid) for quantification.

In vitro kinase assay

SNF1 *in vitro* radioactive kinase assays were performed using WT or T210A (kinase-dead) SNF1 complexes in SNF1 kinase buffer (20 mM HEPES pH 7.5, 100 mM NaCl, 0.5 mM EDTA, 0.5 mM DTT, and 5 mM MgAc). The reactions contained 60 ng SNF1 (quantified with respect to the α-subunit), and either 1 µg His$_6$-Pib2 or 80 ng Sch9$^{N\text{-term}}$ in a total volume of 20 µL. Reactions were initiated by adding the ATP mix (3 µL 10 μCi/μL [γ–^{32}P]-ATP [Hartmann Analytic, SRP-501], 6 µL 200 µM ATP, and 1 µL kinase buffer). The reactions were carried out at 30 °C for 10 min or 30 min for Pib2 or Sch9, respectively.

Pho85 *in vitro* radioactive kinase assays were performed with HA$_2$-Pho85 and HA$_2$-Pho85^{E53A} (kinase-dead) bound to HA magnetic beads, as described in (Wanke et al., 2005). The reactions were carried out in Pho85 kinase buffer (50 mM Tris-HCl pH 7.5, 20 mM $MgCl_2$, and 1 mM DTT) with 50 ng of kinase, 50 ng of Pho80, and 40 ng of the substrate (Sch9$^{C\text{-term}}$). Reactions were initiated by adding the ATP mix (5 μL 20 mM ATP and 5 μL 10 μCi/μL γ-[^{32}P]-ATP [Hartmann Analytic, SRP-501]) and carried out at 30 °C for 30 min.

Reactions were stopped by adding 3X concentrated SDS-PAGE sample buffer (50 mM Tris-HCl pH 6.8, 5% SDS, 0.05% bromophenol blue, 630 mM DTT, and 30% glycerol). Then, samples were denatured at 65 °C for 10 min and proteins were separated by SDS-PAGE.

Gels were stained with SYPRO Ruby (S4942, Sigma-Aldrich) to assess loading. Finally, gels were dried and then analyzed using a phosphoimager (Typhoon FLA 9500, GE Healthcare, Opfikon, Switzerland).

In vitro kinase assays probed by western blot analysis were carried out similarly as described above, with the difference that reactions were performed in a 40 µL volume for 30 min at 30 °C. In the ATP mix, [γ-^{32}P]-ATP was substituted with H_2O. Finally, the presence of proteins and their phosphorylation was probed using the antibodies listed in **Table 9**, and to assess loading, a gel was stained with SYPRO Ruby (S4942, Sigma-Aldrich).

Microscale thermophoresis

We conducted MicroScale Thermophoresis (MST) experiments with a Monolith NT.115 instrument from Nanotemper Technologies. We used a GFP-tagged Snf4 γ-subunit within the Snf1 complex (0.144 µM) as our labeled component. This was mixed with two-fold serial dilution of unlabelled His$_6$-Pib2$^{221\text{-}635}$ (18.1 µM), in its elution buffer (50 mM NaH_2PO_4 pH 8.0, 200 mM imidazole, and 10% glycerol), or with unlabeled Sch9$^{1\text{-}394}$ in its elution buffer (50 mM Tris-HCl pH 8.0, 0.5 mM EDTA, and 10% glycerol). The samples were then placed into Monolith NT.115 Capillaries, and MST measurements were taken at a 20% laser power setting and a temperature of 30 °C. We repeated the experiments in triplicate and analyzed the data using the Kd model in the MO.Affinity Analysis software provided by Nanotemper Technologies. To determine the dissociation constant (Kd), we graphed the fraction of the bound complex against the logarithmic scale of the ligand concentration.

SILAC-based phosphoproteomics conditions

SILAC-based phosphoproteomics analyses were performed in 5 independent replicas. To label the proteins, cells were grown in the presence of non-labeled or labeled lysine and arginine variants (“medium-heavy” L-arginine-$^{13}C_6$ (Arg6) and L-lysine-$^{2}H_4$ (Lys4), or “heavy” L-arginine-$^{13}C_6$-$^{15}N_4$ (Arg10) and L-lysine-$^{13}C_6$-$^{15}N_2$ (Lys8) amino acids (Sigma-Aldrich)). To ensure complete labeling of the proteins, cells were pre-grown overnight in SD-7 medium (0.17% yeast nitrogen base, 0.5% ammonium sulfate [AS], 0.% dropout mix without adenine, arginine, histidine, leucine, lysine, tryptophan, and uracil [USBiological], and 2% glucose) supplemented with 0.03 g/L arginine and 0.03 g/L lysine, depending on the labeling. In the evening, cells were diluted to 0.1 OD_{600nm}/mL in the same medium. The following day, cells were diluted in 250 mL of SD-Arg-Lys medium (0.17% yeast nitrogen base, 0.5% ammonium sulfate [AS], 0.2% dropout mix without adenine, arginine, histidine, leucine, lysine, tryptophan, and uracil [USBiological], 0.1 g/L adenine, 0.05 g/L leucine, 0.05 g/L histidine, 0.05 g/L tryptophan, 0.05 g/L uracil, and 2% glucose) supplemented with arginine and lysine, depending on the labeling, to 0.1 OD_{600nm}/mL.

For the SILAC-based phosphoproteomics analysis described in **Chapter 1**, when cells reached a concentration of approximately 1.0 OD_{600nm}/mL, cultures grown in the presence of "medium-heavy" and "heavy" arginine and lysine were filtered and resuspended in carbon starvation medium (SD-Arg-Lys with 0.05% glucose instead of 2% glucose) for 5 and 15 minutes, respectively, in the presence of the vehicle (DMSO) or 2NM-PP1, then harvested. Cells grown in the presence of unlabeled arginine and lysine were harvested directly.

For the SILAC-based phosphoproteomics analysis described in **Chapter 3**, when cells reached a concentration of approximately 1.0 OD_{600nm}/mL, cultures grown in the presence of unlabeled or "medium-heavy" arginine and lysine were harvested directly. Cells grown in the presence of "heavy" labeled arginine and lysine were filtered and resuspended in carbon starvation medium (SD-Arg-Lys with 0.05% glucose instead of 2% glucose) for 15 minutes, then harvested.

In both experiments, cell collection was performed by filtration, and the nitrocellulose filter was immersed in tubes containing 40 mL of the cell culture medium (without arginine and lysine) containing 6% TCA. Cells were kept on ice for at least 10 minutes, then pelleted and washed with 40 mL of pre-cooled 100% acetone. Cells were pelleted again and washed with 40 mL of pre-cooled 100 mM Tris-HCl pH 7.5. Cell pellets were then dried overnight in a freeze-dryer (ZIRBUS). 30 milligrams of differentially labeled dried cell pellets of each sample were mixed. Cells were lysed using a Precellys homogenizer in 6 mL of urea buffer (8 M urea and 50 mM Tris-HCl pH 8.0) in the presence of acid-washed glass beads, using 2 cycles of 3 rounds of 30 seconds each, followed by a 60-second pause. Cell debris was pelleted, and the supernatants containing cellular proteins were collected, followed by MS sample preparation.

On beads *in vitro* kinase assay (OBIKA)

The proteome substrate used for the SNF1 OBIKA analysis was obtained from cells from 5 independent cultures of exponentially growing *snf1*^{as} cells. Initially, the cells were pre-grown overnight in 5% glucose YP (Yeast extract-Peptone). The following day, they were diluted to a concentration of 0.2 OD_{600nm}/mL in 2 L of 5% glucose YP and grown until the late exponential phase. At this point, they were treated with 10 µM 1NM-PP1 for 20 min. The cells were then collected by filtration and frozen in liquid nitrogen. For cell disruption, 10 mL of primary amine-free lysis buffer (50 mM HEPES pH 7.5, 1% NP-40, 150 mM NaCl, 1 mM EDTA pH 8.0, 1 mM EGTA pH 8.0, and Roche complete protease inhibitor EDTA-free) was used along with acid-washed glass beads. The cells were lysed by beating in a Precellys machine (2 cycles of 3 rounds of 30 seconds each, with a 60-second pause) at 4 °C. Lysates were collected by centrifugation at 4000 rpm at 4 °C. The lysates were then dialyzed using dialysis buffer (50 mM HEPES pH 7.5, 0.1% NP-40, 150 mM NaCl, 1 mM EDTA pH 8.0, 1 mM EGTA pH 8.0, and 1 mM PMSF) and a molecular-porous membrane tubing (14 kDa, Sigma-Aldrich) to remove primary amine-containing metabolites. After 2 h at 4 °C, the buffer was refreshed for overnight dialysis. N-hydroxy-succinimide (NHS)-activated Sepharose beads (5 mL) were washed 3 times with 10 mL of ice-cold 1 mM HCl and twice with 10 mL of lysis buffer before incubating with 60 mg of protein to saturate the beads. The coupling was performed on a rotating wheel at 4 °C overnight. The beads were then spun down to remove the supernatant and washed 3 times with 10 mL of phosphatase buffer (50 mM HEPES, 100 mM NaCl, 0.1% NP-40). 1 mL of phosphatase buffer containing 5000–10000 units of lambda phosphatase with 1 mM $MnCl_2$ was added and incubated overnight at 4 °C on a rotating wheel to dephosphorylate endogenous proteins. The beads were washed twice with 10 mL of kinase buffer (50 mM Tris-HCl pH 7.6, 10 mM $MgCl_2$, 150 mM NaCl, and 1 x PhosSTOP). Endogenous kinases bound to the beads were inhibited by incubation with 1 mM FSBA (5'-(4-Fluorosulfonylbenzoyl)adenosine hydrochloride) in 1 mL of kinase buffer at room temperature on a rotating wheel for 2 h. Additionally, staurosporine was added to a final concentration of 100 µM to inhibit the remaining active kinases for 1 h. The beads were washed 3 times with 10 mL of kinase buffer to remove non-bound kinase inhibitors. The supernatant was completely removed using gel loading tips. Kinase buffer was added to a volume of 860 µL for both kinase-inactive (T210A) and wild-type SNF1 samples. Subsequently, 100 µL of 10 mM ATP, 10 µL of 100 mM DTT, and 30 µL of purified kinase variants were added to each tube. Kinase assays were performed on a rotating wheel at 30 °C for 4 h. Finally, reactions were quenched by snap freezing in liquid nitrogen and samples were lyophilized overnight. Urea buffer (8 M urea and 50 mM NH_4HCO_3 pH 7.8) was added to the dry beads, followed by MS sample preparation (Hu et al., 2021).

Fluorescence microscopy

Confocal microscopy images were captured with an inverted Spinning Disk Confocal Microscope (Nikon Ti-E inverted microscope, VisiScope CSU-W1, Amstelveen, The Netherlands) equipped with a with a dual-camera system (Hamamatsu Orca Quest (C15550-20UP) qCMOS), and a 100x, NA 1.3 oil immersion Nikon CFI series objective. When indicated, FM4-64 staining was performed to stain the vacuolar membranes. Stacks of eleven images with 0.2 μm spacing were taken. Image analysis and processing were performed using the software ImageJ2 (version 2.14.9/1.54f).

Statistical analysis

Statistical significance was assessed using 3 or more independent biological replicates. The analysis was conducted using the Student's t-test analysis with GraphPad Prism 10 software. For comparing normalized data, we employed the paired Student's t-test. We considered values to be significantly different if they had a p-value (or FDR, when specified) below 0.05. The figure legends detail the number of independent replicates, the method of expressing variability, the specific statistical tests used, and the levels of significance.

Supplementary tables

Table 1. Strains used in Chapter 1.

Strain	Genotype	Source
BY4741	*MATα; his3Δ1, leu2Δ0, met15Δ0, ura3Δ0*	Euroscarf
YL515	[BY4741] *MATα; his3Δ1, leu2Δ0, ura3Δ0*	(Binda et al., 2009)
MC037	[YL515] *MATα; snf1Δ::HIS3MX6*	This study
MC012	[YL515] *MATα;* $snf1^{as}$	This study
MC158	[YL515] *MATα; reg1Δ::kanMX*	This study
MB32	[YL515] *MATα; gtr1Δ::kanMX*	(Binda et al., 2009)
Snf1-TAP	[BY4741] *MATa; SNF1-TAP:HIS3MX6*	Open Biosystems(Powis et al., 2015)
MJA5682	[YL515] *MATα; arg4Δ::hisMX4 lys2Δ::hphNT*	(Hu et al., 2019)
NIC078	[MJA5682] *MATα;* $snf1^{as}$	This study
NIC103	[BY4741] *MATa;* $snf1^{T210A}$*-TAP:HIS3MX6*	This study
MC086	[Snf1-TAP] *MATa; SNF4-GFP:kanMX*	This study
MC013	[MC012] *MATα; pib2Δ::HIS3MX6*	This study
MC058	[MC012] *MATα;* $pib2^{SASA}$	This study
MC059	[MC012] *MATα;* $pib2^{SESE}$	This study
MC145	[MC012] *MATα; PIB2-*myc_{13}*:kanMX*	This study
MC152	[MC058] *MATα;* $pib2^{SASA}$*-*myc_{13}*:kanMX*	This study
MC153	[MC059] *MATα;* $pib2^{SESE}$*-*myc_{13}*:kanMX*	This study
MC154	[MC012] *MATα; KOG1-*HA_{3}*:6MX*	This study
MC155	[MC145] *MATα; KOG1-*HA_{3}*:HIS3MX6*	This study
MC156	[MC152] *MATα; KOG1-*HA_{3}*:HIS3MX6*	This study
MC157	[MC153] *MATα; KOG1-*HA_{3}*:HIS3MX6*	This study
MC029	[MC012] *MATα;* $sch9^{S288A}$	This study
MC030	[MC012] *MATα;* $sch9^{S288E}$	This study
MC146	[MC058] *MATα;* $sch9^{S288A}$	This study
MC144	[MC059] *MATα;* $sch9^{S288E}$	This study
MC021	[MC012] *MATα; lst4Δ::HIS3MX6*	This study

Table 2. Plasmids used in Chapter 1.

Plasmid	Genotype	Source
pRS413	*CEN, ARS, amp*^{R}*, HIS3*	(Brachmann et al., 1998)
pRS415	*CEN, ARS, amp*^{R}*, LEU2*	(Brachmann et al., 1998)
pRS416	*CEN, ARS, amp*^{R}*, URA3*	(Brachmann et al., 1998)
pET-24d	*kan*^{R}*, T7p, lacO*	Novagen
p3138	[pET-24d] *His*$_{6}$*-PIB2*$^{221\text{-}635}$	This study
pMC030	[pET-24d] *His*$_{6}$*-pib2*$^{221\text{-}635,S268A}$	This study
pMC031	[pET-24d] *His*$_{6}$*-pib2*$^{221\text{-}635,S309A}$	This study
pMC032	[pET-24d] *His*$_{6}$*-pib2*$^{221\text{-}635,S268,S309A}$	This study
YEplac195	*2µ, amp*^{R}*, URA3*	(Gietz & Sugino, 1988)
pMC013	[YEplac195] *GAL1p-SCH9*$^{1\text{-}394}$*-TAP*	This study
pMC016	[YEplac195] *GAL1p-sch9*$^{1\text{-}394,S288A}$*-TAP*	This study
pMC017	[YEplac195] *GAL1p-sch9*^{K441A}*-TAP*	This study
pYX242-ACC1	*2µ, amp*^{R}*, LEU2, TPI1p-ACC1-GFP-HA*	(Deroover et al., 2016)
pRCC-K	*2µ, amp*^{R}*, kanMX, ROX3p-CAS9, SNR52p*	(Generoso et al., 2016)
pNIC012	[pRCC-K] *SNR52p-SNF1*^{I132} (gRNA)	This study
pNIC015	[pRCC-K] *SNR52p-SNF1*^{T210} (gRNA)	This study
pMC005	[pRCC-K] *SNR52p-SCH9*^{S288} (gRNA)	This study
pMC008	[pRCC-K] *SNR52p-PIB2*^{S268} (gRNA)	This study
pMC009	[pRCC-K] *SNR52p-PIB2*^{S309} (gRNA)	This study

Table 3. Strains used in Chapter 2.

Strain	Genotype	Source
BY4741	*MATa his3Δ1 leu2Δ0 met15Δ0 ura3Δ0*	(Brachmann et al., 1998)
JW 04 038	BY4741 *sch9Δ::NATMX4*	(Wilms et al., 2017)
JW 01 306	BY4741 *sch9Δ::HIS3*	(Smets et al., 2008)
JW 01 307	BY4741 *sch9Δ::LEU2*	(Smets et al., 2008)
JW 03 595	BY4741 *pho85Δ::KANMX4*	YKO collection
JW 12 432	BY4741 *pho81Δ::KANMX4*	YKO collection
JW 10 644	BY4741 *pho80Δ::KANMX4*	YKO collection
JW 03 721	BY4741 *pho80Δ::HIS3*	(Swinnen et al., 2005)
JW 03 604	BY4741 *pcl1Δ::KANMX4*	YKO collection
JW 03 605	BY4741 *pcl2Δ::KANMX4*	YKO collection
JW 12 175	BY4741 *clg1Δ::KANMX4*	YKO collection
JW 03 607	BY4741 *pcl5Δ::KANMX4*	this study
JW 03 608	BY4741 *pcl6Δ::KANMX4*	YKO collection
JW 03 609	BY4741 *pcl7Δ::KANMX4*	This study
JW 03 610	BY4741 *pcl8Δ::KANMX4*	YKO collection
JW 03 611	BY4741 *pcl9Δ::KANMX4*	YKO collection
JW 03 612	BY4741 *pcl10Δ::KANMX4*	This study
JW 03 675	BY4741 *pcl1Δ::KANMX4 pcl2Δ::KANMX4*	This study
JW 03 684	BY4741 *pcl6Δ::KANMX4 pcl7Δ::KANMX4*	This study
JW 03 685	BY4741 *MATα pcl8Δ::KANMX4 pcl10Δ::KANMX4*	This study
JW 01 893	BY4741 *pho80Δ::HIS3 pcl6Δ::KANMX4*	This study
JW 01 894	BY4741 *pho80Δ::HIS3 pcl7Δ::KANMX4*	This study
JW 03 727	BY4741 *pho80Δ::HIS3 pcl6Δ::KANMX4 pcl7Δ::KANMX4*	This study
JW 03 732	BY4741 *pcl6Δ::KANMX4 pcl7Δ::KANMX4 pcl8Δ::KANMX4 pcl10Δ::KANMX4 pho80Δ::HIS3*	This study
JW 03 747	BY4741 *pcl1Δ::KANMX4 pcl2Δ::KANMX4 pcl3Δ::KANMX4 pcl9Δ::Leu2 clg1Δ::KANMX4*	This study
JW 03 591	BY4741 *pho4Δ::KANMX4*	YKO collection
JW 14 686	BY4741 *rim15Δ::KANMX4*	YKO collection
JW 13 780	BY4741 *crz1Δ::KANMX4*	YKO collection
JW 03 664	BY4741 *pho85Δ::KANMX4 pho4Δ::KANMX4*	This study
JW 03 673	BY4741 *pho85Δ::KANMX4 rim15Δ::KANMX4*	(Swinnen et al., 2005)
RG85C1	BY4741 *pho85Δ::KANMX4 crz1Δ::KANMX4*	This study
JW 02 334	BY4741 *pho80Δ::HIS3 pho4Δ::KANMX4*	This study

JW 03 710	BY4741 *pho80Δ::HIS3 rim15Δ::KANMX4*	(Swinnen et al., 2005)
JW 02 430	BY4741 *pho80Δ::HIS3 crz1Δ::KANMX4*	This study
JW 02 338	BY4741 *sch9Δ::LEU2 pho80Δ::HIS3 pho4Δ::KANMX4*	This study
JW 03 594	BY4741 *pho84Δ::KANMX4*	YKO collection
yet36	BY4741 *SCH9::GFP-SCH9*	(Takeda et al., 2018)
JW 05 300	yet36 *pho85Δ:: KANMX4*	This study
JW 05 304	yet36 *pho80Δ::KANMX4*	This study
JW 05 296	yet36 *pho81Δ::KANMX4*	This study
yet234	BY4741 *SCH9::GFP-FYVE-SCH9*	(Takeda et al., 2018)
JW 05 298	yet234 *pho85Δ::KANMX4*	This study
JW 05 302	yet234 *pho80Δ::KANMX4*	This study
JW 05 294	yet234 *pho81Δ::KANMX4*	This study
MC131	BY4741 *sch9-S726A*	This study
MC127	BY4741 *sch9-S726D*	This study
MB32	BY4741 *gtr1Δ::KANMX6*	(Binda et al., 2009)
RKH526	BY4741 *atg13Δ::KanMX*	This study
MC171	BY4741 *ATG13-HA*$_3$*::KanMX*	This study
MC172	BY4741 *ATG13-HA*$_3$*::KanMX pho80Δ::LEU2*	This study
MC173	BY4741 *ATG13-HA*$_3$*::KanMX pho85Δ::LEU2*	This study
MP347-1A	BY4741 *lst4Δ::KanMX*	(Péli-Gulli et al., 2015)
MC174	BY4741 *LST4-V5::KanMX*	This study
MC175	BY4741 *LST4-V5::KanMX pho80Δ::LEU2*	This study
MC176	BY4741 *LST4-V5::KanMX pho85Δ::LEU2*	This study
RKH395	BY4741 *LEU2::GFP-TOR1*	(Hatakeyama et al., 2019)
CDV5410	BY4741 *FAB1-GFP::HIS3*	Euroscarf
yRL649	BY4741 *LEU2::GFP-TOR1*	This study
yRL650	BY4741 *pho85Δ::KANMX4 LEU2::GFP-TOR1*	This study
yRL714	BY4741 *pho80Δ::HIS3 LEU2::GFP-TOR1*	This study

Table 4. Plasmids used in Chapter 2.

Plasmid	Genotype	Source
pRS413	*CEN, ARS, amp*^{R}*, HIS3*	(Brachmann et al., 1998)
pRS415	*CEN, ARS, amp*^{R}*, LEU2*	(Brachmann et al., 1998)
pRS416	*CEN, ARS, amp*^{R}*, URA3*	(Brachmann et al., 1998)
pJU793	[pRS416] *SCH9p-GFP-HA-SCH9*	(Urban et al., 2007)
pJU829	[pRS416] *SCH9p-GFP-HA-sch9*^{5A}	(Urban et al., 2007)
pJU677	[pRS416] *SCH9p-HA*$_{6}$*-SCH9*	(Urban et al., 2007)
pJU790	[pRS416] *SCH9p-HA*$_{6}$*-sch9*^{5A}	(Urban et al., 2007)
pJU675	[pRS416] *SCH9p-SCH9*	(Urban et al., 2007)
pJU822	[pRS416] *SCH9p-sch9*^{5A}	(Urban et al., 2007)
pJU841	[pRS416] *SCH9p-sch9*^{2D3E}	(Urban et al., 2007)
p2809	[pRS413] *SCH9p-GFP-SCH9*	This study
p4048	[p2809] *SCH9p-GFP-sch9*^{S726A}	This study
p4049	[p2809] *SCH9p-GFP-sch9*^{S726D}	This study
pYCPlac33-Sch9-T723A-FLAG	[pYCplac33] *CEN,ARS, SCH9p-SCH9-FLAG-SCH9ter*	(Mudholkar et al., 2017)
pYCPlac33-Sch9-S726A-FLAG	[pYCplac33] *CEN,ARS, SCH9p-sch9*^{S726A}*-FLAG-SCH9ter*	(Mudholkar et al., 2017)
pYCPlac33-Sch9-T737AFLAG	[pYCplac33] *CEN,ARS, SCH9p-sch9*^{S737A}*-FLAG-SCH9ter*	(Mudholkar et al., 2017)
pYCPlac33-Sch9-S758A-FLAG	[pYCplac33] *CEN,ARS, SCH9p-sch9*^{S758A}*-FLAG-SCH9ter*	(Mudholkar et al., 2017)
pYCPlac33-Sch9-S765A-FLAG	[pYCplac33] *CEN,ARS, SCH9p-sch9*^{S765A}*-FLAG-SCH9ter*	(Mudholkar et al., 2017)
pYCPlac33-Sch9-T723A/S726A-FLAG	[pYCplac33] *CEN,ARS, SCH9p-sch9*$^{S726A-S723A}$*-FLAG-SCH9ter*	This study
EB0347	[pRS416] *PHO4p-PHO4-GFP*	(Kaffman et al., 1998)
FAB1	[pRS416] *FAB1*	(Duex et al., 2006)
fab1-14/fab1^{VLA}	[pRS416] *fab1*$^{E1822V/F1833L/T2250A}$	(Duex et al., 2006)

FBp1117	[pRS413] *FAB1*	This study
FBp1118	[pRS413] *fab1*$^{E1822V/F1833L/T2250A}$	This study
p4879	[pRS416] *FAB1p-FAB1-GFP-FAB1ter*	(Chen et al., 2021)
pMC038	[pRS416] *FAB1p-fab1*$^{E1822V/F1833L/T2250A}$*-GFP-FAB1ter*	This study
pRCC-K	[pRS42K] 2*µ, ROX3p-CAS9, SNR52p-gRNA-SUP4ter*	(Generoso et al., 2016)
pMC019	[pRCC-K] *SCH9-near-Ser*^{726}	This study
pVW883	[pCM186] *CEN, ARS, tet07p-HA*$_2$*-PHO85*	(Wanke et al., 2005)
pVW884	[pCM186] *CEN, ARS, tet07p-HA*$_2$*-pho85*^{E53A}	(Wanke et al., 2005)
p946	[pYEX 4T-1] 2*µ*, *CUP1p-PHO80-GST*	(Tan et al., 2003)
pMC014	[pYCplac195] *2µ, URA3, GAL1p-sch9*$^{R650-I824}$*-TAP-Adh1ter*	This study
pMC027	[pYCplac195] *2µ, URA3, GAL1p-sch9*$^{R650-I824-(T723A)}$*-TAP-Adh1ter*	This study
pMC028	[pYCplac195] *2µ, URA3, GAL1p-sch9*$^{R650-I824-(S726A)}$*-TAP-Adh1ter*	This study
pMC029	[pYCplac195] *2µ, URA3, GAL1p-sch9*$^{R650-I824-(T723A-S726A)}$*-TAP-Adh1ter*	This study

Table 5. Strains used in Chapter 3.

Strain	Genotype	Source
BY4741	*MATα; his3Δ1, leu2Δ0, met15Δ0, ura3Δ0*	Euroscarf
YL515	[BY4741] *MATα; his3Δ1, leu2Δ0, ura3Δ0*	(Binda et al., 2009)
MC117	[YL515] *MATα*; *snf1Δ::URA3*	This study
MC220	[YL515] *MATα*; *sip1*^{Q798*} *sip2*^{H380A}	This study
MC212	[YL515] *MATα*; *gal83*^{H384A} *sip2*^{H380A}	This study
MC211	[YL515] *MATα*; *gal83*^{H384A} *sip1*^{Q798*}	This study
MC293	[YL515] *MATα*; *sip1Δ::URA3 sip2Δ::LEU2*	This study
MC292	[YL515] *MATα*; *gal83Δ::kanMX sip2Δ::LEU2*	This study
MC267	[YL515] *MATα*; *gal83Δ::kanMX sip1Δ::URA3*	This study
MC272	[YL515] *MATα*; *gal83Δ::KanMX sip1Δ::URA3 sip2Δ::LEU2*	This study
MC222	[YL515] *MATα*; *SNF1-GFP::kanMX*	This study
PS043	[MC222] *MATα*; *VPH1-mCherry::URA3*	This study
PS030	[YL515] *MATα*; *GAL83-sfGFP::HIS3MX6 VPH1-mCherry::URA3*	This study
PS031	[YL515] *MATα*; *SIP1-sfGFP::HIS3MX6 VPH1-mCherry::URA3*	This study
PS032	[YL515] *MATα*; *SIP2-sfGFP::HIS3MX6 VPH1-mCherry::URA3*	This study
PS043	[MC222] *MATα*; *VPH1-mCherry::URA3*	This study
PS021	[YL515] *MATα*; *GAL83-sfGFP::HIS3MX6 VPH1-mCherry::URA3*	This study
PS022	[YL515] *MATα*; *SIP1-sfGFP::HIS3MX6 VPH1-mCherry::URA3*	This study
PS023	[YL515] *MATα*; *SIP2-sfGFP::HIS3MX6 VPH1-mCherry::URA3*	This study
PS024	[MC220] *MATα*; *GAL83-sfGFP::HIS3MX6 VPH1-mCherry::URA3*	This study
PS025	[MC212] *MATα*; *SIP1-sfGFP::HIS3MX6 VPH1-mCherry::URA3*	This study
PS026	[MC211] *MATα*; *SIP2-sfGFP::HIS3MX6 VPH1-mCherry::URA3*	This study
PS045	[YL515] *MATα*; *SNF1-GFP::HIS3MX6 sip1Δ::kanMX sip2Δ::LEU2 VPH1-mCherry::URA3*	This study
PS046	[MC292] *MATα*; *SNF1-GFP::HIS3MX6 VPH1-mCherry::URA3*	This study
PS047	[YL515] *MATα*; *SNF1-GFP::HIS3MX6 gal83Δ::kanMX sip1Δ::LEU2 VPH1-mCherry::URA3*	This study
PS027	[YL515] *MATα*; *GAL83-sfGFP::HIS3MX6 VPH1-mCherry::URA3 sip1Δ::kanMX sip2Δ::LEU2*	This study
PS028	[MC292] *MATα*; *SIP1-sfGFP::HIS3MX6 VPH1-mCherry::URA3*	This study
PS029	[YL515] *MATα*; *SIP2-sfGFP::HIS3MX6 VPH1-mCherry::URA3 gal83Δ::KanMX sip1Δ::LEU2*	This study
PS044	[MC222] *MATα*; *SV40-NLS-3xmScarlet::URA3*	This study
PS030	[YL515] *MATα*; *GAL83-sfGFP::HIS3MX6 SV40-NLS-3xmScarlet::URA3*	This study
PS031	[YL515] *MATα*; *SIP1-sfGFP::HIS3MX6 SV40-NLS-3xmScarlet::URA3*	This study

PS032	[YL515] *MATα*; *SIP2-sfGFP::HIS3MX6 SV40-NLS-3xmScarlet::URA3*	This study
PS033	[MC220] *MATα*; *GAL83-sfGFP::HIS3MX6 SV40-NLs-3xmScarlet::URA3*	This study
PS034	[MC212] *MATα*; *SIP1-sfGFP::HIS3MX6 S40-NLS-3xmScarlet::URA3*	This study
PS035	[MC211] *MATα*; *SIP2-sfGFP::HIS3MX6 SV40-NLS-3xmScarlet::URA3*	This study
PS048	[YL515] *MATα*; *SNF1-GFP::HIS3MX6 sip1Δ::kanMX sip2Δ::LEU2 SV40-NLS-3xmScarlet::URA3*	This study
PS049	[MC292] *MATα*; *SNF1-GFP::HIS3MX6 SV40-NLS-3xmScarlet::URA3*	This study
PS050	[YL515] *MATα*; *SNF1-GFP::HIS3MX6 gal83Δ::kanMX sip1Δ::LEU2 SV40-NLS-3xmScarlet::URA3*	This study
PS036	[YL515] *MATα*; *GAL83-sfGFP::HIS3MX6 SV40-NLS-3xmScarlet::URA3 sip1Δ::kanMX sip2Δ::LEU2*	This study
PS037	[MC292] *MATα*; *SIP1-sfGFP::HIS3MX6 SV40-NLS-3xmScarlet::URA3*	This study
PS038	[YL515] *MATα*; *SIP2-sfGFP::HIS3MX6 SV40-NLS-3xmScarlet::URA3 gal83Δ::KanMX sip1Δ::LEU2*	This study
MC294	[YL515] *MATα*; *HIS3::pSIVh-TPI1p-ACC1-GFP-HA-ADH1ter*	This study
MC295	[YL515] *MATα*; *HIS3::pSIVh-TPI1p-ACC1-GFP-HA-NLS-ADH1ter*	This study
MC296	[YL515] *MATα*; *HIS3::pSIVh-TPI1p-ACC1-GFP-HA-NES-ADH1ter*	This study
MC297	[YL515] *MATα*; *HIS3::pSIVh-TPI1p-ACC1-GFP-HA-PHO8*^{N}*-ADH1ter*	This study
PS003	[YL515] *MATα*; *HIS3::pSIVh-TPI1p-ACC1-3xGFP-HA-NLS-ADH1ter*	This study
MC281	[YL515] *MATα*; *snf1Δ::natNT2*	This study
MC298	[MC281] *MATα*; *HIS3::pSIVh-TPI1p-ACC1-GFP-HA-ADH1ter*	This study
MC300	[MC281] *MATα*; *HIS3::pSIVh-TPI1p-ACC1-GFP-HA-NES-ADH1ter*	This study
MC301	[MC281] *MATα*; *HIS3::pSIVh-TPI1p-ACC1-GFP-HA-PHO8*^{N}*-ADH1ter*	This study
PS004	[MC281] *MATα*; *HIS3::pSIVh-TPI1p-ACC1-3xGFP-HA-NLS-ADH1ter*	This study
MC304	[MC293] *MATα*; *HIS3::pSIVh-TPI1p-ACC1-GFP-HA-NES-ADH1ter*	This study

MC308	[MC292] *MATα*; *HIS3::pSIVh-TPI1p-ACC1-GFP-HA-NES-ADH1ter*	This study
MC312	[MC267] *MATα*; *HIS3::pSIVh-TPI1p-ACC1-GFP-HA-NES-ADH1ter*	This study
MC320	[MC220] *MATα*; *HIS3::pSIVh-TPI1p-ACC1-GFP-HA-NES-ADH1ter*	This study
MC324	[MC212] *MATα*; *HIS3::pSIVh-TPI1p-ACC1-GFP-HA-NES-ADH1ter*	This study
MC328	[MC211] *MATα*; *HIS3::pSIVh-TPI1p-ACC1-GFP-HA-NES-ADH1ter*	This study
MC305	[MC293] *MATα*; *HIS3::pSIVh-TPI1p-ACC1-GFP-HA-PHO8*^{N}*-ADH1ter*	This study
MC309	[MC292] *MATα*; *HIS3::pSIVh-TPI1p-ACC1-GFP-HA-PHO8*^{N}*-ADH1ter*	This study
MC313	[MC267] *MATα*; *HIS3::pSIVh-TPI1p-ACC1-GFP-HA-PHO8*^{N}*-ADH1ter*	This study
MC321	[MC220] *MATα*; *HIS3::pSIVh-TPI1p-ACC1-GFP-HA-PHO8*^{N}*-ADH1ter*	This study
MC325	[MC212] *MATα*; *HIS3::pSIVh-TPI1p-ACC1-GFP-HA-PHO8*^{N}*-ADH1ter*	This study
MC329	[MC211] *MATα*; *HIS3::pSIVh-TPI1p-ACC1-GFP-HA-PHO8*^{N}*-ADH1ter*	This study
PS005	[MC293] *MATα*; *HIS3::pSIVh-TPI1p-ACC1-3xGFP-HA-NLS-ADH1ter*	This study
PS006	[MC292] *MATα*; *HIS3::pSIVh-TPI1p-ACC1-3xGFP-HA-NLS-ADH1ter*	This study
PS007	[MC267] *MATα*; *HIS3::pSIVh-TPI1p-ACC1-3xGFP-HA-NLS-ADH1ter*	This study
PS008	[MC220] *MATα*; *HIS3::pSIVh-TPI1p-ACC1-3xGFP-HA-NLS-ADH1ter*	This study
PS009	[MC212] *MATα*; *HIS3::pSIVh-TPI1p-ACC1-3xGFP-HA-NLS-ADH1ter*	This study
PS010	[MC211] *MATα*; *HIS3::pSIVh-TPI1p-ACC1-3xGFP-HA-NLS-ADH1ter*	This study
MJA5682	[YL515] *MATα; arg4Δ::HISMX4 lys2Δ::hphNT1*	(Hu et al., 2019)
MC248	[MC220] *MATα*; *arg4Δ::HIS3MX6 lys2Δ::hphNT1*	This study
MC247	[MC212] *MATα*; *arg4Δ::HIS3MX6 lys2Δ::hphNT1*	This study
MC246	[MC211] *MATα*; *arg4Δ::HIS3MX6 lys2Δ::hphNT1*	This study
PS001	[YL515] *MATα*; *snf4Δ::HIS3MX6*	This study
PS002	[MC272] *MATα*; *snf4Δ::HIS3MX6*	This study

MC221	[YL515] *MATα*; *SNF1-HA*$_3$*::kanMX*	This study
MC400	[MC272] *MATα*; *SNF1-HA*$_3$*::kanMX*	This study
MC401	[MC272] *MATα*; *SNF1-GFP::HIS3MX6*	This study

Table 6. Plasmids used in Chapter 3.

Plasmid	Genotype	Source
pRS413	*CEN, ARS, amp^R, HIS3*	(Brachmann et al., 1998)
pRS415	*CEN, ARS, amp^R, LEU2*	(Brachmann et al., 1998)
pRS416	*CEN, ARS, amp^R, URA3*	(Brachmann et al., 1998)
pFA6a-kanMX	*amp^R, TEFp-LEU2*	(Janke et al., 2004)
pFA6a-HIS3MX6	*amp^R, TEFp-HIS3MX6*	(Janke et al., 2004)
pFA-LEU2	*amp^R, LEU2p-LEU2*	(Caligaris & De Virgilio, 2024)
pFA-URA3	*amp^R, URA3p-URA3*	This study
pFA6a-HphNT1	*amp^R, TEFp-HphNT1*	De Virgilio Lab
pFA6a-natNT2	*amp^R, TEFp-natNT2*	(Janke et al., 2004)
pFA6a-GFP^{S65T}-kanMX	*amp^R, GFP^{S65T}-ADH1ter, TEFp-kanMX*	(Janke et al., 2004)
pFA6a-GFP^{S65T}-HIS3MX6	*amp^R, GFP^{S65T}-ADH1ter, TEFp-HIS3MX6*	(Janke et al., 2004)
pGT-URA3-mCherry	*amp^R, mCherry-ADH1ter, TEFp-URA3*	(Wosika et al., 2016)
pGT-HIS3-sfGFP	*amp^R, sfGFP-ADH1ter, TEFp-HIS3*	(Wosika et al., 2016)
pFA6a-myc$_{13}$-HIS3MX6	*amp^R,* myc$_{13}$*-ADH1ter, TEFp-HIS3MX6*	(Janke et al., 2004)
pFA6a-HA$_3$-kanMX	*amp^R, HA$_3$-ADH1ter, TEFp-kanMX*	(Janke et al., 2004)
pSIVh	*Integrative, HIS3*	(Wosika et al., 2016)
pSIVu	*Integrative, URA3*	(Wosika et al., 2016)
pMC058	*[pSIVh], TPIp-ACC1-GFP-HA-ADH1ter*	This study
pMC059	*[pSIVh], TPIp-ACC1-GFP-HA-NLS-ADH1ter*	This study
pMC060	*[pSIVh], TPIp-ACC1-GFP-HA-NES-ADH1ter*	This study
pMC061	*[pSIVh], TPIp-ACC1-GFP-HA-PHO8^N-ADH1ter*	This study
pMC064	*[pSIVh], TPIp-ACC1-3xGFP-HA-NLS-ADH1ter*	This study
pMC052	*[pSIVu], SV40-NLS-3xmScarlet-ADH1ter*	This study

Table 7. Strains used in Chapter 4.

Strain	Genotype	Source
BY4741	*MATa; his3Δ1, leu2Δ0, met15Δ0, ura3Δ0*	Euroscarf
YL515	[BY4741] *MATa; his3Δ1, leu2Δ0, ura3Δ0*	(Binda et al., 2009)
MC380	[BY4741] *MATa; shp1Δ::LEU2*	This study
YSB165-144-1C	[BY4741] *MATa; pph21Δ::kanMX pph22Δ::kanMX*	Euroscarf
YAL016w	[BY4741] *MATa; tpd3Δ::kanMX*	Euroscarf
YDR075w	[BY4741] *MATa; pph3Δ::kanMX*	Euroscarf
YDL047w	[BY4741] *MATa; sit4Δ::kanMX*	Euroscarf

Table 8. Plasmids used in Chapter 4.

Plasmid	Genotype	Source
pRS413	*CEN, ARS,* amp^R*, HIS3*	(Brachmann et al., 1998)
pRS415	*CEN, ARS,* amp^R*, LEU2*	(Brachmann et al., 1998)
pRS416	*CEN, ARS,* amp^R*, URA3*	(Brachmann et al., 1998)
pFA-LEU2	amp^R*, LEU2p-LEU2*	This study

Table 9. Antibodies used in this thesis.

Name	Dilution	Source
Rabbit anti-ACC1-pSer^{79}	1:500	Cell Signaling Technology; 3661S
Rabbit anti-AMPK-phospho-Thr^{172}	1:1000	Cell Signaling Technology; 2535S
Rabbit anti-Lst4-phospho-Ser^{523}	1:10000	De Virgilio lab; N/A
Rabbit anti-human-phospho-S6 ribosomal protein Ser^{235,236}	1:1000	Proteintech; 29223-1-AP
Rabbit anti-Sch9-phospho-Thr^{737}	1:10000	De Virgilio lab; N/A
Rabbit anti-Sch9-phospho-Ser^{288}	1:4000	Rospert lab; N/A
Rabbit anti-ADH	1:50000	Calbiochem; 126745
Mouse anti-GFP	1:3000	Roche; 11814460001
Mouse anti-HA	1:1000	ENZO; ENZ-ABS120
Mouse anti-His$_6$	1:1000	Sigma-Aldrich; H1029
Mouse anti-myc	1:10000	Santa Cruz Biotechnology; sc-40
Guinea pig anti-Rps6	1:1000	(Yerlikaya et al., 2016)
Goat anti-Sch9	1:1000	De Virgilio lab; N/A
Mouse anti-V5	1:5000	Invitrogen; R960-25
Goat anti-mouse HRP conjugated		BIO-RAD; 170-6516
Goat anti-rabbit HRP conjugated		BIO-RAD; 170-6515
Rabbit anti-goat HRP conjugated		BIO-RAD; 5160-2104
Goat anti-guinea pig HRP conjugated		Invitrogen; A18769

REFERENCES

Adachi, A., Koizumi, M., & Ohsumi, Y. (2017). Autophagy induction under carbon starvation conditions is negatively regulated by carbon catabolite repression. *J Biol Chem*, *292*(48), 19905-19918. https://doi.org/10.1074/jbc.M117.817510

Albert, V., & Hall, M. N. (2015). mTOR signaling in cellular and organismal energetics. *Curr Opin Cell Biol*, *33*, 55-66. https://doi.org/10.1016/j.ceb.2014.12.001

Alvaro, C. G., Aindow, A., & Thorner, J. (2016). Differential Phosphorylation Provides a Switch to Control How alpha-Arrestin Rod1 Down-regulates Mating Pheromone Response in *Saccharomyces cerevisiae*. *Genetics*, *203*(1), 299-317. https://doi.org/10.1534/genetics.115.186122

Antoniou, N., Prodromidou, K., Kouroupi, G., Boumpoureka, I., Samiotaki, M., Panayotou, G., Xilouri, M., Kloukina, I., Stefanis, L., Grailhe, R., Taoufik, E., & Matsas, R. (2022). High content screening and proteomic analysis identify a kinase inhibitor that rescues pathological phenotypes in a patient-derived model of Parkinson's disease. *NPJ Parkinsons Dis*, *8*(1), 15. https://doi.org/10.1038/s41531-022-00278-y

Arakel, E. C., Huranova, M., Estrada, A. F., Rau, E. M., Spang, A., & Schwappach, B. (2019). Dissection of GTPase-activating proteins reveals functional asymmetry in the COPI coat of budding yeast. *J Cell Sci*, *132*(16). https://doi.org/10.1242/jcs.232124

Ashrafi, K., Lin, S. S., Manchester, J. K., & Gordon, J. I. (2000). Sip2p and its partner snf1p kinase affect aging in *S. cerevisiae*. *Genes Dev*, *14*(15), 1872-1885. https://www.ncbi.nlm.nih.gov/pubmed/10921902

Baba, M., Hong, S. B., Sharma, N., Warren, M. B., Nickerson, M. L., Iwamatsu, A., Esposito, D., Gillette, W. K., Hopkins, R. F., 3rd, Hartley, J. L., Furihata, M., Oishi, S., Zhen, W., Burke, T. R., Jr., Linehan, W. M., Schmidt, L. S., & Zbar, B. (2006). Folliculin encoded by the BHD gene interacts with a binding protein, FNIP1, and AMPK, and is involved in AMPK and mTOR signaling. *Proc Natl Acad Sci U S A*, *103*(42), 15552-15557. https://doi.org/10.1073/pnas.0603781103

Baker, R. T., Tobias, J. W., & Varshavsky, A. (1992). Ubiquitin-specific proteases of *Saccharomyces cerevisiae*. Cloning of UBP2 and UBP3, and functional analysis of the UBP gene family. *J Biol Chem*, *267*(32), 23364-23375. https://www.ncbi.nlm.nih.gov/pubmed/1429680

Balzi, E., Wang, M., Leterme, S., Van Dyck, L., & Goffeau, A. (1994). PDR5, a novel yeast multidrug resistance conferring transporter controlled by the transcription regulator PDR1. *J Biol Chem*, *269*(3), 2206-2214. https://www.ncbi.nlm.nih.gov/pubmed/8294477

Bar-Peled, L., Schweitzer, L. D., Zoncu, R., & Sabatini, D. M. (2012). Ragulator is a GEF for the rag GTPases that signal amino acid levels to mTORC1. *Cell*, *150*(6), 1196-1208. https://doi.org/10.1016/j.cell.2012.07.032

Baretic, D., Berndt, A., Ohashi, Y., Johnson, C. M., & Williams, R. L. (2016). Tor forms a dimer through an N-terminal helical solenoid with a complex topology. *Nat Commun*, *7*, 11016. https://doi.org/10.1038/ncomms11016

Barrett, L., Orlova, M., Maziarz, M., & Kuchin, S. (2012). Protein kinase A contributes to the negative control of Snf1 protein kinase in *Saccharomyces cerevisiae*. *Eukaryot Cell*, *11*(2), 119-128. https://doi.org/10.1128/EC.05061-11

Becuwe, M., Vieira, N., Lara, D., Gomes-Rezende, J., Soares-Cunha, C., Casal, M., Haguenauer-Tsapis, R., Vincent, O., Paiva, S., & Leon, S. (2012). A molecular switch on an arrestin-like protein relays glucose signaling to transporter endocytosis. *J Cell Biol*, *196*(2), 247-259. https://doi.org/10.1083/jcb.201109113

Bertram, P. G., Choi, J. H., Carvalho, J., Ai, W., Zeng, C., Chan, T. F., & Zheng, X. F. (2000). Tripartite regulation of Gln3p by TOR, Ure2p, and phosphatases. *J Biol Chem*, *275*(46), 35727-35733. https://doi.org/10.1074/jbc.M004235200

Bertram, P. G., Choi, J. H., Carvalho, J., Chan, T. F., Ai, W., & Zheng, X. F. (2002). Convergence of TOR-nitrogen and Snf1-glucose signaling pathways onto Gln3. *Mol Cell Biol*, *22*(4), 1246-1252. https://doi.org/10.1128/MCB.22.4.1246-1252.2002

Betz, C., & Hall, M. N. (2013). Where is mTOR and what is it doing there? *J Cell Biol*, *203*(4), 563-574. https://doi.org/10.1083/jcb.201306041

Binda, M., Péli-Gulli, M. P., Bonfils, G., Panchaud, N., Urban, J., Sturgill, T. W., Loewith, R., & De Virgilio, C. (2009). The Vam6 GEF controls TORC1 by activating the EGO complex. *Mol Cell*, *35*(5), 563-573. https://doi.org/10.1016/j.molcel.2009.06.033

Boeckstaens, M., Merhi, A., Llinares, E., Van Vooren, P., Springael, J. Y., Wintjens, R., & Marini, A. M. (2015). Identification of a Novel Regulatory Mechanism of Nutrient Transport Controlled by TORC1-Npr1-Amu1/Par32. *PLoS Genet*, *11*(7), e1005382. https://doi.org/10.1371/journal.pgen.1005382

Bonfils, G., Jaquenoud, M., Bontron, S., Ostrowicz, C., Ungermann, C., & De Virgilio, C. (2012). Leucyl-tRNA synthetase controls TORC1 via the EGO complex. *Mol Cell*, *46*(1), 105-110. https://doi.org/10.1016/j.molcel.2012.02.009

Brachmann, C. B., Davies, A., Cost, G. J., Caputo, E., Li, J., Hieter, P., & Boeke, J. D. (1998). Designer deletion strains derived from *Saccharomyces cerevisiae* S288C: a useful set of strains and plasmids for PCR-mediated gene disruption and other applications. *Yeast*, *14*(2), 115-132. https://doi.org/10.1002/(SICI)1097-0061(19980130)14:2<115::AID-YEA204>3.0.CO;2-2

Bradford, M. M. (1976). A rapid and sensitive method for the quantitation of microgram quantities of protein utilizing the principle of protein-dye binding. *Anal Biochem*, *72*, 248-254. https://doi.org/10.1006/abio.1976.9999

Braun, K. A., Vaga, S., Dombek, K. M., Fang, F., Palmisano, S., Aebersold, R., & Young, E. T. (2014). Phosphoproteomic analysis identifies proteins involved in transcription-coupled mRNA decay as targets of Snf1 signaling. *Sci Signal*, *7*(333), ra64. https://doi.org/10.1126/scisignal.2005000

Breker, M., Gymrek, M., & Schuldiner, M. (2013). A novel single-cell screening platform reveals proteome plasticity during yeast stress responses. *J Cell Biol*, *200*(6), 839-850. https://doi.org/10.1083/jcb.201301120

Brito, A. S., Soto Diaz, S., Van Vooren, P., Godard, P., Marini, A. M., & Boeckstaens, M. (2019). Pib2-Dependent Feedback Control of the TORC1 Signaling Network by the Npr1 Kinase. *iScience*, *20*, 415-433. https://doi.org/10.1016/j.isci.2019.09.025

Budanov, A. V., & Karin, M. (2008). p53 target genes sestrin1 and sestrin2 connect genotoxic stress and mTOR signaling. *Cell*, *134*(3), 451-460. https://doi.org/10.1016/j.cell.2008.06.028

Caligaris, M., & De Virgilio, C. (2024). Proxies introduce bias in decoding TORC1 activity. *MicroPubl Biol*, *2024*. https://doi.org/10.17912/micropub.biology.001170

Caligaris, M., Nicastro, R., Hu, Z., Tripodi, F., Hummel, J. E., Pillet, B., Deprez, M. A., Winderickx, J., Rospert, S., Coccetti, P., Dengjel, J., & De Virgilio, C. (2023a). Snf1/AMPK fine-tunes TORC1 signaling in response to glucose starvation. *Elife*, *12*. https://doi.org/10.7554/eLife.84319

Caligaris, M., Sampaio-Marques, B., Hatakeyama, R., Pillet, B., Ludovico, P., De Virgilio, C., Winderickx, J., & Nicastro, R. (2023b). The Yeast Protein Kinase Sch9 Functions as a Central Nutrient-Responsive Hub That Calibrates Metabolic and Stress-Related Responses. *J Fungi (Basel)*, *9*(8). https://doi.org/10.3390/jof9080787

Cameroni, E., De Virgilio, C., & Deloche, O. (2006). Phosphatidylinositol 4-phosphate is required for translation initiation in *Saccharomyces cerevisiae*. *J Biol Chem*, *281*(50), 38139-38149. https://doi.org/10.1074/jbc.M601060200

Cameroni, E., Hulo, N., Roosen, J., Winderickx, J., & De Virgilio, C. (2004). The novel yeast PAS kinase Rim 15 orchestrates G0-associated antioxidant defense mechanisms. *Cell Cycle*, *3*(4), 462-468. https://www.ncbi.nlm.nih.gov/pubmed/15300954

Carling, D., Zammit, V. A., & Hardie, D. G. (1987). A common bicyclic protein kinase cascade inactivates the regulatory enzymes of fatty acid and cholesterol biosynthesis. *FEBS Lett*, *223*(2), 217-222. https://doi.org/10.1016/0014-5793(87)80292-2

Carlson, M., Osmond, B. C., & Botstein, D. (1981). Mutants of yeast defective in sucrose utilization. *Genetics*, *98*(1), 25-40. https://doi.org/10.1093/genetics/98.1.25

Catena, V., & Fanciulli, M. (2017). Deptor: not only a mTOR inhibitor. *J Exp Clin Cancer Res*, *36*(1), 12. https://doi.org/10.1186/s13046-016-0484-y

Cecil, J. H., Padilla, C. M., Lipinski, A. A., Langlais, P. R., Luo, X., & Capaldi, A. P. (2023). The Molecular Logic of Gtr1/2 and Pib2 Dependent TORC1 Regulation in Budding Yeast. *bioRxiv*. https://doi.org/10.1101/2023.12.06.570342

Celenza, J. L., & Carlson, M. (1989). Mutational analysis of the *Saccharomyces cerevisiae* SNF1 protein kinase and evidence for functional interaction with the SNF4 protein. *Mol Cell Biol*, *9*(11), 5034-5044. https://doi.org/10.1128/mcb.9.11.5034-5044.1989

Chandrashekarappa, D. G., McCartney, R. R., O'Donnell, A. F., & Schmidt, M. C. (2016). The beta subunit of yeast AMP-activated protein kinase directs substrate specificity in response to alkaline stress. *Cell Signal*, *28*(12), 1881-1893. https://doi.org/10.1016/j.cellsig.2016.08.016

Chandrashekarappa, D. G., McCartney, R. R., & Schmidt, M. C. (2013). Ligand binding to the AMP-activated protein kinase active site mediates protection of the activation loop from dephosphorylation. *J Biol Chem*, *288*(1), 89-98. https://doi.org/10.1074/jbc.M112.422659

Chantranupong, L., Scaria, S. M., Saxton, R. A., Gygi, M. P., Shen, K., Wyant, G. A., Wang, T., Harper, J. W., Gygi, S. P., & Sabatini, D. M. (2016). The CASTOR Proteins Are Arginine Sensors for the mTORC1 Pathway. *Cell*, *165*(1), 153-164. https://doi.org/10.1016/j.cell.2016.02.035

Chantranupong, L., Wolfson, R. L., & Sabatini, D. M. (2015). Nutrient-sensing mechanisms across evolution. *Cell*, *161*(1), 67-83. https://doi.org/10.1016/j.cell.2015.02.041

Chen, L., Jiao, Z. H., Zheng, L. S., Zhang, Y. Y., Xie, S. T., Wang, Z. X., & Wu, J. W. (2009). Structural insight into the autoinhibition mechanism of AMP-activated protein kinase. *Nature*, *459*(7250), 1146-1149. https://doi.org/10.1038/nature08075

Chen, Z., Malia, P. C., Hatakeyama, R., Nicastro, R., Hu, Z., Péli-Gulli, M. P., Gao, J., Nishimura, T., Eskes, E., Stefan, C. J., Winderickx, J., Dengjel, J., De Virgilio, C., & Ungermann, C. (2021). TORC1 Determines Fab1 Lipid Kinase Function at Signaling Endosomes and Vacuoles. *Curr Biol*, *31*(2), 297-309 e298. https://doi.org/10.1016/j.cub.2020.10.026

Coccetti, P., Nicastro, R., & Tripodi, F. (2018). Conventional and emerging roles of the energy sensor Snf1/AMPK in *Saccharomyces cerevisiae*. *Microb Cell*, *5*(11), 482-494. https://doi.org/10.15698/mic2018.11.655

Cowles, C. R., Odorizzi, G., Payne, G. S., & Emr, S. D. (1997). The AP-3 adaptor complex is essential for cargo-selective transport to the yeast vacuole. *Cell*, *91*(1), 109-118. https://doi.org/10.1016/s0092-8674(01)80013-1

Crozet, P., Margalha, L., Confraria, A., Rodrigues, A., Martinho, C., Adamo, M., Elias, C. A., & Baena-Gonzalez, E. (2014). Mechanisms of regulation of SNF1/AMPK/SnRK1 protein kinases. *Front Plant Sci*, *5*, 190. https://doi.org/10.3389/fpls.2014.00190

Crute, B. E., Seefeld, K., Gamble, J., Kemp, B. E., & Witters, L. A. (1998). Functional domains of the alpha1 catalytic subunit of the AMP-activated protein kinase. *J Biol Chem*, *273*(52), 35347-35354. https://doi.org/10.1074/jbc.273.52.35347

Cui, Z., Napolitano, G., de Araujo, M. E. G., Esposito, A., Monfregola, J., Huber, L. A., Ballabio, A., & Hurley, J. H. (2023). Structure of the lysosomal mTORC1-TFEB-Rag-Ragulator megacomplex. *Nature*, *614*(7948), 572-579. https://doi.org/10.1038/s41586-022-05652-7

Dacquay, L., Flint, A., Butcher, J., Salem, D., Kennedy, M., Kaern, M., Stintzi, A., & Baetz, K. (2017). NuA4 Lysine Acetyltransferase Complex Contributes to Phospholipid Homeostasis in Saccharomyces cerevisiae. *G3 (Bethesda)*, *7*(6), 1799-1809. https://doi.org/10.1534/g3.117.041053

Dagon, Y., Hur, E., Zheng, B., Wellenstein, K., Cantley, L. C., & Kahn, B. B. (2012). p70S6 kinase phosphorylates AMPK on serine 491 to mediate leptin's effect on food intake. *Cell Metab*, *16*(1), 104-112. https://doi.org/10.1016/j.cmet.2012.05.010

Dai, X., Jiang, C., Jiang, Q., Fang, L., Yu, H., Guo, J., Yan, P., Chi, F., Zhang, T., Inuzuka, H., Asara, J. M., Wang, P., Guo, J., & Wei, W. (2023). AMPK-dependent phosphorylation of the GATOR2 component WDR24 suppresses glucose-mediated mTORC1 activation. *Nat Metab*, *5*(2), 265-276. https://doi.org/10.1038/s42255-022-00732-4

Dale, S., Wilson, W. A., Edelman, A. M., & Hardie, D. G. (1995). Similar substrate recognition motifs for mammalian AMP-activated protein kinase, higher plant HMG-CoA reductase kinase-A, yeast SNF1, and mammalian calmodulin-dependent protein kinase I. *FEBS Lett*, *361*(2-3), 191-195. https://doi.org/10.1016/0014-5793(95)00172-6

Davie, E., Forte, G. M., & Petersen, J. (2015). Nitrogen regulates AMPK to control TORC1 signaling. *Curr Biol*, *25*(4), 445-454. https://doi.org/10.1016/j.cub.2014.12.034

de Martin Garrido, N., & Aylett, C. H. S. (2020). Nutrient Signaling and Lysosome Positioning Crosstalk Through a Multifunctional Protein, Folliculin. *Front Cell Dev Biol*, *8*, 108. https://doi.org/10.3389/fcell.2020.00108

De Virgilio, C., & Loewith, R. (2006a). Cell growth control: little eukaryotes make big contributions. *Oncogene*, *25*(48), 6392-6415. https://doi.org/10.1038/sj.onc.1209884

De Virgilio, C., & Loewith, R. (2006b). The TOR signalling network from yeast to man. *Int J Biochem Cell Biol*, *38*(9), 1476-1481. https://doi.org/10.1016/j.biocel.2006.02.013

De Vit, M. J., Waddle, J. A., & Johnston, M. (1997). Regulated nuclear translocation of the Mig1 glucose repressor. *Mol Biol Cell*, *8*(8), 1603-1618. https://doi.org/10.1091/mbc.8.8.1603

De Wever, V., Reiter, W., Ballarini, A., Ammerer, G., & Brocard, C. (2005). A dual role for PP1 in shaping the Msn2-dependent transcriptional response to glucose starvation. *EMBO J*, *24*(23), 4115-4123. https://doi.org/10.1038/sj.emboj.7600871

Demetriades, C., Doumpas, N., & Teleman, A. A. (2014). Regulation of TORC1 in response to amino acid starvation via lysosomal recruitment of TSC2. *Cell*, *156*(4), 786-799. https://doi.org/10.1016/j.cell.2014.01.024

Dennis, P. B., Jaeschke, A., Saitoh, M., Fowler, B., Kozma, S. C., & Thomas, G. (2001). Mammalian TOR: a homeostatic ATP sensor. *Science*, *294*(5544), 1102-1105. https://doi.org/10.1126/science.1063518

Deprez, M. A., Caligaris, M., Rosseels, J., Hatakeyama, R., Ghillebert, R., Sampaio-Marques, B., Mudholkar, K., Eskes, E., Meert, E., Ungermann, C., Ludovico, P., Rospert, S., De Virgilio, C., & Winderickx, J. (2023). The nutrient-responsive CDK Pho85 primes the Sch9 kinase for its activation by TORC1. *PLoS Genet*, *19*(2), e1010641. https://doi.org/10.1371/journal.pgen.1010641

Deprez, M. A., Eskes, E., Winderickx, J., & Wilms, T. (2018). The TORC1-Sch9 pathway as a crucial mediator of chronological lifespan in the yeast *Saccharomyces cerevisiae*. *FEMS Yeast Res*, *18*(5). https://doi.org/10.1093/femsyr/foy048

Deroover, S., Ghillebert, R., Broeckx, T., Winderickx, J., & Rolland, F. (2016). Trehalose-6-phosphate synthesis controls yeast gluconeogenesis downstream and independent of SNF1. *FEMS Yeast Res*, *16*(4). https://doi.org/10.1093/femsyr/fow036

Deveryshetty, J., Chadda, R., Mattice, J. R., Karunakaran, S., Rau, M. J., Basore, K., Pokhrel, N., Englander, N., Fitzpatrick, J. A. J., Bothner, B., & Antony, E. (2023).

Yeast Rad52 is a homodecamer and possesses BRCA2-like bipartite Rad51 binding modes. *Nat Commun*, *14*(1), 6215. https://doi.org/10.1038/s41467-023-41993-1

DeVit, M. J., & Johnston, M. (1999). The nuclear exportin Msn5 is required for nuclear export of the Mig1 glucose repressor of *Saccharomyces cerevisiae*. *Curr Biol*, *9*(21), 1231-1241. https://doi.org/10.1016/s0960-9822(99)80503-x

Di Como, C. J., & Arndt, K. T. (1996). Nutrients, via the Tor proteins, stimulate the association of Tap42 with type 2A phosphatases. *Genes Dev*, *10*(15), 1904-1916. https://doi.org/10.1101/gad.10.15.1904

Di Como, C. J., & Jiang, Y. (2006). The association of Tap42 phosphatase complexes with TORC1: another level of regulation in Tor signaling. *Cell Cycle*, *5*(23), 2729-2732. https://doi.org/10.4161/cc.5.23.3516

Dibble, C. C., Elis, W., Menon, S., Qin, W., Klekota, J., Asara, J. M., Finan, P. M., Kwiatkowski, D. J., Murphy, L. O., & Manning, B. D. (2012). TBC1D7 is a third subunit of the TSC1-TSC2 complex upstream of mTORC1. *Mol Cell*, *47*(4), 535-546. https://doi.org/10.1016/j.molcel.2012.06.009

Ding, J., Holzwarth, G., Bradford, C. S., Cooley, B., Yoshinaga, A. S., Patton-Vogt, J., Abeliovich, H., Penner, M. H., & Bakalinsky, A. T. (2015). PEP3 overexpression shortens lag phase but does not alter growth rate in *Saccharomyces cerevisiae* exposed to acetic acid stress. *Appl Microbiol Biotechnol*, *99*(20), 8667-8680. https://doi.org/10.1007/s00253-015-6708-9

Dokládal, L., Stumpe, M., Hu, Z., Jaquenoud, M., Dengjel, J., & De Virgilio, C. (2021a). Phosphoproteomic responses of TORC1 target kinases reveal discrete and convergent mechanisms that orchestrate the quiescence program in yeast. *Cell Rep*, *37*(13), 110149. https://doi.org/10.1016/j.celrep.2021.110149

Dokládal, L., Stumpe, M., Pillet, B., Hu, Z., García Osuna, G. M., Kressler, D., Dengjel, J., & De Virgilio, C. (2021b). Global phosphoproteomics pinpoints uncharted Gcn2-mediated mechanisms of translational control. *Mol Cell*, *81*(9), 1879-1889 e1876. https://doi.org/10.1016/j.molcel.2021.02.037

Dubouloz, F., Deloche, O., Wanke, V., Cameroni, E., & De Virgilio, C. (2005). The TOR and EGO protein complexes orchestrate microautophagy in yeast. *Mol Cell*, *19*(1), 15-26. https://doi.org/10.1016/j.molcel.2005.05.020

Duex, J. E., Tang, F., & Weisman, L. S. (2006). The Vac14p-Fig4p complex acts independently of Vac7p and couples PI3,5P2 synthesis and turnover. *J Cell Biol*, *172*(5), 693-704. https://doi.org/10.1083/jcb.200512105

Duvel, K., Santhanam, A., Garrett, S., Schneper, L., & Broach, J. R. (2003). Multiple roles of Tap42 in mediating rapamycin-induced transcriptional changes in yeast. *Mol Cell*, *11*(6), 1467-1478. https://doi.org/10.1016/s1097-2765(03)00228-4

Egan, D. F., Shackelford, D. B., Mihaylova, M. M., Gelino, S., Kohnz, R. A., Mair, W., Vasquez, D. S., Joshi, A., Gwinn, D. M., Taylor, R., Asara, J. M., Fitzpatrick, J., Dillin, A., Viollet, B., Kundu, M., Hansen, M., & Shaw, R. J. (2011). Phosphorylation of ULK1 (hATG1) by AMP-activated protein kinase connects energy sensing to mitophagy. *Science*, *331*(6016), 456-461. https://doi.org/10.1126/science.1196371

Elbing, K., McCartney, R. R., & Schmidt, M. C. (2006a). Purification and characterization of the three Snf1-activating kinases of *Saccharomyces cerevisiae*. *Biochem J*, *393*(Pt 3), 797-805. https://doi.org/10.1042/BJ20051213

Elbing, K., Rubenstein, E. M., McCartney, R. R., & Schmidt, M. C. (2006b). Subunits of the Snf1 kinase heterotrimer show interdependence for association and activity. *J Biol Chem*, *281*(36), 26170-26180. https://doi.org/10.1074/jbc.M603811200

Eltschinger, S., & Loewith, R. (2016). TOR Complexes and the Maintenance of Cellular Homeostasis. *Trends Cell Biol*, *26*(2), 148-159. https://doi.org/10.1016/j.tcb.2015.10.003

Estruch, F., Treitel, M. A., Yang, X., & Carlson, M. (1992). N-terminal mutations modulate yeast SNF1 protein kinase function. *Genetics*, *132*(3), 639-650. https://doi.org/10.1093/genetics/132.3.639

Fabrizio, P., Pozza, F., Pletcher, S. D., Gendron, C. M., & Longo, V. D. (2001). Regulation of longevity and stress resistance by Sch9 in yeast. *Science*, *292*(5515), 288-290. https://doi.org/10.1126/science.1059497

Feng, W., Wu, T., Dan, X., Chen, Y., Li, L., Chen, S., Miao, D., Deng, H., Gong, X., & Yu, L. (2015). Phosphorylation of Atg31 is required for autophagy. *Protein Cell*, *6*(4), 288-296. https://doi.org/10.1007/s13238-015-0138-4

Fenton, T. R., & Gout, I. T. (2011). Functions and regulation of the 70kDa ribosomal S6 kinases. *Int J Biochem Cell Biol*, *43*(1), 47-59. https://doi.org/10.1016/j.biocel.2010.09.018

Fernandes, S. A., Angelidaki, D. D., Nuchel, J., Pan, J., Gollwitzer, P., Elkis, Y., Artoni, F., Wilhelm, S., Kovacevic-Sarmiento, M., & Demetriades, C. (2024). Spatial and functional separation of mTORC1 signalling in response to different amino acid sources. *Nat Cell Biol*, *26*(11), 1918-1933. https://doi.org/10.1038/s41556-024-01523-7

Fromm, S. A., Lawrence, R. E., & Hurley, J. H. (2020). Structural mechanism for amino acid-dependent Rag GTPase nucleotide state switching by SLC38A9. *Nat Struct Mol Biol*, *27*(11), 1017-1023. https://doi.org/10.1038/s41594-020-0490-9

Galello, F., Portela, P., Moreno, S., & Rossi, S. (2010). Characterization of substrates that have a differential effect on *Saccharomyces cerevisiae* protein kinase A holoenzyme activation. *J Biol Chem*, *285*(39), 29770-29779. https://doi.org/10.1074/jbc.M110.120378

Gander, S., Bonenfant, D., Altermatt, P., Martin, D. E., Hauri, S., Moes, S., Hall, M. N., & Jenoe, P. (2008). Identification of the rapamycin-sensitive phosphorylation sites within the Ser/Thr-rich domain of the yeast Npr1 protein kinase. *Rapid Commun Mass Spectrom*, *22*(23), 3743-3753. https://doi.org/10.1002/rcm.3790

Gao, M., & Kaiser, C. A. (2006). A conserved GTPase-containing complex is required for intracellular sorting of the general amino-acid permease in yeast. *Nat Cell Biol*, *8*(7), 657-667. https://doi.org/10.1038/ncb1419

Garami, A., Zwartkruis, F. J., Nobukuni, T., Joaquin, M., Roccio, M., Stocker, H., Kozma, S. C., Hafen, E., Bos, J. L., & Thomas, G. (2003). Insulin activation of Rheb, a mediator of mTOR/S6K/4E-BP signaling, is inhibited by TSC1 and 2. *Mol Cell*, *11*(6), 1457-1466. https://doi.org/10.1016/s1097-2765(03)00220-x

Gaubitz, C., Oliveira, T. M., Prouteau, M., Leitner, A., Karuppasamy, M., Konstantinidou, G., Rispal, D., Eltschinger, S., Robinson, G. C., Thore, S., Aebersold, R., Schaffitzel, C., & Loewith, R. (2015). Molecular Basis of the Rapamycin Insensitivity of Target Of Rapamycin Complex 2. *Mol Cell*, *58*(6), 977-988. https://doi.org/10.1016/j.molcel.2015.04.031

Gaubitz, C., Prouteau, M., Kusmider, B., & Loewith, R. (2016). TORC2 Structure and Function. *Trends Biochem Sci*, *41*(6), 532-545. https://doi.org/10.1016/j.tibs.2016.04.001

Generoso, W. C., Gottardi, M., Oreb, M., & Boles, E. (2016). Simplified CRISPR-Cas genome editing for *Saccharomyces cerevisiae*. *J Microbiol Methods*, *127*, 203-205. https://doi.org/10.1016/j.mimet.2016.06.020

Georgescu, M. M. (2010). PTEN Tumor Suppressor Network in PI3K-Akt Pathway Control. *Genes Cancer*, *1*(12), 1170-1177. https://doi.org/10.1177/1947601911407325

Gietz, R. D., Schiestl, R. H., Willems, A. R., & Woods, R. A. (1995). Studies on the transformation of intact yeast cells by the LiAc/SS-DNA/PEG procedure. *Yeast*, *11*(4), 355-360. https://doi.org/10.1002/yea.320110408

Gietz, R. D., & Sugino, A. (1988). New yeast-Escherichia coli shuttle vectors constructed with *in vitro* mutagenized yeast genes lacking six-base pair restriction sites. *Gene*, *74*(2), 527-534. https://doi.org/10.1016/0378-1119(88)90185-0

Gonzalez, A., & Hall, M. N. (2017). Nutrient sensing and TOR signaling in yeast and mammals. *EMBO J*, *36*(4), 397-408. https://doi.org/10.15252/embj.201696010

Gonzalez, A., Hall, M. N., Lin, S. C., & Hardie, D. G. (2020). AMPK and TOR: The Yin and Yang of Cellular Nutrient Sensing and Growth Control. *Cell Metab*, *31*(3), 472-492. https://doi.org/10.1016/j.cmet.2020.01.015

Gonzalez, A., Shimobayashi, M., Eisenberg, T., Merle, D. A., Pendl, T., Hall, M. N., & Moustafa, T. (2015). TORC1 promotes phosphorylation of ribosomal protein S6 via the AGC kinase Ypk3 in *Saccharomyces cerevisiae*. *PLoS One*, *10*(3), e0120250. https://doi.org/10.1371/journal.pone.0120250

Gorner, W., Durchschlag, E., Wolf, J., Brown, E. L., Ammerer, G., Ruis, H., & Schuller, C. (2002). Acute glucose starvation activates the nuclear localization signal of a stress-specific yeast transcription factor. *EMBO J*, *21*(1-2), 135-144. https://doi.org/10.1093/emboj/21.1.135

Gu, X., Orozco, J. M., Saxton, R. A., Condon, K. J., Liu, G. Y., Krawczyk, P. A., Scaria, S. M., Harper, J. W., Gygi, S. P., & Sabatini, D. M. (2017). SAMTOR is an S-adenosylmethionine sensor for the mTORC1 pathway. *Science*, *358*(6364), 813-818. https://doi.org/10.1126/science.aao3265

Gwinn, D. M., Shackelford, D. B., Egan, D. F., Mihaylova, M. M., Mery, A., Vasquez, D. S., Turk, B. E., & Shaw, R. J. (2008). AMPK phosphorylation of raptor mediates a metabolic checkpoint. *Mol Cell*, *30*(2), 214-226. https://doi.org/10.1016/j.molcel.2008.03.003

Halford, N. G., Hey, S., Jhurreea, D., Laurie, S., McKibbin, R. S., Paul, M., & Zhang, Y. (2003). Metabolic signalling and carbon partitioning: role of Snf1-related (SnRK1) protein kinase. *J Exp Bot*, *54*(382), 467-475. https://doi.org/10.1093/jxb/erg038

Hara, K., Yonezawa, K., Weng, Q. P., Kozlowski, M. T., Belham, C., & Avruch, J. (1998). Amino acid sufficiency and mTOR regulate p70 S6 kinase and eIF-4E BP1 through a common effector mechanism. *J Biol Chem*, *273*(23), 14484-14494. https://doi.org/10.1074/jbc.273.23.14484

Hardie, D. G. (2013). AMPK: a target for drugs and natural products with effects on both diabetes and cancer. *Diabetes*, *62*(7), 2164-2172. https://doi.org/10.2337/db13-0368

Hardie, D. G., & Ashford, M. L. (2014). AMPK: regulating energy balance at the cellular and whole body levels. *Physiology (Bethesda)*, *29*(2), 99-107. https://doi.org/10.1152/physiol.00050.2013

Hardie, D. G., Schaffer, B. E., & Brunet, A. (2016). AMPK: An Energy-Sensing Pathway with Multiple Inputs and Outputs. *Trends Cell Biol*, *26*(3), 190-201. https://doi.org/10.1016/j.tcb.2015.10.013

Hatakeyama, R. (2021). Pib2 as an Emerging Master Regulator of Yeast TORC1. *Biomolecules*, *11*(10). https://doi.org/10.3390/biom11101489

Hatakeyama, R., & De Virgilio, C. (2019). TORC1 specifically inhibits microautophagy through ESCRT-0. *Curr Genet*, *65*(5), 1243-1249. https://doi.org/10.1007/s00294-019-00982-y

Hatakeyama, R., Péli-Gulli, M. P., Hu, Z., Jaquenoud, M., García Osuna, G. M., Sardu, A., Dengjel, J., & De Virgilio, C. (2019). Spatially Distinct Pools of TORC1 Balance Protein Homeostasis. *Mol Cell*, *73*(2), 325-338 e328. https://doi.org/10.1016/j.molcel.2018.10.040

Hawley, S. A., Ross, F. A., Gowans, G. J., Tibarewal, P., Leslie, N. R., & Hardie, D. G. (2014). Phosphorylation by Akt within the ST loop of AMPK-α1 down-regulates its activation in tumour cells. *Biochem J*, *459*(2), 275-287. https://doi.org/10.1042/BJ20131344

Hedbacker, K., & Carlson, M. (2006). Regulation of the nucleocytoplasmic distribution of Snf1-Gal83 protein kinase. *Eukaryot Cell*, *5*(12), 1950-1956. https://doi.org/10.1128/EC.00256-06

Hedbacker, K., & Carlson, M. (2008). SNF1/AMPK pathways in yeast. *Front Biosci*, *13*, 2408-2420. https://doi.org/10.2741/2854

Hedbacker, K., Hong, S. P., & Carlson, M. (2004a). Pak1 protein kinase regulates activation and nuclear localization of Snf1-Gal83 protein kinase. *Mol Cell Biol*, *24*(18), 8255-8263. https://doi.org/10.1128/MCB.24.18.8255-8263.2004

Hedbacker, K., Townley, R., & Carlson, M. (2004b). Cyclic AMP-dependent protein kinase regulates the subcellular localization of Snf1-Sip1 protein kinase. *Mol Cell Biol*, *24*(5), 1836-1843. https://doi.org/10.1128/MCB.24.5.1836-1843.2004

Hedges, D., Proft, M., & Entian, K. D. (1995). *CAT8*, a new zinc cluster-encoding gene necessary for derepression of gluconeogenic enzymes in the yeast *Saccharomyces cerevisiae*. *Mol Cell Biol*, *15*(4), 1915-1922. https://doi.org/10.1128/MCB.15.4.1915

Heitman, J., Movva, N. R., & Hall, M. N. (1991). Targets for cell cycle arrest by the immunosuppressant rapamycin in yeast. *Science*, *253*(5022), 905-909. https://doi.org/10.1126/science.1715094

Henne, W. M., Buchkovich, N. J., & Emr, S. D. (2011). The ESCRT pathway. *Dev Cell*, *21*(1), 77-91. https://doi.org/10.1016/j.devcel.2011.05.015

Herzig, S., & Shaw, R. J. (2018). AMPK: guardian of metabolism and mitochondrial homeostasis. *Nat Rev Mol Cell Biol*, *19*(2), 121-135. https://doi.org/10.1038/nrm.2017.95

Hindupur, S. K., Gonzalez, A., & Hall, M. N. (2015). The opposing actions of target of rapamycin and AMP-activated protein kinase in cell growth control. *Cold Spring Harb Perspect Biol*, *7*(8), a019141. https://doi.org/10.1101/cshperspect.a019141

Hinnebusch, A. G. (2005). Translational regulation of *GCN4* and the general amino acid control of yeast. *Annu Rev Microbiol*, *59*, 407-450. https://doi.org/10.1146/annurev.micro.59.031805.133833

Hofman-Bang, J. (1999). Nitrogen catabolite repression in *Saccharomyces cerevisiae*. *Mol Biotechnol*, *12*(1), 35-73. https://doi.org/10.1385/MB:12:1:35

Hollstein, P. E., Eichner, L. J., Brun, S. N., Kamireddy, A., Svensson, R. U., Vera, L. I., Ross, D. S., Rymoff, T. J., Hutchins, A., Galvez, H. M., Williams, A. E., Shokhirev, M. N., Screaton, R. A., Berdeaux, R., & Shaw, R. J. (2019). The AMPK-Related Kinases SIK1 and SIK3 Mediate Key Tumor-Suppressive Effects of LKB1 in NSCLC. *Cancer Discov*, *9*(11), 1606-1627. https://doi.org/10.1158/2159-8290.CD-18-1261

Hong, S. P., & Carlson, M. (2007). Regulation of Snf1 protein kinase in response to environmental stress. *J Biol Chem*, *282*(23), 16838-16845. https://doi.org/10.1074/jbc.M700146200

Hong, S. P., Leiper, F. C., Woods, A., Carling, D., & Carlson, M. (2003). Activation of yeast Snf1 and mammalian AMP-activated protein kinase by upstream kinases. *Proc Natl Acad Sci U S A*, *100*(15), 8839-8843. https://doi.org/10.1073/pnas.1533136100

Hu, Z., Raucci, S., Jaquenoud, M., Hatakeyama, R., Stumpe, M., Rohr, R., Reggiori, F., De Virgilio, C., & Dengjel, J. (2019). Multilayered Control of Protein Turnover by TORC1 and Atg1. *Cell Rep*, *28*(13), 3486-3496 e3486. https://doi.org/10.1016/j.celrep.2019.08.069

Hu, Z., Sankar, D. S., Vu, B., Leytens, A., Vionnet, C., Wu, W., Stumpe, M., Martinez-Martinez, E., Stork, B., & Dengjel, J. (2021). ULK1 phosphorylation of striatin activates protein phosphatase 2A and autophagy. *Cell Rep*, *36*(13), 109762. https://doi.org/10.1016/j.celrep.2021.109762

Huang, D., Moffat, J., & Andrews, B. (2002). Dissection of a complex phenotype by functional genomics reveals roles for the yeast cyclin-dependent protein kinase

Pho85 in stress adaptation and cell integrity. *Mol Cell Biol*, *22*(14), 5076-5088. https://doi.org/10.1128/MCB.22.14.5076-5088.2002

Huber, A., Bodenmiller, B., Uotila, A., Stahl, M., Wanka, S., Gerrits, B., Aebersold, R., & Loewith, R. (2009). Characterization of the rapamycin-sensitive phosphoproteome reveals that Sch9 is a central coordinator of protein synthesis. *Genes Dev*, *23*(16), 1929-1943. https://doi.org/10.1101/gad.532109

Huber, A., French, S. L., Tekotte, H., Yerlikaya, S., Stahl, M., Perepelkina, M. P., Tyers, M., Rougemont, J., Beyer, A. L., & Loewith, R. (2011). Sch9 regulates ribosome biogenesis via Stb3, Dot6 and Tod6 and the histone deacetylase complex RPD3L. *EMBO J*, *30*(15), 3052-3064. https://doi.org/10.1038/emboj.2011.221

Hughes Hallett, J. E., Luo, X., & Capaldi, A. P. (2015). Snf1/AMPK promotes the formation of Kog1/Raptor-bodies to increase the activation threshold of TORC1 in budding yeast. *Elife*, *4*. https://doi.org/10.7554/eLife.09181

Humston, E. M., Dombek, K. M., Tu, B. P., Young, E. T., & Synovec, R. E. (2011). Toward a global analysis of metabolites in regulatory mutants of yeast. *Anal Bioanal Chem*, *401*(8), 2387-2402. https://doi.org/10.1007/s00216-011-4800-2

Hung, C. M., Lombardo, P. S., Malik, N., Brun, S. N., Hellberg, K., Van Nostrand, J. L., Garcia, D., Baumgart, J., Diffenderfer, K., Asara, J. M., & Shaw, R. J. (2021). AMPK/ULK1-mediated phosphorylation of Parkin ACT domain mediates an early step in mitophagy. *Sci Adv*, *7*(15). https://doi.org/10.1126/sciadv.abg4544

Ihara, M., Shichijo, K., Takeshita, S., & Kudo, T. (2020). Wortmannin, a specific inhibitor of phosphatidylinositol-3-kinase, induces accumulation of DNA double-strand breaks. *J Radiat Res*, *61*(2), 171-176. https://doi.org/10.1093/jrr/rrz102

Inoki, K., Li, Y., Xu, T., & Guan, K. L. (2003a). Rheb GTPase is a direct target of TSC2 GAP activity and regulates mTOR signaling. *Genes Dev*, *17*(15), 1829-1834. https://doi.org/10.1101/gad.1110003

Inoki, K., Zhu, T., & Guan, K. L. (2003b). TSC2 mediates cellular energy response to control cell growth and survival. *Cell*, *115*(5), 577-590. https://doi.org/10.1016/s0092-8674(03)00929-2

Isom, D. G., Page, S. C., Collins, L. B., Kapolka, N. J., Taghon, G. J., & Dohlman, H. G. (2018). Coordinated regulation of intracellular pH by two glucose-sensing pathways in yeast. *J Biol Chem*, *293*(7), 2318-2329. https://doi.org/10.1074/jbc.RA117.000422

Jablonowski, D., Taubert, J. E., Bar, C., Stark, M. J., & Schaffrath, R. (2009). Distinct subsets of Sit4 holophosphatases are required for inhibition of *Saccharomyces cerevisiae* growth by rapamycin and zymocin. *Eukaryot Cell*, *8*(11), 1637-1647. https://doi.org/10.1128/EC.00205-09

Jacinto, E., Guo, B., Arndt, K. T., Schmelzle, T., & Hall, M. N. (2001). TIP41 interacts with TAP42 and negatively regulates the TOR signaling pathway. *Mol Cell*, *8*(5), 1017-1026. https://doi.org/10.1016/s1097-2765(01)00386-0

Janke, C., Magiera, M. M., Rathfelder, N., Taxis, C., Reber, S., Maekawa, H., Moreno-Borchart, A., Doenges, G., Schwob, E., Schiebel, E., & Knop, M. (2004). A versatile toolbox for PCR-based tagging of yeast genes: new fluorescent proteins, more markers and promoter substitution cassettes. *Yeast*, *21*(11), 947-962. https://doi.org/10.1002/yea.1142

Jiang, R., & Carlson, M. (1997). The Snf1 protein kinase and its activating subunit, Snf4, interact with distinct domains of the Sip1/Sip2/Gal83 component in the kinase complex. *Mol Cell Biol*, *17*(4), 2099-2106. https://doi.org/10.1128/MCB.17.4.2099

Jiang, Y., & Broach, J. R. (1999). Tor proteins and protein phosphatase 2A reciprocally regulate Tap42 in controlling cell growth in yeast. *EMBO J*, *18*(10), 2782-2792. https://doi.org/10.1093/emboj/18.10.2782

Jimenez, J., Bru, S., Ribeiro, M. P., & Clotet, J. (2016). Phosphate: from stardust to eukaryotic cell cycle control. *Int Microbiol*, *19*(3), 133-141. https://doi.org/10.2436/20.1501.01.271

Jin, N., Jin, Y., Oikawa, Y., Nakano, A., Ohsumi, Y., & Weisman, L. S. (2024). A non-canonical CDK, Pho85 regulates the restart of the cell-cycle following stress. *bioRxiv*. https://doi.org/10.1101/2024.08.27.609989

Jin, N., Jin, Y., & Weisman, L. S. (2017). Early protection to stress mediated by CDK-dependent PI3,5P(2) signaling from the vacuole/lysosome. *J Cell Biol*, *216*(7), 2075-2090. https://doi.org/10.1083/jcb.201611144

Jin, N., Mao, K., Jin, Y., Tevzadze, G., Kauffman, E. J., Park, S., Bridges, D., Loewith, R., Saltiel, A. R., Klionsky, D. J., & Weisman, L. S. (2014). Roles for PI(3,5)P2 in nutrient sensing through TORC1. *Mol Biol Cell*, *25*(7), 1171-1185. https://doi.org/10.1091/mbc.E14-01-0021

Jin, Y., Jin, N., Oikawa, Y., Benyair, R., Koizumi, M., Wilson, T. E., Ohsumi, Y., & Weisman, L. S. (2022). Bur1 functions with TORC1 for vacuole-mediated cell cycle progression. *EMBO Rep*, *23*(4), e53477. https://doi.org/10.15252/embr.202153477

Jorgensen, P., Rupes, I., Sharom, J. R., Schneper, L., Broach, J. R., & Tyers, M. (2004). A dynamic transcriptional network communicates growth potential to ribosome synthesis and critical cell size. *Genes Dev*, *18*(20), 2491-2505. https://doi.org/10.1101/gad.1228804

Jung, J., Genau, H. M., & Behrends, C. (2015). Amino Acid-Dependent mTORC1 Regulation by the Lysosomal Membrane Protein SLC38A9. *Mol Cell Biol*, *35*(14), 2479-2494. https://doi.org/10.1128/MCB.00125-15

Kaffman, A., Rank, N. M., & O'Shea, E. K. (1998). Phosphorylation regulates association of the transcription factor Pho4 with its import receptor Pse1/Kap121. *Genes Dev*, *12*(17), 2673-2683. https://doi.org/10.1101/gad.12.17.2673

Kanki, T., Wang, K., & Klionsky, D. J. (2010). A genomic screen for yeast mutants defective in mitophagy. *Autophagy*, *6*(2), 278-280. https://doi.org/10.4161/auto.6.2.10901

Kanshin, E., Giguere, S., Jing, C., Tyers, M., & Thibault, P. (2017). Machine Learning of Global Phosphoproteomic Profiles Enables Discrimination of Direct versus Indirect Kinase Substrates. *Mol Cell Proteomics*, *16*(5), 786-798. https://doi.org/10.1074/mcp.M116.066233

Karim, A. S., Curran, K. A., & Alper, H. S. (2013). Characterization of plasmid burden and copy number in *Saccharomyces cerevisiae* for optimization of metabolic engineering applications. *FEMS Yeast Res*, *13*(1), 107-116. https://doi.org/10.1111/1567-1364.12016

Kawai, S., Urban, J., Piccolis, M., Panchaud, N., De Virgilio, C., & Loewith, R. (2011). Mitochondrial genomic dysfunction causes dephosphorylation of Sch9 in the yeast *Saccharomyces cerevisiae*. *Eukaryot Cell*, *10*(10), 1367-1369. https://doi.org/10.1128/EC.05157-11

Kim, E., Goraksha-Hicks, P., Li, L., Neufeld, T. P., & Guan, K. L. (2008). Regulation of TORC1 by Rag GTPases in nutrient response. *Nat Cell Biol*, *10*(8), 935-945. https://doi.org/10.1038/ncb1753

Kim, J., Kundu, M., Viollet, B., & Guan, K. L. (2011). AMPK and mTOR regulate autophagy through direct phosphorylation of Ulk1. *Nat Cell Biol*, *13*(2), 132-141. https://doi.org/10.1038/ncb2152

Kim, M. D., Hong, S. P., & Carlson, M. (2005). Role of Tos3, a Snf1 protein kinase kinase, during growth of *Saccharomyces cerevisiae* on nonfermentable carbon sources. *Eukaryot Cell*, *4*(5), 861-866. https://doi.org/10.1128/EC.4.5.861-866.2005

Klionsky, D. J. (2007). Monitoring autophagy in yeast: the Pho8Δ60 assay. *Methods Mol Biol*, *390*, 363-371. https://doi.org/10.1007/978-1-59745-466-7_24

Klossel, S., Zhu, Y., Amado, L., Bisinski, D. D., Ruta, J., Liu, F., & Gonzalez Montoro, A. (2024). Yeast TLDc domain proteins regulate assembly state and subcellular localization of the V-ATPase. *EMBO J*, *43*(9), 1870-1897. https://doi.org/10.1038/s44318-024-00097-2

Knight, Z. A., & Shokat, K. M. (2005). Features of selective kinase inhibitors. *Chem Biol*, *12*(6), 621-637. https://doi.org/10.1016/j.chembiol.2005.04.011

Knight, Z. A., & Shokat, K. M. (2007). Chemical genetics: where genetics and pharmacology meet. *Cell*, *128*(3), 425-430. https://doi.org/10.1016/j.cell.2007.01.021

Kuhlee, A., Raunser, S., & Ungermann, C. (2015). Functional homologies in vesicle tethering. *FEBS Lett*, *589*(19 Pt A), 2487-2497. https://doi.org/10.1016/j.febslet.2015.06.001

Kulkarni, A., Buford, T. D., Rai, R., & Cooper, T. G. (2006). Differing responses of Gat1 and Gln3 phosphorylation and localization to rapamycin and methionine sulfoximine treatment in Saccharomyces cerevisiae. *FEMS Yeast Res*, *6*(2), 218-229. https://doi.org/10.1111/j.1567-1364.2006.00031.x

Kumar, P., Awasthi, A., Nain, V., Issac, B., & Puria, R. (2018). Novel insights into TOR signalling in *Saccharomyces cerevisiae* through Torin2. *Gene*, *669*, 15-27. https://doi.org/10.1016/j.gene.2018.05.081

Lang, M. J., Strunk, B. S., Azad, N., Petersen, J. L., & Weisman, L. S. (2017). An intramolecular interaction within the lipid kinase Fab1 regulates cellular phosphatidylinositol 3,5-bisphosphate lipid levels. *Mol Biol Cell*, *28*(7), 858-864. https://doi.org/10.1091/mbc.E16-06-0390

Laplante, M., & Sabatini, D. M. (2012). mTOR signaling in growth control and disease. *Cell*, *149*(2), 274-293. https://doi.org/10.1016/j.cell.2012.03.017

Larochelle, M., Bergeron, D., Arcand, B., & Bachand, F. (2019). Proximity-dependent biotinylation mediated by TurboID to identify protein-protein interaction networks in yeast. *J Cell Sci*, *132*(11). https://doi.org/10.1242/jcs.232249

Laussel, C., Albanese, V., Garcia-Rodriguez, F. J., Ballin, A., Defenouillere, Q., & Leon, S. (2022). 2-deoxyglucose transiently inhibits yeast AMPK signaling and triggers glucose transporter endocytosis, potentiating the drug toxicity. *PLoS Genet*, *18*(8), e1010169. https://doi.org/10.1371/journal.pgen.1010169

Lawrence, R. E., Fromm, S. A., Fu, Y., Yokom, A. L., Kim, D. J., Thelen, A. M., Young, L. N., Lim, C. Y., Samelson, A. J., Hurley, J. H., & Zoncu, R. (2019). Structural mechanism of a Rag GTPase activation checkpoint by the lysosomal folliculin complex. *Science*, *366*(6468), 971-977. https://doi.org/10.1126/science.aax0364

Lee, J. H., Cho, U. S., & Karin, M. (2016). Sestrin regulation of TORC1: Is Sestrin a leucine sensor? *Sci Signal*, *9*(431), re5. https://doi.org/10.1126/scisignal.aaf2885

Lee, M., O'Regan, S., Moreau, J. L., Johnson, A. L., Johnston, L. H., & Goding, C. R. (2000). Regulation of the Pcl7-Pho85 cyclin-cdk complex by Pho81. *Mol Microbiol*, *38*(2), 411-422. https://doi.org/10.1046/j.1365-2958.2000.02140.x

Lee, Y. S., Mulugu, S., York, J. D., & O'Shea, E. K. (2007). Regulation of a cyclin-CDK-CDK inhibitor complex by inositol pyrophosphates. *Science*, *316*(5821), 109-112. https://doi.org/10.1126/science.1139080

Leech, A., Nath, N., McCartney, R. R., & Schmidt, M. C. (2003). Isolation of mutations in the catalytic domain of the Snf1 kinase that render its activity independent of the Snf4 subunit. *Eukaryot Cell*, *2*(2), 265-273. https://doi.org/10.1128/EC.2.2.265-273.2003

Lempiainen, H., Uotila, A., Urban, J., Dohnal, I., Ammerer, G., Loewith, R., & Shore, D. (2009). Sfp1 interaction with TORC1 and Mrs6 reveals feedback regulation on TOR signaling. *Mol Cell*, *33*(6), 704-716. https://doi.org/10.1016/j.molcel.2009.01.034

Lenburg, M. E., & O'Shea, E. K. (1996). Signaling phosphate starvation. *Trends Biochem Sci*, *21*(10), 383-387. https://www.ncbi.nlm.nih.gov/pubmed/8918192

Liang, J., Xu, Z. X., Ding, Z., Lu, Y., Yu, Q., Werle, K. D., Zhou, G., Park, Y. Y., Peng, G., Gambello, M. J., & Mills, G. B. (2015). Myristoylation confers noncanonical AMPK functions in autophagy selectivity and mitochondrial surveillance. *Nat Commun*, *6*, 7926. https://doi.org/10.1038/ncomms8926

Lillo, C., Kataya, A. R., Heidari, B., Creighton, M. T., Nemie-Feyissa, D., Ginbot, Z., & Jonassen, E. M. (2014). Protein phosphatases PP2A, PP4 and PP6: mediators and regulators in development and responses to environmental cues. *Plant Cell Environ*, *37*(12), 2631-2648. https://doi.org/10.1111/pce.12364

Lin, S. S., Manchester, J. K., & Gordon, J. I. (2003). Sip2, an N-myristoylated beta subunit of Snf1 kinase, regulates aging in *Saccharomyces cerevisiae* by affecting cellular histone kinase activity, recombination at rDNA loci, and silencing. *J Biol Chem*, *278*(15), 13390-13397. https://doi.org/10.1074/jbc.M212818200

Ling, N. X. Y., Kaczmarek, A., Hoque, A., Davie, E., Ngoei, K. R. W., Morrison, K. R., Smiles, W. J., Forte, G. M., Wang, T., Lie, S., Dite, T. A., Langendorf, C. G., Scott, J. W., Oakhill, J. S., & Petersen, J. (2020). mTORC1 directly inhibits AMPK to promote cell proliferation under nutrient stress. *Nat Metab*, *2*(1), 41-49. https://doi.org/10.1038/s42255-019-0157-1

Lipatova, Z., Belogortseva, N., Zhang, X. Q., Kim, J., Taussig, D., & Segev, N. (2012). Regulation of selective autophagy onset by a Ypt/Rab GTPase module. *Proc Natl Acad Sci U S A*, *109*(18), 6981-6986. https://doi.org/10.1073/pnas.1121299109

Lippman, S. I., & Broach, J. R. (2009). Protein kinase A and TORC1 activate genes for ribosomal biogenesis by inactivating repressors encoded by Dot6 and its homolog Tod6. *Proc Natl Acad Sci U S A*, *106*(47), 19928-19933. https://doi.org/10.1073/pnas.0907027106

Liu, G. Y., & Sabatini, D. M. (2020). mTOR at the nexus of nutrition, growth, ageing and disease. *Nat Rev Mol Cell Biol*, *21*(4), 183-203. https://doi.org/10.1038/s41580-019-0199-y

Liu, K., Zhang, X., Lester, R. L., & Dickson, R. C. (2005). The sphingoid long chain base phytosphingosine activates AGC-type protein kinases in *Saccharomyces cerevisiae* including Ypk1, Ypk2, and Sch9. *J Biol Chem*, *280*(24), 22679-22687. https://doi.org/10.1074/jbc.M502972200

Liu, Y., Xu, X., & Carlson, M. (2011). Interaction of SNF1 protein kinase with its activating kinase Sak1. *Eukaryot Cell*, *10*(3), 313-319. https://doi.org/10.1128/EC.00291-10

Lizcano, J. M., Goransson, O., Toth, R., Deak, M., Morrice, N. A., Boudeau, J., Hawley, S. A., Udd, L., Makela, T. P., Hardie, D. G., & Alessi, D. R. (2004). LKB1 is a master kinase that activates 13 kinases of the AMPK subfamily, including MARK/PAR-1. *EMBO J*, *23*(4), 833-843. https://doi.org/10.1038/sj.emboj.7600110

Loewith, R., & Hall, M. N. (2011). Target of rapamycin (TOR) in nutrient signaling and growth control. *Genetics*, *189*(4), 1177-1201. https://doi.org/10.1534/genetics.111.133363

Loewith, R., Jacinto, E., Wullschleger, S., Lorberg, A., Crespo, J. L., Bonenfant, D., Oppliger, W., Jenoe, P., & Hall, M. N. (2002). Two TOR complexes, only one of which is rapamycin sensitive, have distinct roles in cell growth control. *Mol Cell*, *10*(3), 457-468. https://doi.org/10.1016/s1097-2765(02)00636-6

Long, X., Lin, Y., Ortiz-Vega, S., Yonezawa, K., & Avruch, J. (2005). Rheb binds and regulates the mTOR kinase. *Curr Biol*, *15*(8), 702-713. https://doi.org/10.1016/j.cub.2005.02.053

Lu, J. Y., Lin, Y. Y., Sheu, J. C., Wu, J. T., Lee, F. J., Chen, Y., Lin, M. I., Chiang, F. T., Tai, T. Y., Berger, S. L., Zhao, Y., Tsai, K. S., Zhu, H., Chuang, L. M., & Boeke, J. D. (2011). Acetylation of yeast AMPK controls intrinsic aging independently of caloric restriction. *Cell*, *146*(6), 969-979. https://doi.org/10.1016/j.cell.2011.07.044

Lucca, C., Ferrari, E., Shubassi, G., Ajazi, A., Choudhary, R., Bruhn, C., Matafora, V., Bachi, A., & Foiani, M. (2024). Sch9(S6K) controls DNA repair and DNA damage response efficiency in aging cells. *Cell Rep*, *43*(6), 114281. https://doi.org/10.1016/j.celrep.2024.114281

Ludin, K., Jiang, R., & Carlson, M. (1998). Glucose-regulated interaction of a regulatory subunit of protein phosphatase 1 with the Snf1 protein kinase in *Saccharomyces cerevisiae*. *Proc Natl Acad Sci U S A*, *95*(11), 6245-6250. https://doi.org/10.1073/pnas.95.11.6245

Ma, X. M., & Blenis, J. (2009). Molecular mechanisms of mTOR-mediated translational control. *Nat Rev Mol Cell Biol*, *10*(5), 307-318. https://doi.org/10.1038/nrm2672

Maegawa, K., Takii, R., Ushimaru, T., & Kozaki, A. (2015). Evolutionary conservation of TORC1 components, TOR, Raptor, and LST8, between rice and yeast. *Mol Genet Genomics, 290*(5), 2019-2030. https://doi.org/10.1007/s00438-015-1056-0

Magnuson, B., Ekim, B., & Fingar, D. C. (2012). Regulation and function of ribosomal protein S6 kinase (S6K) within mTOR signalling networks. *Biochem J*, *441*(1), 1-21. https://doi.org/10.1042/BJ20110892

Malik, N., Ferreira, B. I., Hollstein, P. E., Curtis, S. D., Trefts, E., Weiser Novak, S., Yu, J., Gilson, R., Hellberg, K., Fang, L., Sheridan, A., Hah, N., Shadel, G. S., Manor, U., & Shaw, R. J. (2023). Induction of lysosomal and mitochondrial biogenesis by AMPK phosphorylation of FNIP1. *Science*, *380*(6642), eabj5559. https://doi.org/10.1126/science.abj5559

Mallick, A., & Gupta, B. P. (2021). AXIN-AMPK signaling: Implications for healthy aging. *F1000Res*, *10*, 1259. https://doi.org/10.12688/f1000research.74220.1

Mangat, S., Chandrashekarappa, D., McCartney, R. R., Elbing, K., & Schmidt, M. C. (2010). Differential roles of the glycogen-binding domains of beta subunits in regulation of the Snf1 kinase complex. *Eukaryot Cell*, *9*(1), 173-183. https://doi.org/10.1128/EC.00267-09

Marin, T. L., Gongol, B., Martin, M., King, S. J., Smith, L., Johnson, D. A., Subramaniam, S., Chien, S., & Shyy, J. Y. (2015). Identification of AMP-activated protein kinase targets by a consensus sequence search of the proteome. *BMC Syst Biol*, *9*, 13. https://doi.org/10.1186/s12918-015-0156-0

Martinez-Munoz, G. A., & Kane, P. (2017). Vacuolar and plasma membrane proton pumps collaborate to achieve cytosolic pH homeostasis in yeast. *J Biol Chem*, *292*(19), 7743. https://doi.org/10.1074/jbc.A117.710470

Mayer, F. V., Heath, R., Underwood, E., Sanders, M. J., Carmena, D., McCartney, R. R., Leiper, F. C., Xiao, B., Jing, C., Walker, P. A., Haire, L. F., Ogrodowicz, R., Martin, S. R., Schmidt, M. C., Gamblin, S. J., & Carling, D. (2011). ADP regulates SNF1, the *Saccharomyces cerevisiae* homolog of AMP-activated protein kinase. *Cell Metab*, *14*(5), 707-714. https://doi.org/10.1016/j.cmet.2011.09.009

Mayordomo, I., Estruch, F., & Sanz, P. (2002). Convergence of the target of rapamycin and the Snf1 protein kinase pathways in the regulation of the subcellular localization of Msn2, a transcriptional activator of STRE (Stress Response Element)-regulated genes. *J Biol Chem*, *277*(38), 35650-35656. https://doi.org/10.1074/jbc.M204198200

Maziarz, M., Shevade, A., Barrett, L., & Kuchin, S. (2016). Springing into Action: Reg2 Negatively Regulates Snf1 Protein Kinase and Facilitates Recovery from Prolonged Glucose Starvation in *Saccharomyces cerevisiae*. *Appl Environ Microbiol*, *82*(13), 3875-3885. https://doi.org/10.1128/AEM.00154-16

McCartney, R. R., Rubenstein, E. M., & Schmidt, M. C. (2005). Snf1 kinase complexes with different beta subunits display stress-dependent preferences for the three Snf1-activating kinases. *Curr Genet*, *47*(6), 335-344. https://doi.org/10.1007/s00294-005-0576-2

McCartney, R. R., & Schmidt, M. C. (2001). Regulation of Snf1 kinase. Activation requires phosphorylation of threonine 210 by an upstream kinase as well as a distinct step mediated by the Snf4 subunit. *J Biol Chem*, *276*(39), 36460-36466. https://doi.org/10.1074/jbc.M104418200

McNaughton, R. L., Reddi, A. R., Clement, M. H., Sharma, A., Barnese, K., Rosenfeld, L., Gralla, E. B., Valentine, J. S., Culotta, V. C., & Hoffman, B. M. (2010). Probing *in vivo* Mn^{2+} speciation and oxidative stress resistance in yeast cells with electron-nuclear double resonance spectroscopy. *Proc Natl Acad Sci U S A*, *107*(35), 15335-15339. https://doi.org/10.1073/pnas.1009648107

Measday, V., Moore, L., Retnakaran, R., Lee, J., Donoviel, M., Neiman, A. M., & Andrews, B. (1997). A family of cyclin-like proteins that interact with the Pho85 cyclin-dependent kinase. *Mol Cell Biol*, *17*(3), 1212-1223. https://doi.org/10.1128/MCB.17.3.1212

Menoyo, S., Ricco, N., Bru, S., Hernandez-Ortega, S., Escote, X., Aldea, M., & Clotet, J. (2013). Phosphate-activated cyclin-dependent kinase stabilizes G1 cyclin to trigger cell cycle entry. *Mol Cell Biol*, *33*(7), 1273-1284. https://doi.org/10.1128/MCB.01556-12

Meyuhas, O., & Dreazen, A. (2009). Ribosomal protein S6 kinase from TOP mRNAs to cell size. *Prog Mol Biol Transl Sci*, *90*, 109-153. https://doi.org/10.1016/S1877-1173(09)90003-5

Michel, A. H., Hatakeyama, R., Kimmig, P., Arter, M., Peter, M., Matos, J., De Virgilio, C., & Kornmann, B. (2017). Functional mapping of yeast genomes by saturated transposition. *Elife*, *6*. https://doi.org/10.7554/eLife.23570

Mihaylova, M. M., & Shaw, R. J. (2011). The AMPK signalling pathway coordinates cell growth, autophagy and metabolism. *Nat Cell Biol*, *13*(9), 1016-1023. https://doi.org/10.1038/ncb2329

Mizuno, T., Muroi, K., & Irie, K. (2020). Snf1 AMPK positively regulates ER-phagy via expression control of Atg39 autophagy receptor in yeast ER stress response. *PLoS Genet*, *16*(9), e1009053. https://doi.org/10.1371/journal.pgen.1009053

Moir, R. D., Lee, J., Haeusler, R. A., Desai, N., Engelke, D. R., & Willis, I. M. (2006). Protein kinase A regulates RNA polymerase III transcription through the nuclear localization of Maf1. *Proc Natl Acad Sci U S A*, *103*(41), 15044-15049. https://doi.org/10.1073/pnas.0607129103

Morshed, S., Sharmin, T., & Ushimaru, T. (2020). TORC1 regulates ESCRT-0 complex formation on the vacuolar membrane and microautophagy induction in yeast. *Biochem Biophys Res Commun*, *522*(1), 88-94. https://doi.org/10.1016/j.bbrc.2019.11.064

Moser, B. A., Dennis, P. B., Pullen, N., Pearson, R. B., Williamson, N. A., Wettenhall, R. E., Kozma, S. C., & Thomas, G. (1997). Dual requirement for a newly identified phosphorylation site in p70s6k. *Mol Cell Biol*, *17*(9), 5648-5655. https://doi.org/10.1128/MCB.17.9.5648

Mouillon, J. M., & Persson, B. L. (2006). New aspects on phosphate sensing and signalling in *Saccharomyces cerevisiae*. *FEMS Yeast Res*, *6*(2), 171-176. https://doi.org/10.1111/j.1567-1364.2006.00036.x

Mudholkar, K., Fitzke, E., Prinz, C., Mayer, M. P., & Rospert, S. (2017). The Hsp70 homolog Ssb affects ribosome biogenesis via the TORC1-Sch9 signaling pathway. *Nat Commun*, *8*(1), 937. https://doi.org/10.1038/s41467-017-00635-z

Nair, U., Thumm, M., Klionsky, D. J., & Krick, R. (2011). GFP-Atg8 protease protection as a tool to monitor autophagosome biogenesis. *Autophagy*, *7*(12), 1546-1550. https://doi.org/10.4161/auto.7.12.18424

Nakashima, N., Noguchi, E., & Nishimoto, T. (1999). *Saccharomyces cerevisiae* putative G protein, Gtr1p, which forms complexes with itself and a novel protein designated as Gtr2p, negatively regulates the Ran/Gsp1p G protein cycle through Gtr2p. *Genetics*, *152*(3), 853-867. https://doi.org/10.1093/genetics/152.3.853

Nakatogawa, H., Suzuki, K., Kamada, Y., & Ohsumi, Y. (2009). Dynamics and diversity in autophagy mechanisms: lessons from yeast. *Nat Rev Mol Cell Biol*, *10*(7), 458-467. https://doi.org/10.1038/nrm2708

Napolitano, G., Di Malta, C., & Ballabio, A. (2022). Non-canonical mTORC1 signaling at the lysosome. *Trends Cell Biol*, *32*(11), 920-931. https://doi.org/10.1016/j.tcb.2022.04.012

Napolitano, G., Esposito, A., Choi, H., Matarese, M., Benedetti, V., Di Malta, C., Monfregola, J., Medina, D. L., Lippincott-Schwartz, J., & Ballabio, A. (2018). mTOR-dependent phosphorylation controls TFEB nuclear export. *Nat Commun*, *9*(1), 3312. https://doi.org/10.1038/s41467-018-05862-6

Nayak, V., Zhao, K., Wyce, A., Schwartz, M. F., Lo, W. S., Berger, S. L., & Marmorstein, R. (2006). Structure and dimerization of the kinase domain from yeast Snf1, a member of the Snf1/AMPK protein family. *Structure*, *14*(3), 477-485. https://doi.org/10.1016/j.str.2005.12.008

Nicastro, R., Brohee, L., Alba, J., Nuchel, J., Figlia, G., Kipschull, S., Gollwitzer, P., Romero-Pozuelo, J., Fernandes, S. A., Lamprakis, A., Vanni, S., Teleman, A. A., De Virgilio, C., & Demetriades, C. (2023). Malonyl-CoA is a conserved endogenous ATP-competitive mTORC1 inhibitor. *Nat Cell Biol*, *25*(9), 1303-1318. https://doi.org/10.1038/s41556-023-01198-6

Nicastro, R., Gaillard, H., Zarzuela, L., Péli-Gulli, M. P., Fernandez-Garcia, E., Tome, M., Garcia-Rodriguez, N., Duran, R. V., De Virgilio, C., & Wellinger, R. E. (2022). Manganese is a physiologically relevant TORC1 activator in yeast and mammals. *Elife*, *11*. https://doi.org/10.7554/eLife.80497

Nicastro, R., Raucci, S., Michel, A. H., Stumpe, M., García Osuna, G. M., Jaquenoud, M., Kornmann, B., & De Virgilio, C. (2021). Indole-3-acetic acid is a physiological inhibitor of TORC1 in yeast. *PLoS Genet*, *17*(3), e1009414. https://doi.org/10.1371/journal.pgen.1009414

Nicastro, R., Sardu, A., Panchaud, N., & De Virgilio, C. (2017). The Architecture of the Rag GTPase Signaling Network. *Biomolecules*, *7*(3). https://doi.org/10.3390/biom7030048

Nicastro, R., Tripodi, F., Gaggini, M., Castoldi, A., Reghellin, V., Nonnis, S., Tedeschi, G., & Coccetti, P. (2015a). Snf1 Phosphorylates Adenylate Cyclase and Negatively Regulates Protein Kinase A-dependent Transcription in *Saccharomyces cerevisiae*. *J Biol Chem*, *290*(41), 24715-24726. https://doi.org/10.1074/jbc.M115.658005

Nicastro, R., Tripodi, F., Guzzi, C., Reghellin, V., Khoomrung, S., Capusoni, C., Compagno, C., Airoldi, C., Nielsen, J., Alberghina, L., & Coccetti, P. (2015b). Enhanced amino acid utilization sustains growth of cells lacking Snf1/AMPK. *Biochim Biophys Acta*, *1853*(7), 1615-1625. https://doi.org/10.1016/j.bbamcr.2015.03.014

Nishizawa, M. (2015). The regulators of yeast PHO system participate in the transcriptional regulation of G1 cyclin under alkaline stress conditions. *Yeast*, *32*(3), 367-378. https://doi.org/10.1002/yea.3064

Noda, T. (2017). Regulation of Autophagy through TORC1 and mTORC1. *Biomolecules*, *7*(3). https://doi.org/10.3390/biom7030052

Noda, T., Matsuura, A., Wada, Y., & Ohsumi, Y. (1995). Novel system for monitoring autophagy in the yeast *Saccharomyces cerevisiae*. *Biochem Biophys Res Commun*, *210*(1), 126-132. https://doi.org/10.1006/bbrc.1995.1636

Novarina, D., Guerra, P., & Milias-Argeitis, A. (2021). Vacuolar Localization via the N-terminal Domain of Sch9 is Required for TORC1-dependent Phosphorylation and Downstream Signal Transduction. *J Mol Biol*, *433*(24), 167326. https://doi.org/10.1016/j.jmb.2021.167326

O'Donnell, A. F., McCartney, R. R., Chandrashekarappa, D. G., Zhang, B. B., Thorner, J., & Schmidt, M. C. (2015). 2-Deoxyglucose impairs *Saccharomyces cerevisiae* growth by stimulating Snf1-regulated and alpha-arrestin-mediated trafficking of hexose transporters 1 and 3. *Mol Cell Biol*, *35*(6), 939-955. https://doi.org/10.1128/MCB.01183-14

O'Donnell, A. F., & Schmidt, M. C. (2019). AMPK-Mediated Regulation of Alpha-Arrestins and Protein Trafficking. *Int J Mol Sci*, *20*(3). https://doi.org/10.3390/ijms20030515

Oh, S., Lee, J., Swanson, S. K., Florens, L., Washburn, M. P., & Workman, J. L. (2020). Yeast Nuak1 phosphorylates histone H3 threonine 11 in low glucose stress by the cooperation of AMPK and CK2 signaling. *Elife*, *9*. https://doi.org/10.7554/eLife.64588

Ostling, J., & Ronne, H. (1998). Negative control of the Mig1p repressor by Snf1p-dependent phosphorylation in the absence of glucose. *Eur J Biochem*, *252*(1), 162-168. https://doi.org/10.1046/j.1432-1327.1998.2520162.x

Pacitto, A., Ascher, D. B., Wong, L. H., Blaszczyk, B. K., Nookala, R. K., Zhang, N., Dokudovskaya, S., Levine, T. P., & Blundell, T. L. (2015). Lst4, the yeast Fnip1/2 orthologue, is a DENN-family protein. *Open Biol*, *5*(12), 150174. https://doi.org/10.1098/rsob.150174

Pan, Y., & Shadel, G. S. (2009). Extension of chronological life span by reduced TOR signaling requires down-regulation of Sch9p and involves increased mitochondrial OXPHOS complex density. *Aging (Albany NY)*, *1*(1), 131-145. https://doi.org/10.18632/aging.100016

Panchaud, N., Péli-Gulli, M. P., & De Virgilio, C. (2013a). Amino acid deprivation inhibits TORC1 through a GTPase-activating protein complex for the Rag family GTPase Gtr1. *Sci Signal*, *6*(277), ra42. https://doi.org/10.1126/scisignal.2004112

Panchaud, N., Péli-Gulli, M. P., & De Virgilio, C. (2013b). SEACing the GAP that nEGOCiates TORC1 activation: evolutionary conservation of Rag GTPase regulation. *Cell Cycle*, *12*(18), 2948-2952. https://doi.org/10.4161/cc.26000

Papamichos-Chronakis, M., Gligoris, T., & Tzamarias, D. (2004). The Snf1 kinase controls glucose repression in yeast by modulating interactions between the Mig1 repressor and the Cyc8-Tup1 co-repressor. *EMBO Rep*, *5*(4), 368-372. https://doi.org/10.1038/sj.embor.7400120

Papinski, D., Schuschnig, M., Reiter, W., Wilhelm, L., Barnes, C. A., Maiolica, A., Hansmann, I., Pfaffenwimmer, T., Kijanska, M., Stoffel, I., Lee, S. S., Brezovich, A., Lou, J. H., Turk, B. E., Aebersold, R., Ammerer, G., Peter, M., & Kraft, C. (2014). Early steps in autophagy depend on direct phosphorylation of Atg9 by the Atg1 kinase. *Mol Cell*, *53*(3), 471-483. https://doi.org/10.1016/j.molcel.2013.12.011

Paulsel, A. L., Merz, A. J., & Nickerson, D. P. (2013). Vps9 family protein Muk1 is the second Rab5 guanosine nucleotide exchange factor in budding yeast. *J Biol Chem*, *288*(25), 18162-18171. https://doi.org/10.1074/jbc.M113.457069

Pedruzzi, I., Dubouloz, F., Cameroni, E., Wanke, V., Roosen, J., Winderickx, J., & De Virgilio, C. (2003). TOR and PKA signaling pathways converge on the protein kinase Rim15 to control entry into G0. *Mol Cell*, *12*(6), 1607-1613. https://doi.org/10.1016/s1097-2765(03)00485-4

Péli-Gulli, M. P., Raucci, S., Hu, Z., Dengjel, J., & De Virgilio, C. (2017). Feedback Inhibition of the Rag GTPase GAP Complex Lst4-Lst7 Safeguards TORC1 from Hyperactivation by Amino Acid Signals. *Cell Rep*, *20*(2), 281-288. https://doi.org/10.1016/j.celrep.2017.06.058

Péli-Gulli, M. P., Sardu, A., Panchaud, N., Raucci, S., & De Virgilio, C. (2015). Amino Acids Stimulate TORC1 through Lst4-Lst7, a GTPase-Activating Protein Complex for the Rag Family GTPase Gtr2. *Cell Rep*, *13*(1), 1-7. https://doi.org/10.1016/j.celrep.2015.08.059

Peng, M., Yin, N., & Li, M. O. (2017). SZT2 dictates GATOR control of mTORC1 signalling. *Nature*, *543*(7645), 433-437. https://doi.org/10.1038/nature21378

Perera, R. M., Di Malta, C., & Ballabio, A. (2019). MiT/TFE Family of Transcription Factors, Lysosomes, and Cancer. *Annu Rev Cancer Biol*, *3*, 203-222. https://doi.org/10.1146/annurev-cancerbio-030518-055835

Perez-Sampietro, M., Casas, C., & Herrero, E. (2013). The AMPK family member Snf1 protects *Saccharomyces cerevisiae* cells upon glutathione oxidation. *PLoS One*, *8*(3), e58283. https://doi.org/10.1371/journal.pone.0058283

Peterson, T. R., Laplante, M., Thoreen, C. C., Sancak, Y., Kang, S. A., Kuehl, W. M., Gray, N. S., & Sabatini, D. M. (2009). DEPTOR is an mTOR inhibitor frequently overexpressed in multiple myeloma cells and required for their survival. *Cell*, *137*(5), 873-886. https://doi.org/10.1016/j.cell.2009.03.046

Petrenko, N., Chereji, R. V., McClean, M. N., Morozov, A. V., & Broach, J. R. (2013). Noise and interlocking signaling pathways promote distinct transcription factor dynamics in response to different stresses. *Mol Biol Cell*, *24*(12), 2045-2057. https://doi.org/10.1091/mbc.E12-12-0870

Piao, X., Kobayashi, T., Wang, L., Shiono, M., Takagi, Y., Sun, G., Abe, M., Hagiwara, Y., Zhang, D., Okimoto, K., Kouchi, M., Matsumoto, I., & Hino, O. (2009). Regulation of folliculin (the BHD gene product) phosphorylation by Tsc2-mTOR pathway. *Biochem Biophys Res Commun*, *389*(1), 16-21. https://doi.org/10.1016/j.bbrc.2009.08.070

Plank, M. (2022). Interaction of TOR and PKA Signaling in *S. cerevisiae*. *Biomolecules*, *12*(2). https://doi.org/10.3390/biom12020210

Polge, C., & Thomas, M. (2007). SNF1/AMPK/SnRK1 kinases, global regulators at the heart of energy control? *Trends Plant Sci*, *12*(1), 20-28. https://doi.org/10.1016/j.tplants.2006.11.005

Popelka, H., Reinhart, E. F., Metur, S. P., Leary, K. A., Ragusa, M. J., & Klionsky, D. J. (2021). Membrane Binding and Homodimerization of Atg16 Via Two Distinct Protein Regions is Essential for Autophagy in Yeast. *J Mol Biol*, *433*(5), 166809. https://doi.org/10.1016/j.jmb.2021.166809

Powis, K., & De Virgilio, C. (2016). Conserved regulators of Rag GTPases orchestrate amino acid-dependent TORC1 signaling. *Cell Discov*, *2*, 15049. https://doi.org/10.1038/celldisc.2015.49

Powis, K., Zhang, T., Panchaud, N., Wang, R., De Virgilio, C., & Ding, J. (2015). Crystal structure of the Ego1-Ego2-Ego3 complex and its role in promoting Rag GTPase-dependent TORC1 signaling. *Cell Res.*, *25*(9), 1043-1059. https://doi.org/10.1038/cr.2015.86

Prouteau, M., Bourgoint, C., Felix, J., Bonadei, L., Sadian, Y., Gabus, C., Savvides, S. N., Gutsche, I., Desfosses, A., & Loewith, R. (2023). EGOC inhibits TOROID polymerization by structurally activating TORC1. *Nat Struct Mol Biol*, *30*(3), 273-285. https://doi.org/10.1038/s41594-022-00912-6

Prouteau, M., Desfosses, A., Sieben, C., Bourgoint, C., Lydia Mozaffari, N., Demurtas, D., Mitra, A. K., Guichard, P., Manley, S., & Loewith, R. (2017). TORC1 organized in inhibited domains (TOROIDs) regulate TORC1 activity. *Nature*, *550*(7675), 265-269. https://doi.org/10.1038/nature24021

Qi, W., Acosta-Zaldivar, M., Flanagan, P. R., Liu, N. N., Jani, N., Fierro, J. F., Andres, M. T., Moran, G. P., & Kohler, J. R. (2022). Stress- and metabolic responses of Candida albicans require Tor1 kinase N-terminal HEAT repeats. *PLoS Pathog*, *18*(6), e1010089. https://doi.org/10.1371/journal.ppat.1010089

Ramirez Reyes, J. M. J., Cuesta, R., & Pause, A. (2021). Folliculin: A Regulator of Transcription Through AMPK and mTOR Signaling Pathways. *Front Cell Dev Biol*, *9*, 667311. https://doi.org/10.3389/fcell.2021.667311

Ratnakumar, S., Kacherovsky, N., Arms, E., & Young, E. T. (2009). Snf1 controls the activity of Adr1 through dephosphorylation of Ser230. *Genetics*, *182*(3), 735-745. https://doi.org/10.1534/genetics.109.103432

Rebsamen, M., Pochini, L., Stasyk, T., de Araujo, M. E., Galluccio, M., Kandasamy, R. K., Snijder, B., Fauster, A., Rudashevskaya, E. L., Bruckner, M., Scorzoni, S., Filipek, P. A., Huber, K. V., Bigenzahn, J. W., Heinz, L. X., Kraft, C., Bennett, K. L., Indiveri, C., Huber, L. A., & Superti-Furga, G. (2015). SLC38A9 is a component of the lysosomal amino acid sensing machinery that controls mTORC1. *Nature*, *519*(7544), 477-481. https://doi.org/10.1038/nature14107

Reinke, A., Anderson, S., McCaffery, J. M., Yates, J., 3rd, Aronova, S., Chu, S., Fairclough, S., Iverson, C., Wedaman, K. P., & Powers, T. (2004). TOR complex 1 includes a novel component, Tco89p (YPL180w), and cooperates with Ssd1p to maintain cellular integrity in *Saccharomyces cerevisiae*. *J Biol Chem*, *279*(15), 14752-14762. https://doi.org/10.1074/jbc.M313062200

Roczniak-Ferguson, A., Petit, C. S., Froehlich, F., Qian, S., Ky, J., Angarola, B., Walther, T. C., & Ferguson, S. M. (2012). The transcription factor TFEB links mTORC1 signaling to transcriptional control of lysosome homeostasis. *Sci Signal*, *5*(228), ra42. https://doi.org/10.1126/scisignal.2002790

Roelants, F. M., Torrance, P. D., & Thorner, J. (2004). Differential roles of PDK1- and PDK2-phosphorylation sites in the yeast AGC kinases Ypk1, Pkc1 and Sch9. *Microbiology (Reading)*, *150*(Pt 10), 3289-3304. https://doi.org/10.1099/mic.0.27286-0

Roosen, J., Engelen, K., Marchal, K., Mathys, J., Griffioen, G., Cameroni, E., Thevelein, J. M., De Virgilio, C., De Moor, B., & Winderickx, J. (2005). PKA and Sch9 control a molecular switch important for the proper adaptation to nutrient availability. *Mol Microbiol*, *55*(3), 862-880. https://doi.org/10.1111/j.1365-2958.2004.04429.x

Roth, S., Kumme, J., & Schuller, H. J. (2004). Transcriptional activators Cat8 and Sip4 discriminate between sequence variants of the carbon source-responsive promoter element in the yeast *Saccharomyces cerevisiae*. *Curr Genet*, *45*(3), 121-128. https://doi.org/10.1007/s00294-003-0476-2

Roustan, V., Jain, A., Teige, M., Ebersberger, I., & Weckwerth, W. (2016). An evolutionary perspective of AMPK-TOR signaling in the three domains of life. *J Exp Bot*, *67*(13), 3897-3907. https://doi.org/10.1093/jxb/erw211

Rubenstein, E. M., McCartney, R. R., & Schmidt, M. C. (2006). Regulatory domains of Snf1-activating kinases determine pathway specificity. *Eukaryot Cell*, *5*(4), 620-627. https://doi.org/10.1128/EC.5.4.620-627.2006

Rubenstein, E. M., McCartney, R. R., Zhang, C., Shokat, K. M., Shirra, M. K., Arndt, K. M., & Schmidt, M. C. (2008). Access denied: Snf1 activation loop phosphorylation is controlled by availability of the phosphorylated threonine 210 to the PP1 phosphatase. *J Biol Chem*, *283*(1), 222-230. https://doi.org/10.1074/jbc.M707957200

Rudolph, M. J., Amodeo, G. A., Bai, Y., & Tong, L. (2005). Crystal structure of the protein kinase domain of yeast AMP-activated protein kinase Snf1. *Biochem Biophys Res Commun*, *337*(4), 1224-1228. https://doi.org/10.1016/j.bbrc.2005.09.181

Ruiz, A., Xu, X., & Carlson, M. (2011). Roles of two protein phosphatases, Reg1-Glc7 and Sit4, and glycogen synthesis in regulation of SNF1 protein kinase. *Proc Natl Acad Sci U S A*, *108*(16), 6349-6354. https://doi.org/10.1073/pnas.1102758108

Sadria, M., Seo, D., & Layton, A. T. (2022). The mixed blessing of AMPK signaling in Cancer treatments. *BMC Cancer*, *22*(1), 105. https://doi.org/10.1186/s12885-022-09211-1

Sager, R. A., Woodford, M. R., & Mollapour, M. (2018). The mTOR Independent Function of Tsc1 and FNIPs. *Trends Biochem Sci*, *43*(12), 935-937. https://doi.org/10.1016/j.tibs.2018.09.018

Saitoh, M., Pullen, N., Brennan, P., Cantrell, D., Dennis, P. B., & Thomas, G. (2002). Regulation of an activated S6 kinase 1 variant reveals a novel mammalian target of rapamycin phosphorylation site. *J Biol Chem*, *277*(22), 20104-20112. https://doi.org/10.1074/jbc.M201745200

Salt, I., Celler, J. W., Hawley, S. A., Prescott, A., Woods, A., Carling, D., & Hardie, D. G. (1998). AMP-activated protein kinase: greater AMP dependence, and preferential nuclear localization, of complexes containing the alpha2 isoform. *Biochem J*, *334 (Pt 1)*(Pt 1), 177-187. https://doi.org/10.1042/bj3340177

Sampaio-Marques, B., Burhans, W. C., & Ludovico, P. (2014). Longevity pathways and maintenance of the proteome: the role of autophagy and mitophagy during yeast ageing. *Microb Cell*, *1*(4), 118-127. https://doi.org/10.15698/mic2014.04.136

Sancak, Y., Bar-Peled, L., Zoncu, R., Markhard, A. L., Nada, S., & Sabatini, D. M. (2010). Ragulator-Rag complex targets mTORC1 to the lysosomal surface and is necessary for its activation by amino acids. *Cell*, *141*(2), 290-303. https://doi.org/10.1016/j.cell.2010.02.024

Sancak, Y., Peterson, T. R., Shaul, Y. D., Lindquist, R. A., Thoreen, C. C., Bar-Peled, L., & Sabatini, D. M. (2008). The Rag GTPases bind raptor and mediate amino acid signaling to mTORC1. *Science*, *320*(5882), 1496-1501. https://doi.org/10.1126/science.1157535

Sancak, Y., Thoreen, C. C., Peterson, T. R., Lindquist, R. A., Kang, S. A., Spooner, E., Carr, S. A., & Sabatini, D. M. (2007). PRAS40 is an insulin-regulated inhibitor of the mTORC1 protein kinase. *Mol Cell*, *25*(6), 903-915. https://doi.org/10.1016/j.molcel.2007.03.003

Sanz, P., Alms, G. R., Haystead, T. A., & Carlson, M. (2000). Regulatory interactions between the Reg1-Glc7 protein phosphatase and the Snf1 protein kinase. *Mol Cell Biol*, *20*(4), 1321-1328. https://doi.org/10.1128/MCB.20.4.1321-1328.2000

Sanz, P., Viana, R., & Garcia-Gimeno, M. A. (2016). AMPK in Yeast: The SNF1 (Sucrose Non-fermenting 1) Protein Kinase Complex. *Exp Suppl*, *107*, 353-374. https://doi.org/10.1007/978-3-319-43589-3_14

Saxton, R. A., Knockenhauer, K. E., Wolfson, R. L., Chantranupong, L., Pacold, M. E., Wang, T., Schwartz, T. U., & Sabatini, D. M. (2016). Structural basis for leucine sensing by the Sestrin2-mTORC1 pathway. *Science*, *351*(6268), 53-58. https://doi.org/10.1126/science.aad2087

Saxton, R. A., & Sabatini, D. M. (2017). mTOR Signaling in Growth, Metabolism, and Disease. *Cell*, *168*(6), 960-976. https://doi.org/10.1016/j.cell.2017.02.004

Schmidt, A., Beck, T., Koller, A., Kunz, J., & Hall, M. N. (1998). The TOR nutrient signalling pathway phosphorylates NPR1 and inhibits turnover of the tryptophan permease. *EMBO J*, *17*(23), 6924-6931. https://doi.org/10.1093/emboj/17.23.6924

Schmidt, M. C., & McCartney, R. R. (2000). beta-subunits of Snf1 kinase are required for kinase function and substrate definition. *EMBO J*, *19*(18), 4936-4943. https://doi.org/10.1093/emboj/19.18.4936

Schmitt, D. L., Curtis, S. D., Lyons, A. C., Zhang, J. F., Chen, M., He, C. Y., Mehta, S., Shaw, R. J., & Zhang, J. (2022). Spatial regulation of AMPK signaling revealed by a sensitive kinase activity reporter. *Nat Commun*, *13*(1), 3856. https://doi.org/10.1038/s41467-022-31190-x

Sekiguchi, T., Hirose, E., Nakashima, N., Ii, M., & Nishimoto, T. (2001). Novel G proteins, Rag C and Rag D, interact with GTP-binding proteins, Rag A and Rag B. *J Biol Chem*, *276*(10), 7246-7257. https://doi.org/10.1074/jbc.M004389200

Serra-Cardona, A., Petrezselyova, S., Canadell, D., Ramos, J., & Arino, J. (2014). Coregulated expression of the Na^+/phosphate Pho89 transporter and Ena1 Na^+-ATPase allows their functional coupling under high-pH stress. *Mol Cell Biol*, *34*(24), 4420-4435. https://doi.org/10.1128/MCB.01089-14

Shah, O. J., Ghosh, S., & Hunter, T. (2003). Mitotic regulation of ribosomal S6 kinase 1 involves Ser/Thr, Pro phosphorylation of consensus and non-consensus sites by Cdc2. *J Biol Chem*, *278*(18), 16433-16442. https://doi.org/10.1074/jbc.M300435200

Shashkova, S., Wollman, A. J. M., Leake, M. C., & Hohmann, S. (2017). The yeast Mig1 transcriptional repressor is dephosphorylated by glucose-dependent and -independent mechanisms. *FEMS Microbiol Lett*, *364*(14). https://doi.org/10.1093/femsle/fnx133

Shaw, R. J., Bardeesy, N., Manning, B. D., Lopez, L., Kosmatka, M., DePinho, R. A., & Cantley, L. C. (2004). The LKB1 tumor suppressor negatively regulates mTOR signaling. *Cancer Cell*, *6*(1), 91-99. https://doi.org/10.1016/j.ccr.2004.06.007

Shen, K., Huang, R. K., Brignole, E. J., Condon, K. J., Valenstein, M. L., Chantranupong, L., Bomaliyamu, A., Choe, A., Hong, C., Yu, Z., & Sabatini, D. M. (2018). Architecture of the human GATOR1 and GATOR1-Rag GTPases complexes. *Nature*, *556*(7699), 64-69. https://doi.org/10.1038/nature26158

Shen, K., Valenstein, M. L., Gu, X., & Sabatini, D. M. (2019). Arg-78 of Nprl2 catalyzes GATOR1-stimulated GTP hydrolysis by the Rag GTPases. *J Biol Chem*, *294*(8), 2970-2975. https://doi.org/10.1074/jbc.AC119.007382

Shi, S., Chen, Y., Siewers, V., & Nielsen, J. (2014). Improving production of malonyl coenzyme A-derived metabolites by abolishing Snf1-dependent regulation of Acc1. *mBio*, *5*(3), e01130-01114. https://doi.org/10.1128/mBio.01130-14

Shin, H. R., Citron, Y. R., Wang, L., Tribouillard, L., Goul, C. S., Stipp, R., Sugasawa, Y., Jain, A., Samson, N., Lim, C. Y., Davis, O. B., Castaneda-Carpio, D., Qian, M., Nomura, D. K., Perera, R. M., Park, E., Covey, D. F., Laplante, M., Evers, A. S., & Zoncu, R. (2022). Lysosomal GPCR-like protein LYCHOS signals cholesterol sufficiency to mTORC1. *Science*, *377*(6612), 1290-1298. https://doi.org/10.1126/science.abg6621

Shin, S., Wolgamott, L., Yu, Y., Blenis, J., & Yoon, S. O. (2011). Glycogen synthase kinase (GSK)-3 promotes p70 ribosomal protein S6 kinase (p70S6K) activity and cell proliferation. *Proc Natl Acad Sci U S A*, *108*(47), E1204-1213. https://doi.org/10.1073/pnas.1110195108

Shinoda, J., & Kikuchi, Y. (2007). Rod1, an arrestin-related protein, is phosphorylated by Snf1-kinase in *Saccharomyces cerevisiae*. *Biochem Biophys Res Commun*, *364*(2), 258-263. https://doi.org/10.1016/j.bbrc.2007.09.134

Shirra, M. K., McCartney, R. R., Zhang, C., Shokat, K. M., Schmidt, M. C., & Arndt, K. M. (2008). A chemical genomics study identifies Snf1 as a repressor of *GCN4* translation. *J Biol Chem*, *283*(51), 35889-35898. https://doi.org/10.1074/jbc.M805325200

Shvarev, D., Schoppe, J., Konig, C., Perz, A., Fullbrunn, N., Kiontke, S., Langemeyer, L., Januliene, D., Schnelle, K., Kummel, D., Frohlich, F., Moeller, A., & Ungermann, C. (2022). Structure of the HOPS tethering complex, a lysosomal membrane fusion machinery. *Elife*, *11*. https://doi.org/10.7554/eLife.80901

Simpson-Lavy, K., & Kupiec, M. (2023). Glucose Inhibits Yeast AMPK (Snf1) by Three Independent Mechanisms. *Biology (Basel)*, *12*(7). https://doi.org/10.3390/biology12071007

Simpson-Lavy, K. J., & Johnston, M. (2013). SUMOylation regulates the SNF1 protein kinase. *Proc Natl Acad Sci U S A*, *110*(43), 17432-17437. https://doi.org/10.1073/pnas.1304839110

Simpson-Lavy, K. J., & Kupiec, M. (2022). Regulation of yeast Snf1 (AMPK) by a polyhistidine containing pH sensing module. *iScience*, *25*(10), 105083. https://doi.org/10.1016/j.isci.2022.105083

Simpson-Lavy, K. J., & Kupiec, M. (2023). The polyHIS Tract of Yeast AMPK Coordinates Carbon Metabolism with Iron Availability. *Int J Mol Sci*, *24*(2). https://doi.org/10.3390/ijms24021368

Smets, B., De Snijder, P., Engelen, K., Joossens, E., Ghillebert, R., Thevissen, K., Marchal, K., & Winderickx, J. (2008). Genome-wide expression analysis reveals TORC1-

dependent and -independent functions of Sch9. *FEMS Yeast Res*, *8*(8), 1276-1288. https://doi.org/10.1111/j.1567-1364.2008.00432.x

Smiles, W. J., Ovens, A. J., Kemp, B. E., Galic, S., Petersen, J., & Oakhill, J. S. (2024). New developments in AMPK and mTORC1 cross-talk. *Essays Biochem*. https://doi.org/10.1042/EBC20240007

Smith, F. C., Davies, S. P., Wilson, W. A., Carling, D., & Hardie, D. G. (1999). The SNF1 kinase complex from *Saccharomyces* cerevisiae phosphorylates the transcriptional repressor protein Mig1p *in vitro* at four sites within or near regulatory domain 1. *FEBS Lett*, *453*(1-2), 219-223. https://doi.org/10.1016/s0014-5793(99)00725-5

Soulard, A., Cremonesi, A., Moes, S., Schutz, F., Jeno, P., & Hall, M. N. (2010). The rapamycin-sensitive phosphoproteome reveals that TOR controls protein kinase A toward some but not all substrates. *Mol Biol Cell*, *21*(19), 3475-3486. https://doi.org/10.1091/mbc.E10-03-0182

Stein, S. C., Woods, A., Jones, N. A., Davison, M. D., & Carling, D. (2000). The regulation of AMP-activated protein kinase by phosphorylation. *Biochem J*, *345 Pt 3*(Pt 3), 437-443. https://www.ncbi.nlm.nih.gov/pubmed/10642499

Steinberg, G. R., & Carling, D. (2019). AMP-activated protein kinase: the current landscape for drug development. *Nat Rev Drug Discov*, *18*(7), 527-551. https://doi.org/10.1038/s41573-019-0019-2

Steinberg, G. R., & Hardie, D. G. (2023). New insights into activation and function of the AMPK. *Nat Rev Mol Cell Biol*, *24*(4), 255-272. https://doi.org/10.1038/s41580-022-00547-x

Stracka, D., Jozefczuk, S., Rudroff, F., Sauer, U., & Hall, M. N. (2014). Nitrogen source activates TOR (target of rapamycin) complex 1 via glutamine and independently of Gtr/Rag proteins. *J Biol Chem*, *289*(36), 25010-25020. https://doi.org/10.1074/jbc.M114.574335

Sullivan, A., Wallace, R. L., Wellington, R., Luo, X., & Capaldi, A. P. (2019). Multilayered regulation of TORC1-body formation in budding yeast. *Mol Biol Cell*, *30*(3), 400-410. https://doi.org/10.1091/mbc.E18-05-0297

Sutherland, C. M., Hawley, S. A., McCartney, R. R., Leech, A., Stark, M. J., Schmidt, M. C., & Hardie, D. G. (2003). Elm1p is one of three upstream kinases for the *Saccharomyces cerevisiae* SNF1 complex. *Curr Biol*, *13*(15), 1299-1305. https://doi.org/10.1016/s0960-9822(03)00459-7

Sutter, B. M., Wu, X., Laxman, S., & Tu, B. P. (2013). Methionine inhibits autophagy and promotes growth by inducing the SAM-responsive methylation of PP2A. *Cell*, *154*(2), 403-415. https://doi.org/10.1016/j.cell.2013.06.041

Swinnen, E., Ghillebert, R., Wilms, T., & Winderickx, J. (2014). Molecular mechanisms linking the evolutionary conserved TORC1-Sch9 nutrient signalling branch to lifespan regulation in *Saccharomyces cerevisiae*. *FEMS Yeast Res*, *14*(1), 17-32. https://doi.org/10.1111/1567-1364.12097

Swinnen, E., Rosseels, J., & Winderickx, J. (2005). The minimum domain of Pho81 is not sufficient to control the Pho85-Rim15 effector branch involved in phosphate starvation-induced stress responses. *Curr Genet*, *48*(1), 18-33. https://doi.org/10.1007/s00294-005-0583-3

Tafur, L., Hinterndorfer, K., Gabus, C., Lamanna, C., Bergmann, A., Sadian, Y., Hamdi, F., Kyrilis, F. L., Kastritis, P. L., & Loewith, R. (2022). Cryo-EM structure of the SEA complex. *Nature*, *611*(7935), 399-404. https://doi.org/10.1038/s41586-022-05370-0

Takeda, E., Jin, N., Itakura, E., Kira, S., Kamada, Y., Weisman, L. S., Noda, T., & Matsuura, A. (2018). Vacuole-mediated selective regulation of TORC1-Sch9 signaling following oxidative stress. *Mol Biol Cell*, *29*(4), 510-522. https://doi.org/10.1091/mbc.E17-09-0553

Tan, Y. S., Morcos, P. A., & Cannon, J. F. (2003). Pho85 phosphorylates the Glc7 protein phosphatase regulator Glc8 *in vivo*. *J Biol Chem*, *278*(1), 147-153. https://doi.org/10.1074/jbc.M208058200

Tang, X., Zhang, Y., Wang, G., Zhang, C., Wang, F., Shi, J., Zhang, T., & Ding, J. (2022). Molecular mechanism of S-adenosylmethionine sensing by SAMTOR in mTORC1 signaling. *Sci Adv*, *8*(26), eabn3868. https://doi.org/10.1126/sciadv.abn3868

Tanigawa, M., Yamamoto, K., Nagatoishi, S., Nagata, K., Noshiro, D., Noda, N. N., Tsumoto, K., & Maeda, T. (2021). A glutamine sensor that directly activates TORC1. *Commun Biol*, *4*(1), 1093. https://doi.org/10.1038/s42003-021-02625-w

Tate, J. J., Rai, R., & Cooper, T. G. (2015). Nitrogen starvation and TorC1 inhibition differentially affect nuclear localization of the Gln3 and Gat1 transcription factors through the rare glutamine tRNA_{CUG} in *Saccharomyces cerevisiae*. *Genetics*, *199*(2), 455-474. https://doi.org/10.1534/genetics.114.173831

Tatebe, H., & Shiozaki, K. (2017). Evolutionary Conservation of the Components in the TOR Signaling Pathways. *Biomolecules*, *7*(4). https://doi.org/10.3390/biom7040077

Tavares, M. R., Pavan, I. C., Amaral, C. L., Meneguello, L., Luchessi, A. D., & Simabuco, F. M. (2015). The S6K protein family in health and disease. *Life Sci*, *131*, 1-10. https://doi.org/10.1016/j.lfs.2015.03.001

Tee, A. R., Manning, B. D., Roux, P. P., Cantley, L. C., & Blenis, J. (2003). Tuberous sclerosis complex gene products, Tuberin and Hamartin, control mTOR signaling by acting as a GTPase-activating protein complex toward Rheb. *Curr Biol*, *13*(15), 1259-1268. https://doi.org/10.1016/s0960-9822(03)00506-2

Teng, X., & Hardwick, J. M. (2019). Whi2: a new player in amino acid sensing. *Curr Genet*, *65*(3), 701-709. https://doi.org/10.1007/s00294-018-00929-9

Thedieck, K., Polak, P., Kim, M. L., Molle, K. D., Cohen, A., Jeno, P., Arrieumerlou, C., & Hall, M. N. (2007). PRAS40 and PRR5-like protein are new mTOR interactors that regulate apoptosis. *PLoS One*, *2*(11), e1217. https://doi.org/10.1371/journal.pone.0001217

Tian, W., Li, W., Chen, Y., Yan, Z., Huang, X., Zhuang, H., Zhong, W., Chen, Y., Wu, W., Lin, C., Chen, H., Hou, X., Zhang, L., Sui, S., Zhao, B., Hu, Z., Li, L., & Feng, D. (2015). Phosphorylation of ULK1 by AMPK regulates translocation of ULK1 to mitochondria and mitophagy. *FEBS Lett*, *589*(15), 1847-1854. https://doi.org/10.1016/j.febslet.2015.05.020

Toyama, E. Q., Herzig, S., Courchet, J., Lewis, T. L., Jr., Loson, O. C., Hellberg, K., Young, N. P., Chen, H., Polleux, F., Chan, D. C., & Shaw, R. J. (2016). Metabolism. AMP-activated protein kinase mediates mitochondrial fission in response to energy stress. *Science*, *351*(6270), 275-281. https://doi.org/10.1126/science.aab4138

Trefts, E., & Shaw, R. J. (2021). AMPK: restoring metabolic homeostasis over space and time. *Mol Cell*, *81*(18), 3677-3690. https://doi.org/10.1016/j.molcel.2021.08.015

Treitel, M. A., Kuchin, S., & Carlson, M. (1998). Snf1 protein kinase regulates phosphorylation of the Mig1 repressor in *Saccharomyces cerevisiae*. *Mol Cell Biol*, *18*(11), 6273-6280. https://doi.org/10.1128/MCB.18.11.6273

Tripodi, F., Castoldi, A., Nicastro, R., Reghellin, V., Lombardi, L., Airoldi, C., Falletta, E., Maffioli, E., Scarcia, P., Palmieri, L., Alberghina, L., Agrimi, G., Tedeschi, G., & Coccetti, P. (2018a). Methionine supplementation stimulates mitochondrial respiration. *Biochim Biophys Acta Mol Cell Res*, *1865*(12), 1901-1913. https://doi.org/10.1016/j.bbamcr.2018.09.007

Tripodi, F., Fraschini, R., Zocchi, M., Reghellin, V., & Coccetti, P. (2018b). Snf1/AMPK is involved in the mitotic spindle alignment in *Saccharomyces cerevisiae*. *Sci Rep*, *8*(1), 5853. https://doi.org/10.1038/s41598-018-24252-y

Ukai, H., Araki, Y., Kira, S., Oikawa, Y., May, A. I., & Noda, T. (2018). Gtr/Ego-independent TORC1 activation is achieved through a glutamine-sensitive interaction with Pib2 on the vacuolar membrane. *PLoS Genet*, *14*(4), e1007334. https://doi.org/10.1371/journal.pgen.1007334

Urban, J., Soulard, A., Huber, A., Lippman, S., Mukhopadhyay, D., Deloche, O., Wanke, V., Anrather, D., Ammerer, G., Riezman, H., Broach, J. R., De Virgilio, C., Hall, M. N., & Loewith, R. (2007). Sch9 is a major target of TORC1 in *Saccharomyces cerevisiae*. *Mol Cell*, *26*(5), 663-674. https://doi.org/10.1016/j.molcel.2007.04.020

Valbuena, N., Guan, K. L., & Moreno, S. (2012). The Vam6 and Gtr1-Gtr2 pathway activates TORC1 in response to amino acids in fission yeast. *J Cell Sci*, *125*(Pt 8), 1920-1928. https://doi.org/10.1242/jcs.094219

Valenstein, M. L., Lalgudi, P. V., Gu, X., Kedir, J. F., Taylor, M. S., Chivukula, R. R., & Sabatini, D. M. (2024). Rag-Ragulator is the central organizer of the physical architecture of the mTORC1 nutrient-sensing pathway. *Proc Natl Acad Sci U S A*, *121*(35), e2322755121. https://doi.org/10.1073/pnas.2322755121

Valenstein, M. L., Rogala, K. B., Lalgudi, P. V., Brignole, E. J., Gu, X., Saxton, R. A., Chantranupong, L., Kolibius, J., Quast, J. P., & Sabatini, D. M. (2022). Structure of the nutrient-sensing hub GATOR2. *Nature*, *607*(7919), 610-616. https://doi.org/10.1038/s41586-022-04939-z

van Eunen, K., Bouwman, J., Daran-Lapujade, P., Postmus, J., Canelas, A. B., Mensonides, F. I., Orij, R., Tuzun, I., van den Brink, J., Smits, G. J., van Gulik, W. M., Brul, S., Heijnen, J. J., de Winde, J. H., de Mattos, M. J., Kettner, C., Nielsen, J., Westerhoff, H. V., & Bakker, B. M. (2010). Measuring enzyme activities under standardized *in vivo*-like conditions for systems biology. *FEBS J*, *277*(3), 749-760. https://doi.org/10.1111/j.1742-4658.2009.07524.x

Van Nostrand, J. L., Hellberg, K., Luo, E. C., Van Nostrand, E. L., Dayn, A., Yu, J., Shokhirev, M. N., Dayn, Y., Yeo, G. W., & Shaw, R. J. (2020). AMPK regulation of Raptor and TSC2 mediate metformin effects on transcriptional control of anabolism and inflammation. *Genes Dev*, *34*(19-20), 1330-1344. https://doi.org/10.1101/gad.339895.120

Vincent, O., & Carlson, M. (1998). Sip4, a Snf1 kinase-dependent transcriptional activator, binds to the carbon source-responsive element of gluconeogenic genes. *EMBO J*, *17*(23), 7002-7008. https://doi.org/10.1093/emboj/17.23.7002

Vincent, O., & Carlson, M. (1999). Gal83 mediates the interaction of the Snf1 kinase complex with the transcription activator Sip4. *EMBO J*, *18*(23), 6672-6681. https://doi.org/10.1093/emboj/18.23.6672

Vincent, O., Townley, R., Kuchin, S., & Carlson, M. (2001). Subcellular localization of the Snf1 kinase is regulated by specific beta subunits and a novel glucose signaling mechanism. *Genes Dev*, *15*(9), 1104-1114. https://doi.org/10.1101/gad.879301

Voordeckers, K., Kimpe, M., Haesendonckx, S., Louwet, W., Versele, M., & Thevelein, J. M. (2011). Yeast 3-phosphoinositide-dependent protein kinase-1 (PDK1) orthologs Pkh1-3 differentially regulate phosphorylation of protein kinase A (PKA) and the protein kinase B (PKB)/S6K ortholog Sch9. *J Biol Chem*, *286*(25), 22017-22027. https://doi.org/10.1074/jbc.M110.200071

Wang, J., Cervantes, S., Davis, S., & Ferro-Novick, S. (2015). Identifying a Rab effector on the macroautophagy pathway. *Methods Mol Biol*, *1298*, 117-125. https://doi.org/10.1007/978-1-4939-2569-8_10

Wang, L., Harris, T. E., Roth, R. A., & Lawrence, J. C., Jr. (2007). PRAS40 regulates mTORC1 kinase activity by functioning as a direct inhibitor of substrate binding. *J Biol Chem*, *282*(27), 20036-20044. https://doi.org/10.1074/jbc.M702376200

Wang, L., Kobayashi, T., Piao, X., Shiono, M., Takagi, Y., Mineki, R., Taka, H., Zhang, D., Abe, M., Sun, G., Hagiwara, Y., Okimoto, K., Matsumoto, I., Kouchi, M., & Hino, O. (2010). Serine 62 is a phosphorylation site in folliculin, the Birt-Hogg-Dube gene product. *FEBS Lett*, *584*(1), 39-43. https://doi.org/10.1016/j.febslet.2009.11.033

Wang, S., Tsun, Z. Y., Wolfson, R. L., Shen, K., Wyant, G. A., Plovanich, M. E., Yuan, E. D., Jones, T. D., Chantranupong, L., Comb, W., Wang, T., Bar-Peled, L., Zoncu, R., Straub, C., Kim, C., Park, J., Sabatini, B. L., & Sabatini, D. M. (2015). Metabolism. Lysosomal amino acid transporter SLC38A9 signals arginine sufficiency to mTORC1. *Science*, *347*(6218), 188-194. https://doi.org/10.1126/science.1257132

Wang, X., Campbell, L. E., Miller, C. M., & Proud, C. G. (1998). Amino acid availability regulates p70 S6 kinase and multiple translation factors. *Biochem J*, *334 (Pt 1)*(Pt 1), 261-267. https://doi.org/10.1042/bj3340261

Wang, Z., Wilson, W. A., Fujino, M. A., & Roach, P. J. (2001). Antagonistic controls of autophagy and glycogen accumulation by Snf1p, the yeast homolog of AMP-activated protein kinase, and the cyclin-dependent kinase Pho85p. *Mol Cell Biol*, *21*(17), 5742-5752. https://doi.org/10.1128/MCB.21.17.5742-5752.2001

Wanke, V., Cameroni, E., Uotila, A., Piccolis, M., Urban, J., Loewith, R., & De Virgilio, C. (2008). Caffeine extends yeast lifespan by targeting TORC1. *Mol Microbiol*, *69*(1), 277-285. https://doi.org/10.1111/j.1365-2958.2008.06292.x

Wanke, V., Pedruzzi, I., Cameroni, E., Dubouloz, F., & De Virgilio, C. (2005). Regulation of G0 entry by the Pho80-Pho85 cyclin-CDK complex. *EMBO J*, *24*(24), 4271-4278. https://doi.org/10.1038/sj.emboj.7600889

Warden, S. M., Richardson, C., O'Donnell, J., Jr., Stapleton, D., Kemp, B. E., & Witters, L. A. (2001). Post-translational modifications of the beta-1 subunit of AMP-activated protein kinase affect enzyme activity and cellular localization. *Biochem J*, *354*(Pt 2), 275-283. https://doi.org/10.1042/0264-6021:3540275

Wei, J., Zhang, Y., Yu, T. Y., Sadre-Bazzaz, K., Rudolph, M. J., Amodeo, G. A., Symington, L. S., Walz, T., & Tong, L. (2016). A unified molecular mechanism for the regulation of acetyl-CoA carboxylase by phosphorylation. *Cell Discov*, *2*, 16044. https://doi.org/10.1038/celldisc.2016.44

Willows, R., Navaratnam, N., Lima, A., Read, J., & Carling, D. (2017). Effect of different gamma-subunit isoforms on the regulation of AMPK. *Biochem J*, *474*(10), 1741-1754. https://doi.org/10.1042/BCJ20170046

Wilms, T., Swinnen, E., Eskes, E., Dolz-Edo, L., Uwineza, A., Van Essche, R., Rosseels, J., Zabrocki, P., Cameroni, E., Franssens, V., De Virgilio, C., Smits, G. J., & Winderickx, J. (2017). The yeast protein kinase Sch9 adjusts V-ATPase assembly/disassembly to control pH homeostasis and longevity in response to glucose availability. *PLoS Genet*, *13*(6), e1006835. https://doi.org/10.1371/journal.pgen.1006835

Wilson, W. A., Hawley, S. A., & Hardie, D. G. (1996). Glucose repression/derepression in budding yeast: SNF1 protein kinase is activated by phosphorylation under derepressing conditions, and this correlates with a high AMP:ATP ratio. *Curr Biol*, *6*(11), 1426-1434. https://doi.org/10.1016/s0960-9822(96)00747-6

Wiza, C., Nascimento, E. B., & Ouwens, D. M. (2012). Role of PRAS40 in Akt and mTOR signaling in health and disease. *Am J Physiol Endocrinol Metab*, *302*(12), E1453-1460. https://doi.org/10.1152/ajpendo.00660.2011

Wolfson, R. L., Chantranupong, L., Saxton, R. A., Shen, K., Scaria, S. M., Cantor, J. R., & Sabatini, D. M. (2016). Sestrin2 is a leucine sensor for the mTORC1 pathway. *Science*, *351*(6268), 43-48. https://doi.org/10.1126/science.aab2674

Wolfson, R. L., Chantranupong, L., Wyant, G. A., Gu, X., Orozco, J. M., Shen, K., Condon, K. J., Petri, S., Kedir, J., Scaria, S. M., Abu-Remaileh, M., Frankel, W. N., & Sabatini, D. M. (2017). KICSTOR recruits GATOR1 to the lysosome and is necessary for nutrients to regulate mTORC1. *Nature*, *543*(7645), 438-442. https://doi.org/10.1038/nature21423

Woods, A., Cheung, P. C., Smith, F. C., Davison, M. D., Scott, J., Beri, R. K., & Carling, D. (1996). Characterization of AMP-activated protein kinase beta and gamma subunits.

Assembly of the heterotrimeric complex *in vitro*. *J Biol Chem*, *271*(17), 10282-10290. https://doi.org/10.1074/jbc.271.17.10282

Wosika, V., Durandau, E., Varidel, C., Aymoz, D., Schmitt, M., & Pelet, S. (2016). New families of single integration vectors and gene tagging plasmids for genetic manipulations in budding yeast. *Mol Genet Genomics*, *291*(6), 2231-2240. https://doi.org/10.1007/s00438-016-1249-1

Wu, X., Xie, W., Xie, W., Wei, W., & Guo, J. (2022). Beyond controlling cell size: functional analyses of S6K in tumorigenesis. *Cell Death Dis*, *13*(7), 646. https://doi.org/10.1038/s41419-022-05081-4

Wullschleger, S., Loewith, R., & Hall, M. N. (2006). TOR signaling in growth and metabolism. *Cell*, *124*(3), 471-484. https://doi.org/10.1016/j.cell.2006.01.016

Xiao, W., Fontanie, T., & Tang, M. (1994). UBP5 encodes a putative yeast ubiquitin-specific protease that is related to the human Tre-2 oncogene product. *Yeast*, *10*(11), 1497-1502. https://doi.org/10.1002/yea.320101114

Yang, H., Jiang, X., Li, B., Yang, H. J., Miller, M., Yang, A., Dhar, A., & Pavletich, N. P. (2017). Mechanisms of mTORC1 activation by RHEB and inhibition by PRAS40. *Nature*, *552*(7685), 368-373. https://doi.org/10.1038/nature25023

Yang, S., Zhang, Y., Ting, C. Y., Bettedi, L., Kim, K., Ghaniam, E., & Lilly, M. A. (2020). The Rag GTPase Regulates the Dynamic Behavior of TSC Downstream of Both Amino Acid and Growth Factor Restriction. *Dev Cell*, *55*(3), 272-288 e275. https://doi.org/10.1016/j.devcel.2020.08.006

Yang, X., Hubbard, E. J., & Carlson, M. (1992). A protein kinase substrate identified by the two-hybrid system. *Science*, *257*(5070), 680-682. https://doi.org/10.1126/science.1496382

Yang, Y., Reid, M. A., Hanse, E. A., Li, H., Li, Y., Ruiz, B. I., Fan, Q., & Kong, M. (2023). SAPS3 subunit of protein phosphatase 6 is an AMPK inhibitor and controls metabolic homeostasis upon dietary challenge in male mice. *Nat Commun*, *14*(1), 1368. https://doi.org/10.1038/s41467-023-36809-1

Yao, W., Chen, Y., Chen, Y., Zhao, P., Liu, J., Zhang, Y., Jiang, Q., Wu, C., Xie, Y., Fan, S., Ye, M., Wang, Y., Feng, Y., Bai, X., Fan, M., Feng, S., Wang, J., Cui, Y., Xia, H.,…Yi, C. (2023). TOR-mediated Ypt1 phosphorylation regulates autophagy initiation complex assembly. *EMBO J*, *42*(19), e112814. https://doi.org/10.15252/embj.2022112814

Yao, W., Chen, Y., Zhang, Y., Zhong, S., Ye, M., Chen, Y., Fan, S., Ye, M., Yang, H., Li, Y., Wu, C., Fan, M., Feng, S., He, Z., Zhou, L., Zhang, L., Wang, Y., Liu, W., Tong, J.,…Yi, C. (2024). Ca^{2+}-triggered Atg11-Bmh1/2-Snf1 complex assembly initiates autophagy upon glucose starvation. *J Cell Biol*, *223*(9). https://doi.org/10.1083/jcb.202310049

Yao, W., Li, Y., Wu, L., Wu, C., Zhang, Y., Liu, J., He, Z., Wu, X., Lu, C., Wang, L., Zhong, H., Hong, Z., Xu, S., Liu, W., & Yi, C. (2020). Atg11 is required for initiation of glucose starvation-induced autophagy. *Autophagy*, *16*(12), 2206-2218. https://doi.org/10.1080/15548627.2020.1719724

Yerlikaya, S., Meusburger, M., Kumari, R., Huber, A., Anrather, D., Costanzo, M., Boone, C., Ammerer, G., Baranov, P. V., & Loewith, R. (2016). TORC1 and TORC2 work together to regulate ribosomal protein S6 phosphorylation in *Saccharomyces cerevisiae*. *Mol Biol Cell*, *27*(2), 397-409. https://doi.org/10.1091/mbc.E15-08-0594

Yi, C., Tong, J., Lu, P., Wang, Y., Zhang, J., Sun, C., Yuan, K., Xue, R., Zou, B., Li, N., Xiao, S., Dai, C., Huang, Y., Xu, L., Li, L., Chen, S., Miao, D., Deng, H., Li, H., & Yu, L. (2017). Formation of a Snf1-Mec1-Atg1 Module on Mitochondria Governs Energy Deprivation-Induced Autophagy by Regulating Mitochondrial Respiration. *Dev Cell*, *41*(1), 59-71 e54. https://doi.org/10.1016/j.devcel.2017.03.007

Yoon, M. S. (2017). The Role of Mammalian Target of Rapamycin (mTOR) in Insulin Signaling. *Nutrients*, *9*(11). https://doi.org/10.3390/nu9111176

Yorimitsu, T., Zaman, S., Broach, J. R., & Klionsky, D. J. (2007). Protein kinase A and Sch9 cooperatively regulate induction of autophagy in *Saccharomyces cerevisiae*. *Mol Biol Cell*, *18*(10), 4180-4189. https://doi.org/10.1091/mbc.e07-05-0485

Young, E. T., Dombek, K. M., Tachibana, C., & Ideker, T. (2003). Multiple pathways are co-regulated by the protein kinase Snf1 and the transcription factors Adr1 and Cat8. *J Biol Chem*, *278*(28), 26146-26158. https://doi.org/10.1074/jbc.M301981200

Zeng, Q., Araki, Y., & Noda, T. (2024). Pib2 is a cysteine sensor involved in TORC1 activation in *Saccharomyces cerevisiae*. *Cell Rep*, *43*(1), 113599. https://doi.org/10.1016/j.celrep.2023.113599

Zhang, J., Olsson, L., & Nielsen, J. (2010). The beta-subunits of the Snf1 kinase in *Saccharomyces cerevisiae*, Gal83 and Sip2, but not Sip1, are redundant in glucose derepression and regulation of sterol biosynthesis. *Mol Microbiol*, *77*(2), 371-383. https://doi.org/10.1111/j.1365-2958.2010.07209.x

Zhang, T., Péli-Gulli, M. P., Zhang, Z., Tang, X., Ye, J., De Virgilio, C., & Ding, J. (2019). Structural insights into the EGO-TC-mediated membrane tethering of the TORC1-regulatory Rag GTPases. *Sci Adv*, *5*(9), eaax8164. https://doi.org/10.1126/sciadv.aax8164

Zhang, Y., Gao, X., Saucedo, L. J., Ru, B., Edgar, B. A., & Pan, D. (2003). Rheb is a direct target of the tuberous sclerosis tumour suppressor proteins. *Nat Cell Biol*, *5*(6), 578-581. https://doi.org/10.1038/ncb999

Zong, Y., Zhang, C. S., Li, M., Wang, W., Wang, Z., Hawley, S. A., Ma, T., Feng, J. W., Tian, X., Qi, Q., Wu, Y. Q., Zhang, C., Ye, Z., Lin, S. Y., Piao, H. L., Hardie, D. G., & Lin, S. C. (2019). Hierarchical activation of compartmentalized pools of AMPK depends on severity of nutrient or energy stress. *Cell Res*, *29*(6), 460-473. https://doi.org/10.1038/s41422-019-0163-6

APPENDIX

Acknowledgments

This was an important chapter of my life, my first adventure far from home, and it wouldn't have been possible without the support and help of many friends and colleagues. So, I would like to thank:

Claudio, you have been an incredible supervisor. Every time I entered your office, I came out enriched, with more suggestions, ideas, or even funny comments and stories. From you, I learned to never be satisfied and always strive for better. Thank you for guiding me in these years and believing in me in the first place.

Professors Claudio De Virgilio, Robbie Loewith, and Sébastien Leon, for being part of my PhD thesis committee and for reading and correcting this thesis.

Jörn, thank you for being part of my thesis committee until almost the end. You gave me great insights and participated in the decisions throughout my different projects.

Prof. Joris Winderickx, even though we never had the chance to meet in person, you allowed me to take part in different projects, which led to significant successes in my career. Thank you for your consideration.

Raffa, sei stato un tutor in laboratorio, un amico e un fratello fuori. Mi hai accolto qui e mi hai sfamato durante i tempi del COVID. Se posso dire di essere uno scienziato, è perché mi hai insegnato il metodo scientifico, come pensare e fare le cose fatte bene. Se il mio dottorato è andato liscio, è certamente grazie al tuo aiuto e supporto. Grazie.

Prof. Paola Coccetti e Farida: il mio amore per i lieviti e SNF1 mi è stato trasmesso da voi. Avete creduto in me fin dal Bachelor e mi avete permesso di prendere il volo e vivere questa avventura. Farida, mi hai formato e impostato come scienziato, grazie di cuore.

Marie-Pierre, Malika, and Susi, you have always been kind and helpful to me. You made my work smoother in the lab. I learned a lot from you and I am grateful I met you.

Riko, Ladislav, Guille, Aurélien, Cyril, Rebe, Fra, and Saloni, you have been incredible lab mates. We laughed a lot together, inside and outside the lab.

Olga, ton aide a été inestimable. Tu as rendu mon travail beaucoup plus facile et rapide. Aussi, tu m'as beaucoup aidé en français et tu m'as toujours donné le sourire.

Evelyn, Jean-Daniel, Laura, Céline, and Luisa, vous faisiez également partie de ce voyage, avec des rôles différents, mais merci pour votre aide.

Justine, Lisa, Lucie, and Siria, it was a pleasure and honor teaching you all. A special mention goes to Pauline; a huge part of this thesis was possible thanks to your invaluable help.

To my best friend and Mexican brother Alfonso. I would be completely lost without you in my life. I am incredibly grateful that I met you; you changed me and always supported me outside the lab, in the most difficult decisions. Te quiero.

The gossip queens Sibilla (my surfing buddy) and Melanie (la mia massista di fiducia (= my mass spec trustworthy person)). I loved coming to your lab and laughing and gossiping with you.

All my friends Juliette, Davide, Ema, Alex, Ibby, Séb, Deva, Nacho, Bich, Josephine, Jenny, Zehan, and Gloria. You, and the friends mentioned above, have been like a family to me. When I moved far from home, I met you and you filled a gap in my life.

Cri, Andre, Gabri, Enrico e Luchyo, ho passato momenti meravigliosi con voi. Siete stati grandi amici e un tocco di italianità nella mia avventura svizzera.

I would also like to thank all the friends and people I met during these years in Fribourg and at the University. It was a pleasure spending nice moments with you.

Oti, mi sei sempre stato vicino e mi hai tenuto tanta compagnia. Sono contento che nonostante la distanza non ci siamo persi.

La mia famiglia, mamma, papà, Michi, e Marti. Anche se da lontano, ho sempre sentito la vostra vicinanza. Se sono arrivato qui è grazie al supporto che mi avete dato fin da quando ero piccolo.

I miei nonni Maria, Gianguido, Burnella, Claudia, and zio Gio. Purtroppo non tutti siete arrivati fino a questo momento, ma vi porto nel mio cuore. Mi avete cresciuto e mi avete sempre sostenuto. Anche se non di persona, vi sento vicini in questo momento.

Karen, these years and the distance were sometimes a challenge. We had our ups and downs, but you accompanied me throughout this adventure. Thank you for being there, listening to me like no one else did, for always giving the right suggestion and using the right words, and especially for spending lovely moments with me.

Lastly I thank you, *Streptococcus pneumoniae*. You infected me in 2013 and caused me sepsis. Before, I wanted to become an engineer (before even a fireman), but you made me ask myself, *"How is it possible that we, human beings, were able to go to the moon but still such a teeny-tiny organism can almost kill me?"*. Well, thanks to you I found out that the microscopic world is incredibly fun and that there is still much more to discover.

Curriculum Vitae

Marco Caligaris

PhD Candidate in Biochemistry

Route des Arsenaux, 6, Fribourg CH-1700, Switzerland
+41 77 259 18 72 marco.caligaris@outlook.com Google Scholar

Professional Experience

PhD candidate in Biochemistry (Oct. 2020 – Today)

University of Fribourg (Switzerland) - Prof. Claudio De Virgilio's lab

- Managed and collaborated on 7 research projects involving international groups.
- Published 4 scientific articles in peer-reviewed journals.
- Presented data at 4 international congress.
- Summarized and exposed data in written reports and monthly oral presentations.
- Implemented Biochemical methods by designing and optimizing protocols.

Master's degree thesis project (Sep. 2019 – Jul. 2020)

University of Fribourg (Switzerland) – Prof. Claudio De Virgilio's lab
University of Milan-Bicocca (Italy) – Prof. Paola Coccetti's lab

- Initiated and developed 2 research projects between 2 international laboratories.
- Prepared samples for phosphoproteomics analysis and identified key phosphorylation targets from the resulting data.
- Mastered the most common Biochemical and Molecular Biology techniques.

Education

PhD candidate in Biochemistry (Oct. 2020 – Jan. 2025)

University of Fribourg (Switzerland)

- Continuing education by attending certified courses, seminars, and workshops.

MSc in Industrial Biotechnologies (Oct. 2018 – Jul. 2020)

University of Milan-Bicocca (Italy)

- Result: 110/110 with honors.
- 6 months exchange period at the University of Fribourg with awarded fellowships.

BSc in Biotechnologies (Oct. 2015 – Jul. 2018)

University of Milan-Bicocca (Italy)

- Result: 110/110 with honors.

Awards

Best oral presentation

- 6th European Workshop on AMPK (October 2024).

Fellowships

- SEMP (Swiss European Mobility Programme); awarded by *University of Fribourg* (2020)
- Erasmus exchange Extra-EU programme; awarded by *University of Milan-Bicocca* (2020)

Standard methods

Molecular Biology | CRISPR/Cas9, cloning, PCR, qPCR, genetic screenings.
Biochemistry | Western blotting, CoIPs, protein purification, radioactive kinase assays, microscale thermophoresis.
Others | Confocal fluorescent microscopy, planification of omic analyses (SILAC phosphoproteomics, proteomics, interactomics, TurboID proximity labeling).

Supervising and teaching

Teaching in Biochemistry practical courses (2021 – 2024)
University of Fribourg and University of Bern (Switzerland)

- Bachelor's level – between 40 to 100 students per semester.

Teaching in Biology and Biochemistry theoretical courses (2021 – 2024)
University of Fribourg and University of Bern (Switzerland)

- Master's level – between 5 and 30 students per lecture
- Two 15 minutes presentations and 1 lecture

Mentored and trained students (2021 – Today)

- 1 apprentice student (4 months)
- 3 Bachelor's students (100 hours each)
- 1 post-Master's intern (6 month)
- 1 visiting PhD student (4 month)
- 1 PhD student (from Sep. 2024) – ongoing

Membership and Professional Organizations

Elected PhD student representative in Department Council (2023 - 2024)
University of Fribourg (Switzerland)

- Represented PhD students' interests in the Biology Department Council.

Student representative in graduate school committee (2022)
University of Fribourg (Switzerland)

- Co-organized 1 scientific retreat and 4 seminars for 40 PhD students.

IT skills

Science related | GraphPad Prism, Fiji (ImageJ), SnapGene, Cytoscape
OS | Windows, MacOS
Others | Microsoft Office suite, Adobe Illustrator, Adobe Photoshop, Python basis

Languages

Italian | Native
English | Fluent
French | Intermediate (B2 level, certified by the *University of Fribourg*)

Publications

1. **Caligaris, M.**[†], & De Virgilio, C.* (2024). Proxies introduce bias in decoding TORC1 activity. MicroPubl Biol, 2024. https://doi.org/10.17912/micropub.biology.001170
2. **Caligaris, M.**[†], Sampaio-Marques, B., Hatakeyama, R., Pillet, B., Ludovico, P., De Virgilio, C., Winderickx, J., & Nicastro, R.* (2023). The Yeast Protein Kinase Sch9 Functions as a Central Nutrient-Responsive Hub That Calibrates Metabolic and Stress-Related Responses. J Fungi (Basel), 9(8). https://doi.org/10.3390/jof9080787
3. Deprez, M. A.[†], **Caligaris, M.**[†], Rosseels, J.[†], Hatakeyama, R., Ghillebert, R., Sampaio-Marques, B., Mudholkar, K., Eskes, E., Meert, E., Ungermann, C., Ludovico, P., Rospert, S., De Virgilio, C.*, & Winderickx, J.* (2023). The nutrient-responsive CDK Pho85 primes the Sch9 kinase for its activation by TORC1. PLoS Genet, 19(2), e1010641. https://doi.org/10.1371/journal.pgen.1010641
4. **Caligaris, M.**[†], Nicastro, R.*, Hu, Z., Tripodi, F., Hummel, J. E., Pillet, B., Deprez, M. A., Winderickx, J., Rospert, S., Coccetti, P., Dengjel, J., & De Virgilio, C.* (2023). Snf1/AMPK fine-tunes TORC1 signaling in response to glucose starvation. Elife, 12. https://doi.org/10.7554/eLife.84319

Conferences

1. Selected talks:
    - 6th European Workshop on AMPK (France – September-October 2024)
2. Selected poster presentations:
    - 3rd edition of the TOR de France (France - October 2023)
    - 31st International Conference on Yeast Genetics and Molecular Biology (Italy - August 2023)
    - 15th International Congress on Yeast meets the 30th International Conference on Yeast Genetics and Molecular Biology (Austria - August 2021)

References

Available upon request.